AGARD-CP-240

AGARD

ADVISORY GROUP FOR AEROSPACE RESEARCH & DEVELOPMENT

7 RUE ANCELLE 92200 NEUILLY SUR SEINE FRANCE

AGARD CONFERENCE PROCEEDINGS No. 240

Guidance and Control Design Considerations for Low-Altitude and Terminal-Area Flight

NORTH ATLANTIC TREATY ORGANIZATION

DISCLAIMER NOTICE

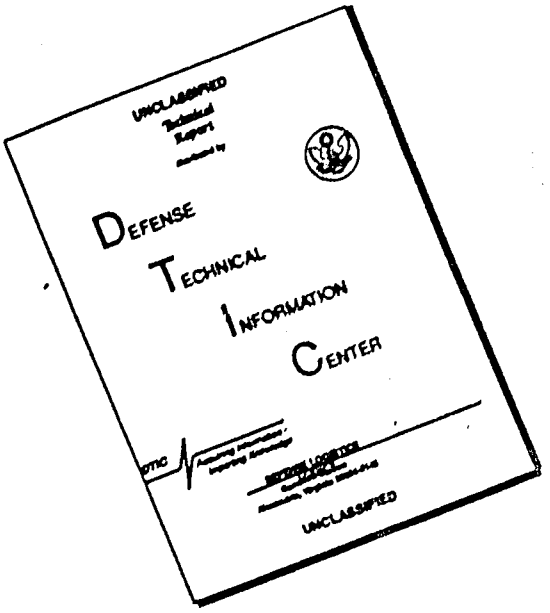

THIS DOCUMENT IS BEST QUALITY AVAILABLE. THE COPY FURNISHED TO DTIC CONTAINED A SIGNIFICANT NUMBER OF PAGES WHICH DO NOT REPRODUCE LEGIBLY.

NORTH ATLANTIC TREATY ORGANIZATION

ADVISORY GROUP FOR AEROSPACE RESEARCH AND DEVELOPMENT

(ORGANISATION DU TRAITE DE L'ATLANTIQUE NORD)

(9) Conference proceedings.

(6) AGARD Conference Proceedings No.240

GUIDANCE AND CONTROL DESIGN CONSIDERATIONS FOR LOW-ALTITUDE AND TERMINAL-AREA FLIGHT.

(11) Apr 78

(12) 317p.

Papers presented at the Guidance and Control Panel
Symposium held in Dayton, Ohio, USA, 17–20 October 1977

THE MISSION OF AGARD

The mission of AGARD is to bring together the leading personalities of the NATO nations in the fields of science and technology relating to aerospace for the following purposes:

- Exchanging of scientific and technical information;
- Continuously stimulating advances in the aerospace sciences relevant to strengthening the common defence posture;
- Improving the co-operation among member nations in aerospace research and development;
- Providing scientific and technical advice and assistance to the North Atlantic Military Committee in the field of aerospace research and development;
- Rendering scientific and technical assistance, as requested, to other NATO bodies and to member nations in connection with research and development problems in the aerospace field;
- Providing assistance to member nations for the purpose of increasing their scientific and technical potential;
- Recommending effective ways for the member nations to use their research and development capabilities for the common benefit of the NATO community.

The highest authority within AGARD is the National Delegates Board consisting of officially appointed senior representatives from each member nation. The mission of AGARD is carried out through the Panels which are composed of experts appointed by the National Delegates, the Consultant and Exchange Program and the Aerospace Applications Studies Program. The results of AGARD work are reported to the member nations and the NATO Authorities through the AGARD series of publications of which this is one.

Participation in AGARD activities is by invitation only and is normally limited to citizens of the NATO nations.

Published April 1978

ISBN 92-835-1278-2

Printed by Technical Editing and Reproduction Ltd
Harford House, 7–9 Charlotte St, London, W1P 1HD

PREFACE

Future operational needs dictate that conventional and VTOL aircraft and helicopters will be operated close to the ground in a wide range of operational tasks and weather conditions. The proximity of the ground produces many common factors that apply in all such situations. In particular, these relate to the precision and modes of control of the aircraft subject to special environmental conditions near the ground, the requirements for sensing position relative to ground features and the high importance of establishing the necessary safety, integrity standards commensurate with the vulnerability to enemy defenses.

This symposium presented recent state-of-the-art in technology to achieve operational capability under adverse weather conditions, and stressed the need for integrity and safety while operating in close proximity to the ground. Of interest for some are the advanced techniques in achieving direct lift control and technology to improve the aircraft resistance to disturbances such as wind shear and gust.

The Guidance and Control Panel expresses sincere appreciation to all the authors and participants that made this symposium a success.

GUIDANCE AND CONTROL PANEL OFFICERS

Chairman: Mr M.A.Ostgaard, Flight Control Division, AFFDL/FG, Wright-Patterson Air Force Base, Ohio 45433, USA
Deputy Chairman: Mr P.Kant, National Aerospace Laboratory (NLR), Voorsterweg 31, Post Emmeloord, Netherlands

PROGRAMME OFFICERS FOR 25th GCP MEETING

Mr G.C.Howell (co-Chairman), Royal Aircraft Establishment, Clapham, Bedford MK41 6AF
Mr M.A.Ostgaard,(co-Chairman), Flight Control Division, AFFDL/FG, Wright-Patterson Air Force Base, Ohio,45433, USA

HOST COORDINATOR

Mr L.J.Urban, Avionics Engineering, Aeronautical Systems Division/ENA, Wright-Patterson Air Force Base, Ohio 45433, USA

PANEL EXECUTIVE

Lt Colonel M.H.Cavenel, FAF

CONTENTS

† Published in CP-240 (Supplement). Classified

* Not available at time of printing

KEYNOTE ADDRESS

by

Charles H.Hausenfleck, Col., USAF
Vice Commander, AFTEC, Kirtland AFB NM

Distinguished members of AGARD, guests, ladies and gentlemen. It is a great pleasure for me to be with you at this 25th meeting of the Guidance and Control Panel. I know the subject of this Panel's meeting is of widespread interest and concern to all member nations represented here. It is of vital importance, as General Rushworth has so aptly pointed out. It is also a very meaningful subject to me as a result of some experience on both the development and operational sides of the question. So I am very much delighted to be with you and be a part of your deliberations today.

For my part, I would like to attempt to set the stage for the next four days – to describe in a very general way the possible events which cause us to have to consider so precisely the requirements for effective operations in the low altitude and terminal area flight regimes. The presentations by other speakers which will then follow over the next several days will get to the heart of the matter in great detail.

I would like to speak to a conventional air/land battle as could conceivably occur between NATO and the Warsaw Pact forces in Central Europe. My presentation is a concept only and it is intended as a framework for discussion; to challenge your thinking, if I may. It emphasizes the role of tactical aircraft in the teamwork between air and ground forces as they seek to counter massive attack. I recognize some of the tactics implied may not be accepted by everyone here. But again, I use them only to illustrate the spectrum of operations, primarily at low altitude, for aircraft involved in the battle. There may also be a difference of opinion on the nature and the magnitude of the threat we face in Central Europe. Nevertheless, an air/land battle in Europe presents the most critical problems in terms of strategy, timing, force ratios, and of special interest to us here today, operational environments for aircraft.

There is also a wide range of scenarios that we may be faced with, and I am sure all will not agree upon which is most likely. But I think we can agree that, regardless of the scenario, we must be prepared to win the opening battle.

In the past we were unprepared for the first battle. We relied upon technology and time, particularly, to work in our favor. Neither of these crutches works to our advantage any longer. We must plan and train now and equip our forces now to win now. Once hostilities begin, it will be too late.

Let's consider a 23/30 scenario since there is a wide understanding of content of that scenario. However, the application of the concept is not limited to any single scenario. The focus is on achieving a tactical aircraft, or tac air, allocation and ground force application mix, to generate combat power throughout the depth of the battlefield.

First of all, what do we mean by the air/land battle? The US Army Field Manual 100-5, "Operations", gives us a good point of departure. It points out that our air and land forces are interdependent (Fig.1). Both can deliver fire power against the enemy, both can kill tanks, both can conduct intelligence gathering, air defense, logistics, electronic warfare operations, and a lot of other functions that comprise the totality of combat power. But neither the Army nor the Air Force alone can fulfill any one of those functions, completely, or by itself. The combination of Army and Air Force capabilities – and limitations – make the services a natural team. And it is the sum or synergistic effect of that activity, the concentration of their combined combat power against enemy forces conducting a major attack, that we have come to describe as the air/land battle.

Looking now at our scenario, the Warsaw Pact launches a massive attack following the period of build-up. Now the defender, I'm sure, would prefer that events follow an ideal case as shown here (Fig.2). We may consider this ideal for several reasons. Since the required Warsaw Pact attrition is achieved prior to major ground force engagement, the Army would be able to defeat Pact ground forces without dependence on close air support. Moreover, the character and depth of Warsaw Pact target arrays prior to engagement offer significant advantages to attacking aircraft. Targets are relatively densely packed in march column formation and they can be identified as hostile simply by location.

The minimum case (Fig.3), that is to say the least desirable, or the maximum risk case that will still satisfy our objective of successfully defending with a minimum loss of territory, is shown on this slide. In this case, the Pact forces have not been attrited to the required level prior to ground force engagement. Therefore, the tactical air forces and Army must mass their fire power at the critical points in time to achieve the combined combat power to halt the enemy.

Here are some of the basic requirements of the air/land battle as we see them (Fig.4). Army and Air Force commanders must be able to see the battlefield to ascertain the location and direction of the main enemy effort. Both services have reconnaissance and surveillance systems capable of making inputs to the overall intelligence and combat information needs. Once the main thrusts are identified, it is the job of the commanders to bring about a winning concentration of force at the critical points. Air and land elements must fight as an integrated team to achieve the needed concentration. As an example, the Air Force may provide close air support to engaged ground forces in those areas where success of the overall effort hangs in the balance. The Army, in turn, provides support in the suppression of enemy air defenses through fire power and electronic means. In addition, the Army contributes to effective close air support through its capabilities for intelligence collection and target designation. I think the remaining factor is self evident. Winning in the European context means winning the first battle with minimum loss of territory.

Now, let's examine how tac air impacts on the air/land battle. First of all, the air/land battle is a tactical battle fought against enemy forces on a major axis of attack. Therefore, it is a critical battle. Within the theatre, there will be a number of air/land battles, all critical and all competing for limited combat resources, tac air included. The tac air missions which most directly influence the air/land battle are primarily close air support of friendly ground forces, air interdiction and, of course, reconnaissance-surveillance to find the targets. Each of these missions presents a unique set of problems in terms of low altitude and terminal area operations. Also, these can be accomplished only by achieving local air superiority for a period of time. From a broader theater perspective, we recognize that offensive and defensive counter air operations will be required to provide security from air attack to our own ground elements and air bases. The airlift mission also contributes to the successful operation. It is the job of the theatre commander to apportion available tac air assets to the various air missions. The remainder of the concept will suggest how that percentage of the overall air effort which has been apportioned to support for the ground forces might best be used.

Because of the likelihood of more than one air/land battle, the first task facing the defender from a theatre perspective is to see across the enemy side with sufficient accuracy to determine where those critical battles will be fought. This is a tall order because the Pact has such a preponderance of force that it will be difficult to identify his major axes of attack. Nevertheless, this must be done and it must be done right or we will be in trouble from the outset. We must check and cross-check data from every available source. We need a lot of confidence in our estimates to permit timely decision-making and the concentration of our forces at the right places, preferably before the hostilities begin, but certainly soon enough afterward to enable them to execute their mission.

If we reduce our focus from the theatre down to, for example, a NATO corps (and in this case, I am going to use US Corps) faced with one of the major attacks, we might find two Warsaw Pact combined arms armies deployed opposite the corps. The combined arms army conducting the main attack could be concentrated on a narrow front in deep echelon. The Army Corps in the defense, two divisions plus an armored cavalry regiment, would have a heavy covering force forward of the main battle area. The covering force, a heavily reinforced cavalry regiment, spread across the corps sector, is no match for the heavier enemy force. But the covering force is strong enough to accomplish four important tasks. First, force the enemy into revealing his strength, location, and general direction of his main attack, or attacks, and force early commitment of his main attack echelons against the covering force. Second, gain time so that the corps commander can concentrate his combat power in the main battle area to meet the main attack. Third, divest the enemy of his air defense umbrella, or at least require him to displace his air defense before attacking the main battle area. Fourth, deceive the enemy as to the composition and location of friendly forces, especially those in the main battle area.

Figures 5 to 10 present a series of conceptual snapshots showing events in a kind of stop action. The first (Fig.5) shows the initial contact between the Pact reconnaissance screen of battalion size force, and a portion of the covering force. Main ground force engagement has not occurred. The lead regiments of the Pact first echelon division are still some distance behind. We think that the covering force may require little close air support in this initial situation. Army attack helicopters can deal with points of pressure. The two most critical threats to the defending division commander back in the main battle area are the first and second echelon regiments of the lead division, in that order. So, we depict a heavy level of tac air effort on the first echelon regiments, and a lesser but still substantial level of effort on the second echelons. The weights shown represent estimated proportions of the tac air assets available for air/ground attack and air defense suppression in this division sector. To carry out their missions, aircraft are penetrating heavy defenses at low and medium altitudes. Terminal air operations will primarily involve low level attacks against armored targets, artillery, and air fields.

Figure 6 carries us forward a short span of time to the point where the first echelon regiments are closing with a covering force. We chose to stop action at this point to show that the heavy tac air pressure on the lead regiments has been maintained while they advanced to closure. Meanwhile, ground forces have been engaging the enemy's first echelon forces, first with artillery fire, and then as they draw closer, with anti-tank missiles, tank gun fire, and attack helicopters.

As the first echelon regiments engage the covering force (Fig.7), the intensity of army fire power increases. This, coupled with damage inflicted by tac air on the first echelon from detection to closure, may free some tac air for redistribution. It seems logical that the most critical target for tac air to strike now is the second echelon regiments, and that is where we show the bulk of air-to-ground attack effort. A light level of close air support is maintained against the lead regiments of the approaching second echelon division. Exact meanings for light, moderate, and heavy are

unknown. These are subjective judgments and so we show them with question marks. The covering force must not allow itself to become decisively engaged. It must live to fight another day as part of the forces in the main battle area. But the covering force must offer sufficient resistance to force the enemy to deploy his main forces, thereby slowing down his forward progress. As enemy pressure continues to mount, the covering force begins to delay rearward, maintaining contact and providing resistance.

Figure 8 picks up the action after the covering force has completed its delay and deployed in the main battle area. The first and second echelon regiments of the lead divisions are engaging our main battle forces. We assume we have been successful, at least up to this point, in identifying the enemy's main attack, positioning our ground forces to defend, and inflicting the necessary level of damage on the enemy's first echelon division. This requisite level of damage is hard to quantify because it must be translated into a ratio of enemy vs friendly ground combat power at the critical time and place. As a rule of thumb, ground forces should not be outgunned by more than 3 to 1 in order to defend and win. This ratio can pulse higher, but not for long. Now, if we have been successful so far, our rationale for the distribution of tac air air-to-ground assets remains the same as in the preceeding snapshot: light in the main battle area, heavy on the lead regiments in the second echelon division, and substantial on the second echelon regiments of that division.

If our intelligence has not been good enough, chances are that we will not be fully successful in concentrating our ground forces to meet the main enemy thrust. This means we will need substantially higher level of close air support. In this case, the tac air effort on the less critical targets would be reduced and redistributed where it is needed (Fig.9). Such a redistribution demands a great deal of flexibility in command and control. More than that, it means that the Army and Air Force command and control systems must be talking to each other to such a degree that both services have the same awareness of what is happening, both at the line of contact and deeper. I might add two points here with respect to this graphic: one, we show the problem in depth and on a single axis, but the rationale supports diversion of aircraft to lateral problem areas in the vicinity of secondary attacks if necessary. For example, movement of attack helicopters and close air support aircraft to an adjacent corps sector. The second point is that the graphic does not represent a flightpath. Such a redistribution of effort need not be an airborne diversion, it may well be preplanned beforehand.

Finally, Figure 10 deals with a successful breakthrough, a very dangerous and not unlikely situation. In order to mass sufficient combat power at the critical time and place, the ground commander will have to draw forces from elsewhere, thereby reducing his combat capability at other places in his sector. This involves risk. We must be prepared to accept breakthoughs, but only of a magnitude that we can deal with. The ground commander will have to draw units from where he can find them without jeopardizing the defense against the enemy's main attack. Combat units in reserve and those in unthreatened areas will be drawn in to halt the breakthough. The most flexible unit of combat power is tac air, and a heavy concentration of tac air and Army attack helicopters will be required to cope with the threat. In this case, we show the heaviest tac air effort against the exploitation forces on the presumption that the breakthrough units have a lesser combat effectiveness due to attrition, fatigue, and a reduced level of ammunition and fuel.

So much for our scenario and pictures. Basically what has been said is that, given the requirement to reduce the enemy's ground strength advantage, we apply tac air against the lead echelon prior to engagement, then against follow-on echelons. Very importantly, this will require a high degree of teamwork between the air and the ground forces.

Now, what does all this mean to the guidance and control designer? I believe it points up some of the severe demands on military hardware as applied across a wide spectrum. Helicopters operating from nap-of-the-earth profiles must be able to pop up, see, and launch ordnance in a very short space of time. Highspeed aircraft are now operating at the altitudes once reserved for helicopters. They must be able to navigate over longer distances, utilizing terrain following or other techniques, locate targets precisely, and deliver their weapons with a high probability of striking the target on the first pass. Low-level operations must be relatively free from the adverse effects of turbulence, gust loadings, and maneuver restrictions. In other words, pilot fatigue as a result of the low altitude regime must be minimal and the aircraft must retain its characteristics as a stable weapons platform.

In the total view, from takeoff through a variety of missions, to final recovery and landing, a man/machine interface must be achieved that enables full utilization of system capabilities without human overload. Integrated avionics, digital subsystems, and the like, I think, are affording us great progress in this area.

By way of conclusion, I would like to say again that there are many more considerations, I realize, in the field of guidance and control than I have alluded to here, and you will be hearing about some of these over the course of the next several days. What I have tried to do is take a worst case situation, a wartime scenario, and relate it to the matter at hand and emphasize the importance of the work that is being done. I think how well we do our jobs in designing and testing the equipment needed in low level flight operations could have a very profound affect on any major air/land battle of the future.

I wish you an enjoyable and very productive symposium. Thank you.

- COMMON CAPABILITIES
  - FIREPOWER
  - INTELLIGENCE
  - AIR DEFENSE
  - ELECTRONIC WARFARE

Fig.1 Army-air force interdependence

PRIOR TO GROUND FORCE ENGAGEMENT –

TACTICAL AIR FORCES REDUCE PACT GROUND FORCE LEVEL TO POINT WHERE ARMY ALONE CAN SUCCESSFULLY DEFEND

Fig.2 Ideal case

PRIOR TO GROUND FORCE ENGAGEMENT –

TACTICAL AIR FORCES REDUCE PACT GROUND FORCE LEVEL TO POINT WHERE ARMY AND TACTICAL AIR FORCES TOGETHER CAN SUCCESSFULLY DEFEND

Fig.3 Minimum case

ARMY AND AIR FORCE TOGETHER MUST –

- SEE THE BATTLEFIELD
- CONCENTRATE COMBAT POWER AT CRITICAL TIMES AND PLACES
- FIGHT AS A TEAM
- WIN

Fig.4 Air/land battle requirements

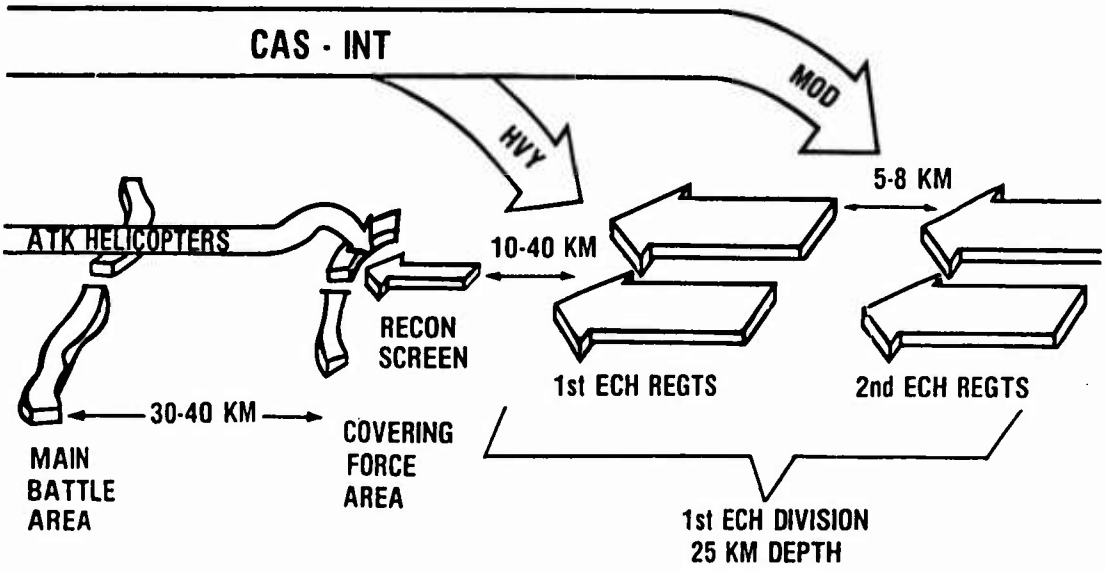

Fig.5 Initial contact

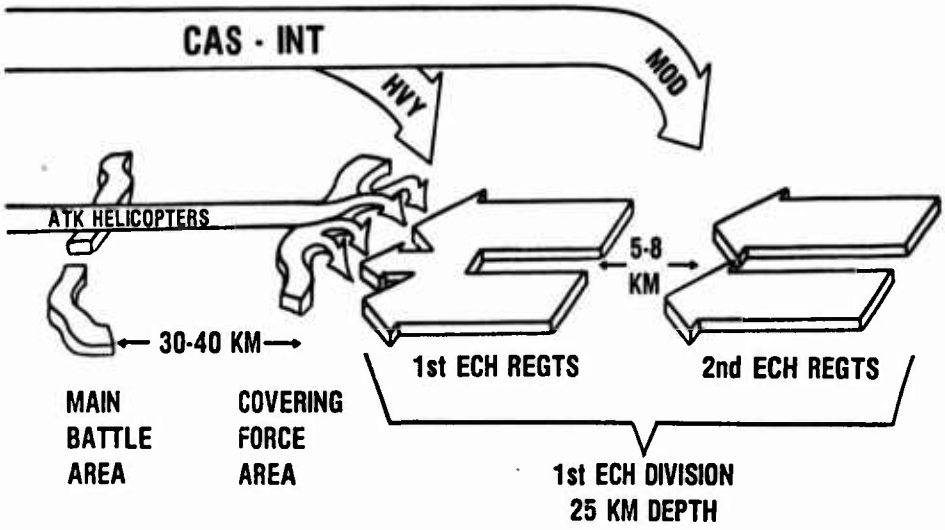

Fig.6 Closure of lead regiments

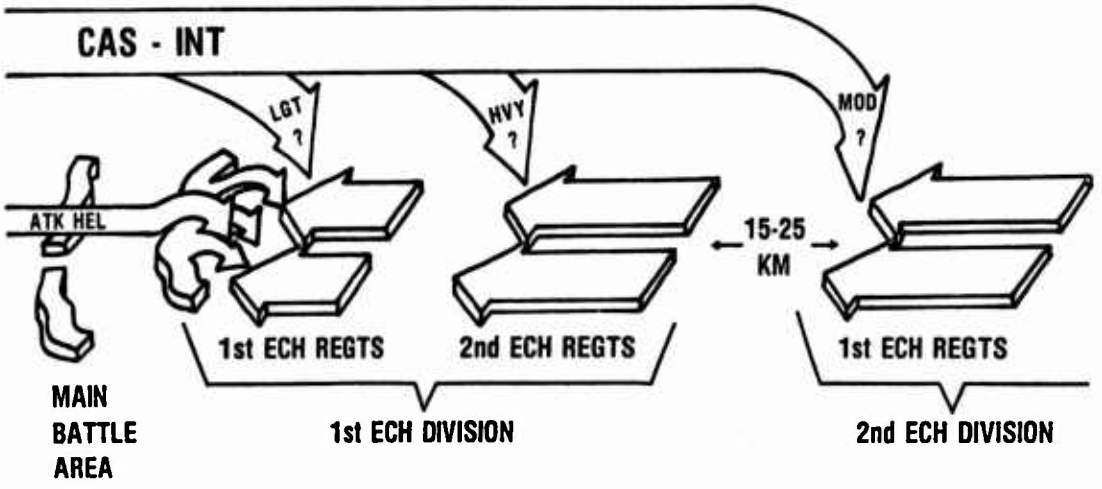

Fig.7 Covering force delay

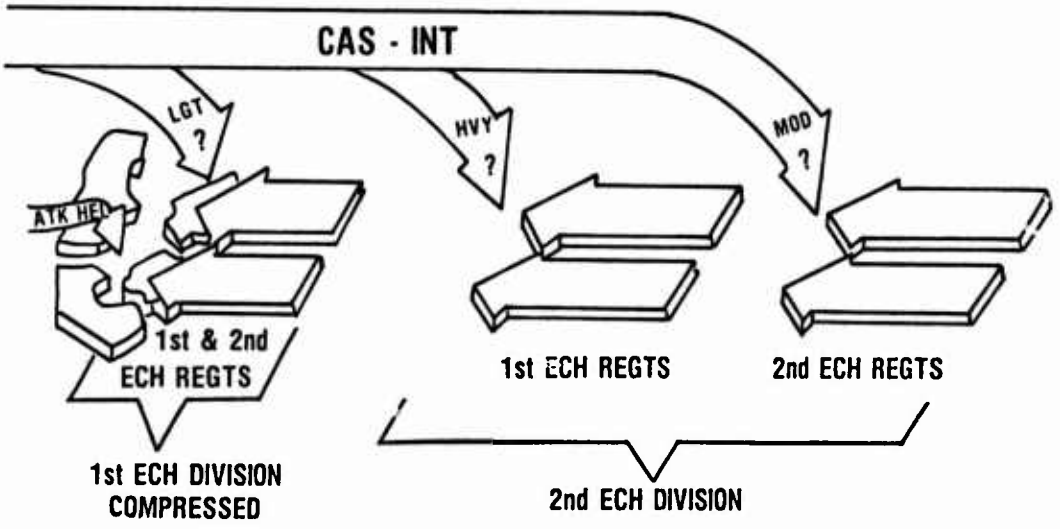

Fig.8 Engagement – main battle area

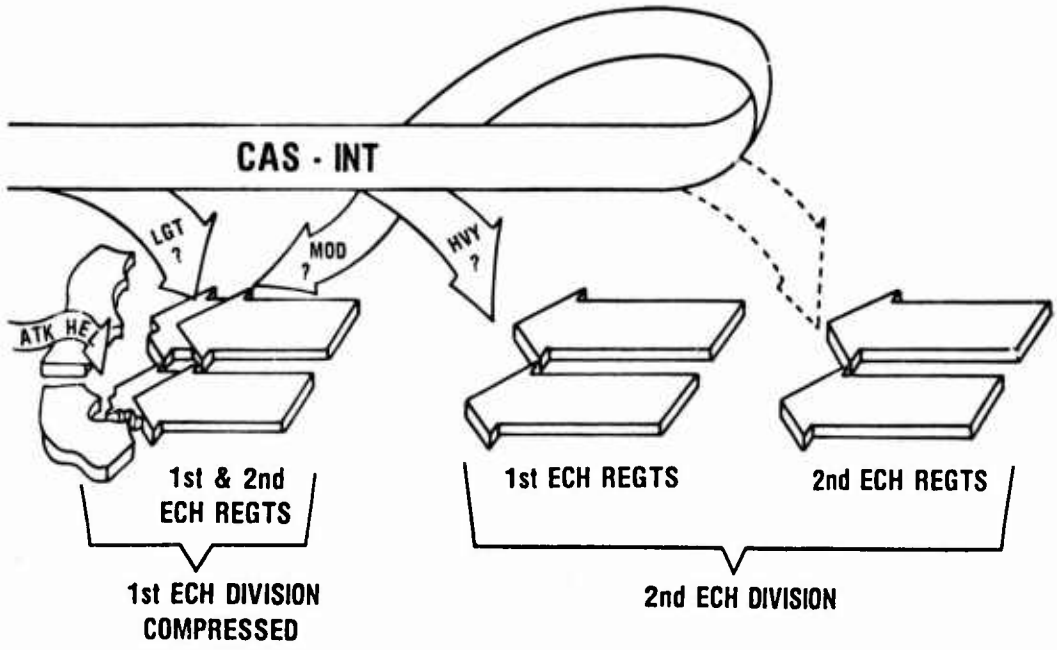

Fig.9 Redistribution of effort

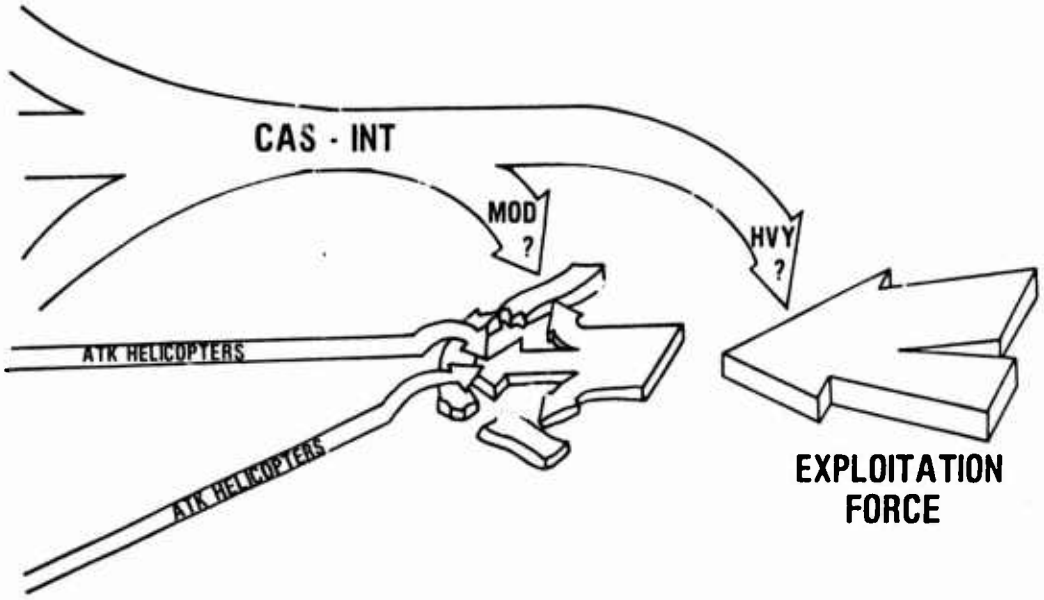

Fig.10 Breakthrough

GUIDANCE AND CONTROL FOR LOW LEVEL OFFENSIVE AIRCRAFT - A ROYAL AIR FORCE VIEW

by

Squadron Leader G A Barnes

OR52(RAF) Ministry of Defence (Air)
Whitehall London SW1 UK

Summary

The operational requirements for guidance and control systems for offensive aircraft employed on the Central Front depend both on the weapon delivery accuracy required and on the penetration tactics and weapon delivery profiles employed. The latter are affected both by the enemy's anti-aircraft defence system and by the weather conditions which are likely to prevail. This paper examines these aspects and suggests possible parameters for aircraft to be employed in the counter-air, interdiction and close air support roles.

Introduction

1. The Scenario for this paper is set in the Central Region of Europe where the Warsaw Pact forces and those of NATO stand arrayed looking at each other across a 600 mile strip of barbed wire and minefields. For years after World War II we were confident in the overwhelming superiority of the West over the communist forces relying on our nuclear striking power, delivered by missile and by aircraft, to enforce a 'trip wire' policy. This has now changed. The Soviets have prosecuted a policy of intensive military expansion far beyond the needs of a defensive force. For example the ratio by which our tanks are outnumbered is about 3 to 1, their air defence systems are being reinforced both by increased numbers and by continuously improving designs, and the air threat has changed from being a predominantly defensive force to one with a considerable offensive capability. In the past we have been encouraged by the knowledge that the Soviet forces although superior in numbers were inferior in technology, and that their training standards were inferior to those of the West. Even if this were true in the past we cannot expect such a state of affairs to continue into the future. Another aspect in the favour of the Eastern Bloc is the interoperability of equipment which their forces enjoy, whereas we in NATO, despite the exhortations of right minded men, find interoperability next to impossible - a drawback of a democratic society.

2. Faced with the excessive and still growing forces of the Warsaw Pact, the fire power and flexibility of our airforces are cited as being major contributors toward the defence of the West. The aim of this paper is to examine the realistic methods by which air power can help the land forces on the Central Front and thence to outline the operational requirements for the guidance and control systems which perhaps this symposium should be considering. In doing this I must emphasise that the views contained in this paper should not be ascribed either to the Royal Air Force or to the British Government - they are mine alone.

The Central Region Environment and Airpower Roles

3. Before discussing the roles for airpower in the Central Region it is necessary to examine the environment of the Region including the enemy air defence capabilities and the weather. Both are hostile.

4. Firstly we must consider the enemy anti aircraft defences. I have no intention here of listing the full AD threat as it is readily available in detailed intelligence summaries and, of course, this information is classified. Suffice it to say that the threat ranges from the SA-7 and ZSU-23/4 at low level to the SA-2, 3 and 8 at high altitude. The alarming aspect for us airmen is that the Soviet now has an incredible anti-aircraft shield around even his fast moving leading tank columns, consisting of the overlapping (vertically as well as horizontally) coverage of SA6, 7, 8 and 9 missile as well as the ubiquitous ZSU-23/4 gun. Fig 1 shows some representative envelopes of the Soviet AD systems culled from unclassified sources. This most lethal area extends up to and beyond the FEBA and presents two main options to the penetrating aircraft either to go low and fast or to go high using extensive active electronic counter measures.

5. Secondly, we must consider the weather. Fig 2 is a graphical representation of cloud and visibility data obtained in the Berlin region of Germany over the months of January to March. It can be seen that at 5000 ft there is only a 0.25 probability of there being no cloud obscuring the ground.

6. Fig 1 shows that penetration avoiding the most varied anti-aircraft threat systems could be achieved at above 15000 ft using active ECM against the remaining 4 or 5 systems (SAM 8 and 9 are not shown in Fig 1). However when this is considered in relation to Fig 2 it can be seen that the ground will very probably be obscured from this height. Therefore, unless blind and probably inaccurate attacks are to be made from medium to high altitude, Close Air Support missions will call for low level attacks in the FEBA areas.

7. When examining counter air (Airfield) types of targets beyond the FEBA other considerations should be taken into account. It is likely that such targets will be very

heavily defended and will include SAM 3 but there will probably be a less severe AD environment between the FEBA and the point target. This allows 3 options of attack to be considered:

a. A medium to high level penetration of the FEBA followed by an attack from the same altitude using a stand-off weapon which would need to have a blind capability in order to have a reasonable probability of success.

b. Low level penetration of the FEBA followed by a low level attack using either a stand off weapon (possibly clear weather), a toss attack, or an overflying attack.

c. A medium to high level penetration followed by a descent to low level using either of the 3 types of attack suggested in b above.

All penetrations could be vulnerable to Soviet fighters.

8. The writer considers that due to weather considerations the only realistic options are the low level attack in the FEBA area and either High-low or low-low profiles for targets beyond the FEBA. This deduction is based on the lack of a suitable blind medium/high altitude weapon system of an accuracy acceptable for conventional attacks. Radars with the resolution capable of approaching the required accuracies will be of a frequency likely to be affected by weather. It must be remembered that the only way in which a medium/high altitude penetration can be considered is by the use of jamming which may well affect our own sensors. Also the transmissions from our radar could provide a convenient target for the use of an anti radar missile (ARM) by the defence. Of course there are times (23% - 50% of the time depending on the season) when there will be no weather to hinder a visual attack but we must assume that about 50% of these occasions will occur after dusk. For air power to remain flexible it cannot be limited by weather and light conditions for long periods.

9. In summary, for the next 10 years we shall need to carry out nearly all attacks at low level but it may be considered acceptable to fly high-low profiles on some missions that penetrate well behind the FEBA.

Operational Requirement over the next 10 years

10. This paper will not give detailed parameters. It will discuss the requirements more in the form of military characteristics. This will avoid a limiting security classification. The paper has been prepared to preface the technical discussions of this Symposium with an explanation of what we are really trying to achieve in the cockpit. For simplicity the classical roles of counter air, interdiction and close air support are taken in descending order of severity to illustrate the requirements. For all roles a high probability of achieving a successful first pass attack is required.

Counter Air

11. There are three main ways of prosecuting a counter air programme: destroying the enemy aircraft in the air, destroying them on the ground and by neutralising their operating bases. The first method will not be discussed in this paper as no attempt is being made to cover air defence aircraft. Destroying enemy aircraft on the ground used to be a favoured way of carrying out the aims of counter air. The Israeli success in 1967 was a superb example. However, aircraft are no longer soft targets; they are sheltered in dispersed hangarettes which are most resistant to normal air delivered weapons. Even if a weapon suitable for the attack of aircraft shelters is produced there remains the doubt as to which shelters are occupied. In a conventional war therefore we have to resort to attacks on the runways and harassment of the ground services to prevent the enemy aircraft from being operated from their bases. This requires fairly large numbers of aircraft per raid to deliver the required ordnance and to overcome the final point defences. Attacks are required at frequent intervals as even when the runways have been successfully holed and delayed action bombs have been strewn, the airfields will only be neutralised for a finite time. This requires that the attacks need to be made irrespective of the weather or of the light conditions as well as being made at low level. Hence we are faced with the requirement for accurate attacks, at high speed (M 0.9) low level (200 ft max) and probably blind. This calls for three systems.

12. Firstly a nav/attack suite is required capable of allowing the crew to deliver ordnance to an accuracy commensurate with the nature of the target, the mean area of effect of the weapon, and the number of weapons which are to be delivered against the target. Added to this is the strong possibility that any radiating sensor will be jammed especially in the target area. This means we are looking for something better than an accuracy of 200ft CEP in jamming conditions. Currently an IN with an accuracy of around 1 nm/hr CEP updated by an accurate ground mapping radar fix whilst outside the area of the target is called for. In the future TERCOM or NAVSTAR GPS mixed with an accurate IN will probably form the basis of a superior Nav/attack system.

13. Secondly a terrain follow radar (TFR) capable of guiding the aircraft at MO.9 at 200 ft AGL safely and with as few excursions above the desired height as possible. The nature of the terrain is an obvious limiting factor but so also is the sensitivity of the aircraft to turbulence.

14. Thirdly the automatic flight control system (AFCS) must take the inputs from both the nav/attack system and the terrain follow system and accurately steer the aircraft in three dimensions as smoothly as possible. This is most important for two main reasons. The pilot will be unable to manually follow navigation and TF demands accurately enough, and the crew will have plenty to do on the run in to the target without having to steer the aircraft as well. Electronic warfare, weapon management and look-out (attacks will not always be blind) will be crucial in the final stages of the attack.

15. For counter air missions, the offensive aircraft will need the following guidance and control system.

a. Nav/attack system capable of achieving a CEP of less than 200 ft in jammed blind attacks at 0.9M at 200 ft approach height.

b. A terrain follow system capable of holding a height of 200 ft with the minimum of excursions at 0.9M and capable of safely transitioning the aircraft from high to low level.

c. An AFCS capable of fully automatic pilotage of the aircraft whilst at 200 ft 0.9M smoothly enough for the crew to carry out other crucial activities.

Such an aircraft will almost certainly require a minimum of two crew members.

Interdiction

16. The term interdiction covers attacks on those rear forces which can have an effect on the land battle. The Warsaw Pact have enough armour and equipment already stationed near the demarcation line to advance at a rapid rate across West Germany and beyond in a few days unless NATO puts up a very stout defence. The future interdiction targets will be second echelon armour waiting to be called forward to the FEBA. Such forces are likely to be no more than 50 Kms back so there is little to commend a high-low attack profile. It is likely that these forces will wish to move forward under cover of darkness and/or bad weather and it follows therefore that the ideal aircraft for the interdiction role should have the same guidance and control requirements as the counter air aircraft. However, some measure of fairweather daytime effectiveness could be obtained from an aircraft with a less comprehensive avionics suite and with only one crew member. These requirements will be covered in the next paragraphs concerning Close Air support.

Close Air Support

17. Discussions on close air support often get quite emotional, probably due to several factors. Aircraft find the FEBA to be an intensely hostile area caused by the anti-aircraft systems of both sides, the targets are often small, hard to acquire and attacks cannot normally be preplanned. In the writers view conventional close air support can only be justified if there is no other way of neutralising the target, especially when the effectiveness of the attacks are taken into account. However, there are times when the need for a form of close air support is unquestionable. This is on the occasion of a massive breakthrough of enemy armour. It will then be necessary to assign as many aircraft as are required to stem the enemy attack. This could mean re-assigning counter air, interdiction, and dual-role air defence fighters.

18. If the specialist close air support aircraft is only required to operate by daytime in clear or marginal weather it will probably need only a single pilot. No terrain follow system will be required, nor will their be a need for a comprehensive AFCS. An accurate navigation system and a weapon system precise enough to neutralise armour will however, be needed. Such an aircraft would be relatively cheap and simple and could possibly be an air superiority fighter with ground attack as its secondary role.

19. If the aircraft is required to operate at night or in bad weather a terrain follow system coupled with an AFCS will certainly be needed and possibly a second crew member. The aircraft is now looking increasingly like the counter air aircraft discussed earlier except it may be trying to attack smaller targets with a more accurate CEP requirement. There is no doubt that if the enemy achieve a major armoured breakthrough it will have to be repulsed by air power. If the breakthrough occurs at night or in bad weather aircraft of the calibre of the counter air aircraft will have to be re assigned to this blind close air support role until such a time as the simpler aircraft can take over.

20. Turning back to interdiction the same sort of arguments apply. In daylight a single seat, fairly simple aircraft could do the job but in more exacting conditions the more complex multi seat aircraft would be called into service.

21. The weather is not always either good or bad however. Often in the Central Region there are marginal weather conditions. There could be patches of blind conditions en route, but the target areas may be relatively clear. In such conditions the simple single seat aircraft would almost certainly be unable to cope, but the use of the complex counter air aircraft would be excessive and would divert the aircraft from their main task. Hence, a need for an aircraft some way between the complexity of the counter air aircraft and the simplicity of the air superiority fighter can be argued. Such an aircraft could be procured in sufficient numbers to carry out effectively the roles of interdiction and close air support in poor weather conditions and at night in clear weather and would be capable of the penetration of occasional blind conditions.

22. This aircraft could be crewed by a single pilot but would have a higher probability of success if a second crew member were employed. The navigation system would still require to have an accuracy of 1nm per hour CEP and the weapon systems must be able to deliver ordnance with sufficient accuracy to neutralise armour.

23. The full TF/AFCS of the counter air aircraft will not be required. Instead a simple pilot-interpreted terrain warning system, should be adequate. As this system would be simplex it should not be linked to an AFCS. However, a simple auto-pilot would help to reduce the pilot's work load.

Summary of Requirements

24. In summary there is a need for three type of offensive aircraft.

a. A multicrew aircraft with a full blind capability suitable for counter air and bad weather/night interdiction and CAS.

b. A single or two seat aircraft with a terrain warning system and an auto-pilot suitable for marginal weather interdiction and CAS.

c. An air superiority fighter with a ground attack capability suitable for clear weather daytime CAS.

The Future

25. Flying at high speed and low level at night and in blind conditions is a very difficult way to go to war. Future research and development could well be directed to improving the aircraft's invulnerability to air defence systems by use of ECM, and to enabling the aircraft to deliver weapons, either stand-off or free fall, with the required precision through several thousands of feet of cloud. The sensors will almost certainly need to be self contained and non radiating. Therefore, whilst striving to improve the operational effectiveness of our offensive air power over the next ten years we must look ahead for entirely new concepts and technologies, which will help us to go to war in a less onerous manner.

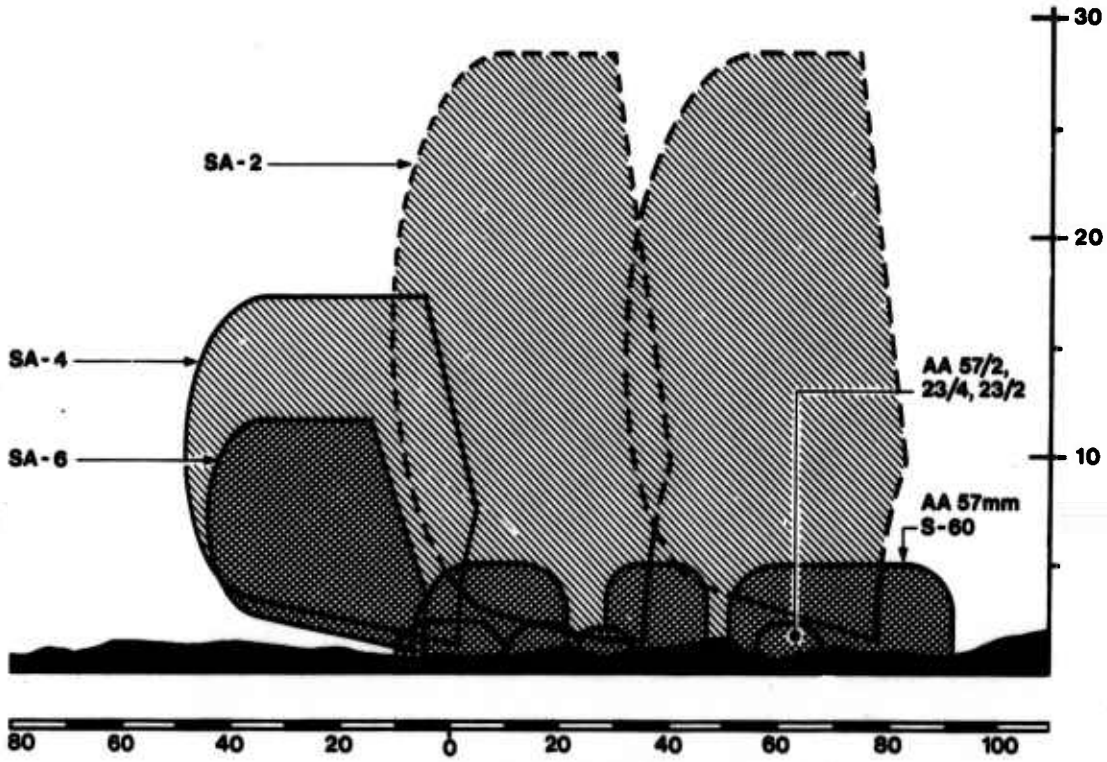

Fig 1. Possible Soviet Air Defence Threat at the FEBA

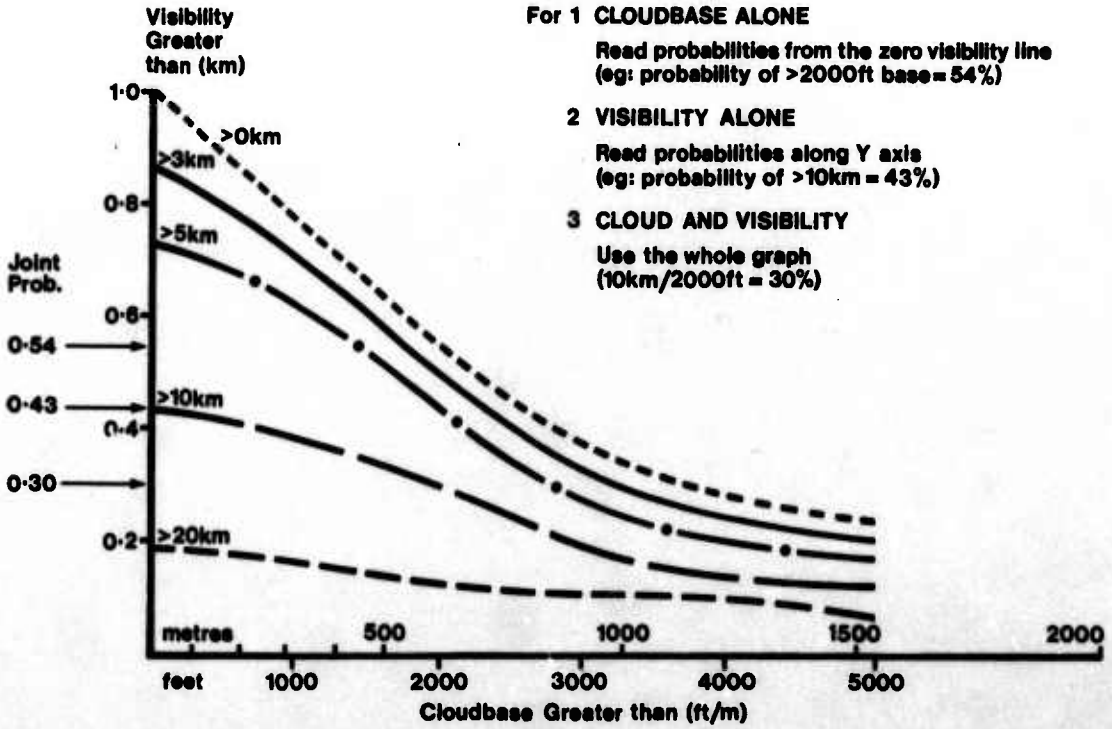

Fig. 2 Joint Probabilities of Cloudbase and Visibility for Berlin – Winter (Jan-March 1956-60)

THE "GROUND-ATTACK/PENETRATION" MODEL: A MONTE CARLO SIMULATION MODEL TO ASSESS THE SURVIVABILITY AND TO EVALUATE TACTICS FOR LOW-ALTITUDE MILITARY MISSIONS IN AN ENVIRONMENT OF GROUNDBASED AIRDEFENCE SYSTEMS

by

M.H.W. Bovy
Operations Research Engineer
National Aerospace Laboratory NLR
Anthony Fokkerweg 2
1059 CM Amsterdam
The Netherlands

SUMMARY

In order to be able to assess the survivability and to evaluate tactics for low-altitude military missions in an environment of groundbased airdefence systems the NLR has developed the "Ground-attack/Penetration" simulation model. A review of the main aspects of the model and some typical conclusions obtained with the model are presented.

1. INTRODUCTION

In behalf of the Royal Netherlands Air Force (RNLAF) the National Aerospace Laboratory NLR carries out operations research studies on the evaluation of tactics for low-altitude fighter aircraft and helicopter missions in order to reduce their vulnerability to groundbased airdefence systems.

The basic problem in such studies is to find the best compromise between the various, often conflicting mission parameters, such as penetration-speed and -altitude, type of formation, crossing distance to airdefence systems, attack profile and attack direction in order to ensure maximum aircraft survivability.

To this end the NLR has developed the "Ground-attack/Penetration" model which is a Monte Carlo computer simulation model of interactions between a groundbased anti-aircraft defence system and penetrating and attacking fighter aircraft or helicopters. The model basically uses a critical event technique for running and updating the sequence of the defence system operations during an engagement with an aircraft.

In the "Ground-attack/Penetration" model the following three sets of parameters, each describing an essential component of the aircraft/defence system interaction, are distinguished:

1. the defence system data (examples: detection performance data, fire control computer performance data, missile data, etc.),
2. environmental factors (examples: terrain features, meteorological conditions),
3. the aircraft characteristics (examples: aircraft trajectory, radar cross section, ECM capabilities).

In order to give an impression of the possibilities of the model the most essential characteristics of the three components mentioned will be discussed in more detail in the next chapter, in particular the methods which have been developed for the simulation of each component. The methods have a mainly statistical nature which implies that the occurrences of those events which are of interest for the investigation of an aircraft/defence system interaction, demonstrate a random aspect. A short review of the total operation of the "Ground-attack/Penetration" model which results after the various sub-models and procedures have been combined, is given in chapter 3. Examples of simulation results obtained with the model are given in chapter 4.

This paper gives only the most important characteristics of the "Ground-attack/Penetration" model. For more details of the model or sub-models separate documents are available; also documents containing typical results of special studies have been published. Because of the classified character of most of the documents, release is only possible after authorization of the RNLAF. At the end of this paper points of contact for further information are given.

2. SURVEY OF MODEL COMPONENTS

2.1 The defence system characteristics

Starting point for the assessment of the aircraft vulnerability to an airdefence system is a separate study of the characteristics of the defence system. Information and relevant data are obtained from RNLAF Intelligence Sources in case of hostile defence systems and from company-documentation in case of friendly systems. Technical and operational aspects of the defence system are studied as far as they are relevant to a realistic simulation. The most important defence system characteristics incorporated in the "Ground-attack/Penetration" model are:

- sensor (radar-, IR- and/or visual) detection performance,
- fire control computer performance,
- projectile/missile trajectory,
- firing doctrine,
- time-delays, inclusive human factor effects.

Up to now the NLR has studied a number of groundbased airdefence systems, both anti-aircraft artillery (AAA) as well as surface-to-air missile (SAM) systems and hostile as well as friendly systems. The great diversity in the defence systems analized and, by consequence, the great diversity in methods developed for the simulation of these systems do not permit to mention in brief all methods. However, two general methods can be mentioned here.

For the simulation of the process of aircraft detection by a weapon system using radar a universal theory (Refs. 1 and 2) has been developed at NLR which determines the detection probability as a function

of the various radar and aircraft characteristics (e.g. radar signal characteristics, aircraft radar cross section, etc.), taking into account environmental factors (e.g. groundclutter). The theory is valid for classical radar systems. The following radar systems can be considered as classical:

- the pulse radar; the method of detection may be single-hit or multiple-hit radar detection or both
- the continuous wave radar.

For the simulation of the trajectory of a surface-to-air missile, a computer program has been developed (Ref. 3) which simulates the kinematics of flight in three-dimensional space of any SAM. The kinematics of the missile are determined according to the navigation law applied. Various guidance laws can be incorporated.

2.2 The environmental factors

Results of survivability studies concerning low-altitude flight of aircraft engaging groundbased airdefence often appear to be considerably affected by the representation of the terrain. In most of those studies a direct method is applied by which specific data on a real terrain are introduced into the research model. Such a direct method has the advantage that the terrain-screening can always be determined quite accurately for the underlying specific area, but on the other hand the results obtained are uniquely related to the particular situation involved. Moreover, a large amount of terrain data has to be stored in the memory of the computer running the simulated interaction. To realize a method which permits a manageable assessment of terrain-screening in a more general context, the NLR has developed an original theory (Ref. 4) to describe a type of terrain (homogeneous or non-homogeneous) in statistical terms. The quintessence of this theory is that terrain elevations are described by geometrical cones characterized by three probability distribution functions, respectively for the altitude of summits, for the sharpness of summits and for their density in the area considered (see Fig. 1). By assigning values to the set of terrain parameters which occur in the three distribution functions mentioned, different types of terrain (flat, hilly, mountainous terrain, etc.) can be generated in a relatively simple way. In combination with the method for terrain generation special calculation techniques have been developed for determining the probability that an object (e.g. aircraft) can be "seen" (is unmasked) or not (is masked) by a sensor (e.g. radar). This probability can be given as a function of parameters which characterize the type of terrain involved and of the positions of the observer and aircraft in the terrain.

Much effort has been spent on the validation of the described techniques by comparing the results obtained with the statistical terrain and terrain screening models with realistic terrain data. The conclusion is that the methods are very powerful techniques for terrain and terrain screening simulation.

Concerning the simulation of groundclutter effects on radar detection performance, a clutter model has been developed incorporating the statistical terrain and radar characteristics in such a way that for the subsequent points of the aircraft flight path the degradation in detection performance due to clutter can be established.

Finally, meteorological conditions can be taken into account by their interference with the IR and/or visual detection capability of a defence system mentioned in section 2.1.

2.3 The aircraft characteristics

The aircraft low-altitude flight performance has a great impact on the effectiveness of a groundbased airdefence system. This impact arises from the fact that low-altitude performance (in combination with terrain features) is the main factor which determines the establishing and maintaining of (e.g. radar-)contact between the defence system and the aircraft. This contact plays a preponderant role during an aircraft/defence system interaction, especially during the firing phase of an interaction.

The low-altitude flight performance of an aircraft is strongly dependent on the type of terrain underneath the flight path. The statistical simulation of terrain (see section 2.2) made it necessary to develop adjusted procedures for the generation of low-altitude flight profiles with a likewise statistical character. On the other hand it was thought necessary to use operational flight data because of the important influence of the shape of the aircraft trajectory on the performance of a defence system, especially in case of a radar guided gun system. In order to satisfy both requirements the NLR has developed a method (Ref. 5) involving spectral theory which utilizes operational flight data obtained during field trials. The quintessence of the method is that power spectra are calculated from actually flown flight profiles under different conditions (type of aircraft, speed, pilot experience, etc.). These spectra are calculated in connection with an analysis of the corresponding terrain. From these power spectra flight altitude profiles as a function of terrain parameters can be generated (see Fig. 2). It has been proven that the flight altitude profiles as generated with this method are in good agreement with actual flight profiles concerning both altitude fluctuations and the average altitude above the terrain. This correspondence is uniquely related to the selected set of values for the (statistical) terrain parameters. The advantage of the method outlined is that it enables the generation in a relatively simple way of flight altitude profiles for any time range which have the same statistical characteristics as the profiles measured. It can be remarked that the method is until now only applied for the generation of low-altitude penetration profiles, in particular for terrain follow (as low as possible) profiles.

For the generation of realistic attack trajectories (e.g. pitch-up trajectories) a curve fitting technique (Ref. 6) is used in order to represent real aircraft trajectories by simple functions of time (polynomials for the position). It has been proven that these polynomials fit the original set of positions within the measurement accuracy. The real trajectories are available as a discrete set of aircraft positions as measured during simulated attacks on realistic ground-targets (Ref. 7).

The detection of an aircraft by a weapon system using radar depends, besides the radar and the terrain characteristics, also on the aircraft radar cross section. A model has been developed, which is also based on data measured during field trials, for the calculation of the radar cross section of fighter bomber types of aircraft as a function of the aircraft position and attitude with respect to a radar system location.

In order to be able to simulate the (tactical) use and the related effect of aircraft ECM equipment on defence system performance, computer programs have been developed or are being developed. These programs are also based on measured data from field trials.

3. THE OPERATION OF THE "GROUND-ATTACK/PENETRATION" MODEL

After incorporating and integrating the characteristics of the defence system, the terrain and the aircraft trajectory, as represented by the separate models as mentioned in the foregoing chapter, in the "Ground-attack/Penetration" model, defence system/aircraft interactions can be simulated. An interaction is simulated from the very beginning when an aircraft comes in range of e.g. the search-radar(s) of a radar controlled defence system, until either the last moment the aircraft is within fire range, or the moment of aircraft kill. In between a sequence of actions is performed by the defence system versus the aircraft. A complete sequence of actions consists for example of the following events: detection, assignment, lock-on, fire, interception and kill. However, such a complete sequence can be easily interrupted for a number of reasons, e.g. definite loss of radar contact, system restrictions (e.g. tracking limit) or threat priority, if some other, more threatening aircraft is detected. If an interruption occurs, re-detection can be realized, and may as yet result in a kill.

The probabilistic character of many of the data which are applied in the simulation of an interaction between a defence system and an aircraft renders the outcome of each run different. So, if in one run the aircraft is destroyed, it might survive in the following run. For a reliable estimation of the survivability it is necessary to perform a run several times. In mathematical terms this means that the Monte Carlo technique is applied. The survivability can be estimated by dividing the number of runs not resulting into an aircraft kill by the total number of runs.

4. RESULTS

4.1 Scope of investigations

The "Ground-attack/Penetration" model as it has been described shortly in the preceding chapters can be applied to a nearly infinite number of operational situations concerning the three main elements in the problem statement:

- the defence system
- the environment
- the aircraft.

In order to restrict the investigations to an acceptable number of discrete problems, a set of "standards" has been defined with respect to these three elements. The selection rules applied result in a number of standards which cover approximately the whole range of operational situations which an aircraft may encounter in performing a low-altitude mission.

Concerning the defence system, it can be remarked that positions (heights) of the defence system in the terrain are chosen which are in accordance with the nature (mobile, semi-mobile, static) of the system.

As regards the environment, three types of terrain are distinguished: flat, hilly and mountainous terrain. These types of terrain are defined by the maximum altitude variations which may occur. These variations are:

- for flat terrain in the order of 100 m (300 ft),
- for hilly terrain in the order of 200 m (700 ft),
- for mountainous terrain in the order of 650 m (1950 ft).

Concerning the meteorological conditions two extreme situations are considered: the situation of optimal visibility corresponding to a maximum visibility range of appr. 15 km and the situation of bad visibility corresponding to visibility ranges less than ca. 1000 m.

As regards the type of aircraft trajectory, mainly two types of low-altitude trajectories are unalized: terrain follow (as low as possible) penetration profiles and pitch-up attack profiles. Parameters describing both types are given in figures 3 and 4. Concerning the values of the various aircraft trajectory parameters (e.g. ground clearance, aircraft speed, apex altitude, etc.) it can be remarked that standards are taken into account which correspond to current operational RNLAF low-altitude tactics.

Starting from the above mentioned "standards" proper simulations can be carried out. Investigations are mostly bearing on the most elementary problem: interactions between one defence system and one aircraft. Output of the "Ground-attack/Penetration" model is a value of the aircraft survivability as a function of the input-"standards". By simulating defence system/aircraft interactions for different input-standards, the influence of different tactics, as represented by the standards, on the aircraft survivability can be established.

There are many ways to present results of a survivability analysis. An approach often chosen by the NLR is to present survivability curves as sketched in the figures 5 and 6. In figure 5 the survivability of a penetration mission, which is always executed with constant heading is given as a function of the crossing distance [a] for given input standards. In case of attack missions curves like figure 6 are given. In this figure a number of curves are drawn, each curve representing the collection of defence system locations with respect to the ground target and the aircraft trajectory which correspond to the same aircraft survivability.

4.2 Some general conclusions and tactical recommendations

The overall purpose of carrying out simulation studies concerning interactions between groundbased air defence systems and low flying aircraft with the "Ground-attack/Penetration" model is to throw some light on questions such as: "Is it more advantageous (from the point of aircrart survivability) to fly as-low-as possible above the terrain at a low speed than at a higher speed but perforcing on the average somewhat higher?" or "How can characteristics of the terrain be utilized optimally?" or "Which formations have the highest survivability against enemy defence?". The answers to such questions are of course

---

a) i.e. the perpendicular distance from the defence system location to the aircrafts' track (see also Fig. 3).

crucial to the type of defence system under consideration and the aircraft tactics to be employed. In this section some typical conclusions obtained by carrying out simulations with the "Ground-attack/Penetration" model are presented. Results of simulations of interactions between specific defence systems and specific aircraft can not be presented here because of the classified character of these results. So, the conclusions presented here are formulated in general terms and have to be interpreted as general tendencies.

There are many ways for a low flying aircraft to defeat a groundbased air defence system. From a great number of analyses carried out with the "Ground-attack/Penetration" model and related to different types of defence systems (SAM as well as AAA systems) and to different types of aircraft it has been established that the aircraft survivability depends mainly, but certainly not exclusively, on the so-called exposure time, i.e. the length of the time-interval(s) an aircraft is exposed unhampered to the defence system during an interaction with that system. Exposure time can be mainly reduced by flying lower and flying faster. However, in case of low-altitude missions, these two aims can often not be pursued independently, for at a given speed one is limited as to the altitude that can be maintained because of pilot fatigue, danger of ground collision and technical (or physiological) limits. At a given low altitude one is limited in speed for the same reasons. So, in reducing exposure time one has to compromise. Concerning this compromise it can be remarked that there is an optimum speed/ground-clearance combination that minimizes exposure time. This optimum depends on the type of defence system (AAA or SAM, short range or long range system), the pilot/aircraft low-altitude performance, the crossing distance and the type of terrain.

Beside reducing the exposure time by flying lower and/or faster, the exposure time can also be effectively reduced by using ECM. The general effect of ECM on weapon system performance is a delay in system reaction time which favourably influences the aircraft survivability.

Additional to the conclusions given above which are applicable to both AAA and SAM systems it must be mentioned that AAA systems can also be defeated by aircraft manoeuvring. The underlying reason for this is that in most current AAA systems fire control computers are in use which employ linear prediction for the calculation of the interception point and lead angle. By manoeuvring, which introduces deviations from the assumptions on which linear prediction is based, the defence system performance can be reduced considerably.

From many simulations with the "Ground-attack/Penetration" model, the following general guidelines can be given for the execution of low-altitude military missions in order to optimize aircraft survivability:

- Use the terrain as much as possible by flying as-low-as possible
- For a given ground-clearance level fly at the highest possible speed
- Use ECM
- Manoeuvre in case of AAA.

The relative importance of each of these guidelines depends on the defence system and the type of aircraft mission under consideration and has to be established for each specific operational situation.

5. POINTS OF CONTACT

As has been stated earlier, this paper gives a survey of only the main aspects of the "Ground-attack/Penetration" model. Those who like to have more information on the model are advised to contact one of the following points:

. Royal Netherlands Air Force RNLAF
Assistant Chief of Staff for Operational Requirements (AOB)
Section Operations Research and Evaluation (ORE)
Prins Clauslaan 8
The Hague
The Netherlands

. National Aerospace Laboratory NLR
Department of Flight
Military Operations Research Group
Anthony Fokkerweg 2
1059 CM Amsterdam
The Netherlands.

6. REFERENCES

1. Hagenberg, Th.H.M. A description of radar detection techniques in aid of simulation models for military aircraft missions, NLR Memorandum VG-72-012 C (Confidential), 1972.

2. Klinker,F. and Pietersen, O. Detection probability of pulse modulated radars, NLR Memorandum, to be published.

3. Bovy, M.H.W. Missile: a digital computer program for simulating three-dimensional flight trajectories of surface-to-air missiles, NLR Memorandum, to be published.

4. Baas, S.M. and Veldhuyzen, R.P. A statistical method for the simulation of terrain and terrain-masking features to be used in simulation models for military aircraft missions. NLR Memorandum VG-72-003 C (Confidential), 1972.

5. Veldhuyzen, R.P. and Hanekamp, J. A new approach to the generation of flight altitude profiles of low level penetration missions. NLR Memorandum VM-71-048 C (Confidential), 1972.

6. Stahlie, T.J. A curve fitting technique for representing the "Inbreker" III attack trajectories as simple functions of time. NLR Memorandum VG-73-040 C (Confidential), 1972.

7. Stahlie, T.J. The analysis of operational mission execution: an assessment of low-altitude performance, navigation accuracy and weapon delivery performance. Paper 41 of Proceedings of 25th GCP/AGARD meeting on "Guidance and Control Design Considerations for Low Altitude and Terminal Area Flight", Dayton, Ohio, USA, October 1977.

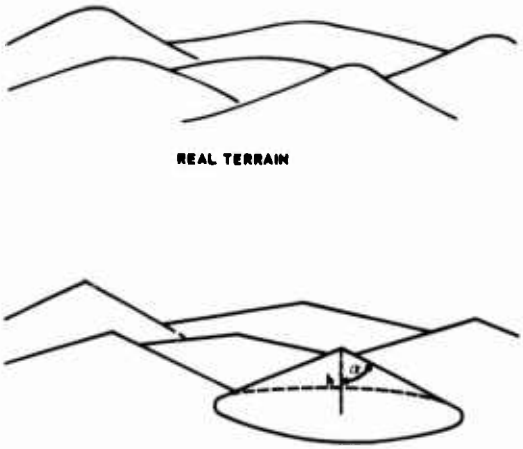

Fig. 1 Terrain simulation

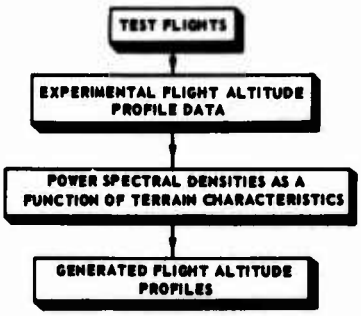

Fig. 2 Generation of low-altitude penetration profiles

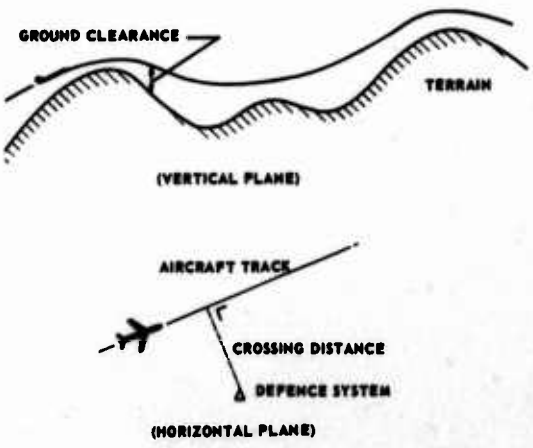

Fig. 3 Terrain follow penetration profile

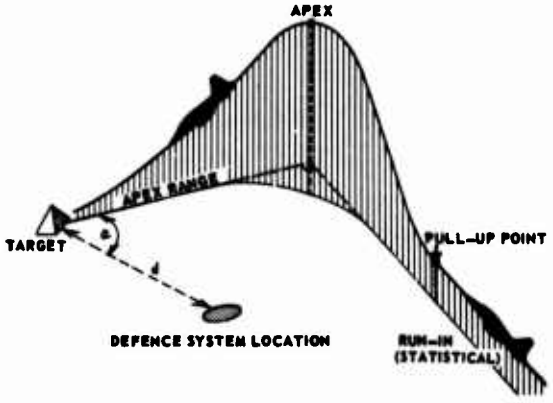

Fig. 4 Pitch-up attack manoeuvre

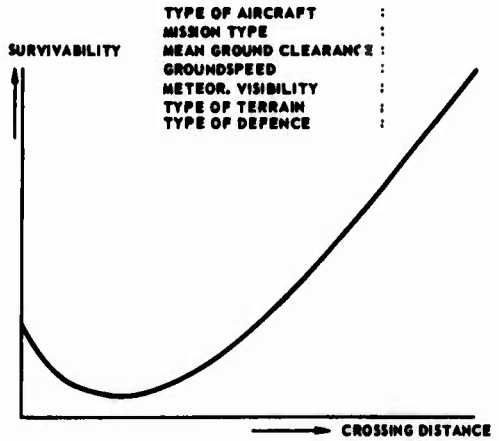

Fig. 5 Example of presentation of survivability results for penetration missions

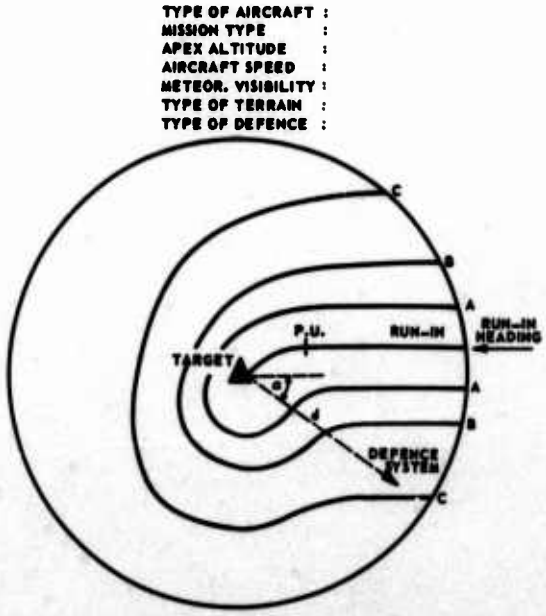

Fig. 6 Curves of defence system positions relative to the ground-target which correspond to an equal aircraft survivability

Open-Loop Compensation of Wind-Shear Effects in Low Level Flight

by
Rudolf Brockhaus
Prof. Dr.-Ing.
Technische Hochschule
D-33 Braunschweig
and
Peter Wuest
Dipl.-Ing.
Bodenseewerk Gerätetechnik GmbH
D-7770 Überlingen
Germany

SUMMARY

Low frequency wind changes, especially wind shear,require important and highly time variant thrust changes if an aircraft has to maintain the glide path. As efficient closed loop control of wind shear produces high throttle activity, an open loop control law has been developed that proves to be very efficient without the short-comings of closed loop control.An open loop activation of throttle and eventually spoilers turns out to be adequate to minimize the wind shear effects and thereby to discharge the closed loop system.

A complete estimation of the wind-variables necessary to generate the control signals would demand for a high amount of information, which can only be generated if an inertial navigation system or other precise navigation systems are available. The horizontal wind components can, on the other hand, be estimated with reduced information as shown in the paper.

The serious problem of separating the low frequency wind shear from higher frequency gusts has to be solved by use of nonlinear estimation filters. A very simple Kalman-filter with a nonlinear limitation of the second derivative of wind velocity proves to be adequate to solve the separation problem.

SYMBOLS

b	accelerometer signal
C_D	drag coefficient
C_L	lift coefficient
D	drag force
F	thrust
g	gravity factor
Δh	height above glide-path
L	lift force
R	slant distance
S	$= du_W/dt$
t	time
u	x-velocity component
u_{Wz}	$\partial u_W/\partial z$
V	airspeed (TAS)
V_K	flight path velocity
W	aircraft weight
w	z-velocity component
α	angle of attack
α_W	angle between $\vec{V}$ and $\vec{V}_K$ in the vertical plane
γ	flight path angle
γ_a	air path inclination angle
ε_F	aircraft elevation angle
ε_L	glide-path elevation angle
θ	pitch angle
σ	standard deviation

SUBSCRIPTS

a	air path axes
c	command variable
g	earth-fixed axes
W	wind velocities
$\hat{}$	estimated variable

INTRODUCTION

Wind shear has often led to dangerous situations,especially during approach,and has caused several major accidents during these last years. It is well known that an aircraft in final approach has to be accelerated in a decreasing head-wind to maintain airspeed without deviation from the glide-path. If this is not done in time the safety margin to minimum airspeed can be reduced rapidly, leading to critical situations. In effect the demanded thrust-settings in a wind shear are very time variant as is shown in fig. 1 for a wind shear situation that occured on June 24th, 1975, at the John F. Kennedy airport, resulting in a fatal accident /1/ /2/.

This example shows clearly that both pilot and autopilot can only manage such situations if they have sufficient information on the wind variables as well as a precise knowledge of the control laws suited to suppress the wind effects on the aircraft. The reasons for the difficulties to cope with wind-shear situations are twofold:

- wind shear implies rapid changes of the aircraft's energy management and therefore it must be compensated through rapid and exactly quantized thrust changes, which is the only means of on board energy-supply. At the same time the aerodynamic state of the aircraft must be kept constant through coordinated spoiler and elevator activity.

- As long as there is no measurement of wind velocity on board, pilot and autopilot both get too poor and too late wind shear-information, this information being only perceptable in steadily increasing flight-path and airspeed deviations. Autopilots can cope with wind shear through high gain and strong integrating terms, but this leads to intolerably high throttle activity in the presence of higher frequency gusts.

Modern system theory tells us to make use of all available information on the controlled process for control actions /3/. Consequently, if disturbances can be measured or estimated, this information should be used for open-loop control to unburden the closed loop system (see fig. 2).

Looking at open loop control, the first question is to find a simple control law that could improve flight-path accuracy in conjunction with a closed loop control system. Having in mind that the open loops should balance the coarse effects of input signals, whereas the closed control system should provide for control refinement as well as for parameter-sensitivity problems, the open loop control law may be determined starting from simplifying assumptions so that small effects can be neglected. In addition the primary objective of open loop wind-shear suppression is to counteract large energy changes which do not occur with high rate of change. Therefore it seems reasonable to restrict the open loop control to the low frequency range. This allows to restrain at the same time the generation of necessary signals to low frequencies.On the other hand in wind shear situations the aircraft is in an accelerated flight where some variables (e.g. the ground speed) are changing to a great extent. Therefore it is no longer admissible to investigate the wind effects by the usual linearized equations, but the control laws in question must be calculated from the nonlinear equations of the process.

The second question concerns the statement, which amount of information (quantity of measured variables) is necessary to generate the additional control signals. At the same time it must be examined if these signals can be measured or estimated on-line with adequate costs and sufficient signal quality.

In the following paper first an open loop control law will be developed and discussed starting from the nonlinear equations of the process /4/. The efficiency of this additional control will be demonstrated through simulation results. Secondly it will be shown

which variables must be available for the generation of the control signals. Finally, simple filters are proposed to estimate the necessary wind-information by aid of radio-signals used as an alternative to inertial navigation signals /4/, /5/.

2. EQUATIONS OF THE PROCESS

The airspeed $\vec{V}$ acting on an aircraft, i.e. the vector of relative velocity between aircraft and surrounding air is related to the inertial velocity of the aircraft, $\vec{V}_K$ and the local wind velocity $\vec{V}_W$ by the vector equation

$$\vec{V} = \vec{V}_K - \vec{V}_W \tag{2.1}$$

which is illustrated in the case of pure longitudinal flight by fig. 3. The angle γ_a of the airspeed vector relative to the earth-fixed coordinates (air path climb angle) is equal to

$$\gamma_a = \gamma + \alpha_W \tag{2.2}$$

where α_W is the angle between the two vectors $\vec{V}$ and $\vec{V}_K$. The definition of α_W may be deduced from fig. 3 as

$$\sin\alpha_W = \frac{u_{Wg}}{V} \sin\gamma + \frac{w_{Wg}}{V} \cos\gamma \tag{2.3}$$

Therefore γ_a is a function of γ, V and of the wind components in earth-fixed axes u_{Wg} and w_{Wg}. The latter can be expressed as sum of the components of $\vec{V}_K$ and $\vec{V}$ in earth-fixed axes according to fig. 3:

$$\begin{aligned} u_{Wg} &= V_K\cos\gamma - V\cos\gamma_a \\ w_{Wg} &= V\sin\gamma_a - V_K\sin\gamma \end{aligned} \tag{2.4}$$

The wind velocity as a function of time is given by the local wind field distribution on one hand and the aircraft's flight path on the other. The effective wind acting upon the aircraft is characterized by the following total differential (in earth-fixed axes):

$$\frac{d\vec{V}_W}{dt} = \frac{\partial\vec{V}_W}{\partial\vec{R}} \frac{d\vec{R}}{dt} + \frac{\partial\vec{V}_W}{\partial t} \tag{2.5}$$

in which the second term is usually neglected, assuming that the aircraft velocity is high in relation to the wind field changes with time. $\vec{R}$ is the vector from an earth-fixed point to the aircraft center of gravity and $\partial\vec{V}_W/\partial\vec{R}$ is the local wind field gradient /6/. For pure longitudinal flight without sidewind, Eq. (2.5) reads in components:

$$\begin{bmatrix} \dot{u}_W \\ \dot{w}_W \end{bmatrix}_g = \begin{bmatrix} u_{Wx}(\vec{R}) & u_{Wz}(\vec{R}) \\ w_{Wx}(\vec{R}) & w_{Wz}(\vec{R}) \end{bmatrix} \begin{bmatrix} \cos\gamma \\ -\sin\gamma \end{bmatrix} V_K \tag{2.6}$$

where $u_{Wx}=\partial u_W/\partial x$ ect. are the wind derivatives with respect to the space coordinates. For an aircraft flying in a wind shear which is alone a function of height as in fig. 6 this gives (in earth-fixed coordinates)

$$\begin{aligned} \dot{u}_{Wg} &= -u_{Wz}(h)\ V_K \sin\gamma \\ \dot{w}_{Wg} &= 0 \end{aligned} \tag{2.7}$$

which means that the rate of change of u_W is proportional to the windshear-gradient u_{Wz} and to the rate of descent $V_K\sin\gamma$. The X- and Z-force equations in air path axes (x_a-axis equal to $\vec{V}$) can be set up from fig. 4 as follows:

$$m\begin{bmatrix}\frac{d}{dt}(V_K\cos\alpha_W) + \dot\gamma_a V_K\sin\alpha_W\\ \frac{d}{dt}(V_K\sin\alpha_W) - \dot\gamma_a V_K\cos\alpha_W\end{bmatrix} = m\begin{bmatrix}\dot V_K\cos\alpha_W + \dot\gamma V_K\sin\alpha_W\\ \dot V_K\sin\alpha_W - \dot\gamma V_K\cos\alpha_W\end{bmatrix} =$$

(2.8)

$$= \begin{bmatrix}-D\\ -L\end{bmatrix} + \begin{bmatrix}-\sin\gamma_a\\ \cos\gamma_a\end{bmatrix} W + \begin{bmatrix}\cos\alpha\\ -\sin\alpha\end{bmatrix} F$$

The situation of an aircraft flying on an earth-fixed glide-path is illustrated in fig. 5 for the pure longitudinal case. From this figure the following differential equation for the flight path can be derived:

(2.9)
$$\begin{bmatrix}\dot R\\ \Delta\dot h\end{bmatrix} = \begin{bmatrix}-\cos(\gamma+\varepsilon_F)\\ \frac{\sin(\gamma+\varepsilon_L)}{\cos\varepsilon_L}\end{bmatrix} V_K \approx \begin{bmatrix}-1\\ (\gamma+\varepsilon_L)\end{bmatrix} V_K$$

Δh and R being the distance of the aircraft c/g to the glide path center line and origin respectively and ε_L being the elevation angle of the straight glide-path.

3. CALCULATION OF THE THRUST REQUIREMENT

Having compiled all necessary equations, we now have to define the flight condition that should be maintained by open loop control, in other words, we have to choose those variables that shall be held constant. Certainly the first demand is to minimize the glide-path deviation, this can be expressed by

(3.1)
$$\Delta\dot h \overset{!}{\equiv} 0 \quad \text{or} \quad \gamma \overset{!}{\equiv} -\varepsilon_L$$
$$\dot\gamma \overset{!}{\equiv} 0$$

The other demand relates to the aircraft velocity and here we will make the usual choice that airspeed is to be held constant because this minimizes variations of aerodynamic lift and drag and guarantees a safe margin to the minimum (stall) speed. Therefore the second demand is:

(3.2)
$$\dot V \overset{!}{\equiv} 0$$

This implies that the absolute speed V_K will vary in accordance with Eq. (2.4). These two demands determine the control law which we will now derive under idealized conditions, i.e. neglecting measurement and actuation lag effects. Moreover, for usual approach situations, all angles and the angular rates of γ_a and α_w may be assumed to be small (products of small terms are neglected in the following). From fig. 3 it can be seen that

(3.3)
$$V_K\cos\alpha_W = V + u_{Wa}$$

Deriving this with respect to time

(3.4)
$$\frac{d}{dt}(V_K\cos\alpha_W) = \dot V + \dot u_{Wa}$$

and introducing into the first row of Eq. (2.8)

(3.5) $$m\left[\dot{V} + \dot{u}_{Wa} + \dot{\gamma}_a V_K \sin\alpha_W\right] = -D - \sin\gamma_a W + \cos\alpha\, F$$

we get for small angles and condition (3.2):

(3.6) $$m\,\dot{u}_{Wa} = -D - W\gamma_a + F$$

Rearranging the terms the required thrust-to-weight ratio results to be

(3.7) $$\frac{F}{W} = \frac{D}{W} + \gamma_a + \frac{\dot{u}_{Wa}}{g} \qquad \text{with}$$

(2.3) $$\gamma_a = \gamma + \alpha_W$$

For small values of $\dot{V}_K$, α_W and α the second row of Eq. (2.8) is simplified under condition (3.1) to:

(3.8) $$0 = -L + W$$

This means that the lift should always balance the weight

(3.8a) $$L \approx W$$

Introducing these simplifications we get the final relation for the demanded thrust /4/:

(3.9) $$\frac{F}{W} = \frac{C_D}{C_L} + \gamma_a + \frac{\dot{u}_{Wa}}{g}$$

4. PHYSICAL INTERPRETATION OF THE WIND-DEMANDED THRUST

In the no-wind case (α_W, $\dot{u}_W = 0$), the steady state thrust-to-weight ratio must be

(4.1) $$\frac{F}{W} = \frac{C_D}{C_L} + \gamma$$

equal to the sum of the actual glide angle C_D/C_L and the commanded flight path angle $\gamma_c = -\varepsilon_L$. This corresponds to the stationary thrust setting in an inclined flight path.

If the wind is not zero, the thrust-to-weight ratio is changed to

(4.2) $$\frac{F}{W} = \frac{C_D}{C_L} + \gamma_a + \frac{\dot{u}_{Wa}}{g}$$

where the additional thrust is proportional to

- the angle $\alpha_W = \gamma_a - \gamma$ between the commanded flight path (vector $\vec{V}_K$) and the new direction of $\vec{V}$
- the actual wind acceleration $\dot{u}_W$ in relation to g.

In other words: In a constant wind field the thrust must guarantee the necessary angle γ_a of the vector of relative speed between aircraft and surrounding air, $\vec{V}$, to maintain the desired flight path angle. Therefore γ_a in Eq. (4.2) has to be interpreted as a command variable: it is the value of γ_a which should exist in the actual wind situation so that the nominal (commanded) value of flight-path angle γ_c can be maintained. In addition to this the thrust must hold the airspeed V constant by accelerating or decelerating the aircraft corresponding to the wind acceleration.

The wind components can be introduced when α_W is substituted by Eq. (2.2):

$$\gamma_a = \gamma + \alpha_W = \gamma + \frac{u_{Wg}}{V}\gamma + \frac{w_{Wg}}{V} \tag{4.3}$$

which leads to the thrust control law for the nominal state where $\gamma = \gamma_c$ and $V = V_c$

$$\frac{F}{W} = \frac{C_D}{C_L} + \gamma_c + \frac{u_{Wg}}{V_c}\gamma_c + \frac{w_{Wg}}{V_c} + \frac{\dot{u}_{Wa}}{g} \tag{4.4}$$

Corresponding to this equation, the thrust must be augmented

- proportional to a head-wind (negative u_{Wg}) if the aircraft is on a glide (γ negative) to reduce the rate of descent in accordance to the decreasing ground-speed. This effect, which does not occur in level flight is due to a rotation of the resultant aerodynamic force, as illustrated by fig. 6,

- proportional to a down wind (positive w_{Wg}) to counteract its effect by an opposite relative velocity between air and aircraft (see fig. 7).

In a wind shear an additional thrust change must be applied proportional to the rate of increasing tailwind or decreasing headwind ($\dot{u}_W$ positive) to accelerate the aircraft and hold the airspeed V constant without glide path deviation (i.e. without additional loss of potential energy). These three effects are well known qualitatively from flight experience.

The last term of Eq. (4.4) is proportional to the horizontal wind acceleration encountered by the aircraft, which is a function of the flight path as shown in Eq. (2.7). To interpret the effect of a certain space-fixed wind field on the aircraft, $\dot{u}_W$ has to be substituted. For the simplified case where the x-component of the wind changes linearly with height (u_{Wz}) and the z-component is constant, Eq. (2.4) and (2.6) yield:

$$\dot{u}_{Wa} \approx \dot{u}_{Wg} = - u_{Wz}\,\gamma\,V_K = - u_{Wz}\,\gamma\,(V + u_{Wg}) \tag{4.5}$$

This leads with Eq. (4.4) to the relation of the required thrust as a function of height (for w_{Wg} = const.):

$$\begin{aligned}\frac{F}{W} &= \frac{C_D}{C_L} + \gamma_c + u_{Wg}(h)\,\frac{\gamma_c}{V_c} + w_{Wg}\,\frac{1}{V_c} - u_{Wz}\,\frac{\gamma_c}{g}\left[\,V_c + u_{Wg}(h)\,\right] \\ &= \frac{F_o}{W} + \frac{\Delta F_1}{W} + \frac{\Delta F_2}{W} + \frac{\Delta F_3}{W}\end{aligned} \tag{4.6}$$

To get a qualitative survey of the relative importance of the four terms of Eq. (4.6), F_o/W, $\Delta F_1/W$ and $\Delta F_3/W$ as well as their sum are shown in fig. 8 as a function of height. The wind-profile is assumed to have piecewise segments of linear gradients of

$$u_{Wz} = 0 \text{ and } \pm 0{,}2 \text{ 1/sec} \triangleq 12 \text{ kts/100 ft}$$

to visualize the different effects. The thrust-to-weight ratios are drawn for $\gamma_c = -3^o$ and $C_D/C_L = 0{,}18$ as typical values and for two approach speeds: V_c = 35 m/sec in fig. 8a for a typical STOL-aircraft and V_c = 70 m/sec in fig. 8b for a typical CTOL-transport. From the idealized curves the following can be stated:

- $\Delta F_1/W$ and $\Delta F_3/W$ are of opposite sign in a tailwind shear (increasing tailwind) and of equal sign in a headwind shear. The slope of the total F/W is therefore of different magnitude in the two cases (this effect is inverted in climb, i.e. γ_c positive).

- The relative importance of $\Delta F_1/W$ is higher for low airspeed, where the proportion of u_W to V_c is higher, and for steeper glide-paths. Therefore the slope of the total

F/W can be positive, negative or zero in a headwind-shear.

The maximum value of the four parts of F/W are listed in table 1 for the two speed cases to show their relative importance. They have been calculated on the basis of the wind components and the wind gradient u_{Wz} of the example shown in fig. 1. First it can be seen that the influence of the u_W-term is small, especially in the case of higher approach speed (see fig. 8). Therefore this term could possibly be neglected in the open-loop control law if the generation of the control signal turns out to be too complicated or expensive.

V_c	$\frac{F_o}{W}$	$\frac{\Delta F_{1max}}{W}$	% of $\frac{F_o}{W}$	$\frac{\Delta F_2}{W}$	% of $\frac{F_o}{W}$	$\frac{\Delta F_{3max}}{W}$	% of $\frac{F_o}{W}$
35 m/sec	0,128	0,018	14	0,174	134	0,050	39
70 m/sec	0,128	0,009	7	0,084	67	0,088	67

Table 1: Relative magnitude of wind-required thrust ($\gamma_c = -3^o$, u_{Wg} = 12 m/sec, w_{Wg} = 6 m/sec, u_{Wz} = 0,2 1/sec)

The thrust demand $\Delta F_2/W$ that is caused by the vertical wind component is related to wind amplitudes of w_W = 6 m/sec. This magnitude has been experienced in conjunction with wind shears of the order of u_{Wz} = 0,2 1/sec in the proximity of thunderstorms (e.g. in the example cited in fig. 1). This seems therefore to be a reasonable guess for a mean value in a greater extension of space, i.e. for long term vertical wind influence. On the other hand it is well known that vertical wind (e.g. downdrafts) exist with a magnitude of 20 m/sec and above. But such high vertical wind components are confined to an extension of the order of 50 m which means that their influence on the aircraft is limited to a time interval of the order of one second. Such high and rapid vertical gusts cannot be counteracted immediately due to the limited performance of the aircraft. Their effect must be suppressed at long term through adequate closed loop control.

The third term which results from the wind shear increases with aircraft velocity, ΔF_2 and ΔF_3 being of same magnitude in the CTOL-example. These two parts should at any rate be incorporated in the open loop control law.

5. SIMULATION RESULTS

In /7/ the efficiency of a thrust control law equal to Eq. (4.7) has been investigated by a nonlinear simulation for a Boeing 707 approaching at $\gamma = -3^o$ and V = 74 m/sec through a wind shear as shown in fig. 1. To the thrust control an open loop cross-coupling to the elevator has been added to compensate the effect of pitching moments due to thrust changes

$$\Delta\eta = \frac{M_F}{M_\eta}\,\Delta F \tag{5.1}$$

but there have been no closed control loops.Traces A of fig. 9 show the flight path and airspeed deviations when neglecting the engine time constants. Even in this excessive wind shear which caused a fatal accident the deviations are very small, the touch down point being 50 m ahead of the threshold.Traces B and C show the effect of engine time constants of 0.25 and 1.0 sec, where a time constant of 0.25 sec has proven to be characteristic for a JT3D-engine regarding the small necessary thrust rates /7/. This shows that the engine lag has only a minor effect on the flight path deviations.

It has to be emphasized here that the simulation proves the surprising fact that the deviations of the two aircraft states V and γ in the presence of wind-shear can be reduced substantially by open loop control to one actuating variable, i.e. to the throttle only. The only additional condition is, that the lift (or the angle of attack) must be held approximately constant by elevator control to satisfy the condition $L \approx W$ which has been used to determine the thrust control law

$$\frac{F}{W} = \frac{C_D}{C_L} + \gamma_a + \frac{\dot{u}_{Wa}}{g} \tag{4.2}$$

So Eq. (4.2) and (5.1) can be considered as the only necessary open loop supplement to usual flight control systems to cope even with difficult wind situations.

6. REALISATION OF THE CONTROL LAW

The first term of Eq. (4.2) C_D/C_L can be assumed to be constant, this is well satisfied in approach flight were the aircraft speed is near the point of minimum drag speed, despite of small possible deviations in angle of attack. In addition to that the airspeed deviations are minimized by thrust control (see fig. 9).

As has been pointed out above, the second term, γ_a, is a command variable. The actual value of γ_a or α_w cannot be used for thrust control because they depend not only on the wind components but on the flight path angle as well, so it would give wrong information in the case of flight path deviations. As can be seen from fig. 10, a control law $\Delta F = W\,\Delta\gamma_a$ would even cause instability. The control law must therefore be derived from Eq.(4.4) as follows:

$$\frac{\Delta F}{W} = \Delta\gamma_c + u_{Wg}\frac{\gamma_c}{V_c} + w_{Wg}\frac{1}{V_c} + \frac{\dot{u}_{Wa}}{g} \tag{6.1}$$

It is applicable to both the control of curved flight paths (γ_c varying) and to the suppression of wind effects. Indeed, the variables u_{Wg}, w_{Wg} and $\dot{u}_{Wa}$ cannot be measured directly but must be calculated or estimated from available variables. To assess the amount of necessary information Eq. (6.1) shall be expressed in measurable variables. From Eq. (2.4) and (3.4) follows for small angles:

$$u_{Wg} = V_K - V \tag{6.2}$$

$$w_{Wg} = V\gamma_a - V_K\gamma \tag{6.3}$$

$$\dot{u}_{Wa} = \dot{V}_K - \dot{V} \tag{6.4}$$

which leads to the final thrust control law

$$\frac{\Delta F}{W} = \Delta\gamma_c + (V_K - V)\frac{\gamma_c}{V_c} + (V\gamma_a - V_K\gamma)\frac{1}{V_c} + (\dot{V}_K - \dot{V})\frac{1}{g} \tag{6.5}$$

The following variables have to be measured or estimated with high precision (small differences of big terms!):

V_K - INS-signal or estimation from DME and accelerometer-signals

V - TAS (air data computer)

$\gamma_a = \theta - \alpha$ - precision attitude and angle of attack sensors

$V_K\gamma = w_{Kg}$ - INS-signal or estimation from radio-height, vario- and accelerometer signals

$\dot{u}_{Wa} = \dot{V}_K - \dot{V}$ - estimation from V_K, V and accelerometer signals.

This makes evident that the full open loop suppression of wind effects requires a great amount of information and can only be achieved if an inertial platform and precise radio signals and estimation filters are available.

As we only want so suppress the low frequency part of the wind effects, we may limit the estimation to the low frequency portion of these signals. But even under this restriction the third term in Eq. (6.5) seems to be very difficult to generate because it represents a small difference of two terms that must be estimated from four or five different signal sources.

If the deviations of airspeed can be neglected ($V = V_c$), the first two terms of Eq. (6.5) reduce to

$$\frac{\Delta F_1}{W} = \frac{\gamma_c V_K}{V_c} = \frac{\dot{h}_c}{V_c} \tag{6.6}$$

This control law has already been implied in the integrated flight control system FRG 70 of Bodenseewerk giving a high improvement of flight path control in steep approaches /8/. To cope with horinzontal wind-shear, the $\dot{u}_W$-term has to be added to this control law.

7. ESTIMATION OF THE WIND COMPONENTS u_W and $\dot{u}_W$

According to Eq. (2.4) the horizontal wind velocity u_W is equal to the difference between the aircraft inertial velocity V_K and the true airspeed V. The latter can be supplied by an air data computer. If there is no inertial platform on board, V_K must be estimated from other available signals. In /4/ and /5/ a very simple Kalman-filter has been proposed and tested for the estimation of the aircraft absolute velocity V_K from DME and accelerometer signals according to the process equations

$$\begin{aligned} \dot{R} &= V_K \\ \dot{V}_K &= f + (b_x - g\sin\theta) \end{aligned} \tag{7.1}$$

R - DME-distance
b_x - accelerometer signal
f - constant accelerometer error

This filter is shown in fig. 11. It has been stated in /5/ that good estimation of V_K is attainable even without the acceleration reference. For the following discussion it can therefore be assumed that V_K is available without the existance of an inertial navigation system.

The low frequency estimation of the variable u_W and its derivative $\dot{u}_W$ can equally be realised by a stationary Kalman-filter under the premises that a model of the signal process is known /9/. A very simple but adequate model of the time history of the low frequency portion of u_W is the following:

$$u_W(t) = u_{Wo} + \int_{t_o}^{t} S\, dt \tag{7.2}$$

where

$$S = \frac{du_W^*}{dt} = S_o \tag{7.3}$$

is first assumed to be constant. This process-model can be realised with two integrators as is shown in fig. 12. It is the heart of the proposed filter. To complete the filter the estimated value $\hat{u}_W$ must be subtracted from the measured value $u_W' = V_K' - V'$ and the difference fed back to the two integrator inputs as is shown in fig. 13. The feedback

factors k_1 and k_2 have to be determined for good filter dynamics. If the real wind process corresponds to the filter model, $\hat{u}_W$ and $\hat{S}$ will match the exact values after the filter transition time when starting from the unknown initial conditions. But in the real process, higher frequency gusts (u_W^{**}) are superposed to the low frequency wind changes (u_W^*).

(7.4) $$u_W = u_W^* + u_W^{**}$$

The low frequency part u_W^* (wind shear) that shall be used for open loop control has to be separated from the gusts because the latter should not be fed to the throttle to avoid rapid thrust changes and high throttle activity.

The problem is, that the higher frequency gusts are dominating in known wind-models (e.g. the Dryden spectrum). Therefore a linear low pass filter as that shown in fig. 13 cannot damp out the gusts sufficiently without loss of the wanted windshear information. Better results in the separation of gusts form the low frequency wind shear can be expected from the use of a nonlinear filter. The linear filter of fig. 13 has therefore been modified by limiting the rate of change of $S = \dot{u}_W^*$ as is shown in fig. 14. The efficiency of this filter, where the limitation has been set to

$$\dot{\hat{S}}_{max} = 0{,}05 \text{ m/sec}^3$$

has been investigated in a simulation where gusts at medium turbulence (σ = 1 m/sec) have been superimposed to wind shear. From fig. 15 it can be seen very clearly that the introduction of the nonlinearity has a positive effect on the estimated $\dot{u}_W$-signal: the higher frequency parts are reduced considerably whereas the mean value of $\dot{u}_W$ reproduces well the wind shear amplitude. The eigenvalues of the filter as well as the limitation value will be verified in flight tests.

In section 4 it has been pointed out that the effect of $\dot{u}_W$ in the thrust control equation is dominant and that the u_W-effects could possibly be left to the closed loop if the signal generation proves to be too difficult. This has led to the question whether the estimation of $\dot{u}_W$ alone could be achieved without knowledge of V_K which can only be determined with relatively high expense as has been pointed out. Fig. 16 which can be developed from the block diagram of fig. 15 by elementary transformations shows a nonlinear filter for the estimation of $S = \dot{u}_W^*$. It turns out that the wind shear part of $\dot{u}_W$ can be estimated from the signals of true airspeed v and the horizontal acceleration $\dot{u}_K$ without use of the absolute speed V_K. The value of $\dot{u}_K$ can be generated by usual means from

(7.4) $$\dot{u}_K = b_x - g\theta$$

or from a strap down system if higher signal accuracy is needed.

For the estimation of the low frequency vertical wind component w_W which is essential for the generation of the control signal (see section 4), no concrete proposition can be made at the moment. It can only be stated, that sureley one has to refer to inertial signals (strap down platform) to ensure the accuracy needed. As the same problem arises for the separation of the high- and low-frequency portions, nonlinear filtering will also be necessary.

8. CONCLUDING REMARKS

In conclusion it can be said that an open loop control of the X-forces by use of throttle and spoilers proves to be very efficient to minimize airspeed and glide-path deviations in the presence of wind shear even under consideration of engine time lag. The open loop

control has the great advantage that high gains can be realized without stability problems and that high frequency signals can be kept away from the throttle by separating them through nonlinear filtering. Full wind-shear suppression can on the other hand not be achieved without the availability of precise inertial and radio signals, this is especially true for the elimination of long term vertical wind effects. The utilisation of inertial navigation systems as well as the introduction of microwave landing systems with precise DME-information will be the essential steps to overcome wind shear problems and will therefore contribute greatly to the increase of flight safety.

9. REFERENCES

/1/ - Aircraft Accident Report: Eastern Airlines Inc. Boeing 727-225, N 8845E, John F. Kennedy International airport, June 24, 1975, National Transportation Safety Board Rept. No. NTSB-AAR-76-8

/2/ P. Krauspe - Die Gefährdung der Flugsicherheit durch Scherwind Paper presented at the DGLR Annual Conference Berlin 13.-15. Sept. 77

/3/ G. Schänzer, H.H. Böhret - Integrated Flight Control System for Steep Approach and Short Landing Paper presented at the AGRAD Symposium, "Advances in Control Systems" 1974

/4/ Barth, R. Brockhaus, Lonn, P. Wuest - Entwurf und Erprobung von Schätzverfahren zur Ermittlung von Wind- und Böenstörungen zur Störgrößenkompensation ZTL-76 Bodenseewerk Gerätetechnik TB D 1264/77

/5/ G. Schänzer - The Influence of Microwave Landing Systems on Guidance and Control Paper presented at the AGARD G&P-Symposium, "Night and All-Weather Guidance and Control Systems for Fixed-Wing Aircraft", May 1976

/6/ R. Brockhaus - Flugregelung I Oldenbourg, München 1977

/7/ P. Krauspe, J. Bergunde - Untersuchung der Verzögerungs- und Totzeiteinflüsse bei Scherwind-landungen Arbeit 77-2 am Lehrstuhl für Flugmechanik der TU Braunschweig, August 1977

/8/ G. Schänzer - Auslegung von Flugreglern mit Hilfe moderner Systemtheorie Zeitschrift für Flugwissenschaften, 23 page 129-137, 1975

/9/ P. Wuest - Probleme der Messung von Windgrößen mit bordüblichen Sensoren Paper presented at the DGLR Annual Conference Berlin, 13.-15. Sept. 77

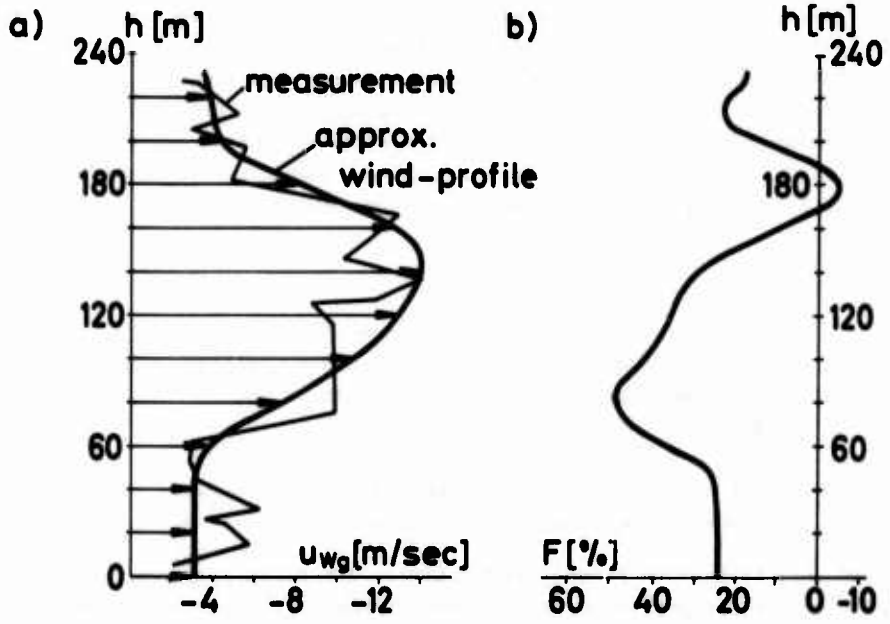

Fig. 1 Required thrust in a strong wind-shear (from /2/)
a) wind profile
b) required thrust setting

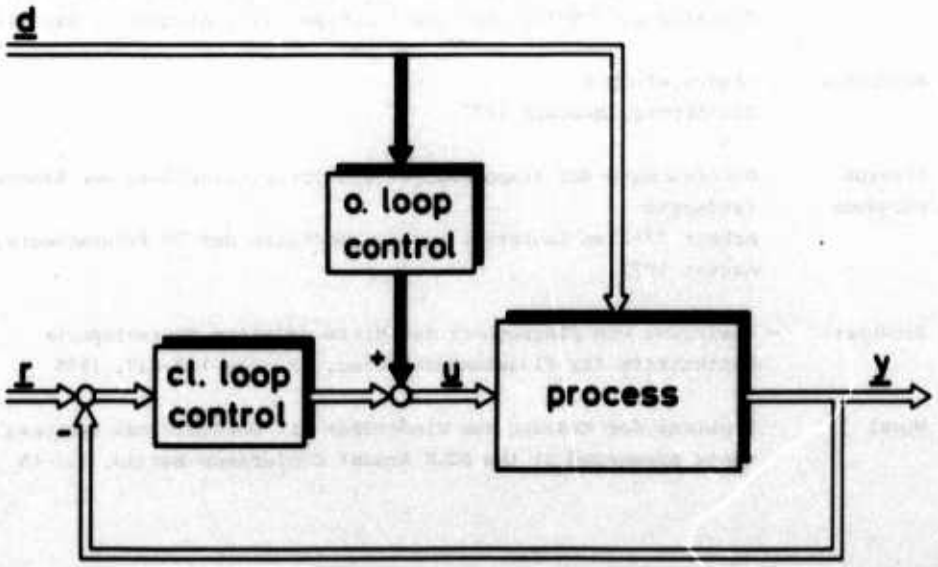

Fig. 2 Control system with open-loop disturbance suppression

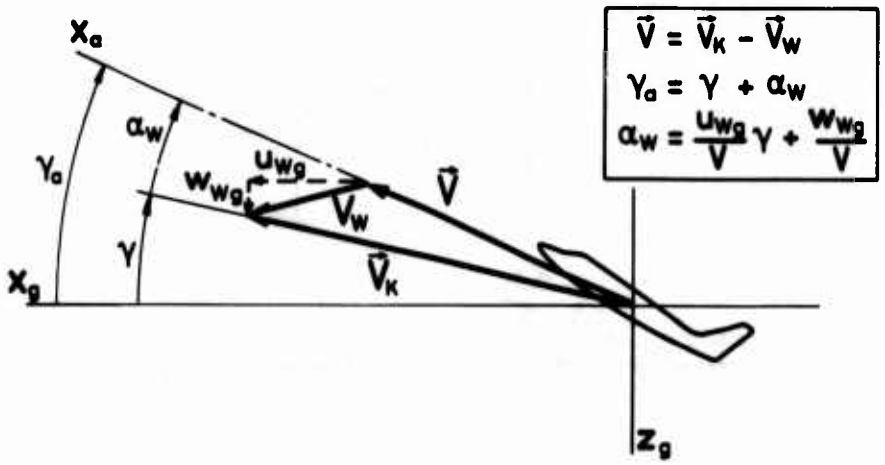

Fig. 3 Relation of aircraft and wind velocities

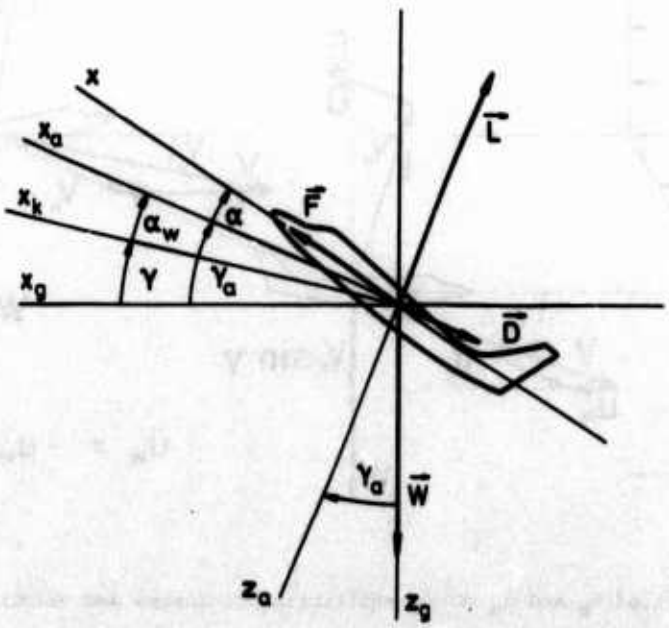

Fig. 4 Definition of forces and angles

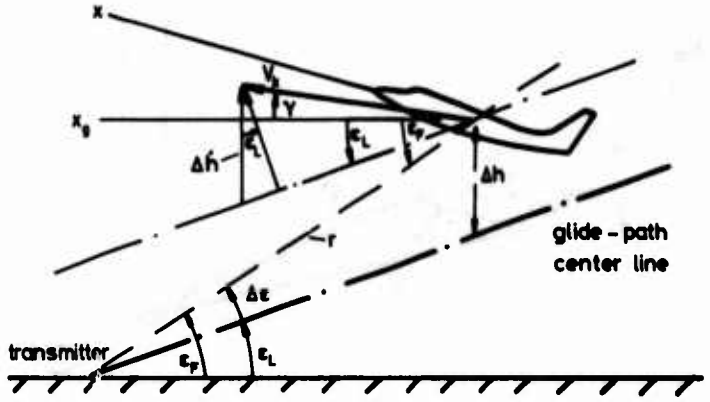

Fig. 5 Geometry of an aircraft relative to the glide-path

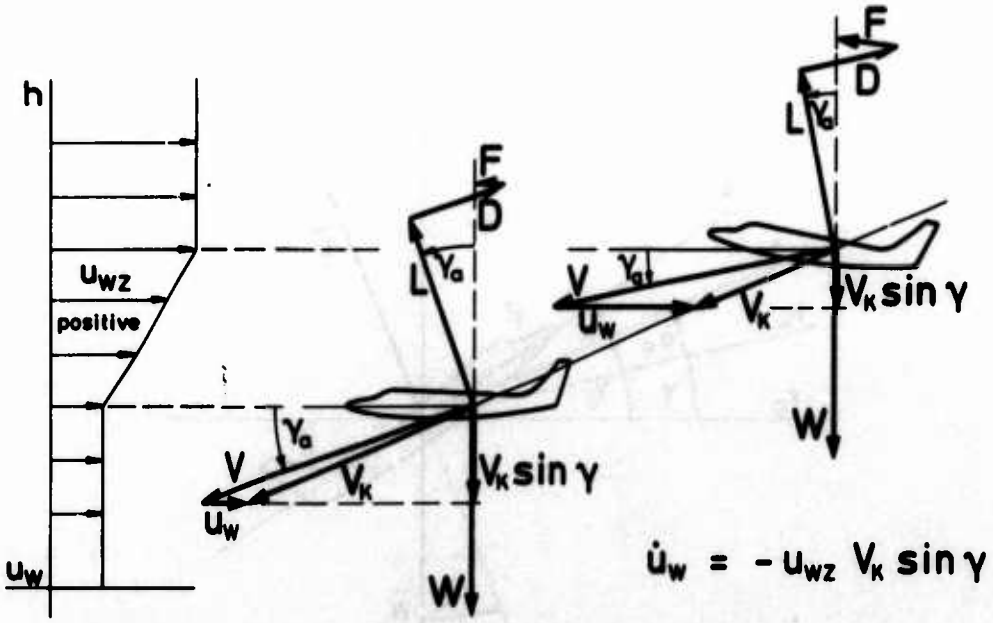

Fig. 6 Effect of u_w and $\dot{u}_w$ on the equilibrium of forces and velocities

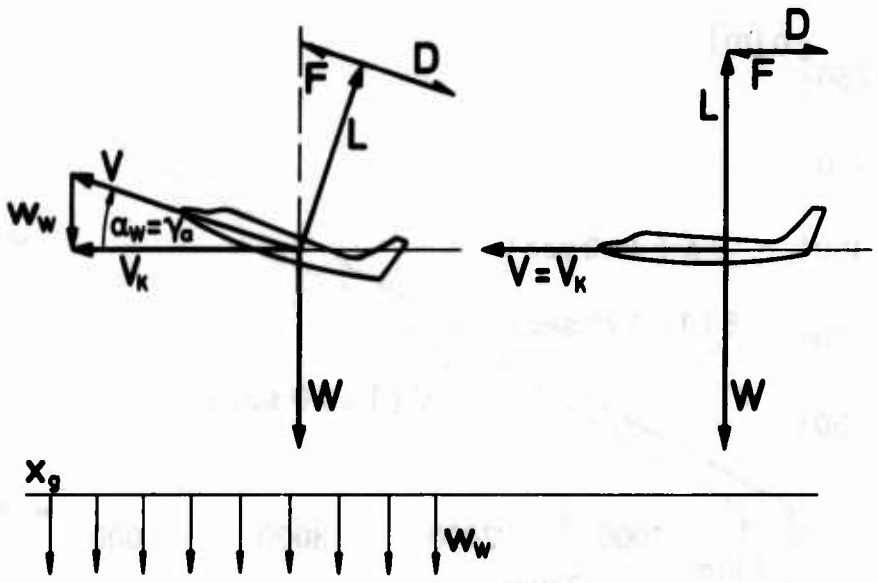

Fig. 7 Effect of w_w on the equilibrium of forces

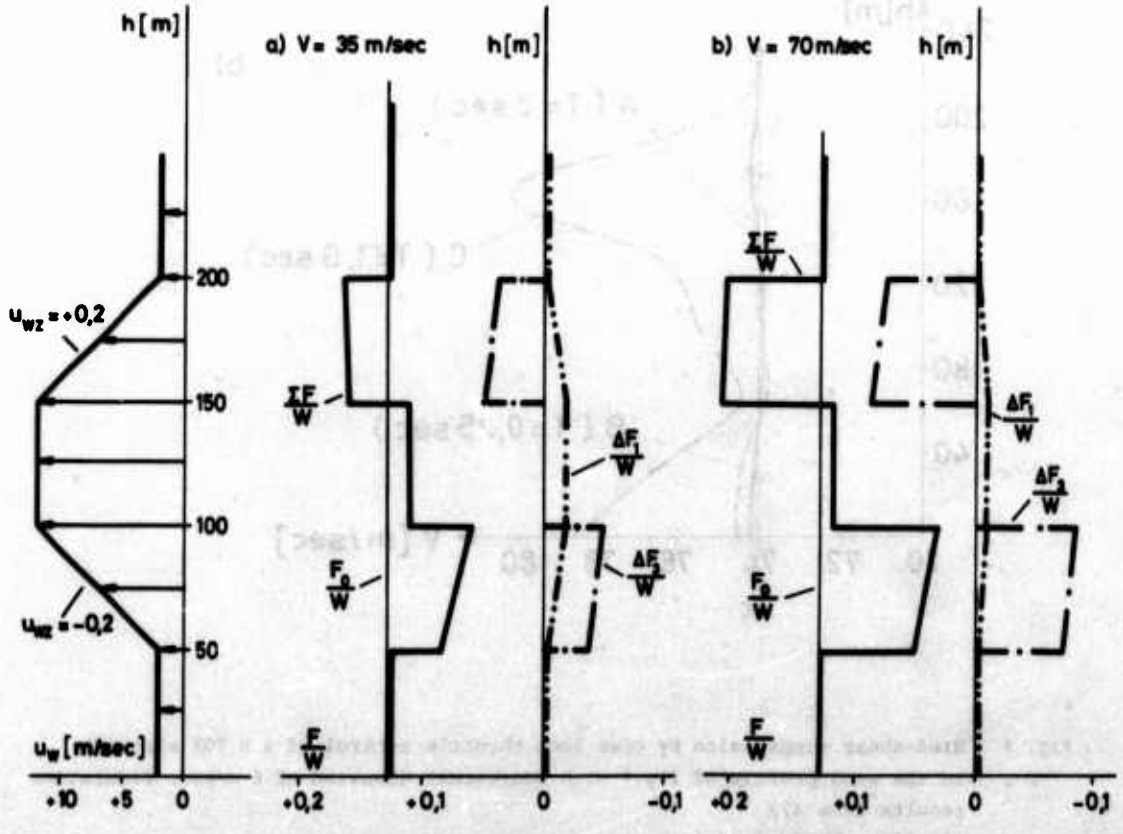

Fig. 8 Required thrust as function of wind-shear ($\gamma_c = -3^\circ$; $C_D/C_L = 0,18$)
a) STOL-aircraft
b) CTOL-aircraft

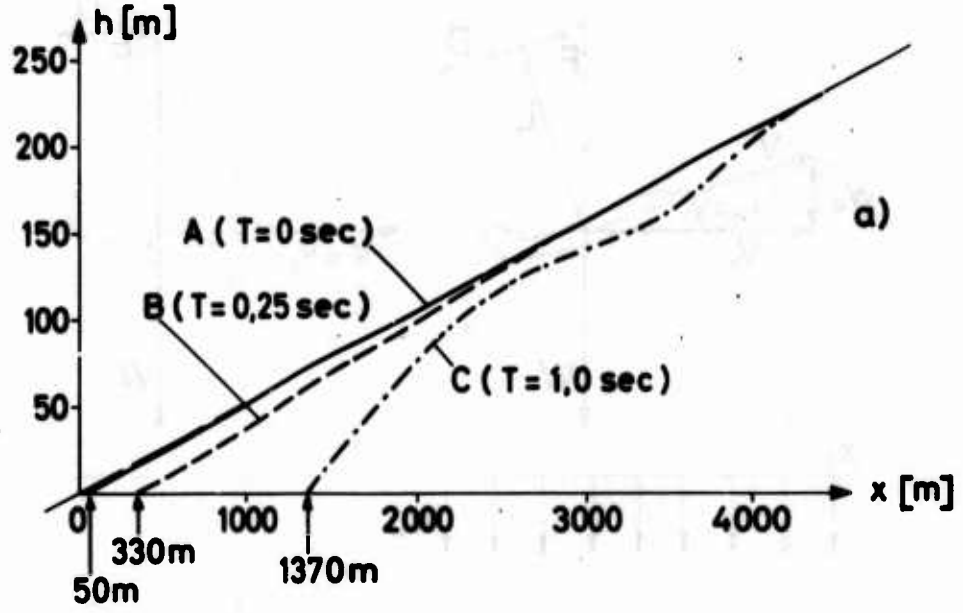

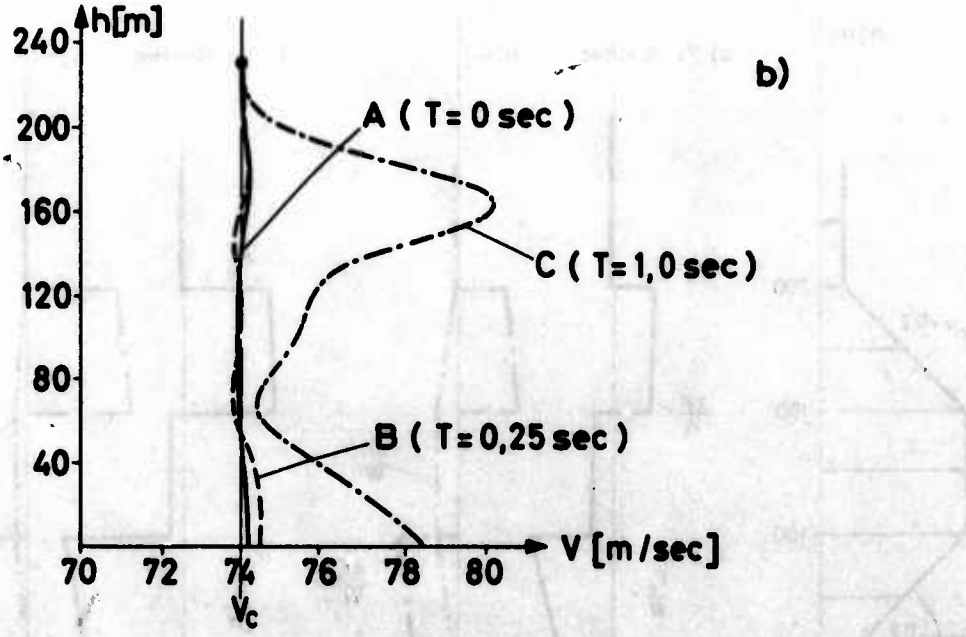

Fig. 9 Wind-shear suppression by open loop throttle control of a B 707 aircraft in the wind profile of fig.1 with additional downwind of 6 m/sec. Simulation results from /7/

a) glidepath-deviations

b) airspeed-deviations

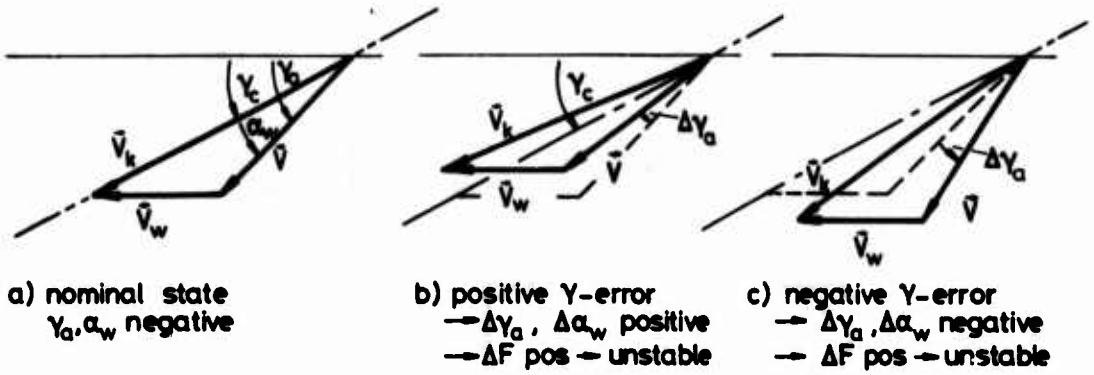

Fig. 10 Influence of flight path error on the value of γ_a and α_w

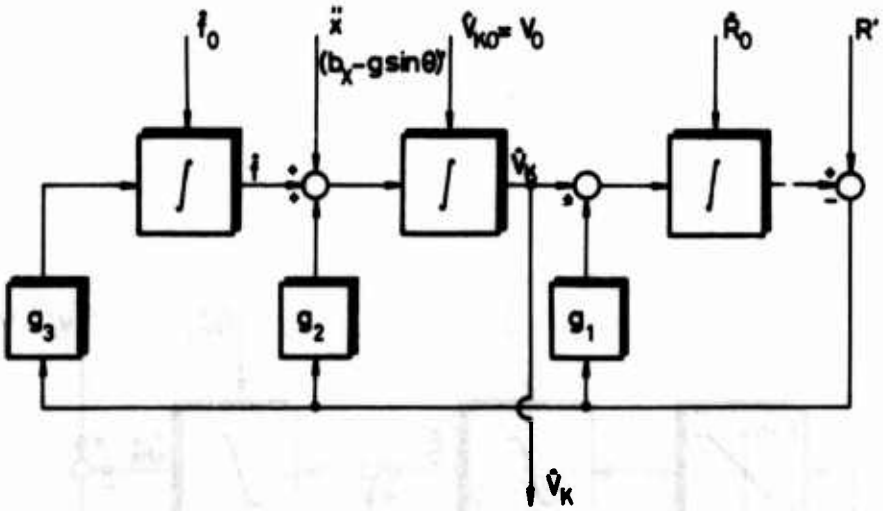

Fig. 11 Flight path velocity estimation filter

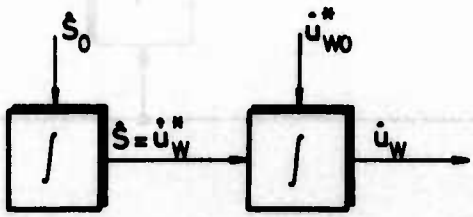

Fig. 12 Simplified wind-shear model

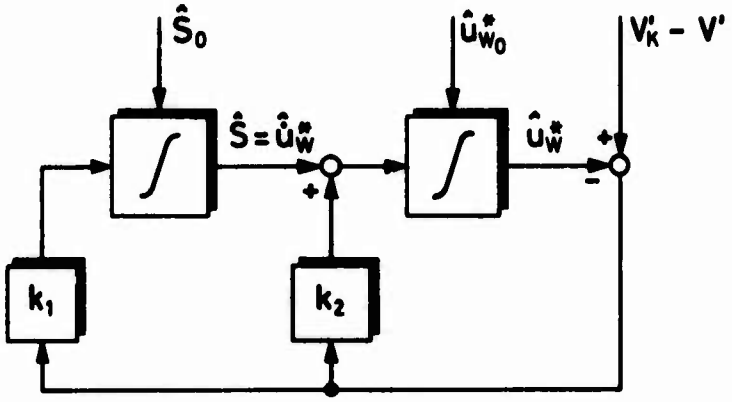

model equation :

$$u_w(t) = u_{w_0} + \int_{t_0}^{t} S\,dt \quad ; \qquad S = \frac{du^*_w}{dt} = S_0$$

Fig. 13 Horizontal wind-shear estimation filter

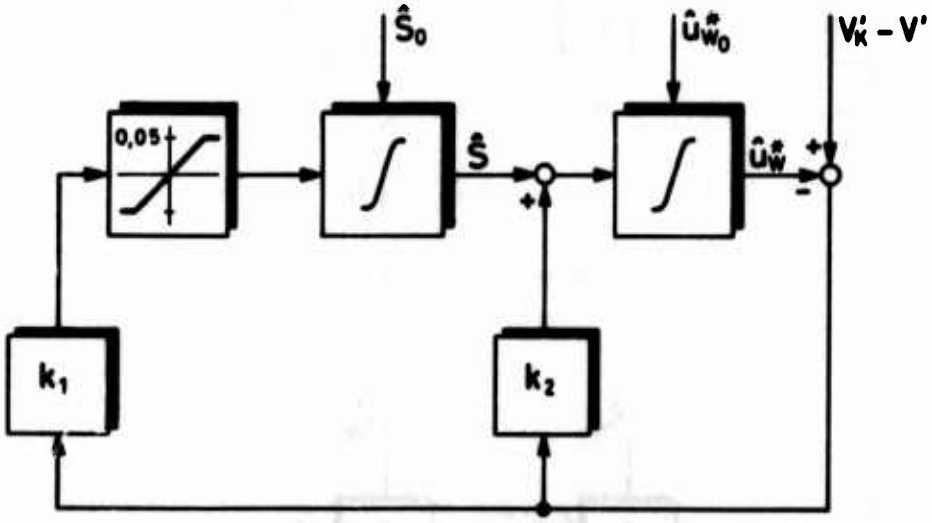

Fig. 14 Nonlinear filter for the estimation of horizontal wind-shear

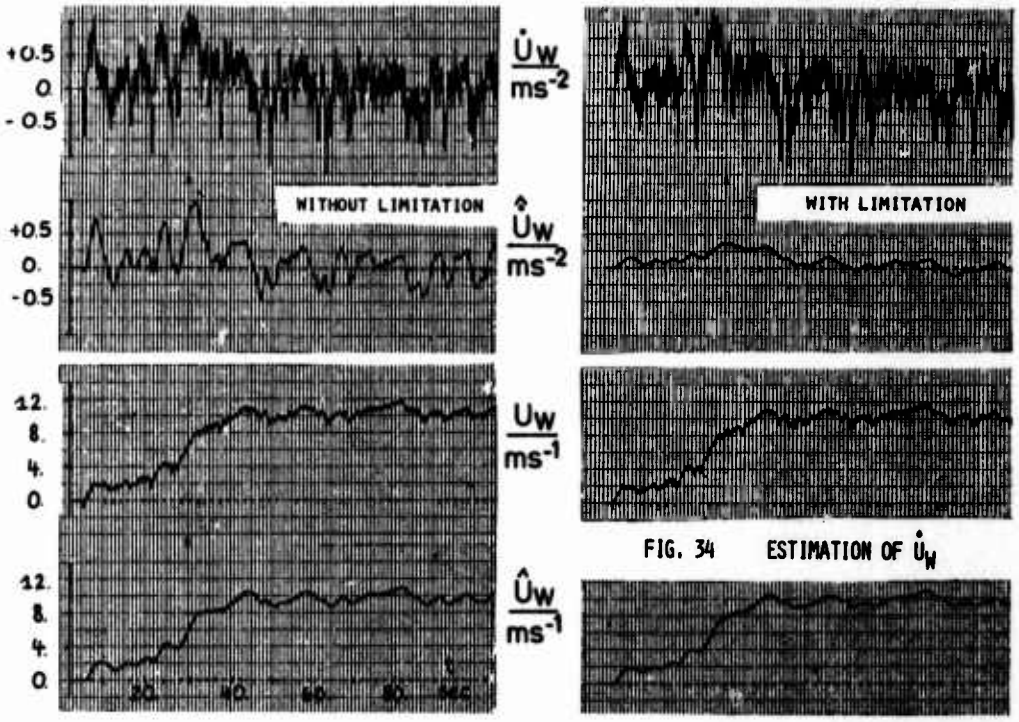

FIG. 34 ESTIMATION OF $\dot{U}_W$

Fig. 15 Effect of the nonlinearity on the separation of the low frequency wind-shear from gusts

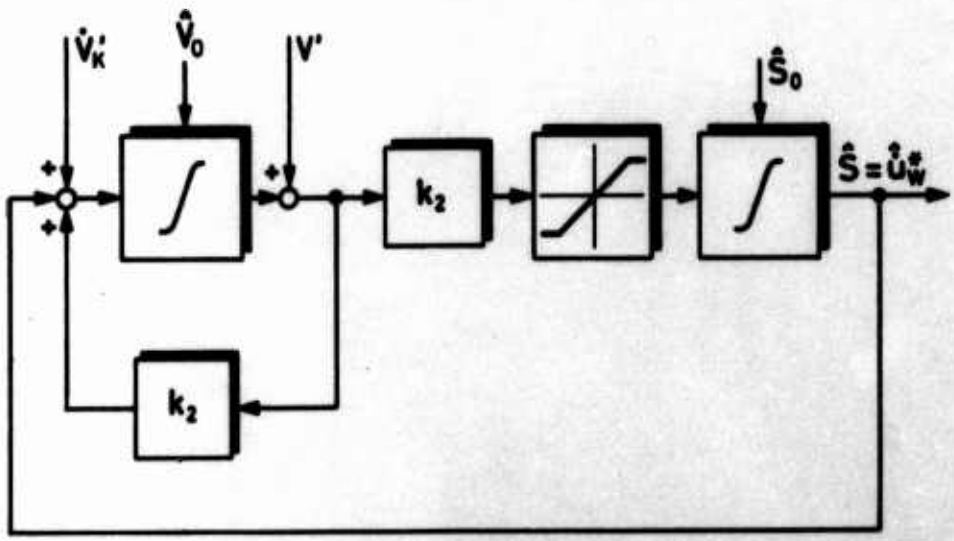

Fig. 16 Filter for the estimation of $\dot{u}_W$ without flight path velocity measurement

AIRCRAFT RIDE-BUMPINESS AND THE DESIGN OF RIDE-SMOOTHING SYSTEMS

by

J. G. Jones and D. E. Fry, Flight Systems Department,
Royal Aircraft Establishment,
Farnborough,
Hampshire
GU14 6TD, UK

SUMMARY

Aircraft longitudinal ride-bumpiness due primarily to aircraft rigid-body response is discussed in this paper. Results obtained for flight at high speeds and low altitude are described and the implications for aircraft design deduced, both in terms of basic airframe considerations and in terms of the use of active controls.

Bumpiness is distinguished from vibration, the former being characterised by a sequence of separately-identifiable g fluctuations, referred to as bumps, the latter being associated with quasi-sinusoidal oscillations. In the case of small combat aircraft, bumpiness is in general influenced predominantly by aircraft rigid-body response whereas vibration may usually be related to the response of the flexible structure.

Using statistical discrete-gust theory, bumpiness is described in terms of g counts per unit time. In addition to providing a quantitative measure of exceedance counts of arbitrary g levels, this theory allows the straightforward computation of the sharpness of a bump in the sense of the rise-time of a typical discrete fluctuation in normal acceleration.

Primary effects of aircraft wing loading, lift slope and speed are discussed. An increase in the airframe-dependent parameter $\frac{W/S}{a}$, where W/S is the wing loading and a is lift slope, gives a double benefit, both reducing the bump amplitudes and decreasing the total number of bumps. In contrast, assessments of ride-smoothing systems using either a normal-acceleration sensor or an incidence sensor in conjunction with direct-lift-control indicate that a reduction in the amplitude of the bumps is in general achieved at the expense of an increase in their total number. Subsequent work has been aimed at reducing bump amplitudes whilst constraining their rate of occurrence. Both open and closed-loop systems have been considered and the formulation of appropriate cost functions for control-system optimisation has been investigated.

1 INTRODUCTION

As the level of atmospheric turbulence increases, not only do the handling qualities of an aircraft deteriorate but the disturbances cause discomfort to the aircrew and make it harder for them to perform control and weapon aiming tasks. The low-altitude high-speed flight mission is particularly liable to give a rough ride both because there is usually a significant amount of turbulence at low altitudes, associated with shear in the earth's boundary layer (possibly aggravated by the proximity of rough terrain), and because the magnitude of fluctuations in normal g due to vertical turbulence is directly proportional to aircraft speed.

Various characteristics of aircraft motion which influence ride quality may be distinguished. One is 'ride-bumpiness', related subjectively to discrete fluctuations in acceleration normal to the flight path. Another is 'vibration', mainly due to the response of the flexible airframe structure in which distinct frequencies of oscillatory motion may perhaps be detectable subjectively at the resonances of the lower-order structural modes. A third aspect of ride quality is the possible tendency of aircraft motion to produce nausea or air-sickness. This may overlap to some extent with the ride-bumpiness and vibration characteristics already mentioned, but may also be influenced by relatively low frequency modes of aircraft motion (similar to the frequencies of motion which produce sea-sickness). In this paper we shall concentrate on the concept of ride-bumpiness and will, furthermore, consider only motion in an approximately vertical plane.

The contents of this paper may be summarised as follows. Section 2 briefly reviews available methods for the theoretical prediction of ride-bumpiness statistics and describes the gust modelling techniques used throughout the remainder of the paper. Section 3 summarises analytical results which allow the rapid evaluation of the effects of varying aircraft wing-loading, lift-slope and speed and also illustrates typical effects of longitudinal stability characteristics in terms of static margin and pitch damping. In section 4 the use of active control systems to improve ride-bumpiness characteristics is discussed and the structures of particular systems employing direct-lift-control (DLC) are outlined. Section 5 confirms the validity of the theoretical results in terms of computer simulations.

The emphasis in this paper upon ride quality associated with longitudinal aircraft response in no way implies that lateral ride characteristics are less significant as a source of discomfort. It is, rather, because longitudinal ride qualities prove more amenable to general conclusions which may be conveniently summarised in relatively simple analytical form. To a large degree, longitudinal ride qualities associated with the basic airframe are dominated by the influence of relatively few parameters, principally aircraft wing-loading and effective lift-slope. This is particularly convenient in the early stages of project assessment when aircraft weight, wing area, aspect ratio and sweep are among those parameters for which quantitative estimates are readily available. Lateral ride qualities, on the other hand, depend to a higher degree upon the stability characteristics of the aircraft and thus are less amenable to general conclusions applicable in the early stages of project assessment. On the other hand, they tend to be more amenable to subsequent improvement by the use of conventional techniques of aircraft autostabilisation.

An associated subject not discussed in this paper is the influence of pitching motion in turbulence on the stability of the aircraft as a weapons-platform. Whilst this aspect is closely related to 'ride-quality' we have taken the view that it is better treated as a separate topic. It should be noted, however, that the techniques (including the gust models) employed in this paper to investigate ride-bumpiness are equally applicable to the prediction of aircraft pitching response in turbulence.

2 THEORETICAL PREDICTION OF RIDE-BUMPINESS STATISTICS

Statistical measures of aircraft motion that have been traditionally regarded as relevant to ride-quality assessment may be separated into two distinct classes:

(i) measures based on probability distributions for the amplitude of acceleration response peaks;

(ii) measures based on frequency-dependent or power-spectral properties of response.

Measures of type (i) have in the past been expressed in terms of, for example, '½g bumps per minute' (see for instance Ref 1). This type of criterion has been applied in particular in the context of high-speed low-altitude flight of military aircraft and is largely dependent on aircraft rigid-body motion. To assess aircraft response in this form, the usual tool has been some form of discrete-gust turbulence model, traditionally of the 'derived-gust' type. However, we believe the 'statistical' discrete-gust technique[2,3] to be particularly appropriate in this context and using it we have presented in Ref 4 a framework for the assessment of aircraft longitudinal ride-bumpiness comprising a statistical model in which families of discrete gusts are used to represent patches of continuous turbulence. The turbulence model takes the form of an aggregate of discrete ramp gusts which for present purposes are considered either singly (Fig 1) or in pairs (Fig 2). Families of 'equiprobable' ramp gusts follow a law $v_m \sim H^{\frac{1}{3}}$ as illustrated in Fig 3. It should be noted that whilst this approach may be used to generate 'synthetic' turbulence time-histories for use, for instance, in ground-based simulators[5], in the present paper it is used simply as a basis for purely theoretical predictions. The theoretical analysis of aircraft response in the time plane involves a search over families of equiprobable gusts, including both isolated gusts and gust-pairs, for the 'tuned gust' or 'tuned gust pattern' which produces maximum response. The theoretical prediction for the rate-of-occurrence of bumps then takes the form[4]

$$n_y = \frac{\alpha}{\lambda \bar{H}} \exp\left\{-\frac{y}{\beta \bar{\gamma}}\right\} \qquad (1)$$

where n_y is the average number, per unit distance flown, of aircraft normal acceleration peaks greater than an arbitrary magnitude y

α, β are parameters which define the statistical properties of the patch of turbulence through which the aircraft is flying

$\bar{H}$ is the tuned gust length (critical gust length)

$\bar{\gamma}$ is the tuned response (response to tuned gust or critical gust pattern)

λ is the gust length sensitivity.

As described in Refs 3, 4 and 8, the tuned response $\bar{\gamma}$ may be associated either with a single isolated gust or with a gust-pair combination, depending upon the system characteristics. The precise condition is:

$$\bar{\gamma} = \max\begin{cases}\bar{\gamma}_1 \\ 0.85\bar{\gamma}_2\end{cases}$$

where $\bar{\gamma}_1$ and $\bar{\gamma}_2$ are respectively the maximum response to a single isolated ramp gust (Fig 1) and the maximum resonant response to a pair of gusts (Fig 2), where the individual component gusts are chosen from the same (equiprobable) family (Fig 3). It should be noted that (for linear systems) the principal of superposition allows the easy evaluation of $\bar{\gamma}_2$ in terms of the largest positive and largest negative (*ie* overswing) peaks in the system response to a single ramp gust.

It is usual for the search for the tuned gust or gust pattern to be made using a computer routine which evaluates the response to a single ramp gust for a range of values of gust length H. In some simple situations, however, where the aircraft response may be adequately approximated in terms of first or second order differential equations, general analytical results can be obtained. This is the procedure followed in Ref 4 where analytical results have been presented which are intended for use both in simple project assessments and as a basis for comparison with more detailed computer studies incorporating, for instance, dynamic equations for the response of active controls.

The statistical result given by equation (1) may be supplemented by the evaluation of the quantity

$$\bar{T} = \bar{H}/V \qquad (2)$$

which is strictly a measure of the time taken to traverse a tuned-gust gradient distance but may also be used as an approximation to the rise-time to peak amplitude of the associated response. Equivalently $\bar{T}$ may be regarded as an approximate measure of the 'duration' of the response peak. In particular, in the case of normal acceleration response, $\bar{T}$ may be used as a measure of the 'sharpness of the bump'.

Measures of type (ii), defined at the beginning of this section, based upon frequency-dependent or power-spectral properties of response, are being widely studied at the present time. For instance, the International Standard Organisation has been working for some time now on vibration criteria in the frequency range 0.1 to 1 Hz. However, nothing definite has emerged yet and there is also doubt as to

whether a general criterion as developed by ISO will be applicable in the extreme environment, for instance, of terrain-following flight. Possible developments along these lines include simple measures proposed for aircrew sensitivity as a function of frequency, and relatively sophisticated power spectral concepts in which a so-called 'rms of annoyance'[6], or 'crew task performance index'[7], is expressed as an integral, with respect to frequency, of the product of the spectral density of aircraft motion (acceleration) and a crew-sensitivity weighting function using equations closely analogous to those employed in aircraft structural analysis. The appropriate applications of measures of this type, however, which are largely based on human response to sinusoidal motions, arise in situations dominated by response of a highly oscillatory character. In qualitative terms the motion then takes the form of relatively continuous vibration rather than irregular sequences of individual bumps. We take the view that the use of data based on quasi-sinusoidal vibration to treat aircraft ride bumpiness in turbulence is a suspect procedure.

In the case of small combat aircraft, for which the high-speed low-altitude mission can be critically influenced by ride considerations, the rigid-body modes and structural response modes are often sufficiently separated with respect to frequency for measures of type (i), related to bumps, to be based mainly on rigid-body motion and measures of type (ii), related to vibration, to depend purely on structural flexibility.

It should be noted that the statistical characteristics of the discrete-gust model employed in Ref 4 and used to derive results presented in this paper are consistent with the energy distribution defined in standard forms of the power-spectrum turbulence model (von Karman spectrum). On this basis it is possible to employ co-ordinated discrete-gust and power-spectrum turbulence models, both related to a common turbulence reference intensity $\overline{\sigma}$ which acts as an overall measure of atmospheric disturbance and for which probabilities of exceedance are available based on overall global statistics (see Appendix B of Ref 4 and also Ref 8).

For the purpose of ride-quality assessment at low altitudes it is proposed in Ref 4 that nominal patch lengths of 5 miles (8 km) be assumed, an overall mission being regarded as a sequence of such patches with varying turbulence intensity from patch to patch. It must be emphasised that the assumption of 5 mile patch lengths is a simplified representation of the patchiness properties of real atmospheric turbulence. In fact, intense patches can sometimes be very short, describable as a burst or cluster of gusts. However, the nominal patchiness postulated is believed to be adequate as a basis for the comparison of the ride characteristics of differing aircraft configurations.

In terms of the assumption of 5 mile patch lengths, the statistical model proposed in Ref 4 takes the form

$$\left.\begin{aligned} \alpha &= 0.38 \quad \text{(dimensionless)} \\ \beta &= \begin{cases} 0.07\overline{\sigma} & \text{(ft/s units)} \\ 0.10\overline{\sigma} & \text{(m/s units)} \end{cases} \end{aligned}\right\} \qquad (3)$$

where α,β appear in equation (1) and $\overline{\sigma}$ is a turbulence reference intensity introduced in Ref 8. The relationship between $\overline{\sigma}$ and the rms intensity σ_i of a component of turbulence with scale length L is illustrated in terms of power spectra in Fig 4.

Turbulence intensity is often described qualitatively as light, severe, etc. Such terms may be approximately related to specific values of the reference intensity according to the following table

Grades of turbulence and reference intensities

Nominal grade of turbulence	Values of reference intensity $\overline{\sigma}$	
	m/s	ft/s
Light	0.9	3
Moderate	1.8	6
Severe	3.7	12

Further details on the use of $\overline{\sigma}$ as a reference intensity, providing a joint power-spectrum and discrete-gust model for turbulence, may be found in Refs 3 and 8.

3 RIDE-BUMPINESS IN HIGH-SPEED FLIGHT

3.1 Influence of wing-loading and lift-slope

The results presented in this section are based on approximate equations of motion which take account of aircraft translational motion but which neglect the influence of aircraft pitching motion. The results derived in Ref 4, for use in equations (1) and (2), are as follows

$$\left.\begin{aligned} \overline{H} &= \frac{1.6W/S}{\rho g a} \\ \lambda &= 0.15 \quad \text{(dimensionless)} \\ \overline{\gamma} &= 0.74V\left(\frac{2W/S}{\rho g a}\right)^{-2/3} . \end{aligned}\right\} \qquad (4)$$

In order to illustrate the effects of wing loading W/S and lift-slope a on exceedance frequencies equations (4) above have been used in conjunction with equation (1), where numerical values of α and β (which characterize the turbulence) are given by equations (3). Typical exceedance frequencies in units of bumps per minute (aggregate of positive and negative bumps) are presented in Figs 5 and 6 for a gust sensitive aircraft (W/S = 60 lb/ft^{-2}, a = 4.5) and a gust insensitive aircraft (W/S = 100 lb/ft^{-2}, a = 3.5), in both moderate and severe turbulence, at a Mach number M = 0.7 .

On the basis of results in the form of Figs 5 and 6, carpet plots have been derived to illustrate effects of wing-loading, lift-slope and Mach number on the rate of occurrence of ±g bumps in moderate (Fig 7) and severe (Fig 8) turbulence. The data in Figs 7 and 8 have been combined in Fig 9, where it can be seen that the rate of occurrence of ±g bumps, at low altitude, depends to quite a good approximation on the single parameter $M\sigma\left(\frac{W/S}{a}\right)^{-1}$.

As indicated in section 2, an additional quantitative measure of ride-bumpiness that may be derived on the basis of statistical discrete-gust theory is the rise-time to peak amplitude of a typical normal-acceleration fluctuation, or 'sharpness' (or hardness) of the bump. This measure is given by $\bar{T} = \bar{H}/V$, where $\bar{H}$ is the tuned gust length. Carpet plots showing the dependence of $\bar{T}$ on wing-loading, lift-slope and Mach number are presented in Fig 10 (this measure is independent of the turbulence intensity).

3.2 Influence of aircraft pitching motion

In this section we go on to illustrate the ways in which the predicted aircraft ride quality is modified, through the influence of aircraft pitching motion, when the aircraft longitudinal stability characteristics are taken explicitly into account. Whilst these characteristics are less likely to be known than wing-loading and lift-slope in the early stages of project assessment, they do tend to be easier to modify subsequently by the use of conventional autostabilisation techniques. In fact, as the results of this section refer to the idealised and somewhat unrealistic case of aircraft response with 'elevator fixed', they are not intended to be used as a means of improving the practical utility of the approximations made in section 3.1 but rather are to illustrate what would happen in the absence of any form of attitude control. They may thus be used as a datum for assessing the influence of various forms of control.

The aircraft pitching degree-of-freedom can influence smoothness of ride through several mechanisms:

(a) In the case of an isolated ramp gust, the peak value of normal acceleration may be either increased or decreased, depending on aircraft characteristics, owing to the competing effects of positive longitudinal stability and gust penetration (*ie* gradient of gust velocity between wing and tailplane).

(b) The influence of pitching motion in general changes the tuned gust length and the associated gust amplitude for a given equiprobable family of gusts.

(c) If the damping of the short-period mode of the aircraft is sufficiently low, amplification of fluctuations in normal acceleration can occur due to the combined resonant effect of sequential gusts.

(d) Angular acceleration influences the local normal acceleration in a manner that varies along the length of the aircraft, depending on the moment arm about the instantaneous centre of rotation.

(e) Human perception of angular motion has a direct effect upon assessment of ride smoothness.

In the following we concentrate upon the effects of aircraft stability on ride-bumpiness measured near the centre of gravity, and incorporate the influence of mechanisms (a) to (c) above. However, we draw attention in the following two paragraphs to contexts in which items related to (d) and (e) are of importance.

The influence of moment arm is most marked when ride quality, as measured by fluctuations in normal acceleration, is compared at two well separated stations along the length of the aircraft. This effect has been emphasised in recent years through incidents in which passengers sitting (or, worse, standing) near the rear of large transport aircraft have been injured through aircraft penetrations of relatively isolated gusts when the aircrew at the other end of the aircraft have not been aware of a disturbance of any great severity. For an adequate overall assessment of the ride qualities of such an aircraft it is clearly essential to evaluate the gust response over a range of longitudinal positions.

The direct effect of angular motion upon ride smoothness is probably considerably less than that of normal acceleration from the point of view of subjective assessment of crew and/or passengers. However, in the context of combat aircraft, where the quality of the aircraft as a platform for weapon release is of prime importance, the effects of gust-induced pitch disturbances on weapon accuracy are of major concern. In this paper we will not, however, discuss these wider aspects of gust response, concentrating on ride-bumpiness as it directly influences aircrew capability and efficiency.

The principal parameters influencing the aircraft longitudinal stability characteristics are static margin (depends on CG position) and damping in pitch (aerodynamic derivative - m_q). To illustrate the influence of these parameters, the discrete-gust response has been evaluated in Ref 4 for a particular numerical example corresponding to a small combat aircraft.

The effects of changing static margin (strictly the CG margin) by moving the CG position are illustrated in Fig 11 in terms of the influence on tuned gust length $\bar{H}$ and tuned response $\bar{\gamma}$. Fig 11a shows that the tuned gust length $\bar{H}$ decreases with increasing static margin (*ie* CG moving forward). Thus the bumps become sharper (equation (2)) with forward motion of the CG and the overall rate of occurrence of bumps increases (as can be seen from the influence of $\bar{H}$ in equation (1)).

Fig 11b shows that the overall effect of increasing static margin is to decrease the tuned response amplitude. This arises partly from the alleviating influence of pitch response which tends to reduce the total wing incidence and partly because of the reduction in tuned gust length and associated reduction in tuned gust amplitude (see Fig 3).

Fig 12 illustrates the analogous variations in $\bar{H}$ and $\bar{\gamma}$ for a range of values of the damping in pitch derivative $-m_q$. It can be seen that decreasing the pitch damping results in an increase in the normal acceleration response and also an increase in the tuned gust length, thus making the bumps both less sharp and less frequent.

4 RIDE-SMOOTHING SYSTEMS EMPLOYING DIRECT LIFT CONTROL

We turn now to the changes in aircraft ride-bumpiness characteristics that may be achieved by the use of active controls, specifically by the use of ride-smoothing systems employing direct-lift-control (DLC). The results presented are based on a study described in Ref 11.

The earlier results of this paper have confirmed the well-known fact that high wing loading and low lift-curve slope contribute to good longitudinal ride qualities. Typical results have been presented in Figs 5 and 6. However, the choice of such airframe characteristics generally has to be a compromise between the requirements for ride and the requirements for manoeuvrability. A possible course in this situation is to choose (low) values of wing loading and (high) values of lift slope primarily to achieve good manoeuvrability and to attempt to recover adequate ride qualities by means of a ride-smoothing system.

In the following, we discuss some possible control-system structures and compare the changes in ride characteristics that may be achieved in this manner with analogous improvements that would result from an increase of the airframe parameter $\left(\frac{W/S}{a}\right)$.

The type of gust-alleviation system considered in this paper is aimed to reduce ride-bumpiness associated with rigid-body response and the discussion is particularly relevant to relatively rigid aircraft. We shall not at all be concerned with the use of active control systems whose primary objective is to alleviate vibration associated with the response of the flexible structure. Such systems (variously referred to as modal suppression or mode-stabilisation systems) have been demonstrated, for example, on the XB-70 and B-52 aircraft[9,10].

We first discuss two types of closed-loop control:

System A - employs normal-acceleration feedback to a DLC motivator.

System B - employs incidence feedback to a DLC motivator.

In addition to the DLC loop, each system has a pitch stabilisation loop which employs pitch-rate feedback to an elevator or tailplane motivator.

The system representations in the following analysis, based on Ref 11, are idealised in the sense that, for example, a single first-order lag filter is used in some cases to represent the overall lag introduced into a loop by both sensors and motivators. In addition, idealised sensor positions are assumed; in particular, the incidence sensor is taken to measure the effective incidence of the wing. These simplifying assumptions are of course not intended for use in practical engineering design but are adequate to illustrate at least qualitatively some of the problems that arise in an assessment of the capabilities of ride-smoothing systems.

A simplified representation of System A is illustrated in Fig 13. Typical effects on aircraft stability of varying the gain B_h'' in the DLC loop are illustrated by means of a root locus plot in Fig 14. Three system poles exist, a complex conjugate pair (of which only one is illustrated) dependent only on the pitch stabilisation loop and the other, lying on the real axis, moving away from the origin as loop gain B_h'' is increased. Thus, with this idealised representation there are no stability limits associated with increasing amounts of acceleration feedback to the DLC motivator. On the other hand, if we employ a more realistic representation of the feedback loop, incorporating an additional second-order filter to represent actuator response, it can be seen from the root locus plot of Fig 15 that additional complex poles are introduced, corresponding to a higher-frequency mode. These poles move towards the imaginary axis with increasing loop gain; thus in practice there does exist a stability boundary on the usable amount of acceleration feedback, the boundary corresponding to a loss of damping in the (higher-frequency) control mode.

Having made the point that increases in the loop gain B_h'' are ultimately limited by a stability boundary, we revert to the simplified representation corresponding to Figs 13 and 14 for the remainder of this analysis. For this system, Fig 16 illustrates the effects of changing the feedback gain B_h'' on the rms values of various parameters including $\sigma_{h''}$ (normal acceleration), σ_q (pitch rate activity) and σ_δ (DLC motivator rate) calculated on a power-spectral basis. As B_h'' is increased the fluctuations in normal acceleration $\sigma_{h''}$ decrease at the expense of an increase in motivator activity σ_δ. On the other hand, the pitching activity σ_q remains relatively unaltered. Also illustrated is the rms of rate-of-change of acceleration $\sigma_{h'''}$ which increases with B_h''. The significance of this measure arises through the so-called 'zero crossing rate' given theoretically by

$$n_0 = \frac{\sigma_{h'''}}{\sigma_{h''}} \quad . \tag{5}$$

This quantity plays a role in power-spectral theory analogous to the quantity $\left(\frac{aV}{\lambda \bar{H}}\right)$ in statistical-discrete-gust theory, where V is aircraft speed and $\frac{a}{\lambda \bar{H}}$ is a factor appearing in equation (1). It represents an

overall measure of the total number of fluctuations in normal acceleration, or 'bumps'. A consequence of the increase in $\sigma_{\ddot{h}}$ with increasing $B_{\ddot{h}}$, illustrated in Fig 16, is that whilst the amplitude of the bumps (as measured by $\sigma_{\ddot{h}}$) is decreased the zero crossing-rate n_0, as defined by equation (5), is increased. An exactly analogous trend is predicted[11] using statistical discrete-gust theory where the effect of increasing $B_{\ddot{h}}$ is to decrease the predicted amplitude of the bumps as measured by $\bar{\gamma}$ but to increase their total number as measured by $\frac{a}{\lambda H} V$ (see equation (1)).

The above effects contrast with the analogous effects of increasing the airframe parameter $\frac{W/S}{a}$, where decreasing amplitude of bumps occurs in conjunction with a decrease in their total number (as reflected in Figs 5 and 6 for example). In qualitative terms, the contrast is illustrated in Fig 17. On this basis it thus appears that the improvements in ride quality obtainable using a closed-loop ride-smoothing system employing acceleration feedback are dissimilar in character from the improvements due to increasing $\frac{W/S}{a}$, for example by increasing wing sweep, with which pilots are familiar. This point is discussed in some detail in Ref 4 where the conclusion is drawn that further work on the human factors aspects is required in order to define a cost function for control-system design that properly reflects the 'quality of the ride'. Possible options that take into account both the amplitude and frequency of bumps are considered[4]. These aspects are discussed further in the following section on the basis of computer simulation studies.

Similar results are obtained[11] using System B which employs incidence feedback to a DLC motivator. Fig 18 illustrated the trends associated with increasing the incidence loop gain B_α, comparable with the results already discussed, Fig 16. It can be seen that the trends are qualitatively identical, decreases in bump amplitude as measured by $\sigma_{\ddot{h}}$ being accompanied by an increase in the overall bump rate n_0. However, one difference between Systems A and B is that, with incidence feedback, there exists a stability boundary with increasing gain even with only a simple first-order lag in the feedback loop.

In Ref 11 various attempts are described to design a ride-smoothing control system which qualitatively reproduces the improvements obtainable aerodynamically by increasing the parameter $\frac{W/S}{a}$, for instance by increasing the wing sweep (see Fig 17). To this end, cost functions have been formulated that penalise the increase in overall bump rate n_0, and the effects of alternative or additional feedback loops, for example with a lead-lag filter acting on $\dot{h}$ in the loop driving the DLC motivator, have been investigated[11]. On the whole these attempts have proved unsuccessful, although subsidiary benefits such as a reduction in motivator activity to achieve a given benefit have been demonstrated for such loops.

Moreover, it is shown in Ref 11 that replacing closed-loop control (as in Systems A and B discussed above) by open-loop control employing feedforward of measured vertical gust velocity to a DLC motivator may not in practice give much improvement. Results obtained for an idealised system in which vertical gust velocity measurements (obtained in practice by combining the output of an incidence sensor with the outputs of (integrated) pitch rate and normal acceleration sensors) are fed forward though a simple first-order lag (representing PCU and actuator lags) to a DLC motivator in fact closely resemble the results obtained with the closed-loop systems. Of course, a gust sensor mounted far enough forward (for example, on a long boom) could in theory provide sufficient lead to counteract the motivator and sensor lag effects, but the practical feasibility of such an idealised sensor position is open to doubt.

In all the above cases, the results of the theoretical studies reported in Ref 11 emphasise the importance of reducing lags in the sensor and motivator channels. The two principal limitations to the benefits theoretically obtainable by ride-smoothing systems are constraints on motivator activity (*ie* maximum amplitudes or rates) and constraints imposed by degradation of stability leading to oscillatory behaviour of a control loop. Both of these deficiencies may be reduced by decreasing the lags in PCUs and actuators.

There are, in practice, additional constraints that limit the practical benefits to be achieved using ride-smoothing systems. Overall performance assessments need to take account, for example, of penalties associated with motivator weights and of the effects of the system on structural loads. The latter can be quite large. In addition to increases in local loads such as those on a tailplane associated with cancellation of pitching moments introduced by the DLC motivator, wing torsion loads tend to be large due to the fact that whilst the incremental lift produced by the deflection of a DLC motivator acts so as to oppose the overall gust-induced lift, these two lift forces are generally located at differing chordwise positions on the wing. The out-of-balance moment thus has to be counter-balanced by the structure. These examples are, of course, simply two factors in the spectrum of benefits and costs that must be incorporated in an overall performance study.

5 COMPUTER SIMULATION STUDY

The results illustrated in this section refer to a particular case of System A, employing normal-acceleration feedback, as discussed in section 4 and illustrated in Fig 13. A digital computer simulation of the system has been used to produce response time histories corresponding to a turbulence input comprising a digitised sample of low-altitude (300 m) turbulence measured by NAE, Canada, using an instrumented T 33 aircraft. Short extracts from the response time histories are illustrated in Figs 19 to 21.

In the case described here the gain G_q in the pitch-stabilisation loop (Fig 13) was held constant and the gain $B_{\ddot{h}}$ in the DLC loop varied. Systems analysis in terms of statistical discrete-gust theory gave the results in the following table:

	$B_h^{\ddot{}}$					
	0	4	8	12	16	20
$\bar{\gamma}$	3.30	2.65	2.21	1.90	1.69	1.53
$\bar{H}$ (m)	112	104	99	87	71	51

The parameters $\bar{\gamma}$ and $\bar{H}$ are defined in section 2. The gust length sensitivity λ, also defined in section 2, has been found on the basis of previous studies to vary significantly less with changes in system characteristics than the other relevant terms and for the present study has been taken to be constant.

It follows theoretically from equation (1) that, if n_γ is found by counting the average number of peaks in response greater than level γ, then a plot of $\log \bar{H} n_\gamma$ against $\gamma/\bar{\gamma}$ should result in a straight line dependent only on α and β (λ has been assumed constant, as explained above) and hence invariant for any particular sample of turbulence. The results of this process are illustrated in Fig 22, where a value of the response has been counted as a peak whenever it exceeded (in modulus) the values of γ within a 'window' extending a distance equal to $\bar{H}/2$ on either side (the process of peak-counting by this and other means has been discussed in Appendix A of Ref 2).

It may be seen from the above table that the theoretical results for this particular study reflect the trends discussed earlier in this paper. With increasing loop gain $B_h^{\ddot{}}$ the tuned response $\bar{\gamma}$ (equivalent to $\sigma_h^{\ddot{}}$ in a power-spectral treatment) decreases but, for the larger gain values, at the expense of a decrease in $\bar{H}$ and thus an equivalent increase in both the sharpness of the bumps and their overall rate of occurrence (see equation (1)). The computer simulation results illustrated in Fig 22 confirm the theoretical trends in terms of the rate of occurrence of peaks counted. However, in order to obtain this good agreement between theory and numerical simulation, it was found necessary to refine the derivation of $\bar{H}$ outlined in previous prescriptions of the theory[2-4]. In contrast to cases previously investigated, the incorporation of the DLC loop tended to render the definition of $\bar{H}$, *ie* the length of the tuned gust, somewhat ambiguous in the sense that a plot of peak-response amplitude $\gamma(H)$ as a function of H resulted in a comparatively flat-topped curve sometimes containing weak local maxima. A satisfactory solution to this problem, used to obtain the results illustrated in Fig 22, was to define a 'global' maximum of $\gamma(H)$ to be the centre of area of the region enclosed by $\gamma(H)$ itself and a line at 90% $(\gamma(H))_{max}$, where $(\gamma(H))_{max}$ is the largest local maximum. The co-ordinates of this global maximum were then used to define $\bar{\gamma}$ and $\bar{H}$. Whilst this revised procedure had negligible influence on $\bar{\gamma}$, in some cases it had a substantial effect on $\bar{H}$. It should be noted that, in situations where such a procedure does have a strong influence on $\bar{H}$, the PSD method is likely to encounter analogous problems in the definition of n_0 (equation (5)). The difficulty is not so much mathematical as conceptual, as the number of peaks counted depends on the precise manner in which a peak is defined (as discussed in Appendix A of Ref 2). In the present context, we are concerned with counting not simply the number of mathematically-defined local maxima in the response but the number of those, referred to as 'bumps', which are associated with a perceivable energy fluctuation. The method outlined above appears to achieve this objective with some success.

However, the simulated time histories shown in Figs 19 and 20 show that the theoretical trends need to be interpreted with some care. The predicted decrease in bump amplitude with increasing $B_h^{\ddot{}}$ is clearly apparent. On the other hand, it may be seen that the theoretical increase in total bump rate, associated with a reduction in $\bar{H}$, is largely due to the removal of low-frequency components of the fluctuations whilst the higher-frequency content remains relatively unaltered.

For comparison, the effect on the response of the basic aircraft (Fig 19) of increasing the parameter $\frac{W/S}{a}$ by a factor of 2.14 is illustrated in Fig 21 (this factor corresponds to a change from $W/S = 60$ lb/ft^{-2}, $a = 4.5$ to $W/S = 100$ lb/ft^{-2}, $a = 3.5$, compare Figs 5 and 6). Comparing Figs 20 and 21 it may be seen that whilst superficially the trends are similar, the immediately apparent effect being the decrease in bump amplitudes as compared with Fig 19, the bumps are distinctly sharper edged in the case of Fig 20 which corresponds to the smaller value of $\bar{H}$. The influence of this phenomenon on the performance and subjective assessment of aircrew is an area requiring further study. However, its potential significance is underlined by the fact that cases have been reported where pilots have remarked on a 'cobblestone ride' in an aircraft with a ride-smoothing system. Moreover, the simulation illustrated in Figs 19 to 21 was based on rigid-body equations of motion. With structural flexibility included, particularly wing-bending, the relative sharpness of the bumps in the case of Fig 20 would probably be accentuated.

REFERENCES

1. G.F.H. Hemsley, Considerations of air turbulence in aircraft design. Proceedings of a Symposium 'Atmospheric Turbulence and its Relation to Aircraft', Farnborough 1961, Her Majesty's Stationery Office, 1963

2. J.G. Jones, Statistical discrete gust theory for aircraft loads. A progress report, RAE Technical Report 73167 (1973)

REFERENCES (concluded)

3. J.G. Jones, Influence of atmospheric gusts and turbulence on aircraft flying qualities at low altitudes. RAE Technical Memorandum FS 64 (1976) (Corrigendum Technical Memorandum FS 85)

4. J.G. Jones, Aircraft longitudinal ride-bumpiness: An application of statistical discrete gust theory. RAE Technical Report 77020 (1977)

5. B.N. Tomlinson, Developments in the simulation of atmospheric turbulence. AGARD CP 198 (1976)

6. J. Koo, Ride qualities of aircraft. National Aerospace Laboratory, Japan, TM 181, RAE Library Translation 1605 (1970)

7. J.W. Rustenburg, Development of tracking error frequency response functions and aircraft ride quality design criteria for vertical and lateral vibration. ASD-TR-70-18 (1971)

8. Joint Airworthiness Committee, Proposed revision for AvP 970, Vol 1, Part 6: Requirement for flying qualities of service aeroplanes. Appendix B to JAC Paper No 925 (1975)

9. J.H. Wykes, E.E. Kordes, Analytical design and flight tests of a modal suppression system on the XB-70 airplane. Aeroelastic effects from a flight mechanics standpoint, AGARD Conference Proceedings NO 46 (1970)

10. P.M. Burris, J.B. Dempster, R.P. Johannes, Flight testing structural performance of the LAMS flight control system. AIAA Paper No 68-244 (1968)

11. D.E. Fry, J.S. Winter, The design of aircraft ride smoothing systems using direct lift control. RAE Technical Report (unclassified report in preparation)

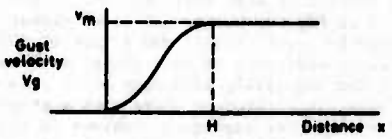

Fig 1 Smooth ramp gust

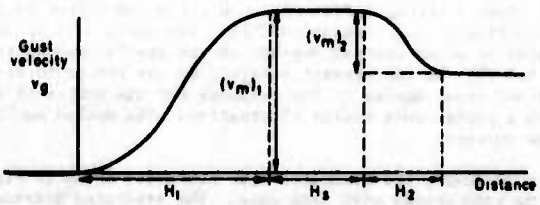

Fig 2 Pair of ramp gusts

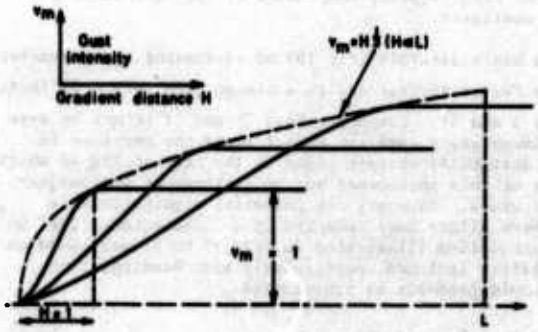

Fig 3 Family of equiprobable ramp gusts defined for H < L

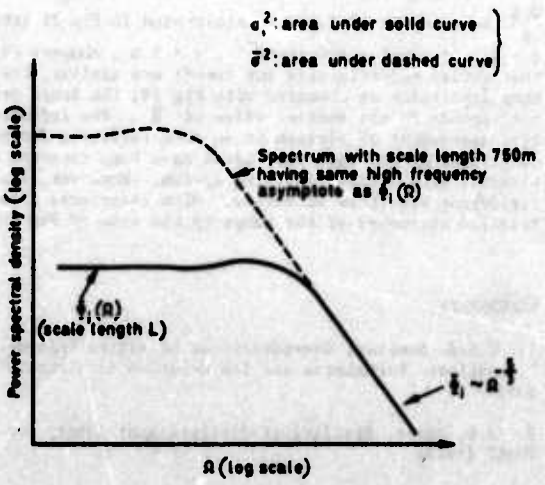

Fig 4 Relationship between σ_1 and $\bar{\sigma}$

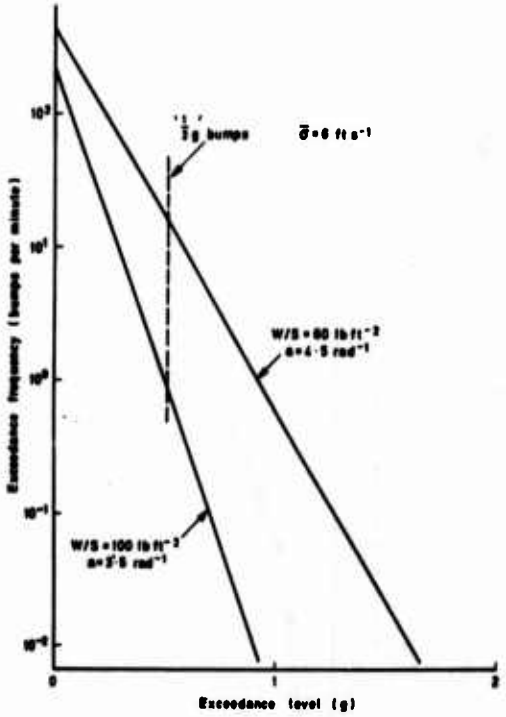

Fig 5 Influence of wing loading and lift slope on aggregate of positive and negative bumps in moderate turbulence at low altitude, M = 0.7

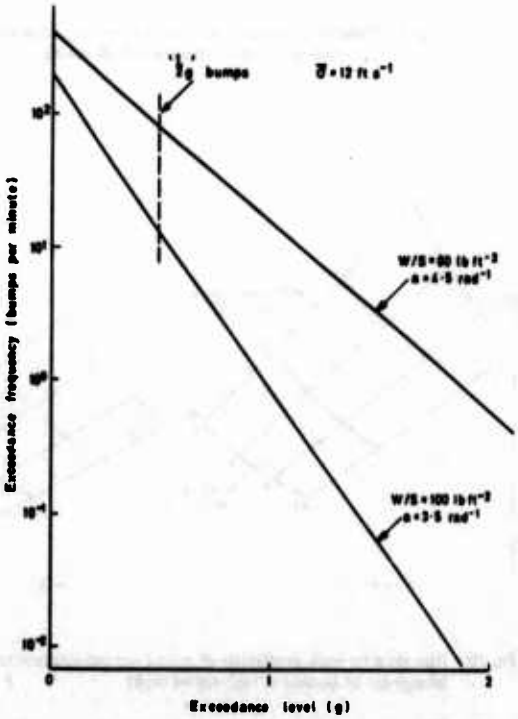

Fig 6 Influence of wing loading and lift slope on aggregate of positive and negative bumps in severe turbulence at low altitude, M = 0.7

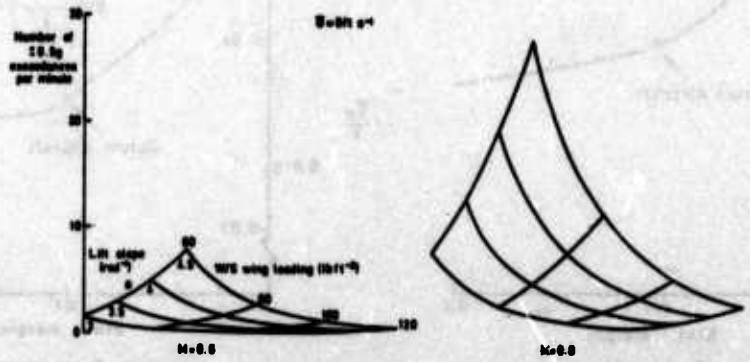

Fig 7 Rate of occurrence of bumps exceeding ±0.5 g in moderate turbulence at low altitude and high speeds

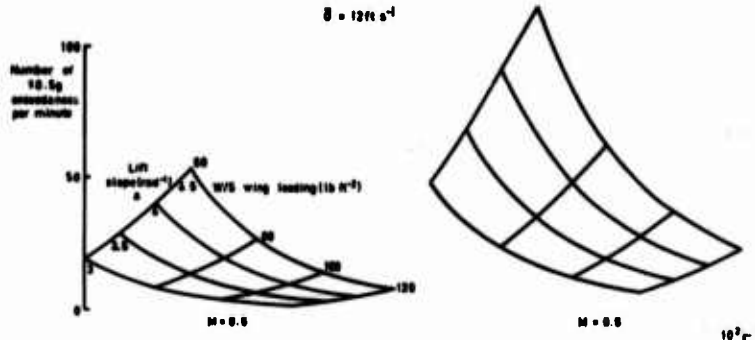

Fig 8 Rate of occurrence of bumps exceeding ±0.5 g in severe turbulence at low altitude and high speeds

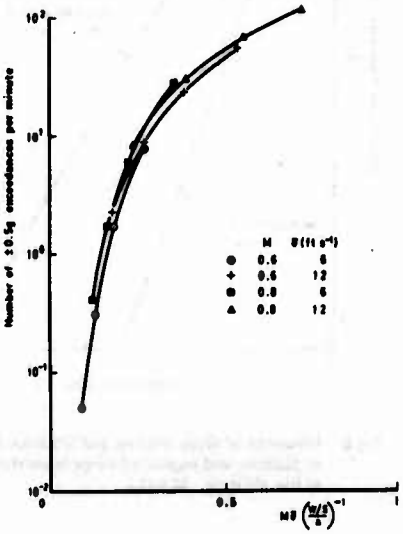

Fig 9 Approximate dependence of rate of occurrence of ±0.5 g bumps at low altitude on single parameter $M\sigma\left(\frac{W/S}{a}\right)^{-1}$

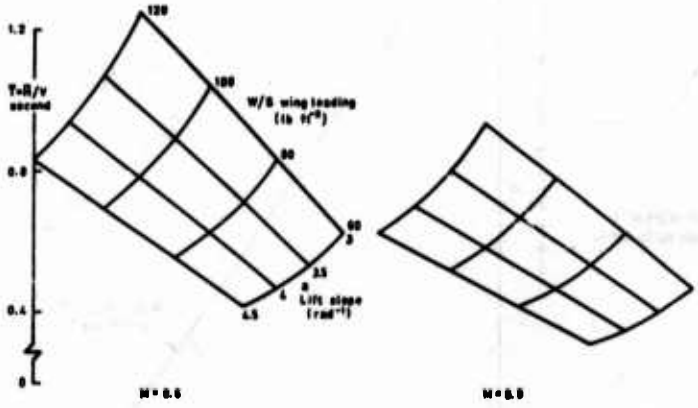

Fig 10 Rise time to peak amplitude of tuned normal-acceleration response (sharpness of bump) in high-speed flight

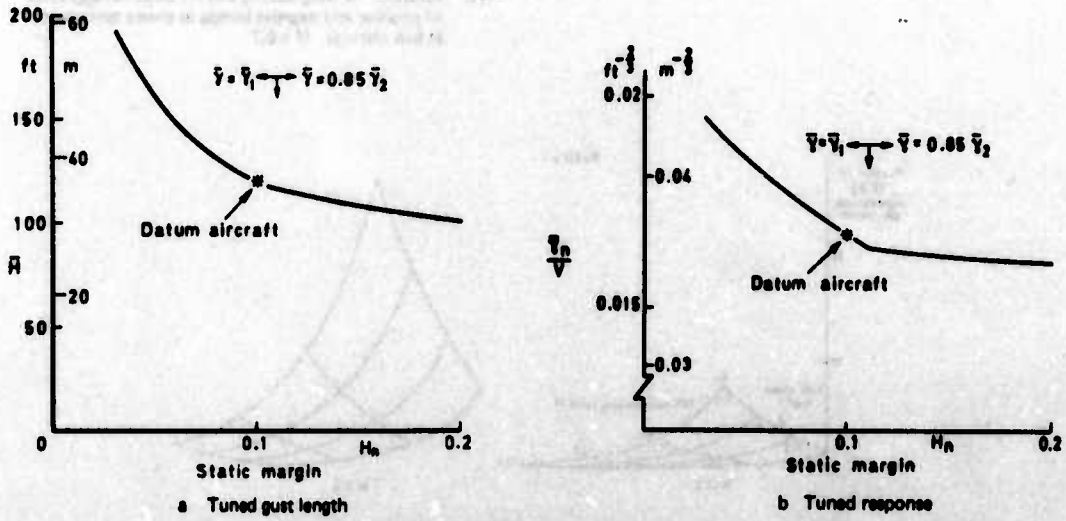

a Tuned gust length

b Tuned response

Fig 11a&b Example of effect of static margin on normal acceleration response

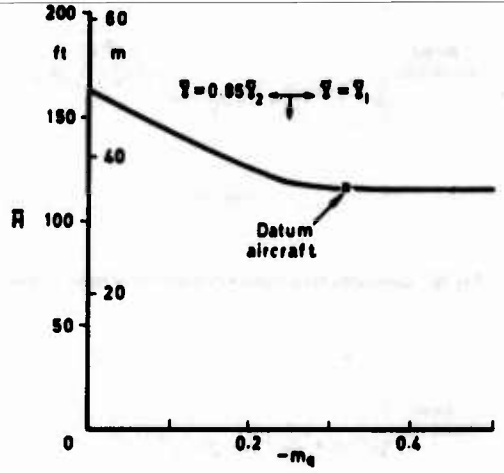

a Tuned gust length

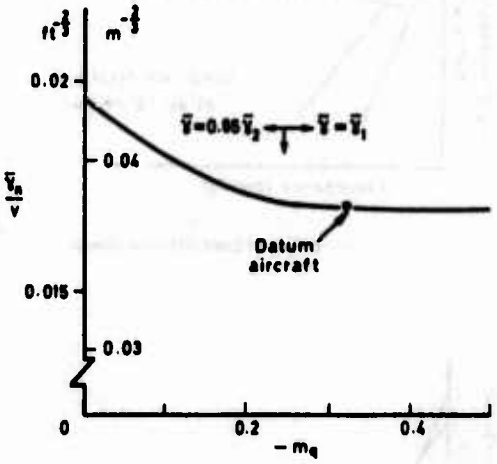

b Tuned response

Fig 12a&b Example of effect of damping in pitch on normal acceleration response

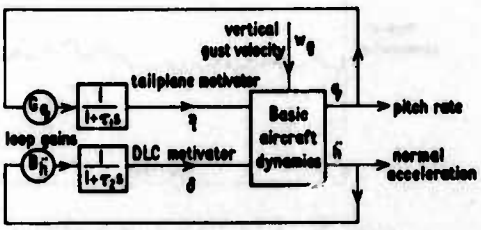

Fig 13 Closed-loop ride-smoothing system employing normal-acceleration feedback (System A)

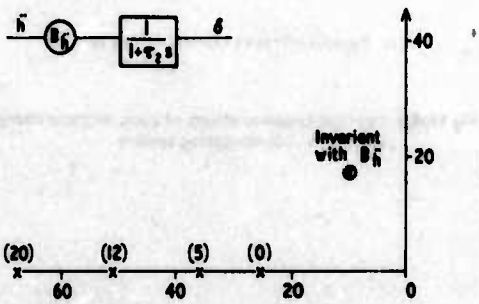

Fig 14 Root locus of $B_{\bar{n}}$ with simple lag

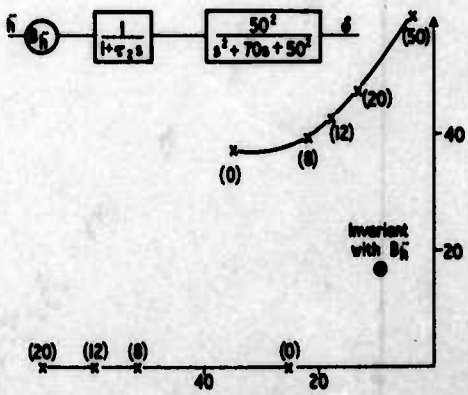

Fig 15 Root locus of $B_{\bar{n}}$ with simple lag plus second order actuator

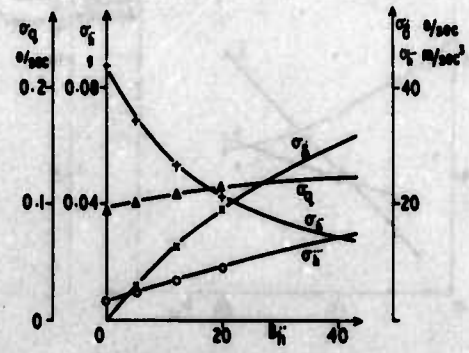

Fig 16 Effect of loop gain, System A

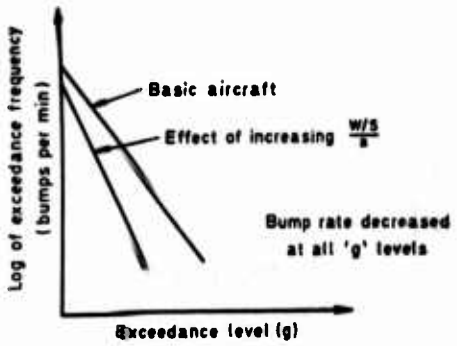

a Effect of basic airframe change

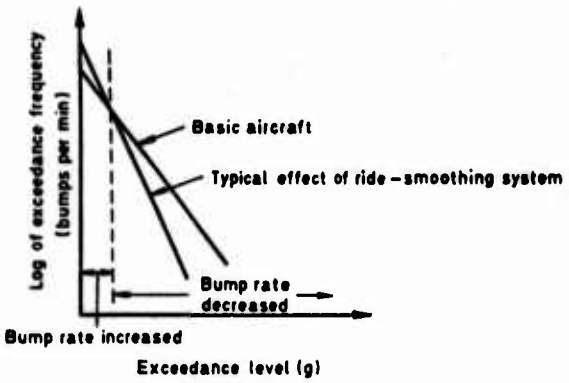

b Typical effect of ride-smoothing system

Fig 17a&b Contrast between effects of basic airframe changes and active ride-smoothing system

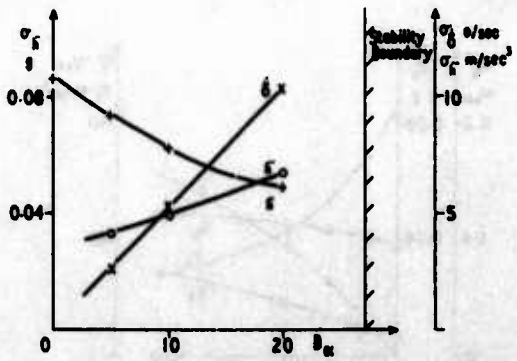

Fig 18 Effect of loop gain, System B

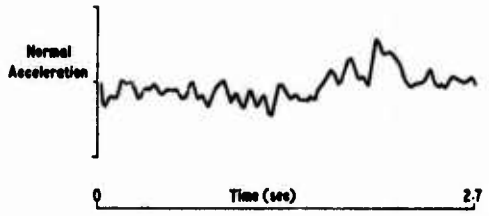

Fig 19 Simulated time history of response of basic aircraft

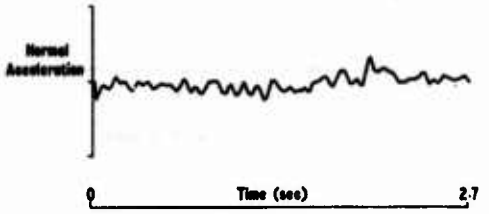

Fig 20 Simulated time history of response with ride smoothing system ($B_{\dot{h}}$ = 20)

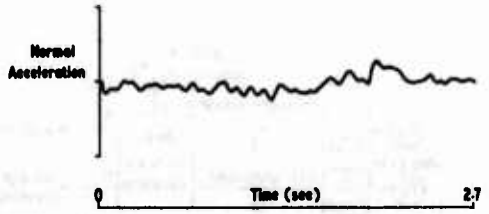

Fig 21 Simulated time history of response with $\frac{W/S}{a}$ increased by a factor of 2.14

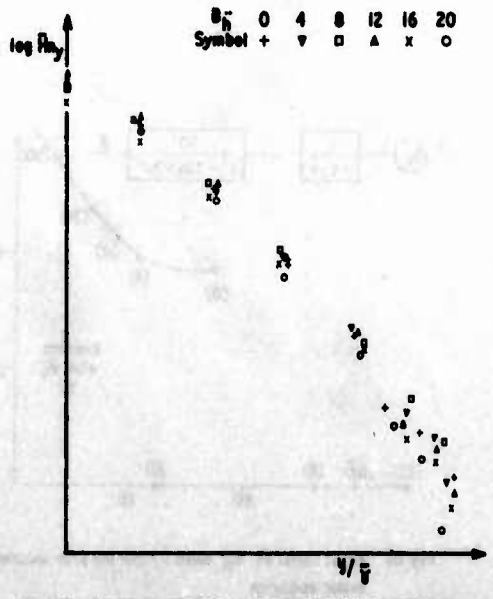

Fig 22 Normalised plots of acceleration count rate as functions of amplitude, for a range of loop gains

FLIGHT CONTROL SYSTEM DESIGN FOR

RIDE QUALITIES OF HIGHLY MANEUVERABLE FIGHTER AIRCRAFT

By

J. F. Moynes, J. T. Gallagher
Northrop Corporation
Aircraft Group
Hawthorne, California, 90250, U.S.A.

SUMMARY

A flight control system design is presented that utilizes a ride improvement mode system (RIMS) in conjunction with a control augmentation system to achieve desired ride smoothing for low altitude high speed flight conditions.

The Northrop Large Amplitude Flight Simulator and the Continuous System Modeling Program were used as the tools to analyze and evaluate ride qualities of a highly maneuverable fighter aircraft in low-altitude, high-speed flight conditions. Analysis included the effect of the first body bending mode on ride quality and pilot evaluations of the RIMS as flown on the Large Amplitude Flight Simulator.

It is demonstrated that significant improvement in ride quality on a low wing loaded multipurpose combat airplane could be achieved without adverse impact on the handling qualities.

SYMBOLS

$\bar{A}$	– Root mean square acceleration response, g's/fps
AR	– Aspect ratio
C^*	– Particular blend of aircrafts n_z, $\dot{\theta}$ and $\ddot{\theta}$ responses, developed by Boeing Corp. used for an indication of handling qualities[2]
C_{L_α}	– Lift curve slope, per radian
F_S	– Stick force, lbs.
G(s)	– Gaussian input
K_g	– w-gust scale factor
K_H	– First body bending mode input scale factor for horizontal tail
K_T	– First body bending mode input scale factor for trailing edge
K_w	– First body bending mode input scale factor for w-gust
K_1	– Aerodynamic parameter used to determine C_{L_α} (Ref. 18)
L	– Scale of atmospheric turbulence, ft.
S	– Wing surface area, $ft.^2$
$T_{AF}(\Omega)$	– Transmissibility of airframe at pilot station, g's/fps
$W(\Omega)$	– Acceleration weighting function, 1/g
b	– Wing span, ft.
g	– Acceleration of gravity, 1 g = 32.2 ft/sec^2
ℓ_p	– Distance of pilot's station ahead of center of gravity, ft.
n_z	– Vertical load factor of aircraft, n_z = 1 for level flight, g's
n_{zc}	– LAS computed vertical load factor at the pilot station, g's
n_{zs}	– Vertical load factor measured in the LAS pilot station, g's
n_{zp}	– Vertical load factor measured at the pilot station, g's
n_{zp_1}	– Vertical load factor at pilot station due to first body bending mode, g's
$n_{zp_{1H}}$	– First body bending mode vertical load factor due to horizontal tail, g's
$n_{zp_{1T}}$	– First body bending mode vertical load factor due to trailing edge, g's
$n_{zp_{1w}}$	– First body bending mode vertical load factor due to w-gust, g's
q	– Pitch rate, degrees/sec
q_{gust}	– Pitching gust velocity, degrees/sec
s	– Laplace operator
V_{gust}	– Side gust velocity, ft/sec
W_{gust}	– Vertical gust velocity, ft/sec
θ	– Pitch attitude, radians
Λ_{LE}	– Leading edge sweep
$\Phi(\Omega)$	– Gust power spectral density
Ω	– Frequency, Hz
Ω_c	– Cutoff frequency (beyond which aeroelastic responses are of no significance in turbulence)
α	– Angle of attack, degrees
δ_H	– Horizontal tail surface position, degrees

δ_{TE} – Trailing edge surface position, degrees

ζ_1 – Damping coefficient of first body bending mode

ρ – Density of air, slugs/ft.^{3}

σ_w – RMS turbulence level, fps

ω_{n1} – Natural frequency of first body bending mode

$\sqrt{\frac{I(k,s)}{\pi}}$ – Gust response factor

FLIGHT CONTROL SYSTEM DESIGN FOR RIDE QUALITIES OF HIGHLY MANEUVERABLE FIGHTER AIRCRAFT

by

J. F. Moynes, J. T. Gallagher

Northrop Corporation, Aircraft Group

INTRODUCTION

In the design of multi-purpose military aircraft the conflict of design features is nowhere more obvious than in the airplane characteristics necessary for excellent air combat capability and those necessary for low altitude high speed (LAHS) penetration. The low wing loading which maximizes turn rate capability essential for survival in air combat also potentially deteriorates the ride quality during high speed penetration, which can lead to reduced mission success in attacking heavily defended ground targets.

Fortunately the application of modern active control technology makes possible achievement of excellent ride qualities without measurable impact on the agility of modern multi-purpose aircraft. In fact, as indicated in Ref. 1, the application of active control technology to ride quality enhancement is the least risk application of the technology. Perhaps this results from the extended time period that such activity has interested the aeronautical engineer. As early as 1937, a French scientist (Ref. 2) had determined that the response of an airplane to turbulence could be controlled by simple control techniques. Shortly after this, NACA researchers demonstrated in the tunnels at Langley (Ref. 3) that a simple overbalanced flap could be employed to reduce the response to turbulence of a low wing loaded aircraft. It was possible in these tests to achieve a forty percent reduction in loadfactor response to turbulence.

Research in the United Kingdom in the mid 1950's (Ref. 4) on the Lancaster and in support of the development of the Brabazon aircraft confirmed the potential for ride quality improvement, and if we are to believe the folklore of Ref. 5 this was possible from a pilot's point of view in spite of improper mechanization of the control system. Quoting from Ref. 5:

> "So they tried to develop a gust alleviation system employing a vane sensor on the pitot boom projecting from the aircraft's nose that would sense gusts and then signal to the ailerons to deflect very rapidly up or down to counteract the gust. Would this have worked? Well, there is a lovely story of a test system being installed in a Lancaster; it is said that the Lancaster pilot tried it out during the delivery flight to Bristol, and reported to Bill Pegg that it seemed really to do the trick, and give a smooth ride. Only later did they find the system was hooked up backwards, making gusts worse rather than lighter!"

Perhaps the most lucid explanation and identification of the challenges of ride quality enhancement is contained in the work of Phillips of NACA in Ref. 6. Here the potential for using angle of attack or acceleration sensing and wing flap motion to reduce the response of aircraft to wind gusts was explored in great detail. This was followed by continuing research at NACA and NASA involving the techniques of stochastic analysis, optimal control, and flight test (Ref. 7 through 10) to demonstrate that theoretical reductions of up to 90 percent in the loadfactor response to gusts were possible on low wing loaded transport aircraft.

In Reference 11, Notess had quantified the influence of loadfactor response to wind gusts on the ability of pilots to perform mission tasks, in essentially rigid aircraft during low altitude high speed flight. Extensive testing under simulated flight conditions further extended the understanding of the impact of gust response on crew performance (Ref. 12) to large supersonic flexible military aircraft in prolonged low altitude flight.

Later, NASA and Boeing Company research refocused on the reduction of gust response to improve the ride comfort of passengers in low wing loaded STOL transport aircraft (Ref. 13). Complementing this work, the potential for applying the techniques of modern control practices to the design of ride quality enhancement was thoroughly explored in Reference 14, where it was demonstrated that significant improvement in ride qualities was possible without measurable impact on flying qualities.

The culmination of this research spanning almost 40 years was the incorporation of design requirements in MIL-F-9490D (Ref. 15) for those systems used to improve the ride qualities of military aircraft. It was against this background that Northrop conducted research employing the Northrop Large Amplitude Flight Simulator (LAS) to confirm that significant improvement in ride quality was possible on a highly maneuverable air combat fighter without compromising the flying qualities essential to air combat effectiveness.

$\bar{A}$, AN INDICATOR OF RIDE QUALITY

In this study the root mean square acceleration response, $\bar{A}$, was used as an indicator of longitudinal ride quality where $\bar{A}$ is the rms loadfactor at the pilot station divided by the rms gust level (fps) as defined in Equation 1.

$$\bar{A} = \left[\frac{\int_0^{\Omega_0} |T_{AF}(\Omega)|^2 \Phi(\Omega) d\Omega}{\int_0^{\infty} \Phi(\Omega) d\Omega} \right]^{1/2} \qquad \text{Eq. 1}$$

$\bar{A}$, rather than the discomfort index as outlined in MIL-F-9490D, was used because it permits direct correlation with various forms of analysis including comparison with simulator results and from previous experience it was considered a good indicator of ride smoothing.

For analytical purposes Equation 2, which is derived from Equation 1 (Refs. 16 and 17), can be used to represent $\bar{A}$ of the rigid body.

$$\bar{A} = \frac{\rho V S C_{L_\alpha}}{2W} \sqrt{\frac{I(k,s)}{\pi}} \qquad \text{Eq. 2}$$

In this derivation, the gust response factor, $\sqrt{\frac{I(k,s)}{\pi}}$, represents a partial fraction expansion of the integrals contained in Equation 1.

Effect of C_{L_α} and W/S on $\bar{A}$

As Equation 2 indicates, the dominant factors determining the level of $\bar{A}$ at a given flight condition are the wing loading, W/S, and the lift curve slope, C_{L_α}. The lift curve slope is strongly influenced by the aspect ratio, AR, and leading edge sweep, Λ_{LE}, as indicated by Equation 3, Ref. 18.

$$C_{L_\alpha} = \frac{2\pi\ AR}{2 + \sqrt{K_1 AR \left(1 + \frac{\tan^2 \Lambda_{LE}}{\sqrt{1 - MACH^2}}\right) + 4}} \qquad \text{Eq. 3}$$

Figure 1 summarizes the influence of aspect ratio, wing loading and wing sweep on $\bar{A}$. As an example, a fighter aircraft with a configuration similar to the aircraft shown in Figure 2 would yield an $\bar{A}$ of 0.080 at a low altitude high speed flight condition of Mach No. 0.9 at 500 feet. For an rms gust level of 6.7 fps the vertical load factor would be 0.54 g's. As shown in Figure 3, the load factor response exceeds the tolerable level boundary suggested by Reference 11.

The ride quality is further aggravated by the influence of the structural mode response to gusts. Typical of fighter aircraft gust response are the data shown in Figure 4. These data were obtained from flight test on the Northrop F-5 and show the contribution of the first body bending mode to the overall power spectral density of the gust response at the pilot station.

To achieve an acceptable ride quality level, these modal responses to gusts must be minimized, particularly at the short period frequency. With a given aircraft design, suppression of these responses can be achieved only through active control techniques.

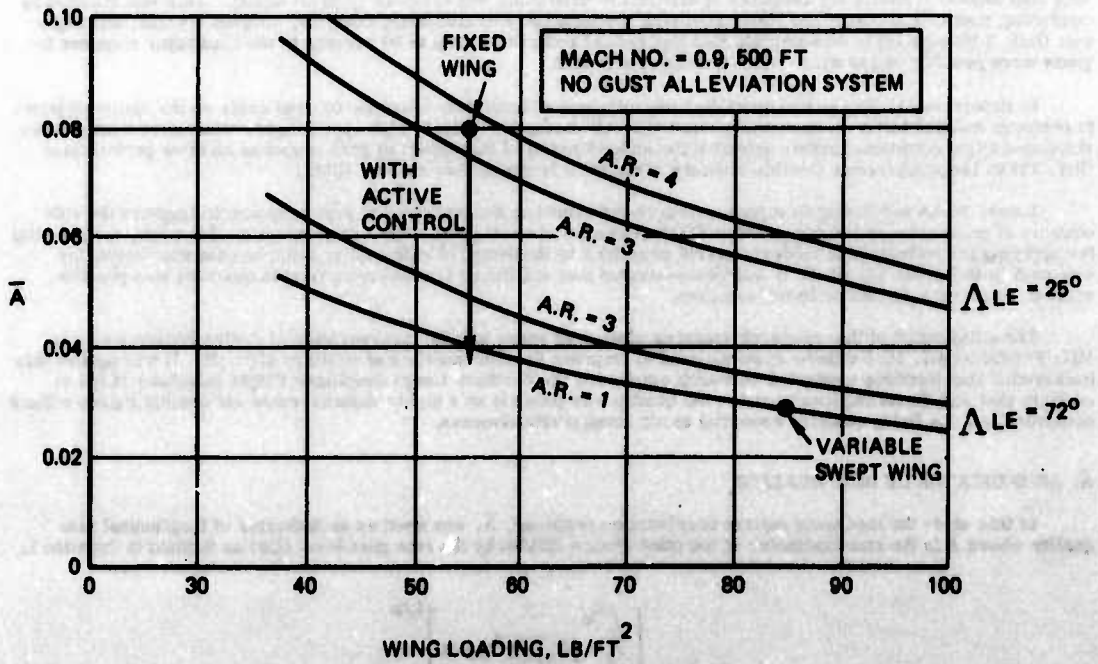

FIGURE 1. EFFECT OF AIRCRAFT PARAMETERS ON $\bar{A}$

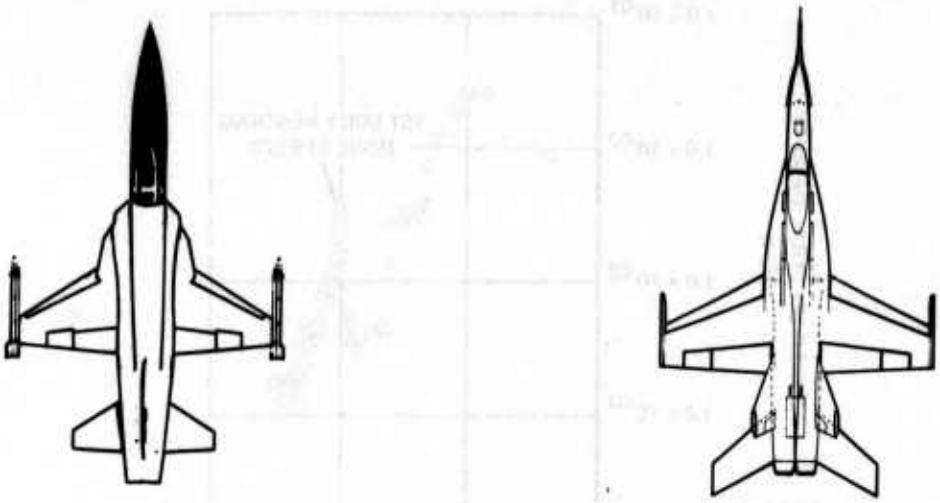

FIGURE 2. EXAMPLE OF HIGHLY MANEUVERABLE FIGHTER AIRCRAFT

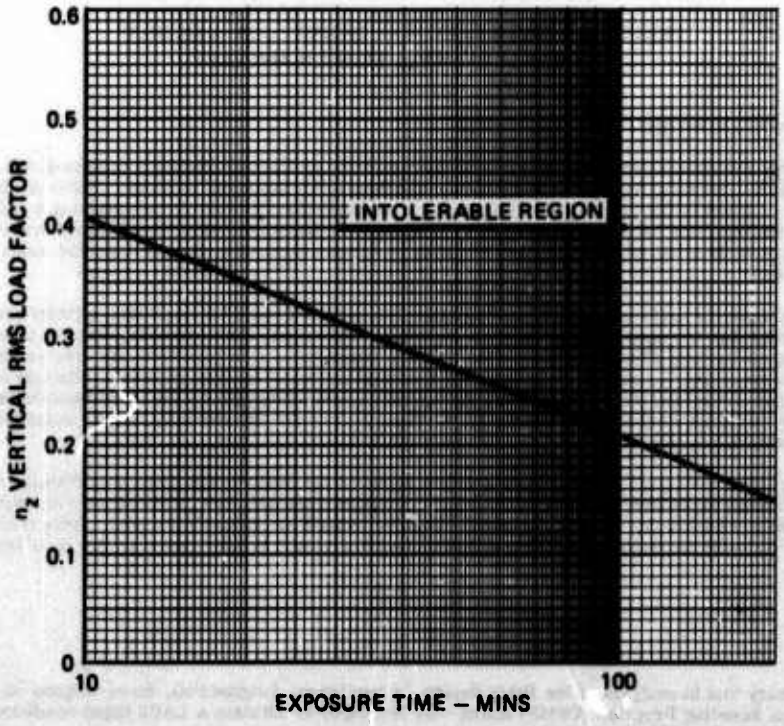

FIGURE 3. RIDE QUALITY CRITERIA

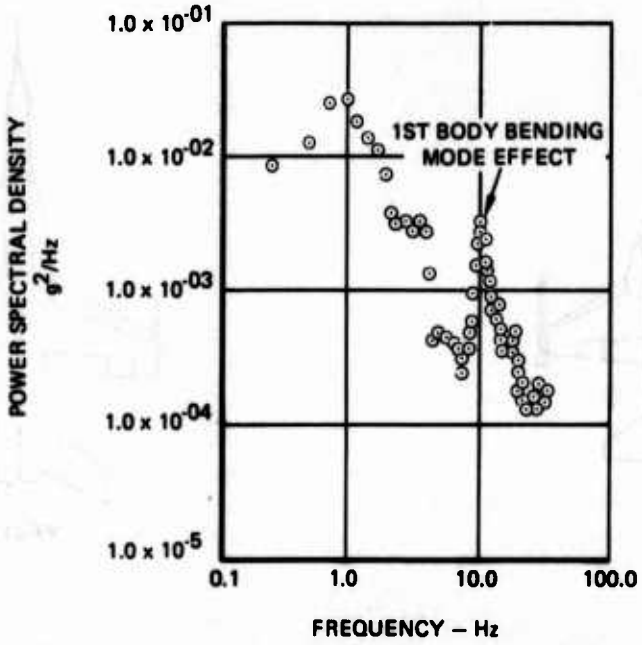

FIGURE 4. POWER SPECTRAL DENSITY FOR A HIGHLY MANEUVERABLE FIGHTER AIRCRAFT

APPROACH TO RIDE SMOOTHING

Given a highly maneuverable fighter aircraft with an existing control augmentation system (CAS), the design approach was to utilize the wing flap surfaces to reduce the load factor response to gusts. These surfaces were to act to minimize variations in the total C_L for changes in α due to vertical gusts. By maintaining a relatively constant C_L in a gust environment, the lift curve slope C_{L_α} is effectively reduced, resulting in a proportionate decrease in $\bar{A}$. As a result, the use of these surfaces minimizes the energy that is contained in the short period mode response of the aircraft to gusts.

Preliminary analysis revealed that the leading edge flap surfaces would be much less effective in lowering C_{L_α} than the trailing edge flap surfaces as illustrated in Figure 5. Therefore, after verifying that the trailing edge flap surfaces had adequate surface effectiveness as well as hinge moment and rate capability for ride smoothing, their implementation as the active control surfaces for ride qualities improvement was pursued. The use of the trailing edge for ride quality control did not interfere with the normal maneuvering flap control function because at the high dynamic pressure and Mach number typifying the LAHS flight regime the flap surfaces, under maneuvering flap control, assume a fixed position.

The measuring of alpha gust for use as the control signal to the trailing edge flaps was dismissed because of the possibility of erroneous signals and associated stability problems. Instead, a dedicated accelerometer at the pilot station was chosen to measure the load factor which would be fedback as the control signal. This control loop of the pilot station load factor to the trailing edge flap surface position, Figure 6, was named as the Ride Improvement Mode System (RIMS).

DESIGN TOOLS

CSMP Model

As the primary tool in analysis of the RIMS design, a non-linear, longitudinal, three-degree-of-freedom Continuous System Modeling Program (CSMP) model was developed to simulate a LAHS flight condition in which the performance of the RIMS could be evaluated.

The program incorporated non-linear, rigid body aerodynamics with corrected aeroelastic terms and downwash effects. Four LAHS flight conditions were used initially for analysis; this was later reduced to just one condition, Mach 0.9 at an altitude of 500 feet, since this condition was determined to be the worst case for ride quality control. Analysis had shown that ride quality was at its worst just below supersonic flight, because of the reduction of effective C_{L_α} above Mach 1.0 due to aeroelastic and compressibility effects.

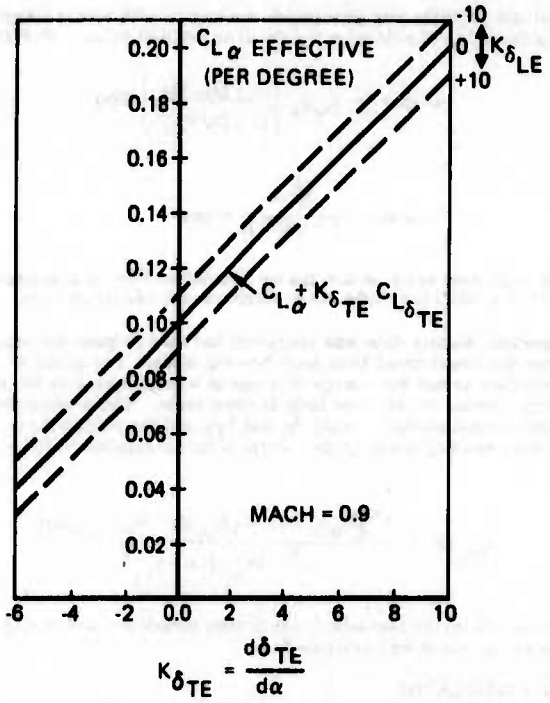

FIGURE 5. EFFECTIVE CL_α AS A FUNCTION OF LEADING AND TRAILING EDGE SURFACES

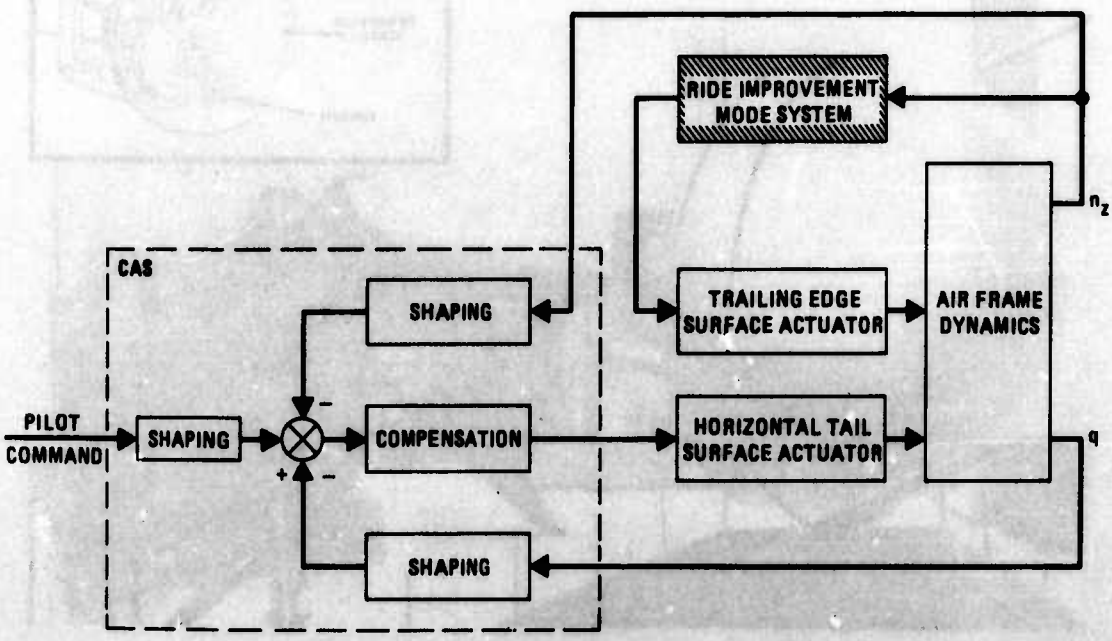

FIGURE 6. LONGITUDINAL CONTROL SYSTEM CONCEPT

The gust turbulence for the analysis was generated as a w-gust with a correlated q-gust, from a Dryden filter model (Equation 4) that had a Gaussian distribution for input as outlined in MIL-F-8785B.

$$\text{w-gust} = K_w \sigma_w \left[\frac{1 + (3L/V)s}{(1 + (L/V)s)^2} \right] G(s) \qquad 4a$$

Eq. 4

$$\text{q-gust} = \frac{\frac{1}{V}s}{1 + (4b/V)s} \text{ w gust} \qquad 4b$$

The w-gust level was scaled to an rms value of 6.6 fps as determined from a gust probability of exceedance of 10^{-2} at 500 feet as set forth in MIL-F-9490D for flight phase duration of 0.5 hour or less.

Acceleration power spectral density data was computed and used to generate equations for the pilot station load factor that resulted from the longitudinal first body bending mode. The effect of the first body bending mode was included to determine whether or not the energy that was to be suppressed in the short period mode would result in an increase of energy content in the first body bending mode. There were three inputs which excited the first body bending mode: The control surface inputs δ_H and δ_{TE} and the w-gust term. The pilot load factor due to the contribution of the first body bending mode is then equal to the summation of the effect of these three inputs represented by:

$$n_{zp_1}(s) = \frac{s^2 \left[K_H \delta_H(s) + K_T \delta_{TE}(s) + K_w w_{gust}(s) \right]}{s^2 + 2w_{n_1} \zeta_1 s + w_{n_1}^2} \qquad \text{Eq. 5}$$

The CSMP model was set up to run for 50 seconds of continuous turbulence and during this time w-gust and n_{zp} were sampled. At the completion of the run $\bar{A}$ was computed.

LARGE AMPLITUDE FLIGHT SIMULATOR

In conjunction with the CSMP analysis, the Northrop Large Amplitude Flight Simulator/Wide Angle Visual System (LAS/WAVS or LAS), Figure 7, was employed to obtain pilot evaluations and data for analysis of the flight control system design. The Large Amplitude Flight Simulator provides the opportunity to verify the CSMP results and to obtain pilot comments pertaining to ride qualities of the CAS/RIMS configurations.

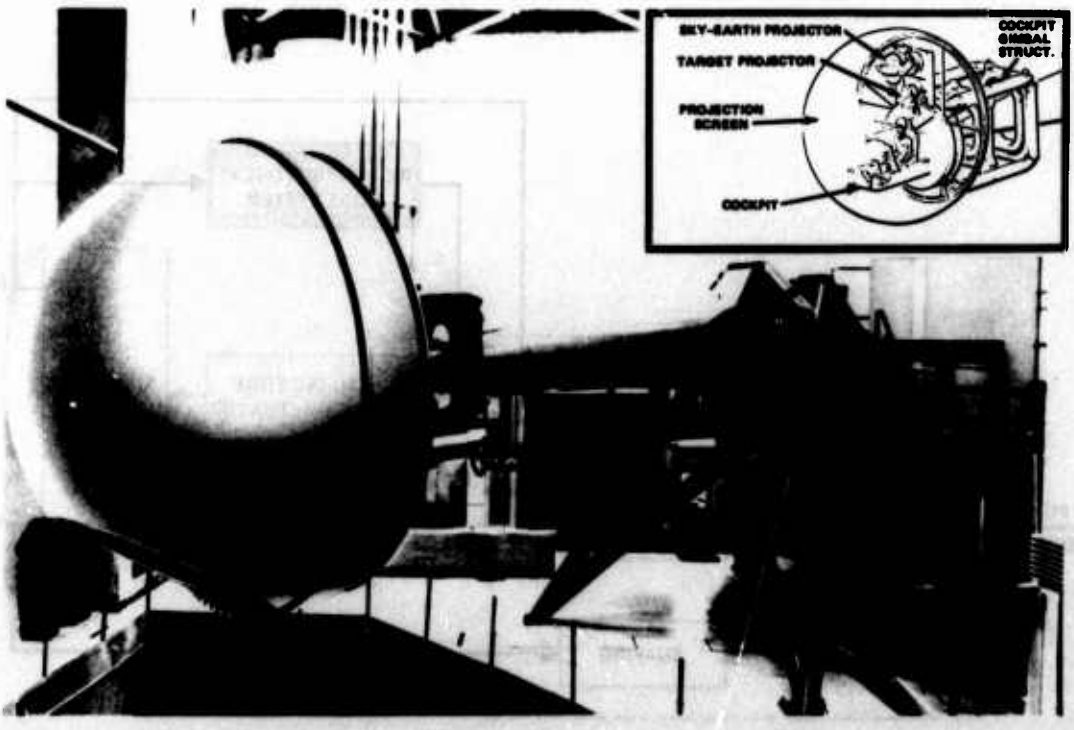

FIGURE 7. LARGE AMPLITUDE FLIGHT SIMULATOR/WIDE ANGLE VISUAL SYSTEM

The model utilized on the LAS included the effect of the first body bending mode on pilot station load factor as incorporated in the CSMP model. The LAS model, however, was a six-degree-of-freedom model rather than three and, in addition to w-gust, there was a Dryden v-gust model with an rms value of 6.6 fps. The simulator gust model also had a provision in it so that as the aircraft got closer to ground level the gust levels became more intense. Aside from these differences and some differences in sampling and integration techniques, the models were the same.

To utilize the LAS for the study of ride qualities, some modifications had to be made to the usual simulation system arrangement. These modifications concerned the vertical drive of the beam. Due to the filtering of the signals to the vertical beam drive, it was not possible to see the effect of the first body bending mode using the normal motion system interface. There were three separate signals which comprised the pilot load factor resulting from the first body bending mode, each signal representing one of the inputs which excited the first body bending mode. These bending mode signals were summed with the normal vertical beam drive signal downstream of the normal motion system interface through implementation of a special motion system interface as depicted in Figure 8.

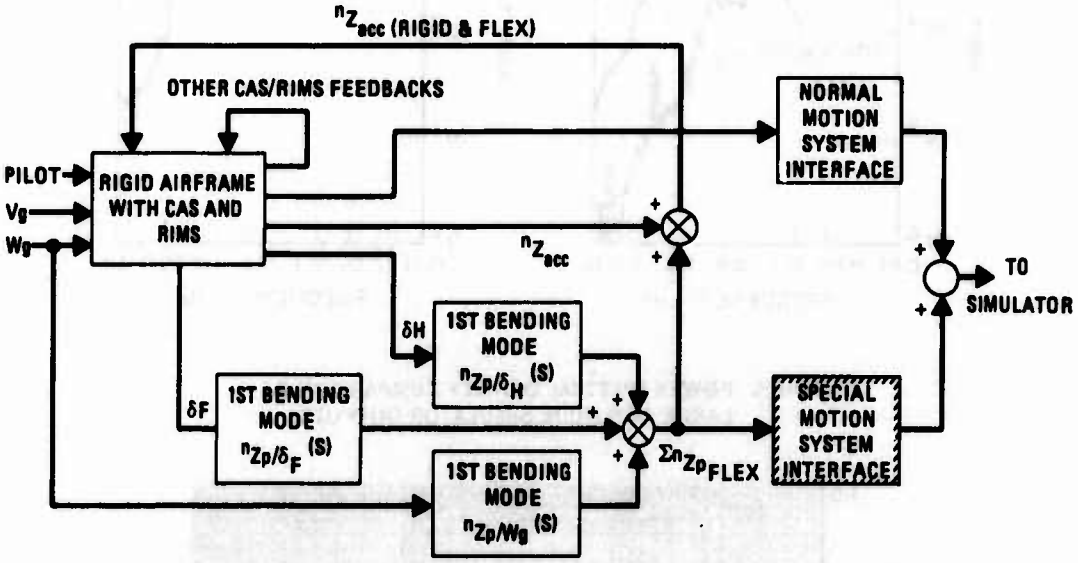

FIGURE 8. RIDE QUALITIES SIMULATION BLOCK DIAGRAM

To prevent the vertical beam drive from encountering its mechanical stops there is an adjustable gain on the vertical beam drive that results in a reduced level of normal acceleration at the pilot station. Thus the Large Amplitude Flight Simulator has two pilot station load factors, where one is the computed load factor, n_{zc}, that is used in computation and the other is the actual load factor, n_{zs}, that is measured by an accelerometer at the pilot station. The power spectral density plots in Figure 9, show the typical differences in n_{zc} and n_{zs} for flying quality and riding quality configurations. For this study the gain was made higher than normal in order to increase the gust response for more relevant pilot evaluation of ride qualities. A comparison of the computed versus simulated load factor is shown for a RIMS off condition in Figure 10. Although Figure 10 looks more like the flying quality plot than the ride quality plot in Figure 9, inspection will indicate that its levels of acceleration are considerably higher than for either of the plots in Figure 9. The ratio between n_{zc} and n_{zs} in Figure 10 is also considerably less than the ratio shown for n_{zc} and n_{zs} in the flying quality plot of Figure 9.

In Figure 11 the acceleration power spectral density for the Large Amplitude Flight Simulator pilot station is compared with those for an F-4C obtained in a study on crew exposure to vibration during LAHS flight (Reference 19). The similarity of the results for identical flight conditions shows the realism of the Large Amplitude Flight Simulator Model in simulating ride qualities for a fighter aircraft.

RIDE QUALITY RESULTS

$\bar{A}$ Comparisons

The fighter design in this study had a wing loading, W/S, of 57.5 lbs/ft^2 and aC_{L_α} of 0.115 per degree for Mach 0.9 at 500 feet, typical of a low sweep, fixed geometry moderate aspect ratio wing. Through the application of equation 2 these parameters and those for three other flight conditions were used to calculate an analytic value of $\bar{A}$ for each of the four flight conditions. The analytic $\bar{A}$ values were used to check the validity of the rigid body CSMP model with no ride improvement mode system. A study of the CSMP and analytic results in Table 1 shows a good level of agreement for the calculated values of $\bar{A}$, particularly for the subsonic condition.

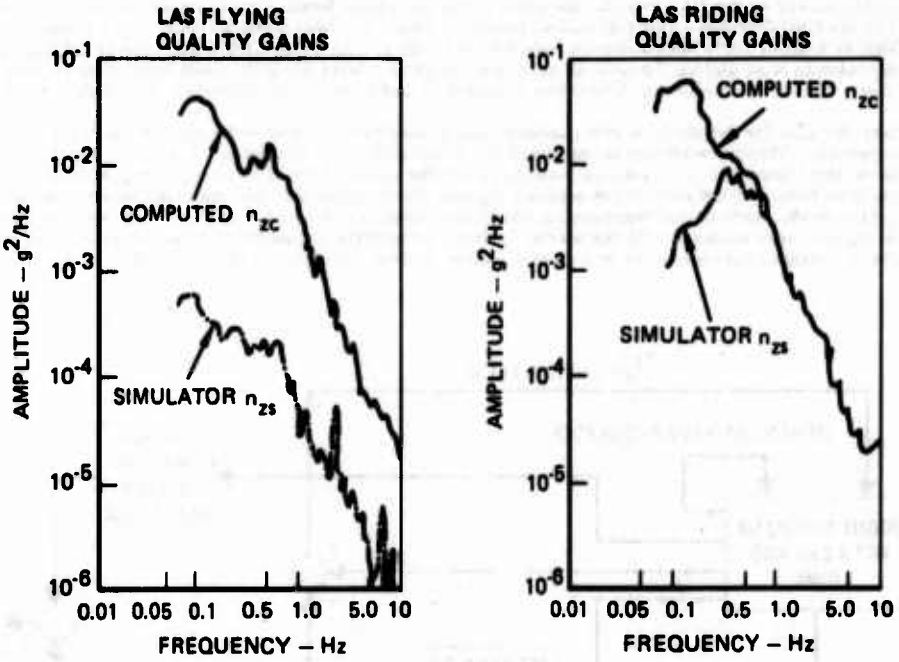

FIGURE 9. POWER SPECTRAL DENSITY COMPARISON OF LARGE AMPLITUDE SIMULATOR OUTPUTS

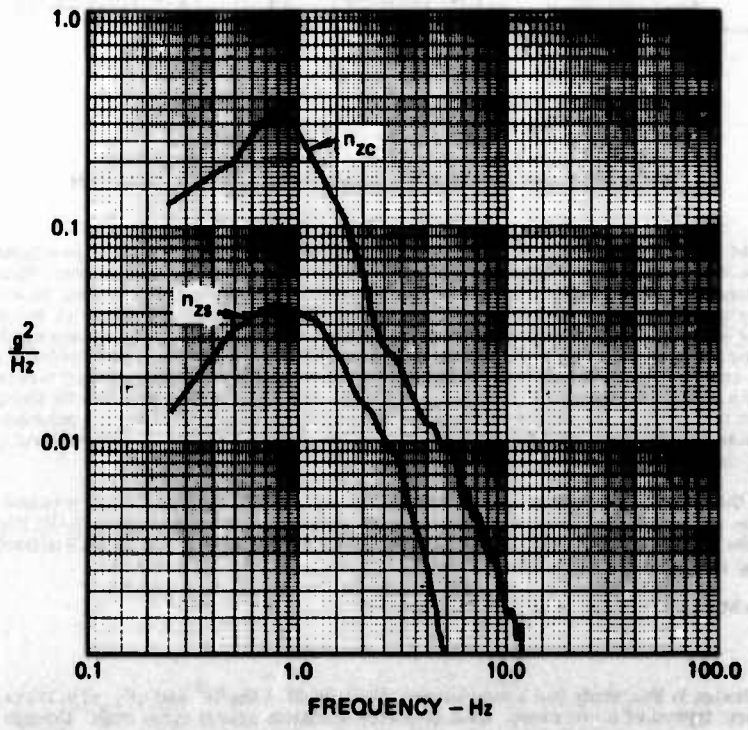

FIGURE 10. POWER SPECTRAL DENSITY OF n_{zs} VERSUS n_{zc} FOR RIMS OFF

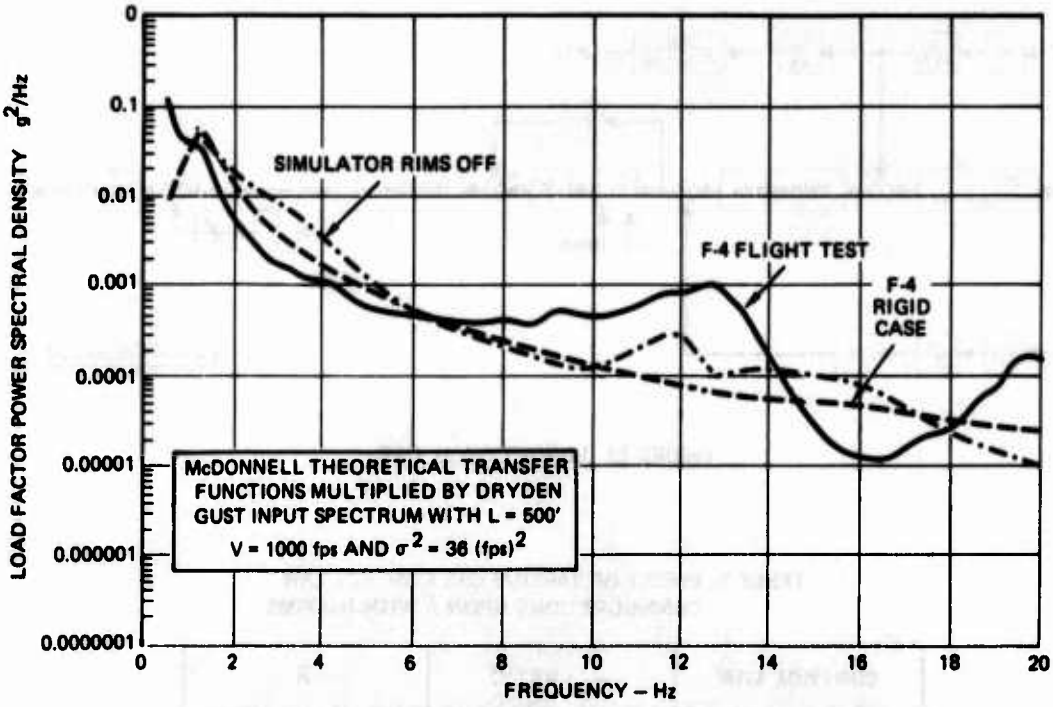

FIGURE 11. COMPARISON OF LAS MODEL POWER SPECTRAL DENSITY WITH THAT OF AN F-4C

TABLE 1. EFFECT OF MACH AND ALTITUDE ON ACCELERATION RESPONSE

MACH NO.	.9		1.2	
ALTITUDE, FT.	CSMP $\bar{A}$	ANALYTIC $\bar{A}$	CSMP $\bar{A}$	ANALYTIC $\bar{A}$
500	.081	.080	.063	.068
1000	.062	.064	.048	.054

Impact of CAS

The existing CAS configuration, Figure 12, with no RIMS was evaluated for different feedback blends of pitch rate and load factor. This was done to see if the control laws could be modified to improve the level of $\bar{A}$ and hence the ride smoothing. The results in Table 2 indicate that while CAS-on is an improvement over CAS-off, the effect of various blends is negligible; therefore, the baseline CAS configuration was used unchanged.

Selection of a Baseline

To obtain a preliminary check of the rigid body LAS model with the rigid body CSMP model a RIMS was configured for the Large Amplitude Simulator model and verified by the CSMP model. For this initial RIMS configuration, referred to as the baseline RIMS, the vertical accelerometer was simulated 20 feet forward of the aircraft cg. This accelerometer signal that was fed back through the CAS was used for the control of the trailing edge surface as was shown in Figure 12. The trailing edge actuator in Figure 12 is represented as an ideal high speed actuator; however, the actuator used in the CSMP and LAS models incorporated both position and rate limiting.

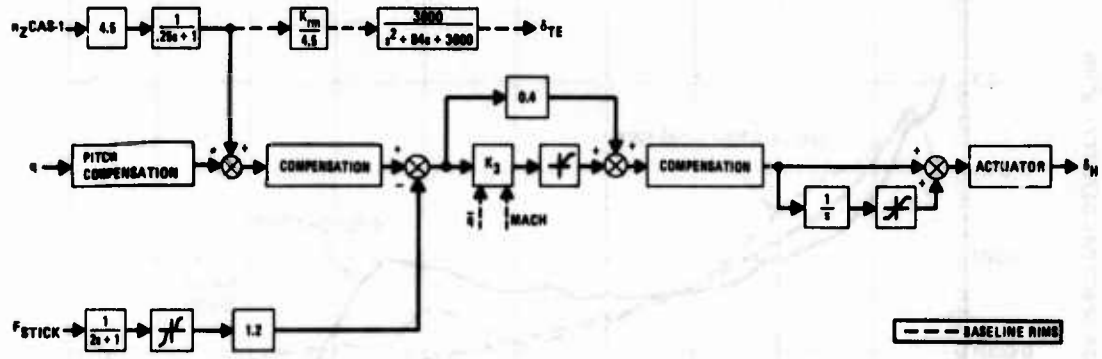

FIGURE 12. LONGITUDINAL CAS

TABLE 2. EFFECT OF VARIOUS CAS CONTROL LAW CONFIGURATIONS UPON $\bar{A}$ WITH NO RIMS

CONTROL LAW	n_z:q RATIO	$\bar{A}$
BASELINE	4.5:1	.081
C*	4.5:1	.082
$\dot{\theta}$	1:2	.083
CAS OFF	–	.087

Comparison of LAS and CSMP Models

This baseline RIMS configuration was then flown for two conditions. One for a RIMS gain, K_{rm}, of -18.0 degrees/g and for a RIMS gain of 0.0, i.e., RIMS off. The -18.0 value was chosen after a parametric study of various RIMS gains. The resulting computed simulator $\bar{A}$ values (Table 3) were 0.075 and 0.056 for the gains 0.0 and -18.0 respectively. Two pilots flew both of the cases for runs of six minutes each. The pilot comments were consistent with the recorded data in confirming that the RIMS mode produced a softer ride with a noticeably lower g level.

The CSMP model with the same baseline RIMS configuration and gain resulted in an $\bar{A}$ of 0.057, thus verifying the LAS model and results (Table 3). This initial RIMS configuration showed that the aircraft's gust response energy in the short period mode could be reduced and that the Large Amplitude Flight Simulator system was an effective tool for the study of ride qualities.

Inclusion of the First Body Bending Mode

The baseline RIMS configuration was then evaluated with the first body bending mode equations (eq. 6) included.

$$\frac{n_{zp_{1H}}(s)}{\delta_H(s)} = \frac{0.18s^2}{s^2+3.2s+4175}$$

$$\frac{n_{zp_{1T}}(s)}{\delta_{TE}(s)} = \frac{-0.056s^2}{s^2+3.2s+4175} \qquad \text{Eq. 6}$$

$$\frac{n_{zp_{1W}}(s)}{w\text{-gust}(s)} = \frac{0.0017s^2}{s^2+3.2s+4175}$$

TABLE 3. ACCELERATION RESPONSE FOR RIMS BASELINE

RIMS GAIN	LAS $\bar{A}$	CSMP $\bar{A}$
0.0	.075	.081
−18.0	.056	.057

By inspection of the baseline RIMS acceleration power spectral density (Figure 13) generated from LAS data, the effect of the first body bending mode can be seen. It was evident that there was a gradual loss in the effectiveness of the baseline RIMS control loop above 0.6 Hz and that the baseline RIMS did not aggravate the first body bending mode. The loss in effectiveness above 0.6 Hz was not unexpected since the low pass filter of the baseline RIMS loop had a breakpoint at 0.63 Hz.

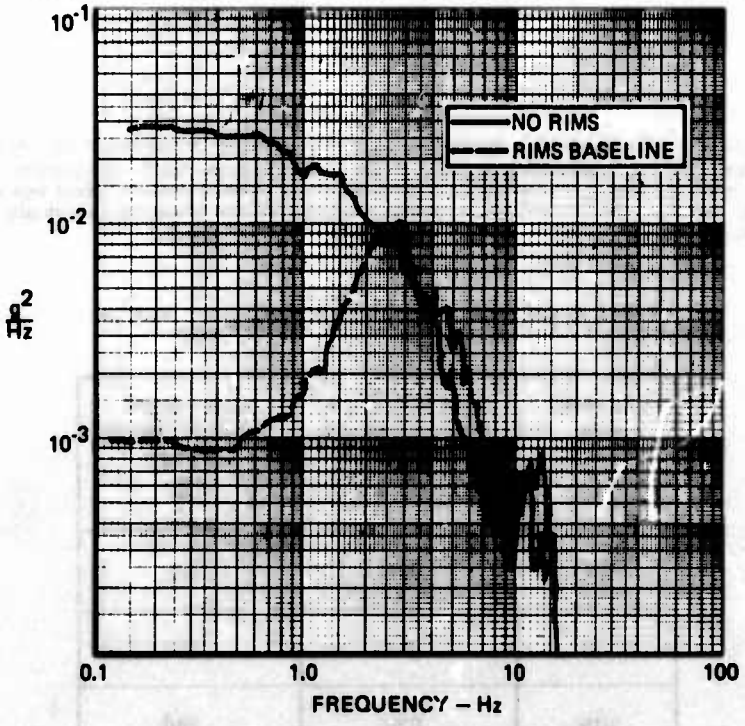

FIGURE 13. n_{zs} POWER SPECTRAL DENSITY

Modified RIMS

To improve the effectiveness of the ride improvement mode system at all frequencies, it was necessary to alter the design of the low pass filter. The simplest approach appeared to be to lower the low pass time constant so that the breakpoint would occur at a high frequency, thus giving less roll off in the desired frequency range, 0 to 10 Hz. However, lowering the time constant of the low pass filter led to phase problems for the ride improvement mode system. Therefore, the low pass filter was abandoned in favor of a laglead. The laglead was chosen because its gain and phase characteristics were desirable in terms of what would be effective for ride smoothing.

The resulting CAS/RIMS configuration was programmed into the LAS and CSMP models. The block diagram in Figure 14 represents this CAS/RIMS configuration with the exception that a Command Model Interconnect (CMI) shown in the figure was not used at this stage of the analysis. The CMI which connects pilot commands to the RIMS will be discussed in a subsequent paragraph.

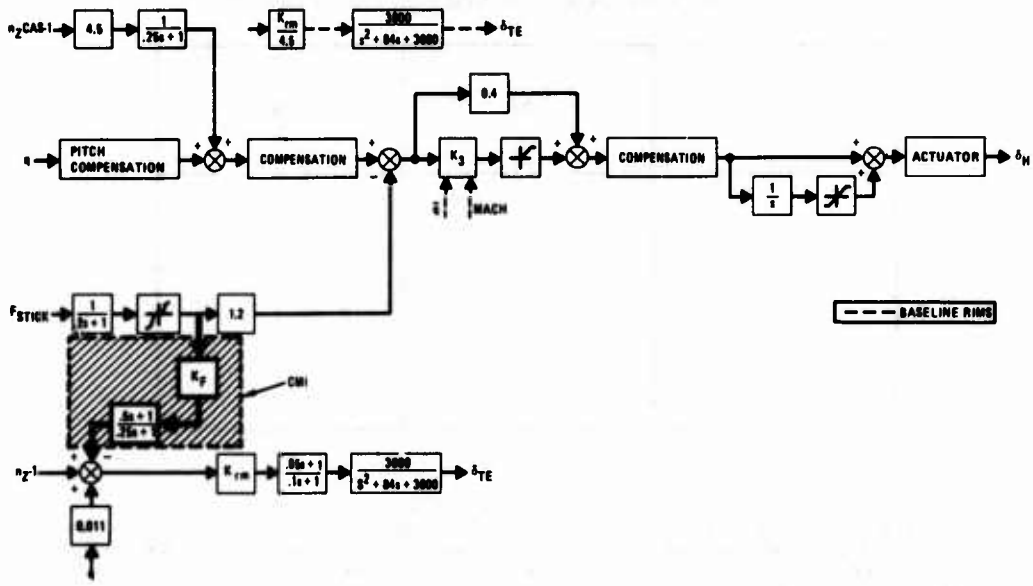

FIGURE 14. LONGITUDINAL CAS/RIMS WITH COMMAND MODEL INTERCONNECT (CMI)

Through the use of the CSMP model, a parametric study was performed to determine the optimum gain for the laglead RIMS. Henceforth, the laglead RIMS will be referred to as simply the RIMS. The results in Table 4 showed that a gain for K_{rm} equal to -15 was optimum and that an $\bar{A}$ reduction of better than 50 percent was attainable for the RIMS configuration. For K_{rm} values above -15 no further improvement was attained and eventually the control loop was driven unstable.

TABLE 4. CAS/RIMS $\bar{A}$ RESULTS FOR $w_{gust_{RMS}}$ = 6.6 fps

LAGLEAD RIMS K_{rm}	w/O 1ST BODY BENDING MODE EFFECT $\bar{A}$	w/1ST BODY BENDING MODE EFFECT $\bar{A}$
0.0	.081	.085
-10	.041	.043
-15	.038	.040
-20	.038	.040

For a RIMS-on $\bar{A}$ value of 0.040 in a 6.6 fps rms gust environment a vertical rms load factor of about 0.26 g's results. A check of the ride quality criteria in Figure 3 indicate that this is well within the acceptable level for a desired exposure of 30 minutes.

The discomfort index as defined by Equation 7, Ref. 15, was also calculated using the RIMS-on computed acceleration power spectral density, where the cutoff frequency, Ω_c, was 20 Hz.

$$D_i = \left[\int_{0.1}^{\Omega_c} \left| W(\Omega) \right|^2 \left| T_{AF}(\Omega) \right|^2 \Phi(\Omega)\, d\Omega \right]^{1/2} \qquad \text{Eq. 7}$$

This calculation resulted in a D_i equal to 0.19 where 0.28 is the specification requirement for the discomfort index for a flight equal to 0.5 hour in length.

The improvement of the RIMS over the baseline RIMS (i.e., the use of the laglead instead of lag) in ride smoothing at frequencies greater than 1 Hz is revealed in a plot of their acceleration power spectral densities, Figure 15, obtained from runs made on the Large Amplitude Simulator for the two configurations. Although the RIMS is not as effective as the baseline for frequencies below 1 Hz, it affords significant improvement between 1 and 6 Hz.

While the CSMP model showed reductions of more than 50 percent, the LAS reductions, both computed and simulated, tended to be more on the order of about 40 to 50 percent. Two factors contributing to the difference in $\bar{A}$ reduction are, one that the LAS also had a v-gust that would contribute some vertical load factor due to the cross coupling of the six degree-of-freedom equations and two, the LAS system had considerably more noise introduced into its model than did the CSMP model.

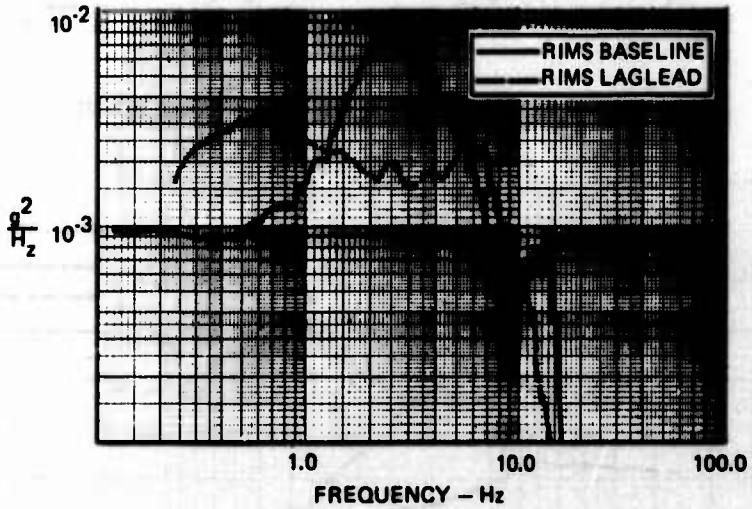

FIGURE 15. RIMS VS BASELINE RIMS, n_{z_s} POWER SPECTRAL DENSITY

First Body Bending Mode Effect

The results in Table 4 also present the effect of the RIMS on the first body bending mode. While the first body bending mode contributes some additional energy to the $\bar{A}$ value of the rigid body, it can be seen that the RIMS does not significantly aggravate or add to the energy that is contributed by the first body bending mode.

The lack of impact of the first body bending mode was also evident from the results obtained from the simulator. A comparison of the RIMS on data with RIMS off data presented in Figures 16 and 17 again indicated that the RIMS was effective in reducing the gust response at the short period frequency without significant energy contribution to the gust response at the first body bending mode frequency.

Pilots Comments

The RIMS configuration was evaluated by two pilots each of whom flew the simulator for RIMS on and off conditions for flights five to six minutes in length for each condition. A table of the pilots comments evaluating the ride quality for the RIMS on and off conditions is presented in Table 5. Both pilots could feel the improvement in ride quality with the RIMS on. In addition both felt they could fly a mission in the RIMS on condition for an hour of exposure in this turbulent environment.

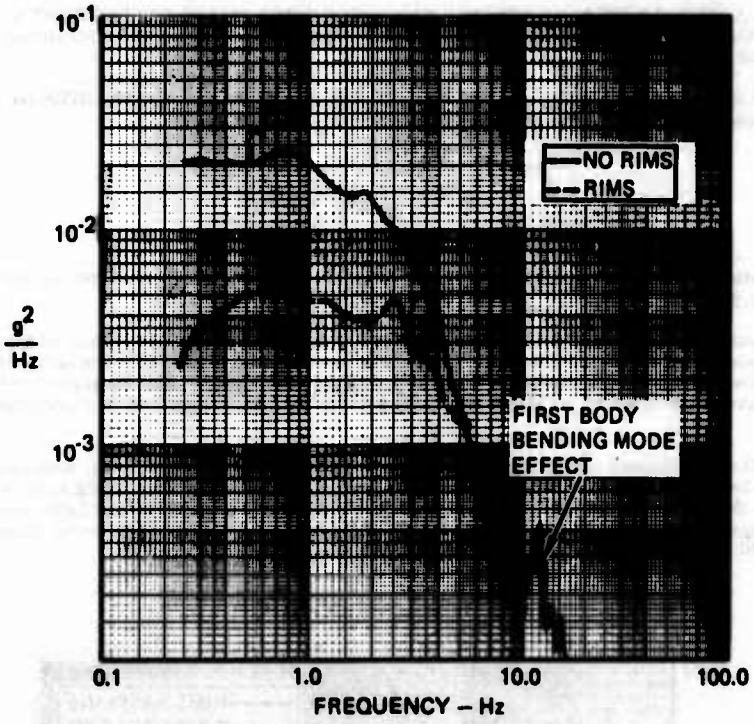

FIGURE 16. RIMS VS NO RIMS, n_{z_s} POWER SPECTRAL DENSITY

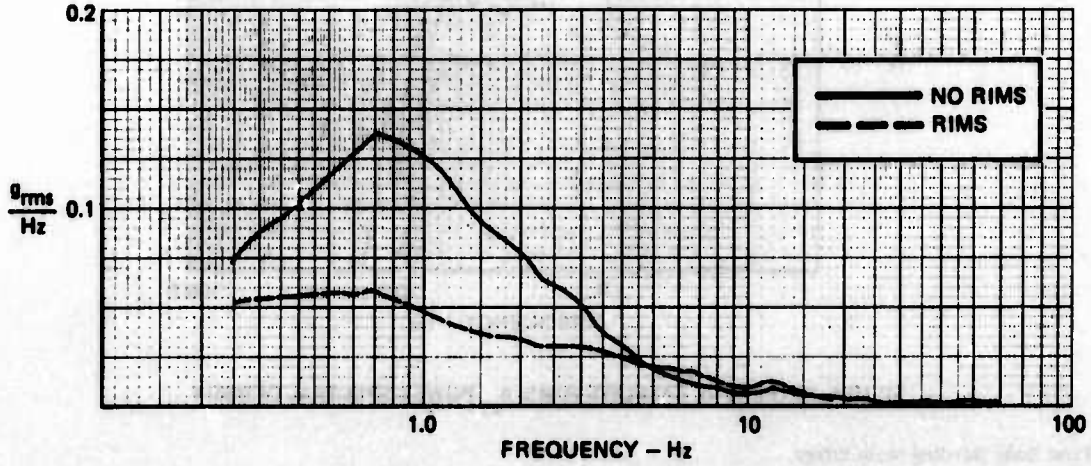

FIGURE 17. LOAD FACTOR REDUCTION OF RIMS VS NO RIMS

HANDLING QUALITIES

Impact of RIMS on Handling Quality

As previously mentioned, the CAS/RIMS configuration evaluated on the LAS did not have the Command Model Interconnect that is shown in Figure 14. The ride quality task that was performed by the pilots to evaluate the CAS/RIMS ride smoothing capabilities did not require the implementation of a Command Model Interconnect; however, while the absence of the Command Model Interconnect had no effect on the ride smoothing performance for the RIMS, it did not allow the pilots to adequately evaluate the overall CAS/RIMS handling qualities. Without the CMI the aircraft response to stick commands with RIMS-on was predictably sluggish. As a pilot input would attempt to command pitch rate and load factor, the trailing edge surface would attempt to reduce any load factor through the RIMS loop with the result being a slow, over-damped response. For the pilot to be able to command load factor without a performance degradation from the RIMS, a CMI was developed to allow for good maneuverability and ride smoothing simultaneously. The interconnect as shown in Figure 14 has a leadlag to give desired transient response characteristics and a gain, KF, which is scaled to give the commanded steady state load factor at the RIMS signal summing junction. Thus configured, the RIMS is designed to operate about some commanded load factor, where for steady level flight and no stick command the RIMS operates about a load factor of 1 g.

TABLE 5. PILOT COMMENTS ON RIDE QUALITY EVALUATION OF CAS/RIMS

PILOT	RIMS OFF	RIMS ON
1	LIGHT TO MODERATE TURBULENCE...CAN FLY INSTRUMENTS. HEAVY TURBULENCE –CAN'T SEE ANYTHING. LOW LEVEL ROUTE IN HILLS UP NORTH, FEELS ABOUT LIKE THIS. EASIER TO FLY WITH GOOD GROUND REFERENCE. HALF HOUR TASK WOULD BE A LOT OF WORK.	SO FAR IT SEEMS A LITTLE SMOOTHER. NOT QUITE SO MANY VIOLENT UP AND DOWNS. TURBULENCE GETS WORSE THE CLOSER YOU GET TO THE GROUND. FEELS SLUGGISH–DEFINITELY. DEFINITE IMPROVEMENT. PEAKS AND VALLEYS NOT SO HARD. NOT AS VIOLENT. DIDN'T HIT MY HEAD ON THIS RUN. (6 OR 7 TIMES LAST RUN.)
2	FLYABLE. TURBULENCE BETWEEN MODERATE AND HEAVY. COULD READ MAPS BETWEEN BUMPS, TRACK A TARGET. MORE UNCOMFORTABLE THAN PREVIOUS TWO RUNS. OSCILLATIONS ARE RELATIVELY MILD, THEN A SHARP PEAK, FAIRLY VIOLENT. HANDLING IS FINE. JUST ROUGH. CAN POINT AIRPLANE OK. JUST AN UNCOMFORTABLE RIDE. HAVE A HARD TIME READING A MAP FOR VERY LONG.	OPERABLE CONDITION. COULD READ MAPS AND HANDLE A TASK. LESS MAGNITUDE ON THE BUMPS; MUCH EASIER TO CONTROL.

C* Criteria

To evaluate the handling qualities of the CAS/RIMS with CMI, the C* criteria was applied as outlined by Neil and Smith in Reference 20. Since the time available did not permit simulator evaluation of handling qualities of the CAS/RIMS with CMI in terms of pilot ratings, the C* criteria was applied as outlined by Neil and Smith in Reference 20. Using the CSMP model, C* responses in accordance with Equation 8 were obtained for three configurations: the CAS-on condition with RIMS-off; the CAS/RIMS with no CMI; and the CAS/RIMS with CMI.

$$\frac{C^*}{F_S} = \frac{n_z}{F_S} + \frac{\ell p}{g}\frac{\ddot{\theta}}{F_S} + \frac{400}{g}\frac{\dot{\theta}}{F_S} \qquad \text{Eq. 8}$$

The three C* responses were then normalized by the steady state C* value and plotted against the C* criteria boundaries in Figure 18. According to the criteria, responses within the boundaries indicate a pilot rating of 3.5 or better.

The CAS/RIMS with no CMI was well outside the C* boundaries as expected. The CAS/RIMS configuration with the inclusion of the CMI, however, provided a response that lies within the C* boundaries and is on par to that of the CAS-only configuration. Hence, the use of the CMI allowed the CAS/RIMS control system to retain excellent handling qualities while improving the ride qualities.

IMPACT OF FEEDBACK RATIO ON THE CAS/RIMS

Once the CAS/RIMS flight control system attained its final configuration, as was shown in Figure 14, the effect on $\bar{A}$ of various blends of CAS feedback gains was re-examined. When the CAS with no RIMS was checked for the influence of various n_z:q feedback ratios on $\bar{A}$, little difference was perceived (Table 2). However, for the CAS/RIMS configuration there is a significant difference for changes in the n_z:q ratios as demonstrated in Table 6. These differences in $\bar{A}$ depending on the n_z:q ratios can be attributed to the heavy reliance of the CAS/RIMS on load factor feedback.

FUTURE PLANS

The focus of this initial study of ride qualities was on the alleviation of load factor at the pilot station. Any pitching moments induced by the trailing edge surface deflections were alleviated through the Control Augmentation System. CSMP results indicated that pitching motions from RIMS on were somewhat less than for RIMS-off. In future investigations, more emphasis will be placed on the study of the pitching motions to see what improvements may be desirable.

Other future plans include further evaluation of the handling qualities on the Large Amplitude Flight Simulator of the Ride Improvement Mode System with the Command Model Interconnect; a check of the RIMS gains performance at other flight conditions; and modifications to improve the RIMS ride smoothing capability.

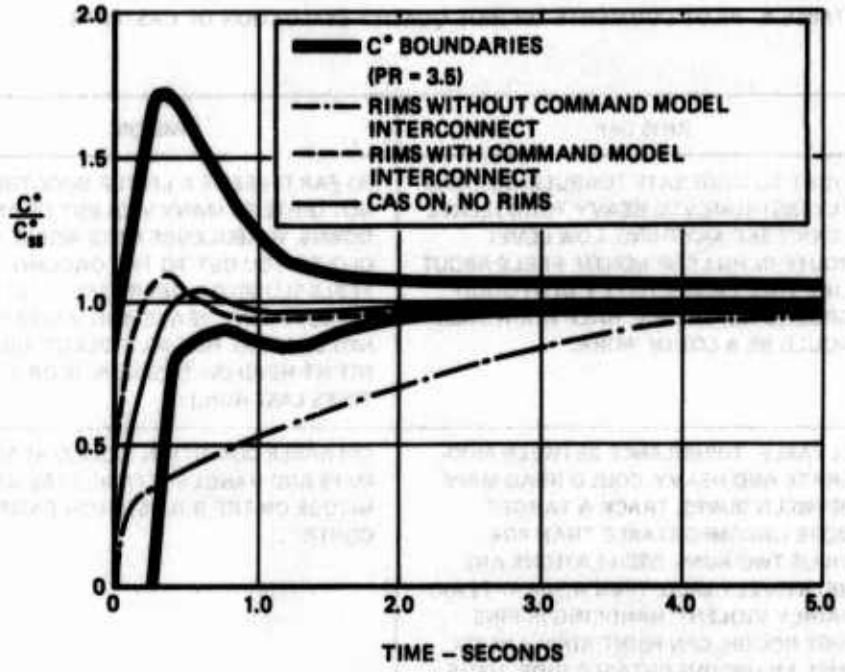

FIGURE 18. C* EVALUATION OF CAS/RIMS HANDLING QUALITIES

TABLE 6. CAS/RIMS $\bar{A}$ RESULTS FOR VARYING $q:n_z$ FEEDBACK BLEND

n_z:q	$\bar{A}$
4.5:1	.043
2:1	.046
1:2	.051
1:4.5	.051

CONCLUSIONS

The study attained its objective: to confirm that a Ride Improvement Mode System could be designed to improve the ride quality of a highly maneuverable low wing loaded air combat multi-purpose airplane without compromise to the flying qualities.

It was demonstrated that:

- Significant reductions in load factor response to gusts were achieved with simple control law implementations.
- Piloted simulation confirmed that improved ride qualities were possible.
- Degradation of flying qualities was avoided by judicious selection of control loops and interconnects.

It was concluded that a simple maneuvering flap system could be employed to achieve both excellent ride qualities and handling qualities in a low wing loaded multi-purpose combat aircraft.

REFERENCES

1. Simpson, A.; Hitch, H. P. Y: Active Control Technology. Aeronautical Journal, p. 231, June 1977.

2. Hirsch, René : Sur la stabilisation automatique des avions. Comptes Rendus, p. 203, no. 24, June 1937.

3. Danley, P; Shufflebarger, C. C.: Tests of a gust-alleviating flap in the gust tunnel. N.A.C.A. TN. No. 745, Jan. 1940.

4. Zbsozek, J.; Smith, K.W.; White, D.: Preliminary Report on a Gust Alleviator Investigation on a Lancaster Aircraft. ARC RAM 2972. Aug. 1953.

5. Gilbert, J.: The Worlds Worst Aircraft, St. Martins Press, 1975.

6. Phillips, W. H.; Kraft, Jr. C. C.; Theoretical Study of Some Methods for Increasing the Smoothness of Light Aircraft Through Rough Air. N.A.C.A. Tech Note 2416, July 1951.

7. Kraft, Jr. C. C.: The Results of a Flight Investigation of a Gust Alleviation System. N.A.C.A. TN. 3612, April 1956.

8. Hunter, P. A.; Kraft, Jr. C. C.; Alford, W. L.: A Flight Investigation of an Automatic Gust Alleviator. NASA TND-532, Jan. 1961.

9. Oehman, W. I.: Analytical Study of the Performance of a Gust Alleviation System with a Vane Sensor. NASA TN D-7431, Feb. 1974.

10. Oehman, W. I.: Optimum Design Characteristics of a Gust Alleviator for Aircraft. NASA TN D-6152, March 1976.

11. Notess, C. B.: Triangle – Flexible Airplanes – Gusts – Crew. C.A.L. (Cornell) Rep. No. FDM 343, May 1963.

12. Coleman, H. J.; Gallagher, J. T.: Moving base simulator studies of crew performance in severe environments. NASA Meeting on Aircraft Response to Turbulence. Langley Research Center, Sept. 1968.

13. Gordon, C. K.; Dodson, R. D.: STOL Ride Quality Feasibility Study, NASA. CR-2276. July 1973.

14. Cunningham, T. B.: Optimal Control of a Low Wing Loading STOL Aircraft. AIAA Paper 76-1954.

15. Anon: Flight Control Systems – Design, Installation and Test of Piloted Aircraft, General Specification for. MIL-F-9490D (USAF) 6 June 1975.

16. Press, Harry; Meadows, May T.; and Hadlock, Ivan: A Reevaluation of Data on Atmospheric Turbulence and Airplane Gust Loads for Application in Spectral Calculations. NACA Rep. 1272, 1956.

17. Fung, Y. C.: Statistical Aspects of Dynamic Loads. Journal of Aeronautical Science, Vol. 20, no. 5, May 1953, pp. 317-330.

18. Finck, R. D.: USAF Stability and Control Datcom, AFFDL, January 1975.

19. Chalk, C. R., et. al., Background Information and User Guide for MIL-F-8785B (ASG), Military Specification – Flying Qualities of Piloted Airplanes, August 1969.

20. Speakman, J. D.; Bonfili, H. F.; et. al.: Crew Exposure to Vibration in the F-4C Aircraft During Low-Altitude, High Speed Flight, AMRL-TR-70-99, Jan. 1971.

21. Neal, T. Peter; Smith, Rogers E.: An In-Flight Investigation to Develop Control System Design Criteria for Fighter Airplanes, AFFDL-TR-70-74, Volume II, Dec. 1970.

FLIGHT PERFORMANCE AND PILOT WORKLOAD IN HELICOPTER FLIGHT UNDER SIMULATED IMC EMPLOYING A FORWARD LOOKING SENSOR

Dipl.-Ing. R. Beyer
Deutsche Forschungs- und Versuchsanstalt für Luft- und Raumfahrt e.V.
Institut für Flugführung
33 Braunschweig-Flughafen
Germany

SUMMARY

The low altitude and terminal area flight of helicopters under IMC is a much desired goal in both civil and military fields. Electro-optical sensors and associated displays may be a part of a future helicopter avionics system to achieve this goal. In order to study some hereto related problems a study was made giving particular emphasis to flight performance and pilot workload in flights under simulated IMC employing a forward looking sensor as well as to the layout of the display and the sensor system. The experiments were flown in a Bell UH-1D helicopter and the paper presents the technical approach which was chosen and some of the results which were obtained.

LIST OF SYMBOLS

A	- mechanical work
h_R	- radio altitude
$h_{R,Min}$	- minimum radio altitude
IAS	- indicated airspeed
IFR	- instrument flight regulations
IMC	- instrument meteorological conditions
m	- mass
M	- torque
r	- product-moment-coefficient of correlation; distance
t	- time
T	- duration of test
v	- velocity
v_{Min}	- minimum indicated airspeed
VFR	- visual flight regulations
VMC	- visual meteorological conditions
α	- angle of rotation
β	- angle between the vertical axis of the helicopter and the projection of the line of sight on the y,z-plane of the helicopter
ϑ	- pitch angle
ϑ_K	- angle between the sensor line of sight and the x,y-plane of the helicopter
φ	- bank angle
Θ	- moment of inertia
ω	- angular velocity
ω_x	- roll rate
ω_y	- pitch rate
ω_z	- yaw rate
ψ_K	- angle between the longitudinal axis of the helicopter and the projection of the sensor line of sight on the x,y-plane of the helicopter
d	- lateral deviation of the helicopter from a given track

1. INTRODUCTION

The guidance and control design considerations for low altitude and terminal area flight of fixed-wing and rotary-wing aircraft are different because helicopters are designed to fly at low altitude most of the time and to take-off and land even at unprepared sites where no ground-based navigation aids are available. Helicopters, therefore, can benefit to a limited degree only from the sophisticated avionics systems available on modern fixed-wing aircraft. As a consequence helicopters are flown manually most of the time and the pilot has to make extensive use of the visual cues provided by the terrain.

The usefulness of a helicopter is limited, therefore, to those cases where the pilot can see the details of the terrain which he needs for orientation and navigation. The limiting conditions are dependent on many factors but may be reached in general when the conditions become worse than flying at a clear night under full moon light.

In order to extend the flexibility of helicopter operation beyond this limit some visual aid for the pilot is required. Electro-optical sensors, for example, produce an image of the area within their field of view, they can intensify this image or convert the signals received from the non-visual to the visual spectrum. The image may be projected then on a screen where it can be seen by the pilot directly as, for example, with night goggles. Alternatively, the electro-optical sensor may produce an electrical output to drive a monitor which displays the image. This latter method has the advantage that additional computer-generated instrument displays can be superposed on the image of the terrain conveniently. In fact, early studies (ref. 1) have shown that this combination of the image of the terrain and instrument displays would be most efficient for an integration of a forward-looking electro-optical sensor and the associated monitor into the existing helicopter avionics system with respect to human engineering considerations and pilot acceptance. But there are other factors affecting flight performance and pilot

workload, too, as, for example, the field of view, the optical magnification, the direction of the line of sight of the electro-optical sensor and so on.

2. THE STUDY AND ITS OBJECTIVES

In order to get some insight into the problems of controlling a helicopter by means of a combined display of the terrain ahead and instruments on a monitor screen an experimental study was set up for a period of two and a half years focussing on human engineering investigations. The objectives of this study were

i) to investigate the influence of certain parameters of the electro-optical sensor on flight performance and pilot workload
ii) to develop a human engineered content and format of the instrument displays to be superposed on the display of the terrain
iii) to compare flight performance and pilot workload in ordinary daylight flights under VMC and in flights under simulated IMC employing the combined terrain/instrument display.

In order to illustrate some of the outcomes of this study within the scope of this paper a selection of topics had to be made. In the following, therefore, the comparison of flight performance and pilot workload for VFR and IFR flights employing the display are discussed in more detail only giving particular emphasis to different control modes of the line of sight of the electro-optical sensor

3. THE TECHNICAL APPROACH

The experiments were flown in a Bell UH-1D helicopter from the left (copilot's) seat (fig. 1). A closed-circuit TV system was used to simulate an electro-optical sensor. The sensor was mounted on a two-axis steerable platform mounted under the helicopter cockpit (fig. 2). All windows at the experimental pilot's seat were covered completely to simulate IMC at night. The sensor field of view was 28° in azimuth and 22° in elevation and the factor of optical magnification was 0.5, i.e. the pilot saw the objects of the terrain on the monitor screen half as large as they appeared when being viewed directly by the pilot. The direction of the line of sight of the sensor could be changed with an angular velocity of 7.5 °/s in azimuth and 4.5 °/s in elevation. The size of the monitor screen was 18 cm wide by 13 cm high. The display is shown in fig. 3 and 4.

Two pilots flew the helicopter at a nominal airspeed of 80 kts and at a nominal height above ground of 200 ft on different courses which are characterized as follows:

a) level terrain well-known to the pilots
b) undulated terrain well-known to the pilots
c) terrain which the pilots passed the first time after preparation by means of a map
d) a river to be followed

Furthermore the flight conditions changed as follows:

e) ordinary daylight VFR flights without the display
f) flights under simulated IMC employing the display and the electro-optical sensor being fixed to the axes of the helicopter, i.e.

$$\psi_K = 0^\circ$$
$$\vartheta_K = -6^\circ$$

g) flights under simulated IMC employing the display and the electro-optical sensor being stabilized in pitch, i.e.

$$\psi_K = 0^\circ$$
$$\vartheta_K = -6^\circ - \vartheta$$

h) flights under simulated IMC employing the display and the electro-optical sensor looking ahead in turns, i.e.

$$\begin{pmatrix} \psi_K \\ \vartheta_K \end{pmatrix} = \begin{pmatrix} \cos\varphi & -\sin\varphi \\ \sin\varphi & \cos\varphi \end{pmatrix} \begin{pmatrix} 0.9\varphi \\ -6^\circ \end{pmatrix}$$

Most of the parameters which were recorded are self-explainatory. Three parameters are explained in more detail in the appendix. These are

$n^2_{\dot{\varphi}}$ - a measure which represents the amount of coordinated flying with respect to bank and yaw

ω^2_{rms} - a relative measure of pilot workload produced by the manual stabilization of the helicopter in one axis

$|\bar{d}|$ - a measure which represents the average absolute lateral deviation of the helicopter from a given track.

Pilots' comments were gathered by means of interviews and specially designed rating scales.

With this set of experimental conditions the hypothesis was tested that neither the different courses a - d nor the various flight conditions e - h produce a statistically significant difference of parameter means. Two-tail tests were applied. However, in the following flight conditions e - h will be discussed only.

4. IMPORTANT ASPECTS

Irrespective of the technical approach which was chosen to achieve the objectives of this study particular attention was given to some more general but nevertheless important aspects. First, many studies of this type have suffered from the fact that the test pilots were given inadequate training only and that the test personnel changed within the course of the experiments. Therefore two experienced test pilots were assigned to this study for the total period of 2 1/2 years. Within the 350 flight hours of this program both pilots could be trained more than adequately and gathered an amount of experience in flying the display which was not available before but was urgently needed for development work. In addition visiting helicopter pilots were given the opportunity to fly the display, too, and their comments balanced some final statements regarding a possible introduction of the display into service and its impact on pilot training.

Second, the simulation of a system employing a forward looking sensor and a combined display of terrain and instruments aboard the helicopter was considered realistic by the potential users. This is a most important factor which determines largely the applicability of the test results for the subsequent development work.

And third, the selection of test courses was not restricted because no ground derived navigation or measurement aids were employed. In addition no technical limitations existed for the layout of the electronically generated instrument displays (fig. 3).

5. RESULTS

A selection of results had to be made to be presented within the scope of this paper. In the following, therefore, particular emphasis is given to the comparison of flight performance and pilot workload for VFR and IFR flights employing the display and to the control of the line of sight of the electro-optical sensor.

Table 1 presents a comparison of parameters obtained from flights under VMC and under simulated IMC employing an electro-optical sensor being fixed to the axes of the helicopter. From this table it can be seen that under simulated IMC employing the display the pilots did not reduce average airspeed significantly compared to VMC flights as it is anticipated sometimes but preferred to increase height above ground by 26 %. This may be due to safety requirements as well as to the fact that the terrain is moving more slowly over the monitor screen which allows more time for orientation. The increased safety requirements for flights under IMC may be recognized also by an increase of minimum height above ground by 26 % and by a decrease of minimum indicated airspeed by 11 %.

An increase of $\omega^2_{x,rms}$ by a factor of 29 and an increase of $\omega^2_{y,rms}$ by 25 % indicate much greater activity in pitch and roll and thus higher pilot workload for flights under IMC. One reason is that a qualitative assessment of pitch and roll and their variation is much easier under VMC than it is by means of the display. Increased pilot workload is also indicated by the measure of coordinated flying r^2_{φ,ω_z} which drops from 52 % under VMC to 39 % under simulated IMC. A major cause may be the higher and more unsteady activity in roll ($\omega^2_{y,rms}$) under simulated IMC already mentioned. It is also interesting to note that the pilots paid less attention to flying wings level under IMC which is indicated by an increase of the average bank angle φ.

Table 2 presents a comparison similar to that of table 1 with the exception that the line of sight of the electro-optical sensor was stabilized in pitch (see chapter 3,g). The table shows that the statistically significant differences of parameter means which appeared in table 1 disappeared for this control mode of the sensor with respect to parameters v(IAS), $\omega^2_{y,rms}$, v_{Min}(IAS) and $h_{R,Min}$ and that the difference for the parameter h_R is reduced. In general the stabilization of the sensor in pitch led to a better conformity of measurements taken in VFR and simulated IFR flights without producing a difference of parameter means in other areas. However, the stabilization of the sensor made the display of the terrain somewhat less realistic and thus less suitable to fly with. Therefore the pilots flew the helicopter to a higher degree according to the information provided by the instrument displays. For example, while the pilots were able to fly steep climbing turns with the sensor being fixed to the axes of the helicopter without difficulties the same manoever could not be flown coordinated when the sensor was stabilized in pitch.

Next a control mode of the sensor was investigated which made the sensor looking ahead in turns (see chapter 3,h). In order to test this feature a river with a number of turns was chosen as the reference course to be followed. A comparison of flights along this course under simulated IMC employing the display with the sensor being fixed to the axes of the helicopter and looking ahead in turns, respectively, is presented in table 3. It can be seen that for the look ahead mode of the sensor there was only a moderate increase of indicated airspeed v(IAS) by 5 %. However, a significant increase of the activity in pitch ($\omega^2_{y,rms}$) and yaw ($\omega^2_{z,rms}$) by 47 % and 52 %, respectively, and thus pilot workload was recorded. Another indication of increased pilot workload is the fact that the pilots devoted less attention to flying wings level resulting in an increased average bank angle φ. But more important the average deviation from the given track (river) was reduced significantly from $|\bar{d}|$ = 109.7 m to $|\bar{d}|$ = 45.0 m when the sensor was in the look ahead mode. In fact, this improvement by approximately 60 % was even larger because the deviation measurement equipment reached its limits sometimes in flights with the sensor being fixed to the axes of the helicopter.

Further results were obtained from these experiments which are related to the influence of the terrain, to flight safety, flight strategy and individual performance of the pilots. However, their presentation would go beyond the scope of this paper. They may be found in refs. 2 and 3.

6. CONCLUSIONS

From the results of this study it can be concluded that with a human engineered layout of the instrument displays and the electro-optical sensor a helicopter can be flown under IMC employing the combined display of instruments and terrain in low altitude flight. A sensor which is fixed to the axes of the helicopter would be adequate for cruise flight. A stabilization of the sensor in pitch, however,

will reduce the deviation of flight performance and pilot workload parameters in IFR flight from their reference values obtained in ordinary daylight VFR flights. As a stabilization of the sensor in pitch has turned out to be most efficient for the landing approach, too, this control mode of the sensor may be maintained for both flight phases. This would also eliminate the need to change the control mode in flight which is undesirable because it requires pilot readaptation each time. Finally, the introduction of a "look ahead in turns" control mode of the sensor will lead to a significant reduction of the deviation from a given track which includes steep turns.

In summary this study has led to quantitative data on flight performance and pilot workload and provided the pilots with long-term experience in flying a helicopter by means of an electro-optical sensor and combined terrain/instrument display under simulated IMC. Both data and personal experience have turned out to be valuable contributions to the guidance and control design considerations for low altitude and terminal area flight of helicopters and to subsequent development work in our country.

7. REFERENCES

1. AGARD, V/STOL Displays for Approach and Landing. AGARD Report No. 594, July 1972.

2. R. BEYER, Untersuchung einer kombinierten Darstellung von Umweltbild und Instrumentenanzeigen in einem Hubschrauber Bell UH-1D. DFVLR Report No. IB 153-76-11, June 1976.

3. R. Beyer, E. Kohnen, Untersuchung unterschiedlicher Ausrichtungen des elektro-optischen Sensors für eine kombinierte Darstellung von Umweltbild und Instrumentenanzeigen in einem Hubschrauber Bell UH-1D. DFVLR Report No. IB 153-77-24, August 1977.

Figure 1: Installation of the combined terrain/instrument display in the Bell UH-1D helicopter instrument panel

Figure 2: Installation of the TV-camera

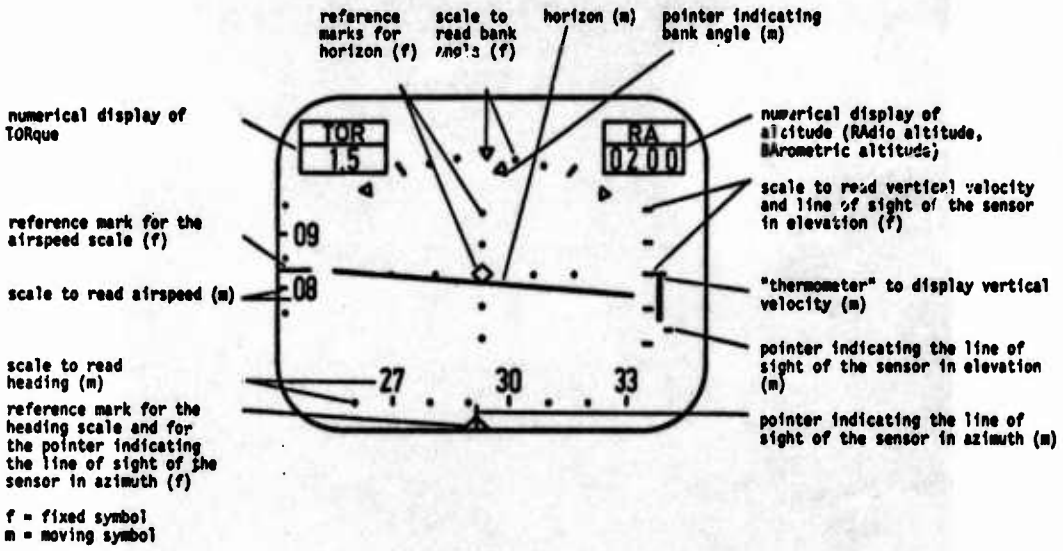

Figure 3: Instrument displays

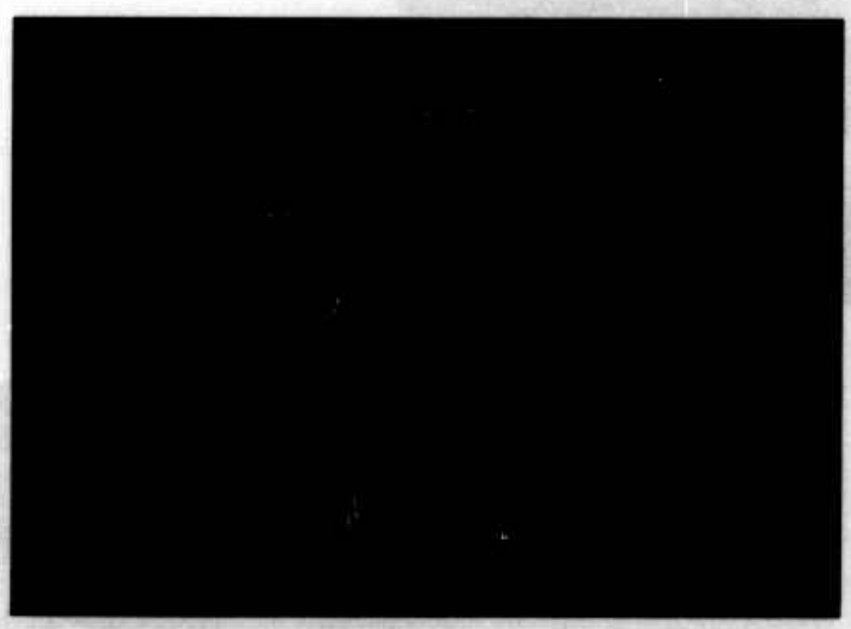

Figure 4: Combined terrain/instrument displays

Parameter	Dim.	VMC	IMC fixed sensor	p
v(IAS)	m/s	43.6 (2.6)	41.9 (1.8)	< 2 o/o
h_R	m	53.8 (5.4)	67.9 (12.7)	< 1 o/oo
φ	deg	-1.5 (0.4)	-2.7 (0.55)	< 1 o/oo
$\omega^2_{x,rms}$	$(deg/s)^2$	0.06 (0.02)	1.72 (1.70)	< 1 o/oo
$\omega^2_{y,rms}$	$(deg/s)^2$	0.73 (0.20)	0.91 (0.11)	< 1 o/oo
$\omega^2_{z,rms}$	$(deg/s)^2$	1.02 (0.49)	1.17 (0.29)	
$v_{Min(IAS)}$	m/s	35.0 (2.9)	31.3 (3.8)	< 1 o/oo
$h_{R,Min}$	m	24.7 (5.0)	31.1 (6.6)	< 1 o/oo
r^2_{φ,ω_z}	-	0.52 (0.09)	0.39 (0.10)	< 1 o/oo

Table 1: Comparison of parameter means obtained in flights under VMC and simulated IMC employing the display and the electro-optical sensor being fixed to the axes of the helicopter. ( ) = standard error. p = error probability for a significant difference of means.

Parameter	Dim.	VMC	IMC stab. sensor	p
v(IAS)	m/s	43.6 (2.6)	43.5 (1.0)	
h_R	m	53.8 (5.4)	61.6 (7.9)	< 1 o/oo
φ	deg	-1.5 (0.4)	-2.6 (0.45)	< 1 o/oo
$\omega^2_{x,rms}$	$(dig/s)^2$	0.06 (0.02)	2.26 (0.69)	< 1 o/oo
$\omega^2_{y,rms}$	$(deg/s)^2$	0.73 (0.20)	0.67 (0.09)	
$\omega^2_{z,rms}$	$(deg/s)^2$	1.02 (0.49)	1.09 (0.33)	
$v_{Min}(IAS)$	m/s	35.0 (2.9)	35.2 (3.3)	
$h_{R,Min}$	m	24.7 (5.0)	27.4 (7.5)	
r^2_{φ,ω_z}	-	0.52 (0.09)	0.41 (0.007)	< 1 o/oo

Table 2: Comparison of parameter means obtained in flights under VMC and simulated IMC employing the display and the electro-optical sensor being stabilized in pitch. ( ) = standard error. p = error probability for a significant difference of means.

Parameter	Dim.	IMC fixed sensor	IMC sensor looking ahead in turns	p
v(IAS)	m/s	37.5 (1.3)	39.2 (2.9)	< 2 o/o
h_R	m	67.7 (4.6)	68.5 (6.1)	
φ	deg	-2.3 (0.62)	-3.3 (0.84)	< 1 o/oo
$\omega^2_{x,rms}$	$(deg/s)^2$	4.80 (1.47)	4.24 (1.05)	
$\omega^2_{y,rms}$	$(deg/s)^2$	1.00 (0.18)	1.47 (0.30)	< 1 o/oo
$\omega^2_{z,rms}$	$(deg/s)^2$	3.88 (1.1)	5.90 (1.25)	< 1 o/oo
$v_{Min}(IAS)$	m/s	31.2 (2.6)	31.3 (3.3)	
$h_{R,Min}$	m	47.3 (4.3)	47.4 (5.1)	
r^2_{φ,ω_z}	-	0.78 (0.07)	0.74 (0.13)	
$\lvert d \rvert$	m	109.7 (16.1)	45.0 (10.4)	< 1 o/oo

Table 3: Comparison of parameter means obtained in flights under simulated IMC employing the display and the electro-optical sensor being fixed to the axes of the helicopter or looking ahead in turns, respectively. ( ) = standard error. p = error probability for a significant difference of means.

APPENDIX

1. THE MEASURE OF COORDINATED FLYING r^2_{φ,ω_z}

Helicopter pilots are trained to fly coordinated with respect to bank and yaw, i.e. to keep the slip indicator centered. Less coordinated flying may be caused by turbulences but also by a detraction of pilot's attention from this task if other tasks are becoming more demanding. Therefore the squared product-moment coefficient of correlation between bank angle φ and yaw rate ω_z was determined because r^2_{φ,ω_z} represents the proportion of coordinated flying, i.e. the proportion of the total variation of yaw rate ω_z which is correlated with a variation of bank angle φ. The parameter r^2_{φ,ω_z} may serve as an indirect measure then to indicate a variation of pilot's attention in this respect if other influencing factors as, for example, turbulences or a variation of torque are less appearing.

2. THE RELATIVE MEASURE OF PILOT WORKLOAD PRODUCED BY THE STABILIZATION TASK ω^2_{rms}

In an unstabilized helicopter pilot workload may be regarded as directly related to the (mechanical) work A required for a rotation of the vehicle in its axes:

$A = M\alpha$
M - torque
α - angle of rotation

The total amount of work may be calculated as the sum of units of work dA:

$$dA = M\,d\alpha = m\frac{dv}{dt}r\,d\alpha$$

m - mass

v - tangential velocity at distance r from the center of rotation

$$\frac{d\alpha}{dt} = \omega \qquad dv = r \cdot d\omega \qquad \Theta = mr^2$$

ω - angular velocity
Θ - moment of inertia

$$dA = mdvr\omega = mr^2\,\omega d\omega = d\left(mr^2\frac{\omega^2}{2}\right) = d\left(\frac{\Theta}{2}\omega^2\right)$$

For Θ = const. the average value of A may be calculated:

$$\bar{A} = \frac{\Theta}{2}\left[\frac{1}{T}\int_0^T \omega^2\,dt\right]$$

T - duration of test

And for

$$\omega^2_{rms} = \frac{1}{T}\int_0^T \omega^2\,dt$$

it is

$$\bar{A} = \frac{\Theta}{2}\,\omega^2_{rms}$$

For Θ = const. and for nearly constant friction loads (to be assumed for a nearly uniform progress of flights which can be examined by means of the flight parameters) and for $\bar{\omega} = 0$ the value of ω^2_{rms} may be taken as a relative measure for pilot workload caused by the control of the work A required to control the helicopter in its axes.

3. MEASUREMENT OF THE LATERAL DEVIATION OF THE HELICOPTER FROM A GIVEN TRACK

In order to measure the lateral deviation of the helicopter from a given track a TV camera was mounted vertically under the helicopter facing the terrain. The image of the terrain was presented on an observer's monitor. Two horizontal lines were placed around the center of the monitor screen to define a given area ahead and aft the helicopter ground position (fig. A1). If, for example, the pilot tried to follow a road the image of the road on this monitor was tracked by the observer who moved an electronically generated cursor horizontally over the monitor screen so that it coincided with the image of the road within the area defined by the two lines. The system was calibrated so that the deflection angle β of the apparent cursor line of sight was known. And as the radio altitude h_R and the bank angle φ were also available the lateral deviation d of the helicopter from the road could be calculated as

$$d = h_R \cdot \tan(\varphi + \beta)$$

Static tests in hover flight at h_R = 150 ft showed that d could be measured with a tolerance of ± 5 %. In cruise flight at h_R = 150 ft and v(IAS) = 80 kts the tolerance was larger and in the order of ± 10 % to ± 15 %.

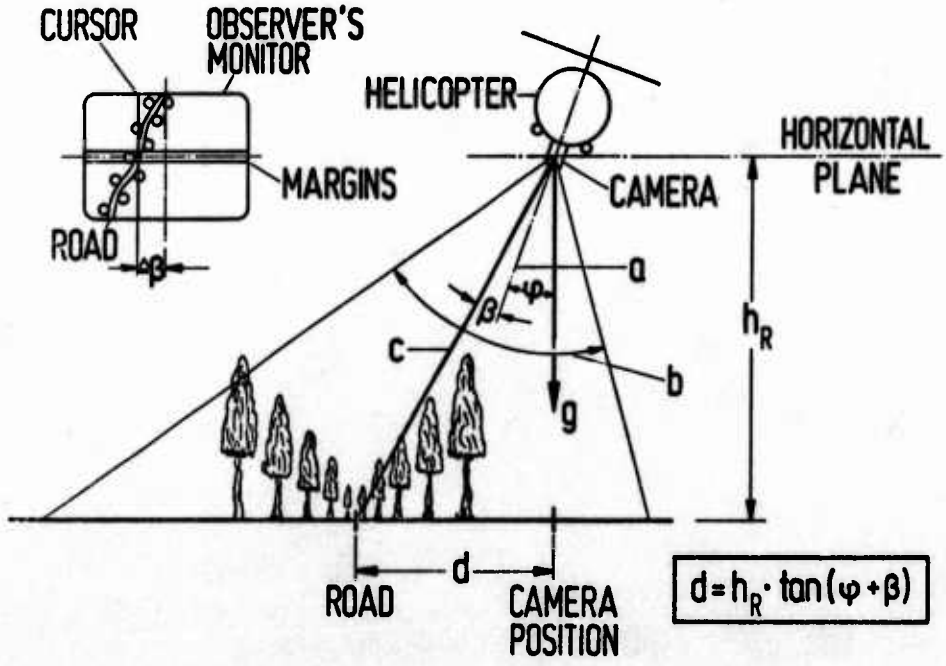

a) CAMERA LINE OF SIGHT
b) CAMERA ANGLE OF VIEW
c) CURSOR LINE OF SIGHT

Figure A1: Measurement of the lateral deviation d of the helicopter from a road

HUMAN ENGINEERING EVALUATION OF A COCKPIT DISPLAY/INPUT DEVICE USING A TOUCH SENSITIVE SCREEN

by

Klaus-P. Gärtner, Klaus-P. Holzhausen

Forschungsinstitut für Anthropotechnik, FAT
(Research Institute for Human Engineering)
D 5309 Meckenheim, Buschstrasse
Germany

SUMMARY

This paper describes a cockpit Touch Input/Output System which in effect integrates and combines several control and display functions of several airborne systems into one space which can be located in the primary control and display areas of the cockpit. This integration is accomplished by the use of touch sensitive virtual switching arrays on a CRT driven by sophisticated computer software. Various technical approaches to the touch sensitive aspect of this system are described. The Touch Input Control Device (TICD) and its possible application to airborne systems are discussed in some detail in terms of its advantages and reliability requirements. Several unique ergonomic problems associated with these new devices are identified. A case history application for selected airborne systems involving use of menu-select hierarchies of virtual keyboards is presented. The authors carried out an actual system simulation to demonstrate the operation and use of a TICD. A film of the simulation was prepared and a series of photos from the film are used as illustrations in the paper.

LIST OF ABBREVIATIONS

The following abbreviations were arbitrarily selected and used in our case study

Main Dispatcher

ENG	Engine Status
NAV	Navigation Receiver Frequencies
ANS	Area Navigation System
SYS	System State (e.g. Fuel System, Anti-Ice)
COM	Communication Transceiver Frequencies
CHK	Check Procedures
RTE	Route Maps (e.g. Departure, Approach)

Subdispatcher and pages

LST	List, of alphanumeric inputs of coordinates and frequencies
MAP	Map, for selections of waypoints and positions through direct touch input on maps presented on the screen
WP -	Waypoint select and readout plus numeral
T --	Track leg select plus numerals
POS	Position select and readout
VRT, UDT, FRQ, TRK, DIS, HDG, WND	Area Navigation related modes
PFL	Preflight checks
POF	Postflight checks
EMY	Emergency checks
DEP	Departure Map
ENR	En Route Map
APP	Approach Map
AL 1, AL 2	Alternate Approach
NXT	Next page
HLD	Hold freezes display
AUT	Automatic/Manual track change
ART	Alert Annunciator and Alert Information Switch
WRN	Warn Annunciator and Warn Information Switch
INS	Insert information to computer
ERS	Erase last entered information
HOM	Home, i.e. return to next higher Dispatcher level

1. INTRODUCTION

Recent advances in aircraft technology include the use of multipurpose displays in aircraft cockpits. A problem facing designers is the trade-off between single purpose and integrated multipurpose displays. Constraints such as limitation in cockpit space, display size and location requirements, and the increase in functional requirements will cause designers more and more to specify multipurpose displays. The use of CRT's gives the designer the possibility to present both symbolic and numeric information to the pilot in one electronic display that was previously presented with several electromechanical displays. This process is normally called display integration. The trend is to separate integrated display information used continuously for primary flight control from that used for other control functions. Primary flight display information is usually presented in fixed dedicated displays which provide information continuously in fixed formats and locations. Other display information used intermittingly for functions such as navigation, communication, weapon etc, can be called-up, modified and dismissed as necessary. Current reliability considerations force the designer to retain some dedicated conventional electromechanical instruments as a backup if a CRT is used for primary flight control. Reliability requirements for other display information can be satisfied by using two or more multipurpose displays.

The success of integrated displays suggests that similar integration measures with controls could provide similar space and operational advantages. Examples of switch integration include multifunction keyboards [1, 2] and multifunction switch designs [3]. Still further integration and advantages may be realised by combining display and control integration concepts to create a powerful integrated Touch Input/Output System which will be discussed later. With increasing use of computers and computer-driven displays in aircraft, the current problem for the aircraft designer is to create a man-machine interface for a Data Management System. The designer must satisfy ergonomic requirements not only for controls and displays but also for the interconnecting software which supports the pilot with strategies, alternatives and control programs. When integrating switch functions, most switch components must necessarily be multilegend switches which have certain inherent problems. Although a large number of switching functions can be combined into a relatively few multilegend switches, satisfactory ergonomic designs of integrated switching arrays are very difficult to achieve because not all switch functions are available at any one time. This means that some switch functions may not be available when needed.

2. A DEVICE FOR INTEGRATING COCKPIT SWITCHING AND DISPLAY FUNCTIONS

The concept of multifunction switching arrays is an essential part of any approach to integration of switch functions in airborne systems. Subsystems which an airborne operator may have to manage include communications, navigation, radar and other sensors, engines, weapons, etc [4, 5, 6, 7].

Operators of modern aircraft may also be provided with a map display of selected areas such as the terminal area or with displays of checklists for making various kinds of systems checks. Also pictorially displayed weapon guidance

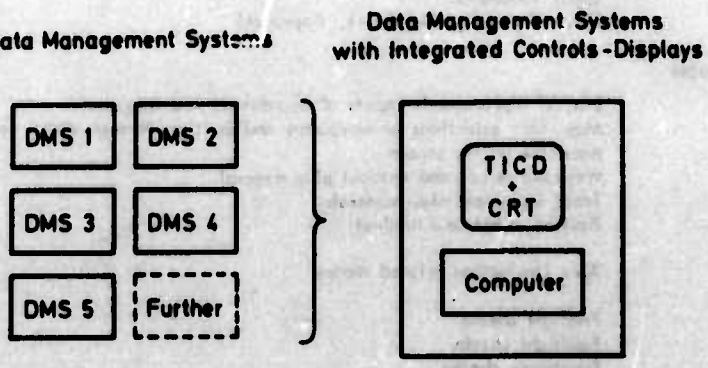

Figure 1. Integration of Data Management Systems' controls and displays by using a touch sensitive screen

information may be necessary. To integrate a variety of display and control functions from these different subsystems into one combined Input/Output System a completely new technical solution has become available. This is comprised of a CRT display with a Touch Input Control Device (TICD) attached to the screen which enables the operator to enter data into the system or perform switch actions by merely touching the screen with the bare finger or some pointing device. This system is symbolically represented on the right side of figure 1. On the left side of the figure the conventional arrangement of several systems, in this case data management systems, are illustrated each with its own dedicated controls and displays. With the TICD, data input manipulations on electronically generated maps or other computer-generated pictorial or graphical presentations are easy to realize. Multifunctional switching areas can also be designed very advantageously and they will appear to the operator as virtual keyboards of function switches. In this way the entire CRT screen can be considered as an integrated display control device and we thereby enter the area of computer driven, multifunctional virtual controls.

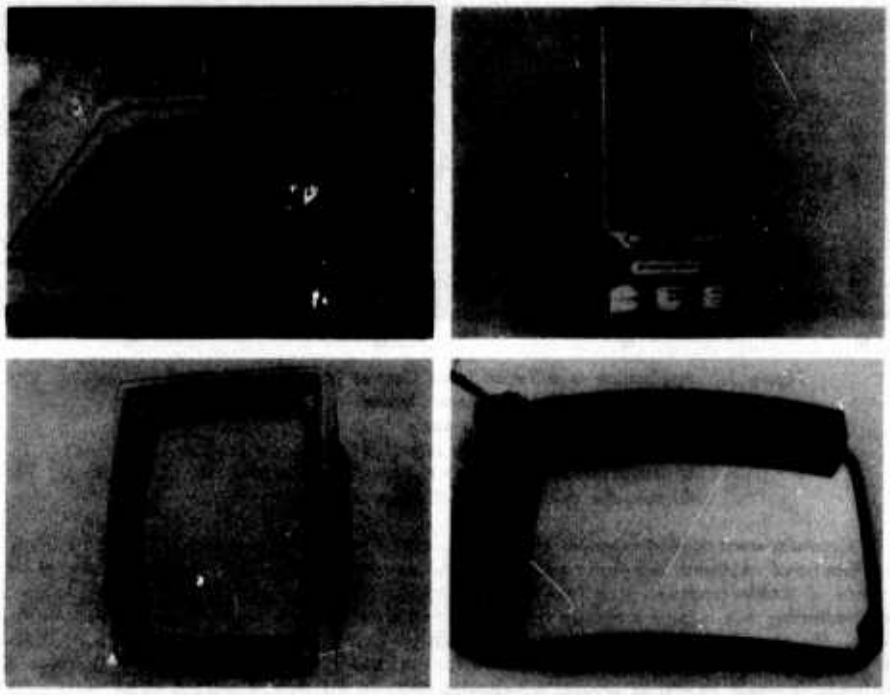

Figure 2. Various types of touch-sensitive screen Input Control Devices (TICD)
a. Touch wire sensor switch
b. Membrane push button switch matrix
c. Integrated LED matrix arrangement
d. Supersonic surface waves principle

Fig. 2 shows various technical solutions for touch-sensitive screens. All TICD's have in common the fact that the control surface is achieved through a "touch panel". This is an attachment over the CRT screen that enables the operator to interact with the computer directly. Fig. 2a illustrates touch wire control [8, 9]. By touching one of the electric contacts the finger produces a capacitance and resistance to earth which unbalances an inductance capacitance bridge. This produces a signal which can be used to activate switch functions by touching switch label or virtual push buttons which will be projected on the CRT screen directly above or below the wire. The activating speed is within a few hundred milliseconds. Figure 2b shows an Interactive Display Terminal [10, 11] consisting of a transparent membrane switch with 54 switch positions covering the display surface consisting of light emitting diodes (LED). Switch action is effected by the lightest touch of the finger on the surface of the membrane with a resolution of just under one centimeter which is quite sufficient for pushbutton or keyboard design purposes. Figure 2c and d illustrate two other systems enabling any part of the screen to be used for both control and display purposes. The one on the left is an integrated LED-matrix arrangement [12, 13]. An array of infrared light beams is projected across the display surface. The LED emitter and detector pairs are mounted opposite each other along the sides of the screen on a surrounding frame. The light transmitted between pairs forms a matrix of intersecting beams. Each point where two beams intersect is a touch point and by interrupting with the finger the signal will be logically decoded to generate the coordinates of the point. Figure 2d illustrates the most sophisticated touching technique involving the use of piezoelectrically excited surface waves on glass [14]. The surface waves are transmitted with ceramic piezoelectric transducers mounted on prisms which are glued to the glass. These waves propagate across the surface until they meet an obstruction such as a finger and are then reflected back to the origin. This returned wave is received by the transducer/prism combination and converted to an electrical signal which represents the touched coordinate or input signal for the system. The last two described touch input devices allow a resolution in the range of a few millimeters.

3. INTEGRATED INPUT/OUTPUT DEVICE APPLIED TO INFORMATION MANAGEMENT SYSTEM USING A TOUCH SENSITIVE SCREEN

A touch-sensitive control capability on CRT screens creates a combined control-display device which can be used to minimize the number of control and display devices required on at the same time improve accessibility for the operator. Accessibility in modern aircraft and airborne systems requires central location of the "universal" Touch Input Control Device combined with the advantage, that the display instrument the pilot is watching is simultaneously the control device. Individuals interacting directly with the computer while carrying out complex interactions may have blurred the distinctions between displays and controls. This is a new problem area for ergonomic and human factors attention. Cathode ray tubes provide fast switching access to graphical, pictorial and alphanumeric information which can be manipulated in many ways with advanced TICD's through programmable software.

a) b) c) d)

Figure 3. Application of a Touch Input Control Device to operation of an Integrated Flight Management System
a) numeric keyboard data entry
b) function keyboard mode selection
c) interactive flight track manipulation via ground map
d) computer controlled check list procedure

Figure 3 illustrates some applied examples of a Touch Input Control Device [also in 15]. In Figures a and b numerical and functional keyboards are displayed. Keyboards are virtual pushbutton arrays with the inherent peculiarity of an absence of tactile feedback. It is from an ergonomic point of view important to investigate conceivable supplementary feedbacks, e.g. visual indicators on the touched screen area or auditory signals after having touched one of the keys. The numeric keyboard in virtual form would be used as any other numeric data input device. The alphanumeric keyboard in virtual form may be unsuitable for use as a typewriter type keyboard because of lack of finger position cues. It would instead be used as a switching array in the form of predetermined function switches or in the form of coded action and object switches. Each functional switch can be used as a main dispatcher which calls up additional switching arrays involving specific subfunctions or lateral functions. Figure 3c illustrates a map design. The screen may be programmed to act as a window on a large scale drawing or map that can be moved continuously or stepped by a switch function to permit a search of relevant information. Techniques for zooming into the display to examine sections in greater detail are available. As shown in the figure, flight track manipulations of the ground map will help a pilot while interacting with the system and gives him a comprehensive picture of his flight situation. Figure 3d finally, illustrates the application to checklists. Checklist items are scanned by the operator and checked-off by touching an associated pushbutton. Check-off actions can be fed into a storage device for later verification.

Since the integrated Input/Output System combines both controls and displays, at least two of them should be present in any cockpit for reliability purposes. In the case of a twin-seated aircraft three such devices may be required. Figure 4 shows a possible arrangement of two integrated Touch Input/Output Devices in a twin seated aircraft. Two CRT's each with touching areas or "writing surfaces", one each for the pilot and copilot can replace considerable number of instruments on the panel. In addition to the two devices configured here as a master control panel, a cockpit should have a master inform panel for radio frequencies to permit constant and immediate access by pilots to this information without going through a menu-select procedure explained later. If a third Input/Output Device is included for reliability reasons it can conveniently be used for auxiliary control display functions, for example such a device could display departure and approach maps.

An inherent aspect of an integrated virtual control/display for Input/Output Systems is the necessity for organizing switching possibilities into functional areas called "pages" and "chapters" and programming an orderly hierarchical summoning procedure for calling-up and dismissing virtual keyboards as needed. In figure 5 is an example of a random and sequential menu page selection hierarchy. The highest level of the hierarchy is frequently called the Main Dispatcher which provides random access to options on the second level. Second level options are called sub-dispatchers which in turn provide random access to selected third level options called "chapters". Within selected "chapters" is a series of sequential "pages". There is a real possibility of overloading the pilot with a variety of manual data input procedures with this menu technique. To minimize the delaying effect of sequencing through the hierarchy of levels to make a switch action, a detailed analysis of supporting software structure is recommended. This involves a thorough planning of access paths using an ergonomically designed menu technique.

4. A CASE STUDY APPLICATION OF AN INTEGRATED INPUT/OUTPUT SYSTEM TO SELECTED AIRBORNE SYSTEMS

To provide the capability for manipulating various flight subsystems through a single Input/Output System, various switching options must be organized into a hierarchy of levels using menu techniques. In the case study we organized our various functions into the hierarchy illustrated in figure 6.

The operator begins with a main "home" menu or Main Dispatcher which is a virtual function switch array shown in the upper left of figure 6 and in figure 7. The operator will always return to this any often having performed sequential functional task. Seven functional options are represented on the Main Dispatcher by separate virtual function switches. Four of these are described in further detail on subsequent levels of figure 6. They are communication frequency selection (COM), checklist selection (CHK), route map selection (RTE), and Area Navigation System (ANS).

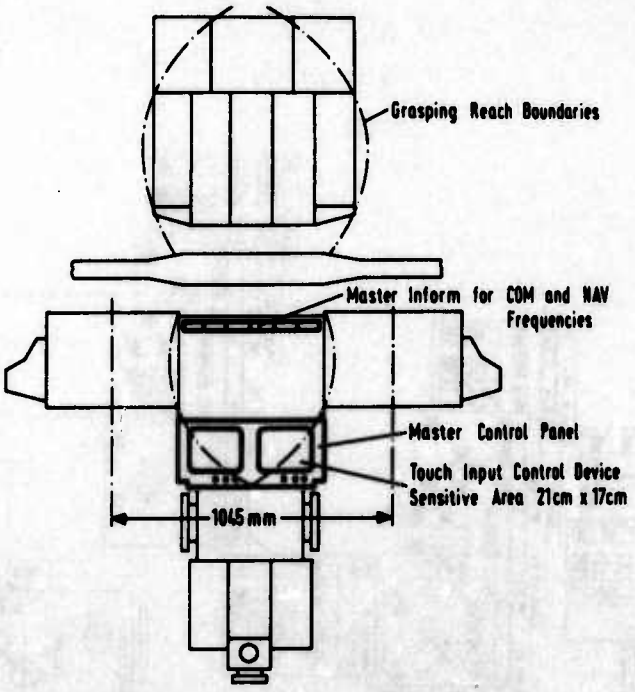

Figure 4. Possible arrangement of two Touch Input/Output Devices in a twin seated aircraft based on an Airbus A 300 B Cockpit

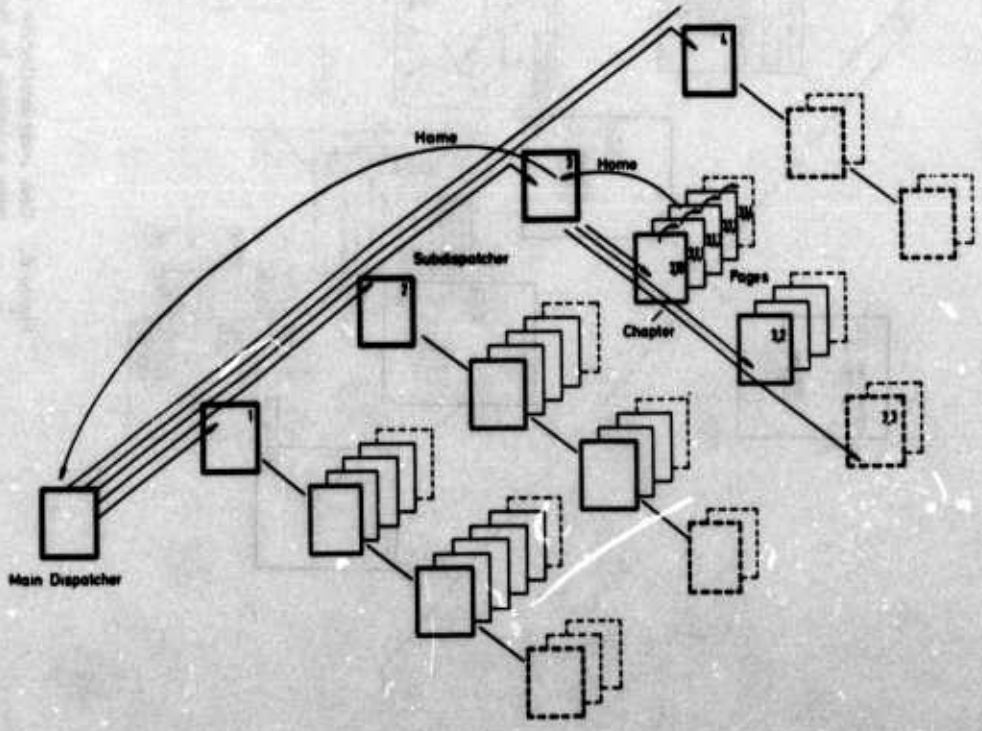

Figure 5. Random and sequential menu page selection hierarchy for information management with a single data Input/Output Device

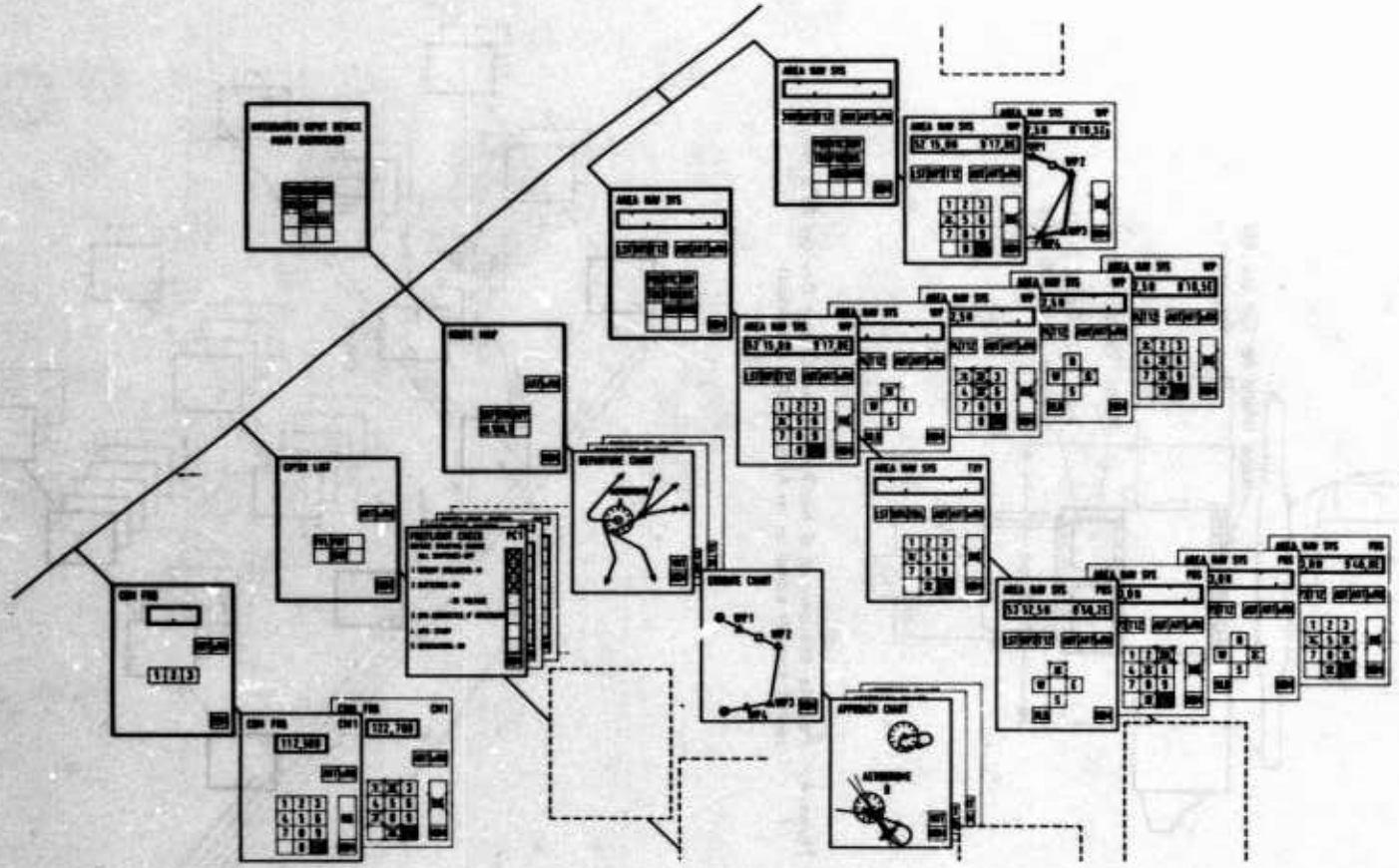

Figure 6. Case study application of an integrated Touch Input/Output System using menu techniques for the operation of various airborne systems in a computer equipped aircraft

Depending on the complexity of each subsystem the random and sequential selection procedure is more or less expanded. For example, the COM frequency selection process is less deeply structured than the Area Navigation System. The Area Navigation System is illustrated with two different possible waypoint selection techniques, one of which is only possible with the virtual Touch Input/Output System. This is the direct touch indication of waypoints on a displayed graphical map to the computer. The other selection technique involves the conventional entry of navigational coordinates.

To illustrate the various operational advantages of the integrated Touch Input/Output System some simulated procedures were filmed and will now be described in more detail. A film of our laboratory simulation was prepared and a series of selected photos from that film are included and discussed. We select as a first example the procedure in calling up and performing a preflight checklist. The category "checks" is selected by touching the appropriate switch (CHK) on the Main Dispatcher (figure 8). As a result of this action the Main Dispatcher disappears and the Checklist Subdispatcher appears (figure 9) . In these and other figures it may be noticed that the operator has a LED attached to his finger. This is part of a Selspot System described in chapter 5. The operator next defines the desired check procedure as the preflight check procedure by touching the virtual switch PFL (figure 10) which results in the appearance of the first page of the checklist. Any number of pages to the checklist can now be operated

Fig. 7 Fig. 8 Fig. 9

Fig. 10 Fig. 11 Fig. 12

upon with computer assistance and automatic documentation (figures 11, 12). Some questions on the checklist can be answered automatically by computer inquiry and sensory feedback. Those which can't will have adjacent virtual pushbuttons on the right hand side which the operator checks-off by touching with his finger when conditions permit it. After checking-off all items on the first page the checklist processor will automatically sequence to the next page. This sequential access is sufficient at this level. The pilot can at any time interrupt the sequence by touching the home key (HOM) in order to return to the Checklist Subdispatcher and finally to the Main Dispatcher.

Before take-off the pilot might require a quick look on a departure map that he selects by activating the Map or Route Subdispatcher (figure 13) and at that level by touching the departure map pushbutton (figure 14). Following these two touch operations a map display (figure 15) of the departure airport is shown on the screen containing departure routes and other information concerning the airport terminal area.

During flight the pilot can tune communication transceivers as well as navigation receivers with the integrated Touch Input/Output System. This is accomplished by touching the COM virtual key on the Main Dispatcher (figure 16) and in case of a triplexed communication transceiver arrangement the appropriate number of the required communication transceiver. If communication 1 is to be selected as an example the pilot would touch the pushbutton containing number 1 on the Route Subdispatcher (figures 17, 18). This action is followed by the display of a numeric keyboard and the selected channel number 1 in the upper right hand corner of the Input/Output System (figure 19). Additionally, the previously selected frequency is displayed. This frequency is also displayed in the Master Inform Panel, so that

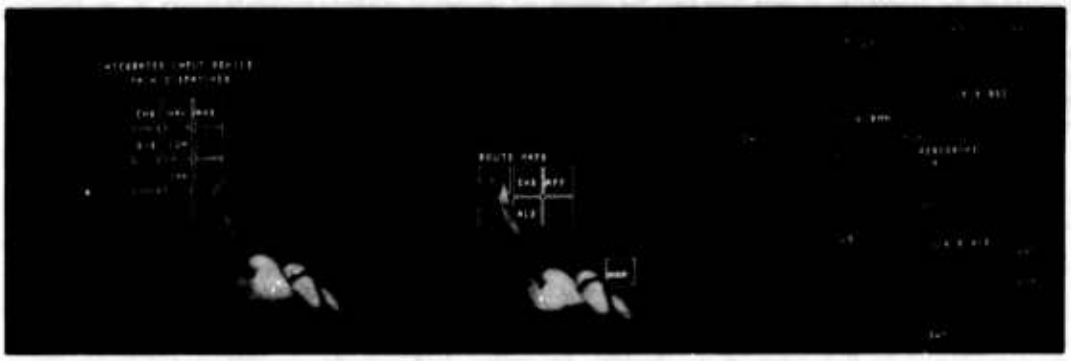

Fig. 13 Fig. 14 Fig. 15

the pilot need not go through the select procedure to find out his current COM frequency. To enter a new frequency the pilot touches the digits on the virtual numeric keyboard (figure 20). After touching the insert virtual button (INS) (figure 21), the system checks whether the entered frequency is acceptable or not and in case of an error, flashes the Alert button. The Alert and Warn buttons are here shown empty to demonstrate nominal operation. The pilot would then correct his error and enter the correct frequency. If the input error is less obvious, the pilot could touch the Alert display switch which also serves as an error status inform request button in order to call-up a detailed error condition list. NAV frequency selection would be accomplished in the same way be touching the NAV button selecting the appropriate receiver and entering the new frequency.

Another system that could be operated through the Touch Input/Output System is the well known Area Navigation System (figure 22). Our simulation is based on Littons LTN 72-R now used by German Lufthansa. After selection, the pilot sees a display area with double lines dedicated to show position and waypoint coordinates as well as six labeled virtual keys that are mainly used for mode display and select purposes and further down a dedicated keyboard with various ANS-function (figures 23, 24).

First shown is a position check during flight by activating the position check button (POS) (figure 23) resulting in the output of the present aircraft position in latitude and longitude. Also displayed is a latitude-longitude select keyboard in case the pilot wants to enter his present position as necessary on the ground after warmup of the ANS.

Fig. 16 Fig. 17 Fig. 18

Fig. 19 Fig. 20 Fig. 21

Fig. 22 Fig. 23 Fig. 24

Another function enables the pilot to request a readout of certain preprogrammed waypoint coordinates and to enter new waypoint data. The waypoint function is selected by touching the waypoint virtual switch (figure 25) which also serves as a readout of the last waypoint previously selected. That calls up a numeric keyboard with which the number of the next waypoint may be selected and inserted into the computer (figures 26, 27). This action normally

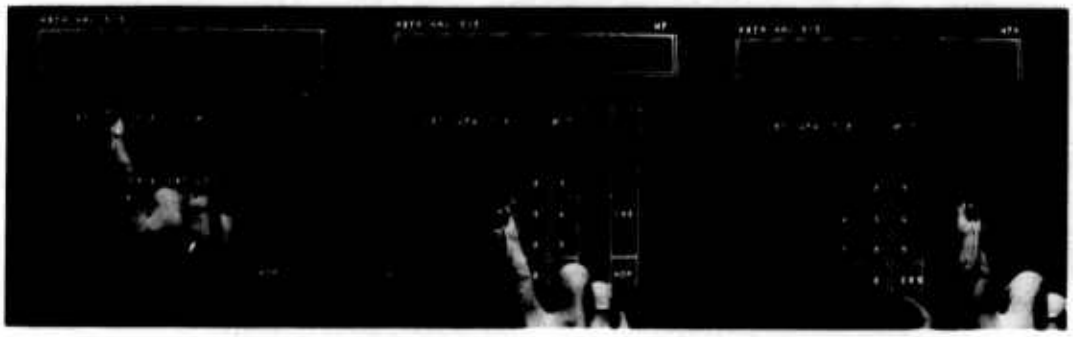

Fig. 25 Fig. 26 Fig. 27

Fig. 28 Fig. 29 Fig. 30

Fig. 31 Fig. 32 Fig. 33

Fig. 34 Fig. 35 Fig. 36

Fig. 37 Fig. 38 Fig. 39

Fig. 40 Fig. 41 Fig. 42

Fig. 43 Fig. 44 Fig. 45

results in a display of the previously entered coordinates for this specific waypoint in latitude and longitude. But since a fourth waypoint had not yet been entered no coordinates are displayed. These must now be entered. A special lat.-long. select keyboard appears which enables the pilot to select North or South latitude and West or East longitude as appropriate for each coordinate input. After selecting North latitude first (figure 28) the lat.-long. select keyboard is again replaced by the numeric keyboard and the first coordinate is keyed in and inserted into the ANS computer (figure 29). This same procedure is repeated for the second half of the coordinate which is East longitude (figure 30, 31, 32, 33).

The same waypoint entry can be accomplished by using the map option instead. This map option is selected by touching a virtual switch which serves both as a list/map switch and as a current mode display (figure 34). After touching this switch its legend changes to MAP and future functions called up in the ANS will use a flight map for appropriate inputs and outputs. Again the desired waypoint is selected by keyboard entry (figures 35, 36, 37). The system now switches to the map display and as such lists preprogrammed waypoints on the intended flightplan (figure 38). To define the fourth waypoint, which was not yet entered into the system, the pilot will touch the appropriate checkpoint on the map itself thereby selecting the fourth waypoint (figure 39). A label is added to the selected waypoint on the map and the planned track is lengthened from waypoint 3 to 4 as indicated with a dashed line. The selection of this waypoint is confirmed and will be accepted by the system as soon as the pilot touches the insert key (figure 40). The waypoint coordinates are then repeated by the system in digital form (figure 41) until the operator uses the HOM key to return to the ANS-Subdispatcher and subsequently to the Main Dispatcher.

En route or in the terminal area the aircraft might be requested to perform a track leg change requiring the pilot to leave the predefined flight track by reprogramming the area navigation system to guide the aircraft directly to the new destination point. This is demonstrated by using either the list or map mode. In any case, the track leg switch is activated (figure 42). This switch normally serves as a readout of the track leg designation the aircraft is currently flying. The numeric keyboard that appears after this action permits the track to be changed. A track leg change to undefined waypoints would cause an error condition. Here in our example the pilot wants to fly from his present position, which is defined as waypoint 0 directly to waypoint 4 such as shortening an approach to the terminal area, for example (figures 43, 44, 45).

In the map mode the flight map is used instead. After selecting the track leg change function (figure 46), the track leg change is performed by touching the aircraft's present position (figure 47) and the next desired waypoint (figure 48).

Before landing the pilot might require an approach map of the destination airport which he can select from the Main Dispatcher and Map-Subdispatcher (figure 49). The approach map (figure 50) is dismissed by touching the HOM-key to return to the subdispatcher level and again to sequence back to the Main Dispatcher (figure 51).

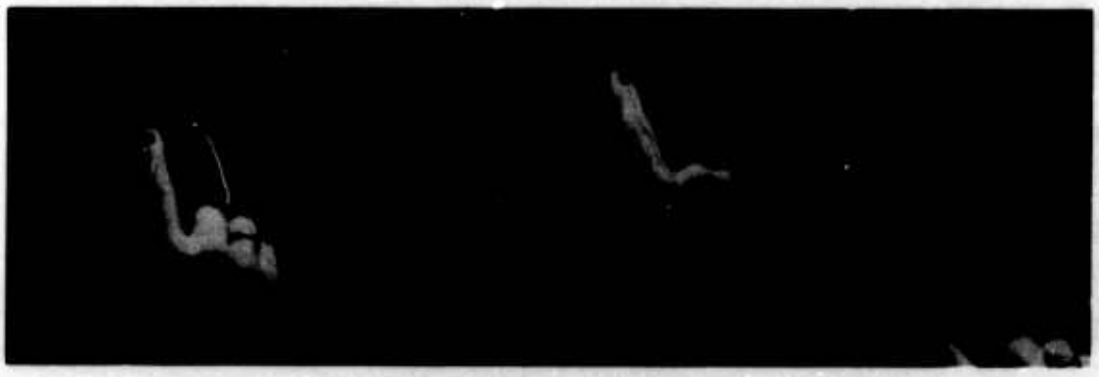

Fig. 46 Fig. 47 Fig. 48

Fig. 49 Fig. 50 Fig. 51

5. ERGONOMIC ASPECTS DISCOVERED DURING SIMULATED OPERATIONS WITH THE INTEGRATED TOUCH INPUT/OUTPUT SYSTEM

An Integrated Touch Input/Output System as discussed earlier was simulated at FAT. The operator's inputs in response to displayed functions were accepted through a Touch Input Control Device (TICD) in real time. The TICD used was different from any of the TICD types described earlier. It was instead a Selspot System [16] consisting of an IR LED attached to the top of the operator's pointing finger and tracked by an overhead camera. A computer program translated position and time data into switch actions and provided a means of storing finger trajectories from the operator's rest position to the virtual switch in a form lending itself to exact dynamic analysis of operator actions. Although the Selspot system is not recommended for use in actual operational systems, it was selected for our simulation because of these experimental advantages. While operating with random and sequential menu techniques described in detail earlier during preliminiary studies, subjective impressions were that TICD operations are convenient, effective and natural.

A comparative ergonomic evaluation of a Touch Input/Output System with current conventional cockpits would be very difficult because of lack of standardization in cockpit equipments and their location. However if the need of integration is accepted, the primary ergonomic objective of optimizing the integrated Input/Output System itself is sufficient. Some design aspects with this new device which requires ergonom's attention include such visible aspects as virtual switch size, distance between them, the number and arrangement required for various applications, switch shape and color. Other less obvious but equally important ergonomic considerations include types of feedback and the interacting software structure and design behind the screen. First experiments with six operators and various sized round virtual switches showed that key activation time decreased significantly when switch size was increased from 11 mm diameter to 22 mm but not with size increases beyond 22 mm up to 33 mm. These results imply that virtual switches may require larger sizes than minimum electro-mechanical pushbutton diameters perhaps due to the lack of tactile feedback of whether or not the key is actually hit properly. The operator must rely more on visual feedback or auditory feedbacks can be added in the form of "on and off" key tones. Total activation time with all switch types include actual switch activation time in addition to finger positioning time. With virtual switches this activation is nearly instantaneous which is an advantage over conventional pushbuttons.

This paper can only illustrate a few of the possibilities for such an integrated system in future aircraft cockpit. Use of integrated Touch Input/Output Systems as described should help to save cockpit space and open up numerous new possibilities for crew interaction with flight systems. Although a large amount of onboard computer capacity is required this is available today with miniaturized airborne computers. Further experimentations with such integrated systems is necessary to provide comprehensive ergonomic design guidelines for designers of further aircraft.

6. REFERENCES

[1] de Callies, R.N. — Development of Human Engineering Standards for Multifunction Keyboard Design
IEEE 1976 International Conference on Cybernetics and Society held Nov. 1-3, 1976 in Washington, DC , 76 CH 1137 - 9 SMC

[2] Fenwick, C.A.; Craig, W.H. — Keyboard Data Entry in Avionics
Society of Automotive Engineers, Business Aircraft Meeting, Wichita, Kan., April 8-11, 1975, Paper 750 522

[3] Graham, D.K. — Multifunctional Switching, Methodology and Evaluation
Boeing Aerospace Company, Research and Engineering Division Seattle, Washington

[4] Elson, B.M. — Navy Expands Simpler Cockpit Displays
Aviation Week & Space Technology, July 11, 1977

[5] Elson, B.M. — Aircraft Systems Monitor Under Study
Aviation Week & Space Technology, August 4, 1975

[6] — Strike Fighter Aircraft
Electronic, Electro-optic and Infrared, Countermeasures, April 1977

[7] Armstrong, L. — DAIS takes center stage
Electronics, February 6, 1975

[8] Orr, N.W.; Hopkin, V.D. — The Role of the Touch Display in Air Traffic Control
The Controller, 11(1972), Nr. 1 - 4

[9] — UAC Maastricht
Europäische Organisation zur Sicherung der Luftfahrt
Rue de la Loi, B-1040 Brüssel, 1974, Belgien

[10] — Interactive Display Terminal (IDT), Technical Data Sheet
Litton Data Systems, 8000 Woodley Avenue, Van Nuys, Cal. 91409, USA

[11] Input/Output Display Communications Terminal
product spec. brochure, Data Systems Division, Litton Industries,
8000 Woodley Avenue, Van Nuys, Cal. 91 409, USA

[12] Digitatron DI 570
product spec. brochure, Thomson-CSF T-VT, Rue de la Grange Dame
Rose, BP 34, 92 360 Meudon la Foret, France

[13] Touch Input System
product spec. brochure, CARROLL MFG.CO., 1212 Hagan,
Champaign Il. 61820, USA

[14] Touch Sensitive Digitizer Direct to Computer Interface
product spec. brochure, Instronics Limited, Stittsville, Ontario, Canada

[15] Holzhausen, K.-P.
Gärtner, K.-P.
Eine Berühreingabe als Alternative zu Tastenfeld und Rollkugel
des Radarlotsen am Schirmbildarbeitsplatz bei der bodenseitigen
Flugführung
Jahresband 1977 of the Deutsche Gesellschaft für Luft- und Raumfahrt
Goethestraße 10, 5000 Köln 51, Germany

[16] The Selspot System
product spec. brochure, Selective Electronic Company
Box 30, S-43 121 Mölndal, Sweden

PROPOSAL FOR A COST EFFECTIVE RADAR NAVIGATION SYSTEM FOR LOW ALTITUDE AND TERMINAL AREA FLIGHT

E. Wildermuth
Institut fuer Flugnavigation der Universitaet Stuttgart
Keplerstrasse 11, 7000 Stuttgart
Bundesrepublik Deutschland

SUMMARY

In a time of considerable economical difficulties and rapidly growing expenses for modern military systems one should spend sufficient time and effort for considerations, how, without high costs, already existent and well proved equipment can be made more useful and effective that it may be kept in service yet for a considerable time.

The Institute of Air Navigation of the University of Stuttgart has designed on this basis a selfcontained Radar Navigation System which in many ways may meet the requirements for a navigation system suited for low altitude and terminal area flight.

1. INTRODUCTION

If we consider the development of navigational performance during the past decade, and if we think, which aims in this respect are already within reach, we find that it should be possible to equip all modern aircraft with navigational systems producing extremely good navigation results, each system permitting always to select that mode and kind of display which seems best for the specific mission.

High costs however and lack of time do often not allow to elaborate the very best solution and to realize it. Thus we meet today sometimes the tendency to provide modern aircraft only with a minimum of navigational equipment which satisfies hardly the most modest navigational requirements.

A solution for this problem could often be found in the integration of the various navigation systems already belonging to the basic equipment of the aircraft, improving thus the operational effectiveness so much, that expensive new developments are not necessary.

In my paper I want to demonstrate on a practical example how the effectiveness of a relatively aged autonomous navigational equipment of a close support aircraft could be improved so considerably, and that nearly without additional costs, that it may comply with numerous demands requested for an autonomous navigational system for low altitude and terminal area flight.

The demand for such a system has been induced to us during a period of flights for the evaluation of an automatic map display, where we were involved simultaneously with data gathering for our researches on "Integrated Air Navigation". During these flights we looked for a means of reliable dead reckoning position fixes which we could include into the "Integrated Air Navigation". Because however we could carry out our intentions only within an already running flight program, we had rather restricting conditions for our plan. These restrictions were: No money, no changes within the existent navigation equipment of the aircraft, very little time for development and no extra flights for flight evaluation.

These four preliminary conditions in mind we started our reflections. First we looked over the present navigational facilities within the aircraft in question. The basic autonomous navigation equipment of the C-160 - Transall - (fig. 1) consisted of the dead reckoning system PHI 3-B-10 of Computing Devices of Canada, the Doppler Radar Set DRA-12B of Bendix, the Sperry Reference Systems CL 11 and SYP 820. To the outfit of the Transall belongs furthermore the Weather Radar Set RDR-1DM of Bendix. This basic navigation equipment had been completed for evaluation purposes by a dead reckoning navigation system, the so called Automatic Map Display AKT5, system Teldix-Ramsayer.

If we now reflect upon figure 1 and if we have in mind the problems connected with radar position finding and with dead reckoning navigation, we instantaneously wish to combine the two systems, because both systems have ideal complementary qualities. Whilst on the one hand the dead reckoning navigation system computes continuously the aircraft position and the distance and course to every target contained within the navigational chart of the map display, simplifying thus very much the identification of radar returns on the radar scope, it is very easy on the other hand, to update automatically from time to time the dead reckoning position by means of radar position fixes.

2. AN ECONOMIC SOLUTION TO SIMPLIFY RADAR POSITION FINDING

Now on account of completeness let me say a few words about problems connected with radar position finding. The plan position indicator of the radar set presents a map like picture of the terrain below and around the aircraft. To use this radar picture as a means for navigation it is necessary to correlate its features with the symbols of the navigation chart. This however is often very difficult because in most cases the radar picture on the PPI is very different from that presented by the navigation chart. Therefore correlation between radar- and chart-picture has been automatized in modern and complex autonomous navigation systems, or it is done semi-automatically by superimposing both pictures.

These methods however are rather expensive. Therefore we used the vector to the target, to combine the two systems with one another (fig. 2). This vector is delivered to the navigator by both systems. On the radar scope the distance R and the relative bearing B_R to a target are measured. If the scope employs no azimuth-stabilization the relative bearing must be added to the true heading respectively grid heading to obtain a grid bearing α_G to the target.

The dead reckoning system as well computes continuously the distance R' and the grid bearing $\alpha_{G'}$, when the target-coordinates are stored in the memory of the navigation computer.

Due to the well known inaccuracies with radar bearing- and distance-measurements and due to dead reckoning errors the vectors to the identical target, delivered by the two systems, will usually not be in full conformity with each other.

Eventually radar slant range must be converted to ground range, which, as you know, could be accomplished automatically with little expense. Besides with low level flying this transformation will not be necessary because here the slant range to the target will always be at least more than twenty times the difference of altitude between aircraft and target, which would lead to a distance error of about .1 %.

If however every now and then - for example every ten to twenty minutes - dependent on the dead reckoning sensors - radar updating is carried out, which can be done very easily and quickly with this integrated system, both systems are always sufficiently in accordance to permit the integration of both systems in this manner.

3. RADAR NAVIGATION SYSTEM

Fig. 3 shows the integration of a dead reckoning navigation system with a radar system. The dead reckoning navigation system is composed of a navigation computer, a map display and a homing indicator. Both systems are switched together by means of a radar coupling unit.

3.1 Radar Coupling Unit (RCU)

The Radar Coupling Unit links the weather radar set with the dead reckoning system without the need for any changes within the aircraft navigation equipment. The RCU is connected with the Radar Display Unit by means of two plugs interconnected to the power supply- and video-lines and it is fed from the dead reckoning system with the range- and bearing-signals to a target. This target will be selected in the navigation chart of the map display. The two signals are used to servo an electronic marking aid on the PPI, produced within the RCU.

Figure 4 shows a functional diagram of the RCU. Due to reasons of simplicity a special kind of electronic marking aid on the PPI has been chosen which could be realized easily. It consists of an additional range marker on the PPI, whose radius and length of arc are variable. By turning the range-knob, the R/C-value of the range marker generator can be changed. Thus the turning angle of the knob corresponds to the distance to the target. The length of arc of the range ring will be determined by adjusting a synchro receiver with the bearing knob. This synchro receiver will stop the range marker generator when it is in coincidence with the respective synchro transmitter within the antenna unit. By this the turning angle of the bearing knob corresponds to the relative direction to the target, if properly adjusted. To measure the distance and relative bearing to a radar target the end of the arc of range will be moved to the radar echo on the PPI. Two synchros, connected with the control knobs, will transmit the data for further indicating and processing purposes. An erase switch can be activated when the marking arc shall be visible within an expanded radar echo. Thus it is possible to set the measuring edge of the marking arc to every point within an extended target return.

To move the marking aid on the PPI automatically two servo systems, driving the control knobs, can be switched in. By this the range and bearing signals of the navigation computer control the two servo systems and the electronic marking aid will lock on the radar echo, selected within the map display.

For updating and averaging purposes the data measured with the control knobs can be corrected by means of two differential control knobs, thus superimposing manually the computer-controlled movement of the marking aid on the PPI (fig. 5).

The RCU had been composed of parts and subsystems already existent. It had been provided with extra dials and a counter for evaluation purposes. Fig. 5 shows the RCU with its four subunits. The upper left subunit contains a bearing control knob with a dial, indicating the relative radar bearing to the target and a bearing correction knob. The upper right one contains a distance control knob with a distance counter and a distance correction knob. The lower left subunit, containing the electronics for TACAN-adaption and coordinate transformation, is furnished with a grid bearing dial. The lower right one serves as control panel. This subunit contains the electronics which produces the marking aid on the PPI.

3.2 Junction Box

Within the Junction Box the navigation signals will be distributed to the respective units, depending on the functional modes, selected on the RCU.

3.3 Automatic Map Display AKT5-2

The basic design of the Map Display (fig. 6) has been made by the Institute of Air Navigation of the University of Stuttgart. It has been produced as a sample map display by Teldix Ltd., Heidelberg at the request of the German Ministry of Defence and was thought to improve the navigation system of the Transall close support aircraft. With little expense it can be adjusted to other aircraft navigation systems too.

To be of optimum use the map device serves not only as a position indicator but it permits the navigator as well, to draw, plot and write on the navigational chart in its usual way.

The map display uses a roller map which can be composed of chart strips, each 40 cm wide. The strips will be pasted together to a maximum length of 37 m resp. 121 ft. The roller map may contain charts of six different scales, i. e. conventional large scale air navigation charts with the scale 1:0,5, 1:1, 1:2 millions and small scale navigation charts with the scales of 1:5, 1:10, 1:20 millions. The small scale charts serve as index diagram for the large scale charts. An area of 6000 km by 6000 km can be covered by a roller map, using hundred chart-leaves, 40 cm by 40 cm of the scale 1:2 millions and ten index-leaves, with the scale 1:20 millions. The actual chart number of each map scale is shown continuously on a digital counter.

The aircraft position is indicated by a light spot bright enough to be seen in full sun shine.

During the flight every scale can be chosen any time without necessity of resetting the light spot.

An important feature is the very simple possibility of updating the system when the exact aircraft position is known otherwise, for example from ground facilities, visual observations or airborne radar. There is no need to read actual position coordinates in the navigational chart and to feed them manually into the computer. It suffices to set the position light spot in the roller map on the actual aircraft position and to press the updating button.

In this simple way the coordinates of every landmark or target, contained within the large-scale-charts can be stored. Thus distance and track to the target will be computed continuously and displayed on the homing indicator of the system.

3.4 Homing Indicator

During the evaluation flights the Homing Indicator could be alternatively fed with navigational data delivered either from the dead reckoning system PHI-3B10 or from the Automatic Map Display AKT5. The control panel of the Roller Map Unit contains the corresponding mode selector switch. The indicator can furthermore be used to indicate radar data. For this purpose the distance and bearing data from the RCU will be switched to the indicator instead of the signals from the dead reckoning systems.

4. THE RADAR NAVIGATION SYSTEM IN PRACTICAL USE

Fig. 7 shows the operational modes of the Radar Navigation System. From these only three basic modes could be tested during the evaluation flights due to shortage of time. These three modes: Radardata-Control, Targetecho-Detection and Radar-Updating however give an impression of the accuracy and advantage of the whole system and permit to draw conclusions with regard to the usefulness of the other three modes: Targetecho-Identification, Aircraft-Radarposition-Display, and PPI-TACAN-Beaconposition.

4.1 Radardata-Control

To be sure that radar data can be used for position updating it is advisable to compare these data with those gained from the navigation computer. For this the distance and bearing information R, B_R gained with the Radarsystem will be frozen simultaneously with the corresponding information R', B_R' of the dead reckoning system. Both informations will be switched quickly one after the other to the homing indicator and be compared. If there exists a considerable difference between the corresponding values, for example a difference of more than 2 naut. miles in distance and more than 3° in bearing the radar position determination should be repeated. This can be done very easily because the marking aid on the PPI is servoed. Therefore only differential corrections must be applied to the marking aid on the PPI by means of the corrections knobs of the RCU.

4.2 Radarecho-Detection

Often it is desirable to find out if special targets or certain objects printed into the navigational chart produce a good radar return on the PPI. For this purpose the navigator sets the position light spot in the store-mode of the map display on the target in the chart and switches to "Targetecho-Detection". The marking aid on the PPI is then servoed to the corresponding spot respectively radar echo with dead reckoning accuracy. It locks on the echo controlled by the navigation computer.

4.3 Targetecho-Identification

The mode Targetecho-Identification will be especially useful in practical radar navigation. To identify a targetecho on the PPI the electronic marking aid will be put on the echo by turning the respective control knobs of the RCU. Thus the distance and relative bearing will be transfered in this RCU-mode to the automatic map display to control the position light spot within the navigation chart, where it indicates now the radar target belonging to the selected radar echo with dead reckoning accuracy.

4.4 Aircraft-Radarposition-Display

To indicate the radar-position of the aircraft in the navigation chart, the RCU will be switched to "aircraft-radarposition" and the marking aid on the PPI will be set manually on a targetecho by means of the two control knobs. The coordinates of the appertaining radar target will be put into the computer store as described before - see 3.3 -. Now the radar-position of the aircraft is indicated in the map display as measured with the radar set.

4.5 Radar-Updating

If in any mode a difference between the radar-position and the dead reckoning position of the aircraft is observed, automatic radar-updating of the dead reckoning system can be executed. For this purpose the map display will be switched to "store" and the position light spot will be set on a radaractive target in the navigation chart. Thereupon, after switching to "Targetecho-Detection", the marking aid on the PPI will be servoed to the respective targetecho, missing it by the error vector $-\underline{E}$ (fig. 8). Then with the correction knobs of the RCU the marking aid will be moved exactly to the radarecho producing thus an updating signal. This signal serves, after pressing the updating button of the map display, to correct the dead reckoning navigation system. When the map display is now switched to "NAV", the updated aircraft position is indicated in the navigation chart.

- This updating feature was not yet embodied into the AKT5 during the evaluation flights. Updating has been executed therefore only manually as described before (see 4.4). -

4.6 PPI-Position of TACAN-Beacon

Sometimes it may be very useful to know the latitude and longitude or the coordinates of a reference point on the PPI in relation to which radar echoes can be identified. If the aircraft is equipped with a TACAN receiver for example, the marking aid on the PPI can be controlled by the TACAN distance and bearing signal, thus indicating the position of the TACAN-beacon. If there is a radar return of this beacon visible on the PPI, the rate of coincidence between marking aid and radar return gives information about the exactness of the radar positioning. For this purpose the RCU contains a TACAN-adapter to transform the signals from the TACAN receiver accordingly.

5. TWO METHODS FOR BETTER RADAR FIXES

5.1 Position-Updating with Averaged Multiple Radar-Position Data

The accuracy of radar fixes can be improved considerably by averaging multiple radar-position data. For this the coordinates of the radar target will be put into store by positioning the light spot of the map display accordingly - see 4.2 -. After switching to "Targetecho-Detection" the marking aid is servoed to the respective echo on the PPI. To get mean position values, the distance and bearing to the target will be measured several times by adjusting the marking aid with the correction knobs only. The values will be averaged and the correction knobs adjusted accordingly. Now an automatic updating can be initiated. Finally the two correction knobs are turned back into their zero position for further measurements.

5.2 Multiple Range Radar Fixes

For reasons of better accuracy, position fixes from multiple range measurements are often preferred. To get good results however the time difference and with that the distance flown between the two or more range measurements must be regarded. This can be done very easily by means of the roller map and it may be explained with a few words.

In figure 9 L_1 and L_2 are the two incorrect dead reckoning positions, indicated in the map display by the light spot at the time t_1 and t_2, when the radar ranges R_1 and R_2 to the targets T_1 and T_2 are determined. To take into account the distance Δs flown by the aircraft between t_1 and t_2, the first radar target T_1 will be moved to T_1' in the navigational chart by the dead reckoning distance Δs. - This will be very accurately equal to the actual distance flown between t_1 and t_2. - The intersection point P of the two range circles with the radii R_1 and R_2 is the radar fix at the time t_2. Optimum results with this method will be obtained if the intermediate distance Δs is approximately equal to the range R_2 to radar target T_2.

6. PRACTICAL EVALUATION OF THE RADAR NAVIGATION SYSTEM

For the evaluation of the radar navigation system the roller map display had been installed into the working table of the navigator, immediately beneath the radar scope. The RCU had been fastened beside the map display. Due to shortage of time and due to instructions for airspace observations all radar measurements have been made in the 50-nautical-miles range of the PPI. At first radar fixes have been carried out in the usual way, measuring range and distance to the target on the PPI and drawing the line of position and range circle into the navigational chart. At the time of radar measurements airial photographs have been taken to determine the accurate actual aircraft position in this moment. The difference between actual and radar-position has been resolved into position errors along and across track to the target and presented graphically in figure 10. As one can see all position errors are to be found within an error circle of 1.1 nautical miles radius. The mean distance to all targets was about 26 nautical miles.

A second number of radar fixes has been carried out in the mode "Targetecho-Detection", where the marking aid is moved with dead reckoning accuracy to the targetecho. Then the "fine"-measurement of distance and bearing has been made with the correction knobs of the RCU. The accuracy of these radar fixes is shown in figure 11. It is considerably better than before and all position errors lie within an error circle of .45 nautical miles.

These better results can be ascribed to the fact that in employing the automatic echo marking, the navigator can concentrate all his efforts on the fine-measurement, because the electronic marking aid does not move off the echo during the measuring period due to aircraft movement.

There is an important tactical aspect too in employing this method. Due to the automatic identification of radar echoes only one or two antenna revolutions are required for a radar fix.

7. LOW FLYING OPERATIONS AND TERMINAL AREA FLIGHT

For low altitude flights a combination of radar picture presentation and automatic aircraft position indication in a navigation chart seems to be ideal, because the chart grants a better general view on the surroundings of the aircraft, whereas the radar range is limited to only about 10 nautical miles in an altitude of 100 ft. This is especially important for give way manoeuvers. Furthermore the chart shows more distinctly obstacles like high tension wires, shipping ropes over rivers, high bridges crossing the flight track etc. The navigator may aid the pilot by selecting dangerous obstacles during low level flights with the target setting device of the map display and servoing the marking aids on the PPIs in the "Echo-Detection"-mode, thus warning the pilot of dangerous objects.

Sometimes it may be very difficult or not possible at all to recognize on the PPI the target position or the landing site in the terminal area. In this case the navigator may select on the PPI an auxiliary radar echo in the near of the target, identify it automatically in the navigation chart - see 4.3 - and put the light spot manually, if necessary, exactly on the radar target, thus updating the dead reckoning system. If the coordinates of the final target are stored in the navigation computer, the pilot can steer now the aircraft to the final target with radar accuracy, reading the homing indicator.

8. CONCLUSIONS

The demand for better accuracy, reliability and effectiveness of self contained navigation systems is increasing steadily. The expenses for development and production of such systems however are growing exponentially, being thus in sharp contrast to the slowly increasing or even diminishing military budgets.

A solution to this paradox may be found in numerous cases in the combination of already existent, well proved and reliable navigational components or systems to a much more effective integrated navigation system. Such a system is not in need of further expensive development and its maintenance does not cause additional problems.

The usefulness of this concept has been demonstrated in this paper on a practical example where a dead reckoning navigation system and a radar set, belonging to the navigation equipment of a close support aircraft, have been integrated to a cost effective radar navigation system. The utility and the advantage of this radar navigation system have been proved on navigation test flights. The results show that the system could be a valuable navigational aid for low altitude and terminal area flight.

ACKNOWLEDGEMENT

The author wishes to thank Lt. Col. T. Krauss and Lt. Col. K. Dremmel of the German Airforce - both students of navigation of the Airforce Base Mather, Cal. - for their excellent assistance and performance during the evaluation flights and Reg.Dir. N. Brießmann, BWB - Airforce Test Center 61, Manching for his technical advice and activities in connection with this project.

The results presented in this paper would not have been possible without the work they have performed.

REFERENCES

1. Ramsayer, K. and Wildermuth, E.: Automatische Koppelkarte AK4T, ein neuer Navigationsrechner zur Integration bordeigener und bodengestützter Navigationshilfen. Ortung und Navigation, Heft 1/1967.

2. Wildermuth, E.: Eine feinwerktechnische Lösung zur Verbesserung der Radarortung an Bord von Flugzeugen. Feinwerktechnik + Micronic, 77. Jahrgang, Heft 8, 1973.

3. Wildermuth, E.: Automatisierung der Radarortung an Bord von Flugzeugen. Feinwerktechnik + Micronic, 78. Jahrgang, Heft 1, 1974.

4. Air Navigation. Air Force Manual, Number 51-40, Vol. I. U.S.Government Printing Office, Washington/D.C. 20 402.

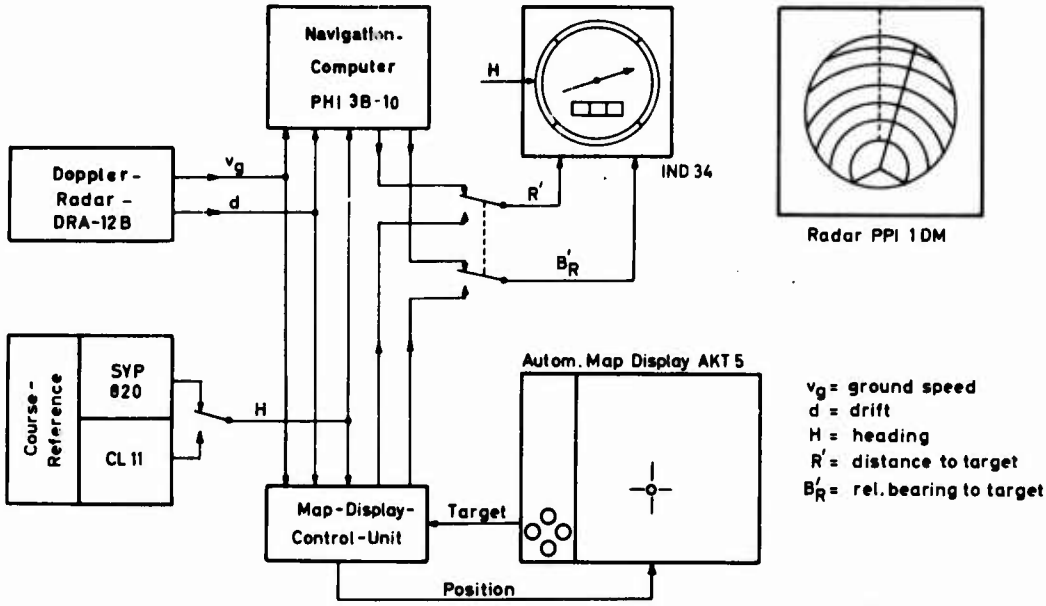

Fig. 1: Autonomous Navigation System of the close support aircraft C 160 -Transall-

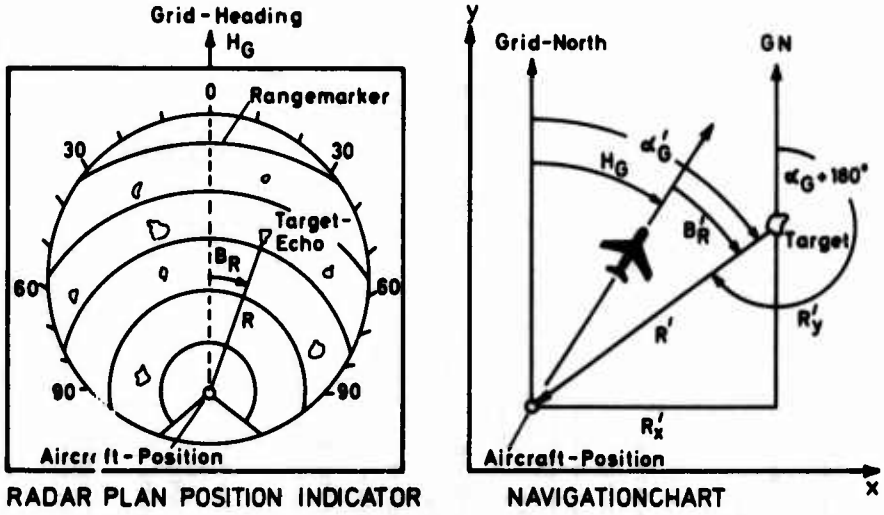

Fig. 2: Aircraft- and Targetposition on the PPI and in the Navigationchart

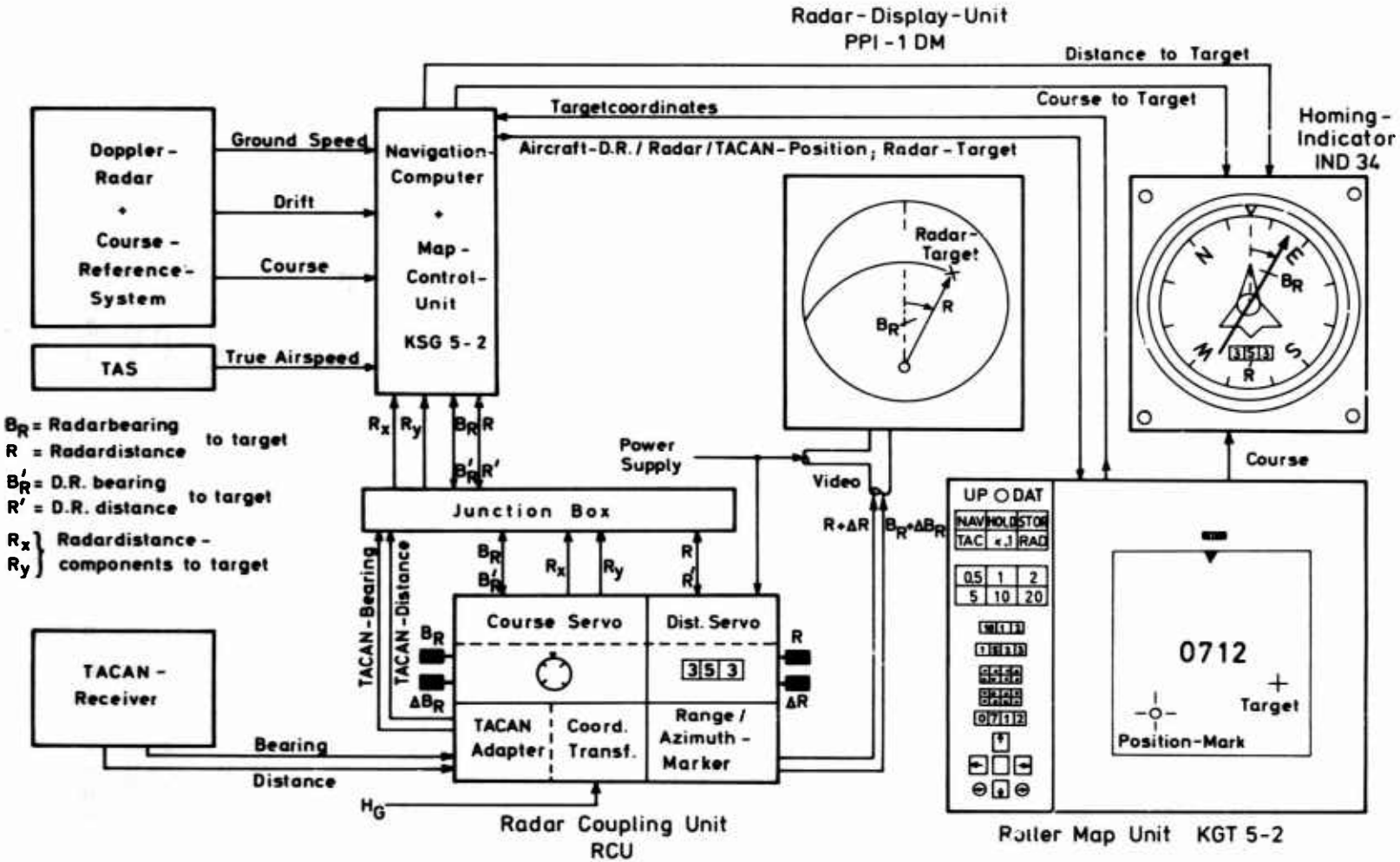

Fig. 3 : Integrated Radar-Navigation-System

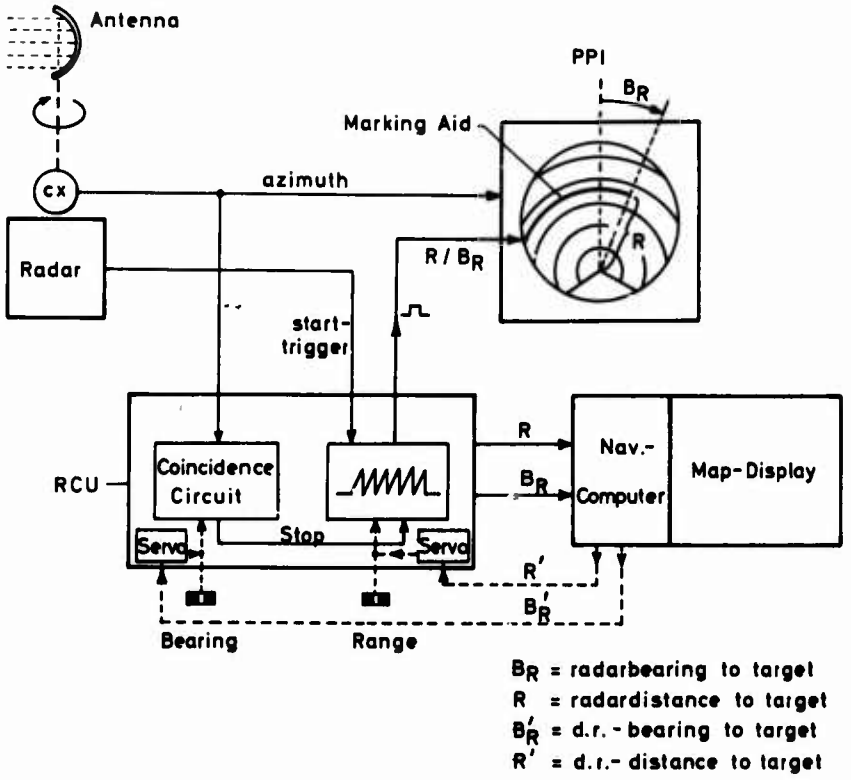

Fig. 4: Functional Diagram of the RCU

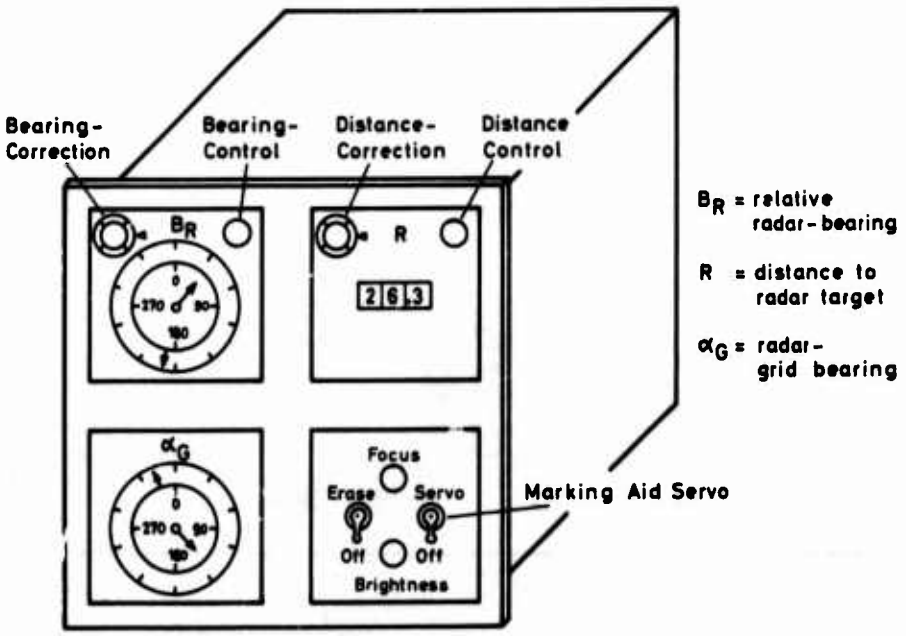

Fig. 5: Radar Coupling Unit

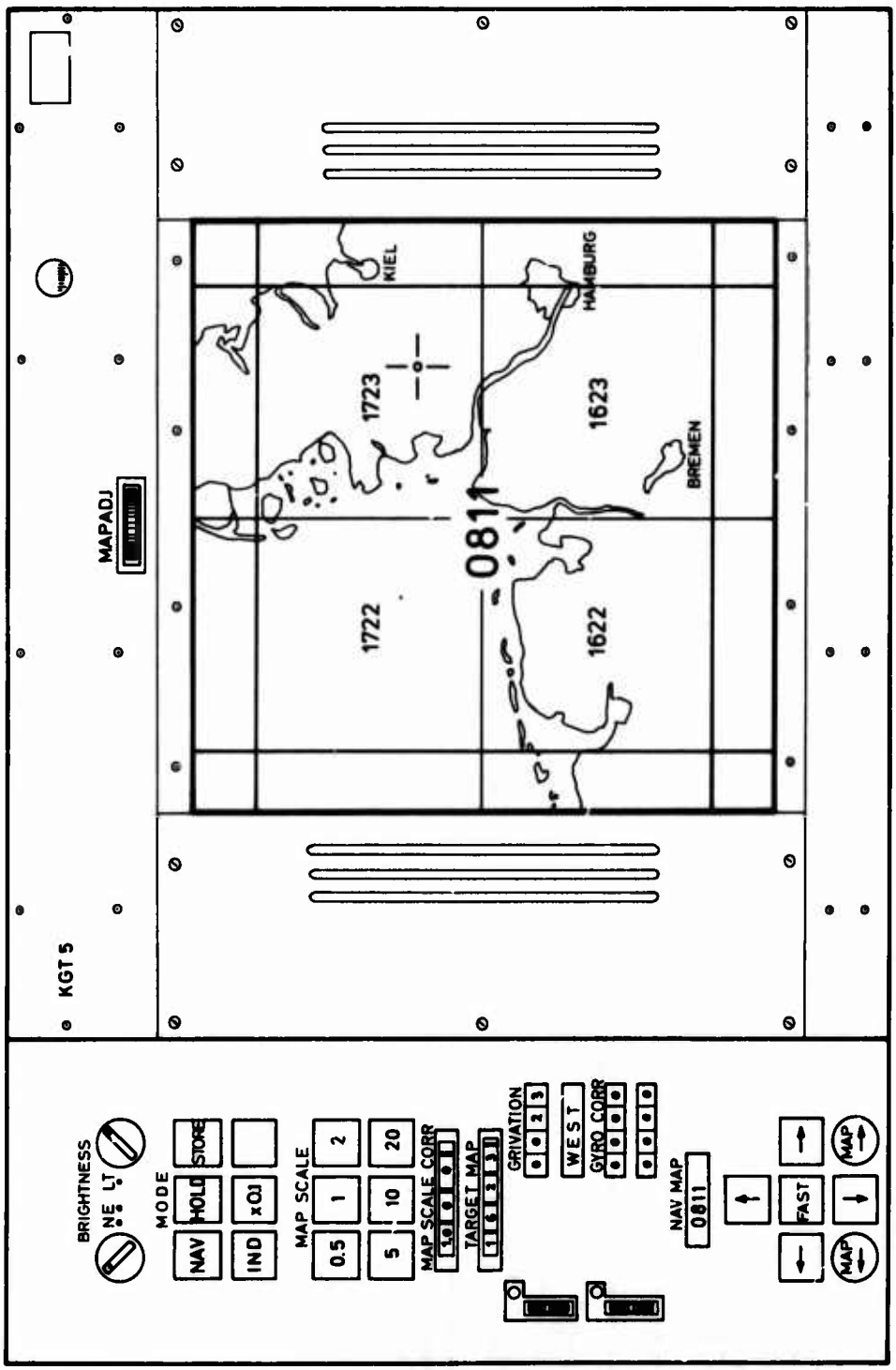

Fig. 6 : Map Display AKT 5-2

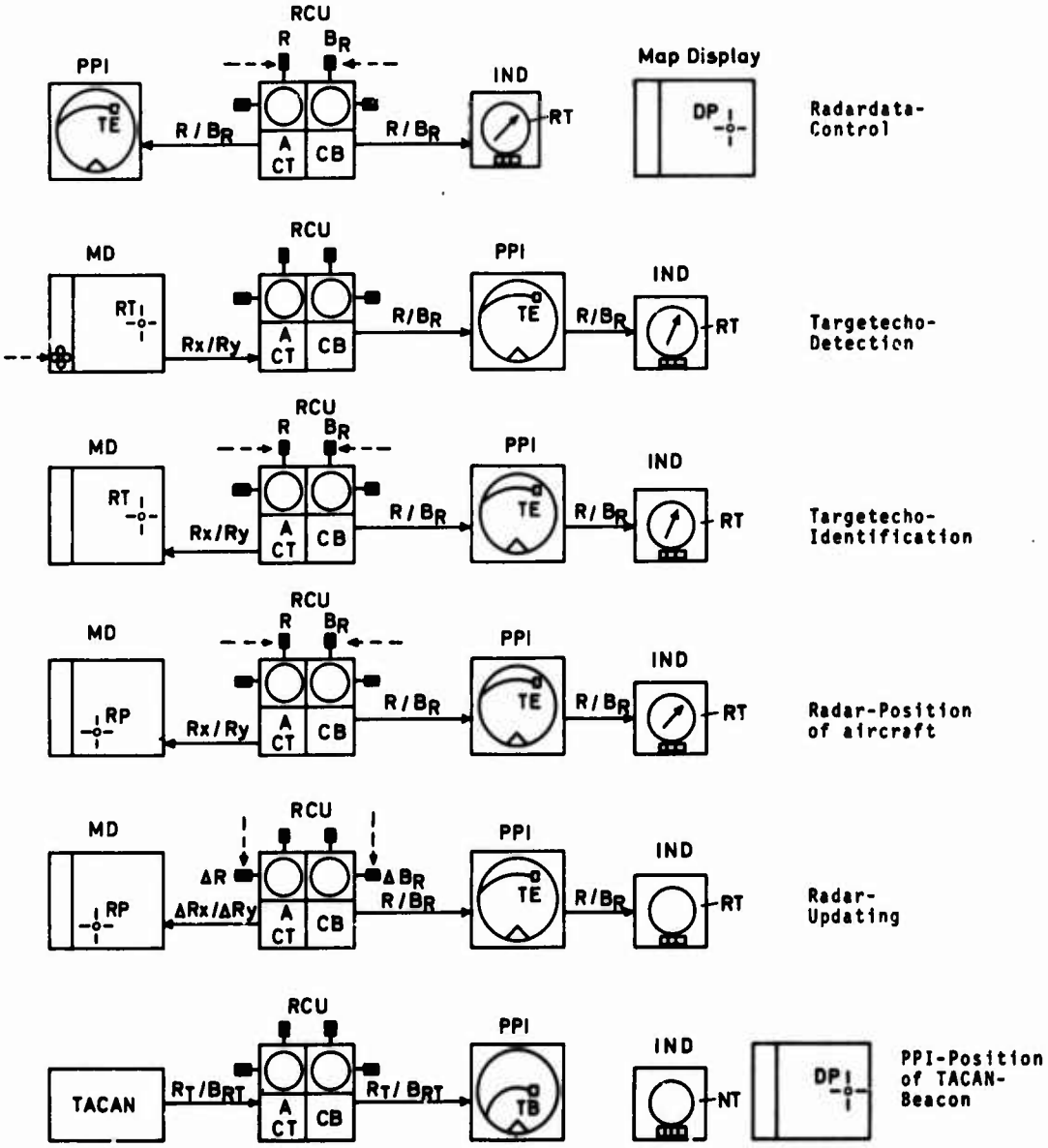

RCU	= Radar Coupling Unit	NT	= Navigation Target
A	= Adapter	TB	= TACAN-Beaconposition
CT	= Coordinate Transformer	R/B_R	= Distance/Bearing to target
CB	= Control Board	$\Delta R/\Delta B_R$	= Dist./Bearing correction
MD	= Map Display	R_x/R_y	= components of distance to a target
RT	= Radar Target	$\Delta R_x/\Delta R_y$	= error components of distance to a target
TE	= Target Echo	R_T/B_{RT}	= dist./rel. bearing of TACAN
DP	= D.R.Position of aircraft	----→	= manual control
RP	= Radar Position of aircraft		

Fig. 7 : Modes of Operation of the Radar-Navigation-System

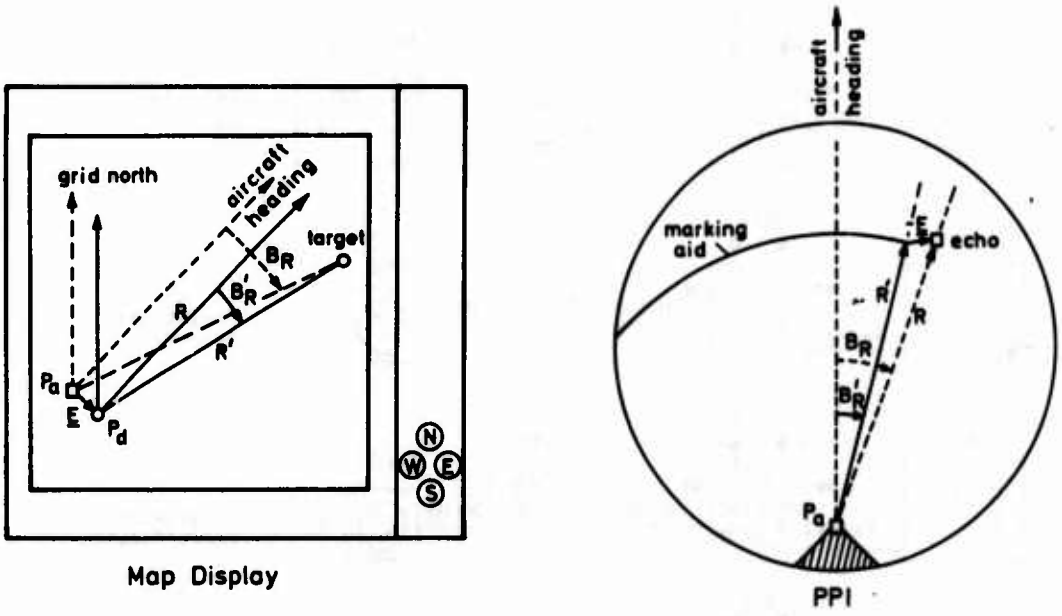

P_a = actual position
P_d = D.R.position
$\underline{E}$ = position error
R = radar distance to target
B_R = relative radar bearing to target
R' = D.R. distance to target
$B_{R'}$ = relative D.R. bearing to target

Fig. 8 : Radarupdating of the D.R. Position

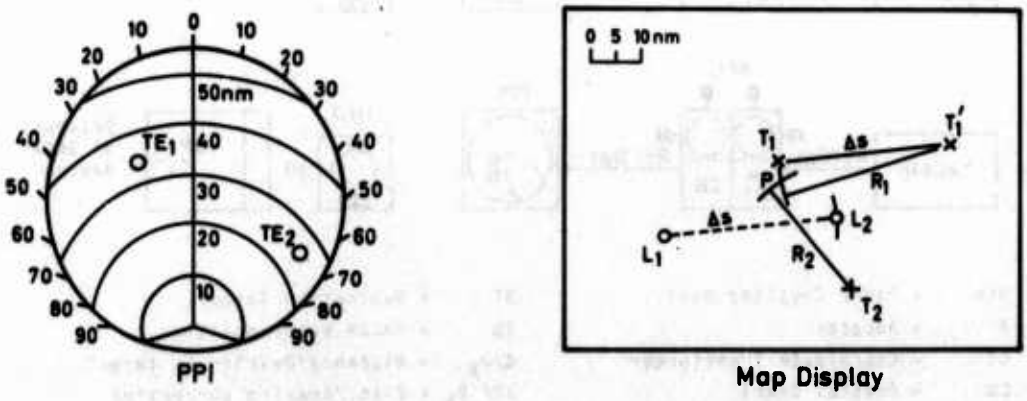

TE_1 = target echo at time t_1
TE_2 = target echo at time t_2

T_1 = first radar target at time t_1
T_2 = second radar target at time t_2
R_1 = distance to target T_1
R_2 = distance to target T_2
L_1 = D.R.position at time t_1
L_2 = D.R.position at time t_2
Δs = distance flown between t_1 and t_2

Fig. 9 : Aircraftposition from two radardistances

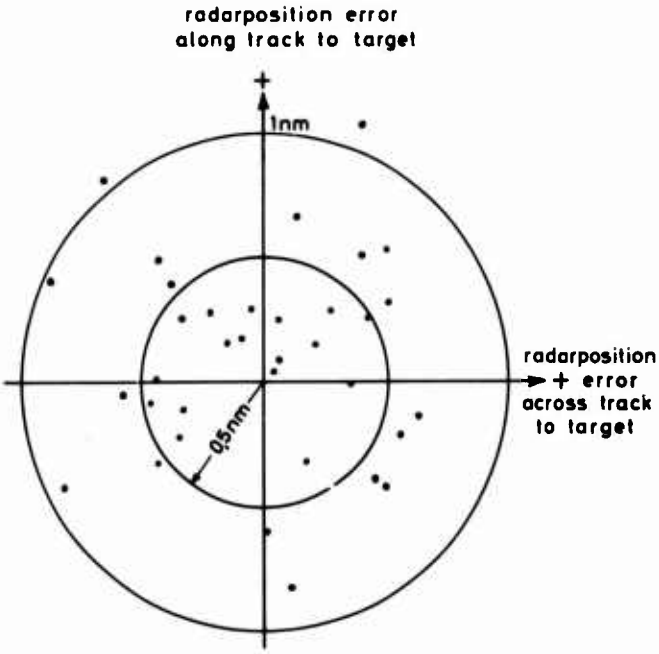

Fig. 10 : Radarposition errors within 50-n.miles range of PPI resulting from normal radarmeasurements

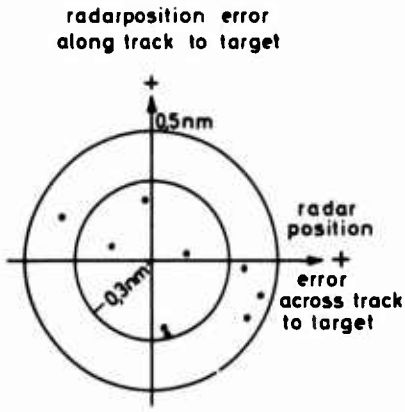

Fig. 11 : Radarposition errors within 50-n.miles range of PPI resulting from radarmeasurements with RNS

DESIGN CONSIDERATIONS FOR A GROUND AVOIDANCE MONITOR FOR FIGHTER AIRCRAFT

D.A. Whittle
British Aircraft Corporation Ltd.
Military Aircraft Division
Warton Aerodrome
Preston PR4 1AX
Lancashire, U.K.

SUMMARY

The problem of ground avoidance, as a consequence of manoeuvres executed by fighter aircraft, is considered and a relatively simple form of monitor is proposed to provide a pilot warning in the event of the aircraft being subjected to a hazardous trajectory. The paper discusses the parametric requirements of the Ground Avoidance Monitor and the difficulties associated with selection of suitable and available sensors, which could be included in the mechanisation of such a facility into a typical fighter aircraft.

LIST OF SYMBOLS AND ABBREVIATIONS

g	gravitational constant of acceleration
h_B	barometric height
h_{BI}	baro-inertial height
h_d	datum height
h_g	height above ground
h_p	pull-out height loss
h_r	height loss due to pilot reaction time
n	aircraft load factor
t_p	pilot reaction time
V	aircraft velocity
V_g	aircraft ground speed
V_t	true airspeed
α	aircraft incidence
γ	aircraft dive angle
θ	aircraft pitch angle

ADC	Air Data Computer
AFDS	Autopilot and Flight Director System
CWP	Central Warning Panel
GAM	Ground Avoidance Monitor
HSI	Horizontal Situation Indicator
HUD	Head-Up Display
INS	Inertial Navigation System
MC	Main Computer
PFCS	Primary Flight Control System
RA	Radio/Radar Altimeter
SAHRS	Secondary Attitude and Heading Reference System
TAS	True Airspeed
TF	Terrain Following

1. INTRODUCTION

The safety of military aircraft flying at high speed and low level has been extensively studied, and system design techniques continue to evolve to provide the increasingly high levels of safety and confidence demanded for these high-risk flight conditions, which are primarily related to ground attack or close support aircraft. This paper discusses the requirements for, and problems of, designing a Ground Avoidance Monitor for fighter aircraft, with particular emphasis on the air-to-air role. The difficulties associated with achieving an acceptable performance from available sensors, and the problems of computing and pilot's interfaces are also considered.

A typical fighter aircraft flying at high speed and high dive angle could require a clearance height above ground of 15,000 ft. to execute a safe pull-out manoeuvre. Medium to low altitude combat flying therefore requires a high degree of awareness from the pilot to obtain the maximum performance from the aircraft, whilst respecting the dangers and limitations of manoeuvres involving large dive angles. The Ground Avoidance Monitor

has been considered as a means of ensuring that the pilot does not encroach upon trajectories which could result in ground impact. In addition to the primary objective of increasing aircraft safety at low altitude, the GAM can also aid in relieving the pilot of the essential task of monitoring the ground situation. This is considered particularly important, since the high workload involved during certain phases of an air-to-air attack tends to lead to the air combat pilot being less aware of the terrain than his ground attack counterpart.

Statistical evidence of the need for a GAM is difficult to obtain. However, a survey of aircraft losses in the Royal Air Force in the period from 1970 suggests that there is a real problem and that it is not uncommon for pilots, particularly those of limited experience, to find themselves in difficulties due to disorientation or misjudgement, leading to serious loss of height, which may not be appreciated by the pilot until it is too late.

The proposed GAM operates by continuously predicting the height loss of the aircraft using speed, dive angle and height as the major parameters. In the event of the predicted height loss being insufficient to achieve a safe pull-out above a pre-determined height threshold, a warning is indicated to the pilot.

A major difficulty facing the system designer arises from the need to compute the GAM during all flight conditions. In true low-level modes such as terrain following and landing approach, the aircraft attitude tends to be limited to the operational range of prime sensors such as Terrain Following Radar and Radar Altimeters. However, an attitude limitation cannot be tolerated during air-to-air combat, therefore the available height sensors are limited to air pressure and inertial types.

Careful consideration must be given to the integrity requirements of sensors and computing, since the GAM could represent a safety critical feature of the aircraft if the pilot comes to rely on it, which he must be allowed to do. In this respect, the GAM function must be mechanised on a fully duplex or self-monitored basis, such that a GAM failure can be detected and indicated to the pilot.

Although the paper is primarily concerned with the air combat fighter, it is suggested that other aircraft types could also benefit from some form of GAM to enhance the safety of medium to low altitude flying.

2. BACKGROUND

2.1 GENERAL AIRCRAFT

Medium/low altitude manoeuvring requires constant awareness by the pilot of his position relative to ground. This is an obvious statement and one which is clearly appreciated by pilots, and the altimeter therefore becomes an object of central importance in the pilot's scan pattern. In normal conditions, such as clear visibility during a sortie with no unexpected occurrences, a pilot would expect no difficulties in maintaining an adequate safety clearance height above ground. However, faced with a sudden change of circumstances such as poor visibility or distraction, an inexperienced pilot can fairly quickly become disoriented and put his aircraft into a downward attitude, which may not be realised until it is too late.

Statistical evidence of aircraft losses resulting from diving manoeuvres is difficult to collate. Invariably, pilots involved in such incidents fail to survive, since almost by definition we are talking about a situation which is not immediately appreciated by the pilot. Even when the criticality is realised, it is natural for the pilot to fight to regain control and a safe altitude, rather than eject.

A survey of R.A.F. Accident reports since 1970 (refer to Table 1) shows that several losses could have been attributable to the aircraft's entering a critical flight profile without the immediate or subsequent awareness of the pilot. It must be emphasised that in each of the reports considered, the Board of Inquiry was unable to reach any firm conclusion as to the cause of the accident. The probable causes mentioned were therefore based on supposition and the circumstances surrounding the incident. In all cases the crew were killed and the aircraft was severely damaged (if recovered) so that the possibility of aircraft malfunction although not in evidence, could not be completely disregarded. However, for most of the incidents tabulated it seems probable that if the causes postulated were in fact valid, then some form of Ground Avoidance Monitor could have been beneficial in preventing the crashes.

Incidents 4, 5, 9 and 12 would almost certainly have required a height loss prediction, in order to provide the advanced warning which is essential to enable the pilot to recover the aircraft. A simple low height warning may have been adequate for the other incidents.

Although it is not the purpose of this paper to discuss the circumstances which may lead to the above types of accident, it is clear that there are several factors which could lead to a degradation of the pilot's awareness of altitude, for example:-

- Visual concentration on an outside object (e.g. target)
- High Radio Transmission activity

. Navigation and Weapons Selections

. Instrument flying in poor visibility

2.2 APPLICATION TO MODERN AIR COMBAT FIGHTER

The problems discussed above are generally relevant to all types of fighter aircraft, both ground attack and air attack. The severe demands imposed by the requirements for fast low flying ground attack aircraft have resulted in the need for automatic terrain following systems, which ensure the maintenance of a safe clearance height. The performance and safety requirements of such a task have led to the development of specialised radars and control systems. The safety requirements of an air combat fighter, however, are fundamentally different, but the need to maintain an adequate terrain clearance, albeit perhaps greater than that of the T.F. aircraft, is equally important. Moreover, the air combat fighter must respect the position of the ground under a wide range of manoeuvres in contrast to the ground attack aircraft, which can adopt a relatively limited attitude range during the sortie. The air combat fighter therefore must seek techniques for ground avoidance other than those available for the ground attack vehicle.

Direct experience of the need for GAM during air combat is difficult to acquire, since a representative scenario can only be achieved in wartime. Training for air-to-air combat manoeuvres is generally performed at 'safe' altitudes so that the peacetime role is not necessarily typical of the real problem. The increasingly recognised importance of air combat superiority however is tending to lead to greater emphasis on more realistic simulation during air combat training (Ref. 1), and this trend may generate more tangible evidence of the requirement for a GAM.

2.3 GROUND PROXIMITY WARNING SYSTEMS

It is perhaps relevant at this point to mention the developments which have taken place in recent years in the civil aviation field to compare with the fighter problems previously described, since the object of the GAM is precisely the same as the GPWS, i.e. to avoid impact with the ground.

The typical GPWS on the market today provides pilot warnings for four different flight conditions. These are:-

. Excessive Sink Rate

. Excessive Terrain Closure Rate

. Descent after Take-off

. Insufficient clearance when not in Landing Configuration

Since a civil aircraft follows a relatively tightly constrained flight profile, the definition of thresholds and the scheduling of thresholds with altitude, is not a difficult task. Thus the GPWS is not directly applicable to the fighter aircraft problem, which needs to accommodate a much wider flight envelope.

3. DESIGN OBJECTIVES

It is considered that the GAM is primarily provided as a pilot/aircraft safety feature for the automatic attack phase of an air combat engagement, where the flight guidance and control system is steering the aircraft towards the target in ignorance of the position of the ground in relation to the manoeuvres being performed. The GAM is of course equally beneficial in a manual Flight Director attack or indeed as a general facility to be available in any phase of the mission, except specific low-level tasks, such as landing, where the GAM would need to be inhibited. Following the above primary objective, the secondary objectives are considered to be as follows:-

i) To devise a simple control law depending on the minimum number of sensors in order to achieve high reliability / availability consistent with a minimum of false warnings.

ii) To employ sensors which can readily be monitored from alternative sources.

iii) To be relatively adaptable to a simple pre-flight confidence check routine.

4. GAM PARAMETER REQUIREMENTS

4.1 GENERAL

The object of the GAM is to calculate the height clearance which the aircraft requires in order to enable a pull-up manoeuvre to be executed at a safe height above the terrain. It is therefore necessary to study the various parameters which influence the pull-up performance of the aircraft and decide which parameters need to be included in the GAM computing. These could include:-

- Fuel content
- Stores
- Configuration (e.g. airbrakes, wing sweep angle)
- Engine thrust
- Atmospheric conditions
- Airspeed
- Dive angle

The effects of variations in these parameters are discussed briefly below.

4.2 FUEL AND STORES

Changes in fuel and stores configurations affect the total aircraft weight which can be considered under two categories. At high speeds where aircraft tend to be 'g' limited, changes in weight have little effect on height lost during a pull-out. However, at lower speeds aircraft tend to be lift limited and the available 'g' increases as weight reduces, thus reducing height loss.

Aircraft weight is not usually required to be computed on aircraft, but fuel contents and stores configuration data is normally available. However, the requirement for an independent source of this information could only be achieved by providing duplicated sensors. Alternatively, the GAM can be designed for the high weight case which will ensure that weight changes will always be in the 'safe' sense. It is predicted that only at the extreme low speeds and high dive angles, which are improbable flight conditions, would the GAM initiate a significantly premature warning. It is therefore concluded that aircraft weight can be excluded from the GAM.

4.3 CONFIGURATION

Changes in wing geometry affect height losses due to variable lift and drag effects, but the effects are not large and can be accommodated by designing for the wings forward case. The effect of deploying airbrakes is to reduce the height loss.

4.4 ENGINE THRUST

Engine setting only becomes significant at high speed and large dive angles, where height losses increase with speed.

4.5 ATMOSPHERIC CONDITIONS

Changes in atmospheric conditions, temperature and pressure can have considerable effect on height losses due to the impact of these parameters on TAS. Fig. 1 shows as an example the variation in TAS as a function of temperature, assuming Mach number is held constant. Thus increases in air temperature will result in corresponding increases in height loss during a pull-out manoeuvre. If a temperature range of $-30^{o}C$ to $+45^{o}C$ is considered, this would equate to a TAS variation of approximately ±5%. It is therefore necessary to allow for this error in the computation of the GAM warning threshold.

Pressure variations have a similar effect as temperature in influencing the height loss. A pressure reduction, for example, will have the effect of increasing the TAS for a given Mach number, thus increasing the height loss.

4.6 AIRSPEED AND DIVE ANGLE

Airspeed, along with dive angle, is a prime parameter for computing height loss and the effect is broadly shown in Fig. 2. Airspeed is required for two functions:-

i) To calculate the distance travelled, and hence the height lost in the period from indicating the low height warning to the pilot, and his initiating the pull-out manoeuvre.

ii) To calculate the height lost during the pull-out manoeuvre itself.

4.7 GAM CONTROL LAW

The major factors affecting the pull-out height loss are speed, dive angle and height. The control law objective is to compute the minimum pull-out height for a given flight condition and to compare this with a pre-determined minimum height for level flight. In the event of the former exceeding the latter, a pilot warning is initiated.

A graphical representation of a simple pull-out manoeuvre is shown in Fig. 3, where:-

$$h_g = h_r + h_p + h_d$$

$$h_r = VT_p \sin\gamma$$

$$h_p = \frac{V^2}{g(n-\cos\gamma)} (1 - \cos\gamma)$$

h_d is the datum height selected by the pilot

This relationship, however, does not take into account the full capability of the aircraft, since if maximum 'g' is applied during the pull-out, level flight could be achieved at a higher altitude. Fig. 2 is a typical pull-out performance carpet, showing height loss during pull-out manoeuvres as a function of speed and dive angle. This carpet can be conveniently represented mathematically by a second or third-order equation, which is the basis for the proposed GAM.

It is concluded therefore that the GAM should be based solely on speed, dive angle and height.

5. SENSOR SELECTION

The GAM is considered primarily as a safety precaution for fighter aircraft equipped with automatic target tracking and following controls (Auto Air Attack). It is this combat situation which could put the aircraft into a dangerous position relative to the ground if the dynamic behaviour of the aircraft is ignored. A typical avionic and flight control system for such an aircraft is shown in Fig. 4. It is assumed that the flight control system includes a duplex full authority autopilot driving a fly-by-wire control system. The fly-by-wire system is not essential but is typical of a modern combat fighter. The duplex autopilot provides integrity and protection against failures occurring in the outer loop. This is an important feature since the availability of monitored sensor data is likely to be fairly extensive. The autopilot, in addition to an auto air attack mode, features the normal modes such as Height, Heading, Speed and Mach Hold, for which data is supplied from an Air Data Computer, HSI, Inertial Navigator System and Radio Altimeter.

For the purposes of the GAM, the following sensors can be considered for the three GAM parameters:-

SPEED	Air Data Computer
	Inertial Navigation System
HEIGHT	Radio Altimeter
	Forward Looking Radar
	Air Data Computer
	Inertial Navigation System
DIVE ANGLE	Inertial Navigation System
	Air Data Computer

Let us consider the above sensors in detail:-

5.1 SPEED

5.1.1 Air Data Computer

True airspeed obtained from an ADC is typically available to an accuracy of ±5 knots which is more than adequate for the GAM application.

5.1.2 Inertial Navigation System

The INS does not normally compute aircraft velocity, but this can be derived from vertical velocity and elevation which are readily available.

5.2 HEIGHT

5.2.1 Radio/Radar Altimeter

The Radio Altimeter provides the most accurate source of height above terrain available. There is, however, one major disadvantage in its use for the GAM; at the present state of the art, the RA can be used only up to aircraft attitudes of 60°. In the application being considered, this represents an unacceptable limitation, since aircraft involved in air combat can expect to exceed these attitudes quite frequently, particularly in bank where 60° represents a normal acceleration of only 2g (assuming zero sideslip). In order to utilise the full manoeuvrability of the fighter aircraft, bank angles of 75° and upward must be available for execution of tight turns. The importance of bank angle in determining the maximum normal acceleration and also turn radius is demonstrated in Fig. 5, which shows that an increase in available bank angle from 60° to 75° approximately halves the turn radius. The extension of RA attitude range beyond 60° does not appear feasible due to the inherent problems of aerial loop gain reduction as the attitude is increased. Improvements could possibly be achieved by the use of multi-aerial installations provided that suitable locations free from interference and masking effects can be found.

Height range, which is usually limited to approximately 5,000 feet, does not appear to be an insurmountable problem since Radar Altimeters can be obtained to operate up to

50,000 ft., but with degraded accuracy.

5.2.2 Air Data Computer

The ADC provides a barometric height signal over the full range of height and attitude, but this is subject to large errors due to atmospheric changes. A 50 mb pressure change will cause an error of approximately 1,800 ft. To ensure reasonable accuracy for the GAM therefore, it would be necessary to compensate for the ground datum pressure, similar to an Altimeter Q_{FE} correction. Although such action is common pre-landing practice to ensure correct runway height, it is not considered desirable to burden the pilot with such a task during a mission, either from the workload or safety viewpoint. Automatic correction is not considered feasible and could only be effected via a ground-to-air data link. Even here, manual involvement would be necessary to input the data.

5.2.3 Inertial Navigation System

The vertical channel of an INS can provide a height output derived from the double integration of vertical acceleration. However, the errors resulting from accelerometer drift lead to large errors in the pure inertial height signal, therefore it is necessary to limit this divergence by comparing the inertial height with barometric height. A typical baro-inertial mix arrangement is shown in Fig. 6. In level flight baro height is allowed to dominate in order to trim accelerometer errors. However, in climbing or diving flight where the barometric channel is less accurate than the inertial channel, baro height is corrected by an amount proportional to the baro/inertial difference. Typically a baro/inertial mix would provide a height signal accurate to about 50 feet.

5.2.4 Forward Looking Radar

As previously described, the prime purpose of the GAM is to augment the safety of an automatically-controlled air attack, particularly where the radar is locked on to a low-level target. Ground returns from an air-to-air radar are, of course, normally avoided. If, however, these could be separately processed, then by compensating for radar inclination and aircraft attitude, height above terrain could be obtained. This technique would also have the advantage of incorporating a look-ahead capability. Unfortunately, the present techniques used in radar systems for tracking fixed and moving objects require the use of different radar modes, i.e. ground tracking employs the use of pulse return measurement and moving target tracking uses frequency difference (Doppler) measurement. Multi-mode radars capable of providing both these facilities simultaneously are not currently available.

5.3 DIVE ANGLE

5.3.1 Inertial Navigation

Dive angle can be computed from vertical velocity and ground speed, both of which are normally available from an INS, using the relationship:-

$$\cos\gamma = \frac{\dot{h}_g}{V_g}$$

5.3.2 Air Data Computer

Dive angle can also be derived by an ADC from the relationship:-

$$\gamma = \theta - \alpha$$

where θ is obtained from an IN or other attitude source.

Due to the errors in the measurement of incidence, for example during sideslip conditions, this method is less accurate than the INS derived dive angle.

6. SYSTEM IMPLEMENTATION

From the foregoing discussion it is concluded that the GAM control law be based on Baro-Inertial height, speed from the ADC and dive angle from the INS. It can be seen from Fig. 4 that this information is already available in the basic auto attack system considered. However, to preserve the integrity of the system, it is necessary to ensure that each parameter used in the GAM computation is monitored against an independent source, such as barometric height from the ADC, independent forward pressure for speed, and ADC-derived dive angle. In the event of an incompatibility between the prime and monitored sensor, the pilot can be warned of the non-availability of the GAM by indicating a 'GAM' warning on the CWP.

A suitable selector switch is required in the cockpit to enable the pilot to pre-select the safe clearance height applicable to the sortie being flown. A general arrangement of the GAM showing the origin of the sensor signals is shown in Fig. 7.

A conservative estimate suggests that the GAM computation would require approximately 200 words of program storage, which should be readily containable within a typical autopilot computer, performing the tasks previously described.

7. SYSTEM OPERATION AFTER LOW HEIGHT WARNING

The major decision to be taken in the design of a system using a GAM is whether to go 'active' or 'passive'. In an 'active' system an automatic wings level and pull-up would be initiated, after which the autopilot would probably be disengaged. A passive system would simply provide the pilot with visual or audio warning so that he may take whatever recovery action he sees to be necessary. The relative merits of each technique are briefly discussed below.

7.1 ACTIVE

The fundamental requirement of an active recovery system is that an autopilot coupling to the flying controls must be assumed. This may or may not be a disadvantage, depending on the application. However, it is important to develop an accurate and reliable monitor law if confidence in the system is to be accumulated.

7.2 PASSIVE

A passive system allows the pilot some room for discretion in terms of the type and severity of the pull-out manoeuvre. As discussed previously, in practice it is not feasible to take account of all parameters which affect aircraft height loss, therefore, the tolerance included on the safe height threshold may in certain circumstances allow the pilot some room for relaxation or delay in obeying the warning. Equally important is the avoidance of uncommanded (as far as the pilot is concerned) manoeuvres during a critical phase of an attack manoeuvre.

Alternative types of pilot warning are available, e.g. audio, visual Central Warning Panel, visual HUD, and opinion regarding the preferred method differs from pilot to pilot, designer to designer. Whatever solution is chosen however, a common feature must be the integrity built in to both the monitor and display sections. Thus the duplex nature of the GAM computing must be extended to the pilot warning system.

8. PRE-FLIGHT CONFIDENCE CHECK

The GAM shares with all outer loop related flight controllers, difficulties in carrying out comprehensive pre-flight confidence checks. The problems arise in attempting to provide all the sensor signals necessary to simulate conditions which would activate the GAM warning. The following methods can be considered:-

i) Fully automatic.

ii) Semi-automatic.

iii) Manual.

The method adopted depends primarily on the importance attached to a rapid pre-flight check, however, whichever method is chosen, it must take account of the following factors:-

. Due to the possibility of dormant failures upstream of the GAM computing the interfacing sensor signals must be checked right back to the transmitting equipment. It is not sufficient to simulate a given sensor signal at the GAM computing itself. This would be achieved ideally by exercising the sensor directly to produce the necessary output, but alternatively an artificial signal transmitted down the line to the GAM, coupled with a separate sensor self-check, would probably be adequate.

. The pilot warning circuit must be fully checked from the GAM through to the warning.

9. IMPACT OF FUTURE FLIGHT CONTROL DEVELOPMENTS

The behaviour of aircraft performing dive attack manoeuvres could be significantly influenced by future developments to airframe and flight control systems. The trend towards greater use of Active Control Technology and high 'g' cockpits, is aimed at squeezing the maximum performance from the aircraft and pilot and places a greater emphasis on the need for safety in low altitude manoeuvres. For example, Direct Lift Control obtained by co-ordination of tailplane and flap demands could be used to minimise altitude loss during dive recoveries, or alternatively to allow initiation of the recovery manoeuvre to be delayed. A second example is the fuselage pitch pointing mode which enables a pitch attitude deviation of several degrees from the normal for a particular flight condition to be held to aim at a ground target. In YF16 tests during simulated ground attacks (Ref. 2), a 3 degrees downward pointing attitude enabled the target to be acquired earlier in the manoeuvre such that for a given length of time on target, the aircraft could pull up at 400 ft. instead of 200 ft., compared with the conventional approach. Significant improvements on these figures could be achieved if pointing angles can be increased.

10. CONCLUSIONS

The requirement for some from of Ground Avoidance Monitor for the air-to-air fighter role has been discussed and the need appears to be supported by evidence of aircraft losses occurring in recent years.

It is suggested that a very simple GAM based on speed, height and dive angle could be effective in providing advance pilot warning of an approaching critical situation. Optimisation of the GAM must be performed depending on the aircraft considered to quantify the variation in height losses with aircraft configuration, etc., and to predict the occurrence and acceptability of nuisance (i.e. early) warnings. In order to arrange for pilot warning of non-availability of the GAM it is necessary to make use of sensors which can be conveniently monitored by independent means.

In addition to the particular case discussed of the air-to-air fighter, it is also suggested that a simple form of GAM could be of benefit to a much wider range of military aircraft, and in many cases a facility similar to the GPWS devices could be of relevance in preventing low-level problems.

Finally, it must be stated that the design of the GAM inevitably presents a conflict between safety and performance which must be compatibly resolved.

11. REFERENCES

11.1 C. Gilson, Tiger on Your Tail, Flight International, March 12th, 1977.

11.2 D.E. Fink, Improved Fighter Capabilities Sought, Aviation Week and Space Technology, July 4th, 1977.

TABLE 1 Examples of RAF Aircraft Losses Relevant to Requirement for a GAM

	AIRCRAFT TYPE	SORTIE	PROBABLE CAUSE	COULD GAM HAVE HELPED?
1.	Jet Provost	Student first night solo	Disorientation.	Possibly
2.	Lightning	Low-level Practice Interception	The pilot inadvertently lost control or flew the aircraft into the sea.	Possibly
3.	Lightning	Night Shadowing and Shepherding of Low Speed Targets	The pilot failed to monitor the height of his aircraft whilst slowing down and acquiring his target and he inadvertently flew his aircraft into the sea.	Probably
4.	Hunter	Formation Training	The pilot experienced disorientation in cloud, lost visual contact with leader, lost height and recovered to level flight at too low an altitude in fog over hilly ground.	Probably
5.	Buccaneer	Navigation and Weapons Training	The pilot had inadvertently allowed the aircraft to adopt an unusual attitude in cloud.	Probably
6.	Hunter	Low Level Navigation Training	When descending to low-level ran into heavy rain which degraded forward visibility to the extent that the pilot did not see the high ground on which the aircraft impacted.	Probably
7.	Buccaneer	Night Formation and Weapons Training	Misjudgement of height during low flying.	Probably
8.	Buccaneer	Simulated Weapons Attack	Lost contact with leader in reduced visibility, resulting in circumstances at very low altitude in which the pilot allowed his aircraft to strike the sea.	Probably
9.	Hunter	Low Level Navigation	Disorientation in cloud leading to circumstances in which the aircraft came out of cloud too steeply for a recovery.	Probably
10.	Hunter	Conversion Training	Disorientation.	Possibly
11.	Phantom	Low Level Range Sortie	The aircraft was inadvertently flown in a shallow dive into the sea.	Probably
12.	Hunter	High Level Battle Formation	The pilot lost sight of his leader during a turn, overbanked and entered a steep, rapidly-accelerating dive and did not immediately appreciate the dangerous situation building up.	Probably

Notes
1. The above information has been extracted from Aircraft Accident Reports published by the Directorate of Flight Safety (RAF) London.
2. The incidents cover the period 1970-1977.
3. The 'Probable Causes' are those postulated by the Board of Inquiry as being the most likely cause. It must be emphasised that in most cases there was little if any evidence to substantiate the statements and therefore the official classification of the cause of each of the above accidents was 'unknown'.

Fig.1 **Example of Variation of True Airspeed With Temperature For Constant Mach Number**

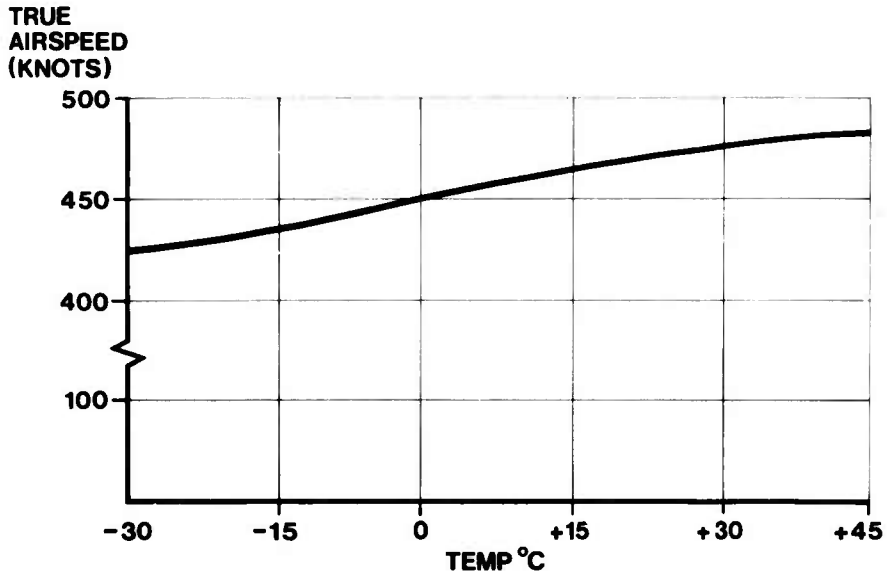

Fig. 2 **Pull-Out Height Loss Carpet As A Function of Speed and Dive Angle**

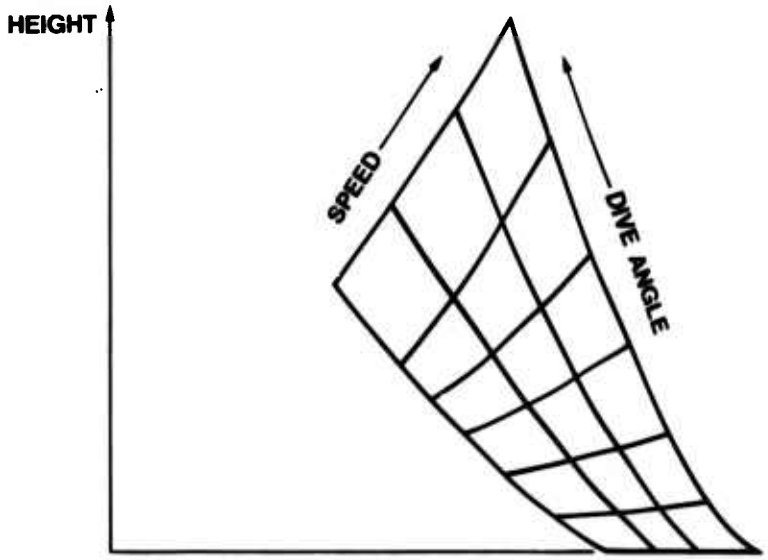

Fig. 3 **Ground Avoidance Parameters**

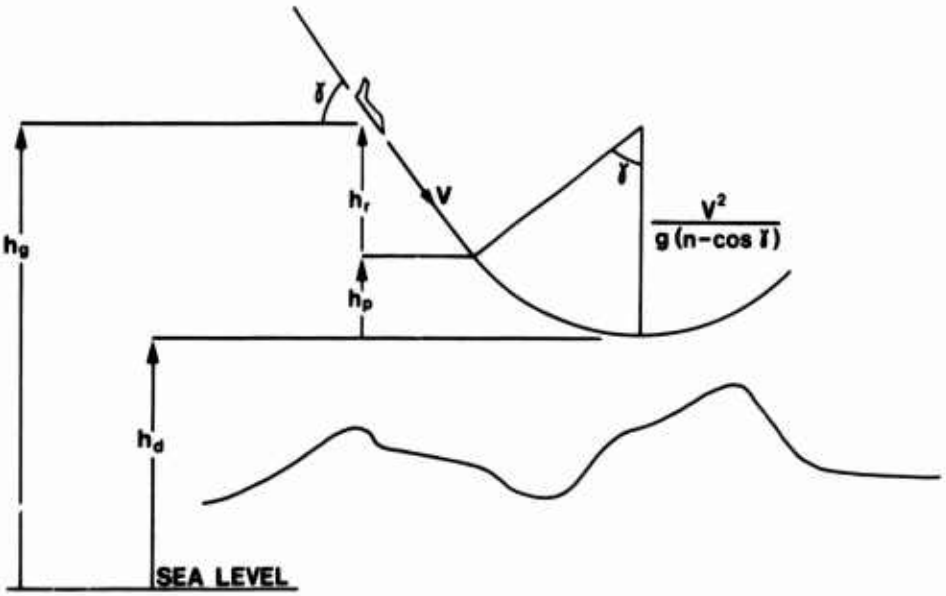

Fig. 4 **Basic Auto-Attack System with GAM**

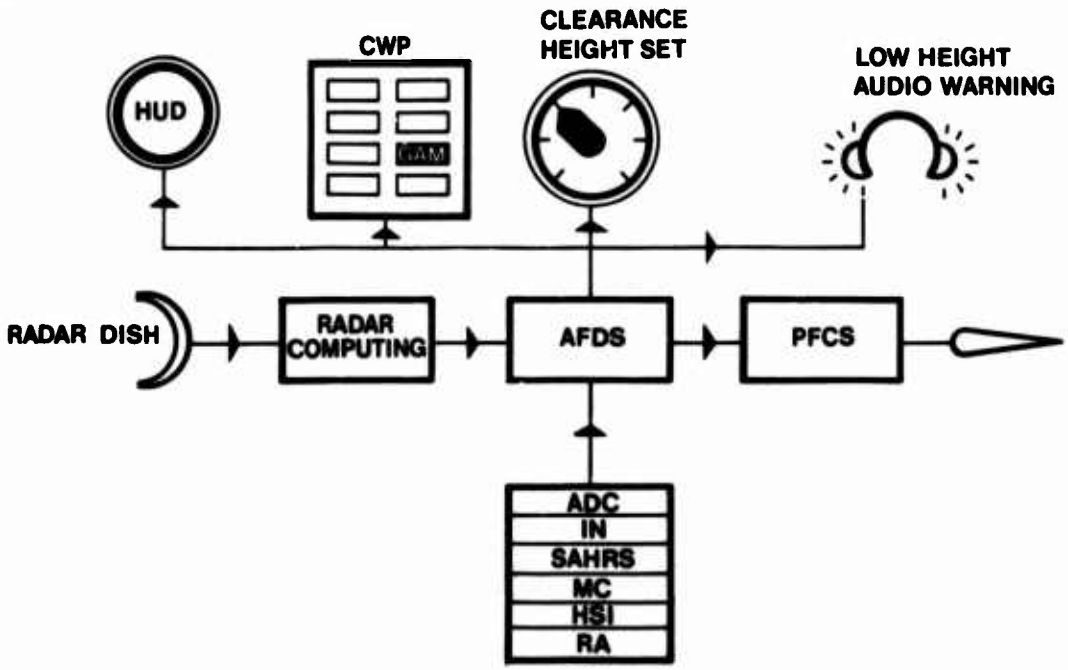

Fig. 5 **Effect of Bank Angle on Normal Acceleration and Turn Radius**

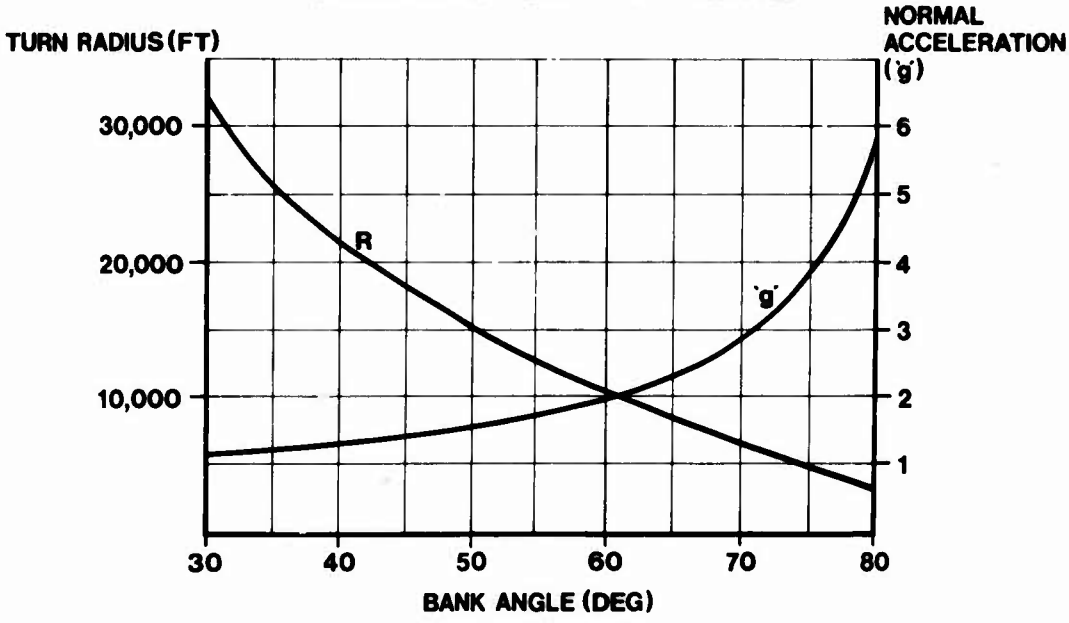

Fig. 6 **Baro-Inertial Height Mix Loop**

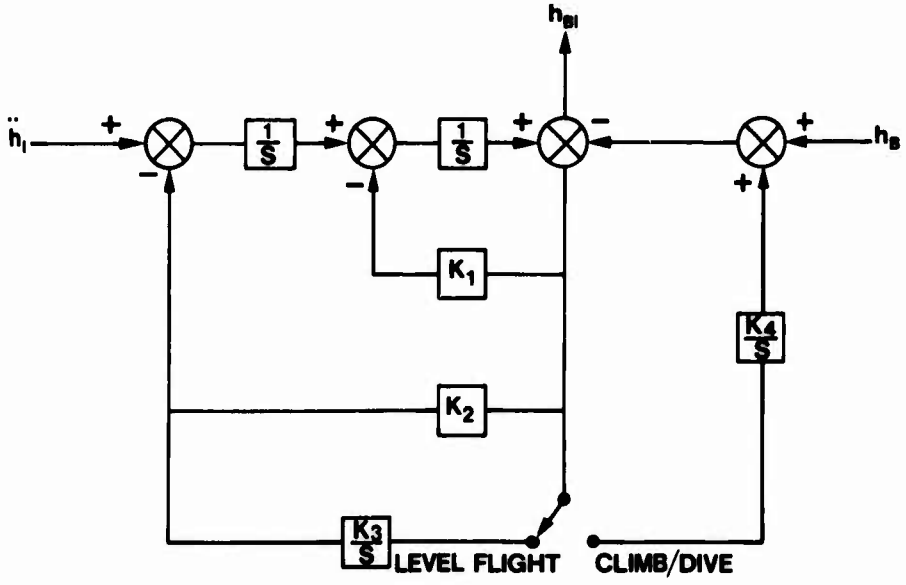

Fig. 7 Ground Avoidance Monitor, General Arrangement

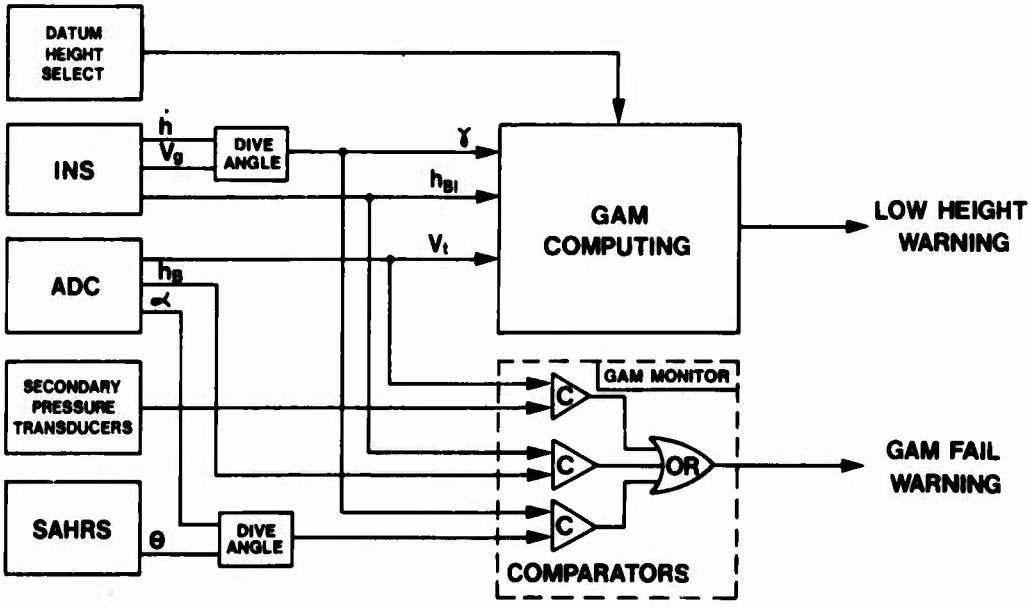

SYSTEM INTEGRATION AND SAFETY MONITORING TO ACHIEVE INTEGRITY IN LOW ALTITUDE FLIGHT CONTROL SYSTEMS

by

D. Sweeting

Flight Controls Division

Marconi-Elliott Avionic Systems Limited

Airport Works, Rochester, Kent, England.

SUMMARY

Low altitude flight, particularly in a Terrain Following mode imposes special requirements on all the avionic systems which are involved. This paper examines the requirements for the various sub-systems and how they are most effectively integrated to achieve the required levels of integrity and performance.

The problems of monitoring the key system elements are examined, in particular the primary TF sensor, and proposals are made for TF sensor monitors which take advantage of digital computing system capability which was not available in the first generation of TF systems.

Current and future improvements in Navigation systems such as Strapdown IN and NAVStar when combined with stored map information can be employed during low altitude operation to give warning of hazardous situations relative to terrain ahead of the aircraft or perform a guidance function independent of forward looking sensors.

1. INTRODUCTION

Automatically controlled flight at low altitude, calls for exacting requirements to be placed on all elements of the low flying system such that stringent safety and performance goals can be reached. If these requirements are examined in relation to the total aircraft avionics system prior to sub-system definition, a safer and more efficient low flying system will result.

The process of integrating the various aircraft sub-systems to meet a total system integrity goal highlights the importance of a full understanding of the redundancy philosophy and monitoring techniques employed in each sub-system.

While recent advances in on-board computing capability have eased the problem of achieving desired integrity levels there are still some problems to be solved in the area of TF sensors and their monitoring methods.

2. LOW ALTITUDE FLIGHT CONTROL SYSTEMS

2.1 System Types

The operational and performance requirements of the low altitude flight control system must be defined before the optimum system configuration for integrity can be examined. In military application, low flying systems fall into two broad categories with quite different operational limits, namely those capable of providing fully automatic blind flying at low altitude, and those with additional operational limits imposed by the absence of forward looking sensors or insufficient integrity in sensors, computing or actuation.

An example of the simpler type of system which uses a Radio Altimeter as the primary height sensor is shown in figure 1. Such a system can be operated at altitudes as low as 100 feet over the sea, but is limited by terrain roughness over land. In conditions of poor visibility the minimum operating height is limited by the pilot's ability to perceive hills, pylons etc, in time to pull-up and avoid them. If such a system is used in the automatic mode, over smooth terrain, the integrity requirements for the total system will be almost as stringent as for automatic TF systems since the failure consequences will be similar. The only advantage is in cost, weight and ease of installation of the Radar Altimeter compared to a forward looking Radar.

Another example of a simple low flying system has been given in a previous AGARD Symposium (1), where a Flight Director System based on a LLTV sensor was examined. This promised enhanced operational capability at night in good visibility, though pilot work load was found to be high compared to daylight operation at the same altitude, and careful integration of the navigation task was required for single seat operation.

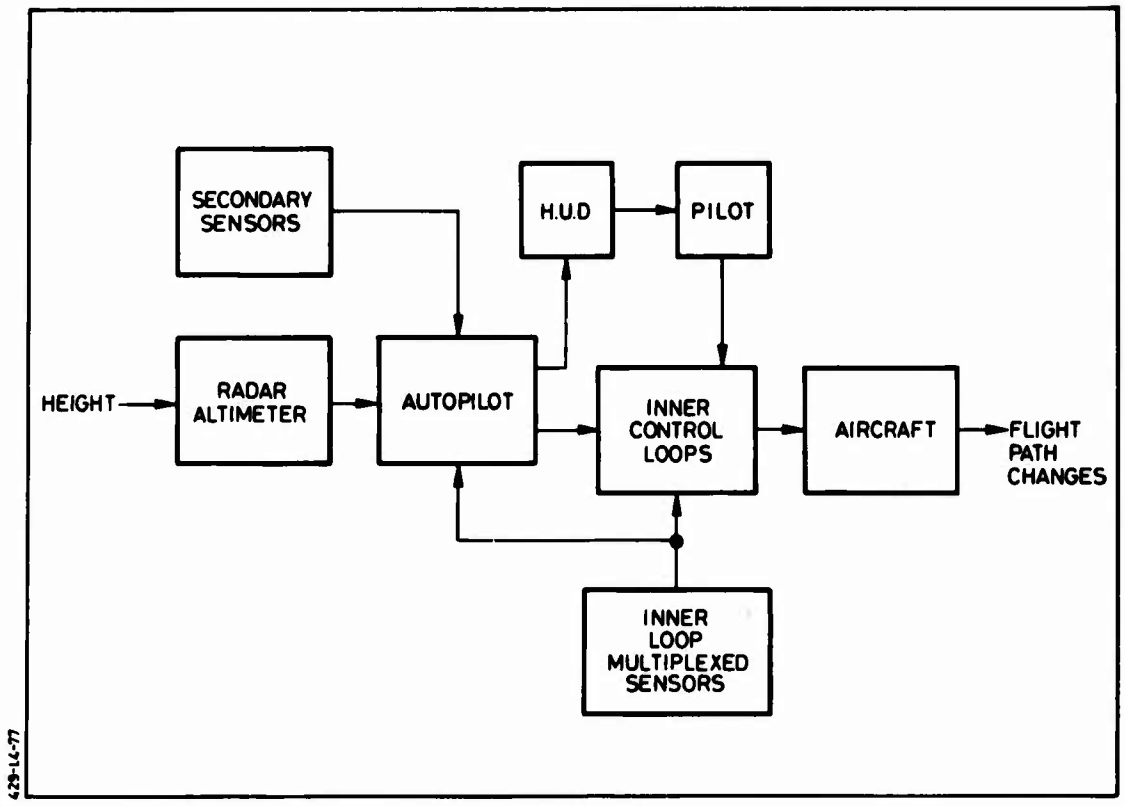

Figure 1 Simple Low Flying System

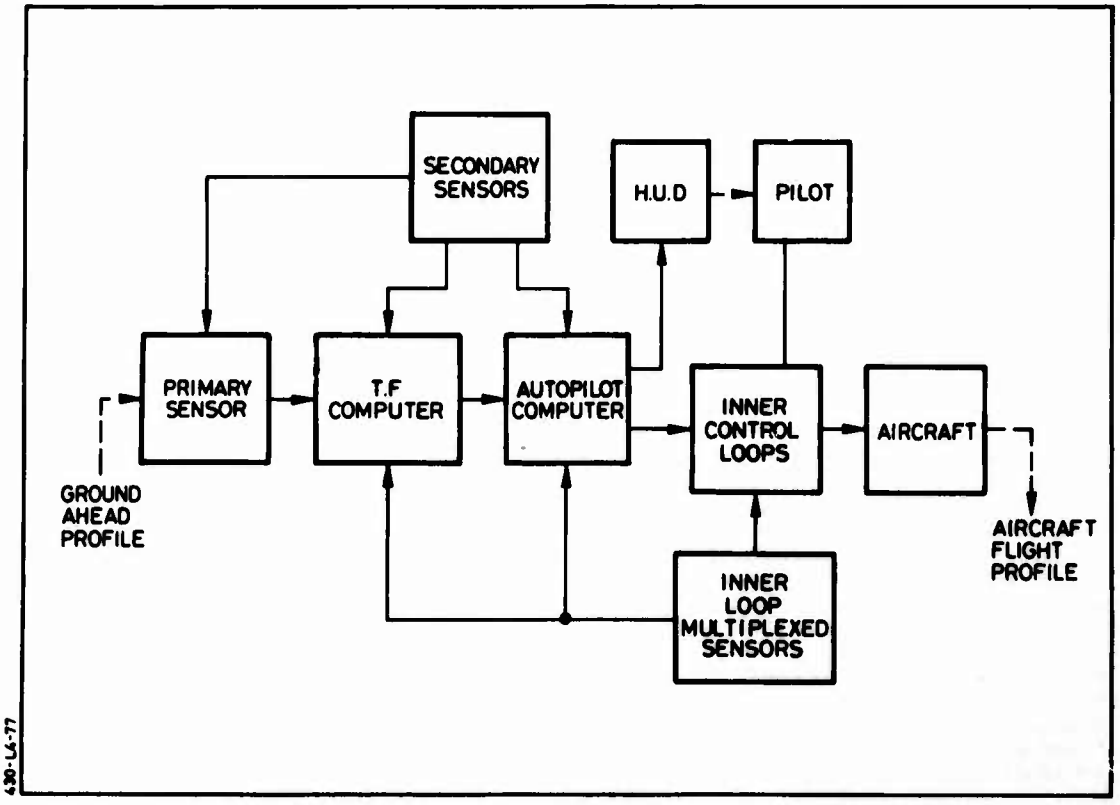

Figure 2 TF System Schematic

The main operational defect of these simple systems is the problem of returning the aircraft to its cruise altitude safely once it has climbed into cloud to avoid an obstacle. This problem is similar to that experienced by civil aircraft on the approach to an airfield where natural obstacles, hills or mountains, lie close to the flight path, where without precise navigational information descent through cloud is hazardous.

A generalised block diagram of a more complex system providing blind flying capability is shown in figure 2. The system depends on a forward looking sensor (normally TF radar) to provide a ground profile of the terrain ahead. In order to cover a sufficiently wide field of view the radar aerial normally scans in both elevation and azimuth axes. An additional computational task must be performed to convert terrain profile information into an equivalent height error signal or a manoeuvre command and this task is usually performed in the Terrain Following Computer (TFC)

Although the low flying system relies heavily upon the TF Radar for its outer loop guidance information the radar data must be corrected for aircraft attitude, incidence and drift angle, and provision must be made for secondary sensors and inner control loops which are matched in performance and integrity.

2.2 System Requirements

2.2.1 Reliability and Integrity

During low altitude TF flight the consequences of undetected failures are more serious than in any other phase of flight, due to the limited ability of the pilot to take recovery action. In addition, the sensor requirements of an automatic TF mode are more comprehensive than any other autopilot mode and hence the integrity of the several other sub-systems will strongly affect the safety in this mode.

During the course of a UK MOD funded study, various TF system architectures were examined with the aim of achieving a target probability of less than 1×10^{-5}/hr for any hazardous undetected failure in the total system. (The low flying system is defined as the chain from TF radar to control surface actuation, but does not include airframe, engines or electric/hydraulic power supplies).

The investigation of various system configurations required collection of reliability data on the constituent units of the system and most important a measure of the extent or effectiveness of the on-line monitoring in each sub-system.

The target probability for undetected failures in a flight director type of system is less easy to define from established safety requirements, since the pilots ability to detect a failure will depend on many factors including the speed of failure application and the location of the failure. However, undetected failure probability should be ' remote', (less than 1×10^{-5} per hour).

2.2.2 Terrain Following Sensors

The forward looking TF sensors that can be considered are TF Radar, Scanning Lasers and LLTV. The requirements for the ideal sensor are shown below with the TF radar meeting most of the requirements with the exception of the last, ECM.

- **Range** — The sensor should have adequate range such that sufficient warning of distant objects can be given at aircraft speeds up to Mach 1.2 at sea level.
- **Resolution** — High resolution at extreme range is an ideal goal. However, finite beam width limits the use that can be made of the information. At mid and close ranges it is highly desirable that credible returns can be received from power cables and pylons, and fluctuations in angular indications should be minimised.

  Azimuth resolution of objects in the beam would also be a desirable feature, if it could be obtained with little penalty, since objects off-track at long range could be ignored.
- **Weather Penetration** — Capability is essential for low altitude flight in rain, cloud and fog. Means to eliminate the possibility of flying over rain or clouds under the impression that it is ground are essential.
- **Terrain** — Type tolerance is required such that returns are not lost or fluctuate over thick vegetation, forest, snow or glassy water, etc.
- **Beam** — Width should be sufficient to allow for aircraft turn manoeuvres, and means should be available for scanning in both elevation and azimuth.
- **ECM** — Vulnerability should be minimal both from the point of view of the TF sensor giving indication of aircraft presence and the ability of the enemy to jam the TF sensor itself.

2.2.3 Terrain Following Computing

The calculations necessary for conversion of radar range and boresight angle returns to guidance signals are well established and are summarised below in Table I.

Table I TF Outer Loop computations

Calculation of 'ski-toe' functions for various ride levels
Calculation of flight path angle command from: Range, set height, boresight and and incidence
Calculation of aircraft manoeuvre limits
Input data checks
On-line BITE
Radio height control law (back-up control).

2.2.4 Secondary Sensors

Secondary Sensors' encompass all the sensors used to align and stabilise the primary TF sensor in its outer loop guidance role together with the sensors required for the inner control loops. Tables II and III give a summary of signals, their application and possible sources within the aircraft avionic systems.

Table II Secondary Signals Used in Outer Loop

SIGNAL	REQUIRED FOR	SOURCES
PITCH ANGLE θ	Computation of elevation commands	(i) IN SYSTEM (ii) VERTICAL GYRO
BANK ANGLE ϕ	Ground stabilisation of TF sensor	(i) IN SYSTEM (ii) VERTICAL GYRO
ELEVATION INCIDENCE α EL	Computation of elevation commands	(i) From INS θ, $\dot{h}$ and V_G (ii) From Doppler V_2 and V_G and θ (iii) Computed from incidence and sideslip signals, resolved and correct to ground axes.
DRIFT ANGLE δ	Track correction of TF radar	(i) IN SYSTEM (ii) From Doppler V_y and V_G (iii) From sideslip vane resolved into ground axes
TURN RATE $\dot{\psi}$	Biasing sensor sightline into turn	(i) From yaw rate (ii) From Compass (iii) Computed from ϕ and V_T
SPEED MACH OR 'g' LIMITS	To adjust ski-toe according to aircraft manoeuvre capability	(i) INS V_G (ii) ADC V_T or M (iii) Autopilot

Table III Secondary Signals Used in Inner Guidance Loops

SIGNAL/PARAMETER	REQUIRED FOR	SOURCES
RADAR HEIGHT h_R	Back up control for outer loop	Radar Altimeter
HEIGHT RATE $\dot{h}$	Damping of radar height control loop	(i) INS (ii) ADS
ANGULAR RATES p q r	Inner loop and stability augmentation	(i) Rate gyros (ii) Strapdown INS (1 lane)
NORMAL ACCELERATION n	Normal acceleration demand inner loop	Accelerometer
HEADING/TRACK ERROR ψ_E χ_E	Azimuth outer loop control	(i) Compass (ii) NAV Computer
BANK ANGLE ϕ	Azimuth control loops, Turn coordination, Pitch priority limits	(i) INS (ii) Vertical Gyro
AIR DATA p-s, s V_T, h_p	Gain schedules, turn coordination, 'g' limit computation	(i) CADC (ii) Multiplexed capsules (iii) Baro-Inertial source

In most aircraft designed for automatic TF flight, the design of the inner loop will be 'failure-survival' with no degradation of performance after a first failure. If this is not so, then some form of automatic pull-up manoeuvre would be required after a failure is identified, since the pilot reaction time and aircraft response time would be too long to prevent collision with the ground following a failure at low altitude.

The most critical secondary parameters are therefore those concerned with the TF loop and those used in the autopilot for intermediate control loops, e.g. attitudes, speed, manoeuvre limit parameters.

The minimum requirement is for dual sources for these signals, which enables a failure to be identified and a pull-up initiated. If a redundancy level better than 'fail passive' is available then a failure does not require an immediate automatic pull-up.

The provision of the secondary signals very much depends on the total aircraft avionic fit and if a choice is available then the following ground rules apply:-

- Use attitude sources with similar accuracy and dynamic response.
- Wherever possible use the highly redundant information available in the inner loop, particularly if accuracy is not critical.

  e.g. Yaw rate, not $\dot{\psi}$

  P-S and S for 'g' limits
- Specify an IN system interface which enables most use to be made of the high quality signals available in the INS, e.g. $\dot{h}$, δ, V_G
- Decide the method of obtaining α_{EL} at an early stage in the design, since it may not be available with the required integrity level.
- Limit as far as possible the number of other sub-systems that the TF system is relying upon for its functioning.

2.2.5 Flight Control System

The flight control system comprises the autopilot and inner loop control functions which may be separated or integrated according to the complexity of the stabilisation function of the inner loop and the redundancy levels required. The main computing tasks for these functions are given in Tables IV and V.

Table IV Autopilot Functions

Axes conversion from ground axes to aircraft axes
Turn Coordination
Pitch Priority System
Lateral coupling to NAV
Auto pull-up
Response shaping in pitch
Additional pitch control loops
'g' limits
Mode and Failure Logic
BITE (on-line and pre-flight)
Flight Director computing

Table V Inner Loop Functions

Stability Augmentation
Redundancy Management (Voters, Monitors Servo Lanes)
Control Surface Servo Loops
Voting and Monitoring on redundant air data sensor signals
Management and scheduling of variable geometry devices, e.g. wing sweep, LE, TE flaps
Structural Filters

The major features arising from the addition of a TF Mode to the other modes are the pitch priority limits, which give pitch commands priority over lateral commands when they are competing for a share of the normal acceleration available, and the provision of an automatic pull-up facility which operates after certain failures have been identified. It is essential from the performance point of view that the outer TF loop feeds into an inner control loop with good normal acceleration response, and because of this a special coupler may be necessary to match the inner loop response to the TF loop requirements.

Because of the large authority required in TF and the likely complexity of the inner loop control system, it is necessary that the actuation system has an adequate level of integrity to match the role that it plays in Auto TF flight. In order that an auto-pull up can be performed after a single system failure, the actuation must retain its performance under these conditions, and preferably, since it is basic to the control of the aircraft it should survive two failures without degradation of performance.

3. SYSTEM ARCHITECTURE FOR HIGH INTEGRITY

Having discussed briefly the system elements and signals required to implement a blind flying TF system the next step is to examine the optimum system design to achieve the required level of integrity.

Unfortunately the choice of system layout for TF operation will be constrained by the other roles the aircraft is called upon to play e.g. The TF radar cannot use the full aperture available at the nose of the aircraft because it must share the available volume with a mapping radar. The constraint of cost may result in the TF system designer having to make do with a secondary sensor signal of insufficient integrity because it happens to be provisioned as part of some other requirement. But if the total avionics package is considered at an early stage across the various operational requirements then a more optimum layout will result than if the various sub-systems are purchased off-the-shelf and assembled into a system.

The method of assessment adopted for this study was to examine various system configurations with the design goal of minimising the probability of undetected failures, while maximising the mean time between defects (MTBD).

The comparative integrity of different sub-systems depends very strongly upon their level of self monitoring and a special effort was made in the study to determine the credibility of monitoring percentages claimed by sub-system designers and manufacturers. In many cases the sub-system e.g. Gimballed IN may be designed with no particular requirements in its specification for self monitoring and the self checking capability will be confined to the digital processor section of the sub-system. A list of assumptions used in this study, based on collected data is given in Table VI. This reflects

currently available equipment entering service now or during the next five years

Table VI Sub-System Reliability and Monitoring

SUB-SYSTEM	TOTAL FAILURE RATE (ppmh)	PERCENTAGE MONITORING	UNDETECTED FAILURE RATE ppmh
TF RADAR TX/RX AND SERVOS	3000	98	60
IN SYSTEM GIMBALLED	2500	10	2250
IN SYSTEM STRAPDOWN	500	97	15
ATTITUDE AND HEADING REFERENCE	1600	50 (VISUAL)	800
TF COMPUTER DIGITAL	1100	95	55
AUTOPILOT COMPUTER DUPLEX APPLICATION	1000	40 (per channel)	600
COMBINED TF C/AP COMPUTER - PER CHANNEL	1250	40	750
RADAR ALTIMETER	660	90	66
CADC	450	15	382
DOPPLER NAV	1600	10	1440
AIR DATA CAPSULES (TRIPLEX)	270	TRIPLEX	0.1 SINGLE FAILURE
FULL AUTHORITY INNER LOOP	5000	TRIPLEX	0.05 FAILURE HAZARDOUS
'E SCOPE'	660	50 (VISUAL)	330
HUD OPTICS AND CRT	1000	90 (VISUAL)	100
DISPLAY COMPUTER	1000	95 (VISUAL)	50
LASER RANGER	2000	60	800
FULL AUTHORITY ACTUATION	1300	QUADRUPLEX	0.015 HAZARDOUS FAILURE
RATE GYRO	140 per gyro	TRIPLEX	NEGLIGIBLE
ACCELEROMETER	50 per sensor	TRIPLEX	NEGLIGIBLE
NAV/WAS COMPUTER	1000	97	30

In this study a total of eight different system architectures are considered, which are variations of the basic system, No. 1, shown in figure 3.

In the basic system some sub-systems, e.g. Inner control loop, have virtually zero probability of undetected failure because of their already high level of redundancy. The secondary sensor signals are also available, in duplex form, from two independent NAV systems, hence the level of success in meeting the design goal of 100,000 hours between undetected failures is solely determined by the efficiency of the self-monitoring function in the 'simplex' elements. In System 1 these critical elements are the TF Computer, TF Radar Receiver/Transmitter and the Radar Altimeter, the latter unit has not such a direct effect on integrity because it is only in control of the aircraft for short durations, over the top of peaks and over glassy lakes, and its undetected failure rate has been reduced to 1/10 of its actual value to allow for this.

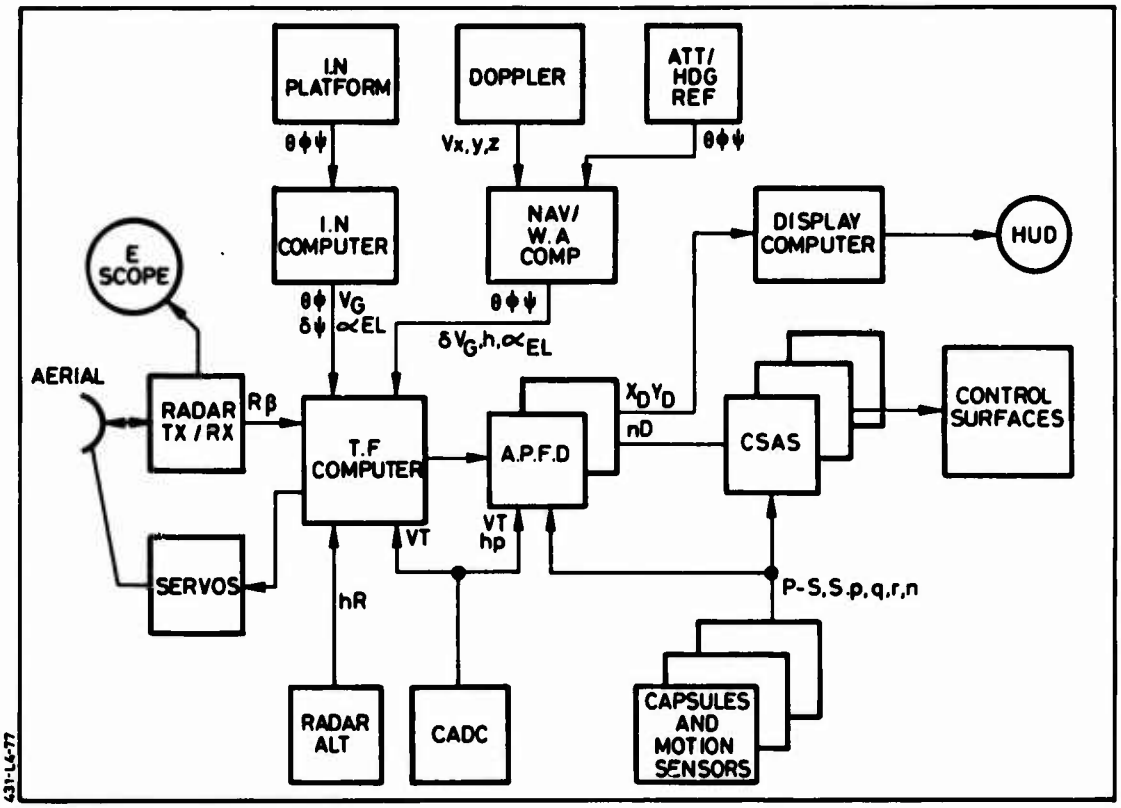

Figure 3 TF System 1

System 1 has an undetected failure time in the region of 8000 hours. See Table VII, which is well below the design goal. The critical elements have already high levels of self monitoring (of the order of 98%) hence there is little to be gained by spending a large amount of effort to obtain the last fractions of percent.

Table VII Reliability and Integrity Comparison - Various Systems

SYSTEM	DEFINITION	MEAN TIME BETWEEN DEFECTS	MEAN TIME BETWEEN UNDETECTED FAILURES
1	BASIC SYSTEM	49.5 hrs	8,213 hrs
2	DUPLEX TFC/APFD	51.0 hrs	14,981 hrs
3	2 WITH SIMPLEX STRAPDOWN IN	74.7 hrs	12,232 hrs
4	2 WITH DUPLEX STRAPDOWN IN	72.0 hrs	14,981 hrs
5	BASIC WITH SIMPLEX STRAPDOWN IN	64.1 hrs	7,312 hrs
6	BASIC WITH LASER MONITOR	45 hrs	16,194 hrs
7	SYSTEM 3 WITH LASER MONITOR	65 hrs	45,977 hrs
8	SYSTEM 4 WITH LASER MONITOR	62.9 hrs	148,148 hrs

The alternative solution is to add extra lanes or elements, but this will have an adverse effect on overall defect rate, and whereas it may be technically easy to duplicate purely computing functions, to improve integrity, the problems of duplication of the primary TF sensor are almost impossible to solve because of space limitations. The results for the 8 systems have been plotted in two ways, figure 4 shows the contribution of the critical elements to the hazardous failure rate, while figure 5 indicates the

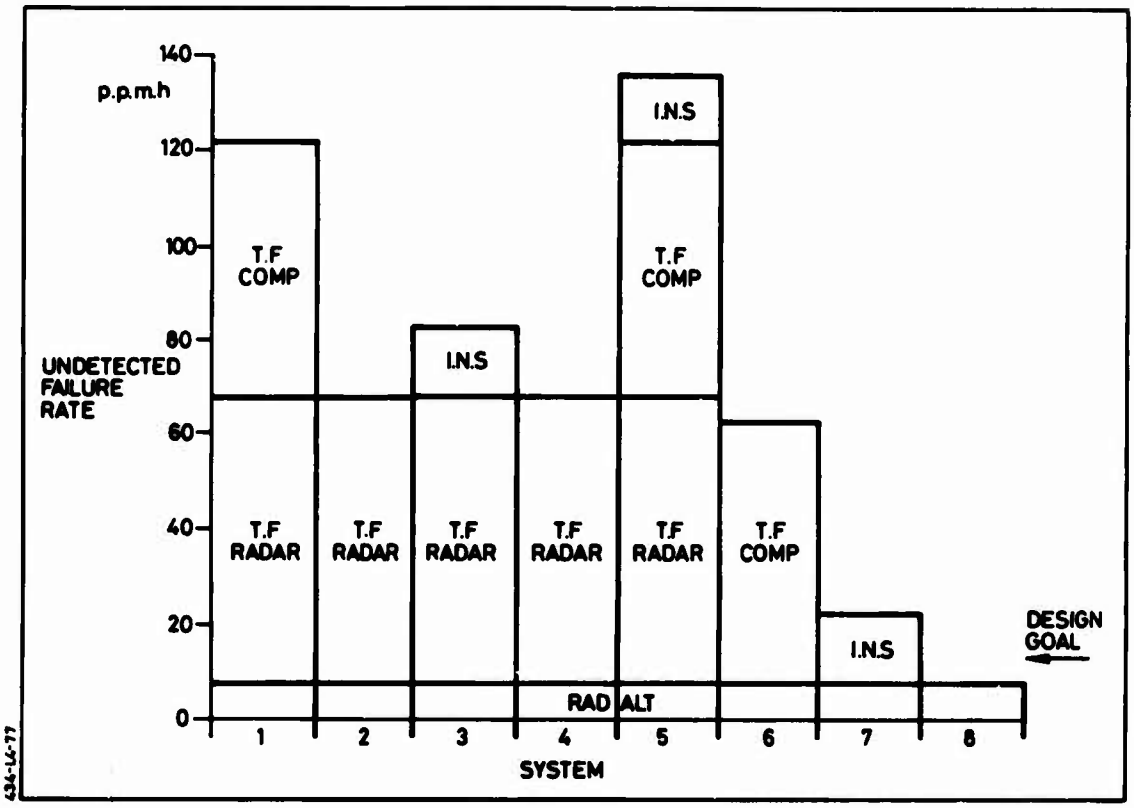

Figure 4 Build up of Undetected Failure Rate

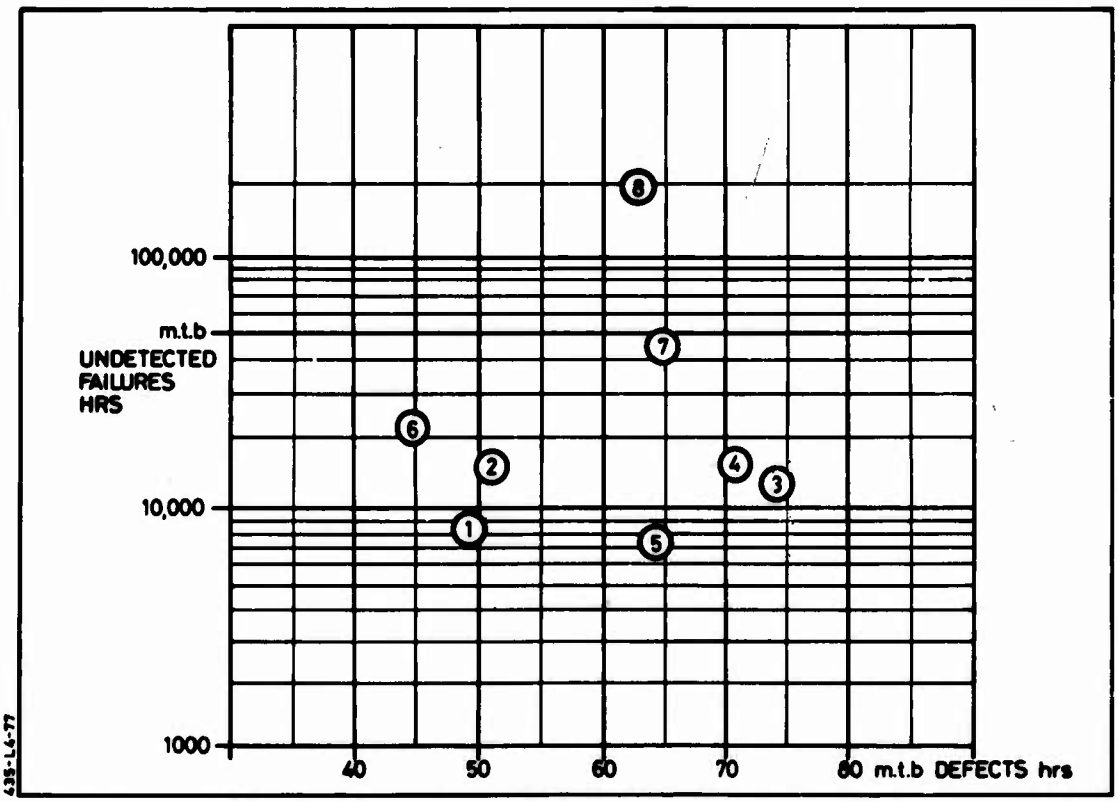

Figure 5 Reliability/Integrity Comparison

balance between system integrity and overall defect rate.

Using this approach several methods of increasing the system integrity are highlighted.

- The simplex monitored TF Computer tasks could be performed in the autopilot, which has duplex redundancy (System 2 - figure 6)

- The provision of secondary control parameters, mainly attitudes, in System 1 carries a penalty in defect rate. A single strapdown IN System substituted for the existing INS/Doppler/Attitude Reference gives a significant reduction in defect rate, and because of its high level of monitoring adds only a small penalty in hazardous failure rate. (System 3).

- The major remaining source of undetected failures is the TF Radar Receiver/Transmitter, and in Systems 6, 7 and 8 it is postulated that this can be fully monitored by an independent sensor in the form of a Laser Range finder. Subject to the feasibility of this, the integrity design goal can be met.

Since the TF Sensor is critical to integrity, and is the one area which cannot be easily duplicated, various monitoring methods were examined in order that integrity levels could be increased by conventional electronic means or by independent monitors.

4. MONITORING OF TF SYSTEMS

The results of the previous section indicate that the primary TF sensor is the most critical area where monitoring is applied since it is unlikely that space is available to duplicate the radar in all but the largest aircraft, while the other sensors including the radar altimeter can be duplicated, if necessary, and the computing functions in the TF system are likely to be almost all digital in nature and are becoming easier to monitor with the extensive use of multiplexed lanes and microprocessors which can efficiently perform a full-time on-line monitoring function.

4.1 TF Sensor Monitoring

Failure of the Aerial Elevation/Azimuth scan servos can be detected by standard servo monitoring methods e.g. position error monitoring. The provision of a power threshold in the receiver channels of the RF head and a small test horn-feed in the tip of the radome can provide monitoring of the transmit/receiver cells. The test horn-feed injects a small amount of power into the receiver via the aerial at top of scan and hence monitors the receiver and aerial. The transmitter output power can be checked at every pulse by an RF power monitor, while a further receiver test can be performed during an inter-pulse period by injection of a wide band signal into the RF head, this also checks the sum and difference circuits. The above methods when applied in conjunction with power supply monitoring, result in a high level of monitoring in the radar. However, it is impossible to achieve a 100% level because of the difficulty of detecting such mechanical faults as cracks and holes in the radome and mechanical faults in the aerial and mounting structure. It is thought that damage or deterioration of the radome or aerial surface would be detected by routine ground maintenance, and would only result in degraded performance as opposed to catastrophic failure. Although the percentage of failures not detected by the monitoring may be small the failure probability is still significantly high relative to the design goal, hence the application of a dissimilar sensor must be considered.

4.2 Laser Monitor

The use of a Laser Ranger for this task was suggested by the fact that many military aircraft already are fitted with such a device. It is unlikely that currently used laser range finders would be directly applicable, but it should be possible to develop a laser capable of performing both tasks.

Features of existing lasers which are unsuitable for TF use are the flash tube life, the pulse repetition frequency, (p.r.f) and the lasers ability to damage eye-sight, which would limit peacetime operation. In TF applications the laser would be called upon to work at longer ranges if it were to exactly mimic the radar and this brings problems of operation over a wide range of ground reflectivity and at shallow angles to the ground. From the point of view of monitoring, problems may arise because of the difference in returns off-boresight due to the different beam width of the two sensors.

The laser will also suffer a relative disadvantage as a result of fog, rain or snow conditions compared to radar, and for this and all the above reasons performance may be marginal except at close ranges. One compromise is to employ a fixed laser at the bottom-of-scan elevation angle, where it has the best chance of detecting a radar range error, this fixed system also has the advantage of requiring a lower p.r.f. and hence longer life and reliability will result.

There are still a number of technical problems to be solved in such a laser design, a requirement to cool the receiver to minimise thermal noise and to develop suitable optical windows capable of withstanding erosion effects expected at low altitudes. Because of the lack of experience in this area, reliability and integrity data is sparse. However, the next few years are likely to bring rapid changes, perhaps enough to merit the use of a laser as the prime TF sensor, which will result in weight saving and a reduction in the warning transmissions propagated ahead of the low flying aircraft.

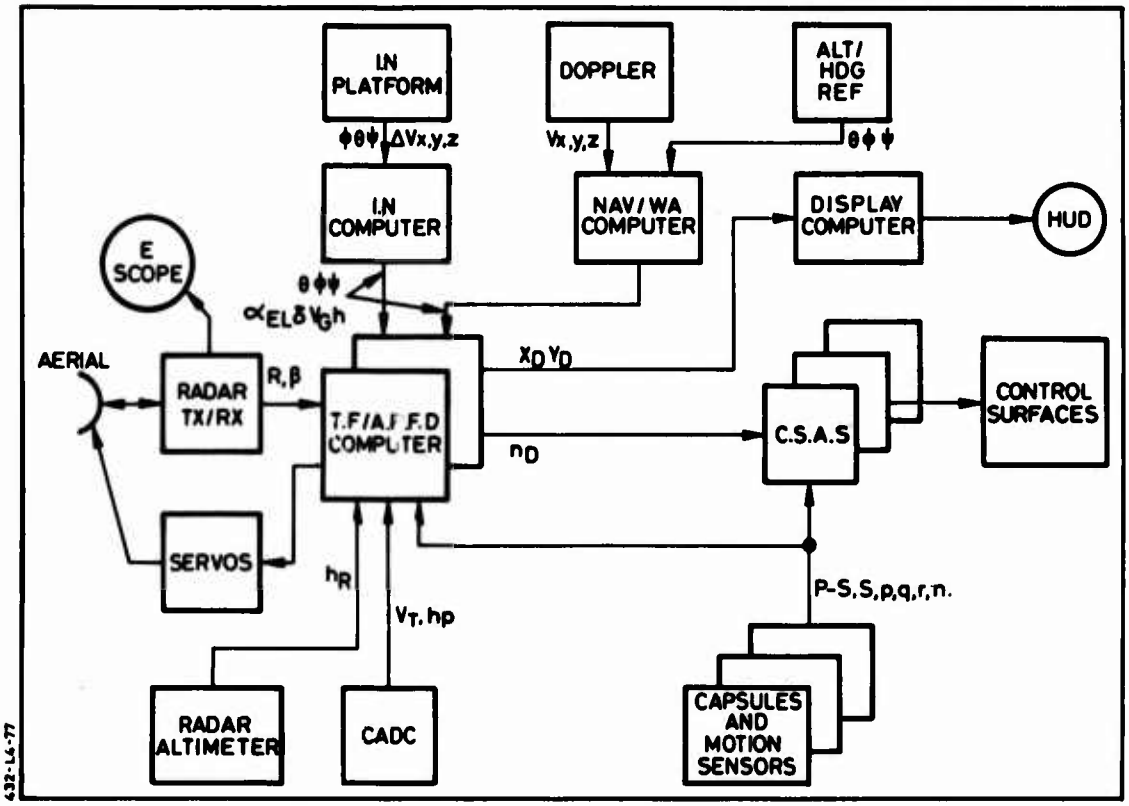

Figure 6 TF System 2

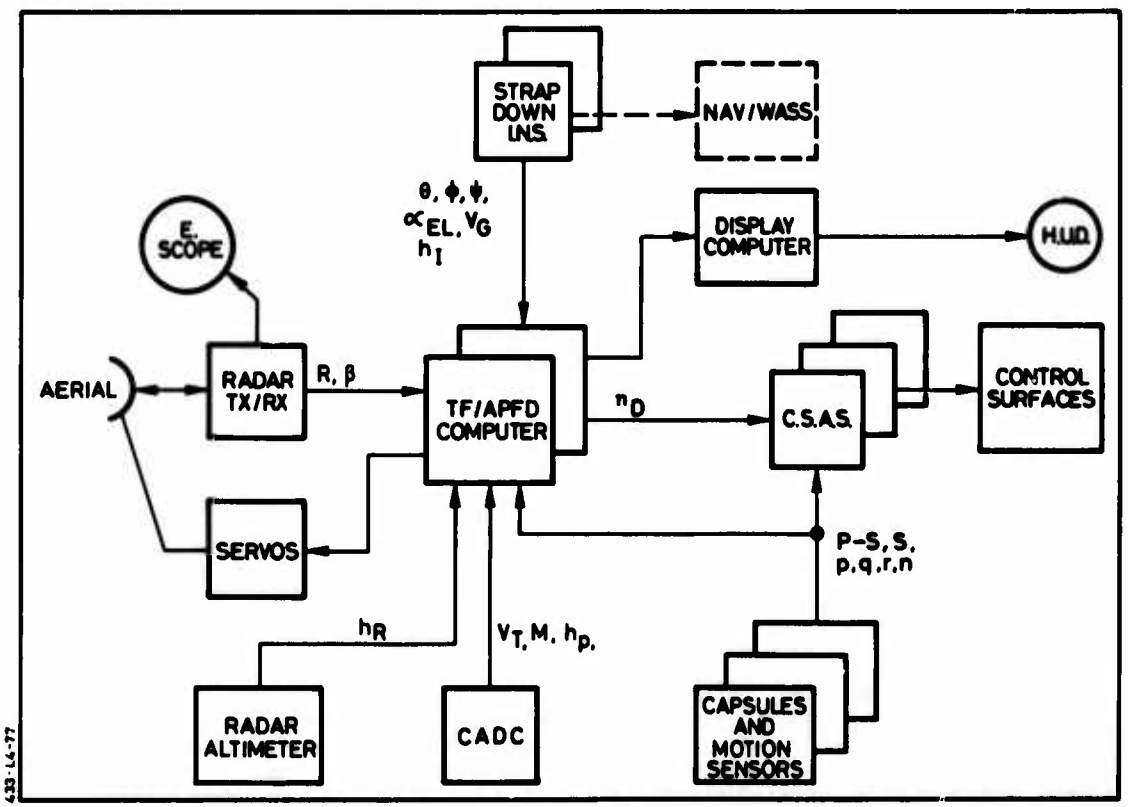

Figure 7 TF System 4

4.3 Terrain Ahead Storage

In current analogue terrain following computers the control algorithm used is based on commanding flight path changes computed from the most nose-up return per scan which requires only two storage circuits. This form of control tends to concentrate on one or two terrain features at a time, while the vast majority of the radar returns are ignored. A terrain following system based on storing a more complete profile of the terrain ahead was discussed at least seven years ago (2), where the stored data was employed to compute and fly a kinematic flight path over the terrain. The work described in ref 2 was carried out to obtain significant performance advantage in achieving an optimum profile, however the same principle can be applied to increase the level of monitoring of the total system.

The terrain storage method can be implemented as part of the TF Computer or in the form of a separate monitor unit. A digital processor is employed to receive the radar range and boresight angles, to convert them to its own axes system, allowing for distance travelled vertically and horizontally and to store them in range segments at intervals of 200 feet or so, see figure 8. Prominent terrain features will generate numerous returns, and as soon as sufficient number are collected in one terrain segment, various smoothing or voting algorithms can be performed upon them. Failures of the radar aerial, incidence references or appearance of a 'chaff mountain' can be detected by logic operations on each segment and the array of segments. It will be possible to use the smoothed terrain data for guidance as well as monitoring if so desired.

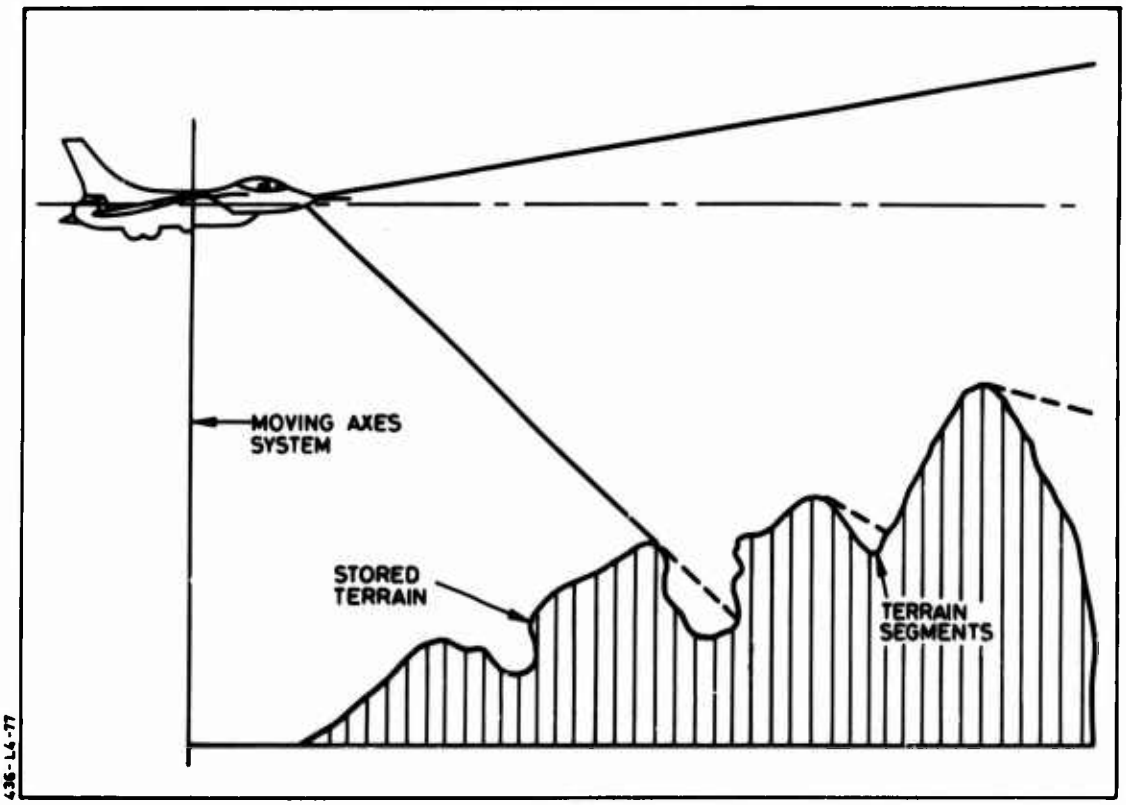

Figure 8 Terrain Ahead Storage

The storage method used must compensate for two major effects, firstly the three dimensional effects of the beam/terrain geometry, which cause objects to pass out of the scanned volume as their range decreases, and secondly errors in the stored terrain profile caused by turning flight. A limited assessment of the necessary smoothing algorithms has been made, based on sparse recorded radar data, and this has shown the need for the use of an algorithm that 'fades out' stale returns in a particular segment, as the range decreases, to eliminate inaccuracies caused by measurements made at longer ranges. Figure 9 shows the height calculated for two range segments as successive returns are received from those segments. At longer ranges the measured height tends to oscillate, but settles down at around 12000 feet range. There are still errors at close ranges compared to the radio altimeter measurements, but this is due to lack of data from this segment, since only most-nose-up points are available. Figure 9 shows that simple averaging is not satisfactory as a smoothing method since the effect of large errors at long ranges tend to contaminate results at closer ranges: a 'faded highest' algorithm gives a good compromise and would give improved results on current algorithms which employ most-nose-up per scan and must tend to fly high. More investigation is required into this method before the effectiveness as a monitor can be established, and thus requires availability of large

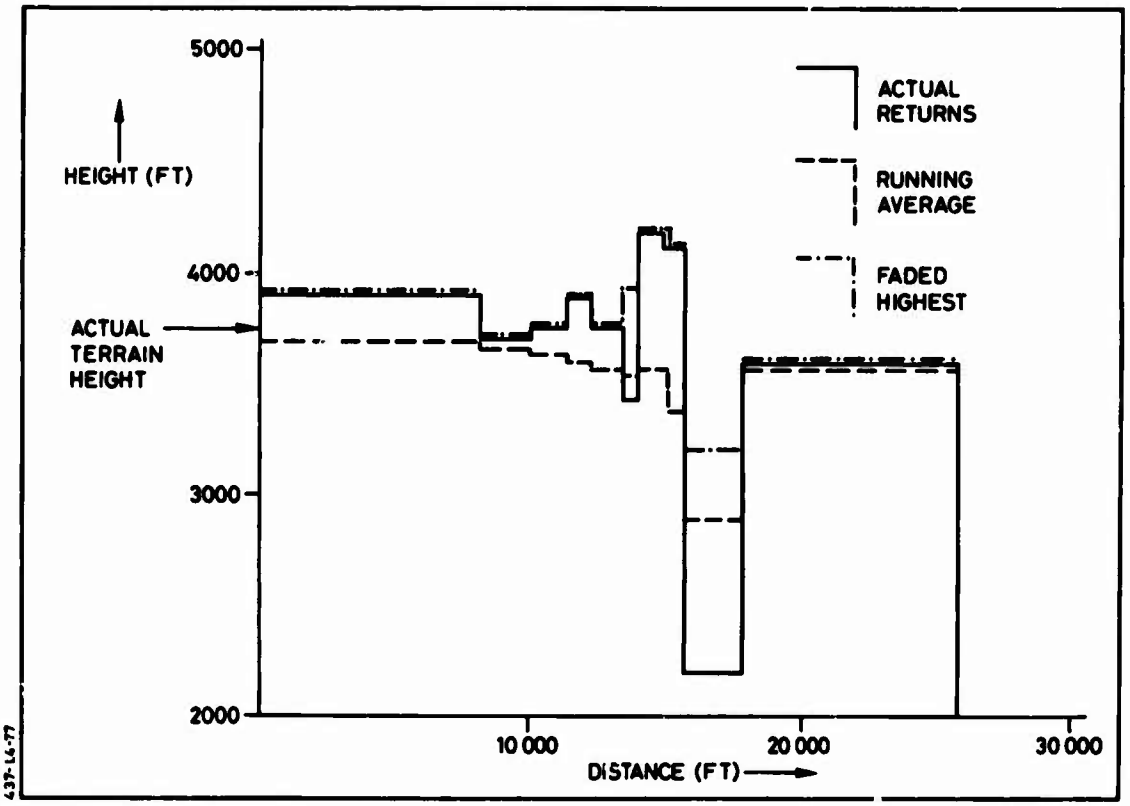

Figure 9 a) Smoothing of Radar Returns - Segment 36

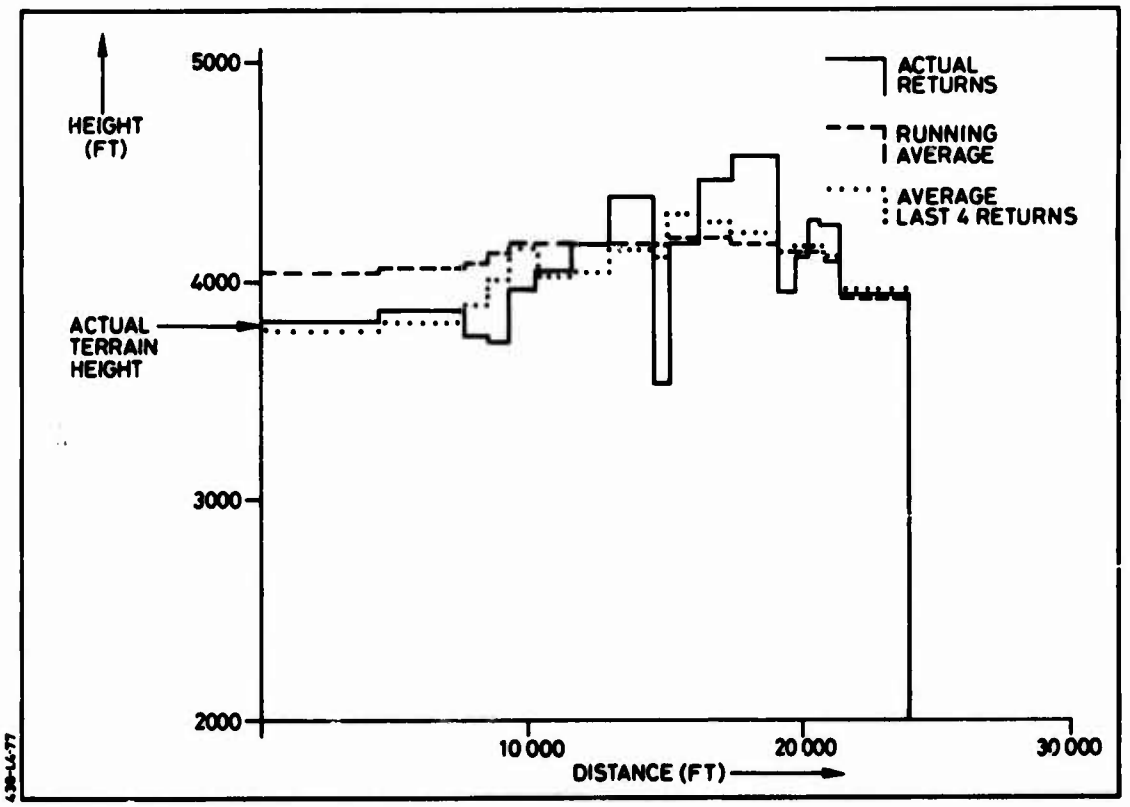

Figure 9 b) Smoothing of Radar Returns - Segment 40

amounts of recorded radar data, at p.r.f. intervals from aircraft flying controlled flight paths in straight lines and steady turns. There is an almost unlimited number of smoothing and monitoring algorithms that can be investigated to obtain trade-offs with nuisance disconnects and monitor logic.

4.4 Overall System Monitors

There is a strong economic case in favour of any relatively simple system monitor that can detect failures in any of the systems elements by detecting performance degredation in the outer control loops. Such monitors can be based on monitoring the height error between the set clearance and radio height or monitoring the flight path angle or normal acceleration command loop errors. The simplicity of these monitors limits their effectiveness, since unless the terrain is smooth, the height error monitor is too late to avoid ground collision and the flight path error monitor is duplicating the task of the usual autopilot monitoring systems. This reinforces the requirement to have an additional independent TF sensor, with ability to monitor radar operation including the TFC and possibly the radar altimeter.

4.5 The Role of Displays

In flight at low altitudes the time available to react to a pilot detected failure is very short e.g. 0.5 seconds or less, and hence visual monitoring is not an acceptable substitute for automatic methods. If the clearance altitude is increased and the pilot concentration level can be maintained, then a HUD based monitor is feasible. A display on the HUD of an appropriate outer loop error signal should be complementary to the automatic monitoring function, since if the parameter can be displayed it can also be used to operate a failure comparator.

The main application of displays should be in areas where the information cannot be presented by HUD symbology but remains as a pictorial representation for example the E-Scope picture of the actual radar returns ' stored on the screen with a natural ' fade-out' of stale data. This presentation is essentially a long-term health monitor which will detect weather or jamming effects and would be a useful means of combining outputs of independent monitor systems e.g. lasers, with the primary TF Radar.

5. A LOW ALTITUDE ADVISORY SYSTEM (LAAS)

5.1 Terrain Matching

Safety during operation of TF flight is of concern to a minority of all aircraft operators. However, the monitoring methods investigated for TF may well be applicable to aircraft not fitted with TF Radar, but which operate, for example, close to the ground in a tactical close air support role.

In searching for an independent monitor for the TF system, methods based on prior knowledge of the terrain profile were examined. Recent developments, notably the cruise missile, have led to highly accurate navigation systems, based on area correlation using radiometric sensors and stored maps, or terrain profile correlation using radar altimeters and stored terrain altitudes. The initial application of these systems was to supply a mid-course navigation correction to the IN System and to give very accurate guidance at the terminal phase for weapon delivery, hence the volume of map data could be limited.

There is a wide spectrum of applications of this improved navigation technology, but of particular interest is the possibility of obtaining information about the terrain ahead which does not depend upon any forward looking sensor. At one end of the spectrum is a TF system with clearance attitudes less than 500 feet, which flies a kinematic flight path over a stored terrain profile using a grid size of say 100 feet spacing. With an aircraft radius of action of 300 miles this system would require storage of around 800 million terrain points, which is well beyond the capacity of even ground based disc storage devices. The map area to be stored would be reduced if a strip of terrain were considered corresponding to specific targets or missions or if larger sized grids were employed for areas where terrain was smooth. In assessing the feasibility of such a system it should be noted that the number of terrain points to be stored is proportional to the inverse square of the grid side length. Also the required grid size can be increased if the terrain clearance height is increased, since not only does the radar altimeter receive returns from a larger area, but accuracy of terrain clearance is less critical and a smoother profile can be flown, using reduced ' g' limits.

The simplest form of system, which has wide application need not guide the aircraft flight profile but merely advise on the aircraft' s vertical situation relative to local terrain features. For this type of system a grid size of $\frac{1}{4}$ mile would be adequate, leading to storage requirements up to 10 million words, much closer to currently available disc storage capacity.

5.2 Advisory System Implementation

The primary implementation problem to be solved is that of storage of terrain data, and this depends on the map area to be covered. For high reliability it is desirable to restrict data storage to ROM devices, hence with reasonably sized current airborne processors, maximum capacity would be in the region of 64K to 256K which would provide data for approximately 4 aircraft pre-planned missions or for civil application, 10 local airfield regions. Beyond this capacity it is necessary to use bulk storage, disc or magnetic tape, which reads blocks of terrain data into a volatile data store as the aircraft flies along. Clearly it is desirable to avoid the use of bulk storage methods because of their effect on reliability, cost and weight, and with the rapid advances in electronic storage devices, particularly recent

developments in bubble memories, the area of map which can be stored is increasing.

A block diagram of a Low Altitude Advisory System (LAAS) is shown in figure 10. It has relatively simple interfaces with the other aircraft sub-systems and consists mainly of a large data store, a simple processor and small control panel.

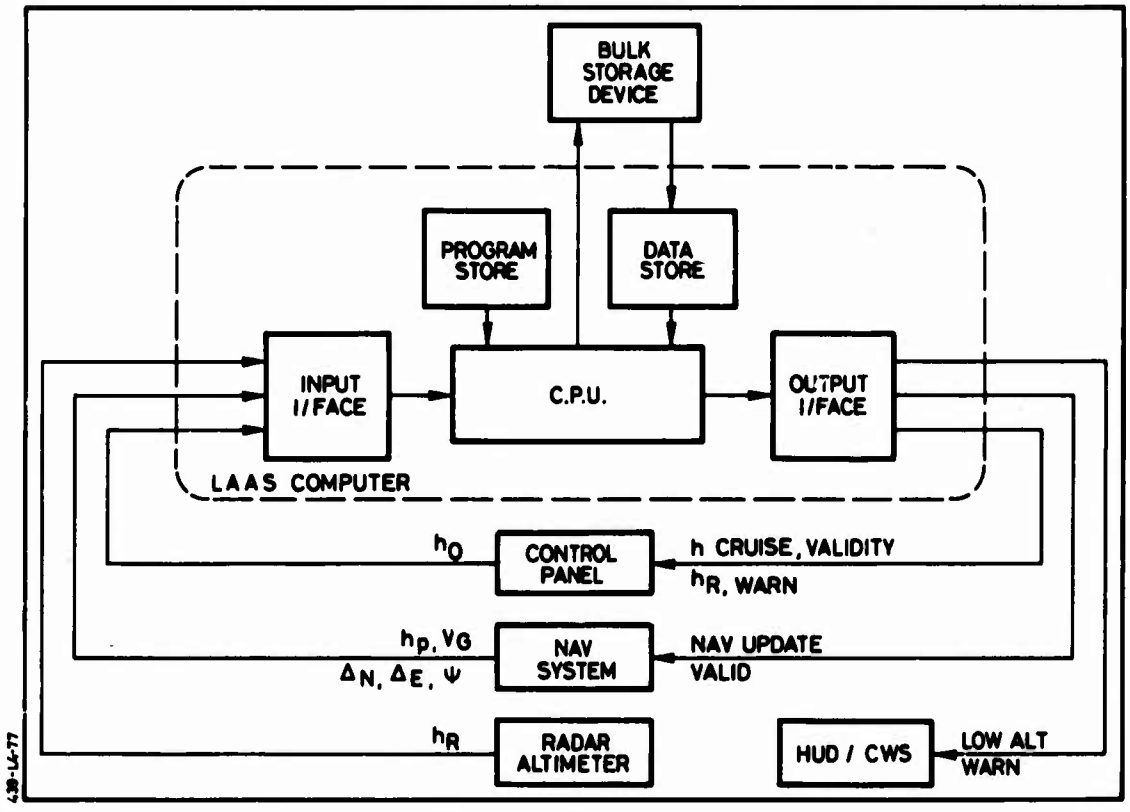

Figure 10 Low Altitude Advisory System (LAAS)

The computer calculates a safe cruise altitude based on a set clearance of the terrain up to say 10 miles ahead of the aircraft. Any penetration of the clearance plane will generate a warning to CWS or HUD.

The terrain matching function is performed continuously, and requires short term incremental position changes from an IN or Doppler based NAV system together with an approximate initial position fix. If a good match is obtained to the stored data an update validity is set to enable the NAV system to be updated if required. Where terrain is flat or smooth the advisory height is computed for a limited time based on dead reckoning.

This type of system has the advantages of being relatively self contained: more passive than FL Radar based systems and is capable of retrofit, with enhancement of NAV system performance over land.

6. FUTURE DEVELOPMENTS

In the quest for high integrity in low altitude flight control systems, improvements are being made in all areas, perhaps with the exception of TF Radars, where monitoring levels are already as high as can be achieved without full duplication. TF radars still have room for improvement in the area of signal processing where digital smoothing techniques can lead to better performance and this can be achieved at little cost penalty.

There is a definite requirement for a simpler, smaller, forward-looking sensor (probably an eye safe laser) which could be installed in a variety of aircraft at a fixed boresight angle to provide a monitor during manoeuvres close to the ground and in mountainous terrain. There is still a large gap between TF Radar performance in all weathers and the capabilities of laser sensors, and this needs to be bridged before this type of monitor is feasible.

A more recent trend which has a significant effect in improving integrity is the use of strapdown IN Systems in place of the traditional gimballed platform system which has relatively low MTBF in military applications. The strapdown INS can have self monitoring levels up to 97% at little extra cost, whereas gimballed systems tend to be largely unmonitored. Since attitude information is crucial to low

flying, and particularly TF flight, the wider use of strapdown IN will have significant effect on total system integrity.

Accurate knowledge of aircraft position must contribute, if only indirectly, to safety in flight and future development of navigation aids in particular NAV-Star will have an impact in both civil and military application. This system based on satellites placed in geosynchronous orbit has a potential positional accuracy of the order of tens of feet. A system using NAV-Star coupled with stored maps for automatic terrain avoidance or driving a moving map display would provide protection to civil aircraft particularly during the terminal flight phase and for military aircraft in specific operational areas. The NAV-Star System is susceptible to jamming on a local basis only, so that a simpler low performance navigation system is required as a back up in military applications. The current and future scene in the area of flight control will be strongly influenced by the flexibility and versatility of digital computing. Optimum control of the aircraft for different tasks can be achieved with fewer compromises although this means additional complication. High integrity is obtained by the inherent self checking capability of digital computers and now that microprocessors are available to military specification they can be applied in many areas as off-line full-time monitors to various sub-systems.

7. CONCLUSIONS

It is essential that all the elements of the low flying system are considered together as a total system in order that an optimum allocation of sub-system interfaces and integrity levels are achieved. This analysis should be performed before sub-system specifications are fixed in order that no 'weak links' exist in the system integrity. A total system view will result in definition of the reliability target, monitoring level and critical functions of each sub-system.

Such a study on Automatic TF Systems has highlighted the problems of monitoring the primary TF sensor effectively, since this is one area where adding additional sensors or computing lanes is not possible. Various monitoring methods have been suggested, including extracting more information from radar returns, utilising stored map data on terrain profile ahead, or using a laser ranger as an independent monitor. The laser sensor solution if developed to be eye-safe has the widest application for both military and civil aircraft and could be easily retrofitted.

A significant contribution to safety at low altitudes can be achieved by more accurate knowledge of aircraft position relative to local terrain hazards. While it will be some years before NAV-Star is generally available, consideration should be given to the enhancement of existing navigation systems by addition of corrections based on terrain matching methods. Subject to the limitations in the volume of data stored, the navigation information can be used to provide advance warning of specific terrain features.

References

1. An initial Flight Assessment of Low Light TV as a Manual Terrain Avoidance Aid

   R.G White, A. Karavis
   AGARD CP 211

2. Optimal Terrain Following Controller
   1/Lt A.F Barfield, D.P Rubertus
   AGARD CP-72-71

3. Automatic Navigation Updating by means of Digital Correlation Using Image or Nonscanning Sensors.

   A Hessel, W Eckl
   AGARD CP211

TERRAIN FOLLOWING CRITERIA
THE NEED FOR A COMMON MEASURE

By

A.F. Barfield
CCV Technical Director
Air Force Flight Dynamics Laboratory
Wright-Patterson AFB, Ohio, USA

SUMMARY

During the advanced development of a new terrain following system, it became evident that, although the basic merits of the system could be validated by flight testing, comparison with other systems based on differing terrain following command generation techniques was extremely difficult and at times misleading. A "common measure" for evaluating terrain following systems did not exist. Detailed criteria were not available for adequately specifying terrain following system needs relative to strategic and tactical requirements. Performance evaluation measures being used varied widely from one system to another, and such measures were generally developed for a specific system being tested. At times little more was required than for a system to follow the terrain in some safe manner. When detailed specifications were established, meeting those specifications did not necessarily mean good operational performance.

Previous efforts have resulted in the separate development of requirements in many important related areas (safety, performance, reliability, stability, vulnerability, structural fatigue, ride comfort and cost). Because of this separate development, application of specific and sometimes conflicting requirements to terrain following has resulted wherein the relative importance of each factor was unknown. A research program, discussed in this paper, was undertaken to organize the results of these efforts into meaningful terrain following criteria. The standards developed were required to be independent of system mechanization. Initially a literature search was conducted to obtain data on various terrain following systems and previously used criteria. Terrain following concepts were categorized and used to define common system elements that would be considered in the study. Criteria were then established based on this previous work and a current simulation effort. Performance measures were quantified and a performance index established. The performance index, in conjunction with a checklist, provided a means of comparing terrain following techniques. A handbook was then formulated but remains to be validated before incorporation into applicable Air Force Specifications can be accomplished. The proposed criteria are intended for use not only in writing terrain following system specifications, but also in determining terrain following equipment design, equating and ranking alternate terrain following methods and allowing the merits of modifications to be assessed.

INTRODUCTION

Flight testing of a new second generation terrain following system was being conducted at Wright-Patterson under the direction of the Air Force Flight Dynamics Laboratory. This new system had been designed by General Electric through the application of Optimal Control Theory to the terrain following problem. The approach offered improved contour following within established aircraft and crew constraints. Simulation evaluations and the flight test effort were demonstrating very good results. The time had come to document the results of this new concept and push for application. Questions about how the new system compared with a currently favored operational system and what impact it would have on cost, reliability, etc. needed to be addressed. In attempting to make the desired comparison using flight test data, it became evident that the criteria for each system were generally developed as the system was designed. Such concept oriented evaluation measures usually evolved in order to insure that specific concept problems were solved in the development and production effort. In actuality the new system provided a definite performance improvement as ascertained by comparison of flight profiles over simulated terrain and examination of acceleration time histories; however, evaluation with system oriented criteria presented an erroneous assessment. The impact on reliability, total cost, aircraft vulnerability, etc. of the new concept could not be easily determined. This emphasized the need for universal terrain following criteria for both manual and automatic systems. It was decided that formulation of such criteria should make maximum use of meaningful existing guidelines.

THE CRITERIA DEVELOPMENT EFFORT

A contracted research effort was initiated with the Boeing Company in Wichita, Kansas. Terrain following criteria were to be developed through analysis, investigation and trade studies. This new criteria would be compiled in a handbook format to allow easy utilization. As a starting point in the effort, a six-month long literature search was conducted to collect information from industry and government sources. Figure 1 provides a general breakdown of the reviewed documents by major topic areas. The search provided several general conclusions: 1) Most of the recent work was concerned with improvement of specific systems and, unfortunately, very little objective criteria had been developed; 2) Safe performance was a common concern; and 3) Only a limited amount of useful data from Low Altitude High Speed (LAHS) flight testing were available. In order to develop meaningful criteria, it became necessary to conduct investigations using a detailed terrain following simulation which included defensive (threat) models for specific penetration routes of interest. Pertinent aircraft dynamics and flight control system characteristics were also represented in the simulation in addition to real world terrain sections. The search also highlighted common performance guidelines being used by the community which are listed below:

- Subjectively evaluate flight path time histories
- Minimize RMS clearance altitude deviation from the reference clearance altitude
- Attain level flight over dominant peaks
- Minimize RMS normal acceleration
- Reduce the maximum clearance altitude deviation

- Reduce minimum and maximum vertical velocity and vertical acceleration
- Minimize time at altitude

It was also apparent that terrain following performance was influenced by parameters dependent on the aircraft's performance capabilities and the penetration mission. These included aircraft forward velocity, terrain roughness and frequency content, defensive threat, aircraft clearance altitude, climb and dive limits and normal acceleration capability. Although trade studies and analyses performed to select an optimum design generally considered the above constraints, survival from terrain clobber and enemy defenses was not assessed.

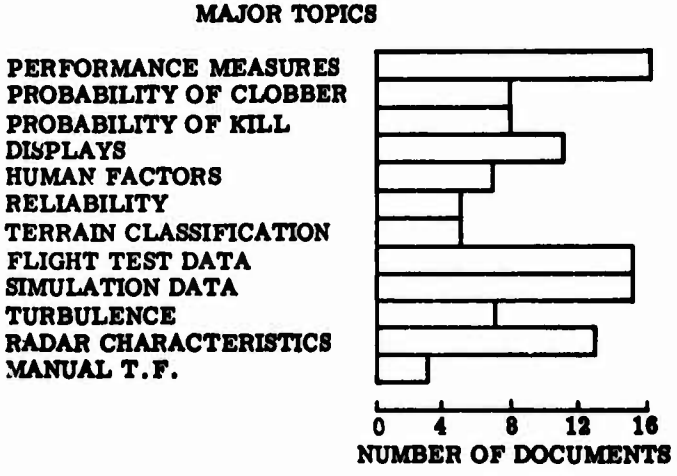

Figure 1 Literature Review Breakdown

The terrain following mechanizations examined varied widely. Command generation concepts included template (scanned range), angle command, advanced low altitude technique (ADLAT) and optimal controller systems. However, basic elements were found to be common to these terrain following systems as shown in Figure 2. General design philosophies for each of the common blocks were then specified. For the terrain following radar, accurate terrain profile sensing in straight and turning flight is crucial to flight safety. Resolution, accuracy and sensitivity must be improved to provide adequate input data to the terrain following system in adverse situations such as the encounter of trees, power cables, relay towers, precipitation, deep snow, jamming, etc. Sufficient minimum range and low angle coverage for adequate control are needed. It has also become apparent that a capability for elevation boresight calibration for a system installed in the aircraft is desirable. Drift stabilization in azimuth during turning flight, self-check and self-calibration are also required. In the command computer means must be included to provide restraints while generating desired flight commands. Safety measures to provide failure detection and annunciation, overrides and emergency maneuvers are needed. These should cover not only the computations in the computer but also aircraft states, internal radar operation and associated subsystem checks. Measurement characteristics of the radar altimeter must be considered in the overall terrain following system design. In some cases the radar altimeter's effective cone of reception can be used to advantage. The difference between altimeter measurement and actual clearance directly beneath the aircraft is a function of aircraft pitch angle, ground slope and the altimeter's effective measurement cone angular coverage. One system analyzed had differences as large as 29 percent of the selected clearance altitude. Compensation would be required if the terrain following system also used inertial quantities for referencing terrain height or aircraft altitude. The display must present adequate data to perform manual terrain following or for operational assessment of an automatic system. Failure warning is vital, and although a visual indication may be acceptable, aural warning for the more serious failures especially ones causing fly-up, warrant consideration. Manual and automatic terrain following displays need to be compatible for fail-safe protection. Overlay cursors on the forward looking terrain following radar video in a form to allow inflight system calibration checks are needed. Display of radar video is an important backup mode for flying in rainfall and jamming situations. The coupler can be used to provide the required control system configuration for good terrain following performance without imposing undue restraints on the basic flight control system which must be designed to accommodate many other mission objectives. Interface logic and signal conditioning for proper operation with the flight control system should be accomplished at this point. The terrain following system, although only a part-time element of the flight control system, directly impacts flight control design. Authority, redundancy and safety requirements must be compatible with the terrain following system's requirements. Studies have also shown that a limited authority automatic flight control system (AFCS) can severely degrade an aircraft's terrain following capability. Pilot assist functions advantageous for the terrain following mission such as an automatic ground track or a wings leveler should be considered for inclusion in the flight control design. In addition, maximum use of the aircraft's available maneuvering capability should be allowed for terrain following within acceptable dynamic constraints. It would be beneficial to develop a design to provide commanded trajectories that minimize stress on the aircraft and crew while maintaining terrain masking. A smooth and well-damped response without excessive excitation by turbulence is needed. Fail-operational capability should be provided to the extent possible. Any fail-safe implementation should result in graceful degradation.

After the review, analyses and simulation investigations, criteria were formulated in eight specific areas:

- Safety
- Performance

- Reliability
- Stability
- Vulnerability
- Structural Fatigue
- Ride Control
- Cost

Highlights of the study results in each area will be covered in the following discussions. A performance index will also be presented that provides a means of addressing the importance of each area. A question and answer checklist was established to allow scoring in each area for this performance index, but a comprehensive simulation capability was also required to evaluate some areas.

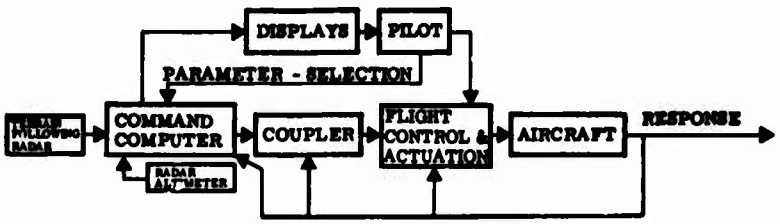

Figure 2 Common Terrain Following System Elements

SAFETY

The failure mode capability of a terrain following system cannot be allowed to be degraded by interfacing systems. After examination of pilot reaction times for recoveries from hardover failures and the associated altitude losses during such conditions, the requirement was established for the terrain following system to be a fail-safe design. To fulfill such a requirement in this mission phase requires fly-up initiation and appropriate pilot warning following a failure. Terrain following operation has a significant impact on the failure mode capability of the automatic flight control system. The AFCS must be operational after a failure to allow exit from the terrain following environment or mission continuation with manual terrain following. The fly-up mechanization must be included in the fail-operate flight control system. Built-in test, self-check, wrap around and redundancy should be considered in realizing this level of failure mode capability. The fly-up mechanization recommended is one in which the command is initiated by either a hardware failure or a predicted excessive clearance altitude undershoot. The predicted undershoot is formulated using the aircraft's present clearance altitude, vertical velocity and normal acceleration. Such undershoots should not exceed 80 percent of the desired clearance altitude. Consideration must be given to the possibility of the loss of the information used in this prediction during certain failure conditions. A fly-up acceleration command inversely proportional to the selected acceleration limit would be desirable.

Due to the critical nature of the mission, the built-in test equipment needs to provide an on-line capability to continuously monitor system performance, inflight pre-engage tests to ensure initial proper operation, and ground tests to allow pre-flight failure detection, and calibration. The pre-engage tests should provide checks on operation of all modes within the system. Automatic letdown to the highest terrain clearance setting provides a useful system confidence check if included as a pre-engage test. In reference to the established probability of aircraft loss, the terrain following system is considered as a part of the flight control system during the terrain following mission phase. Thus, the maximum allowable probability of aircraft loss due to all material failures allocated to the flight control system must include the terrain following equipment.

Clobber considerations were also evaluated in the formulation of a safety measure. A probability of clobber (P_C) value for a single encounter of a terrain obstacle of 2.7×10^{-7} had been determined by previous investigations to be acceptable and safe. However, the computation of P_C was based on a normal distribution of terrain clearance altitude points. Many systems are specifically designed to provide a skewed distribution due to safety and performance considerations. A graphical method of determining P_C was found that allows application to data with non-normal distributions. Figures 3 and 4 illustrate the concept. First, the lower portion of clearance altitude points from actual or simulated system operations is plotted on probability paper. A straight line is fitted through the data points below the selected clearance value, H_Q. This is represented by the dotted line in Figure 3. The clearance altitude value where this fitted line intersects the 50 percent probability line is designated "$\bar{X}$", and the clearance altitude difference between the intersection of the line with the 50 percent line and 15.9 percent line is designated "σ". The values of $\bar{X}$ and σ are used in Figure 4 to determine a P_C value. Examining this graphical technique, it becomes apparent that the ratio of $\bar{X}$ to σ is itself useful as a safety measure. The slope of the plotted lower clearance distribution points defines σ. For high $\bar{X}$ values the slope can be small representing a large deviation of points and still produce the desired ratio and a safe P_C value. As the system's mean clearance $\bar{X}$ is reduced, the slope of the lower clearance distribution line must increase to converge on the same P_C value. It should be remembered that the terms "mean value, $\bar{X}$" and "standard deviation, σ" have been loosely applied to allow meaningful interpretation of plots from actual terrain following systems with skewed distributions. This type of technique can easily be included in a terrain following simulation to evaluate the probability of clobber for various designs as performance is being examined.

PERFORMANCE

Trade studies have illustrated the extreme sensitivity of clearance altitude on aircraft survivability during a penetration mission. To provide flexibility to accommodate various defensive threats and terrain variety, a pilot variable clearance altitude setting is desirable with detents to aid in positive selection and avoid inadvertent alteration. The resolution of this setting needs to be as high as practical design allows. Simulation evaluations indicate the need for a ±10 feet resolution for settings at 300 feet or

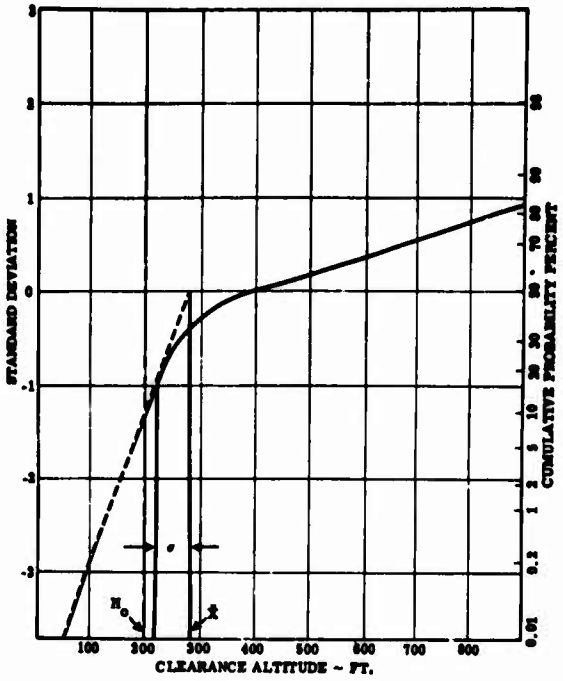

Figure 3 Distribution Plot of Lower Clearance Altitude Points Used to Determine $\bar{X}$ and σ

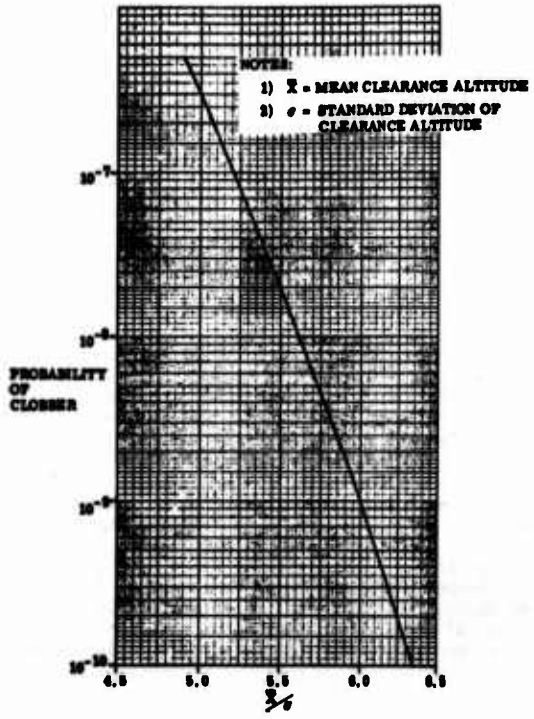

Figure 4 Relationship of $\bar{X}/\sigma$ to Probability of Clobber

lower. The actual clearance altitude chosen will depend on the mission, expected threat and previous knowledge of the system's operation. The extremes at present are 100 feet and 1000 feet. Several of the systems reviewed consistently operated either above or below the selected desired clearance alt'tude. Provisions are needed in the clearance altitude mechanization to allow removal of such a system bias during ground tests.

Terrain following acceleration constraints are usually also pilot adjustable. The review indicated that three settings were normally provided. This appears to be a minimum requirement. It is proposed that maximum climb and dive accelerations for aircraft during terrain following be added to the specification defining maximum aircraft loads by mission class. Table 1 illustrates the proposed addition. Human factors analyses, simulations and trade studies suggested placing the dive limit at 50 percent of the specified climb limit in incremental g's. Other settings provided to the pilot would be equally spaced between zero and the maximum limits. Vertical velocity constraints are needed to prevent excessive sink rates or accidental stalls during terrain following commanded climbs. If the terrain following algorithm does not include vertical velocity limits, a means must be provided to warn the crew of obstacles that require an excessive climb maneuver. Data from the review indicated that a negative vertical velocity of 100 feet/sec for bombers and 150 feet/sec for fighters should not be exceeded. These limits need to be varied with the selected acceleration settings.

Basic Mission Symbol (1)	Symmetrical Flight Limit Load Factor					Max. Ordnance Weight		Time for abrupt cockpit longitudinal control displacement t_p, second	Terrain Following Load Factor	
	Basic Flight Design Weight		All Weights	Max. Design Weight						
	Max	Min at V_H	Min at V_L	Max	Min at V_{H_c}	Max	Min at V_H		Max	Min
A, F, TF (Subsonic)	8.00	−3.00	−1.00	4.00	−2.00	6.00	−2.00	0.2	+3.0	0.
A, F, TF (Supersonic)	6.00	−3.00	−1.00	4.00	−2.00	6.00	−2.00	0.2	+3.0	0.
O, T	6.00	−3.00	−1.00	3.00	−1.00			0.2	+2.5	0.35
U	4.00	−2.00	0	2.50	−1.00			0.3	2.0	0.5
B_I	4.00	−2.00	0	2.50	−1.00			0.3	2.0	0.5
B_{II}	3.00	−1.00	0	2.00	0.00			0.3	2.0	0.5
$C_{Assault}$	3.00	−1.00	0	2.00	0.00			0.3	2.0	0.5
$C_{Transport}$	2.50	−1.00	0	2.00	0			0.4	2.0	0.5

Table 1 Proposed Terrain Following Load Factor Addition to Specified Aircraft Loads

At this point the influence of two operational capabilities in the performance area will be considered. The first is the improvement in survivability due to improved masking if acceleration limits are established inversely proportional to terrain roughness. Over relatively smooth terrain a small altitude increase due to limited acceleration commands could result in aircraft detection. In rough terrain small altitude deviations are generally less significant. The second point concerns automatic engagement. Initial automatic letdown to the highest altitude setting of the system provides a means of inflight check of system operation. It is considered a reasonable system check since experience has shown that the largest undershoots occur during initial letdowns. Due to this the system should be designed to provide a well-damped letdown response. As a maximum, undercutting in this situation should not exceed 40 feet or 10 percent of the desired clearance, whichever is smaller.

In examining a means of assessing a terrain following system's performance, as well as stability, a new evaluation measure was developed. It was based on the use of frequency response information to investigate control system performance and stability. The generally accepted performance measures are dependent on system response characteristics, terrain roughness and terrain frequency. A terrain model that can be used to compare each system is needed. This model must be able to show typical, as well as, worst case operation. The performance measure proposed is shown below:

$$PM_{Test} = 20 \log \left[\frac{(H_o + Mean_{Terr}) - (\bar{c})}{Mean_{Terr}} \right]$$

where:

$\bar{c}$ is the mean clearance altitude of the terrain following system above the terrain.

H_o is the set clearance.

$Mean_{Terr}$ is the mean altitude of the terrain above the terrain's lowest altitude.

The technique was formulated for a 1-cosine terrain representation with a maximum height of 2 $Mean_{Terr}$ but can be extended to real world terrains as will be discussed. PM_{Test} is expressed in decibels. The intent was to have zero db represent a system that follows the terrain in a perfect manner ($\bar{c} = H_o$). As degradation occurs the PM_{Test} value becomes negative.

There are two minor problems with this approach. First, a unique value of $\bar{c}$ is assumed that can be realized only by a perfect system. Unfortunately, this uniqueness does not exist. A $\bar{c}$ value equal to H_o could be achieved by a system whose performance is less than perfect by flying under the desired clearance altitude to compensate for flying above it. However, such a system would be severely penalized by the clobber criteria presented earlier because of the excessive excursions below H_o. The second problem is that this performance measure penalizes any system that deviates from the selected clearance altitude. Deviations are necessary in any practical system since acceleration and vertical velocity constraints must

be imposed, and response lags are present. The best performance that could be obtained in such a case is an "ideal" flight path profile. Such a trajectory would be generated by a system with no response lags which exactly follows the terrain contour within the imposed constraints. Although elimination of response lags may appear unrealistic, the prediction effect in some advanced terrain following techniques can sufficiently compensate for their influences.

Using such an ideal profile generation technique with a specific set of acceleration limits, the terrain following system will eventually be restrained from precise contour following as terrain height or aircraft velocity increases. The PM value will then decrease as shown in Figure 5. The corner or break frequency, f_b, varies with the acceleration limits and $Mean_{Terr}$ heights. In this way, a realistic upper performance boundary can be established. The apparent frequency, f_a, used in the plot is the product of terrain frequency and aircraft velocity. This "frequency response" plot was then normalized by dividing the apparent frequency by the break frequency. Simulation data indicated a necessary but not sufficient condition for survival during a representative mission in that the actual terrain following performance must be maintained within one terrain standard deviation (σ_T) from the ideal response. The resulting performance envelope that was defined is shown in Figure 6 for the 1-cosine terrain. Lower boundaries were tabulated for various real terrain courses presently used for flight test evaluation. Although not acutally employed in flight testing, a minimum boundary for Penn 6201 was also computed since it has long been used for system simulation tests. These were calculated using the equation:

$$PM_{Minimum} = 20 \log \left[\frac{(Mean_{Terr} - \sigma_T)}{Mean_{Terr}} \right]$$

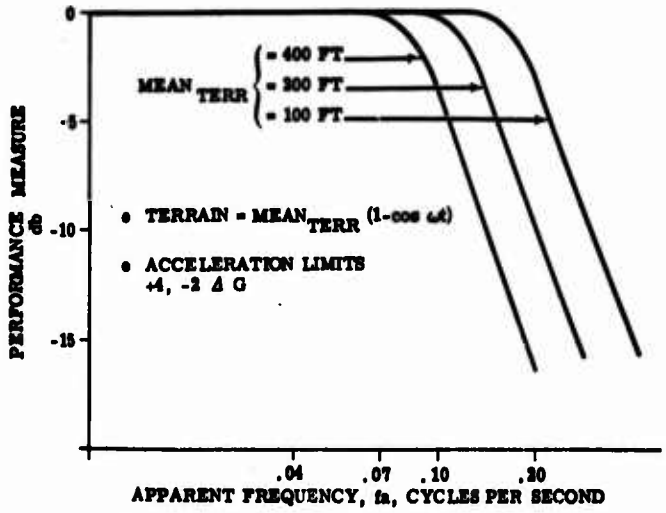

Figure 5 Performance Measure Response Plot

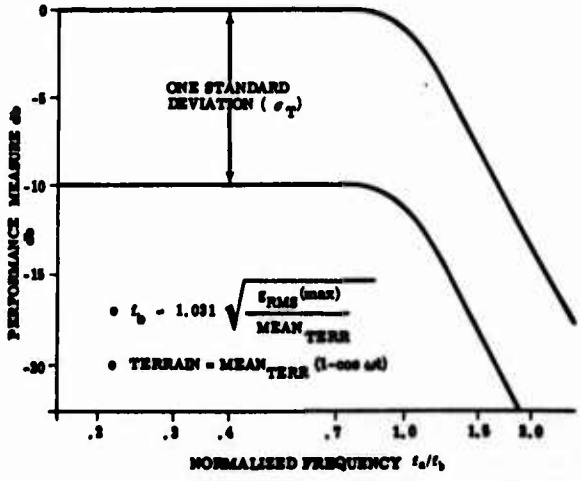

Figure 6 Performance Measure Frequency Response Envelope

A Fast Fourier Transform program was used to obtain magnitude versus frequency plots of various terrain routes to establish the upper frequency range of interest for the performance envelope. Figure 7 shows such a plot for Penn 6201. A normalized frequency of .2 was considered an adequate lower limit based on altitude changes during simulations. For the 1-cosine terrain the maximum terrain frequency was chosen to be 3×10^{-5} cycles per foot. Multiplying by aircraft velocity yields an upper apparent frequency limit. The corner frequency is then calculated for the proper constraints and terrain altitude and used with f_a to determine the maximum normalized frequency of interest.

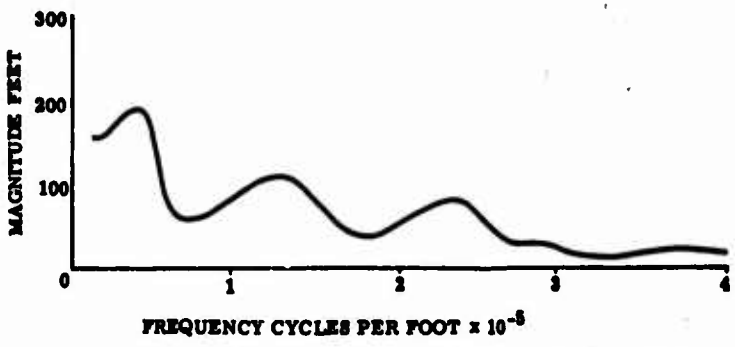

Figure 7 Fourier Series Magnitude vs. Frequency for Penn 6201

An acceleration band shown in Figure 8 can also be generated for system performance over 1-cosine terrain. Such a band provides a means of determining if excessive accelerations were needed to maintain clearance altitudes within the prescribed performance envelope. An index was also generated to allow a comparison of the compromise each terrain following system provides between clearance altitude performance and acceleration. The index is expressed as:

$$PI = \sum_{i=1}^{n} \frac{PI_i}{n}$$

where:

PI_i = 10 (actual Performance Measure-lower limit)+

$$100 \left(\frac{\text{allowed acceleration-actual acceleration}}{\text{allowed acceleration}}\right)$$

n = number of discrete frequency samples

To standardize the evaluation, initial altitudes were specified for actual terrain following systems being tested over 1-cosine terrains. The initial altitudes were chosen based on system acceleration limits, apparent frequency and the terrain's mean altitude.

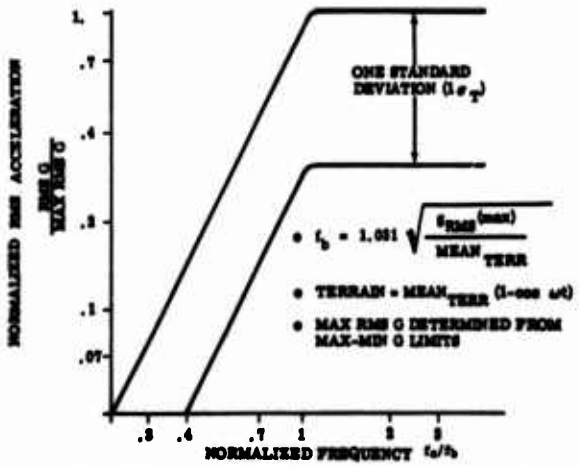

Figure 8 Normalized Acceleration Frequency Response Envelope

Overshoot and ballooning over prominent terrain peaks have long been values to be minimized in a system's design. To be useful a standard means of measuring this "time at altitude" was needed. In this study, $T_{altitude}$ was defined as the time at or above the terrain peak plus desired clearance altitude, H_D, as illustrated in Figure 9. Time at altitude will generally increase the exposure time of the penetrator. Exposure time becomes critical as it approaches the reaction time of the defensive system. If an ideal system clears the peak by a clearance altitude that was established on criteria developed for a total

Probability of Survival (P_S) value, then the ideal system is assumed to have a P_S considered optimum for the threat (probability of kill) and terrain (probability of clobber). In general the nonperfect system will increase the threat P_K as $T_{altitude}$ increases beyond the defense sites' reaction time. Overshooting and ballooning criteria will require terrain following systems to have the $T_{altitude}$ time less than the sites' reaction time for at least 95 percent (2 σ) of the time. Of course, the threat reaction time will vary among the various types of sites (AAA, SAM, etc.).

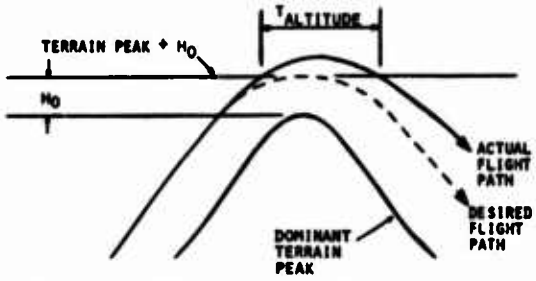

Figure 9 Additional Exposure Time Measurement

Finally, it was realized that an extensive low level penetration simulation was needed to provide a means of performing necessary trade studies between terrain following system parameters with success being measured in terms of probability of survival.

RELIABILITY

Mean Time Between Failure (MTBF) has to be predicted during system design. High MTBF is desired but, unfortunately, redundancy and complexity cause it to decrease. MTBF prediction techniques for terrain following systems need to be adequately substantiated. They must cover components that are likely to experience increasing failure rates with service life. Figures 10 and 11 annunciate the fact that there are significant differences between wartime mission and peacetime safety assumptions used in arriving at system reliability. Selected use of redundancy is recommended to meet mission and safety reliability. A goal for the failure mode capability is that it prevents any single failure from causing loss or major degradation of terrain following capability.

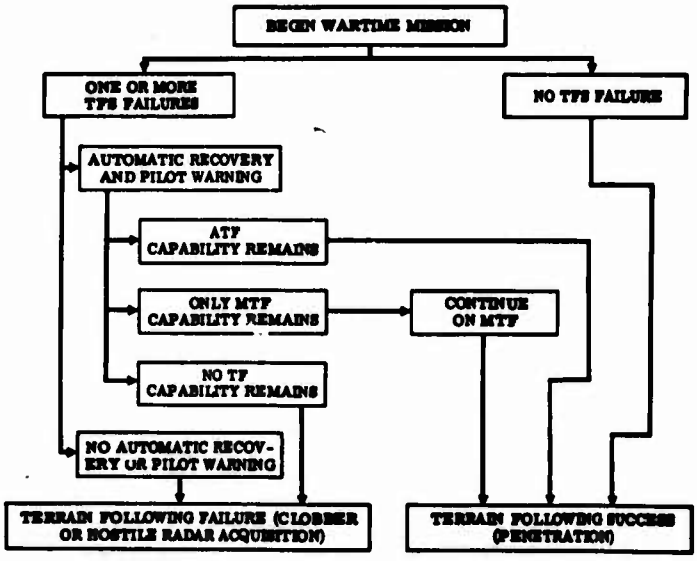

Figure 10 Wartime Reliability Event Diagram

Failure Mode and Effect Analyses are required by military specifications; however, preparation methods are not defined. The criteria developed provide requirements for this preparation. Most important are the treatment of power supply and failure detection circuitry and essential interface equipment failures. These analyses must be accomplished with reliability and system design personnel working closely together to prove useful. In such an investigation the "worst case" approach must be avoided. A degraded or erroneous output may be more difficult to detect and, therefore, more dangerous than a total signal loss or hardover.

Reliability optimization capabilities must be developed to allow the proper tradeoffs to be made between reliability increases and the associated space, cost, weight, etc. Such a capability does not exist at this time. One method proposed would be to directly relate the cost of an increment of mission reliability to overall aircraft and offensive armament cost. This includes operating and maintenance

costs during the intended useful life, and appropriate pro rata shares of costs of bases, depots, training, etc. Assume, for example, that this figure is $50,000,000 per aircraft. Since military effectiveness will be directly proportional to mission reliability, an increment of 0.01 in mission reliability will be worth (0.01) X ($50,000,000) or $500,000 per aircraft.

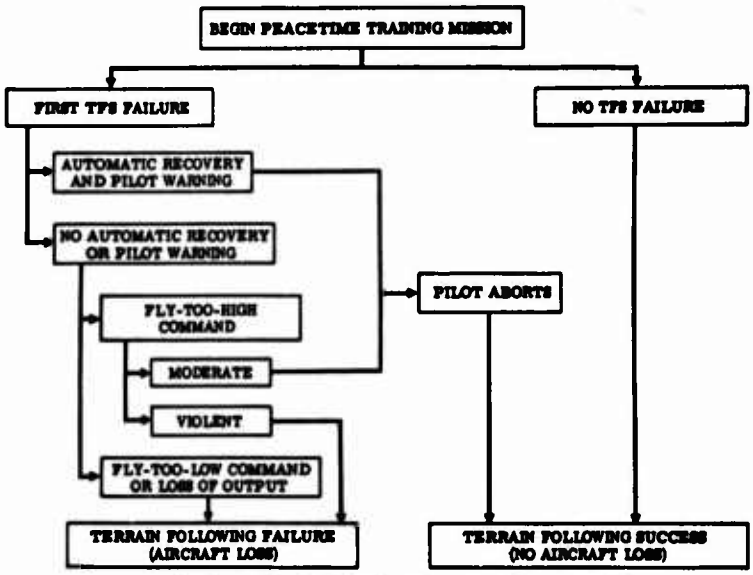

Figure 11 Peacetime Reliability Event Diagram

STABILITY

The terrain following system will have to comply with gain and phase margins specified for flight controls. This is due to the use of feedback control to maintain adequate performance. The terrain following system will also have to meet the residual oscillation limits imposed by handling qualities specifications. Table 2 illustrates the required stability margins for aerodynamically closed loops of the flight control system. A sensitivity analysis is usually needed to define the range of gain and phase errors that may exist. Parameter variation investigations are also required to identify the tolerance of these margins to changes in each significant parameter. The 1-cosine terrain performance and acceleration measures defined previously can be used to verify terrain following system stability. Simulated flight over six or more cycles is needed to obtain terrain following system steady state sinusoidal response characteristics. Evaluation using these measures over simulated real world terrains also appears to be valid.

	Low Frequency Modes	Medium Frequency Modes	High Frequency Modes	Very High Frequency Modes
Airspeed Up to $V_{o_{MAX}}$	GM = $\pm$4.5 dB PM = $\pm30^o$	GM = $\pm$6.0 dB PM = $\pm45^o$	GM = $\pm$8.0 dB PM = $\pm60^o$	$f_M \leq 8$ Hz GM = $\pm$8 dB $f_M > 8$ Hz GM = $\pm f_M$dB
Airspeeds Equal to V_L	GM = $\pm$3.0 dB PM = $\pm20^o$	GM = $\pm$4.5 dB PM = $\pm30^o$	GM = $\pm$6.0 dB PM = $\pm45^o$	Magnitude shall be less than 0 dB at all frequencies

Table 2 Required Gain and Phase Margins

In addition, roll stabilization of the radar sensor during turns is desirable and stabilizing with yaw rate would provide needed lead information. Pilot override capability and ATF commands in series with the pilot's command are preferred. Decoupling of the stick from control surface motion has also been shown to be desirable.

VULNERABILITY

Consideration of the terrain following system's susceptibility to direct hits from munitions, extreme environmental conditions and crew errors has to be examined. Withstanding at least one direct hit from a single round of any size munition up to and including 23mm is a necessary condition. Operation can be degraded but must permit safe termination of precise tracking or maneuvering tasks, and provide a return home and landing capability. Redundancy required to meet normal fail-safe operation will aid in meeting this requirement. Physical separation of all critical equipment will also be an aid and will ensure completeness of redundancy. Shielding is not recommended as a substitute for equipment separation but could be used to supplement the invulnerability of the terrain following system.

Specifications presently cover applicable environmental tests and procedures for airborne equipment. System procurement guidelines should define the extremes postulated. Damage from crew errors presents special design considerations. Clear and distinguishable displays are a necessity. Efforts are needed to minimize the probability of the flight crew having to make hazardous commands during the penetration mission. Nuisance failures that require fly-ups or unnecessary climb or dive commands reduce the aircraft's overall survivability especially in a wartime situation. Concentrated efforts are also needed to design against improper installation and to minimize the on-aircraft adjustments.

STRUCTURAL FATIGUE

The terrain following mission segment consists of a series of repetitive loads which have a significant effect on aircraft service life. The literature review revealed very little analysis and trade study data for the area of structural fatigue. Most published literature pertained to the fighter type aircraft. The total maneuver load spectra specified for fighter aircraft appear adequate for terrain following. The spectra specified for strategic bombers is limited when considering the maneuver loads imposed by the LAHS mission. Studies conducted by Boeing used the criteria of minimizing the magnitude and number of maneuver loads on the aircraft without degrading clearance altitude performance. This was accomplished by designing a terrain following system that produced a smooth, nonoscillating acceleration response characteristic.

A method of obtaining trade data between probability of survival and structural fatigue is to include the aircraft load equations in an extensive penetration simulation program. The maneuvers required for effective penetration and the fatigue damage accrued in the remaining aircraft mission segments will determine the maneuver load spectra allocated to the LAHS mission. The gust spectrum for the low level environment should also be included as part of terrain following system simulation evaluation. Service-load spectra for terrain following operation has to include combined maneuvers and gust loads.

RIDE CONTROL

The crew's ability to perform assigned duties as a function of the ride environment is related by established ride control criteria. Previous investigations into the effects of gust turbulence on a crew member's tracking ability are applicable to the terrain following mission. A crew sensitivity index ($\bar{R}$) was established relating the aircraft, turbulence and human frequency response.

$$\bar{R} = \frac{\sigma_D}{\sigma_u} = \left[\int_0^\infty |T_D(\Omega)|^2 |T_{A/P}(\Omega)|^2 \frac{\phi(\Omega)}{\sigma_u^2} \, d\Omega \right]^{1/2}$$

where:

σ_D = RMS discomfort

σ_u = RMS gust velocity

$\bar{R}$ = Crew sensitivity index (RMS discomfort/RMS gust velocity)

$T_D(\Omega)$ = Human frequency response function

$T_{A/P}(\Omega)$ = Crew compartment acceleration frequency response function

$\frac{\phi(\Omega)}{\sigma_u^2}$ = Turbulence spectrum for unit RMS gust velocity as defined by von Karman PSD function (MIL-A-8861)

Tabulated data are available relating RMS discomfort levels (σ_D) with crew performance and physiological effects.

The components of the $\bar{R}$ integrand in the above equation are constant for a given flight condition allowing a direct relation for terrain following ride criteria. The human frequency response function, shown in Figure 12, is independent of the disturbance source whether it be gusts or terrain contour maneuvering. Terrain roughness and frequency content are the parallel of the von Karman gust spectrum. The discomfort equation can be revised for terrain following as shown below.

$$\sigma_D = \left[\int_0^\infty |T_D(\Omega)|^2 |T_{A/P}|^2 |T_{Terr}(\Omega)|^2 \, d\Omega \right]^{1/2}$$

where

$T_{A/P}$ is the crew compartment acceleration response due to ATF control surface activity, flying over the terrain.

$T_{Terr}(\Omega)$ is the terrain (and radar command) that determines control surface motion.

Unfortunately, a direct solution is impossible since terrain following systems are nonlinear and terrain profiles are random. The approach taken was to fit linear transfer functions to the human frequency response function. These transfer functions were then added to a detailed terrain following penetration simulation and used to filter accelerations produced at the pilot station. In this way, terrain following RMS discomfort levels were determined. By evaluating crew performance and physiological effects at these discomfort levels in conjunction with acceptable exposure durations, the needed ride quality could be specified. Table 3 illustrates the results of this approach. The technique is recommended to allow evaluations to be made of the ride quality of various terrain following systems. Turbulence discomfort at low level must also be considered in such evaluations. The preferred aircraft response caused by a gust is an $\bar{R}_{vertical}$ value equal to .026 or less.

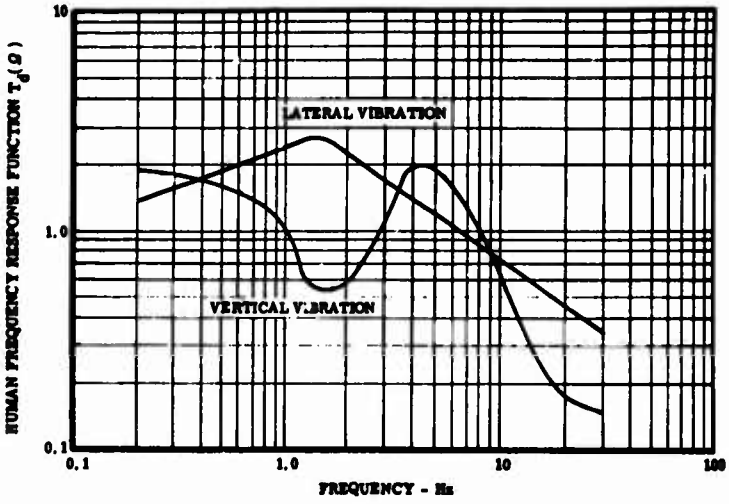

Figure 12 Human Frequency Response Function

RIDE SELECT	$\sigma_a \bar{n}_o$	AIRCRAFT ACCEPTABILITY	MISSION PERFORMANCE AND CREW EFFORT	PHYSIOLOGICAL EFFECTS
Soft	.07	Acceptable for unlimited exposure time.	Mission performance not affected.	No effect on normal tasks.
Medium	.14	Acceptable normal operation.	Mission performance adequate.	No effect on normal tasks, writing becomes difficult, small dials become difficult to read.
Hard	.21	Acceptable normal operation not exceeding allowable exposure time.	Adequate for mission success; reasonable performance requires considerable crew concentration.	Normal tasks still possible. Manual control demands considerable attention and psychomotor coordination is reduced. Time to read instruments and displays and adjust controls increases. Small dials unreadable. Eventual setting in of fatigue.
	.28	Unsatisfactory for normal operations; unacceptable when exceeding allowable exposure times.	Adequate for mission success, but requires maximum available pilot/crew concentration to achieve acceptable performance.	Limits of effective tracking. Manipulation of controls and other psychomotor tasks requires bracing of arms and legs and movements become deliberate. Pilot looks forward with only brief glances at instruments which cannot be read accurately. Cross checks are slowed down and tolerances widened. Rapid increase in fatigue.
	.35	Unacceptable except for emergency conditions.	Inadequate performance for mission success; aircraft controllable with minimum cockpit duties.	Beginning of unworkable level. Control of aircraft requires full pilot attention. Tasks other than stick and throttle control almost impossible. Pilot will establish hierarchy of tasks. Attention cannot be diverted from tracking task without immediate deterioration.
	.42	Unacceptable, dangerous.	Aircraft just controllable requiring maximum pilot skill; mission success impaired.	Performance levels low and all tasks impossible except for gross adjustments. Displays difficult if not impossible to read. Concern for structural integrity.

Table 3 Crew Mission Performance Limitations

COST

Terrain following costs are influenced by factors such as performance, reliability, weight, safety, vulnerability and fatigue effects. A cost performance (CP) index was established to relate these factors to the ultimate objective of the weapon system. The pounds of weapons successfully delivered divided by the total cost of ownership of the weapon system represent a value parameter to be maximized. It may be considered as approximately proportional to:

$$CP = \frac{(P)(W_O - W)\left(\frac{1}{1-P_S}\right)}{C_A + C_M + \frac{C_W}{(1-P_S)}}$$

P = Probability of surviving Y years of peacetime training and successfully delivering offensive weapon to target

$(W_O - W)$ = Weight of offensive weapon carried

W_O = Weight of offensive weapon that could have been carried if the terrain following system had a weight of zero

W = Weight of terrain following system

C_A = Acquisition cost per aircraft (including terrain following system)

C_M = Maintenance and other operational cost per aircraft (including terrain following system) for Y years of peacetime training plus a brief period of wartime operation

C_W = Offensive weapons cost per aircraft sortie launched

P_S = Probability of survival and safe return from a wartime mission

Many probabilities based on items such as terrain following performances, reliability and vulnerability are multiplied together to compute the value of P used above. Some of these probabilities also influence the value of P_S. Using such an index, specific areas for improvement can be identified which will have a significant increase on cost effectiveness. It should be noted that the safety of peacetime training operations for several years may have a significant impact. For example, acceptable overall survival probability for a wartime mission would be unacceptably low for a peacetime training mission. This may force peacetime training to be accomplished at a relatively high clearance setting reserving the lower clearance setting for wartime use; such restrictions tend to decrease the value or peacetime training.

Subjective evaluation was found to be a common technique when comparing concepts, performing trade studies, etc., between performance requirements and their associated costs. The total cost of ownership includes maintenance costs, initial material and engineering burdens. The maintenance plan should include the use of existing ground support equipment as much as possible to minimize the requirement for new AGE. Each system definition should include levels of complexity with its associated dollar and weight/volume costs.

RELATING THE VARIOUS AREAS

Finally, an overall performance index was established to allow system evaluation. The relative importance of each of the eight areas previously discussed had to be integrated into this index. It is expressed as:

$$PI = \sum_{i=1}^{8} (C_i)(Area_i)$$

The Cs are weighting factors which were subjectively selected based on the literature review. Table 4 lists these values. A score from 0 to 100 is assigned to each area from a question and answer checklist. The first section of this checklist is shown in Table 5. The maximum available points listed denotes the importance of each question. The total area score used in the index is obtained by adding the individual question and answer scores. Area weightings will have to be refined as experience with this index is gained.

i	$Area_i$	C_i
1	Safety	0.20
2	Performance	0.25
3	Reliability	0.10
4	Stability	0.10
5	Vulnerability	0.05
6	Structural Fatigue	0.05
7	Ride Comfort	0.05
8	Costs	0.20
	TOTAL	1.00

Table 4 Weighting Factors For Performance Index

CONCLUSIONS

Universal terrain following criteria have been needed for some time. Such criteria must bring together requirements in the related area of safety, performance, reliability, stability, vulnerability, structural fatigue, ride comfort and cost. The program covered by this paper was a first step towards the establishment of a "common measure". Criteria were developed through review of existing standards, analyses and detailed simulation investigations. An attempt has been made to select merit functions associated with the various factors involved in order to identify their relative importance to terrain following. Compilation of the results into a handbook was also accomplished. The handbook has been iterated through several review and revision cycles by an Air Force engineering panel at Wright-Patterson. At the present, several limited trial evaluations are being conducted.

Unfortunately, application is being hindered because many of the proposed evaluation measures are new and untested. Formal validation is needed. Such a verification is being planned as a future Laboratory

effort. Several operational and experimental terrain following systems will be evaluated with the criteria. Comparisons will then be made with existing measures including subjective evaluations. Deficiencies of the proposed criteria in denoting outstanding systems, ranking overall performance and pinpointing problem areas will be identified. Corrections will be formulated, tested and incorporated.

It is the author's hope that this effort has stimulated interest in the development of a "common measure" that will provide a practical means of evaluating and comparing terrain following systems. Establishment of such criteria is needed to allow improved weapon system effectiveness by providing a way to select the best system for low level penetration within the many constraints imposed by aircraft, crew, mission and available resources.

	QUESTION	MAX. POINTS	POINTS AWARDED	COMMENTS
1.	SAFETY			
1.1	Does the TF system include a fail-safe design with flyup?	15		This is a minimum requirement.
1.2	Does the TF system include a fail-operate capability?	10		
1.3	Does the fly-up precaution include a prediction of excessive undershoot?	15		
1.4	Does the TF design predict aircraft loss due to TF failure less than specified in 3.1.3?	15		
1.5	Does the TF design employ the following test capability:			
	a. On-line test	10		
	b. Inflight, pre-engage	10		
	c. Ground test	10		
1.6	Does the TF design predict a PC single $\leq 2.8 \times 10^{-7}$ for the indicated terrain profile?	15		
	TOTAL	100		
2.	PERFORMANCE			
2.1	Does the TF system provide clearance altitude settings as required in paragraph 3.2.1?	15		

Table 5 Area Scoring Checklist

B-1 TERRAIN-FOLLOWING DEVELOPMENT

Charles W. Brinkley and Patrick S. Sharp
Air Force Flight Test Center
Edwards AFB, California 93523

and

Richard Abrams
Los Angeles Division
Rockwell International
Edwards AFB, California 93523

ABSTRACT

The test and evaluation of the B-1 terrain-following (TF) system has been an important part of the overall B-1 flight test program because its successful implementation was considered essential to the operational effectiveness of the B-1 weapon system. The purpose of this paper is to present an overview of the work accomplished to develop, test, and evaluate the B-1 TF system and low-altitude penetration capabilities. First, the B-1 mission, flight test program goals, and test philosophy are discussed. Then, the operating theory of the B-1 TF system, including the forward-looking radar, TF computer, radar altimeter, TF/flight control system adapter, automatic throttle system, and flight control/autopilot system, are briefly outlined, including a discussion of how these components are integrated to produce the total system performance. The test techniques required to verify design concepts and operational requirements are outlined, including the types of terrain used for testing, ground tracking requirements, and types of maneuvers flown. Some of the important aspects of the data acquisition and analysis techniques used during the ongoing test program are discussed, and finally, a progress report of the completed testing and projections for future testing is presented.

INTRODUCTION

The B-1 was designed to be a versatile weapons system able to carry out both nuclear war and limited conflict missions without modifications to its airframe. U.S. Air Force studies conducted in the past have shown that the best way to penetrate the sophisticated defenses expected to be used into the 21st century is by flying at nearly the speed of sound at very low altitudes. This is what the B-1 was designed to do. In addition to being able to follow the terrain at extremely low altitudes, it was also capable of penetrating at high supersonic speeds at high altitude. This high-low capability meant that a potential enemy would have to consider defenses to cover both environments. Radar cross section and infrared emissions were also greatly reduced to make the B-1 considerably less visible to enemy defense systems.

The basic mission profiles of the B-1 - the primary and the alternate - are depicted in figure 1. These missions required that the aircraft loiter on airborne alert for an extended period of time; i.e., for as long as practical by using aerial refueling. Finally, the aircraft had the option if it was to go into the target area, to go either at high subsonic speed and low altitude, as shown on the left, or at high altitude and supersonic speeds. Also shown here graphically is the primary mission weapon, the short-range attack missile (SRAM) AGM-69. The primary mission of the B-1 was, however, low-altitude penetration at near sonic speeds where defensive radar, interceptors, and missiles are considered least effective.

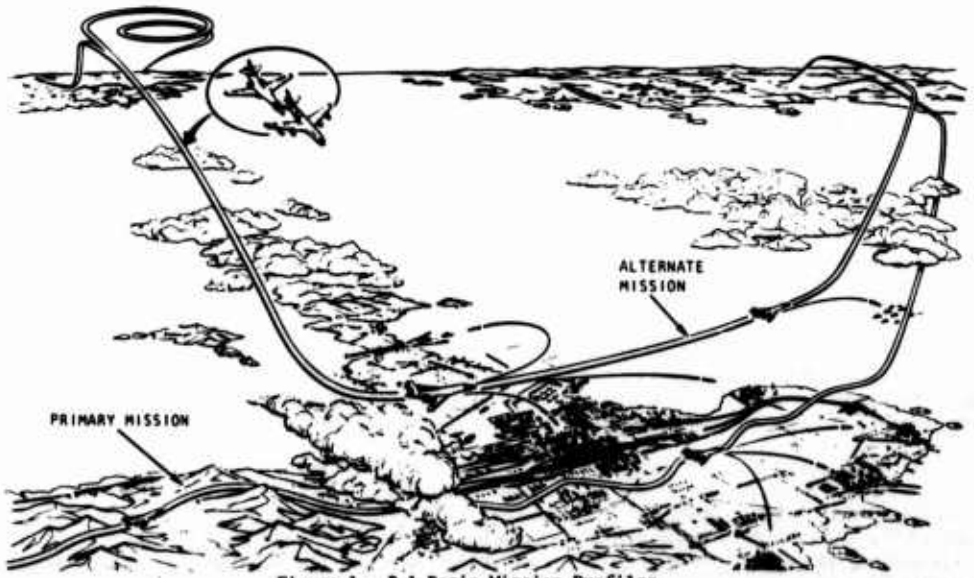

Figure 1. B-1 Basic Mission Profiles

The B-1 flight test program has been mission-oriented from the start, and the primary emphasis has always been placed on the high-speed, low-altitude flight regime. In order to orient the program, the primary mission of the aircraft had to be considered; i.e., low-altitude, high-speed penetration. This mission is shown schematically in figure 2. The key elements that had to be addressed very early in the test program were extracted from this mission. Thus, the initial envelope expansion was aimed at getting to the high-speed, low-altitude flight condition early, rather than moving more conventionally toward the high-speed, high-altitude supersonic regime. This approach was not as glamorous, but to the B-1, it was certainly more meaningful.

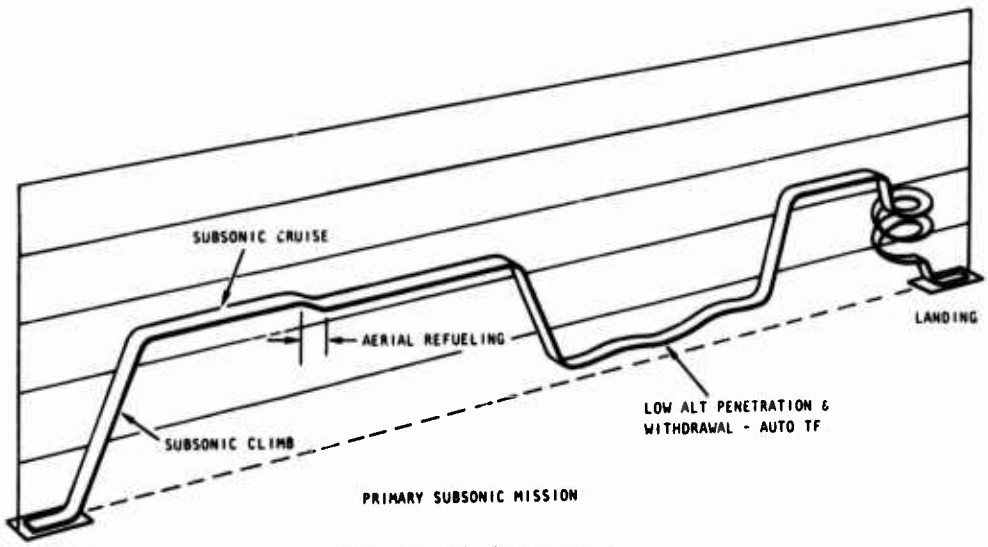

Figure 2. B-1 Mission Elements

Long before the first flight of the No. 1 prototype B-1 in December 1974, flight test program requirements were prioritized with respect to expanding the low-altitude, high-speed envelope of the aircraft and clearing the aircraft for operation at mach 0.85 at sea level. Testing was initially accomplished toward this objective, with primary emphasis on flutter clearance and flying qualities envelope expansion. Aircraft 1 was equipped with a single-channel manual TF system, and the system was also used after this initial envelope expansion effort was completed for a preliminary assessment of the B-1 low-altitude penetration capabilities. Structural mode control system (SMCS) development testing was also accomplished during this phase of the flight test program, as well as other tests that were required to optimize TF/flight control system adapter gains. This test philosophy would ensure that by the time the third prototype B-1 (the primary TF and offensive avionics test aircraft) entered the flight test program in April 1976, manual and automatic TF system testing could be initiated as soon as practical after the first flight of this airplane.

OPERATIONAL REQUIREMENTS

The B-1 TF system was designed to get the aircraft to and from the target safely. Detection could be avoided by flying below radar defensive systems and at night to avoid visual detection. The B-1 has the capability to follow the contour of the earth at selected altitudes above the ground.

The TF portion of an operational mission starts with an automatic letdown to a TF altitude when the aircraft is more than 150 nautical miles from the area being penetrated. The automatic letdown consists of an initial pushover to an 8-degree dive angle until reaching an altitude of 5,000 feet AGL, and then pushing over to a 10-degree dive angle. The pullout is initiated at approximately 2,000 feet AGL, and the penetration is made at whatever altitude is desired.

The aircraft has six selectable clearance planes that can be flown, the highest being 1,000 feet and the lowest being 200 feet. Preflight planning would establish the clearance plane to be selected for each leg of the penetration route based on the defenses to be penetrated and the terrain masking available. In general, the aircraft would never be flown any lower than necessary.

There are three selectable ride settings at each clearance plane setting: soft, medium, and hard. The ride setting controls the magnitude of the "g" forces imposed on the aircraft by the flight control system as it maintains a set clearance above the terrain. The ride setting will vary the degree of closeness that the flight profile matches the contour of the terrain with the hard setting providing the closest match. The medium ride setting is generally considered the most comfortable ride for the crew and is the setting that would normally be used in a training environment.

TF commands are only generated in the longitudinal axis. When the commands are coupled to the autopilot, the pilot or navigation system (through the autopilot) can still maneuver the aircraft in roll without affecting the pitch commands. In other words, the pilot can fly manual terrain avoidance while flying automatic TF. This gives him the capability of following the lowest part of the terrain and using the higher terrain to mask him from detection. TF can be flown as easily at night as in the daytime, practically eliminating the chance of visual interception.

TF SYSTEM OPERATING THEORY

The TF system in the B-1 is basically the same concept as implemented in the F-111 series aircraft. The system consists of a dual-channel, forward-looking multimode radar which provides angle and range information to a TF computer. The TF computer processes this information and provides a signal proportional to the desired "g" required for the system to fly the aircraft at a preselected set clearance above the terrain. The automatic flight control system then takes this signal and provides proper commands to the stabilator to produce the desired response (figure 3).

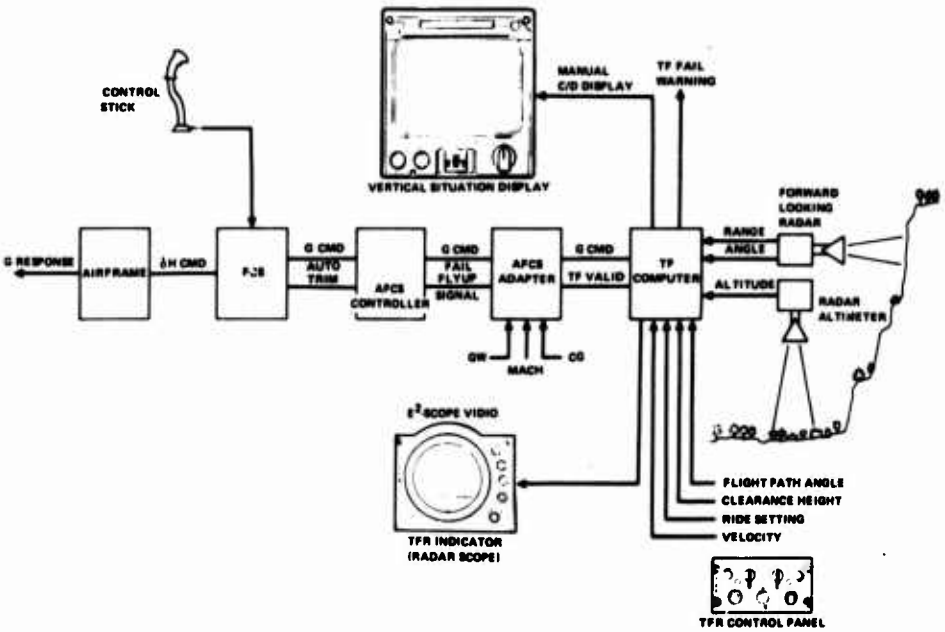

Figure 3. TF System Block Diagram

TF RADAR (TFR)

The synchronizer-transmitter contains the circuits required for the synchronization, modulation, transmission, and monitoring of the TFR radio frequency (RF) power (figure 4). The synchronizer is the clock for the radar, as it provides the timing for all events that take place. It provides a trigger to the modulator circuit at the pulse repetition frequency of the radar set. It also provides a synchronizing pulse for the other TFR. Finally, it provides a blanking pulse to the TFR receiver and to all of the aircraft systems to prevent saturating them during transmission. The modulator supplies the high power required to operate the magnetron. The modulator consists of a high-voltage section, a hydrogen thyratron tube, and a thyratron trigger circuit. The magnetron is tunable and produces a power in excess of 30 kilowatts. The magnetron output is piped through a waveguide to the antenna roll assembly and on to the TFR antenna.

The antenna-receiver accepts the transmitter pulse from the synchronizer-transmitter and beams it out in a direction determined by elevation and azimuth positioning commands. In the receive position, the antenna intercepts the reflected signals and applies these signals to the receiver portion of the antenna-receiver. The receiver converts the received RF signals to video signals for output to the TF computer and indicator.

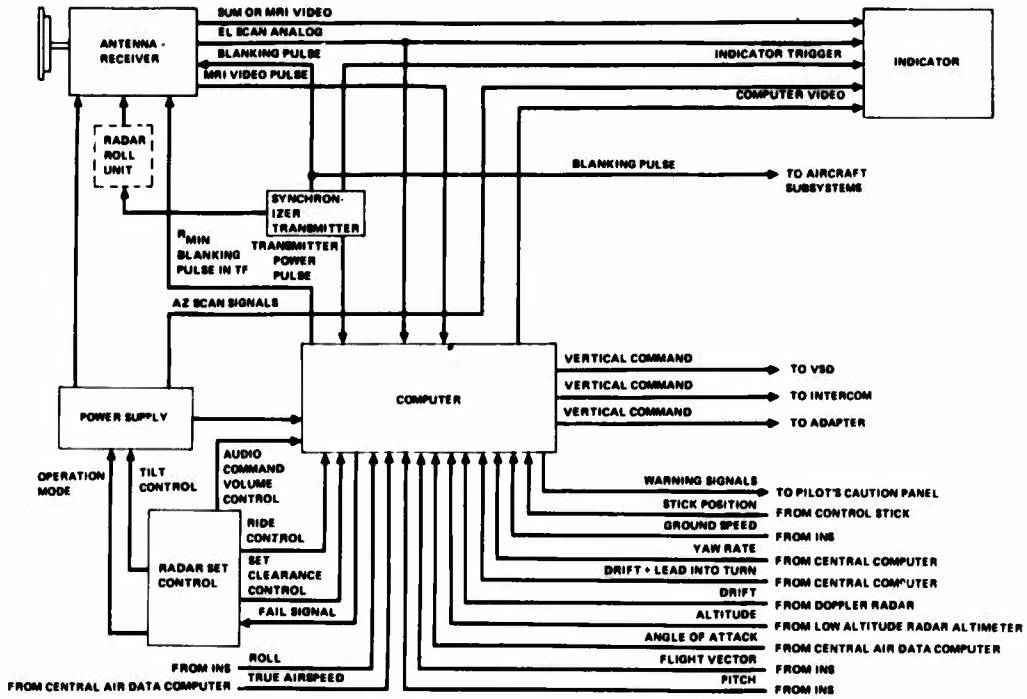

Figure 4. Terrain-Following Radar Set Block Diagram

TF COMPUTER

The TF computer accepts the video information and antenna pointing information from the antenna-receiver and converts the video from an aircraft reference system to an earth reference system. It then compares the received video with a desired flight profile calculation based on the shape of the terrain ahead to arrive at a desired flight path angle. The actual flight path angle is subtracted from the desired flight path angle to determine the climb/dive angle command. The climb/dive command is converted to g's and sent to the adapter set and the command bars on the pilot's vertical situation display (VSD). The TF computer also controls the drift plus lead-into-turn compensation for the pointing of the radar in azimuth for turning flight.

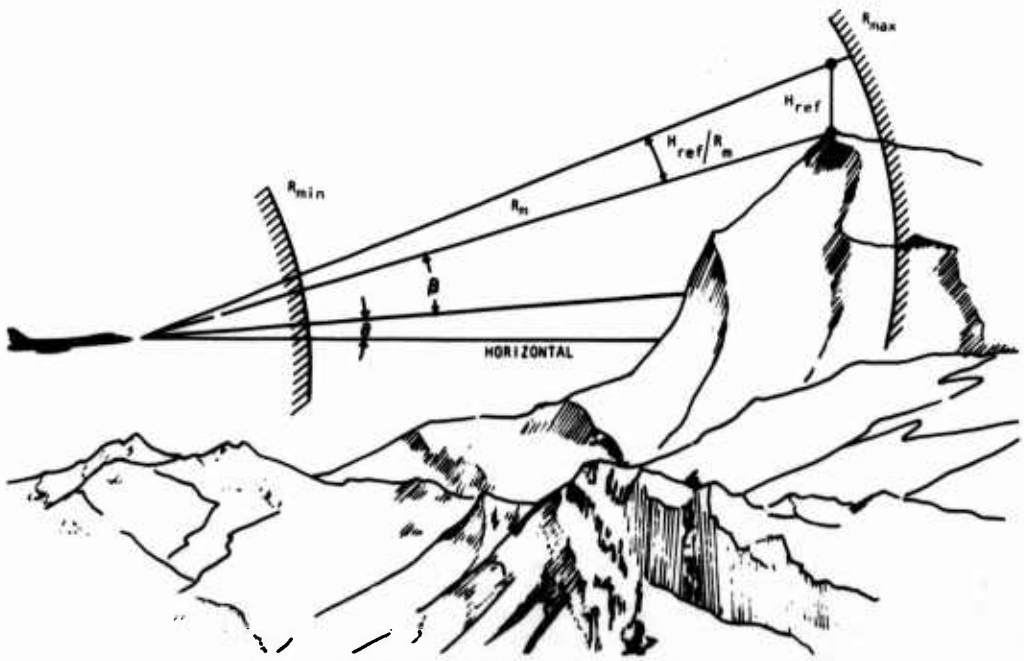

Figure 5. Relative Angle Concept - TF Computer

The system operates on a relative angle concept and reacts to terrain points that lie in the range interval (R_{min}, R_{max}) as shown in figure 5. The most critical terrain point in the interval is that point which results in the most positive flight vector command as determined by the equation:

$$\gamma_c = K\left(\theta + \beta + \frac{H_{ref}}{R} - F_s\right)$$

Where K is a constant coefficient, θ is the aircraft pitch attitude, β is the elevation angle corresponding to the critical point, R is the range to the critical point, H_{ref} is the set clearance, and F_s is a shaped offset function.

If the shaped offset function were not included, the system would command the aircraft to fly at an angle that clears the highest point of terrain within the range of the radar, and the aircraft would fly essentially from peak to peak. The F_s function suppresses the apparent height of targets as a function of range, velocity, flight path angle, and ride control. The terms "F_s" and "K" were chosen to provide the best contour matching within the constraints of maneuverability of the aircraft.

A typical terrain-following situation is illustrated in figure 6, and it can be displayed in terms of the radar look angle. This display is presented to the pilot on what is referred to as an E^2-scope display, as shown in figure 7.

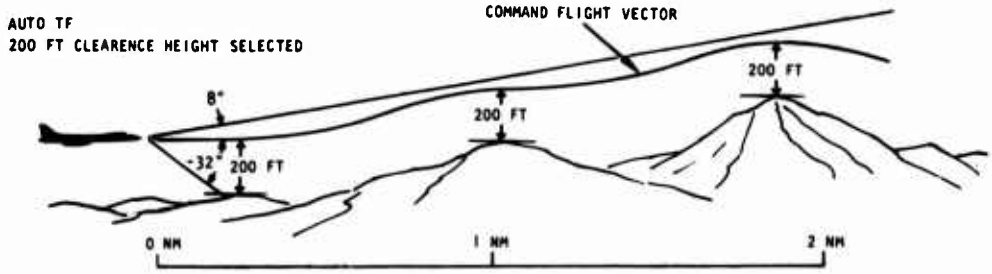

Figure 6. Actual Terrain Profile

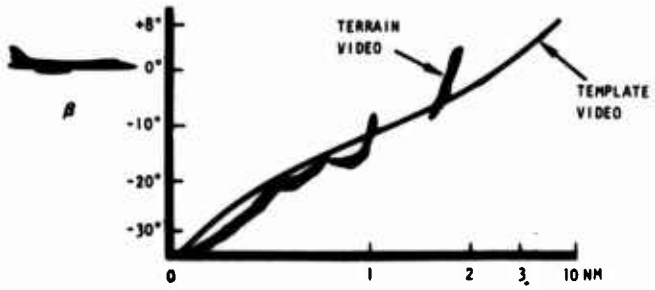

Figure 7. E-Scope Display

RADAR ALTIMETER

The radar altimeter is used as an aid in terrain-following control. It provides altitude information from which the TF computer generates commands when returns are not available to the forward-looking radar, such as over water. In addition, when the aircraft is a given percentage below the selected clearance height, a low-altitude warning is activated, and a maximum g pullup is initiated.

TF ADAPTER

The output of the TF computer is a voltage which is representative of a g-command to the aircraft. However, since the aircraft characteristics vary significantly throughout its envelope, the adapter is provided to condition the command to the elevator as a function of center-of-gravity position, mach number, and gross weight, such that the desired response is attained.

AUTOMATIC FLIGHT CONTROL SYSTEM (AFCS)

The TF adapter signal is next processed by the AFCS where trim and pitch support functions are included. The automatic trim consists of a series integrator which attempts to null the error between actual and commanded response. The pitch support function adds increased pullup commands to compensate for the loss of lift in turns.

The flight director mode of the AFCS in conjunction with the navigation system provides automatic steering while terrain following.

The autothrottle mode of the AFCS can maintain a constant mach number for TF flight by varying engine power from idle to intermediate.

FLIGHT TEST REQUIREMENTS

INSTRUMENTATION/DATA ANALYSIS

The instrumentation requirements for evaluating a TF system are rather complex. In a general sense, it can be said that the input and output of every part of the TF system must be measured. The critical questions to be answered by the instrumentation are (1) what is the aircraft doing with respect to the terrain that it is flying over? (2) how and why was the command generated which caused the aircraft to do what it is doing with respect to the terrain? and (3) was it the proper command that was generated? Rather than produce a parameter list, it will be explained what data are required and, in general, what has to be measured to obtain those data.

The most basic data measurements are those that tell exactly what the aircraft is doing. To determine this, it is necessary to measure aircraft attitude, rates, accelerations, and velocities. Next, it must be determined what the TF commands were. This is determined by measuring elevator position, the output of the TF adapter, control stick position, and the output of the TF computer.

The next level of analysis knowledge requires knowing what caused the TF commands to be generated. This is determined by measuring all of the inputs to the TF computer including the TFR video and the radar altitude. To record the TFR video requires a video recorder or a digital recorder that will sample at video frequency rates. For example, the B-1 was the first aircraft to have its TF computer instrumented to include video returns and radar look angle from the antenna-receiver. As a result, several system characteristics pertinent to not only the B-1, but also to the F-111, were evaluated.

To determine if a command was the proper command, it is necessary to compare the actual flight profile for a specific test condition with the predicted flight profile for the same test condition. This requires using a simulation program that reflects the most accurate model possible of the aircraft and TF system.

All of these instrumentation and data analysis tools have been utilized in both real-time and post-flight modes during the B-1 TF system development program.

TEST COURSES

It is imperative that an instrumented test course is used to determine if the TF system is performing as it should. Aircraft position data should be available at the test course with an accuracy of ±5 feet in all axes. Since this dictates optical tracking data with its long processing time, it is also desirable to have a tracking radar on the test course to provide quick-look data.

The most important feature of a test course is that it have an isolated peak with an altitude in excess of 500 feet above the surrounding terrain. The run-in line to the hill should be as level as possible with optical tracking available for at least 5 miles on each side of the hill. The run-in line should be very closely marked so that the pilot can visually keep the aircraft on the correct ground track. The run-in line to the hill should be surveyed to an accuracy of better than ±2 feet in elevation.

Another important feature is to have an area where the terrain is level within 0.1 degree for at least 5 miles. It is not necessary to have optical tracking for this part of the test course. However, the ground track should be clearly marked so that the pilot can visually keep the aircraft on the proper ground track.

It is also highly desirable to have an area where the terrain has a gradual slope of more than 0.5 degree but less than 2 degrees for a distance greater than 5 miles. Again, the ground track should be clearly marked for the pilot, and optical tracking is not necessarily required.

Two test courses have been utilized during the B-1 TF system development program. The first is referred to as the Edwards AFB Haystack Butte course. Haystack Butte is on the bombing range at Edwards AFB, east of the main base complex, and rises 412 feet above the surrounding terrain. The normal run-in to Haystack is made from west to east over Rosamond Dry Lake and Rogers Dry Lake, followed by the final approach to Haystack over terrain that has a gradual rise of 1.0 to 1.5 degrees. The Haystack Butte profile is shown in figure 8.

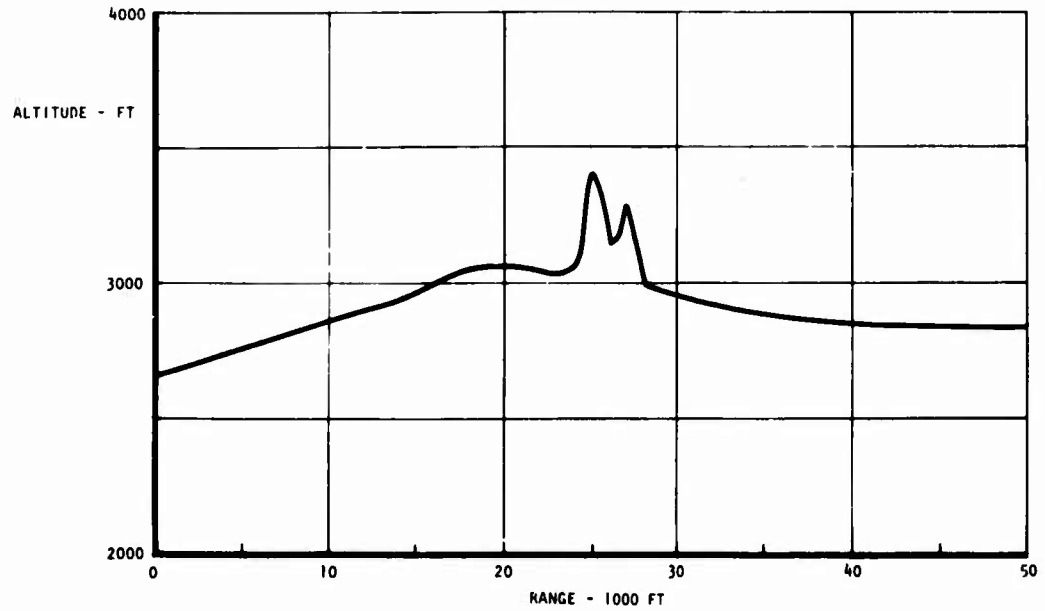

Figure 8. Haystack Butte - Edwards AFB

The second test course utilized during the TF system development program is at the Dugway Proving Ground, in Utah. Granite Peak rises approximately 2,700 feet above the surrounding flat terrain, which itself averages 4,300-foot elevation. The normal run-in to Granite Peak is made from east to west. The Granite Peak profile is shown in figure 9 (0- to 50-thousand-foot range is east to west).

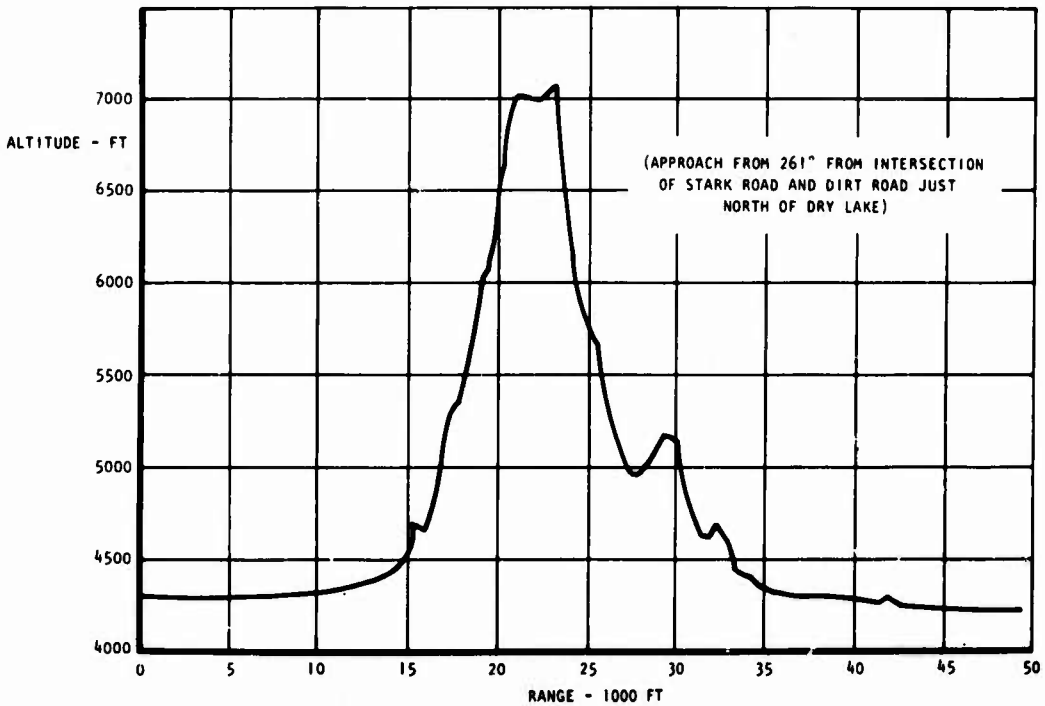

Figure 9. Granite Peak - Dugway Proving Ground

OPERATIONAL COURSES

Several VFR low-altitude training routes (TR) and all-weather, low-altitude Olive Branch routes, which are identified by the prefix OB and a number, were chosen to evaluate and demonstrate the penetration capabilities of the aircraft under realistic operational conditions. These routes were selected on the basis of proximity to Edwards AFB and those differences in terrain characteristics that were considered important for the operational TF evaluation.

The following terrain classifications will be used in the description of these routes:

Ocean	- Flat
Flat	- Less than 300-foot rise in 10 miles
Rolling	- 300- to 1,000-foot rise in 10 miles
Moderate	- 1,000- to 3,000-foot rise in 10 miles
Severe	- 3,000- to 5,000-foot rise in 10 miles
Extremely severe	- Greater than 5,000-foot rise in 10 miles

Hawthorne, Nevada (OB-10), is an Olive Branch route in central Nevada (figure 10). The terrain features on the route vary from flat to severe.

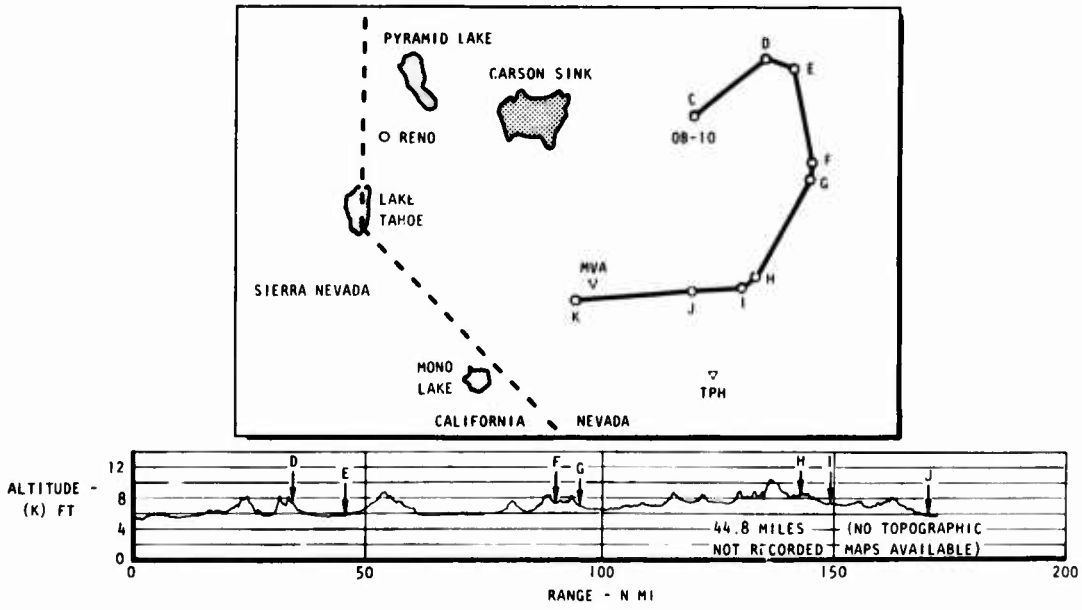

Figure 10. OB-10 (Hawthorne)

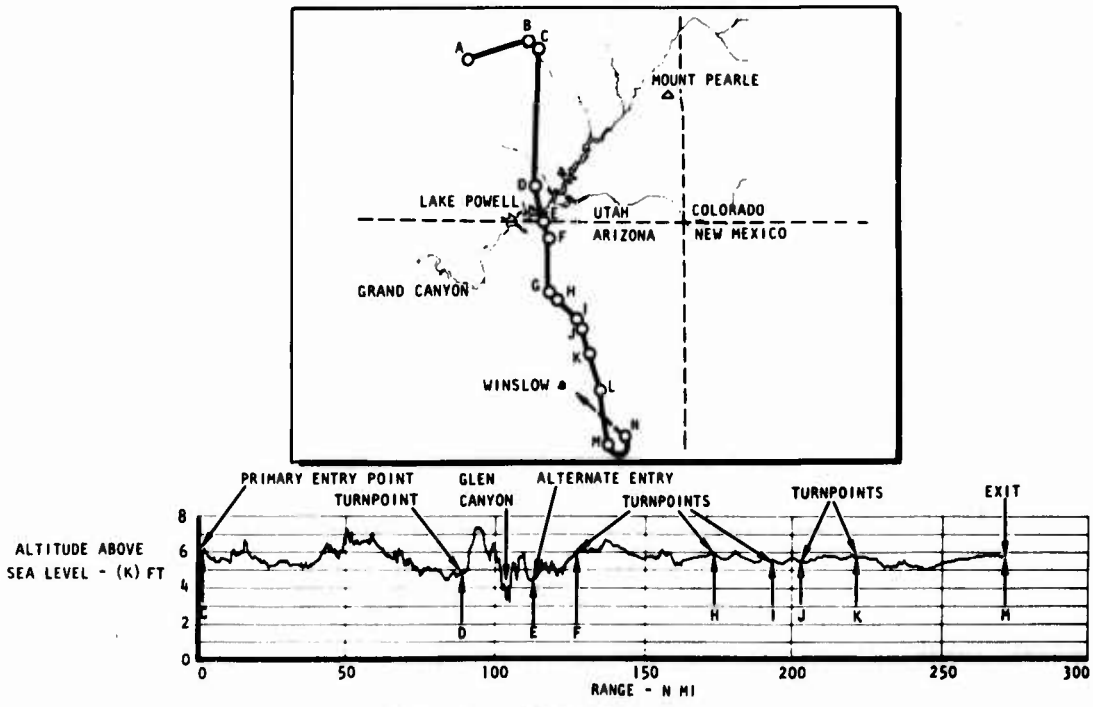

Figure 11. OB-20 (Holbrook)

Holbrook, Arizona (OB-20), is an Olive Branch route that began in central Utah and terminated in eastern Arizona (figure 11). The route was generally moderate north of the Colorado River and became rolling to moderate thereafter. (On 23 July 1977, OB-20 was deleted as a low-altitude training route.)

Low-altitude training route TR-345 (Lancaster, California) starts off the coast of California between Ventura and Malibu and then heads north through the Sierra Nevada mountains and into southern Nevada (figure 12). Turn point C is used as the normal entry point after departing from the Edwards area. Terrain features vary from moderate to extremely severe, with the most severe terrain at turn point H, which crosses Bald Mountain at 9,190 feet.

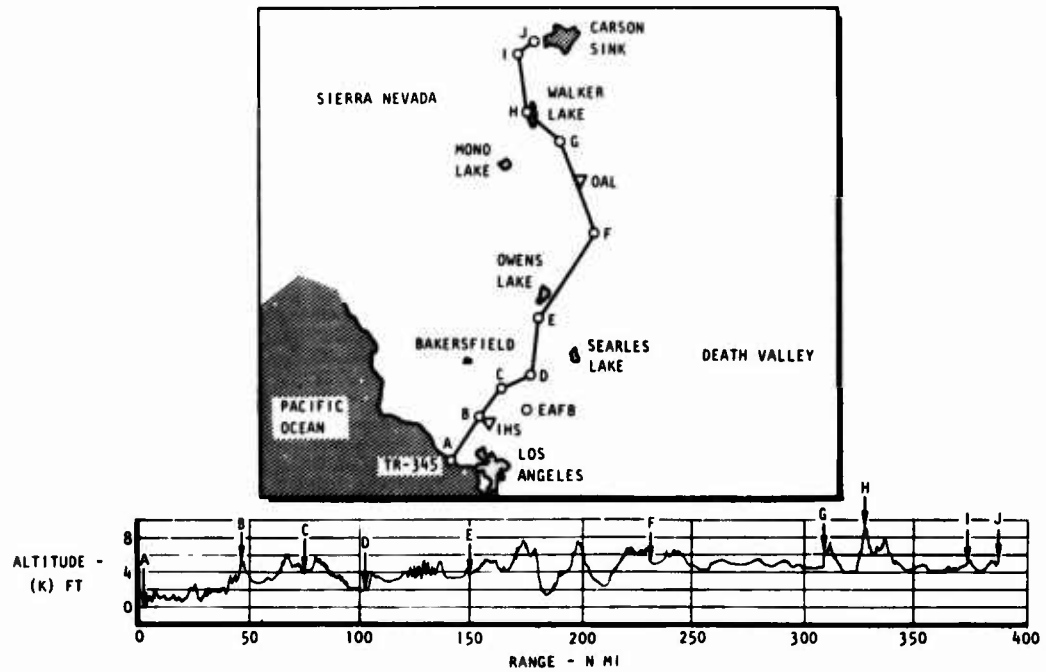

Figure 12. TR-345 (Lancaster)

TR-360 (Los Angeles, California) starts at the Lake Hughes Vortac and heads in a northeastern direction into Nevada. It then turns southbound in a southeastern direction back into California and terminates just west of the Salton Sea (figure 13). Terrain features vary from moderate to extremely severe.

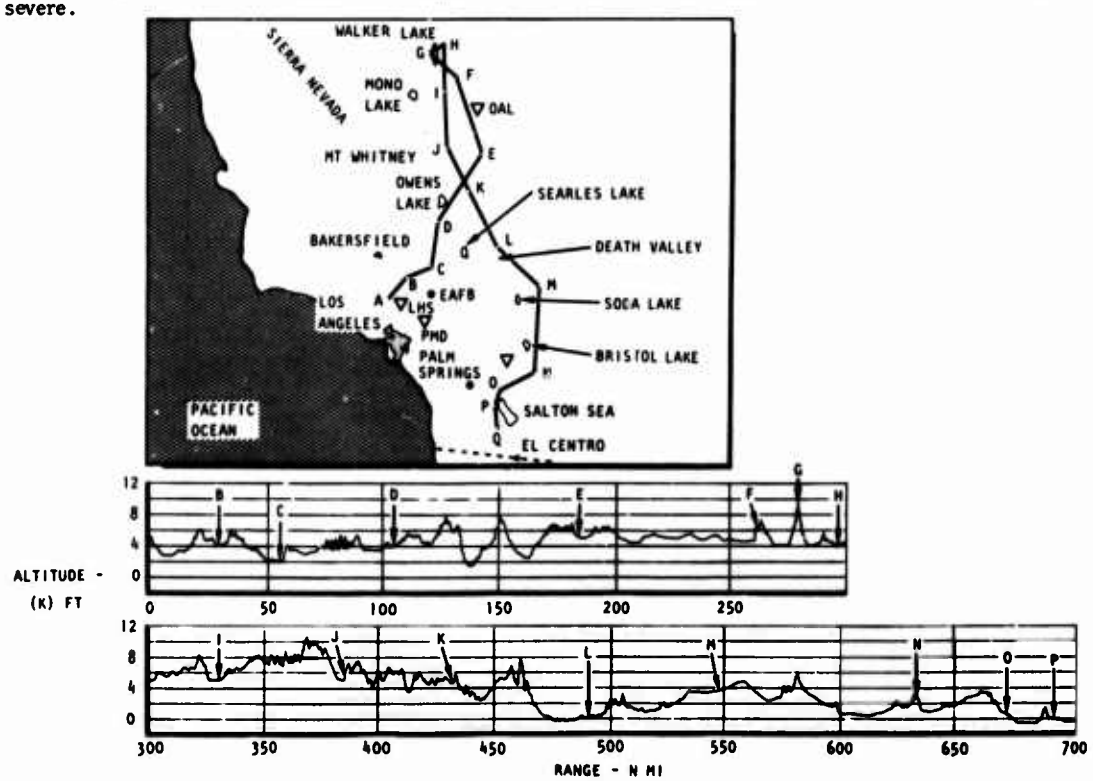

Figure 13. TR-360 (Los Angeles)

TR-368 (Santa Barbara, California) is a low-altitude training route in southern California (figure 14). This route has been considered the primary evaluation route for the B-1 because of its proximity to Edwards AFB and relatively short length, which permits flying multiple runs on a single flight. Terrain features on TR-368 are considered moderate.

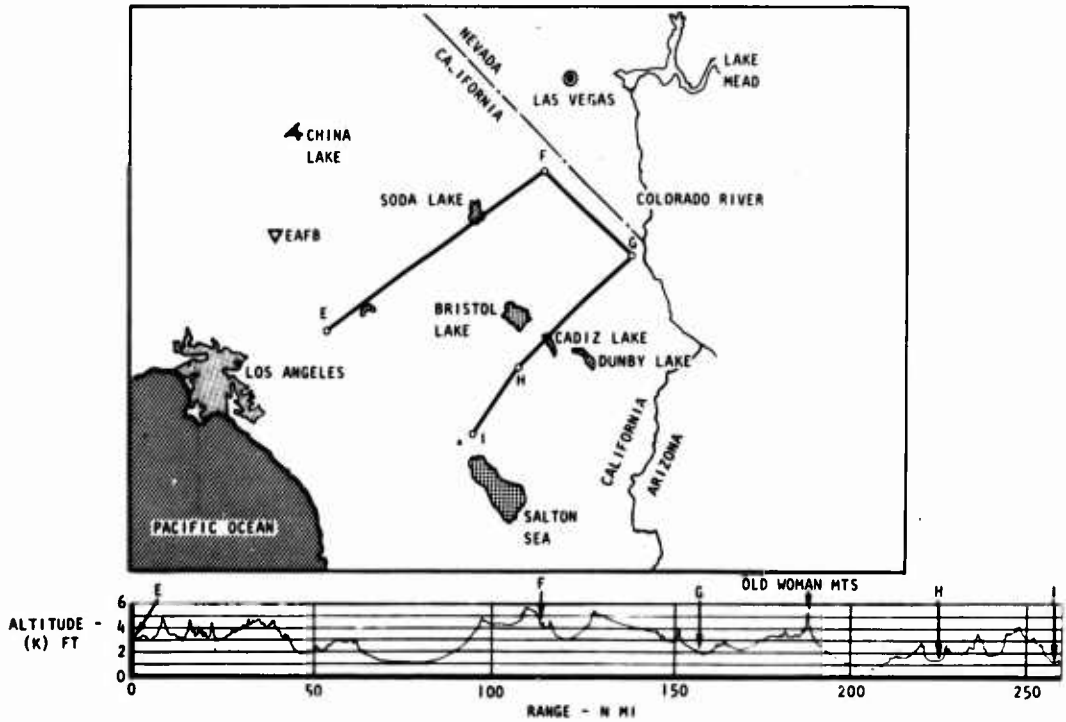

Figure 14. TR-368 (Santa Barbara)

TR-385 (Tonopah) starts in western Nevada and runs southbound into California to a point just east of Edwards AFB (figure 15). Terrain features on TR-385 vary from flat to severe.

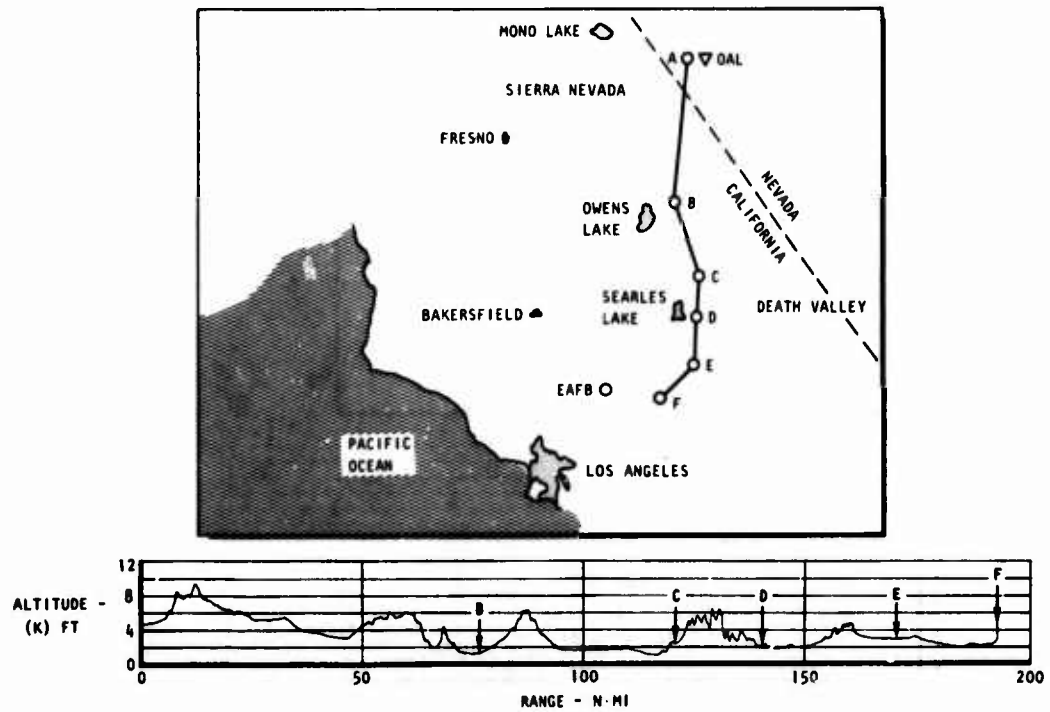

Figure 15. TR-385 (Tonopah)

TR-391 (Ukiah) starts over the Pacific Ocean, runs east across California into western Nevada, and then runs south to a point near Fallon Naval Air Station (figure 16). The route has ocean and generally mild-to-severe terrain. The initial part of this route is heavily forested.

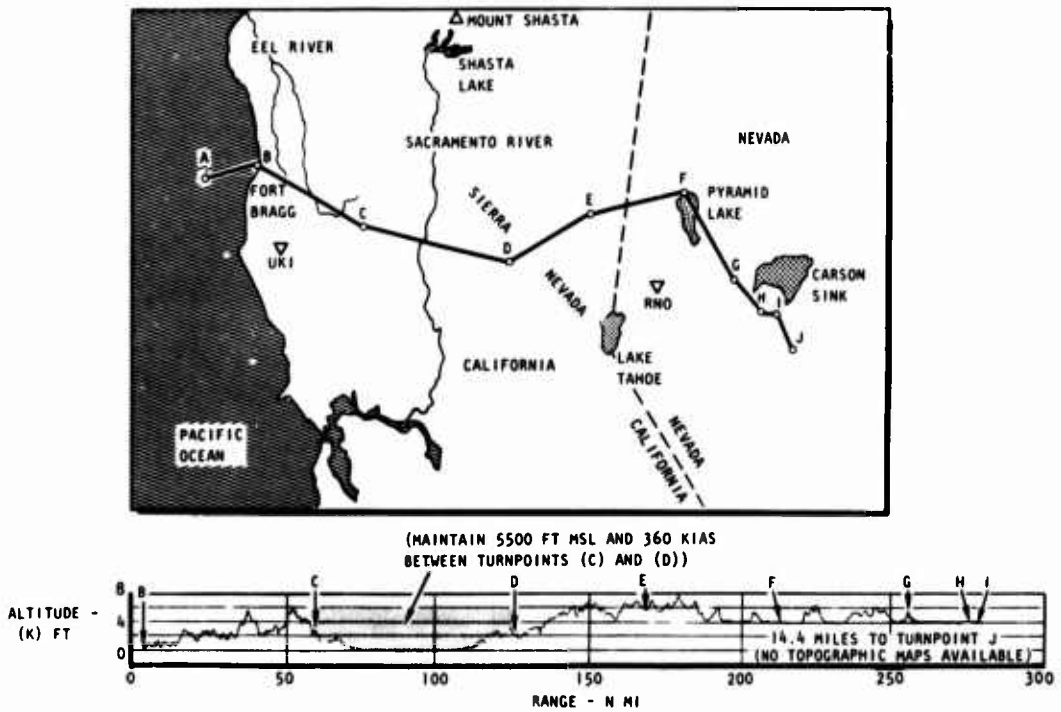

Figure 16. TR-391 (Ukiah)

A composite route has also been used recently which consists of TR-391 (Ukiah) points A through J, TR-360 (Tonopah) points H through I, TR-385 (Los Angeles) points A through F and then westbound into the Edwards AFB area (figure 17).

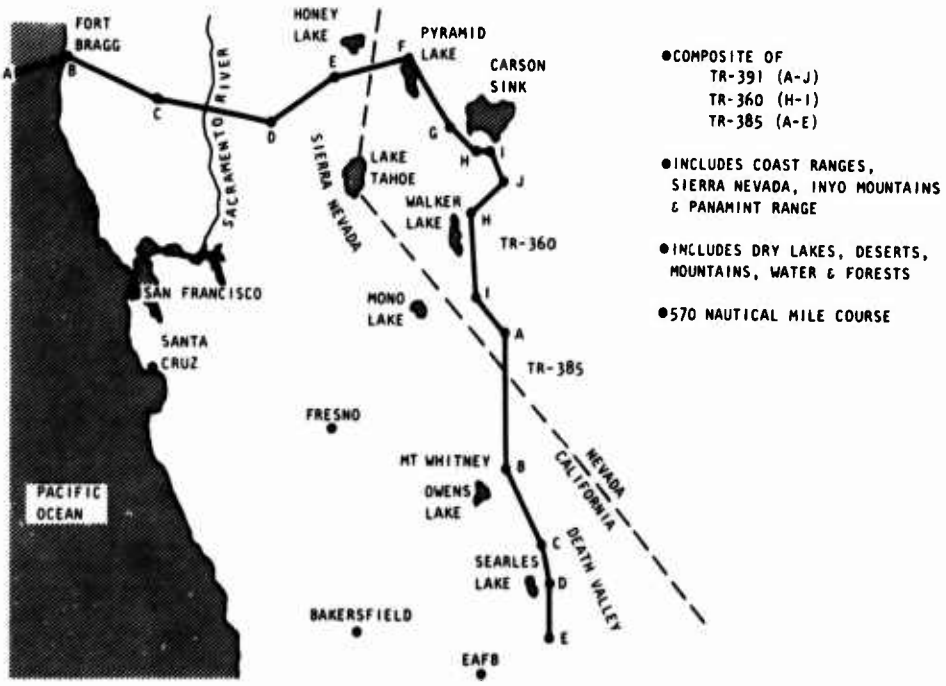

Figure 17. Composite Severe Course

FLIGHT TEST RESULTS

As earlier emphasized, the initial B-1 flight test effort was oriented toward clearing the aircraft for operation at 0.85 M at sea-level flight conditions in order to ensure that by the time the third prototype B-1 entered the flight test program, manual and automatic TF testing could be initiated as soon as practical after the first flight of this aircraft.

Flutter testing was initiated on the seventh flight of aircraft 1, and testing at the final phase I low-altitude, 0.85 M, 500-foot flight condition was completed on flight 18. Flying qualities envelope expansion tests went hand-in hand with the flutter tests. On the 20th flight of aircraft 1, the preliminary flying qualities envelope expansion effort had also been completed at 0.85 M and 500 feet including tests at the extremes of the allowable cg envelope.

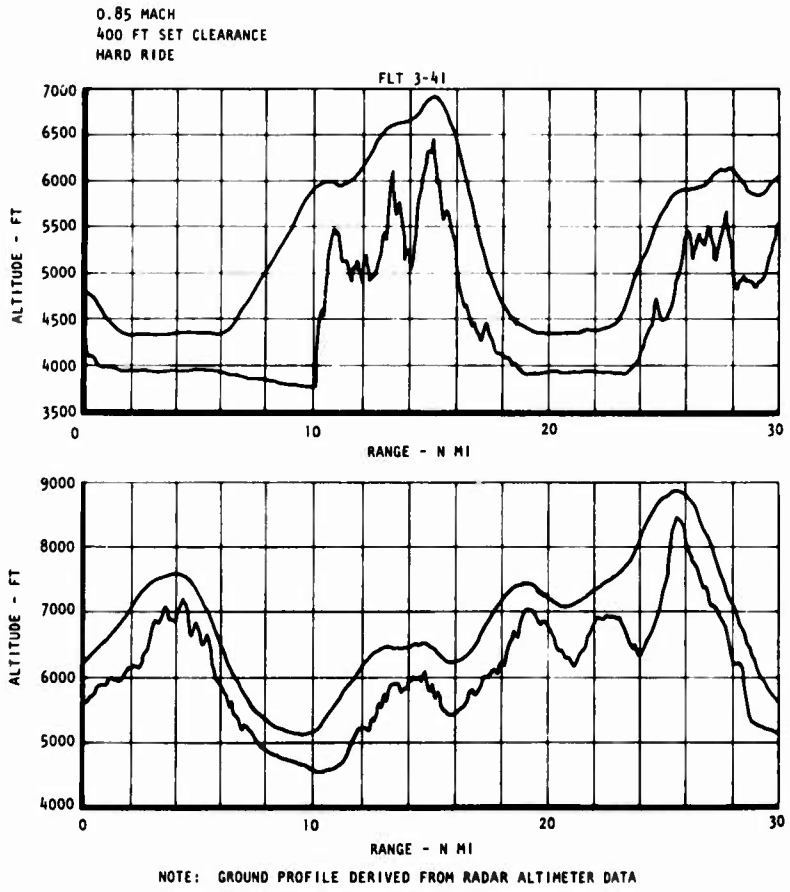

Figure 18. TF Performance - TR-391/360/385

Low-altitude testing on aircraft 1 was then directed at optimizing TF/flight control system adapter gains and defining structural mode control system (SMCS) operating gains. Aircraft 1 was fitted with a pitch control system exciter that was used to optimize the TF system adapter gains, while a SMCS exciter system was used in conjunction with an elaborate and time-consuming series of tests to define the optimum gains for that system.

In conjunction with these tests, the first series of manual TF tests were initiated over a course that extended from Edwards AFB, to Camp Irwin, California, and back to Edwards. The terrain on this route varied from flat to moderate, and this route was considered a very satisfactory one for these initial TF assessments. Testing was initiated at 0.70 M and 1,000-foot AGL, and progressed rapidly to 0.85 M at 500-foot AGL by the 24th flight of the airplane on 26 November 1975.

The results of these initial tests indicated that in the manual TF mode, longitudinal control forces were higher than desired for optimal manual TF performance and acceptable pilot workload, but that lateral control forces were acceptable. The airplane structure was very easily excited by even light turbulence. Turbulence stronger than light caused an uncomfortable ride with the SMCS off, to the point that some runs were discontinued when SMCS was inoperable. With the SMCS operating, the ride was always considered acceptable. Of primary importance is that these initial manual TF tests did indicate that the B-1 was capable of satisfactorily performing its low-altitude primary mission.

TF testing was begun in earnest on the first flight of the No. 3 prototype B-1 on 1 April 1976 when TF system functional checks were accomplished as part of the 4.9-hour shakedown flight. Manual TF testing was initiated on the third flight of aircraft 3 on the Edwards AFB Haystack Butte course at 1,000-foot AGL and 0.68 M and 0.85 M. Soft-, medium-, and hard-ride settings were evaluated at each mach number; in general, the TF system operated well.

The aircraft response to inputs of various TF system adapter gains was verified on the fourth flight, and automatic TF testing was initiated on the fifth flight.

The basic approach used during the TF system development program was to work down from 1,000- to 200-foot AGL set clearance at 0.85 M in the penetration configuration (65-degree wing sweep) on the Edwards AFB Haystack Butte TF course. As performance at the lower set clearance planes was verified at Edwards, runs down low-altitude training routes were initiated, first at the higher set clearance settings, and then again working down in altitude to 200-foot AGL.

The first "offsite" run was completed on the 11th flight on OB-20 (Holbrook, Arizona) at 0.85 M and 1,000-foot AGL. The aircraft negotiated this route (which is classified moderate to rolling) quite easily at the conditions flown. By flight 36, this route had been flown at 300-foot AGL and 0.85 M. Testing on TR-368 (Santa Barbara) was initiated on flight 13. The first 200-foot AGL offsite run was made on TR-368 during flight 28 on 5 May 1977.

To date, 26 hours of automatic and manual TF have been logged in aircraft 3 over many of the previously described routes in California, Utah, and Arizona. One of the latest test flights included a 1.1-hour automatic TF run at 0.85 M and 400-foot set clearance over the composite route TR-391/360/385 (Ukiah/Tonopah/Los Angeles), which has terrain features that vary from ocean to extremely severe. Quantitative test results and qualitative crew comments indicate excellent TF system performance during this extreme test of the aircraft low-altitude capabilities. Typical performance characteristics observed on this route are shown in figure 18, and a summary of all TF testing accomplished to date is shown in figure 19.

COURSE	TYPE	LOWEST CLEARANCE/FT	SUMMARY FINDINGS
HAYSTACK, EAFB	ISOLATED 400 FT HILL	200	LED TO DISCOVERY OF PULSE PHENOMENON APPARENTLY DUE TO WATER TOWER
GRANITE PK, UTAH	ISOLATED 3000 FT MOUNTAIN	200	EXCELLENT PERFORMANCE TO DATE. EMPHASIZED INADEQUACY OF SOFT RIDE
TR-368 (SANTA BARBARA)	MODERATE SOUTHERN CALIF COURSE	200	RECENT PERFORMANCE EXCELLENT. BASELINE OFF-RANGE COURSE. NO ANOMALIES
TR-391/360/385 (UKIAH/TONOPAH/ LOS ANGELES)	OCEAN/FLAT/ MODERATE/SEVERE/ EXT SEVERE	400	EXCELLENT PERFORMANCE TO DATE. CONCERNS ABOUT PERFORMANCE IN TURNS & LATERAL CLEARANCE
OB-10 (HAWTHORNE, NV)	FLAT/ROLLING/ MODERATE/SEVERE	NOT YET FLOWN	
OB-20 (HOLBROOK, AZ)	ROLLING/MODERATE	300	EXCELLENT RECENT PERFORMANCE. ROUTE NO LONGER ACTIVE
TR-345 (LOS ANGELES)	FLAT/ROLLING/ MODERATE/SEVERE	NOT YET FLOWN	

Figure 19. Route Summary

It is intended that TF testing will be continued in the future on both instrumented test courses and on operational low-altitude training routes in order to continue TF system development testing, and at the same time, to continue the evaluation of the capability of the B-1 to operate in the TF environment.

STEEP GRADIENT APPROACH SYSTEMS RESEARCH FOR ALL-WEATHER OPERATIONS

by
A D Brown
Operational Systems Division
Royal Aircraft Establishment
Bedford, UK

SUMMARY

This paper describes some aspects of steep gradient approach research carried out at RAE Bedford between 1973 and 1975 using flight trials, piloted simulation and theoretical studies. Because only conventional aircraft were available, the flight programme was orientated towards establishing the limitations of such types and their associated avionics equipment when used for R/STOL operations. Only performance data for the twin turbojet BAC 1-11 and the twin turboprop HS 748 are presented in the paper. Aspects considered include the determination of the maximum useable glideslope angle and the optimum beamwidths for azimuth and elevation radio guidance to permit R/STOL operations using a standard autopilot. It is suggested that MLS with DME range information will overcome some of the limitations identified.

Manual approach performance results are also presented which indicate the need for 150-200 ft decision heights. Piloted simulation research has shown a requirement for approach lighting comparable to existing Category 2 patterns for poor visibility operations. Even then, it is unlikely that acceptable missed approach rates can be achieved unless RVRs are in excess of 1000 metres.

Future research is anticipated using an MLS system at RAE Bedford in order to validate some of the ideas presented.

1. INTRODUCTION

During 1972, Operational Systems Division (formerly the Blind Landing Experimental Unit) was given a mandate to investigate the problems of carrying out steep approaches in all-weather conditions. The advantages claimed for flying steep gradient approaches include noise abatement, fuel conservation, terrain clearance and the ability to operate from short runways situated close to city centres. In the absence of specialised R/STOL aircraft, the limitations of conventional aircraft and their avionics were investigated using flight trials, piloted simulation and theoretical studies. The types used included a four engined VC10 jet airliner, twin turboprop HS 748 and HS Andover aircraft, a HS 125 executive jet and a Sea Vixen naval jet fighter. This paper describes some of the systems research carried out using the facilities at the Royal Aircraft Establishment, Bedford with particular emphasis on all-weather operations.

2. SCOPE OF THE R/STOL RESEARCH PROGRAMME

Among the aspects considered during the RAE research programme were:-

(a) the limitations of current automatic flight control systems (AFCS) when used to achieve coupled approaches comprising short range beam captures and steep glidepaths.

(b) the factors influencing the steepest operational glideslopes that can be flown.

(c) the determination of decision height.

(d) flare performance from steep glideslopes.

(e) the influence of visual aids on approach and landing performance.

This paper discusses these topics, describing the relevant RAE facilities where necessary.

Two of the aircraft used during the flight trials, namely a Series 201 BAC 1-11 (XX 105) and a Series 1 HS 748 (XW 750) are still being used by Operational Systems Division and the flight results presented will be restricted to these types. The main characteristics of the aircraft are listed in Table 1.

TABLE 1

DETAILS OF BAC 1-11 AND HS 748 RELEVANT TO R/STOL TRIALS

	BAC 1-11 (XX 105)	HS 748 (XW 750)
Max Landing Wt	32,200 Kg	16,330 Kg
Threshold Speed	119 kn	85 kn
Wing Span	27.0 m	30.0 m
Wing Area	91.2 sq m	75.4 sq m
Approach flap for Steep Approaches	45°	$27\frac{1}{2}^{\circ}$
Engines	2 x RR Spey turbojets	2 x RR Dart turboprops

The piloted simulator used for the steep gradient research at RAE Bedford essentially comprises a fixed-base two-seat cockpit, a 200 amplifier analogue flight computer and a collimated computer generated

'outside world' display. The latter presents the pilots with a perspective view of the airfield approach and runway lighting in colour as seen at night (Ref 1). The forward visibility can be readily controlled as a function of height and in a manner representative of fog or cloudbase conditions.

3. APPROACH GRADIENT CAPABILITY

Brief flight trials were carried out using both aircraft to confirm the theoretical predictions covering the maximum approach gradients that could be achieved in still air with the engines set at flight idle. For the BAC 1-11 in the approach configuration - 45° flap, undercarriage down - this was approximately 8°, the precise value depending on aircraft weight and speed. Figure 1 shows the relevant performance carpet as a function of these parameters. It is worthy of comment that on some aircraft the use of additional aircraft services, eg anti-icing equipment, does require the throttles to be forward of the flight idle position, thus reducing the maximum gradient capability. Since, in practice, a margin of at least $1\frac{1}{2}^{\circ}$-2° must be allowed to give some manoeuvre margin, deceleration capability, wind allowance etc, (Ref 2), the steepest operational glideslope that can be contemplated from purely aerodynamic/airframe considerations is 6°. Autopilot performance, the consistency of the flare and landing and decision height requirements could still of course, reduce this angle further.

Unlike the BAC 1-11 where, due to non-linearities in the throttle position - engine thrust relationship, the flightpath angle does not increase significantly for RPMs less than 75% (Ref 1), for the HS 748 the reverse is true. Being a turboprop aircraft, when the throttles are near their back-stops (approximately 20 psi indicated torque), a zero thrust situation is reached beyond which a significant drag increase occurs. This yields an additional 2° of flightpath angle for the last 11% of throttle movement. However, such is the sensitivity of control in this region that it cannot realistically be considered for operational purposes.

Another difference of the HS 748 as compared to the BAC 1-11 is the degree of flap needed to achieve the desired glideslope. Normal approach flap (for a 3° glidepath) is $22\frac{1}{2}^{\circ}$, with an airspeed equivalent to (V_{AT} + 10) of typically 105 knots. In order to achieve a significant steep gradient capability, land flap ($27\frac{1}{2}^{\circ}$) had to be used which, when coupled with the appropriate approach speed of 95 knots, yielded a realistic (zero thrust) maximum gradient of approximately $6\frac{1}{2}^{\circ}$. This limited the operational glideslope to a maximum of 5°. During the course of the R/STOL programme, this approach performance was improved an extra 2° by increasing the flap (and associated tab angle) deflection from $27\frac{1}{2}^{\circ}$ to $29\frac{1}{2}^{\circ}$ - the maximum mechanical limit. This non-standard configuration did however, result in a severe airspeed restriction of 100 knots which presented considerable operational problems to the pilot, especially during the glidepath capture manoeuvre and was eventually abandoned.

4. AUTOPILOT SHORT RANGE BEAM CAPTURE PERFORMANCE

At the time of the research, it was generally considered that if R/STOL aircraft were to be able to operate in Terminal Movement Areas (TMAs) at major airports like London (Heathrow), then they would need to be capable of making accurate azimuth approach intercepts from wide angles and at short ranges (Ref 3). It was also assumed that an MLS guidance system providing wide angle coverage would be available. Current autopilots are not designed for this type of manoeuvre, their function being generally to join the relatively narrow beam ($\pm$ 2°) ILS localiser within a range of 10 miles. It therefore seemed important to determine at the outset the limitations of current standard AFCS in the R/STOL role and to establish how far operational techniques could overcome any deficiencies in the approach performance. The effects of crosswind and radio guidance beamwidth on approach accuracy were considered as part of this work and to assist the programme a digital simulation of the HS 748 (SW 750), the aircraft available for the trial, was used. The aircraft is equipped with a Smiths Industries SEP6 autopilot and flight system certificated for use in ICAO Category 2 visibility limits and which has the normal modes available, ie IAS lock, attitude stabilisation, heading steering, height lock and ILS (beam and glidepath) coupling. An autothrottle provides an alternative means of airspeed control if required. The azimuth control law comprises beam and beam rate and yaw rate terms and beam acquire occurs as the ILS deviation falls below a nominal 160μA (Ref 4). Figure 2 shows a typical circuit pattern for the HS 748 flying steep approaches using the autopilot. Figure 3 shows digital simulation results for the effect of reducing the intercept range (measured from the GPO of the runway) for an azimuth capture manoeuvre from 5 nm to 2 nm using a 90° intercept angle and a typical localiser beamwidth. (At RAE Bedford the ILS localiser is approximately $\pm$ 1.8° with a beam sensitivity of 82.5 μA/deg - due to the considerable length of the main runway). During the simulated approaches an 8 knot crosswind was represented in order to match the runs with the equivalent flight cases.

The progressive reduction in stability is obvious as the range decreases, curve (a), the 5 nm case, representing an ideal situation in terms of response time and damping, whereas curve (c), the 2 nm case, is a totally unacceptable state. It must be remembered that once the glideslope is acquired, the bank limit in an autopilot is generally reduced and for the SEP6, this change is nominally from 30° to 10°. Thus, unless the aircraft is already well established on the extended runway centreline, the azimuth performance will inevitably deteriorate. (Note: for a circuit height of 1500 ft, glide acquire occurs at a range of 2.4 n miles). In Figure 3 case (b) represents a situation considered to be just operationally acceptable to a pilot in IMC conditions.

Figure 4 again shows simulation results for the HS 748, the main variable being azimuth beamwidth. Case (a) representing the $\pm$ 2.5° beamwidth situation, is obviously unstable, whereas cases (b) and (c) are both damped. Case (c) ($\pm$ 10°) is however, very sluggish and unlikely to be acceptable operationally. A number of the simulation runs were validated against flight data and found to agree well enough to allow the model to be used more widely for performance predictions.

Figure 5 shows flightpaths recorded using a Bell SPN 10 tracking radar which also provided via a data link to the aircraft, the experimental azimuth guidance of different beamwidths. Both the simulation and the flight trials revealed an optimum beamwidth for short range captures close to 3°. Figure 5 shows

experimental data for a 3.5° beam and clearly reveals the influence of intercept angle. It can be seen by inference that a 45° intercept would allow acceptable captures to be made at ranges of 2 n miles using the existing AFCS if this was operationally feasible.

Another important parameter influencing the capture manoeuvre is obviously that of windspeed and direction. Simulation showed that even for an optimum beamwidth of 3° at a range of 4 n miles, the maximum overshoot of the beam centreline during a 90° capture could increase from 170 metres to 900 metres if the wind changed direction from 30 knots head to 30 knots tail (Ref 2).

To summarise, with the potential wide azimuth coverage of MLS (at least ± 40°), there will obviously be no problem in achieving short range captures with 90° intercepts using current AFCS, except that gain scheduling using the associated DME range information might be necessary to achieve the optimum beam sensitivity in terms of μA/degree. For short runways of 600 to 900 metres length, even an ILS localiser with a beamwidth of ± 3° would appear to be adequate.

From the AFCS viewpoint, the biggest improvement would come from reducing the bank limit during the approach at some point below glide capture perhaps using a range discriminant.

The ability to overcome the extreme lateral overshoots caused by crosswinds and to perform intercepts at angles in excess of 90° need further research.

5. AUTOPILOT STEEP GRADIENT PERFORMANCE

It follows that a similar exercise can be performed to establish the limitations of the autopilot during the glidepath phase of the approach. For the SEP6 autopilot the glidepath control law primarily comprises beam and beam rate terms together with a pitch damping term and glide acquire occurs when the signal level reduces to 30 μA (Ref 4). For the HS 748 full (land) flap - 27½° - was selected at glide acquire and the speed reduced to the nominal approach speed of 95 knots equivalent to (V_{AT} + 10) knots (see Figure 2).

Figure 6 shows two examples of glidepath captures from nominal circuit heights of 1500 ft and 1000 ft. The Bell lock-follow radar was used to provide the experimental guidance, the glideslope angle being 6° and the beamwidths equivalent to the ILS at ± 0.7°. For the higher circuit the overswing at glide capture is still within the beam coverage and thereafter, the performance is well damped. At the lower circuit height however, the glidepath holding is oscillatory following a very large overshoot at the capture point and is rated as operationally unacceptable. Flight trials indicated that the optimum beamwidth was ± 1.5° and this was used for the remaining R/STOL research.

The capture manoeuvre is more demanding than the azimuth case; a change of configuration has to occur, together with large changes of attitude and speed. Using the existing AFCS, which is optimised for a 3° glideslope, glidepath capture does not begin until the aircraft has virtually reached the centre of the beam (within 0.3°) but the resulting overshoot is small and operationally acceptable. However, for a steep glideslope the late acquire is undesirable and creates a situation where the pitch auto-trim system has difficulty in following the demand. During the course of a research programme using RAE's BAC 1-11 to investigate the problems of two-segment approaches (Ref 2,5), this same problem was overcome using so-called 'easy-on' circuitry as an interface between the guidance signal and the standard Smiths SEP5 AFCS. The glide acquire point was made a function of beam and beam rate and took place early enough to eliminate any overshoot even in the presence of a tailwind. This interface would appear to be essential for steep approaches even using MLS guidance. By using the DME range information, the glideslope sensitivity could effectively be kept constant, thus making the capture performance independent of circuit height - an operationally desirable situation. (This could also be important for manual flight director approaches as well).

6. MANUAL APPROACH PERFORMANCE USING VISUAL GUIDANCE

As explained earlier, the general R/STOL concept was that of aircraft flying steep approaches to short narrow runways relatively close to city centres. Runway widths would probably be no more than 30 metres and the length somewhere between 600 m and 1200 m depending on the size of the aircraft (Ref 6). It follows that the R/STOL touchdown zone must be considerably smaller in length then the conventional runway values of 900 m and the glidepath origin must be closer to the threshold than the usual 300 m. This requirement for more accurate landings means that all the 'system' tolerances producing touchdown scatter must be reduced. One important factor is that of flightpath accuracy since error from the glidepath could well translate into range errors at touchdown. The pilot also faces a more difficult flare and hence needs to be well positioned at the start of each such manoeuvre. Measurements made of manual approach performance using the VASI system for 3° approaches (Ref 7) showed that there could be considerable flightpath variation which would probably be unacceptable in an R/STOL application. To provide an alternative to radio guidance, an improved visual guidance system was developed - the Precision Approach Path Indicator (PAPI), described fully in reference 8 - which has proved extremely effective for steep gradient approaches. Figure 7 shows typical height scatter from the nominal glideslope as a function of range from the glidepath origin. Three cases were considered, namely 6° and 3° approaches to a defined TDZ and a 6° approach to an unmarked runway. At ranges greater than 400 metres, the standard deviations (SDs) for these three approach tasks were essentially the same, ie between 5 and 6 ft. Thereafter, performance for the 3° glideslope and the 6° glideslope using an unmarked runway, continue to improve to between 3 ft and 4 ft. Where, however, the aircraft is required to land within a defined TDZ on the runway from a steep (6°) approach, the height scatter increases to a peak of nearly 8 ft at a range of virtually 300 m. The only plausible explanation was that around a height of 100 ft, the pilots involved were attempting to position the aircraft in a way they each considered to be most appropriate in order to land within the TDZ. (This trial was repeated in view of a possible anomaly but with the same outcome).

If these results are now converted into horizontal scatter from the nominal glidepath as a function of height as shown in Figure 8, it can be seen that now the 3° glideslope yields significantly more scatter

than the 6° glideslope essentially due to the range : height relationship involved (approximately 20:1 for a 3° glidepath). This difference in the two SDs exists right down to touchdown. (This emphasizes the need to use the correct performance parameter).

Of equal interest is the fact that the apparently good approach performance to the unmarked runway referred to earlier, deteriorates rapidly during the last 10 ft of the flare and ends up being comparable to the other two cases. Obviously the pilots have no range constraints and hence concentrate primarily on a smooth touchdown.

7. MANUAL FLARE PERFORMANCE

Figure 9 shows time histories of two typical examples of flares from steep gradient approaches in VMC, one set each for the BAC 1-11 and HS 748. Beginning with the turbojet (solid lines), a slight reduction in flightpath angle is occurring about 75 ft but as the aircraft passes a height of 25 ft, it is still approximately 5°. Thereafter, a progressive nose-up pitch attitude is achieved (approximately 3°) as a result of which flightpath angle reduces rapidly. To prevent any possibility of a balloon, the nose of the aircraft is lowered slightly leading to a virtually perfect touchdown. During most of the flare, the power is retained close to the approach value and only during the last two seconds is the power reduced. This has been termed a 'cautionary' flare in reference 9.

For the HS 748 (dashed line), a significant reduction in the flightpath angle does not begin until a height of 25 ft. Prior to this, a nose-up change of attitude only appears to compensate for the trim change due to the reduction of power which begins about 35ft and is at flight idle, with 1½ seconds to go to touchdown. The nose-up attitude only reaches about 1° and then returns to virtually zero with the result that flightpath angle does not reduce to zero but still results in a nice landing with a rate of descent of less than 2 ft/sec.

Comparing the two aircraft, the BAC 1-11 is flared progressively from about 50 ft, a significant nose-up attitude is achieved early to arrest the descent rate and then, as power is reduced fairly fast, the final adjustment is done by using altitude. The HS 748 is flared much later but power is reduced progressively and slowly due to the associated trim changes and the attitude stays close to zero.

During the course of trials with both aircraft it was found, as might be expected, that there was a definite tendency to produce firmer landings from steep gradients than from a 3° approach in good meteorological conditions (Ref 2). This was particularly so when the pilots were required to touchdown within a defined area on the runway as could well be the case in actual R/STOL operations. In fact, a sample of 49 HS 748 landings involving 3 pilots made on the defined R/STOL TDZ yielded one touchdown in excess of 6 ft/sec and six in excess of 5 ft/sec. It follows that if operations were to continue in more adverse weather conditions, eg fog, the situation could become much worse thus indicating that conventional aircraft are unsuitable for such a role. If however, the restricted runway length requirement is relaxed, then the touchdown performances for 3° and 6° become comparable.

8. ALL-WEATHER OPERATIONS

Two prime parameters govern the all-weather operation of civil aircraft, namely decision height and runway visual range (RVR). R/STOL research at RAE Bedford investigated both aspects and these are discussed in the following sections.

8.1 Decision Height

Assuming that the use of a steep glideslope removes the obstacle clearance problems, the major factors to be considered in determining a realistic decision height are firstly, the missed approach performance of the aircraft and secondly, the side-step capability.

8.1.1 Missed Approach Performance

Beginning with the height loss during the missed approach, for conventional ICAO Category 2 certification requirements (Ref 10) the UK calculates the minimum decision height as the mean value plus 5 standard deviations in order to establish a minimal risk that an accident will occur during this manoeuvre. For the BAC 1-11, the so-called height allowance is specified as 60 ft for a 3° glideslope and this includes a contribution due to a possible engine-out WAT limited situation. Measurements made using the BAC 1-11 flying down a 6° glidepath indicated a mean height loss of 98 ft and an SD of 14 ft, thus yielding a minimum decision height of 170 ft (Ref 2). Because the same flap setting (45°) for the BAC 1-11 was used for both glideslope angles, performance measurements and the crew procedures involved were straightforward even in the single engine case.

For the HS 748, as mentioned earlier, a non-standard flap setting (27½°) had to be used to achieve a realistic steep approach capability. This meant that during the missed approach manoeuvre, two notches of flap had to be raised (this takes 8 seconds) in order to establish a realistic climb rate, thus generating a large nose-up trim change. Additional problems were obvious during the engine-out situation; for example the need to exert considerable pressure on the rudder pedals to maintain directional control. Such was the workload generated that several pilots were observed to forget to raise the undercarriage until reminded.

Another problem experienced was caused by the turbo-propellor engines. Such were their characteristics that careful pilot handling was necessary in order to avoid an initial decrease of speed. Such effects are shown in Figure 10 where three throttle movement rates are shown ranging from slow to slam (curves (a), (b) and (c)). For a stick fixed situation, the effects on pitch attitude and airspeed are obvious; a 'slam' throttle movement leading to a 7 knot speed loss whereas a progressive movement, whilst still producing a nose-up attitude, maintains a virtually constant airspeed.

Such considerations indicated a realistic minimum decision height of 150–200 ft. It follows that such adverse handling characteristics must be avoided in any future purpose-built R/STOL airliner.

8.1.2 Side-step Performance

During the flight trials it was considered important to examine the problems of carrying out lateral side-step manoeuvres in order to align the aircraft with the runway. A comprehensive treatment had already been performed for 3° approaches (Ref 11) and hence the task was really one of briefly validating these data and then determining the extra height penalty due to the steeper glideslope. It was found that the bank angles used for the manoeuvres were always less than 20° and generally around 10°. Of greater importance however, was the additional height needed due to the increased descent rate relative to the 3° case, in order to correct a given lateral offset, an extra 100 ft of height being required for the HS 748 in order to correct a 30 metre lateral offset. Figure 11 shows this so-called 'height penalty' as a function of lateral error. This is obviously a severe operational penalty and indicates the prime requirement for good avionic equipment and guidance so that the aircraft is well positioned during every IMC approach.

8.2 Visibility and Related Aspects

As mentioned earlier, RVR is an important parameter but it is intimately connected with approach and runway lighting patterns and the following sections deal with these aspects.

8.2.1 R/STOL Runway Lighting

As a preliminary investigation into the most effective form of R/STOL lighting, a piloted simulator exercise was carried out initially looking at three runway patterns in VMC at night (Ref 12). Figure 12 shows the minimum arrangement, whilst Figure 13 shows the additional centreline and crossbars. PAPI guidance was used for each manual approach. Although the runway was relatively narrow, (45 metres), the pilots still felt that a centreline was essential, especially in crosswind conditions. In the good visual conditions simulated, two such bars were found to be adequate to define the TDZ, one defining the GPO and the other the end of the touchdown area. However, the length of the TDZ was relatively small for the size of aircraft with the result that pilots tended to duck under the 6° glidepath in order to land or else deliberately to underflare. Equivalent painted TDZ markings were added to the runway for use in daytime fog conditions (Ref 2).

8.2.2 Effects of Poor Visibility

A follow-up experiment using the same simulator with its night visual display examined the low visibility aspects, this time including the approach lighting. A conventional (3°) approach and runway lighting pattern was used as the datum case since all the current AWOP experience was based on this lighting and it was quite conceivable that R/STOL aircraft would from time to time, have to operate from such runways. A second pattern was that of the R/STOL runway referred to previously with a TDZ defined by four crossbars. In an attempt to overcome the previous flare problems, the TDZ was shifted along the runway, beginning at the GPO. Approach lighting was added comprising 450 metres of extended centreline, two crossbars and a limited set of red barrettes. This was considered to be the maximum likely for R/STOL runways. Both lighting arrangements are shown in Figure 14.

In addition to the two patterns, a number of other experimental parameters were investigated. For example, three decision heights were examined, namely 100, 200 and 300 ft, covering the ICAO Category 2 range and extending up to include the values considered realistic for R/STOL operations as described in Section 8.1. The effect of lateral displacement from the extended runway centreline was also examined. The same generalised RTOL jet aircraft was simulated as before, having a mass of 48000 kgs and an approach speed of 90 knots, (Ref 12). For each low visibility approach (automatic down to decision height) the pilot's far point of vision was controlled in a manner representative of fog, giving (a) a definite height at which he made contact with the lighting (generally 30–40 ft above his decision height), (b) a given segment of lighting at the decision height and finally (c) a normal RVR on the runway generally between 400 and 800 metres.

Table 2 shows the global results for the experiment and indicates the excessive number of missed approaches at the 300 ft decision height, especially for the R/STOL pattern. At 200 ft the results are better with the conventional pattern still generating less go-arounds. At 100 ft, the R/STOL pattern appears to be the slightly better of the two. Large (40m) lateral offsets appear to be affecting the approach success but the results are not statistically significant.

We can now look at the results more closely in order to determine the precise effects of visibility on approach success.

TABLE 2

		R/STOL Pattern			Conventional Pattern		
Decision Height	Lateral Offset	No of App.	Land Decisions	Approach Success	No of App.	Land Decisions	Approach Success
300'	40 m	40	13	32.5%	40	28	70.0%
	20 m	40	15	37.5%	40	33	82.5%
	0 m	40	16	40.0%	40	33	82.5%
200'	20 m	40	31	77.5%	40	36	90.0%
	0 m	40	31	77.5%	40	37	92.5%
100'	0 m	40	38	95.0%	40	36	90.0%

Figure 15 shows diagrammatically an aircraft on a steep approach at the two heights in question. The important parameters, visual segment, cockpit cut-off and horizontal visual range are illustrated. The aircraft at 300 ft is positioned such that the pilot has a visual segment (defined by the near point and far point) of 300 metres. The near point is obviously determined by the pilot's view over the nose of the aircraft - a function of cockpit cut-off angle and aircraft attitude - and the far point by the pilot's ability to recognise features on the ground as far ahead of the aircraft as possible - determined by the fog density. It is obvious that when the aircraft reaches 100 ft and assuming that the slant visual range (SVR) remains constant (most unlikely) then the pilot can see well down the runway.

Having defined visual segment, Figures 16 and 17 show examples of the results for the two patterns at decision heights of 300 ft and 100 ft as a function of this parameter. For the former case, lateral offsets up to 20 metres from the centreline did not appear to significantly effect the pilot's decision to land but displacements in the order of 40 metres definitely reduced the approach success. At the 100 ft level, the pilot was always aligned with the runway when he made visual contact.

At the 300 ft decision height (Figure 16) the conventional pattern is clearly superior to the others in terms of approach success (the ratio of the number of landings to the number of approaches). Zero overshoots occur down to a visual segment of 300 metres and thereafter the missed approach rate progressively increases to a level of 50% for a segment between 100 and 125 metres. Corresponding segments for the R/STOL patterns are an estimated 500 metres (point off graph) and 230 metres respectively. This is in general terms obviously due to the 900 metres of approach lighting plus the 300 metres of TDZ prior to the glidepath origin. By contrast, for the R/STOL pattern, the approach lighting extends for only 450 metres and the threshold is only 120 metres before the glidepath origin.

At the 100 ft decision height, it can be seen that the effectiveness of the conventional and the R/STOL patterns in terms of approach success have reversed, implying that the visual cues are more effective in the latter case. (It must be remembered that visual segment is only a meaningful parameter if it contains useful cues for the pilot, eg some elements of the lighting pattern). Zero overshoots occur down to a visual segment of 220 metres but thereafter, the conventional pattern is tending to produce a missed approach rate of 50% for a visual segment of 100 metres whereas for the R/STOL pattern, the missed approach rate appears to be only 10%.

To help clarify these approach success results for the two patterns in terms of the visual cues available to the pilot, we can, be assuming that the aircraft is accurately coupled to the nominal glidepath guidance and using the parameters defined earlier, construct so-called visual sequence charts. (Ref 15). These illustrate how, for different fogs, the pilot's far point of vision changes as the aircraft flies down the glidepath - the result being a so-called visual sequence. At any specific eye-height those major features of the approach and runway lighting pattern visible to the pilot can be readily determined, these being a function not only of the fog which determines the far point but also of the near point as determined by the downward view from the cockpit. Such features can be indicated on the charts.

Figures 18 and 19 show such charts with two typical visual sequences used during the simulator experiment. As just mentioned, at 300 ft, it can be seen that the red barrettes are within view once the pilot has made visual contact and hence he knows his position relative to the runway threshold and can be reasonably confident of making a safe landing.

For the R/STOL pattern, the pilot sees only a few white centreline lights - insufficient to produce a confident land decision since he is still devoid of range or ground plane information. By contrast, at the 100 ft decision height, once the threshold has disappeared from view beneath the nose of the aircraft on the conventional pattern, the pilot only sees a TDZ devoid of positive range cues until the GPO comes into view, just at decision height. For the smaller R/STOL pattern in the same circumstances, the pilot sees some red barrettes and the threshold prior to the GPO and hence, can rapidly assess his situation.

Whilst it is accepted that the pilot is involved in a dynamic situation, the charts illustrate the visual cues that the pilot sees down to decision height and hence can be used successfully as a basis for experimental lighting pattern design. The simulator results show that unless an R/STOL runway is equipped with a reasonable length of approach lighting, then at the decision heights considered to be practical, either the missed approach rate will be high in poor visibility or else the required RVR will be very high - both serious operational penalties.

Fog flying at RAE Bedford using a 3° glideslope has shown that the day and night situations are significantly different in terms of the visual cues available to the pilot. Whilst at night, ie the simulator situation, the lighting pattern and its colour coding are paramount, during day fogs the red barrettes and the green threshold lights are far less effective due to the higher background brightness. In addition, on the runway it is the white painted markings and other textural cues that become dominant over the lighting. To cater for these differences, distinctive changes of lighting pattern should be used to provide range cues, etc for the pilot and colour used purely to enhance the effect, as opposed to being a major factor.

Comparison with past results for 3° Category 2 operations (decision height 100-200 ft) using the conventional pattern (Ref 13) reveals a virtually identical curve to the 300 ft 6° case as shown in Figure 16 bearing in mind the relatively small samples involved. Many changes were made to the simulator during the intervening years between the two experiments and obviously the pilot population was different. This gives confidence to the results since the aircraft would be approximately the same range from GPO in each case and hence seeing the same cues.

In Figure 17 it can be seen that the 6° results are in fact superior to the past 3° data, obviously due to the benefits of being closer to the GPO. Thus, great care must be taken in applying the results to other situations. This is further borne out by the fact that, as an extension to the main simulator exercise, an experimental lighting pattern was used having crossbars in the approach lighting at optional spacings of either 120 m or 60 m. Although obviously an impractical situation, it did result in improved approach success, values of 75% being achieved for visual segments of 75 metres provided that the aircraft

was aligned with the runway, thus eliminating the need for any lateral manoeuvre.

8.2.3 Runway Visual Range Effects

Previous sections have dealt with the problems of decision height and the effect that visibility has on approach success at this point during the approach. In an operational situation, however, the only measurement made of visibility at an airfield is RVR. An attempt to look at this complex problem is made in Reference 14. Using a statistical model of fog based on measured data (including vertical gradients) in combination with known airfield lighting characteristics, it was possible to compute the height at which first visual contact ought to be made on a 6° approach in a range of RVRs. The results ranged from 280 ft at 800 metres RVR to 180 ft at 400 metres RVR, assuming a conventional Category 2 lighting pattern.

If further criteria are applied such as the time for the pilot to assess his position (at least 3 seconds) and the minimum visual segment that is necessary for him to make a 'land' decision on at least 90% of such approaches (approximately 200 metres at 300 ft for a conventional lighting pattern - Figure 16), then either the decision heights must reduce or RVRs increase. The former parameter is based on obstacle clearance and performance considerations and hence is independent of meteorological conditions. A value of 200 ft has been suggested from the performance data presented earlier (Section 8.1) and the RVR required at this height to achieve a reasonable approach success is estimated to be in the order of 1000 metres - again a considerable operational penalty.

9. DISCUSSION

The paper so far has highlighted a number of operational difficulties associated with R/STOL operations, in particular the relationship between decision heights and RVRs for steep approaches. In the absence of new high performance aircraft designs there would appear to be few options available to overcome the problems. The results suggest that without a reasonable length of approach lighting (at least 450 metres), safe operations in fog (RVRs less than 1000 metres) appear remote. Careful design of the approach and runway lighting pattern is necessary to yield the best possible approach success at any height and the most useful visual cues for the flare manoeuvre. A good downward view from the cockpit (at least 20°) is necessary to yield as much visual segment as possible.

A two-segment approach with a low transition height (eg 150 ft), from the 6° slope to the 3° has been considered in an attempt to overcome the difficulties of the steep single segment case (Ref 2). However, this appears unlikely to appeal to pilots in general since it implies aiming for a point short of the runway and also having to disturb the aircraft's stabilised approach path at a low height. The use of a reliable autopilot and MLS wide angle guidance might help to redress the balance. Even then, reference 14 shows that only small benefits accrue in terms of increased visual contact heights and in fact the increased range of the aircraft at a given height merely delays the point at which the pilot sights GPO.

10. CONCLUSIONS

This paper has briefly described some aspects of steep gradient approach research carried out at RAE Bedford between 1973 and 1975 using conventional aircraft. The results suggest that in terms of radio guidance, azimuth beamwidths of $\pm 3^{\circ}$ and elevation beamwidths of $\pm 1.5^{\circ}$ should allow existing AFCS designs to couple aircraft at relatively short ranges. The existence of MLS coupled with DME range information should considerably extend the approach performance capability, for example allowing stable operation in a wide range of wind conditions, AFCS gain scheduling and wide angle (270°) captures to be performed as well as segmented elevation glidepaths, if required in order to mix R/STOL and CTOL traffic in a TMA environment. The maximum operational glideslope angle is a function of many factors and 5°-6° was found to be the maximum using the conventional BAC 1-11 and HS 748 aircraft.

The problems of R/STOL all-weather operations looks pessimistic with decision heights around 200 ft. This leads to a requirement for high RVRs, in the region of 1000 metres, and the concept of a short runway devoid of approach lighting appears unrealistic (at least a length of 450 metres is suggested). However, careful design and approach lighting is essential to optimise the approach success (ie reduce the missed approach rate) obtainable at a given decision height.

During 1978 when a production Doppler Microwave Landing System has been installed at RAE Bedford, then some effort can be devoted to exploring the R/STOL MLS concepts discussed in addition to the conventional airline application. Similarly, during the course of flight research into the problems of improving aircraft avionics to help operations and increase safety in poor visibility conditions, it is hoped that some validation of the piloted simulation results can also be attempted.

REFERENCES

(1) J C Penwill, R J Packwood, Digitally generated outside world display of lighting pattern used in conjunction with an aircraft simulator. RAE Tech Memo FS 45, 1975.

(2) A D Brown, Resume of steep gradient research at RAE Bedford. RAE Tech Memo FS 113, 1977.

(3) N H Hughes, The implications of RTOL terminal area operations on avionics and guidance requirements. RAE Tech Memo Avionics 153, 1973.

(4) R Rawlings, Model Matching of the HS 748 aircraft with SEP6 autopilot. RAE Tech Memo Avionics 161, 1974.

(5) R B Lumsden, P H Collins, The development and evaluation of two-segment approach techniques. IEE Conference: 'The Future of Aircraft All-Weather Operations', November 1976.

(6) D L Button, The development of a prototype STOL System Demonstration, Eighth ICAS Congress, Amsterdam, 1972.

(7) A J Smith, D Johnson, An assessment of the in-service performance of VASI. RAE Tech Memo Avionics 131, 1973.

(8) A J Smith, D Johnson, The Precision Approach Path Indicator - PAPI. RAE Report TR 76123, 1976.

(9) R F A Keating, Steep gradient approach flare studies, Part I. Operational Techniques. RAE Report to be published.

(10) United Kingdom provisional operating requirements for all-weather operations, Category II. Board of Trade CAP 321, 1969.

(11) D Perry, W Port, J Morrall, A Flight study of the side-step manoeuvre during landing. ARC R & M 3347 1964.

(12) A D Brown et al, A Flight simulator investigation of R/STOL Runway Lighting Patterns. RAE Tech Memo Avionics 175, 1974.

(13) A D Brown, Category 2 - A simulation study of low visibility approaches and landings at night. RAE Report TR 71044, 1971.

(14) A J Smith, The performance of visual aids for steep gradient approaches in low visibility conditions. RAE Tech Memo FS 26, 1975.

(15) E A Goodman, L C Brown, An experimental method of forecasting visual sequences in low visibility. RAE Tech Memo BLEU 137, 1967.

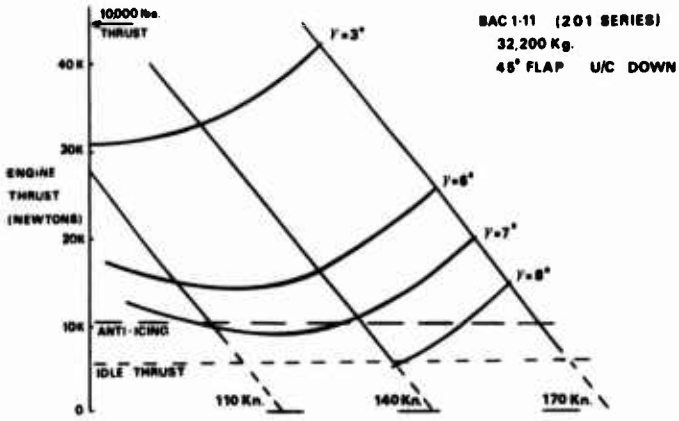

FIG 1: APPROACH GRADIENT CAPABILITY OF BAC 1-11

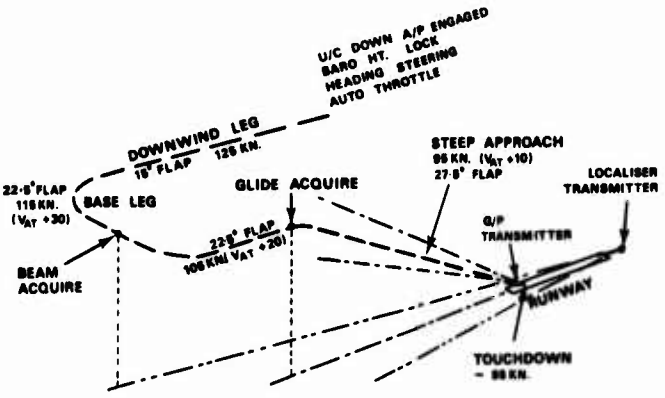

FIG 2: TYPICAL CIRCUIT PATTERN FOR HS 748 FLYING STEEP GRADIENT APPROACHES

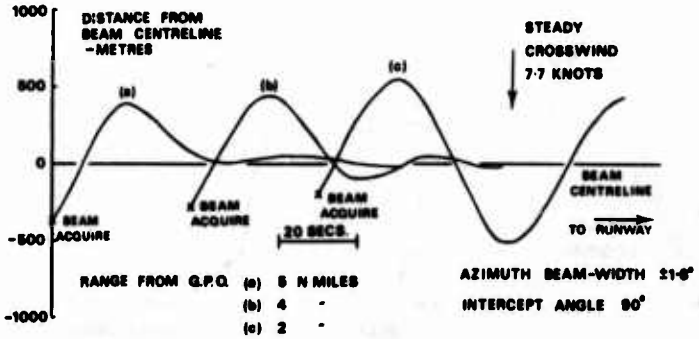

FIG 3: HS 748 - SEP6 AUTOPILOT SIMULATION. EFFECT OF RANGE ON AZIMUTH CAPTURE PERFORMANCE

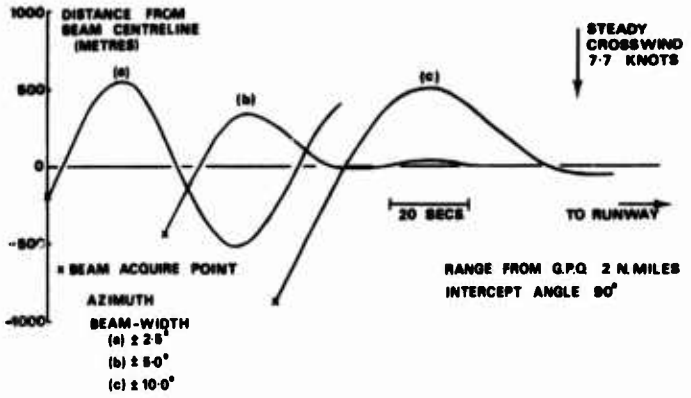

FIG 4: HS 748 - SEP6 AUTOPILOT SIMULATION. EFFECT OF BEAMWIDTH ON AZIMUTH CAPTURE PERFORMANCE

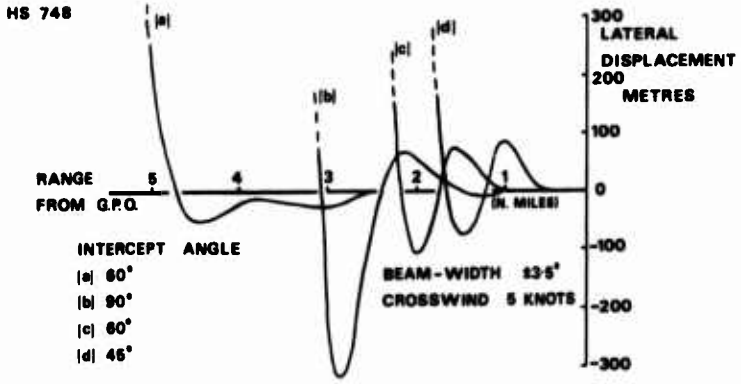

FIG 5: TYPICAL AZIMUTH CAPTURE PROFILES MEASURED USING THE HS 748 AND SEP6 AUTOPILOT

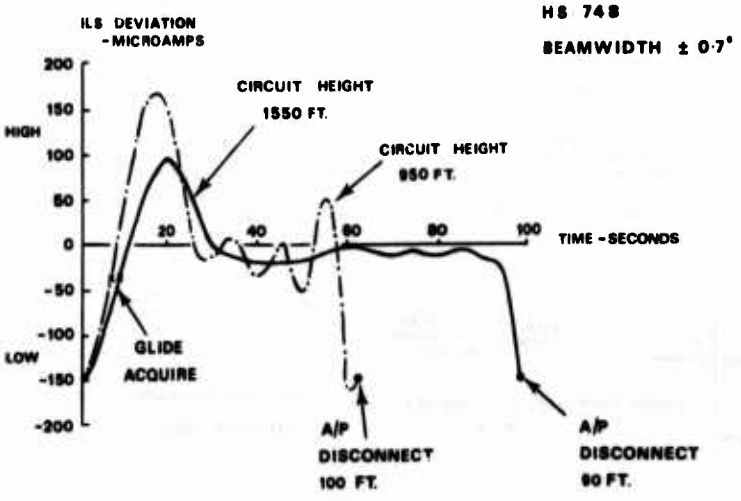

FIG 6: TYPICAL 6° GLIDEPATH PERFORMANCE USING THE HS 748 AND SEP6 AUTOPILOT

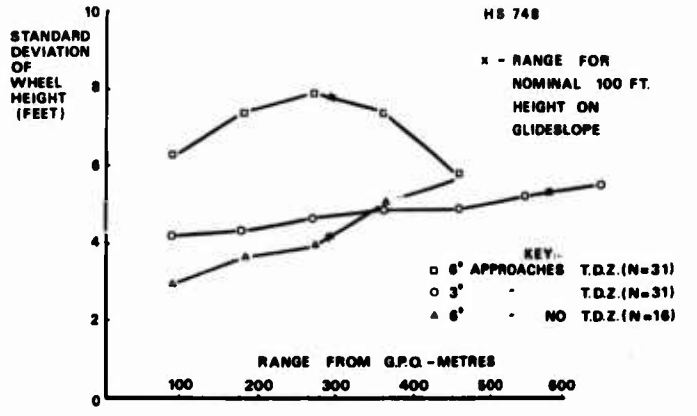

FIG 7: MANUAL APPROACH PERFORMANCE USING THE HS 748 - PAPI GUIDANCE

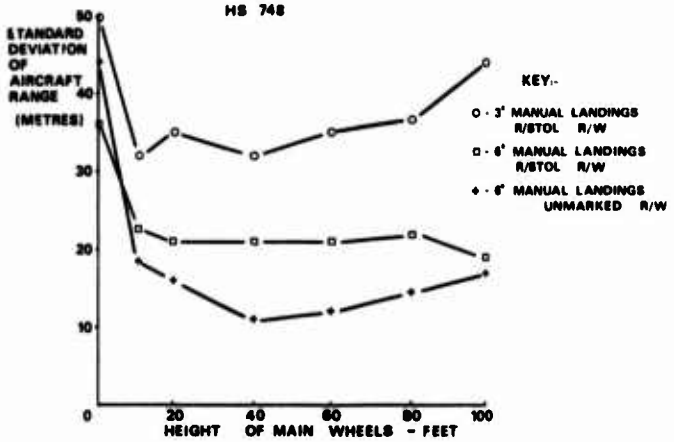

FIG 8: MANUAL APPROACH PERFORMANCE USING THE HS 748 - PAPI GUIDANCE

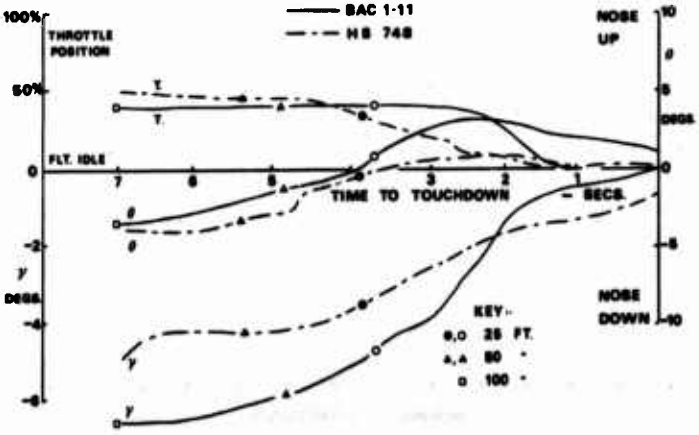

FIG 9: TYPICAL FLARES FROM STEEP APPROACHES FOR THE BAC 1-11 AND HS 748

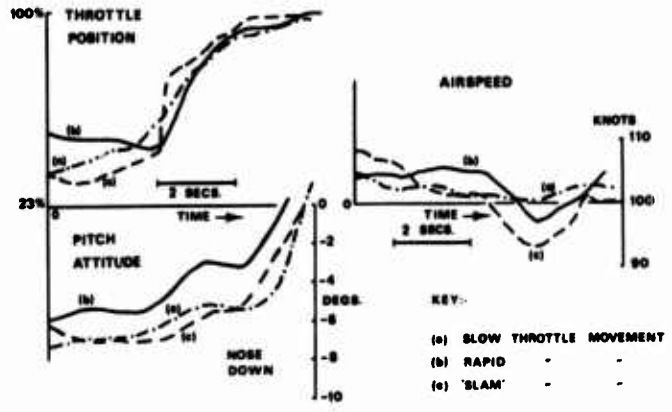

FIG 10: EFFECT OF THROTTLE LEVER MOVEMENT ON AIRCRAFT RESPONSE - HS 748

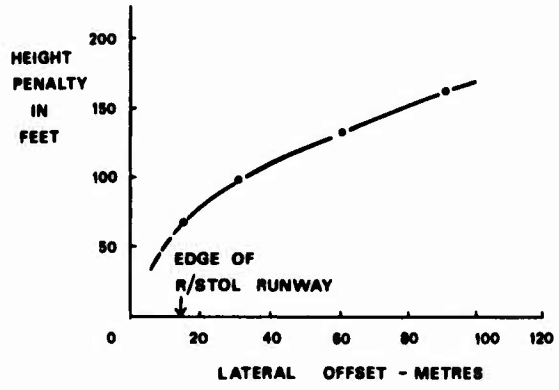

FIG 11: EXTRA HEIGHT INCREMENT RELATIVE TO 3° CASE NEEDED TO CORRECT LATERAL ERROR FOR HS 748

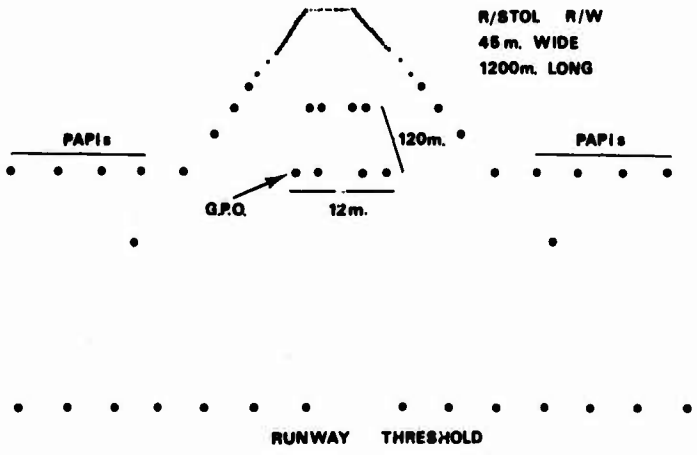

FIG 12: SIMULATED R/STOL RUNWAY - MINIMUM LIGHTING

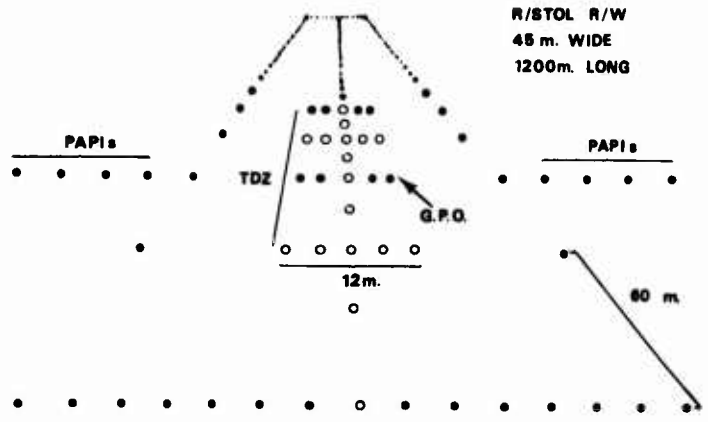

FIG 13: SIMULATED R/STOL RUNWAY - MAXIMUM LIGHTING

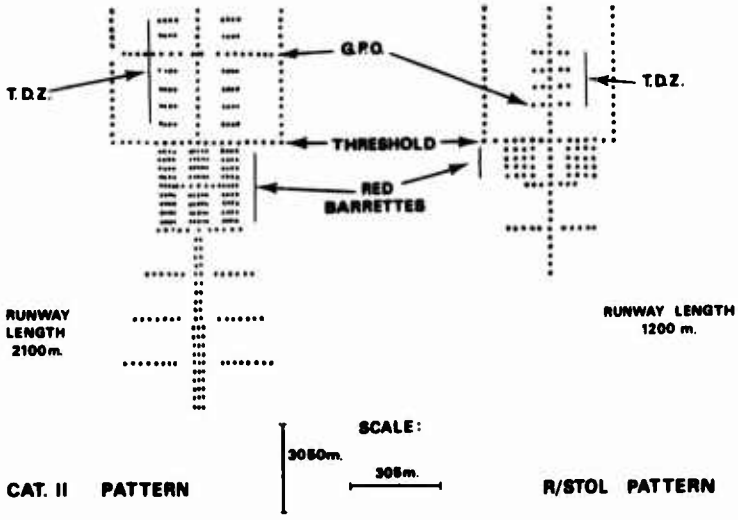

FIG 14: SIMULATOR LIGHTING PATTERNS USED TO STUDY R/STOL POOR VISIBILITY OPERATIONS

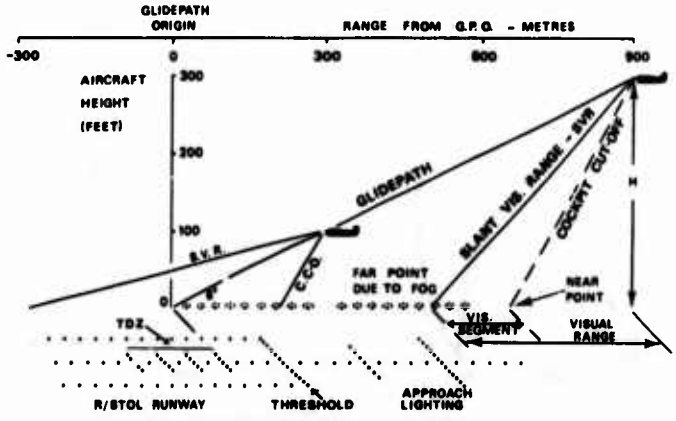

FIG 15: DIAGRAM ILLUSTRATING PARAMETERS USED FOR POOR VISIBILITY OPERATIONS

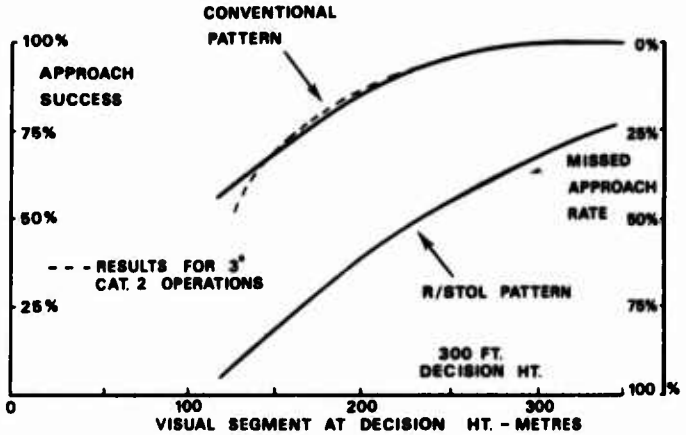

FIG 16: EFFECT OF VISUAL SEGMENT ON APPROACH SUCCESS - 300 FT DECISION HEIGHT (SIMULATION)

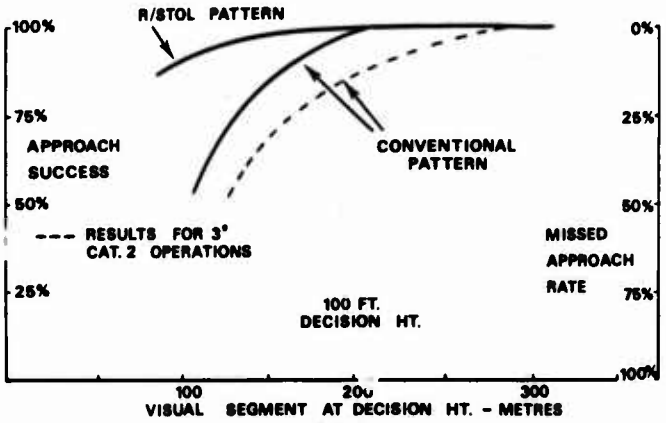

FIG 17: EFFECT OF VISUAL SEGMENT ON APPROACH SUCCESS - 100 FT DECISION HEIGHT (SIMULATION)

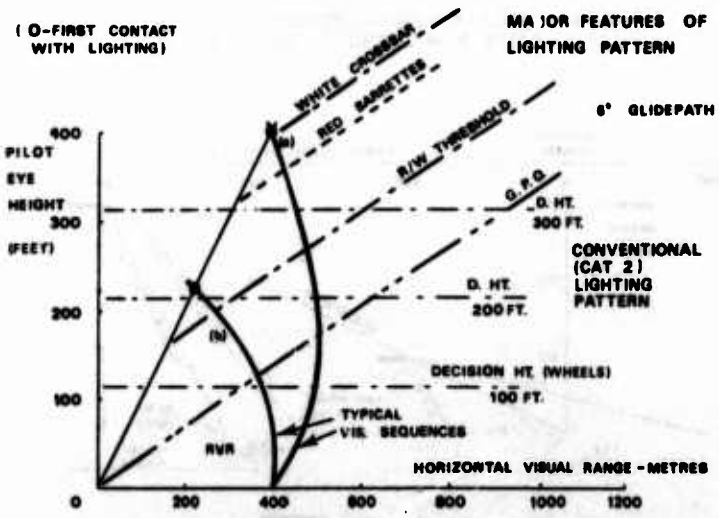

FIG 18: VISUAL SEQUENCE CHART FOR CONVENTIONAL (CATEGORY 2) LIGHTING PATTERN

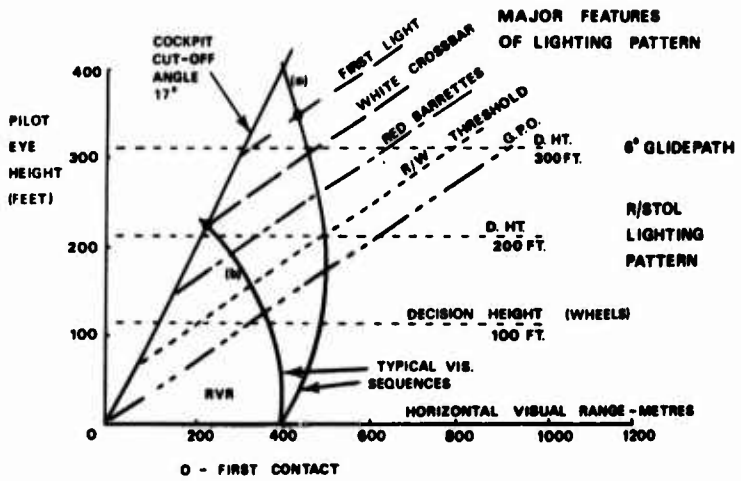

FIG 19: VISUAL SEQUENCE CHART FOR R/STOL LIGHTING PATTERN

RECENT FLIGHT TEST RESULTS USING AN ELECTRONIC DISPLAY FORMAT ON THE NASA B-737

Samuel A. Morello
Aero-Space Technologist
Flight Research Division
NASA Langley Research Center
Hampton, Virginia 23665

SUMMARY

This paper presents the results of a flight evaluation of two electronic display formats for the approach-to-landing under instrument conditions. The evaluation was conducted for a baseline electronic display format and for the same format with runway symbology and track information added. The evaluation was conducted during 3^{o}, manual, straight-in approaches with and without initial localizer offsets. Flight-path tracking performance data and pilot subjective comments were examined with regard to pilot's ability to capture and maintain localizer and glideslope using both display formats.

The results of the flight tests agree with earlier simulation results and show that the addition of a perspective runway symbol with an extended centerline and relative track information to a baseline electronic display format improved both lateral and vertical flight-path tracking. Pilot comments indicated that the mental workload required to assess the approach situation was reduced as a result of integrating perspective runway with extended centerline along with relative track information into the vertical situation display. The limited flight test results also show that the flight-path performance with the integrated situation display format meets Category II Flight-Director performance criteria.

Flight-path tracking results of close-in, curved approaches using the integrated vertical situation display format and predictive information on the horizontal situation display will also be presented.

SYMBOLS

ATTSYNC	Attitude Synchronization
$\dot{h}$	Complementary filtered altitude rate
k	Constant
LAT	Latitude
LONG	Longitude
PCOD	Pitch Control Out of Detent
Pitch PMC	Pitch Panel Mounted Controller
RCE	Roll Computer Enable
RCOD	Roll Control Out of Detent
Roll PMC	Roll Panel Mounted Controller
s	Laplace transform
t	Time
V_E	East velocity
V_N	North velocity
$\ddot{y}$	Crosstrack acceleration as measured in an inertial axis
β	Angle of glide-path deviation
δ_{ac}	Aileron command
δ_{ec}	Elevator command
η	Angle of lateral-path deviation
γ	Flight path angle as measured in an inertial axis
γ_c	Commanded flight path angle
θ	Aircraft pitch angle
$\dot{\theta}$	Aircraft pitch rate

ϕ Aircraft roll angle

$\dot{\phi}$ Aircraft roll rate

ψ Aircraft yaw angle

INTRODUCTION

One of the objectives of the NASA Terminal Configured Vehicle (TCV) Program is the research and development of electronic display concepts that will improve pilot instrumentation for the approach-to-landing task in low visibility. Present-day electromechanical instrumentation has been very beneficial in achieving low visibility landings on long, straight-in final approach paths. This instrumentation, however, is considered to be inadequate for the low visibility approach to landing on close-in, curved, approach paths that may be required in the future. As discussed in reference 1, the increased number of parameters that the flight crew may be required to control or monitor will also demand that information be processed and displayed in an integrated, analog form where possible to convey a naturally assimilated mental picture of a complex situation. The flight experimental systems used in the TCV program incorporate electronic displays which offer capabilities not currently found in electro-mechanical display systems. Considering this increased capability, a specific guideline or philosophy within the display information research is to investigate means of presenting improved situation information to the pilot. A display format is desired that will aid the pilot in maintaining a mental picture of his current situation relative to the runway and extended centerline during the approach to landing under instrument conditions. To achieve this objective, an integrated situation display format was developed that was aimed at presenting, in a single display, the necessary information for the approach-to-landing task, whether flown manually or automatically. This display format was evaluated in a piloted-simulation study where horizontal situation information, in the form of perspective runway and relative track symbology, was integrated into an existing vertical situation display format.

This paper presents the results of flight tests aimed at evaluating a baseline electronic display format and an integrated electronic display format in the actual flight environment. Piloted simulation results, reported in reference 2 and presented in this report, are compared with the flight-test results. The flight tests were conducted in the TCV B-737 utilizing an aft flight deck (AFD) and a velocity vector control mode. Results of straight-in, 3° approaches with and without initial localizer offsets at 3 nautical miles from the runway threshold are discussed. Flight-path accuracy data and pilot comments are presented and compared with Flight-Director performance criteria. Flight-path tracking results and pilot comments are also presented in the Results and Discussion section for close-in, curved approaches with 1.5-and 1.0-nautical mile, straight-in final approach segments.

TEST AIRPLANE AND EXPERIMENTAL SYSTEMS

The flight-test facility used in the TCV program is a modified Boeing 737-100 twin-engine jet transport shown in cutaway form in figure 1. Shown is the arrangement of palletized research installations aboard the test aircraft. Major components consist of a standard forward cockpit, an aft flight deck (AFD), navigation and guidance pallets, flight control computers, and a data acquisition system.

The two-man aft flight deck, shown in figure 2, consists of primary flight controls including conventional rudder pedals and panel-mounted controllers (PMC) for pitch and roll control. This cockpit has a fly-by-wire interface with the basic aircraft systems for both manual (semi-automatic) and fully automatic control of the airplane. With the exception of gear and speed brake actuation, direct electrical tie-in to flaps and throttles is provided to the research pilots. For safety monitoring purposes, control surface inputs are reproduced in the forward cockpit.

Flight control functions are managed through the use of the Advanced Guidance and Control System (AGCS) provided in the aft flight deck. The AGCS concept is shown in figure 3. The digital flight control computer which is triple redundant with a variable-increment capability provides the primary computational function for the flight control system. The fail-operational computer has programmable memory in which controls laws are solved in real time. The system interfaces the pilot and crew with the normal flight functions of navigation, guidance, display, and automatic control. Mode selection is available by using the AGCS mode select panel. The navigation-guidance computer, sensors, and three incremental flight control computers are the major elements of this system.

Crew communication with the navigational computer is made through the Navigation Control/Display Unit (NCDU) which has a keyboard for data input and a cathode-ray tube for data display on which paths can be synthesized during flight. The primary piloting displays of the AGCS are the Electronic Attitude Director Indicator (EADI) and the Electronic Horizontal Situation Indicator (EHSI). Additional details of the navigation, guidance and display systems are shown in block diagram in figure 4.

Depending on the mode selected, the aft flight deck pilot has available an attitude or velocity vector control mode. Only the velocity vector control mode was used in this study. Figures 5 and 6 are block diagrams of the pitch and roll control modes. Basically, these control modes provide the pilot with augmented control of the aircraft laterally and longitudinally. When pitch PMC is applied above the detent level, airplane pitch rate is commanded proportional to controller deflection. When the pilot releases his input and the controllers are recentered, airplane flight-path angle is maintained.

In the roll axis, the velocity vector control mode is designed to hold the airplane's attitude constant after roll PMC if bank angle is greater than 5^{o}. If the bank angle at controller release is less than 5^{o}, the control system maintains the airplane's present ground track by modulating bank angle.

Data were recorded onboard the aircraft on a wide-band magnetic tape recorder at 40 samples per second. Typical recorded data consisted of three-axis body angular position and rate information as well as pilot control inputs. Ground-based tracking data were obtained from a phototheodolite facility. The facility is a four-station optical instrumentation complex which provides accurate space-position-time location of a target within 15 nautical miles of the airport.

FLIGHT EXPERIMENT

The primary objective of the flight experiment was to evaluate the effect of adding horizontal situation information, consisting of a perspective runway symbol with extended centerline and a relative track-angle indicator, to a previously established vertical situation display format. (See Ref. 2.)

Figure 7 presents the information that can be presented on the EADI. The perspective runway symbology, drawn on a 30^{o} by 40^{o} field of view, includes the basic outline of the runway, a centerline drawn one nautical mile before the runway threshold to the horizon. The magnification factor was between 0.3 and 0.5, depending on pilot seat position. The runway symbol represents a runway 3,048 meters (10,000 feet) in length and 45.72 meters (150 feet) in width. Four equally spaced lines were drawn perpendicular to the centerline of the runway at 304.8 meters (1,000 feet) intervals. Two lines parallel to the centerline of the runway were drawn on the runway dividing it into equal quarters. The mathematics of drawing the runway symbology are detailed in reference 2.

The relative track angle indicator pictorially shows the inertially referenced track angle of the airplane relative to the runway heading. Relative track angle information was indicated by a tab that moved along the horizon line of the EADI. A track scale with 10^{o} increments referenced to the runway heading was drawn on the horizon line of the EADI. The pilot using the track pointer and scale could determine the magnitude of the relative track angle of the airplane to the runway.

The evaluation process was both qualitative and quantitative. Pilot opinion concerning the ability to understand and use the displayed information as well as tracking performance data were analyzed for the final approach-to-landing task. Onboard data instrumentation and ground-based tracking theodolite data were recorded and analyzed.

DISPLAY FORMATS TESTED

The navigation, guidance, and display subsystems have been integrated into a single system, as can be seen in figure 4. The system utilized digital computation, information processing, and transmission techniques, together with cathode-ray tube (CRT) displays. The EADI was the primary display used by the evaluation pilots and measures 12.70- by 17.78-centimeters (5- by 7-inches).

Two display formats were presented on the EADI for evaluation purposes. Figure 8 is a drawing of the baseline format on the EADI, which consists primarily of the airplane's attitudes, flight-path information, and flight-path deviations. Included in the baseline display format is the EHSI, also shown in this figure. Presented on the EHSI are the airplane symbol for present position information, a 30-second curved trend vector (predicted position information 30 seconds ahead), runway and extended centerline, and digital readout and scale of present track angle.

Figure 9 is a drawing of the integrated situation information format and basically contains the addition of the perspective runway symbology and relative track information.

The flight tests reported here were flown using the Time Referenced Scanning Beam Microwave Landing System (MLS) located at the National Aviation Facilities Experimental Center. The airplane's basic navigation, guidance, and display system was modified, as shown in figure 10, for compatibility with the MLS. The MLS receiver processor provided raw decoded MLS elevation and azimuth angular information and filtered range data to the MLS guidance signal processor. The MLS guidance signal processor utilized the MLS information and data from the aircraft sensors to prefilter the raw data, perform coordinate transformation, and process the transformed data into position, velocity, and acceleration estimates. These data were then sent to the navigation and guidance computer for display information computation. The MLS processed signals used for display computations are shown in figure 11. Position (LAT, LONG), velocity (V_N, V_E, $\dot{h}$), acceleration ($\dot{V}$), and path error (η,β) signals are utilized to compute displayed information for both the EADI and EHSI. Airplane attitudes, from onboard sensors, were also used in the perspective runway computation. Detailed information concerning the MLS receiver and guidance signal processors are presented in reference 3.

EXPERIMENTAL TASK

The experimental task required the pilot to track a straight-in MLS path to the runway threshold. The MLS path was a 3^{o} ($\pm 1^{o}$) glideslope that terminated on the runway 304.8 meters (1,000 feet) past the runway threshold. The localizer course was $\pm 2.5^{o}$ wide and emanated from a point 2,605.8 meters (8,547 feet) past the runway threshold.

A localizer offset approach task was used to evaluate the benefits of the integrated display information for correcting relatively large lateral path errors. A planview of the 3-nautical mile, straight-in approach, with an initial segment consisting of a 130° turn on a 3° descent, is illustrated in figure 12. Guidance in the form of a dashed curved path was presented on the EHSI so that an initial localizer offset of approximately 0.1 nautical mile was obtained. The airplane was in the landing configuration (flaps 40°, gear down) prior to the turn and the autothrottle system was used to maintain the approach speed.

TEST SUBJECTS

Four NASA test pilots were used during the evaluation. Only three pilots, however, flew the localizer offset approach task. Two of the pilots were type-rated for the B-737, and the other two pilots had some flight experience in the B-737. All of the pilots had previous experience in the AFD simulator.

TEST PROCEDURE

The test procedure required the pilot to execute the 130° curved approach (without localizer offset) shown in figure 12 using both the EADI and EHSI display information. Once the turn had been completed (Waypoint FAF3M), the pilot was instructed to use primarily the display information in the EADI to track localizer centerline while maintaining the 3° glideslope.

Since the principle objective of the flight tests was to evaluate the use of presenting horizontal information in the EADI or vertical situation display, the second series of approaches concentrated on the localizer offset task. During these runs, the pilot was required to fly the localizer offset path (shown dashed in figure 12) to a point 0.1 nautical mile left of Waypoint FAF3M. At this point he was instructed to use primarily the displayed information on the EADI to capture and hold the localizer centerline, while tracking the glideslope.

The approaches, with and without the localizer offset, were flown using both the baseline and integrated display formats. The display format runs were randomized so that environmental conditions and pilot learning curve factors would be reduced. Although the pilot was told to use the EADI as the primary display, he was allowed to scan the EHSI and the basic flight instruments for information that might be missing in the EADI.

RESULTS AND DISCUSSION

Three-Nautical Mile Approach Tests

Localizer tracking performance was analyzed for both display formats to determine the benefits or disadvantages of integrating horizontal information into the vertical situation display. Figures 13 and 14 are plots of localizer deviation versus range from runway threshold for the approaches without localizer offset. Figure 13 presents the localizer tracking results of four approaches using the baseline situation display format as the primary display. As can be seen, the tracking is oscillatory in nature and the lateral deviations at times are larger than the runway width. Pilot comments indicated that pilot mental workload was high using the baseline format since the pilot had to scan the map display (EHSI) to obtain track information from the airplane symbol, trend vector symbolgy and the digital readout of track angle. The pilots felt that the lateral path guidance provided by the map display was not sufficient for a close-in final approach even with the map scale set for greatest resolution, 0.394 nautical mile per centimeter (1 nautical mile per inch).

The localizer tracking performance using the integrated situation display format is presented in figure 14. This lateral tracking data show that the pilots could consistently complete the approach to landing with only small deviations from the runway centerline. Pilot comments indicated that the integrated display format on the EADI eliminated the need to scan the EHSI during the approach. The runway and relative track information enabled the pilot to better understand his position and trajectory relative to the extended runway centerline.

Figure 15 presents cross plots of glideslope and localizer deviations at 61- and 30.5-meter altitude windows. The data for the integrated display format show better localizer tracking and more consistent glideslope tracking. The integrated format reduces the amount of time the pilot needs to build the mental picture of his lateral position and predicted trajectory and enables him to spend more time on the glideslope task. It should be remembered that the displayed information of glideslope deviation is the same for both display formats, however, the runway symbology provides a reference point on the EADI for the flight-path angle symbols.

Figures 16 and 17 present the lateral tracking results of several approaches flown with the initial localizer offset (see Fig. 12) at 3 nautical miles from runway threshold. The lateral tracking results using the baseline display format are shown in figure 16 and illustrate the deficiency of this format to provide adequate close-in localizer path capture information. The tracking is oscillatory in nature with the final corrections back toward the extended centerline occurring very close to the threshold. Only one approach actually crosses the centerline, and none of the approaches ever achieves the proper track angle to the runway. The lack of good lead information and the fear of a large localizer overshoot brought about the centerline undershoots seen in this figure.

The lateral tracking results using the integrated situation display format are shown in figure 17. The data show that the pilots are able to make a precision capture of the localizer and maintain runway centerline tracking using only the integrated format presented on the EADI. After the flight-path corrections are made to capture the localizer, it can be seen that the track angle to the runway threshold is proper and stabilized for all the approaches.

Figure 18 presents cross plots of glideslope and localizer deviations at 61- and 30.5-meter altitude windows for the offset approaches. The data show that both glideslope and localizer errors are smaller for the integrated display format at both windows. Pilot comments indicated that the integrated format reduced the lateral task mental workload and allowed more time to be spent on the glideslope tracking task.

Figure 19 is a comparison of the 30.5-meter window data from the offset approaches with previous simulation data and with Category II Flight-Director criteria as stated in FAA Advisory Circular, AC 120-29. Figure 19(a) illustrates that the flight results for the integrated situation display format lie within the mean and standard deviation of the simulation results for the same format. The flight and simulation data for the baseline display format also show similar trends. The lateral bias in the simulation data is due to a steady left crosswind that was part of the experiment.

Figure 19(b) illustrates that the glideslope and localizer path performance with the integrated situation display format compares very favorably with Category II Flight-Director criteria. Three of the approaches made with the baseline display pass through the window criteria, but the pilots considered these approaches unsatisfactory because the airplane's attitudes and track were not stabilized.

Close-In Approach Tests

Following the approach tests with the 3-nautical mile final approach segments, both 1.5- and 1.0-nautical mile final approach path tasks were evaluated. The geometry of the close-in approach paths, including the 3^{o} descent and 130^{o} turn onto the final segment, was identical to the previous approaches. The only difference was the length of the final approach segment. The velocity vector control mode was used in this evaluation.

The EADI display format used during these tests was the integrated situation format that was used in the previous experiment. The format on the EHSI differed only in the curved trend vector displaying predicted airplane position 30, 60, and 90 seconds ahead. The pilots used the EHSI as the primary display for initiating and during most of the turn onto the final straight segment. The pilot could readily determine the initiation point for the turn and then attempted to position the curved trend vector upon the referenced path also presented on the display. The EADI was monitored during this period to assure that the vertical path (3^{o} descent) was being maintained. The pilot's attention switched to the EADI near the end of the turn as the computer generated runway symbology came into the display's field of view. From this point down to about 15 meters (50 feet) altitude, the pilot used the integrated situation format presented on the EADI as the primary display.

Figure 20 presents the flight-path tracking results of the approaches on the 1.5-nautical mile test path. Although these were the first such approaches made by two pilots, it can be seen that the vertical and lateral tracking are smooth and consistent. An expanded plot of the final portion of the approaches is presented in figure 21. Note that one of the approaches overshoots the referenced path by approximately 100 meters (300 feet). The pilot commented that he had not tracked tightly the lateral path, but that he knew his situation clearly during and at the end of the turn. It can be seen that all the approaches have attained a stable track to the runway by approximately 1.5 kilometers (5,000 feet) from the runway threshold.

Figure 22 presents the vertical and lateral path tracking results for the approaches on the 1.0-nautical mile test path. Again, these are the first such approaches flown by the pilots. The lateral tracking data show overshoots of approximately 30.5 meters (100 feet) but the pilots have stabilized the airplane's track to the runway at approximately 0.92 kilometers (3,000 feet) from the runway threshold.

CONCLUDING REMARKS

Three-Nautical Mile Approach Tests

The results of these flight tests show that the addition of perspective runway symbology and relative track information to a baseline EADI format increased flight-path tracking accuracy during the approach to landing task under instrument conditions.

Pilot comments indicated that the integrated situation display format brought about a better understanding of the airplane's position and trajectory relative to the runway and runway extended centerline. The integrated display also enabled the pilots to quickly recognize and recover from a close-in, large lateral path deviation with confidence. Limited flight-path performance results using the integrated display compare very favorably with previous fixed-based simulation results. Flight-Director criteria for glideslope and localizer performance for Category II approach conditions were also met with the limited data acquired. The integrated situation format allows the pilot to assess the information and make the corrective flight control inputs, depending on the size of the error and the remaining distance to the runway threshold.

Close-In Approach Tests

The results of the flight evaluation of the 1.5- and 1.0-nautical mile approach tests show good flight-path performance during the turn and on the short-final approach segments. The display information content and format, however, is not considered to be optimized. Further display and control efforts are needed to define the display information requirements for the close-in curved approach-to-landing task.

REFERENCES

1. Reeder, John P.; Taylor, Robert T.; Walsh, Thomas M.: New Design and Operating Techniques and Requirements for Improved Aircraft Terminal Area Operations. NASA TM X-72006, 1974.

2. Steinmetz, G. G.; Morello, S. A.; Knox, C. E.; and Person, L. H., Jr.: Piloted Simulation Evaluation of Two Electronic Display Formats for Approach and Landing. NASA TN D-8183, April 1976.

3. Walsh, T. M.; Morello, S. A.; and Reeder, J. P.: Review of Operational Aspects of Initial Experiments Utilizing the U.S. MLS. Presented at the NASA Aircraft Safety and Operating Problems Conference, Langley Research Center, Hampton, VA, October 18-20, 1976.

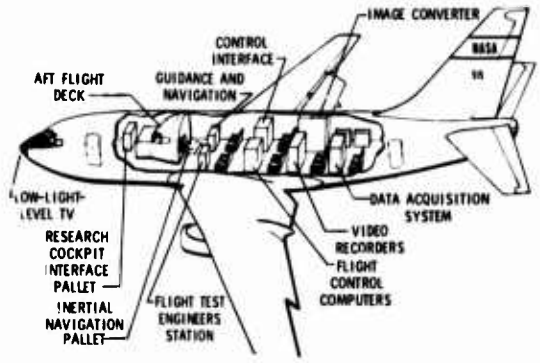

Figure 1.- TCV B-737 internal arrangement.

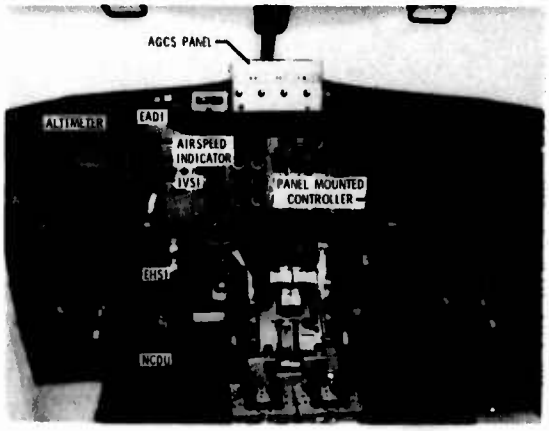

Figure 2.- AFD cockpit control and display layout.

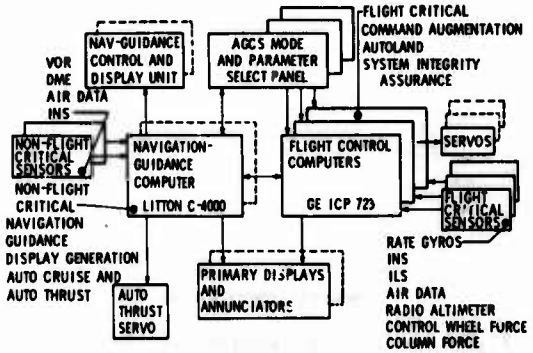

Figure 3.- Advanced guidance and control system (AGCS) concept.

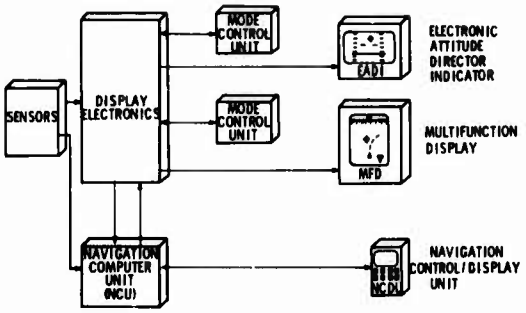

Figure 4.- Navigation, guidance, and display system block diagram.

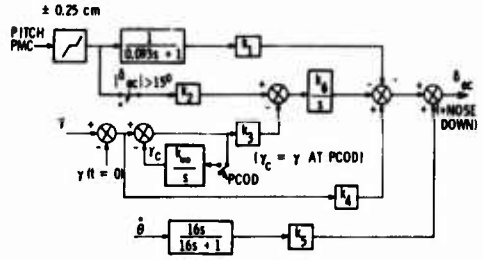

Figure 5.- Velocity vector control mode for pitch axis.

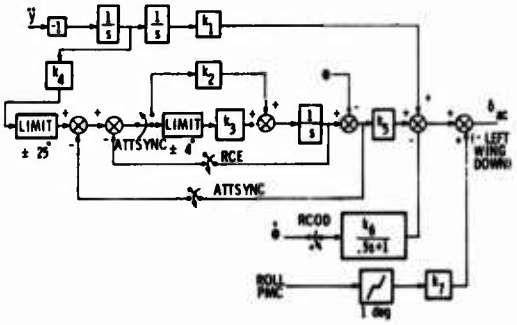

Figure 6.- Velocity vector control mode for roll axis.

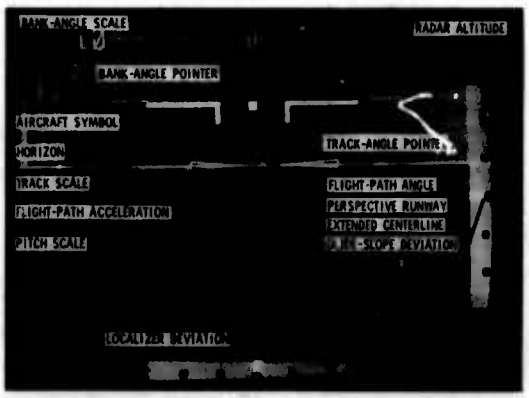

Figure 7.- EADI display information.

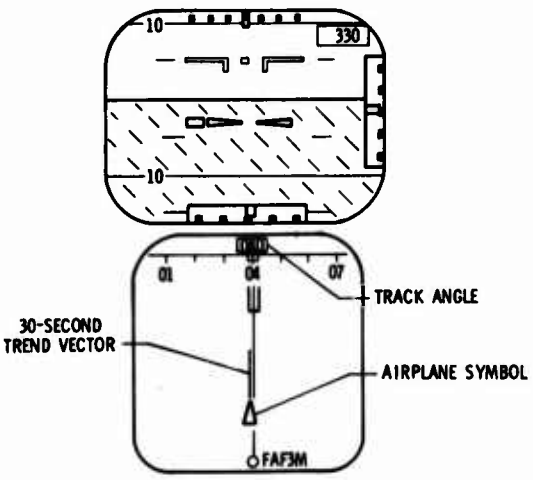

Figure 8.- Baseline situation display format.

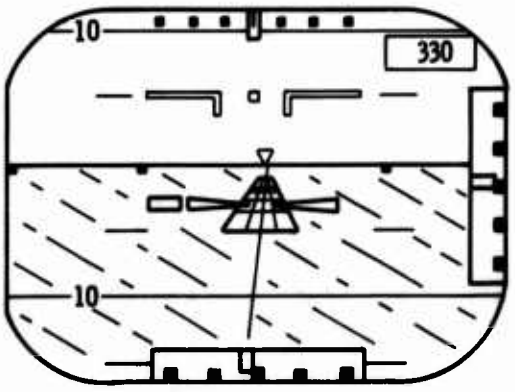

Figure 9.- Integrated display format.

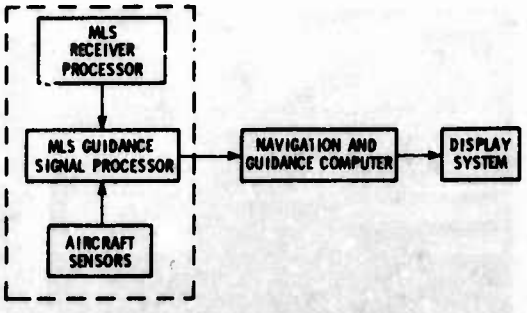

Figure 10.- MLS signal integration with navigation, guidance and display systems.

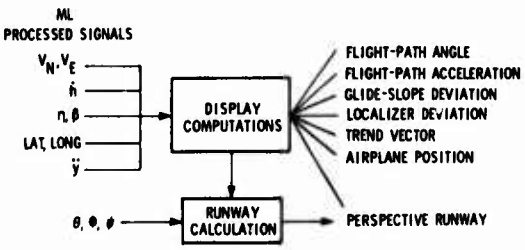

Figure 11.- MLS processed signals used for display information.

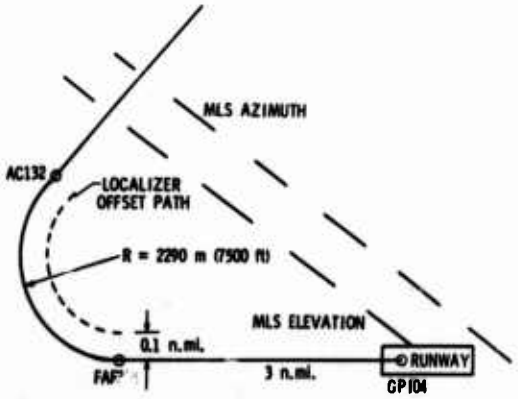

Figure 12.- Plan view of approach path to runway 04 at the NAFEC.

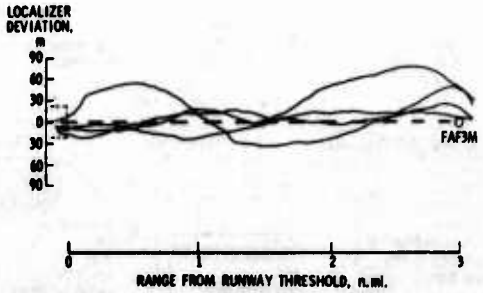

Figure 13.- Localizer tracking performance using the baseline situation display format.

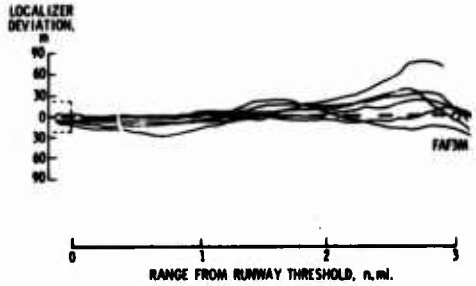

Figure 14.- Localizer tracking performance using the integrated situation display format.

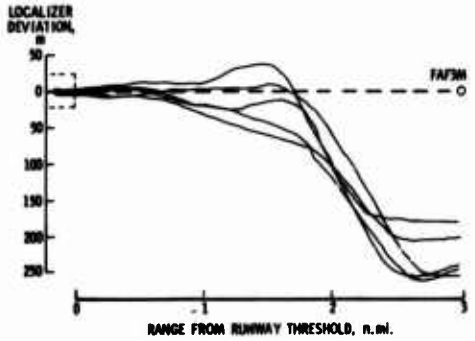

Figure 17.- Localizer tracking using the integrated situation display format.

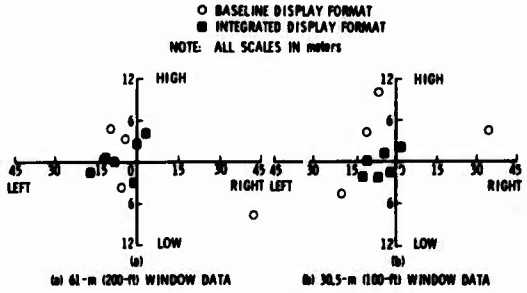

Figure 15.- Window data of glideslope and localizer deviations.

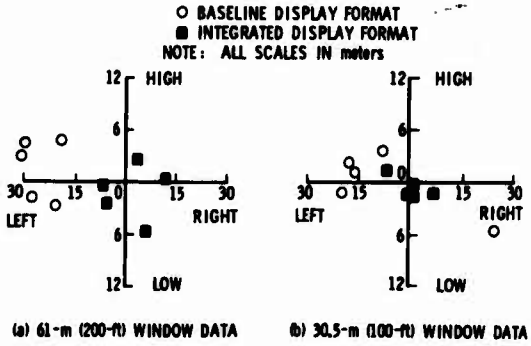

Figure 18.- Window data of glideslope and localizer deviations.

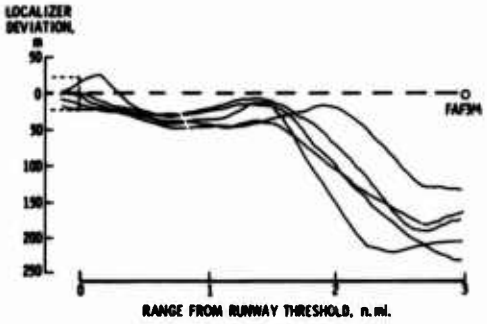

Figure 16.- Localizer tracking using the baseline display format.

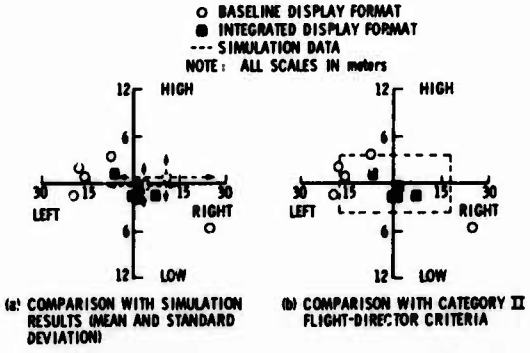

Figure 19.- Flight-path performance comparisons at the 30.5-m (100 ft) window.

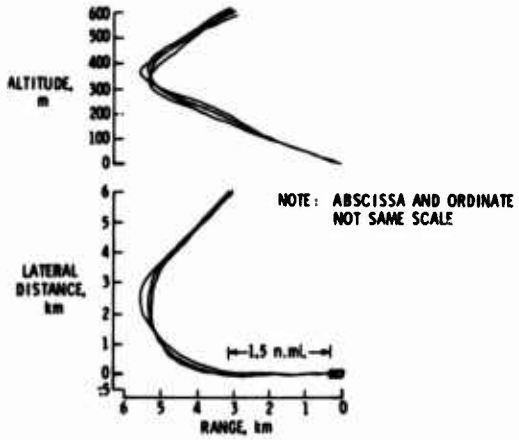

Figure 20.- Manual tracking on 2.78 km (1.5 n.mi.) approach path.

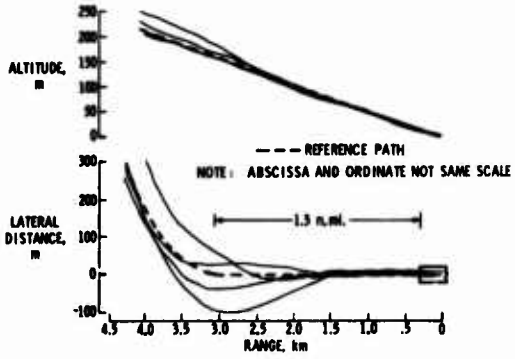

Figure 21.- Manual tracking results on 2.78 km (1.5 n.mi.) approach path.

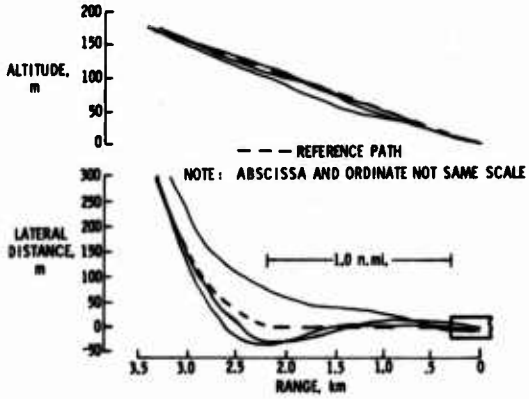

Figure 22.- Manual tracking on 1.85 km (1.0 n.mi.) approach path.

AIRLINE PILOT SCANNING BEHAVIOR DURING APPROACHES AND LANDING IN A BOEING 737 SIMULATOR

Amos A. Spady, Jr.
National Aeronautics and Space Administration
Langley Research Center
Hampton, Virginia 23665

SUMMARY

A series of approaches using airline-rated Boeing 737 pilots in an FAA qualified simulator has been conducted. The test matrices include both manual and coupled approaches for VFR, Category I and Category II conditions. A nonintrusive oculometer system was used to track the pilot's eye-point-of-regard throughout the approach. The results indicate that, in general, the pilots use a different scan technique for the manual and coupled (auto-pilot with manual throttle) conditions. For the manual approach 73 percent of the time was spent on the Flight Director and 13 percent on airspeed as opposed to 50 percent on Flight Director and 23 percent on airspeed for the coupled approaches. For the visual portion of approach from less than 100m (300 ft) to touchdown or when the touchdown point came into view, the pilots tend to fixate on their aim or touchdown area until the flare initiation, at which time they let their eye-point-of-regard move up the runway to use the centerline lights for rollout guidance.

INTRODUCTION

The scanning patterns used by pilots during various phases of flight have been of extreme interest for a number of years. A number of techniques have been developed to measure subject lookpoint; however, each has either intruded on the pilot or has been difficult to correlate with the state of the aircraft. For this study a non-instrusive real-time oculometer system, which allows the subject $0.3m^3$ (a cubic foot) of head motion was used.

A number of studies of pilot scanning behavior during approach and landing have been conducted by Langley. This paper will highlight parts of two studies which used Piedmont Airlines' Boeing 737 FAA certified training simulator and Boeing 737 rated airline pilots as test subjects. The first study dealt with pilot instrument scanning behavior during Category II approaches, the second with what a pilot looks at out-of-the-window in VFR, Category I and Category II ILS approaches.

The information obtained from these studies provide an insight into how a pilot scans the information available in the cockpit and out-the-window during ILS type approaches. This information should be useful in the development and evaluation of future aircraft displays.

EQUIPMENT

The Boeing 737 simulator used is an FAA certified initial and recurrent training facility operated by Piedmont Airlines. The only changes in the cockpit were the incorporation of the oculometer optical head which was mounted below the Automatic Direction Finder (ADF) behind the instrument panel (fig. 1) for the instrument scanning study and to the left of the airspeed indicator for the visual studies. A TV camera was mounted behind the pilot to view the instrument panel and the TV monitor for this camera was located behind the pilot's seat to allow the test conductor to observe the pilot lookpoints superimposed in the scene. For the visual studies a TV camera mounted outside the cockpit viewed a CRT displaying the nighttime scene. Again, pilot lookpoints were superimposed on the scene to provide the test conductor a real-time monitoring capability.

A highly modified Honeywell Mark 3 oculometer was used for the study. The modifications to the system consists primarily in a redesign of the electro-optical head resulting in a unit one-fourth the original size, simplification of the operating system, and modifications to software to adapt the system to provide out-the-window tracking capability. The oculometer has two primary subsystems: the electro-optical system generates a beam of infrared light which is directed through a beam splitting mirror toward the subject's eye. Reflections from the eye are directed by the beam-splitter to an infrared-sensitive TV camera. The high reflectivity of the human retina for infrared leads to a backlighting of the pupil, so that the camera sees the pupil of the eye as a bright, circular area (fig. 3). It also sees a small bright spot due to reflection at the corneal surface. The relative positions of the center of the pupil and the corneal reflection depend on the angle of rotation of the eyeball with respect to the infrared beam. The signal processing unit uses

the signal from the TV camera to compute this angle of rotation and the coordinates of the lookpoint on the instrument panel. The output of the signal processor is a set of calibrated digital or analog signals representing the subject's lookpoint coordinates and pupil diameter.

Several constants were set in the aircraft program as follows: (1) the simulated aircraft weight was 42,640 kg (94,000 lbs) for all approaches; (2) the aircraft c.g. was set at 25 percent; (3) winds were either at 0 or 5 kt at 90 degrees with respect to the runway heading; (4) turbulence, when used, was the maximum available on the simulator (pilots rated this turbulence as moderate); (5) at no time were emergency conditions imposed on the pilots except that during each session of the visual study for one approach (chosen at random) the RVR and ceiling were lowered below minimum to require the approach to be aborted and a go-around executed.

All tests were conducted at the Piedmont Airlines Training Facility in Winston-Salem, North Carolina. A Vital II out-the-window system was used to provide the pilots a nighttime scene of the Winston-Salem area and airport.

PROCEDURES AND SUBJECTS

All tests were started at 19 Km (12 miles) from runway threshold and approximately 415m (1360 ft) above ground level (runway 33 at Smith-Reynolds Airport). The first 6 Km (4 miles) were used by the pilot to stabilize the aircraft on the correct flight path and to check the oculometer calibration. At 13 Km (8 miles) data recording was started and continued through capture and descent down the 3 degree glide slope, touchdown and rollout or until the approach was aborted as a result of the pilot choosing to go around.

All airline pilots used in the program were qualified Boeing 737 pilots who fly for a scheduled airline. Prior to starting the test program each pilot was given a briefing on the operation of the oculometer, which was the only thing different in the cockpit. Also, the pilots were asked to assume that they were flying an aircraft full of passengers, and if they would normally elect to go around, they should do so. At the end of the last test period the pilots were asked to fill out a questionnaire concerning various aspects of instrument scanning and visual scene usage.

All tests were conducted using the same copilot. The copilot functioned in the same manner as he would in a normal approach and provided all required callouts.

RESULTS AND DISCUSSION

The scanning patterns of pilots are expected to differ between pilots and even from approach to approach for the same pilot; however, there should be a consistency in terms of the primary information scanned for a particular type approach (manual or coupled (auto-pilot with manually controlled throttles)) and what is looked at in the visual (out-the-window) scene as a function of visibility.

In order to show this consistency for the instrument scan portion of the study this paper will deal with only the summary data obtained for three runs each for seven pilots. A more complete discussion of these data can be found in references 1 and 2. The discussion on the visual portion of the approach will be based on the observations noted during the tests and review of the TV tapes. This part of the study has just been completed, consequently the data reduction showing statistical information on scan behavior is not yet available.

Instrument Scan

Observation of the pilot scan patterns during the instrument portion of the test indicated that the pilots used the center of the flight director as the primary lookpoint and moved from there to an instrument and then came back to the center of the flight director. Only rarely did a pilot check more than one instrument before returning to the center of the flight director. This is demonstrated in figure 4 which is a time history of one pilot's scan from approximately 213m (700 ft) altitude down to 30m (100 ft) altitude. Figure 4(a) shows the manual case (with no turbulence), and figure 4(b) shows the coupled case (with no turbulence). The ordinate indicates the instruments at which the pilot was looking, with the flight director being broken into its information blocks as indicated in figure 5. The abscissa indicates flight time in seconds. The sections T and n/T indicate eye tracking (upper level) and not tracking (lower level). The majority of the out-of-track time was caused by the pilot looking at the center console engine instruments. As can be seen from the time histories, the pilot changes fixations more rapidly and looks at more instruments in the coupled mode as compared with the manual mode.

The bar graphs presented in figure 6 show a comparison of the percent time spent on the instruments for both the manual and coupled modes with no atmospheric turbulence. Each contains the summary data for the entire approach. It was found that the percent times for various instruments do not vary but a few percent for the different phases of the flight (straight and level, glide slope capture or descent along the glide slope). The crosshatched sections define the mean percent time on the instrument while the open section, at the top, defines the standard deviation. The clock, radar altimeter, and A.D.F. are not included in this figure as they are used very little

by the pilots during the type of approaches being flown. Of particular interest is the comparison of percent time spent in the flight director (approximately 73 percent for the manual mode as compared to 50 percent for the coupled mode) and the airspeed indicator (13 percent in manual and 22 percent in coupled).

The increase in time on airspeed for the coupled conditions can in part be due to the fact that the 737 aircraft as flown by Piedmont do not have auto-throttle; consequently, the pilot is required to manually control airspeed. The percent time on the other instruments increased slightly for the coupled mode as compared to the manual mode.

Pilot comments from the questionnaire indicate that while they were not necessarily aware of the differences in scan as a function of control mode they attribute the change to the different type of mental picture required. For the manual mode they must keep a mental image of where they are and where they are going, which is best obtained from the flight director. Any looks away from it require that they rebuild the mental picture upon returning to the flight director. For the coupled mode they are primarily checking needle positions and consequently are free to scan more as indicated by both the time histories in figure 3 and the percent time on instruments in figure 6.

The introduction of turbulence did not greatly affect the pilots' scanning behavior in terms of the percent time he spent on various instruments. For both the manual and coupled cases the time on flight director increased by about 3 percent with this being taken away primarily from airspeed.

Visual Scene Study

This study considered a number of factors such as pilot instrument scan, both manual and coupled standard approaches (SA) and Pilot Monitored Approaches (PMA) for both VFR, Category I (720m Runway Visual Range (RVR), 60m Decision Height (DH) (2400 ft RVR and 200 ft DH)), and Category II (360m RVR, 30m DH (1200 ft RVR and 100 ft DH)), takeoff as well as where and at what a pilot looks during takeoff and the visual part of the approach, flare and rollout. The Standard Approach is the type currently flown by the airlines where the pilot flies hands on the controls. For the pilot monitored approach, the copilot flies the aircraft with the pilot monitoring down to approximate DH. If the pilot elects to land, he states, "landing, I have the aircraft." If he does not so state, the copilot automatically starts a go-around. Only the real-time video tapes and very limited data on two of the eight pilots are available at this time. Therefore, only general trends of these two pilots and observations from the video tape will be discussed. It should be noted that for both the PMA and SA the pilot actually lands the aircraft so all runs from Decision Height (DH) to roll-out are manually flown by the pilot.

In general, pilot 1 tended to spend an average of 40 percent looking outside in VFR straight and level flight, 20 percent during glide slope capture, 40 percent from on glide slope down to about 91m (300 ft). From approximately 91m (300 ft) pilot 1 spent from 75 to 95 percent of his time out the window (4 runs) coming inside primarily to check airspeed and the flight director. Pilot 2, on the other hand, spend better than 90 percent of his scan time out the window from 300 feet to touchdown.

Pilot 1 tended to check the outside scene for the Category I condition starting at 30m (100 ft) above minimum (60m (200 ft)). He averaged three transitions in and out before DH and two transitions from DH to touchdown with the last look at the instruments at 15m (50 ft) above the field. Pilot 2, on the other hand, for the Category I runs, stayed inside on the instrument panel until the copilot called runway-in-sight at which time he looked out the window and for three out of four runs stayed out until touchdown. In one run he transitioned inside to the airspeed, moved to the flight director then transitioned back outside. For both the VFR and Category I conditions, when looking outside, pilots tend to fixate on their aim or impact point on the runway. This point is nominally between 300 and 360m (1000 and 1200 ft) from runway threshold depending on how tight the pilot has held the glide slope. The pilots generally hold this fixation point until flare initiation at which time they let their lookpoint drift up the runway for rollout guidance.

For the Category II (360m RVR, 30m DH (1200 ft and 100 ft)) pilot 1 again started taking quick looks out the window at 30m (100 ft) above DH or minimums. After DH he transitioned back into the instrument three times to check the flight director and airspeed. Pilot 2, however, did not look out until the copilot called runway in sight and did not transition back inside except once in five approaches. In that case the approach speed was a little high and he came inside to check airspeed. In the Category II condition the pilots are not able to see their impact point when they initially look out the window due to the limited visibility. Consequently, they tend to look just below the apparent horizon or visibility line and move along the runway in small jumps until the impact point comes into view. They then held their lookpoint at the impact point until flare initiation at which time they let their lookpoint move farther up the runway for rollout guidance.

In general, the pilots tend to do very little scanning around the runway during the final part of the approach. They appear to fixate on their impact point and obtain from that point the information needed to judge when to initiate the flare maneuver.

CONCLUSIONS

The results obtained from the two studies covered will provide a data base on how pilots scan the existing flight instruments and where they are looking during the final part of the approach, flare and rollout. The preliminary results indicate that:

1. Pilots use different instrument scanning strategies for manual versus coupled approaches. The strategies differ in percent time spent on Flight Director (73 percent for manual to 50 percent for coupled) and airspeed (13 percent for manual versus 22 percent for coupled) and in scanning rate which is significantly higher in the coupled mode.

2. Introduction of turbulence does not grossly change the pilot scanning behavior.

3. From 91m (300 ft) or breakout to flare initiation in both VFR and Category I conditions the pilots fixate at their aim or impact point on the runway.

4. In Category II conditions the pilots look just below the apparent horizon or visibility line, with their lookpoint moving in small jumps up the runway until their impact point comes into view. They then fixate on the impact point until flare initiation at which time they let their lookpoint move up the runway for rollout guidance.

REFERENCES

1. SPADY, Amos A., Jr.: Preliminary Report on Airline Pilot Scan Patterns During Simulated ILS Approaches; NASA Aircraft Safety and Operating Problems Conference; SP-416, 1974.

2. DICK, A. O.; and BAILEY, George: A Comparison Between Oculometer Data and Pilot Opinion on the Usefulness of Instruments During Landing. Center for Visual Science Technical Report No. 3-76, 1976.

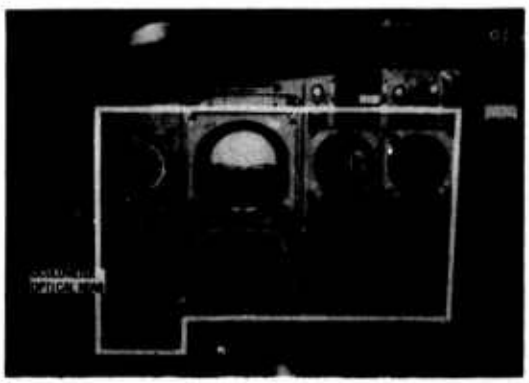

Figure 1. - Captain's flight instrument panel.

Figure 2. - Picture of TV monitor as viewed by the Test Director.

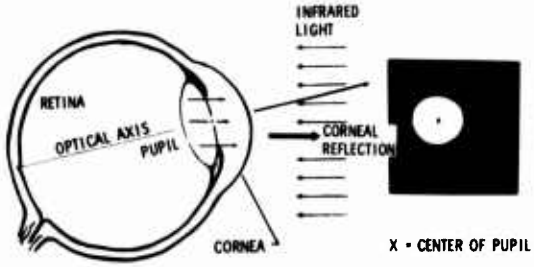

Figure 3. - Oculometer basic sensing principle.

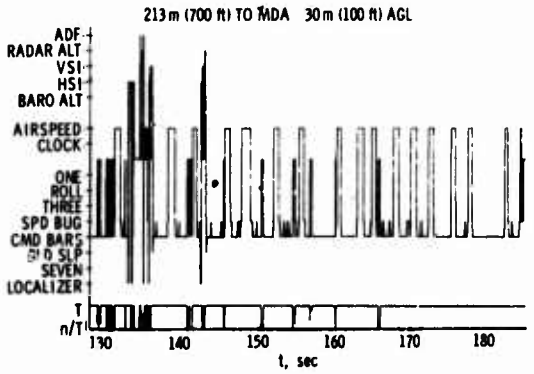

(a) Manual

Figure 4. - Time histories of one pilot's scan during an approach.

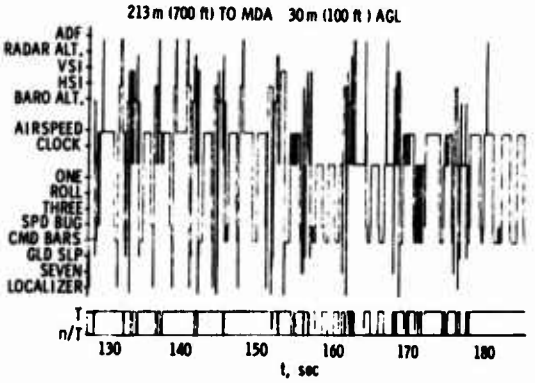

(b) Coupled

Figure 4. - Concluded.

Figure 5. - Flight Director breakdown.

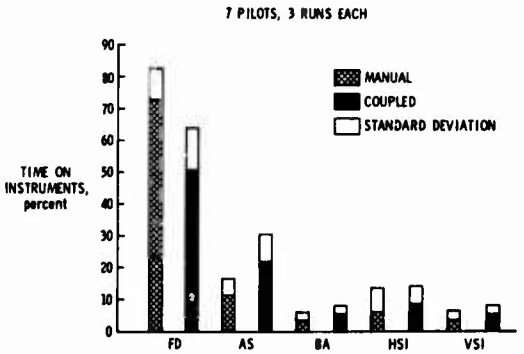

Figure 6. - Percent time on instruments for manual and coupled approaches.

Evaluation of Digital Flight Control Design for VTOL Approach and Landing

Paul W. Berry and John R. Broussard
Members of the Technical Staff
The Analytic Sciences Corporation
6 Jacob Way
Reading, Mass. 01867, U.S.A.

Robert F. Stengel
Associate Professor
Princeton University
Department of Aerospace and Mechanical Sciences
Princeton, N.J. 08540, U.S.A.

Summary

Methods and results in the design and evaluation of a digital flight control system (DFCS) for a CH-47B helicopter are presented. The DFCS employs proportional-integral control logic to provide rapid, precise response to automatic or manual guidance commands while following conventional or spiral-descent approach paths. It contains attitude-and velocity-command modes, and it adapts to varying flight conditions through gain scheduling. Extensive use is made of linear systems analysis techniques -- the DFCS is designed using linear-optimal estimation and control theory and the effects of gain scheduling are assessed by examination of closed-loop eigenvalues and time responses. The pre-flight-test evaluation described here provides a direct comparison of alternate navigation, guidance, and control philosophies; confirms the practical merits of the DFCS design approach; and demonstrates techniques which will aid the development of future guidance and control systems.

INTRODUCTION

Vertical takeoff and landing (VTOL) aircraft are able to operate from small landing areas and in the vicinity of obstacles which would prevent the operation of conventional aircraft. The VTOL Approach and Landing Technology (VALT) Program of the National Aeronautics and Space Administration is developing and demonstrating concepts for guidance and control which will enable such operations in the congested terminal airspace; the work reported here is a contribution to these goals. This paper describes digital flight control design and evaluation procedures that are being applied to the VALT Research Aircraft, a CH-47B helicopter that is equipped to test a variety of manual and automatic flight management alternatives.

Figure 1 illustrates the program's experimental facilities. The VALT Research Aircraft contains state-of-the-art digital computing equipment, actuators, and sensors. The digital flight control system (DFCS) includes velocity-command and attitude-command guidance logic, state estimators, control laws containing proportional-integral compensation for stability augmentation and precise command response as well as guidance, estimator and controller gain scheduling (Refs. 1 and 2). Ground facilities support advanced format displays and simulate existing or future navigational aids, e.g., a microwave landing system (MLS), using tracking radar data.

Development of the VALT DFCS is following a four-step sequence consisting of theoretical formulation, control law design, computational evaluation, and flight test evaluation. The first two steps, reported in Refs. 1 and 2 and summarized below, provide the methodology for designing discrete-time (digital) controllers to continuous-time (analog) specifications, resulting in quantitative designs for three VALT DFCS command modes -- a velocity-command and two attitude-command control laws (of differing structure). Evaluation of the DFCS begins with the computation of eigenvalues and time responses for linear-time-invariant models of helicopter dynamics, defined throughout a wide range of flight conditions. This evaluation proceeds with the computation of time responses of helicopter models that contain linear-time-varying inertial and aerodynamic coefficients and selected nonlinearities in control linkages and feedback measurement geometries. An independent hybrid computer evaluation of the VALT DFCS also is conducted by NASA engineers during the third step. The DFCS is coded and stored in the VALT Research Aircraft's on-board computer for hybrid simulation and flight test evaluation.

This paper treats guidance laws and approach paths, summarizes VALT DFCS design, and provides examples of computer evaluation results. The combination of optimal control

theory and modern systems analysis is shown to provide a unified, easily understood basis for practical control system design, defining potential problem areas at an early stage of the process where they are most readily assessed.

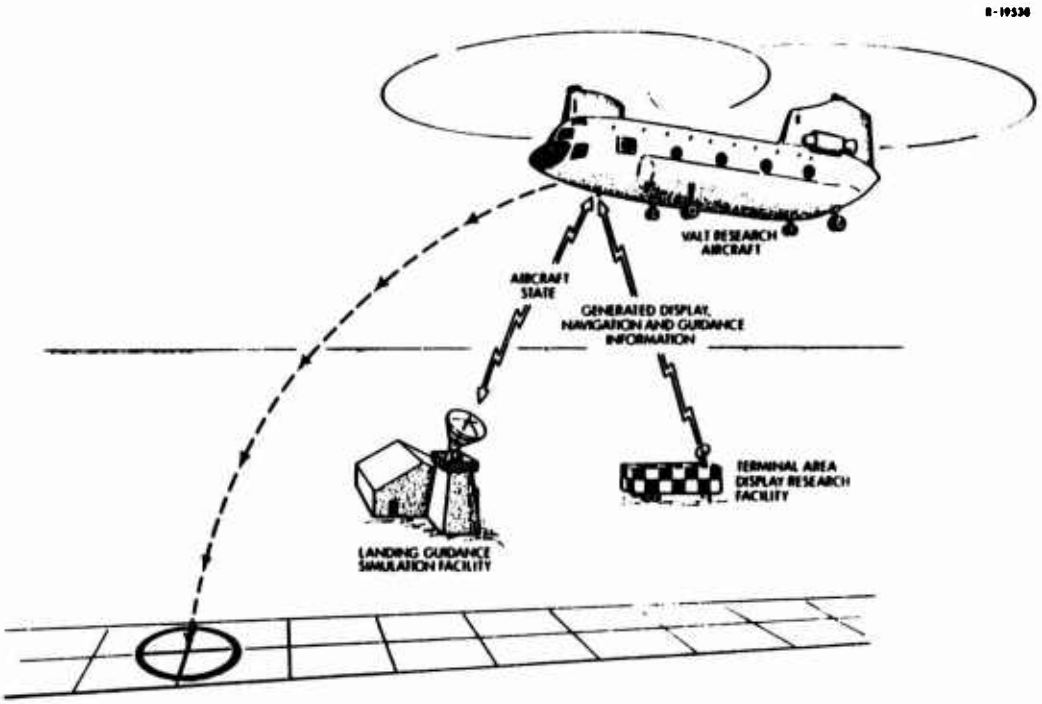

Figure 1 VALT Flight Test Program

GUIDANCE LAWS AND APPROACH PATHS

The guidance laws in the VALT DFCS issue commands to the control laws that cause the helipcopter to follow a nominal flight path. These commands are composed of a nominal and a perturbation portion; the former is a function solely of the helicopter's position along the path. The perturbation commands correct errors normal to the path, and may include velocity and acceleration-based terms. A fourth guidance command serves to control the helicopter body yaw angle.

The velocity command vector (Eq. 1) contains earth-relative velocity commands as well as body yaw angle.

$$y_d = \begin{bmatrix} V_{x_c} \\ V_{y_c} \\ V_{z_c} \\ \psi_c \end{bmatrix} = \begin{bmatrix} V_{x_o} \\ V_{y_o} \\ V_{z_o} \\ \psi_o \end{bmatrix} + \begin{bmatrix} \Delta V_x \\ \Delta V_y \\ \Delta V_z \\ 0 \end{bmatrix} \qquad (1)$$

The body yaw angle is commanded to follow the air relative heading,

$$\psi_c = \tan^{-1}\left((V_{y_o} - W_y)/(V_{x_o} - W_x)\right) \qquad (2)$$

where W_x and W_y are components of the estimated earth-relative wind vector. Figure 2 illustrates the geometry in the horizontal plane. The perturbation velocity commands are calculated by a feed-back law (eq. 3) operating in guidance axes, which are yawed by the heading angle ξ. H_E^G performs this transformation.

$$\Delta\underline{V}_E = \begin{bmatrix}\Delta V_x \\ \Delta V_y \\ \Delta V_z\end{bmatrix} = H_G^E(\xi_0) \left\{K_1 H_E^G(\xi_0)(\underline{x}_E - \underline{x}_{E_0}) + K_2 H_E^G(\xi_0)(\underline{V}_E - \underline{V}_{E_0}) + K_3 H_E^G(\xi_0)(\dot{\underline{V}}_E - \dot{\underline{V}}_{E_0})\right\} \quad (3)$$

The gain matrices are sparse and very nearly diagonal, with the specific values taken from Refs. 3 or 4.

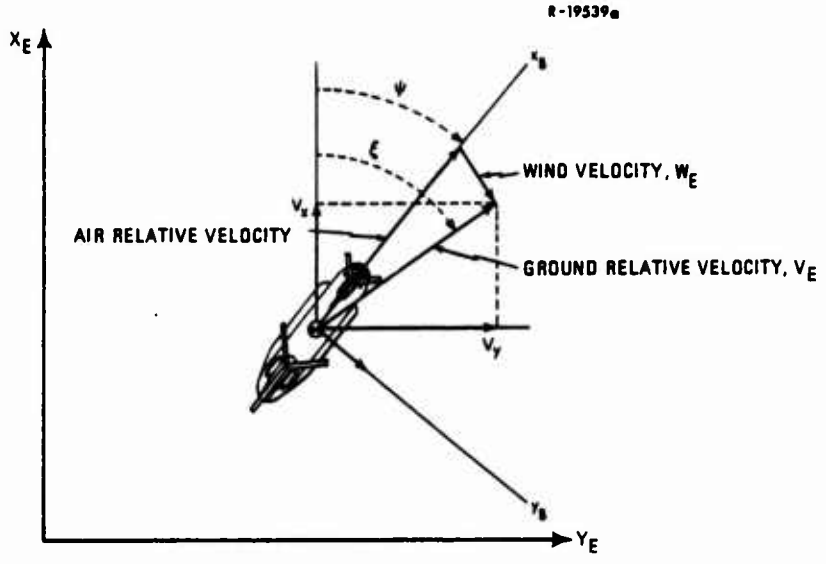

Figure 2 Horizontal Plane Guidance Command Geometry

An approach path used for many of the tests presented in this paper is shown in Fig. 3. Except for the final section, it is flown at constant speed and altitude, and includes a holding pattern. The final section is composed of a decelerating descent. The deceleration profile, taken from Refs. 5 and 6, has been found to be quite acceptable to test pilots.

An alternative command vector, the attitude command vector, is also tested. It is composed (Eq. 4) of roll and pitch angle commands for horizontal velocity control, as well as vertical velocity and body yaw angle commands.

$$\underline{y}_d = \begin{bmatrix}\phi_c \\ \theta_c \\ \psi_c \\ V_{z_c}\end{bmatrix} = \begin{bmatrix}\phi_o \\ \theta_o \\ \psi_o \\ V_{z_o}\end{bmatrix} + \begin{bmatrix}\Delta\phi_c \\ \Delta\theta_c \\ 0 \\ \Delta V_{z_c}\end{bmatrix} \quad (4)$$

Yaw angle commands are calculated according to Eq. 2, while the perturbation commands are calculated from velocty perturbations in a local-level reference frame yawed to the body yaw angle, ψ_c, i.e.

$$\begin{bmatrix}\Delta\theta \\ \Delta\phi \\ \Delta V_z\end{bmatrix} = K_A \left\{K_1 H_E^{LL}(\psi_c)(\underline{x}_E - \underline{x}_0) + K_2 H_E^{LL}(\psi_c)(\underline{V}_E - \underline{V}_{E_0}) + K_3 H_E^{LL}(\psi_c)(\underline{V}_E - \underline{V}_{E_0})\right\} \quad (5)$$

The gain matrices are the same as in Eq. 4 except that K_A transforms downrange and crossrange velocity perturbations to pitch and roll perturbation commands. The nomunal roll (Eq. 6) is calculated to cause the net specific force to lie in the body x-z plane, while the nominal pitch angle (Eq. 7) comes from a pitch trim integrator

$$\phi_o = \tan^{-1}(V_{DR}\dot{\xi}/g) \quad (6)$$

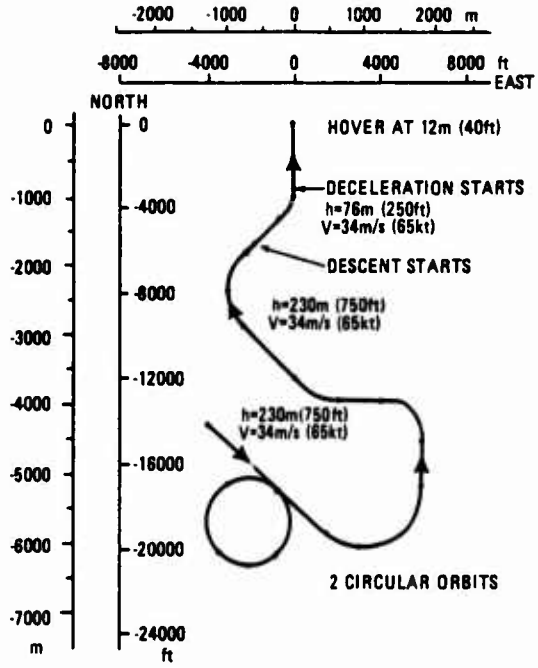

Figure 3 Ground Path of the Conventional Approach

$$\theta_o = K_I \int \Delta\theta \, dt \tag{7}$$

where V_{DR} is the downrange velocity and $\dot{\xi}$ is the turn rate.

One approach path that is especially suited to VTOL aircraft in a dense terminal environment is the spiral descent, shown in Fig. 4. The major portion of this trajectory involves steady, turning, descending flight. The final sigment is a decelerating descent similar to that used in the approach trajectory. A guidance law specifically designed for the spiral descent is given in Ref. 4. It is used in this work as an attitude command guidance law with the perturbation law implemented as in Eq. 8.

$$\begin{bmatrix} \Delta\theta \\ \Delta\phi \\ \Delta V_z \end{bmatrix} = K_A \left\{ K_1 H_E^G(\xi_o)(\underline{x}_E - \underline{x}_{E_o}) + K_2 \left(H_E^{LL}(\psi_c)(\underline{V}_E - \underline{W}_E) - \underline{V}_{A_o} \right) \right\} \tag{8}$$

$\underline{V}_{A_o}$ in Eq. 8 is the desired air-relative velocity in local level axes.

The gains are chosen to feed back crossrange and vertical position errors using guidance axes and air-relative velocity errors in local-level body axes. Although this law is chosen for constant air-relative velocity spiral descents, it and the other guidance laws discussed here are capable of guiding the helicopter along either of the flight paths described above.

VALT DIGITAL FLIGHT CONTROL SYSTEM

Estimator Design

The digital control laws require estimates of the aircraft states to achieve the desired command response. The available sensors that can be used to estimate the states consist of three body mounted accelerometers, three angular rate gyros, a vertical gyro, a gyromagnetic compass, a barometric altimeter, an airspeed indicator, and a sideslip sensor. Navigation information in the terminal area is provided by either a microwave landing system (MLS) providing range, azimuth, and elevation or a multilateration system (TRI) providing cartesian coordinate position, $\underline{x}_E$, and velocity, $\underline{v}_E$, information transmitted via an integral data link to the aircraft. The VALT instruments measure all states

needed for control in the terminal area: vehicle angular rates, $\underline{\omega}_B^E$, vehicle velocity $\underline{v}_B$, and vehicle position, $\underline{x}_E$, but the measurements require filtering and, in some instances, coordinate transformation.

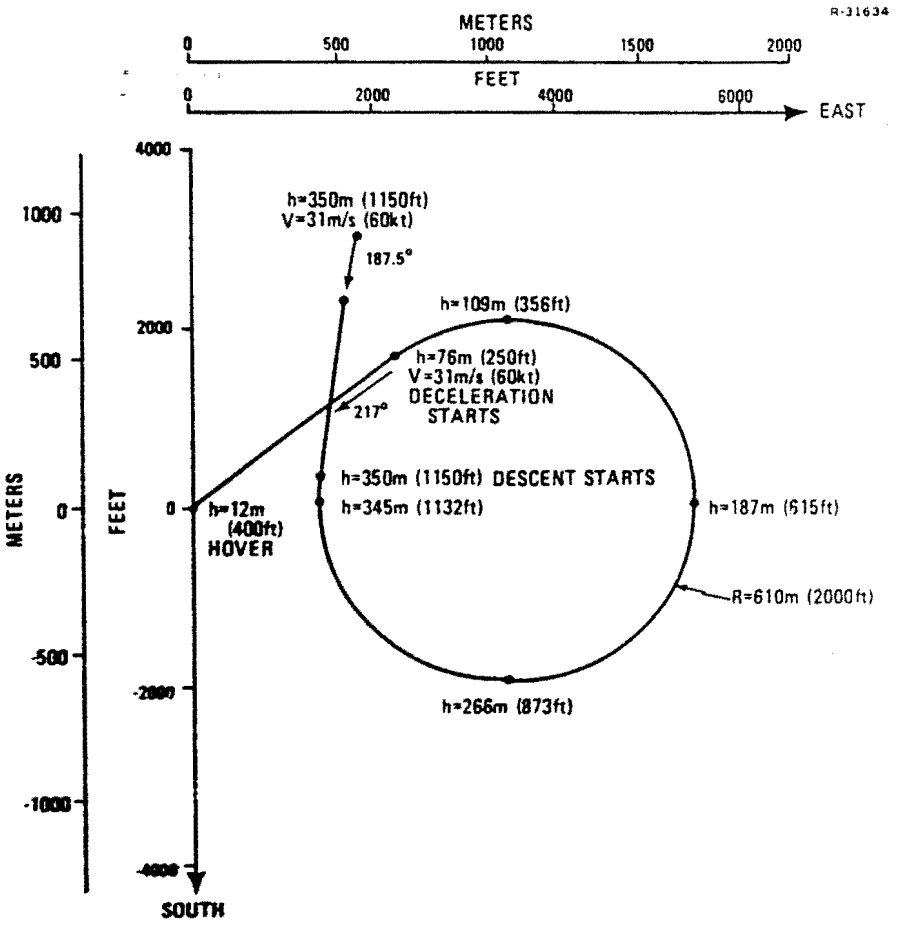

Figure 4 Ground Path of the Spiral Descent

A useful estimator for combining the dissimilar nonlinear measurements is the extended Kalman filter (EKF, Ref. 7); however, such a filter is overly complex for this application. Two approaches are taken to simplify the estimation problem. The first approach partitions the vehicle's dynamic model into random walk and first-order markov processes, transforms all measurements to similar coordinates, and groups sensor errors into white Gaussian observation noise. The estimators that result are constant gain, low-order digital Kalman filters which are found to be analogous to low-pass and complementary filters commonly used in conventional aircraft control systems. The first approach is discussed more extensively in Ref. 2.

The second approach for estimating helicopter states incorporates many of the concepts of the EKF without requiring on-line covariance propagation to compute the EKF gain. Using the Taylor series expansion and incorporating white Gaussian "process noise" for unmodeled forcing functions, the twelve rigid body states of the helicopter are expressed as

$$\underline{x}_{E_{k+1}} = \underline{x}_{E_k} + \Delta t\left[H^E_{B_k}\underline{v}_{B_k}\right] + \frac{\Delta t^2}{2}\left[H^E_{B_k}\dot{\underline{v}}_{B_k} + H^E_{B_k}\tilde{\omega}^E_{B_k}\underline{v}_{B_k}\right] + \frac{\Delta t^3}{3}\underline{w}'_x \qquad (9)$$

$$\underline{v}_{B_{k+1}} = \underline{v}_{B_k} + \Delta t \left[\dot{\underline{v}}_{B_k}\right] + \frac{\Delta t^2}{2} \underline{w}'_{v_k} \tag{10}$$

$$\underline{\omega}_{B_{k+1}} = \underline{\omega}_{B_k} + \Delta t \left[L_B^{-1} \underline{\omega}^E_{B_k}\right] + \frac{\Delta t^2}{2} \underline{w}'_{v_k} \tag{11}$$

$$\underline{\omega}^E_{B_{k+1}} = \underline{\omega}^E_{B_k} + \Delta t \underline{w}'_{\omega_k} \tag{12}$$

with the observations

$$\underline{z}_k = h_k \left[\underline{x}_k\right] + \underline{v}'_k \tag{13}$$

In these equations H^E_B is the body-to-earth axis transformation matrix, L_B^{-1} is the body-angular-rate-to-Euler-angular-rate transformation matrix, and the $\underline{v}'_k$ and $\underline{w}'_k$ vectors are Gaussian, uncorrelated sequences.

The second approach to the filter design proceeds by assuming Euler angles and body angular rates zero and then propagating the EKF covariance equations to steady state at a number of flight conditions along the approach trajectory. The perturbation transformation matrix,

$$H_k \left[\underline{x}_k(-)\right] = \left.\frac{\partial \underline{h}_k(\underline{x}(t_k))}{\partial \underline{x}(t_k)}\right|_{\underline{x}(t_k) = \hat{\underline{x}}_k(-)} \tag{14}$$

is factored from the EKF gains and the remaining significant gains are scheduled with flight condition. The following equations show the terminal area filter for estimating vehicle position, $\underline{x}_E$, velocity, $\underline{v}_B$, wind velocity, $\underline{w}_E$, and accelerometer bias, $\underline{b}_B$, using multilateration measurements, true airspeed measurements, sideslip measurements and accelerometer measurements (all subscript m).

$$\begin{bmatrix} \hat{\underline{x}}_E(+) \\ \hat{\underline{w}}_E(+) \\ \hat{\underline{v}}_B(+) \\ \hat{\underline{b}}_B(+) \end{bmatrix}_k = \begin{bmatrix} \hat{\underline{x}}_E(-) \\ \hat{\underline{w}}_E(-) \\ \hat{\underline{v}}_B(-) \\ \hat{\underline{b}}_B(-) \end{bmatrix}_k + \left[\begin{array}{c|c|c} KTRI1 & KTRI2 & \begin{matrix} E & B \\ aH(-)H(-) \\ B & A \end{matrix} KTRI3 \\ \hline aKTRI4 & aKTRI5 & \begin{matrix} E & B \\ bH(-)H(-) \\ B & A \end{matrix} KTRI6 \\ \hline \begin{matrix} B \\ H(-) \\ E \end{matrix} KTRI7 & \begin{matrix} B \\ H(-) \\ E \end{matrix} KTRI8 & \begin{matrix} B \\ aH(-) \\ A \end{matrix} KTRI9 \\ \hline \begin{matrix} B \\ H(-) \\ E \end{matrix} KTRI10 & \begin{matrix} B \\ H(-) \\ E \end{matrix} KTRI11 & \begin{matrix} B \\ aH(-) \\ A \end{matrix} KTRI12 \end{array}\right]_k \left[\begin{array}{c} \underline{x}_{E_m} - \hat{\underline{x}}_E(-) \\ \hline \underline{v}_{E_m} - \hat{\underline{v}}_E(-) \\ \hline TAS_m - \hat{TAS}(-) \\ \hline \beta_m - \hat{\beta}(-) \end{array}\right]_k \tag{15}$$

$$\begin{bmatrix} \hat{\underline{x}}_E(-) \\ \hat{\underline{w}}_E(-) \\ \hat{\underline{v}}_B(-) \\ \hat{\underline{b}}_B(-) \end{bmatrix}_{k+1} = \begin{bmatrix} I & 0 & \Delta t \begin{matrix} E \\ H(+) \\ B \end{matrix} & 0 \\ 0 & \Phi_w & 0 & 0 \\ 0 & 0 & I & 0 \\ 0 & 0 & 0 & \Phi_b \end{bmatrix}_k \begin{bmatrix} \hat{\underline{x}}_E(+) \\ \hat{\underline{w}}_E(+) \\ \hat{\underline{v}}_B(+) \\ \hat{\underline{b}}_B(+) \end{bmatrix}_k + \begin{bmatrix} DTRI1 \begin{matrix} E \\ H(+) \\ B \end{matrix} \left[\underline{a}_m - \hat{\underline{b}}_B(+)\right] \\ 0 \\ DTRI2 I \left[\underline{a}_m - \tilde{\underline{\omega}}(+) \begin{matrix} E \\ B \end{matrix} \hat{\underline{v}}(+) - \hat{\underline{b}}_B(+)\right] \\ 0 \end{bmatrix}_k \tag{16}$$

In Eq. 16, H^B_A is the air-relative to body-axis perturbation transformation matrix and $\underline{a}$ is the accelerometer output. The gains KTRI1 to KTRI12, DTRI1 and DTRI2 have only the diagonal elements scheduled; the off-diagonal elements are zeroed. The scalars a and b are used to phase out the air-data sensors as they become unreliable at a vehicle velocity below 25.7 m/s (50 kt). The barometric altimeter is phased into $\underline{x}_{E_m}$ as a function

of range before the measurement is sent to the filter.

State estimators that use MLS are similar to Eqs. 15 and 16 in that range, azimuth, elevation, air data and acceleration measurements are complemented to estimate translational velocity and earth-relative position. We term estimators designed using the EKF approach but implemented with scheduled filter gains as extended complementary filters (ECF); Eqs. 15 and 16 are thus referred to as the TRI-ECF design.

The ECF approach is not required for the angular position and angular rate filters, which are implemented as

$$\begin{bmatrix} \hat{\underline{\nu}}_B(+) \\ \hat{\underline{\omega}}_B^E(+) \end{bmatrix}_k = \begin{bmatrix} \hat{\underline{\nu}}_B(-) \\ \hat{\underline{\omega}}_B^E(-) \end{bmatrix}_k + \begin{bmatrix} K_\nu & 0 \\ 0 & K_\omega \end{bmatrix} \begin{bmatrix} \underline{\nu}_{B_m} - \hat{\underline{\nu}}_B(-) \\ \underline{\omega}_{B_m}^E - \hat{\underline{\omega}}_B^E(-) \end{bmatrix}_k \tag{17}$$

$$\begin{bmatrix} \hat{\underline{\nu}}_B(-) \\ \hat{\underline{\omega}}_B^E(-) \end{bmatrix}_{k+1} = \begin{bmatrix} I & D_\nu L_B^{-1}(+) \\ 0 & I \end{bmatrix}_k \begin{bmatrix} \hat{\underline{\nu}}_B(+) \\ \hat{\underline{\omega}}_B^E(+) \end{bmatrix}_k \tag{18}$$

where K_ν, K_ω, and D_ν are diagonal and constant. An angular rate bias estimator could be readily added to the filter if the additional complexity becomes necessary. Although the angular position and rate filters do not use translational information, the MLS-ECF and TRI-ECF are dependent on the Euler angle filter because they require the earth-to-body transformation matrix H_B^E.

Controller Design

The design model of the helicopter for the PIF (Proportional-Integral-Filter) laws is the linear-time-invariant differential equation

$$\begin{bmatrix} \Delta\dot{\underline{x}}(t) \\ \Delta\dot{\underline{u}}(t) \\ \Delta\dot{\underline{\xi}}(t) \end{bmatrix} = \begin{bmatrix} F & G & 0 \\ 0 & 0 & 0 \\ H_p & 0 & 0 \end{bmatrix} \begin{bmatrix} \Delta\underline{x}(t) \\ \Delta\underline{u}(t) \\ \Delta\underline{\xi}(t) \end{bmatrix} + \begin{bmatrix} 0 \\ I \\ 0 \end{bmatrix} \Delta\underline{v}(t) + \begin{bmatrix} 0 \\ 0 \\ -I \end{bmatrix} \Delta\underline{y}_d(t) \tag{19}$$

where $\Delta()$ indicates a perturbation variable. Equation 19 is obtained by local linearization of the helicopter's nonlinear model (Ref. 2). The command perturbations ($\Delta\underline{y}_d$) correspond to the previous total-value definitions, $\Delta\underline{\xi}$ represents "command integrator states" to be added in the control system, and $\Delta\underline{v}$ is the control rate. The state vector contains body axis velocity and angular rate ($\Delta\underline{\nu}_B$, $\Delta\underline{\omega}_B^E$) as well as Euler angle ($\Delta\underline{\nu}_B$) perturbations. The four control perturbations form $\Delta\underline{u}$. The helicopter's kinematics, stability derivatives, and inertial effects are contained in the (9×9) matrix F and the control derivatives are contained in the (9×4) matrix G, as in Ref. 8. In symmetric flight, F and G contain rotor-induced coupling but otherwise partition into the conventional longitudinal and lateral-directional equation sets. In turning flight, F and G also contain certain turn-induced coupling terms. The (4×9) matrix H_p transforms the perturbation state vector to command-vector corrdinates.

The VALT digital control laws are developed assuming that longitudinal, lateral, and directionsl motions are coupled, in order to assure that no potentially significant cross-axis effects are overlooked (e.g., the helicopter's normal tendency to pitch up when turning in one direction and to pitch down when turning in the opposite direction). If the coupling is not significant, that fact will be reflected in the control laws, which will partition accordingly.

The derivation of the proportional-integral-filter control law is presented in Ref. 1 and is not repeated here. The design objective is to find the digital feedback control law which minimizes the continuous time quadratic cost function

$$J = \int_0^\infty \left\{ \begin{bmatrix} \Delta\underline{x}^T(t) & \Delta\underline{u}^T(t) & \Delta\underline{\xi}^T(t) \end{bmatrix} Q \begin{bmatrix} \Delta\underline{x}(t) \\ \Delta\underline{u}(t) \\ \Delta\underline{\xi}(t) \end{bmatrix} + \Delta\underline{v}^T(t) R \Delta\underline{v}(t) \right\} dt \tag{20}$$

Q and R in Eq. 20 are weighting matrices that are used as design parameters in creating a control law which satisfies the response criteria. This continuous-time cost function is expressed as an equivalent sampled-data cost function, as in Ref. 9. Minimizing the cost function provides a PIF control law, which is shown in Fig. 5, and can be written as

$$\underline{u}_k = \underline{u}_{k-1} + \Delta t \underline{v}_k \tag{21}$$

$$\underline{v}_k = (I-\Delta tC_2)\underline{v}_{k-1} - C_1(\underline{x}_{k-1}-\underline{x}_{k-2}) - \Delta tC_3(\underline{y}_{k-2}-\underline{y}_{d_{k-1}}) + C_4(\underline{y}_{d_k}-\underline{y}_{d_{k-1}}) \tag{22}$$

where Δt is the sampling interval, and the coefficient matrices C_1 to C_4 are defined in Ref. 1.

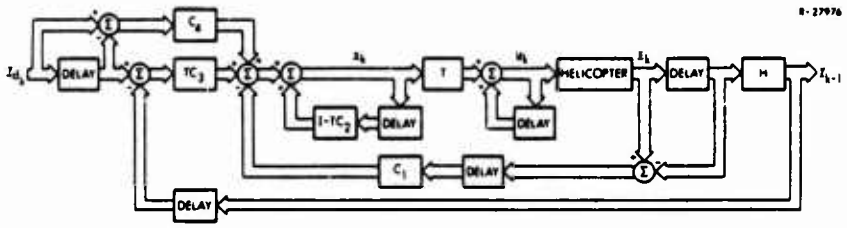

Figure 5 Structure of Proportional-Integral-Filter Control Law

Figure 5 shows the incremental form of the PIF controller, which accepts total guidance command and state inputs and issues total commands to the helicopter's rotors. The position-form controller presented in the earlier reference operates on perturbation variables and requires explicit specification of nominal values to form total commands; the incremental PIF controller effectively generates its own nominal values (by incorporating past values of $\underline{u}$ and $\underline{v}$ in the current command) and operates on differences in the state and command variables. The differences "wash out" the nominal values; hence, the controller can interface with a nonlinear model of the helicopter (or with the helicopter itself) as well as with the linear-time-invariant model used for design. The only difference is in the use of the nonlinear $\underline{x}$ to $\underline{y}$ transformation. In either case, the PIF controller described by Eqs. 21 and 22 results in Type 1 command response.

The attitude-command and velocity-command PIF control laws both are described by Fig. 5; the difference between the two is in the definition of $\underline{y}$, H and the gain matrices. The Q and R matrices used in the design process assign equal costs to the state and control perturbations shown in Table 1. For both control laws, once acceptable step responses are established at a single flight condition the values of Q and R are frozen, and control gains are generated for the remaining 27 flight conditions. With this approach, most step response criteria have been met at all flight conditions for both control laws. The simpler PI control law does not include the "low-pass" filtering of the control signals (Ref. 1).

Gain Scheduling

The control laws are adapted to the helicopter flight condition by scheduling their gains as functions of true airspeed (V), body z-axis velocity (w), and yaw Euler angular rate ($\dot{\psi}$). The gain schedules are developed in a 3-step process:

Determination of means and standard deviations of all gains (summed over all flight conditions), determination of correlation coefficients between gains and flight conditions, and curve fitting by regression analysis (Ref. 8). The objective of the first step is to determine which gains can be zeroed or held constant; the second step indicates which functional relationships are most appropriate for gain scheduling; and the last step provides the scheduling coefficients.

The PIF control law for the helicopter, described by Eqs. 21 and 22 contains 84 gains; however, 29 and 25 gains are zeroed in the attitude-command and velocity-command controllers, respectively. The zeroed gains have mean values which are generally less than 5% of comparable gains, and the standard deviations also are small. The remaining gains are scheduled in three sets, which take the following forms:

$$\text{Gain} = a_1V+a_2V^2+a_3w+a_4\dot{\psi} + a_5 \tag{23}$$

$$\text{Gain} = a_1 V + a_2 w + a_3 \dot{\psi} V^2 + a_4 V^2 / \left[1+(V/V_N)^2\right] + a_5 \quad (24)$$

$$\text{Gain} = a_1 V + a_2 V^2 + a_3 \dot{\psi} w + a_4 / \left[1+(V/V_N)^2\right] + a_5 \quad (25)$$

TABLE 1
DESIGN PARAMETERS FOR HELICOPTER CONTROL LAWS

ALLOWABLE PERTURBATION	ATTITUDE COMMAND	VELOCITY COMMAND
Δu, fps	—	16.
Δv, fps	—	18.
Δw, fps	7.	6.
Δp, deg/sec	7.	10.
Δq, deg/sec	15.	10.
Δr, deg/sec	7.5	10.
$\Delta\phi$, deg	3.3	6.5
$\Delta\theta$, deg	2.8	7.
$\Delta\psi$, deg	3.	3.5
$\Delta\xi_1$(ϕ or V_x)	4.4 deg-sec	10. ft
$\Delta\xi_2$(θ or V_y)	3.4 deg-sec	12. ft
$\Delta\xi_3$(ψ or V_z)	3.8 deg-sec	3.5 ft
$\Delta\xi_4$(V_z or ψ)	3.2 ft	2.5 deg-sec
$\Delta\dot{u}$, fps^2	—	0.2
$\Delta\dot{v}$, fps^2	—	0.2
$\Delta\dot{w}$, fps^2	0.2	0.3
$\Delta\delta_B$, in	6.5	6.5
$\Delta\delta_C$, in	4.6	4.6
$\Delta\delta_S$, in	3.6	3.5
$\Delta\delta_R$, in	4.2	4.2
$\Delta\dot{\delta}$(all), in/s	2.	2.

In these scheduling equations V is true airspeed, and V_N is 27 m/s (53 kt). One-sixth of the scheduled gains have standard deviations which are less than 10% of their mean values, and they are candidates for being considered constant.

The optimal gains computed at 28 flight conditions generally have correlation coefficients with the scheduled gains of 0.8 or better. An example of gain variations with forward airspeed is given by Fig. 6, which shows the pitch rate feedback (C_1) gains to differential collective, gang collective, and differential cyclic rotor deflections for the velocity-command controller. The scheduled gains are represented by Eqs. 23, 24, and 24, respectively, and all their correlation coefficients are greater than 0.96.

Because the scheduling only approximates the progression of the optimal gains, evaluation of the scheduled controller is a particularly important step in the design process. The next section discusses the use of eigenvalues, eigenvectors, and simulation responses for this purpose

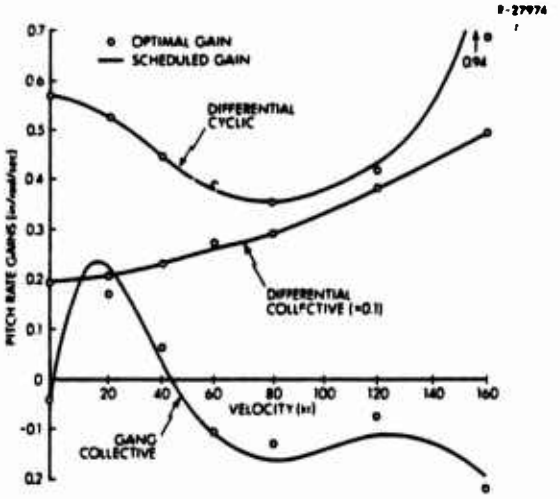

Figure 6 Optimal and Scheduled Pitch Rate Gains

DFCS EVALUATION MODEL

The VALT DFCS described above is evaluated using a digital simulation of the helicopter and on-board sensors. This simulation is implemented using a variable time-step Runge-Kutta integration routine which is driven by subroutines describing the continuous-time helicopter models, the discrete-time sensor models, and flight computer (DFCS) coding. Figure 7 illustrates the simulation structure. The helicopter model which is implemented in the evaluation simulation is outlined in Fig. 8, and the details of this model are discussed in the next paragraphs.

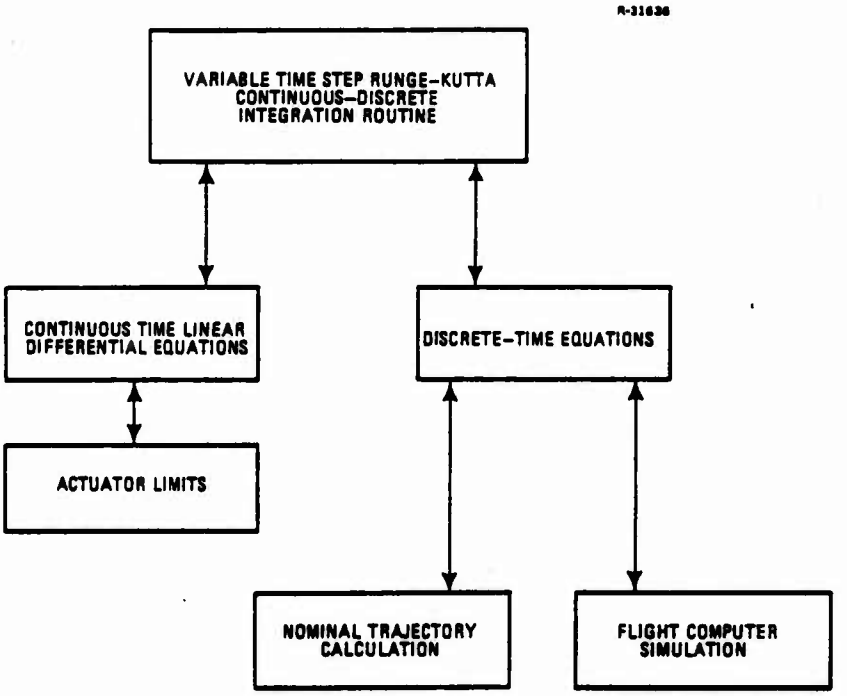

Figure 7 DFCS Evaluation Simulation Structure

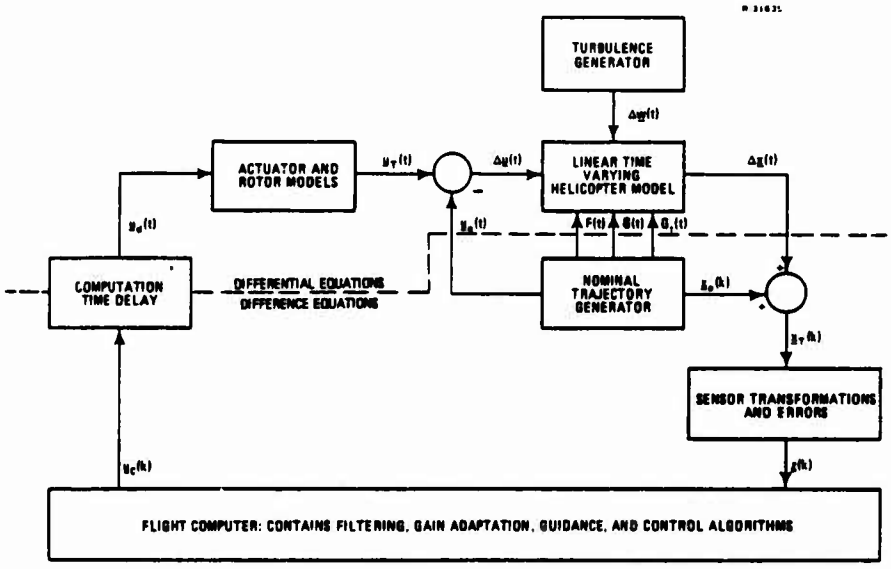

Figure 8 Helicopter Model Structure

The rigid-body dynamics of the helicopter are simulated by implementing the linear time-varying system

$$\Delta\dot{\underline{x}}(t) = F(t)\Delta x(t) + G(t)\Delta\underline{u}(t) + G_t(t)\Delta\underline{w}(t) \qquad (26)$$

where $\Delta\underline{x}$ contains the 12 rigid-body states, $\Delta\underline{u}$ is the 4-element control position vector and $\Delta\underline{w}$ is the 3-element wind and turbulence vector. The 12×12 F(t) matrix contains linearized dynamic equations. Helicopter stability derivatives are incorporated which result in a fully-coupled system even in straight-and-level flight.

The helicopter simulation contains identical models of the first-order actuator and second-order rotor dynamics in each of the four control channels (Figs. 9 and 10). The actuator model also incorporates control position and rate limits. These nonlinearities can be important in certain extreme maneuvers. The actuator time constant is 1/80 sec, while the rotor response has a steady-state gain of 1.0 and a natural frequency and damping ratio of 24 rad/sec and 0.6, respectively. The actuator limits are given in Table 2.

TABLE 2

ACTUATOR LIMITS

CHANNEL	POSITION LIMIT	RATE LIMIT
Differential Collective	-50.8 to +50.8 mm (-2.0 to +2.0 Inches)	± 76.2 mm/s (± 3.0 in/sec)
Collective	0.0 to 101.6 mm (0.0 to +4.0 Inches)	
Cyclic	-50.8 to +50.8 mm (-2.0 to +2.0 Inches)	
Differential Cyclic	-50.8 to +50.8 mm (-2.0 to +2.0 Inches)	

The computation time delay (which is restricted to be less than one flight computer sample period long) is simulated so that the sensitivity of the control laws to these delays can be tested. It is important to insure that a computational lag will not adversely affect stability.

Some of the sensor transformations included in the evaluation model are nonlinear, as are some of the sensor errors (scale factor errors). Table 3 details the sensor suite and indicates which errors are included in these models. It is intended that only one of the two radio navigation methods be used at a time, and it should be noted that the air-relative velocity sensors (airspeed and sideslip) are not used below 25.7 m/s (50 knots) air speed.

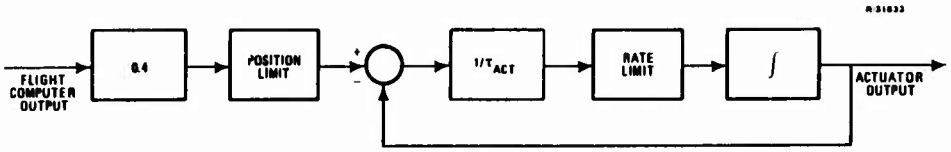

Figure 9 Actuator Model

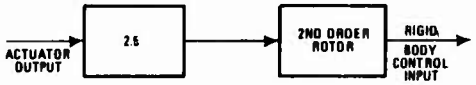

Figure 10 Rotor Dynamics Model

The nominal trajectory generator calculates both the nominal state and control vectors and the linear system matrices as a function of time along a nominal trajectory. The trajectory is made up of segments, some of which involve non-zero nominal dynamic state rates. The dynamic states are u, v, w, p, q and r. The time-varying nominal is constructed so that the total-value linear time-varying system responds to total-value control commands, $\underline{u}_T(t)$, much as a nonlinear simulation would. Hence, as the nominal trajectory moves from one segment to another, the total system state should not respond if a constant control command, $\underline{u}_T(t)$ is applied. Figure 11 illustrates the implications of this. Assume the nominal dynamic state is constant for $t<t_1$ and $t>t_2$. Hence, these two values imply a nominal state rate $\dot{\underline{x}}_o$. For $\underline{x}_T$ to remain constant (as it should in the face of constant $\underline{u}_T$), the perturbation state rate must exactly cancel the nominal state rate ($\Delta\dot{\underline{x}} = -\dot{\underline{x}}_o$). However, to induce this six-element perturbation state rate, discontinuities in a six element nominal "control" vector must be allowed. The six-elements are formed from the four controls (δ_B, δ_C, δ_S, δ_R) and the pitch and roll Euler angles (ϕ,θ). The resulting dynamic trim problem can be stated as follows:

$$\begin{bmatrix}\Delta(\Delta u)\\ \Delta(\Delta v')\end{bmatrix} = \begin{bmatrix}G' & F_{xv}\end{bmatrix}^{-1}\left[\dot{\underline{x}}_0 - F_{xx}\,\Delta(\underline{x}_0)\right] \qquad (27)$$

where $\Delta v'$ contains the two Euler angles, F_{xx} (6×6) defines the effects of the dynamic states on their own state rates and F_{xv} (6×2) defines the effect of the roll and pitch Euler angles on the dynamic state rates. G' is the 6×4 control input matrix describing the control effect on the six dynamic states. The vector $\Delta(\underline{x}_o)$ contains the discontinuity in angular rates due to rolling and pitching on turn entry. Implementation of these nominal state and control discontinuities $\left(\Delta(\underline{x}_o),\ \Delta(\Delta\underline{u}),\ \text{and}\ \Delta(\Delta v')\right)$ results in a total-value linear-time-varying helicopter simulation which responds much as a nonlinear simulation would, but which can be implemented using linear system models.

TABLE 3

SENSOR SUITE AND ERROR SOURCES

SENSOR	MEASUREMENT	BIAS	SCALE FACTOR	MEASUREMENT NOISE
Angular Rate Gyro	Roll Rate	Yes	Yes	Constant RMS
	Pitch Rate	Yes	Yes	Constant RMS
	Yaw Rate	Yes	Yes	Constant RMS
Heading Gyro	Yaw	No	No	Constant RMS
Attitude Gyro	Roll	Yes*	Yes*	Constant RMS
	Pitch	Yes*	Yes*	Constant RMS
Accelerometer	Longitudinal	Yes	Yes	Constant RMS
	Lateral	Yes	Yes	Constant RMS
	Normal	Yes	Yes	Constant RMS
Airspeed	Air Relative Velocity	Yes	Yes	Constant RMS
Sideslip	Sideslip	Yes	Yes	Constant RMS
Altitude	Pressure Altitude	Yes	Yes	Constant RMS
Spherical MLS	Range	Yes	Yes	Constant RMS
	Azimuth	Yes	No	Range-Dependent
	Elevation	Yes	No	Range-Dependent
or				
Trilateration MLS	North Position	No	No	Range-Dependent
	East Position	No	No	Range-Dependent
	Altitude	No	No	Range-Dependent
	North Velocity	No	No	Range-Dependent
	East Velocity	No	No	Range-Dependent
	Altitude Rate	No	No	Range-Dependent

*The attitude gyro incorporates an erection mechanism which nulls the bias. However, the erection mechanism cuts out during a steady-turn, allowing the attitude gyro to drift.

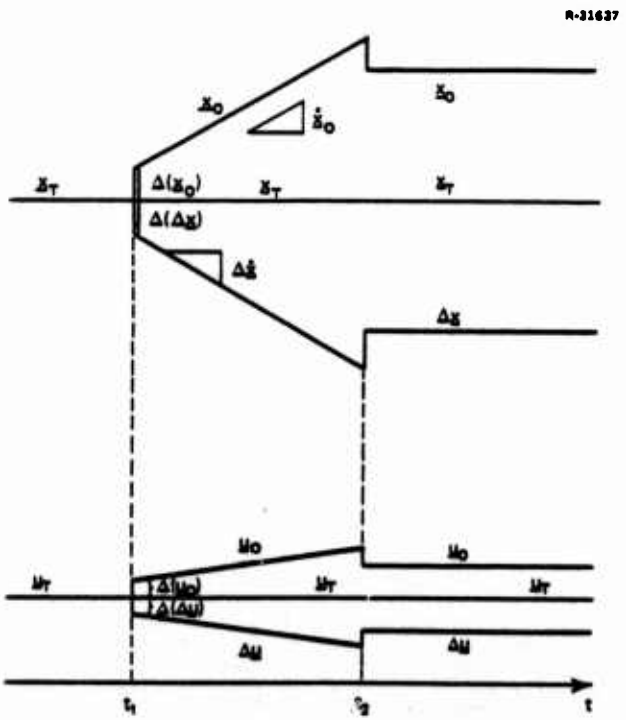

Figure 11 System Response Along an Accelerated Nominal Trajectory for Constant Total States and Controls.

$\{\underline{x} = [u,v,w,p,q,r],\ \underline{u} = [\delta_B, \delta_C, \delta_S, \delta_R]\}$

SIMULATION RESULTS

Linear Time-Invariant Model

The DFCS and helicopter comprise a hybrid system, some of whose components are described by differential equations and some by difference equations. For linear-time-invariant response analysis, a closed loop system is formed in discrete time and transformed into a continuous-time equivalent system by a matrix logarithm. The eigenvalues and eigenvectors of the resulting continuous-time equivalent system can be used to compare optimal to scheduled controller accuracy and to compare the different controller designs. Table 4 compares open loop and scheduled closed-loop eigenvalues at a primary design point (80 kt straight and level flight). In addition to the classical aircraft modes, the controllers introduce new modes associated with the control system integrators and low-pass filters.

Although closed-loop eigenvalue locations are not used as an indicator in controller design, they exhibit good control characteristics. Short period and Dutch roll complex pairs fall well within the requirements of military specifications MIL-F-83300 (Ref. 10) as does the roll mode time constant. All other complex pairs have damping ratios greater than 0.5. Noteworthy observations are 1) the attitude systems have slow velocity modes (real phugoid (speed) and closed-loop "spiral") in order to meet the angle command steady-state requirements, 2) the low-pass filter natural frequency locations are in close proximity to open-loop natural frequencies, and 3) the scheduled eigenvalues remain near their optimal counterparts (not shown), but with increased damping in most cases.

TABLE 4

COMPARISON OF SCHEDULED EIGENVALUES AT
41.2 m/s (80 kt) STRAIGHT AND LEVEL FLIGHT

DYNAMIC MODE	OPEN LOOP			PI ATTITUDE			PIF ATTITUDE			PIF VELOCITY		
	ω_n rad/sec	ζ, –	τ, sec	ω_n rad/sec	ζ, –	τ, sec	ω_n rad/sec	ζ, –	τ, sec	ω_n rad/sec	ζ, –	τ, sec
SHORT PERIOD	0.359	-1.77*	–	2.92	0.630	–	4.05	0.892	–	3.73	0.875	–
PHUGOID	0.256	0.342	–	1.63	0.754/40.6		2.10	0.592/41.7		0.405 1.99	0.681 0.590	–
DUTCH ROLL	0.394	-0.190	–	2.60	0.595	–	2.81	0.635	–	3.06	0.665	–
ROLL	–	–	0.899	–	–	0.322	–	–	0.630	–	–	0.685
SPIRAL	–	–	25.77	–	–	13.6	–	–	13.77	0.524	0.757	–
HEADING	–	–	∞	2.26	0.563	–	2.27	0.594	–	2.35	0.661	–
ζ_θ OR ζ_{V_x}	NONE			–	–	0.462	–	–	1.41	0.405	0.681	–
ζ_ϕ OR ζ_{V_y}				–	–	0.423	–	–	1.18	0.524	0.757	–
ζ_ψ				2.26	0.563	–	2.27	0.594	–	2.35	0.661	–
ζ_{V_z}				1.63	0.754	–	2.10	0.592	–	1.99	0.590	–
A_B	NONE			NONE			1.32	0.961	–	1.29	0.979	–
B_C							1.32	0.961	–	1.29	0.979	–
B_B							1.12	0.948	–	1.00	0.775	–
B_R							1.12	0.948	–	1.00	0.775	–

*Two real roots

Comparisons of eigenvalues over a range of velocities shows that PIF increases the natural frequency of Dutch roll and short period as velocity increases, while concurrently decreasing the low-pass filter bandwidths. Eigenvalues for PI remain fairly constant over the operating range.

Controller-Filter Simulations Without Measurement Errors

Command responses of the scheduled-gain DFCS with operational filters in the feedback loops (but without measurement errors or noise) are presented in Figs. 12 to 16. Figure 12 illustrates the response of the PI attitude command law to a 3.28 m/s (10 fps) step command in vertical velocity at hover using the TRI-ECF filter. The TRI filter relies heavily on the velocity measurements from the multilateration system at the hover point to produce this accurate response. The PIF attitude command control law response to a 0.1 rad step command in roll angle is shown in Fig. 13, and it can be seen that the design criteria are met.

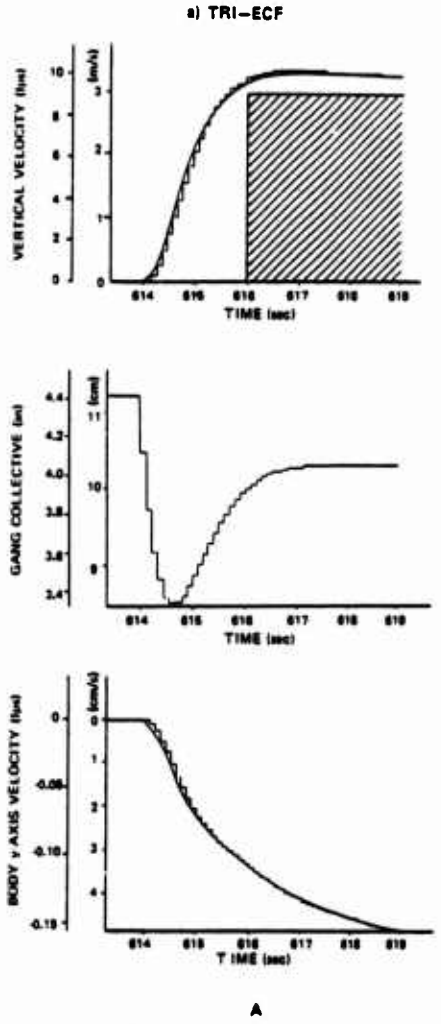

Figure 12 PI-Attitude Vertical Velocity Command Response at Hover

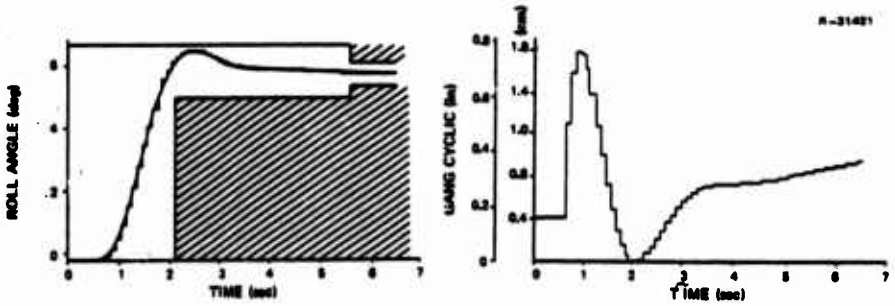

Figure 13 PIF-Attitude Roll Response With the TRI-ECF (TAS = 30.9 m/s (60kt), S&L Flight)

The PIF attitude command control law response to a 0.1 rad yaw command is shown in Fig. 14. This command is not accompanied by the appropriate turn coordination subcommand; hence the aircraft is held at a sideslip by the steady-state gang cyclic command. The yaw angle response has a slightly excessive overshoot using the filtered measurements, although rise time is unaffected. This is caused by the filter lags, which also result in the errors in the northerly velocity estimate.

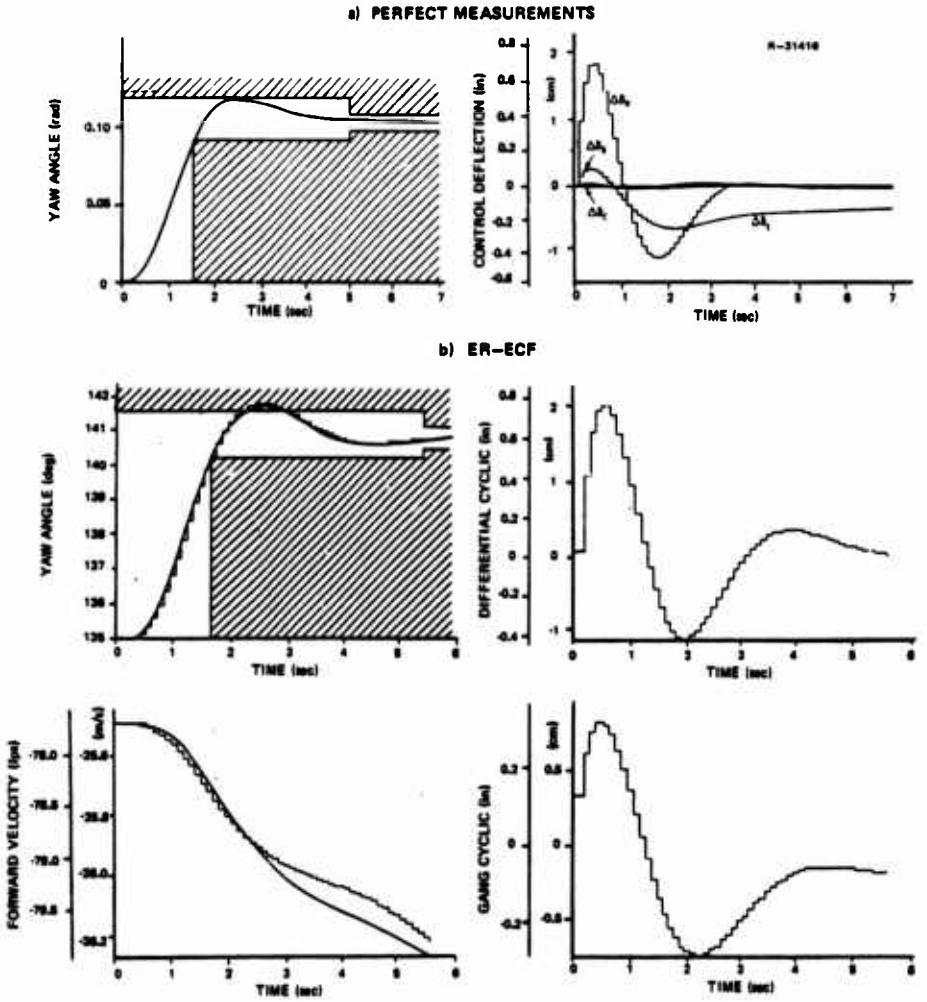

Figure 14 PIF-Attitude Yaw Angle Response (TAS=41.2 m/s (80 kt), Heading = 135 deg, S&L Flight)

The pitch response of the PIF attitude control law with the rotor and actuator dynamics included is shown in Fig. 15. The response requirements and response without actuator and rotor models are also shown. The figure illustrates the reduction in damping caused by the additional lags in the vehicle model. Figure 16 shows both the differential collective command and the value actually exerted on the helicopter after the command is passed through the actuator and rotor dynamics. Computational time delays have a similar effect on the vehicle response: the damping decreases (shown by increased overshoot), but the rise time remains constant. Time delays up to 90% of the controller sample period have been tested without producing an instability, although the vertical velocity overshoot increases to 17.3% at 90% sample period delay as compared to its zero-delay value of 11.1%.

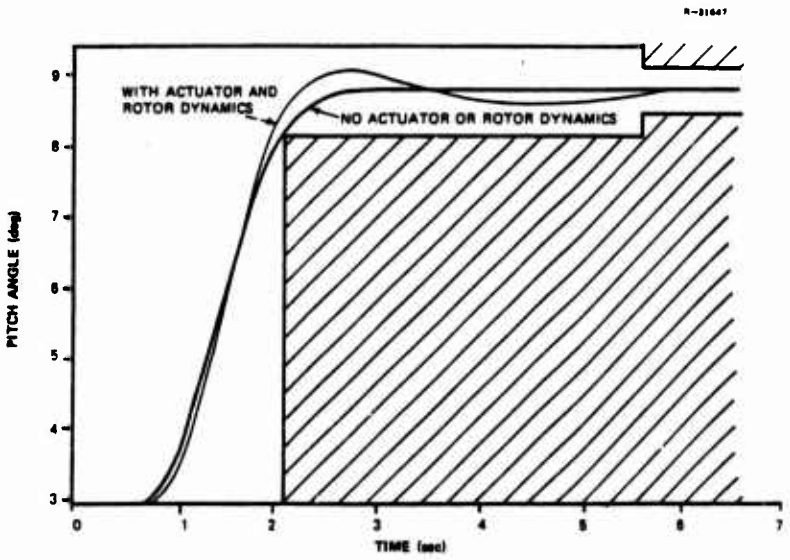

Figure 15 Pitch Command Response as Affected by Actuator and Rotor Dynamics

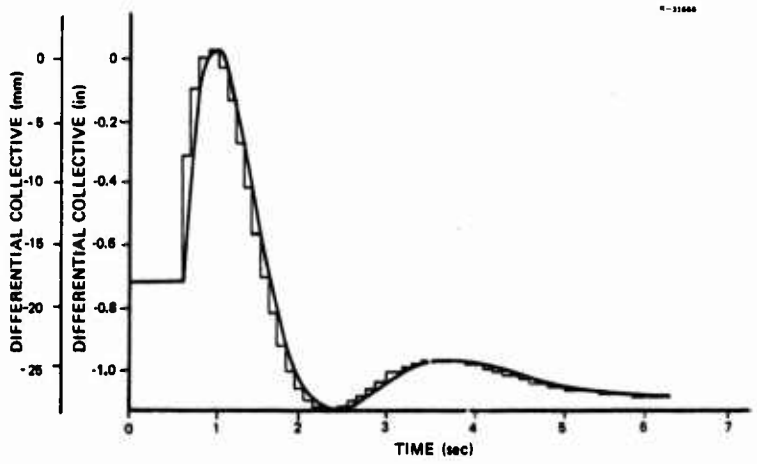

Figure 16 Differential Collective Command and Actuator/Rotor Output

Measurement Error Effects

The selection of command vector, controller structure and sensor suite to provide best vehicle response in the presence of unavoidable sensor errors and measurement noise is discussed in this section. Both attitude and velocity command vectors have been tested. Although the velocity command vector provides better body-axis velocity control (Table 5), its angular control (especially roll) is worse than the attitude command vector's performance (Table 6). Hence, the earth-relative velocity is controlled more effectively by the attitude command vector (Table 7). The northerly and easterly velocity errors are correlated such that most of the horizontal velocity command error is normal to the velocity vector. This is caused by velocity command controller roll control which is insufficient for these noise levels.

TABLE 5

BODY-AXIS VELOCITY STANDARD DEVIATIONS
33.5 m/s (65 kt) STRAIGHT FLIGHT

VELOCITY COMPONENT	PIF, VELOCITY COMMAND	PIF, ATTITUDE COMMAND
u	0.04 m/s (0.12 fps)	0.04 m/s (0.12 fps)
v	0.3 m/s (1.0 fps)	0.7 m/s (2.3 fps)
w	1.2 m/s (4.0 fps)	1.3 m/s (4.1 fps)

TABLE 6

BODY ATTITUDE STANDARD DEVIATIONS
33.5 m/s (65 kt) STRAIGHT FLIGHT

ATTITUDE ANGLE	PIF, VELOCITY COMMAND	PIF, ATTITUDE COMMAND
ϕ	1.3 deg	0.15 deg
θ	0.5 deg	0.4 deg
ψ	1.1 deg	1.0 deg

TABLE 7

EARTH-RELATIVE VELOCITY STANDARD DEVIATIONS
33.5 m/s (65 kt) STRAIGHT FLIGHT AT 135 DEG HEADING

VELOCITY COMPONENT	PIF, VELOCITY COMMAND	PIF, ATTITUDE COMMAND
V_x	0.3 m/s (1.0 fps)	0.12 m/s (0.4 fps)
V_y	0.3 m/s (1.0 fps)	0.05 m/s (0.15 fps)
V_z	1.2 m/s (4.0 fps)	1.2 m/s (4.0 fps)

The PIF controller structure does provide a smoother control output than the PI controller, as can be seen by comparing the yaw command responses in Figs. 17 and 18. The control signal deviation from its trim value is about three times larger in the PI system than in the PIF system, and the PI control signal contains higher frequency deviations. PIF and PI produce comparable magnitude outer loop responses, although the angular rates and control deflections the PI controller produces are much larger than those from the PIF controller.

The choice of sensors primarily revolves around air-data and radio navigation sensors. Body-axis velocity estimation errors are listed in Table 8 for three situations. The fourth possibility (MLS at short range) can be expected to perform almost as well as TRI at close range. The true air-speed and sideslip sensors provide significant information in the long-range cases, as can be seen in the w channel, where no angle of attack sensor is available. Short range velocity estimates by the TRI estimator are very accurate.

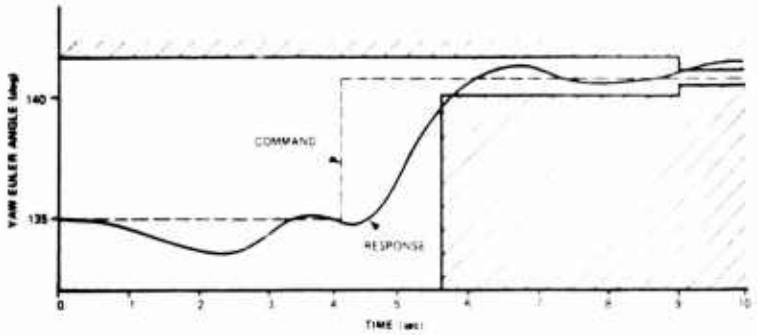

Figure 17 Yaw Angle Response Due to PIF Attitude Command Controller: Pilot Command $\Delta\psi_c$=5.73 Deg at T=4.1 Sec

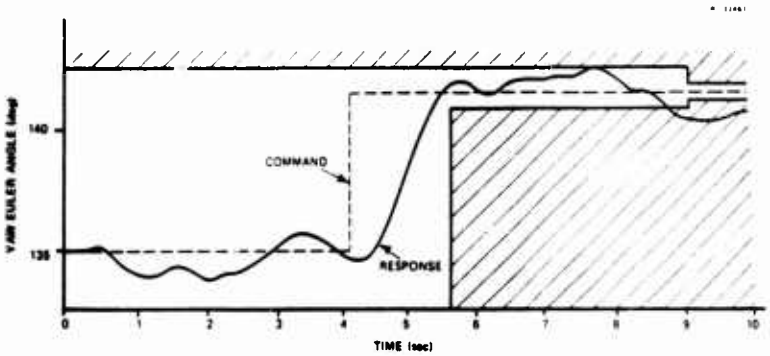

Figure 18 Yaw Angle Response Due to PI Attitude Command Controller: Pilot Command $\Delta\psi_c$=5.73 Deg at T=4.1 Sec

TABLE 8

BODY AXIS VELOCITY ESTIMATION ERROR STANDARD DEVIATIONS AS A FUNCTION OF RADIO NAVIGATION AID

VELOCITY COMPONENT	TRI SHORT RANGE (1 km, 1/2 nm)	TRI LONG RANGE (5 km, 2.5 nm)	MLS LONG RANGE (5 km, 2.5 nm)
u	0.1 m/s (0.4 fps)	0.2 m/s (0.7 fps)	0.3 m/s (1.0 fps)
v	0.24 m/s (0.8 fps)	0.46 m/s (1.5 fps)	0.3 m/s (1.0 fps)
w	0.15 m/s (0.5 fps)	1.5 m/s (5.0 fps)	0.9 m/s (3.0 fps)

The inaccurate w channel estimate at long range translates to errors in vertical velocity of a similar magnitude. These errors result in altitude estimation errors as listed in Table 9. At the long range, the TRI system produces its altitude estimate primarily from the relatively inaccurate baro altimeter. Note that this range is somewhat longer than the TRI designed maximum range of 4 km (2 nm). In summary, the MLS system performs better than the TRI system at ranges beyond about 4 km (2 nm), but the TRI system, with its all-aspect capability and excellent close range position and velocity estimates, may be desirable for actual landing zone navigation. A radar altimeter could

improve the long-range TRI vertical channel, as well as being useful to an MLS system at close range.

The choice of command vector and sensor suite are closely linked. A velocity command vector appears to require more accurate state measurements than the sensor suite used in this simulation series provides, except possibly at short range with trilateration. However, if this velocity estimation accuracy can be achieved, the velocity command structure seems ideally suited to precision position and velocity control, especially at low speeds. The attitude command vector is more oriented to on-board angular sensors, and seems ideal for enroute control, and is probably a desirable command vector for pilot control of the vehicle.

TABLE 9

ALTITUDE ESTIMATION ERROR STANDARD DEVIATIONS AS A FUNCTION OF RADIO NAVIGATION AID

TRI SHORT RANGE (1 km, 1/2 nm)	TRI LONG RANGE (5 km, 2.5 nm)	MLS LONG RANGE (5 km, 2.5 nm)
0.4 m (1.4 ft)	>15 m (>50 ft)	2.4 m (8 ft)

For both command vectors, the PIF structure provides smoother response with much less control motion than the PI controller. The low-pass filter dynamics in PIF assist in filtering out residual noise in the state estimates. It appears that more sophisticated filters with smoother state estimates could operate well with a PI controller structure. The proper trade-off between filter and controller complexity is certainly an area of possible further research.

CONCLUSIONS

The development and computational testing of the VALT DFCS are outlined in this paper. The digital flight control system is based on the design of gain-scheduled controller and filter algorithms using linear systems analysis techniques. Specific conclusions follow:

Controller Design - The controllers are designed using digital control techniques, but they minimize an analog performance index. The slow sampling rates which are possible using this design method produce good vehicle response even in the presence of large computation delays, actuator lags and estimator lags. Although both the PI and PIF structures provide fast and accurate response to commands when using accurate state estimates, the PIF controller structure produces more desirable response in the presence of noisy state feedback.

Gain Scheduling - Control and filter gains can be scheduled as a function of a few flight condition variables and still capture most of the gain variation from flight condition. Response quality of the scheduled gain controller is essentially unchanged relative to the optimal design.

Command Vectors - In a noisy environment, the attitude command controller actually regulated vehicle velocity more accurately than the velocity command controller. Velocity control laws are superior to attitude control laws in the presence of vehicle disturbances, such as wind. The choice between the two command modes depends on the intended application.

State Estimators - The filters implemented here performed reasonably well in the simulation tests, despite their simplicity relative to a complete EKF implementation. Because the filters are sub-optimal, with many unmodeled error sources, there is a strong connection between filter design policy and controller design policy. The DFCS operates in a much smoother manner with a PIF controller than with a PI controller, but smooth response could probably be produced also by a more complex state estimator and a PI controller.

Many of these conclusions will be tested by the planned flight tests of the NASA VALT helicopter.

REFERENCES

1. Stengel, R.F., Broussard, J.R. and Berry, P.W., "Digital Controllers for VTOL Aircraft," Proceedings of the 1976 IEEE Conference on Decision and Control, Clearwater, Dec. 1976, pp. 1009-1016.

2. Stengel, R.F., Broussard, J.R. and Berry, P.W., "Digital Flight Control Design for a Tandem-Rotor Helicopter," Proceedings of the 33rd Annual National Forum of the American Helicopter Society, Paper No. 77.33-44, Washington, May 1977.

3. Hoffman, W.C., Zvara, J., Bryson, A.E., Jr. and Ham, N.D., "An Automatic Guidance Concept for VTOL Aircraft, AIAA Paper No. 70-1035, New York, Aug. 1970.

4. Hoffman, W.C. and Hollister, W.M., "A Spiral Guidance Approach Concept for Commercial VTOL Operations," NASA CR-132651, Burlington, MA, May 1975.

5. Moen, G.C., "Simulation and Flight Studies of an Approach Profile Indicator for VTOL Aircraft, "NASA TN D-8051, Washington, Nov. 1975.

6. Moen, G.C., DiCarlo, D.J. and Yenni, K.R., "A Parametric Analysis of Visual Approache for Helicopters," NASA TN D-8275, Washington, Dec. 1976.

7. Gelb, A. ed., Applied Optimal Estimation, M.I.T. Press, Cambridge, 1974.

8. Stengel, R.F., Broussard, J.R. and Berry, P.W., "The Design of Digital-Adaptive Controllers for VTOL Aircraft," NASA CR-144912, Mar. 1976.

9. Dorato, P. and Livis, A.H., "Optimal Linear Regulators: The Discrete-Time Case, IEEE Transactions on Automatic Control, Vol. AC-16, No. 6, Dec. 1971, pp. 613-620.

10. Anon., "Flying Qualities of Piloted V/STOL Aircraft, "U.S. Air Force, Dec., 1970.

AUTOMATIC FLIGHT PERFORMANCE OF A TRANSPORT AIRPLANE ON COMPLEX MICROWAVE LANDING SYSTEM PATHS

by

Thomas M. Walsh
NASA Langley Research Center
Hampton, VA U.S.A. 23665
and
Earl F. Weener
The Boeing Company
Seattle, WA U.S.A. 98124

SUMMARY

In May 1976, the National Aeronautics and Space Administration, through its Langley Research Center Terminal Configured Vehicle (TCV) Program, participated with the Federal Aviation Administration (FAA) in a demonstration of the U.S.A. microwave landing system. This demonstration was conducted for the All Weather Operations Panel of the International Civil Aviation Organization at the FAA's National Aviation Facilities Experimental Center. During this demonstration the microwave landing system was utilized to provide the TCV B-737 airplane with guidance for automatic control on complex, curved descending paths with precision turns into short final approaches terminating in landing and roll-out, even when subjected to strong and gusty tail- and cross-wind components and severe wind shear. The data collected from more than fifty approach flights during the demonstration provided an opportunity to analyze airplane flight performance on a statistical basis rather than on a single flight record basis as is customarily done with limited data replication. Mean and standard deviation data are presented for approach flight path tracking parameters. In addition, the adverse wind conditions encountered during these flights are described using three-dimensional wind vector characteristics computed from the extensive on-board sensor data.

1. INTRODUCTION

The National Aeronautics and Space Administration's Terminal Configured Vehicle (TCV) Program is conducting analytical, simulation, and flight research which will support improvements in (1) terminal area capacity and efficiency, (2) approach and landing in adverse weather, and (3) operating procedures to reduce noise impact. (Reference 1) In this research major emphasis is being placed on the development of advanced concepts for application to avionics and display systems for aircraft operations in future terminal area air traffic control systems. Particular emphasis is being placed on operations in microwave landing systems (MLS) environments. One example of this effort is the participation of the NASA through the TCV Program with the Federal Aviation Administration (FAA) in the demonstration of the U.S. national MLS to the All Weather Operations Panel (AWOP) of the International Civil Aviation Organization (ICAO). This demonstration took place at the FAA's National Aviation Facilities Experimental Center (NAFEC) in May 1976. During this demonstration the MLS was utilized to provide the TCV B-737 research airplane with guidance for automatic control during transition from conventional to MLS area navigation in curved, descending flight and in flare, touchdown and roll-out. It is the purpose of this paper to describe the operational aspects and performance achieved during the demonstration. Flight profiles, system configuration, and operating procedures used in the demonstrations are described, and performance results of the automatic flights are discussed.

The demonstrations to the ICAO of automatic flight performance of a transport type aircraft on complex MLS paths consisted of a large number of replicated flights in the same basic configuration. With these data as a basis, airplane flight performance can be analyzed statistically on an ensemble basis across similar runs, rather than along the time axis as is more customarily done with limited data replication. Mean and deviation type data are presented for airplane approach tracking parameters. Finally, these flights were conducted in rather adverse wind conditions. Hence, this atmospheric environment will also be described using three-dimensional wind vector characteristics computed from the extensive on-board sensor data.

This paper will briefly describe the U.S. MLS and the TCV B-737 airplane used in the demonstration flights, followed by a description of the demonstration scenario and approach paths. The tracking performance achieved on these paths under MLS guidance will be examined in some detail. Finally, the wind environment, within which these flights were conducted, will be quantified.

2. U.S. MLS

The U.S. MLS basically transmits three time-reference scanning fan-shaped radio beams from the runway, as illustrated in Figure 1. One beam scans $\pm 60^{\circ}$ from side to side of the runway center at a rate of 13½ times per second to provide azimuth (Az) referencing. The second beam scans up 20° and down to a reference plane parallel to the runway surface at a rate of 40 times per second to provide basic glide slope guidance (EL1). The third beam, which scans up $7\frac{1}{2}^{\circ}$ and down to the same plane parallel to the runway at a rate of 40 times per second, is used for flare guidance (EL2). A fourth nonscanning fan-shaped beam

transmitted from a distance measuring equipment (DME) site provides ranging information. This DME beam is transmitted at a rate of 40 times per second and has an angular coverage of 120° in azimuth and 20° in elevation. Time reference means that receiving equipment on-board the aircraft will measure the time difference between successive "to" and "fro" sweeps of the scanning beams to determine aircraft position relative to the runway center line and to a pre-selected glide path. This time-difference measurement technique gives rise to the designation of the U.S. MLS as a Time Reference Scanning Beam MLS.

3. TCV B-737 RESEARCH AIRPLANE

The equipment aboard the TCV B-737 research airplane includes all-digital integrated navigation, guidance, control and display systems. A cut-away view of the airplane shown in Figure 2 illustrates the palletized installation of the avionics and depicts a second cockpit for research (aft flight deck, AFD). The value of the airplane for research purposes is enhanced by several notable design features:

(a) The system functions are controllable and variable through software.

(b) The hardware is easily removed, modified, repaired, and installed.

(c) Flight station changes are readily accomplished in the research cockpit, which has a fly-by-wire implementation for control of the airplane.

The arrangement of the AFD is shown in the photograph of Figure 3. The center area of the cockpit is seen to resemble a conventional 737 cockpit, whereas the area immediately in front of the pilot and copilot has been opened up by removing the wheel and wheel column and replacing them with "brolly handle" controllers. This open area has been utilized as the location for advanced electronic displays. The displays illustrated in Figure 3 consist of an electronic attitude director indicator (EADI) at the top, the electronic horizontal situation indicator (EHSI) in the middle, and the navigation control display unit (NCDU) at the bottom. A control mode select panel, through which the pilot may select from a variety of automatic and manual control modes, is shown located at the top of the instrument panel and centered between the two pilots. The display system is all digital and can be readily reprogramed with regard to formats and symbology for research purposes. The NCDU is used to call up preplanned routes and flight profile information or for entering new or revised information to be displayed. Inserted information and flight progress information can be called up on the NCDU for review. The EADI instrument provides basic attitude information to control the airplane; the EHSI shows the horizontal plan of the flight, either with a heading-up or north-up mode, and the flight progress. On it can be displayed moving time slots in which the pilot can maintain position, manually or automatically, for sequencing. Also, the dashed leader line projected from the nose of the aircraft in the figure shown presents predictive information to the pilot as to where the airplane will be (at its present turn rate) in 30, 60, and 90 seconds from the present. Although the entire flight plan could be flown from the EADI alone, the EHSI adds greatly to the clarity of the situation and provides long-term anticipation for the pilot.

4. DEMONSTRATION SCENARIO AND APPROACH PATHS

In July 1975, at the request of the FAA, the NASA agreed to participate in a flight demonstration of the U.S. MLS capabilities to the All Weather Operations Panel (AWOP) of the ICAO at NAFEC. The ground rules adopted for the demonstration were:

(a) Fly three-dimensional path (3-D) automatic, curved, descending approaches with TCV B-737 navigation control laws and MLS guidance used for the curved-path portions.

(b) Make transition from curved-path portions to short, straight final approaches and land with the autoland control laws modified to use MLS guidance.

(c) Perform flares using EL2 and/or radio altimeter signals.

(d) Perform roll-out using MLS guidance.

(e) Drive the TCV B-737 displays with MLS derived information.

The philosophical approach taken by Langley Research Center was to make minimum modifications in the existing navigation, guidance, and control system and to derive all necessary parameters from the MLS data for interface with these systems.

The prescribed approach paths flown during the demonstration are shown in Figure 4 and consist of two paths typical of the types of curved, three-dimensional complex paths which might be used to reduce overflight over noise-sensitive areas, or eliminate congestive or interfering flight traffic patterns. The first prescribed approach path was called the 130°-turn approach because of the curved, descending 130° left turn onto a short, three mile final approach. The second prescribed approach path consisted of two opposite 90° turns separated by a short intervening straight segment prior to the final approach turn, and was designated the S-turn approach. Both of these prescribed approach paths started at a nominal altitude of 4,000 feet and descended at a local 3° angle to the runway.

As seen in Figure 4, take-off for the 130°-turn approach path was from runway 22 with the airplane controlled manually from the front cockpit during take-off. Shortly after take-off, control was shifted to the aft cockpit, where a manual control wheel steering (CWS) mode had been selected by the AFD pilot. Prior to encountering the first way point, the AFD pilot selected a 3-D automatic area navigation (RNAV) mode for airplane control. This control mode used inertially smoothed DME/DME as the source of guidance information. Altitude was maintained at 4000 feet until the way point indicated by "Begin 3° descent" was passed. From this point the airplane continued descending 3° until flare was initiated. After crossing the Az boundary and approximately 15 seconds after crossing the EL1 boundary, the pilot received an indication of valid MLS data, at which time he selected the MLS RNAV mode which used MLS data as the source of guidance information. This latter event is noted as "MLS enable" in Figure 4. Just prior to entering the final turn, the pilot selected Land Arm. The airplane continued to fly under the MLS RNAV mode until both selected glide slope and lateral path were acquired; then the control of the airplane was switched to autoland for control along the 3 nautical mile final approach. At an altitude consistent with the sink rate and altitude criteria of the flare laws in the autoland mode, flare was initiated. Flare was executed using EL2 and DME data as the source of vertical guidance information on most of the touchdowns. On a few flights during the demonstration, a radio altimeter was used as the source of vertical guidance information for comparison purposes.

The events along the S-turn profile are very similar to the events of the 130°-turn profile, as shown in Figure 4. It may be noted that the S-turn profile resulted in a greater time period of MLS RNAV than did the 130°-turn profile. On touch-and-go approaches, control was switched from aft flight deck automatic control to front flight deck manual control for the take-off portion of repeat flights. On landings that continued to a full stop, roll-out was conducted in an automatic mode that used the Az beam for runway centerline guidance information.

A typical demonstration flight consisted of five approaches, four 130°-turns, and one S-turn. Of these five approaches, the first four were touch-and-go landings while the final one was a full stop with roll-out guidance on the runway. Both automatic approaches continued through flare, decrab, touchdown, and roll-out. In total, over 50 separate automatic approaches were conducted during this demonstration. It should be noted that approximately 150 additional automatic approaches were conducted at NAFEC during pre-demonstration development flights and post-demonstration flight experiments (Reference 2). Over 40 manually controlled approaches were also flown after the demonstration using the advanced displays of the TCV B-737 (Reference 2).

5. TCV B-737 CONFIGURATION FOR MLS OPERATION

The basic configuration of the TCV B-737 that was used during the ICAO Demonstration is illustrated by the simplified block diagram of Figure 5. It should be noted that the original airplane was not configured to use MLS data for navigation, guidance, or control. The principal task addressed was the integration of the MLS signals into the navigation, guidance, and control laws and display formats of the original airplane that had been designed to use INS, DME, ILS, and radio altimeter data. The major development effort was directed at aircraft antenna design and location, interface of the MLS receiver with the navigation, guidance, and control system, and design of the MLS guidance signal processor. Wherever possible, the functions of this signal processor were designed to permit integration of MLS derived navigation, guidance, and control parameters with existing laws of the navigation and guidance computer and the autoland computer with minimal modifications to these computers. Minor changes were made to the existing display formats, with features added to indicate validity of MLS signals.

Details of the MLS processor are illustrated in Figure 6. As shown in this figure, the inputs to the MLS processor from the MLS receiver are Az, R, EL1, and EL2. These signals were prefiltered to remove extraneous noise and then transformed to a runway-referenced coordinate frame which produced position data (x, y, z) relative to the selected glide-path intercept point.

The function of the closed-loop estimator of Figure 6 was to produce estimates of position and velocity parameters required for interface with the navigation and guidance computer, the autoland computer, and the displays. The Air Data input to the closed-loop estimator consisted of calibrated airspeed and sink rate as derived from a barometric altimeter. These two pieces of data were used to initialize the closed-loop estimator. The Accelerations input to the closed-loop estimator was used to produce the quality of velocity data required in the flight control system. These acceleration data were extracted from the INS during the ICAO Demonstration.

The parameters derived from MLS data for navigation were latitude and longitude deviations from the origin of the MLS runway-referenced coordinate frame. The latitude and longitude origin values were known a priori and stored in the navigation computer. It is then a simple task to determine the aircraft latitude and longitude. The MLS processor outputs used for guidance are latitude, longitude, altitude to mean sea level, north velocity, east velocity, and sink rate. These MLS processor outputs and way points defining the desired flight path which are prestored in the navigation and guidance computer are then operated upon by the guidance laws to produce path correction commands to the autopilot while operating in an automatic RNAV mode.

The MLS processor outputs to the autoland computer are glide-path-angle deviation, lateral-path-angle deviation, altitude to touchdown, vertical velocity, or sink rate, and cross runway velocity. These inputs to the autoland guidance laws are processed in the autoland computer along with a prestored runway heading during the final approach to produce pitch and roll commands to the autopilot. It should be noted here that airspeed is controlled by the autothrottle according to a preset airspeed selected by the pilot.

Changes to the TCV B-737 configuration for the ICAO Demonstration may be seen by comparing Figure 7 with Figure 2. As shown in Figure 7, three antenna locations were selected for the demonstration. The C-band antennas on the tail and lower aft fuselage were used for diagnostic purposes during the development flights. The C- and K_u-band antennas located above the front cabin were the primary antennas used for guidance. The cabin-mounted C-band antenna was used to receive Az, EL1, and R signals, and the K_u-band antenna was the receiving antenna for EL2 signals. The MLS receivers, processor, and special MLS signal recorders are shown located just in front of the aft flight deck. Special in-flight diagnostic oscillographs and a backup MLS receiver are shown located at the right rear of the airplane.

6. DATA ACQUISITION SYSTEMS

The TCV B-737 on-board, real-time data acquisition systems consisted of the Piloted Aircraft Data System (PADS), the Flight Control Computer (FCC) data formatter, and the Navigation Computer Unit (NCU) output bus. The TCV B-737 PADS constitutes a general purpose data acquisition and retrieval system. For the MLS flight demonstrations, the PADS was configured to digitize at the rate of 40 samples/second. The basic word length is 10 bits per word. Data recorded on this data acquisition system originate in the MLS Processor, the NCU, the FCC and several dedicated instrumentation transducers located throughout the airplane. The data formatter receives digital inputs from the Flight Control Computer Interface Unit (FCI) and reformats them into a serial, digital signal that is recorded on wideband magnetic tape. Twenty-five different triplex sets of FCC sources are selectable for recording. The sample rate of this data acquisition system is approximately 20 samples/second with a 16 bit word length.

On-board data are also acquired from the data output bus of the NCU. This ARINC 561 format data bus is software controlled within the NCU. The sample rate of this system is approximately 8 samples/second with a word length of 24 bits. Outputs of these three data acquisition systems were recorded on wideband magnetic tape.

The NAFEC phototheodolite tracking system was employed to optically track the aircraft during the initial and final approach phases. Position information in an orthogonal coordinate system with origin located at the center of the MLS azimuth antenna array was derived from tracking elevation and azimuth angles from at least two and usually three tracking towers. These data were digitally filtered to reduce the noise level of the position information. The sample rate of the theodolite data is 10 position samples/second.

7. DATA ORGANIZATION AND PROCESSING

The MLS demonstration consisted of numerous flights on either of two specific prescribed approach paths, with the configuration of the TCV B-737 experimental systems remaining unchanged throughout. Because of the unusually large numbers of flights, it becomes meaningful to ask what the average values and statistical variations of the flight parameters were. In other words, the flight data acquired constituted a data base suitable for across approach ensemble statistical analyses.

However, several fundamental obstacles had to be circumvented before statistical summarization. First, the time-referenced data describing any single approach were contained on four physically separate magnetic tapes at different sample rates. Data from these four sources had to be combined on a single storage device with a common time index. Secondly, after the data sources from a specific approach were correlated, there was still no means to readily align the data from separate approaches. Ground speeds were not the same from one approach to another. Consequently, a given time interval did not correspond to the same distance along the approach path from one approach to another.

Without a common independent or reference variable it was difficult to compare performance on one approach with that of another approach at an equivalent point on the prescribed approach path. To facilitate this comparison, an independent variable which was common to all approaches was defined.

The occurrence of most events during an approach was systematically correlated to the progress or position along the prescribed approach path. Since only two different prescribed approach paths were utilized during the demonstration flights, a reasonable independent variable with which to correlate data between flights on the same approach was the distance from the glide path intercept point along the prescribed path.

The value of this independent variable, L, was defined to be the point on the prescribed path closest to the actual tracked position as shown in Figure 8. With the data subsequently referenced to points along the prescribed path, data corresponding to a particular point on the approach could be calculated by a linear interpolation. Consequently, for each of the two approach paths all the respective flight data could be

compared at common spatial points. In addition, since all flights had identical final approach segments, this final data set consisted of all approaches combined. This process is illustrated graphically in Figure 9.

To recapitulate, it was desired to compare performance data from similar approaches. To do this, the basic time-referenced data were transformed to a distance reference. The chosen distance reference was the scalar distance from the glide path intercept point (GPIP) along the prescribed approach path. With the resulting distance-referenced data base, statistical analyses of the flight data could be performed across the set of similar approaches at equivalent points along the prescribed approach paths. For example, the mean value of some variable at a specific distance from the GPIP could be readily computed from this distance-referenced data base. In fact, these computations have been performed at relatively small intervals along the initial and final approach segments, resulting in mean and standard deviation descriptions that appear to be almost continuous along the prescribed approach path.

It is important to note that this across-run, ensemble approach was necessary because the system characteristics are not stationary in a statistical sense: gains, sensitivities, modes and control laws vary with progression along the approach path.

8. TRACKING PERFORMANCE

The automatic flight control system operation during the MLS portion of the approach consisted of two segments. The outer curved position prior to final approach was flown in an area navigation mode while the straight final approach through flare, touchdown and roll-out was flown in an autoland mode. The guidance control laws associated with each of these modes were substantially different. Concurrently, there are two sets of lateral and vertical deviation variables, one set corresponding to each of these two guidance modes.

Figure 10 presents the lateral guidance signals for a typical 130°-turn approach culminating in a full stop landing. The upper trace is the lateral deviation from the prescribed path during the area navigation mode and the lower trace is a similar deviation for the autoland portion. It should be noted that these two quantities are defined with reversed signs, as indicated on the left of the figure. The independent variable is the along-path distance from the glide path intercept point, GPIP. The path length in this figure corresponds to the interval starting from navigation about 8 nautical miles out and ending about 2/3 nautical miles past the GPIP. The change to autoland operation occurred at approximately L = 19,000 feet from the GPIP, shortly after completion of the turn-to-final.

The initial value of lateral deviation, XTK, at TRSB ENABLE (right-hand side) indicated an apparent error in tracking. This initial XTK deviation was the result of: (1) the transition from DME area navigation to the more accurate MLS area navigation, and (2) the initialization of the MLS Processor which produced transient MLS area navigation outputs. Frequently, in excess of 10,000 feet of path after TRSB ENABLE was required for the initialization transient for this particular filter to decay. This is exemplified in Figure 10 by the rapid swing from an initial left (negative) XTK to a right (positive) XTK of approximately 125 feet.

Following the change to MLS autoland control laws, the lateral deviation is represented by the variable DELYSK. As illustrated in Figure 10, the maximum values of DELYSK are much smaller than those of XTK. Also, the system dynamics indicated by the behavior appear to be stiffer, with higher frequency components than are evident on the XTK signal. The tighter control of the airplane, as manifested by the decrease in the magnitude of the DELYSK guidance signal, was a result of the higher gains in the autoland localizer track control law.

Vertical path tracking performance for the same flight is shown in Figure 11. As was the case for the lateral axis, two control laws were used during the MLS guidance portion of the approach. However, the point of transition from MLS area navigation to MLS autoland occurred earlier than in the lateral case. For this particular approach, transition occurred at approximately 27,000 feet from GPIP. This corresponds to a point approximately halfway around the 130° turn-to-final approach.

As in the lateral case, two variables represent vertical deviation: HER during area navigation and DELHSK during autoland operation. HER and DELHSK have reversed signs: positive HER means the airplane is below the prescribed approach path while positive DELHSK means the airplane is above the prescribed approach path, as indicated on the left side of Figure 11. The disparity between the two vertical deviation variables at the transition point from one control law to the other is primarily due to the difference in descent profiles. On the outer curved portion, the descent angle is 3°, but measured with respect to the local vertical. On the inner portion, the descent angle is still 3° but now measured along the extended runway centerline and with respect to the horizontal runway plane which is tangent to the earth surface at the GPIP. The outer curved portion of the approach is above this 3° glide path plane, descending into it from the side during the turn-to-final. Consequently, the switch to autoland control laws prior to interception of the straight final approach course results in an apparent error above the course.

As stated previously, the demonstration flight series consisted of more than fifty approaches with more than forty of them being 130°-turn approaches and about ten S-turn approaches. All valid tracking data for the 130°-turn approaches were restructured and transformed to dependence on path length, as described earlier. With all similar approaches indexed in this manner the average deviation occurring at specific distances from GPIP could be calculated. In fact, the average deviation was computed across the ensemble of 130°-turn approaches at 200 foot intervals along the path starting at GPIP. This is shown for the outer segment of the 130°-turn approach course in the upper portion of Figure 12. In general, the beginning of valid data occurred at different points for the various individual approaches. Consequently, the right-hand side of Figure 12 has greater variability (the progression of time along these approaches is from right to left). The lower portion of this figure shows the 2σ (twice the standard deviation) value of the deviation about the mean at the corresponding distances along the path. For distances further out than approximately 40,000 feet, the mean and 2σ values show the effects of MLS filter initialization transients. The mean deviation at 40,000 feet is about 60 feet to the right with a 2σ of almost 250 feet. However, during most of the 130°-turn-to-final the mean position is to the left side of path and somewhat closer. The tracking also becomes much less variable as indicated by the decrease of 2σ to about 70 feet. In other words, throughout the 130°-turn, the airplane tracked the computed path with a mean error of less than 50 feet.

Similar data for the S-turn approach is shown in Figure 13. Note immediately the absence of the initialization transient that was encountered for the 130°-turn approach. Because of the particular geometry of the S-turn approach, the MLS signal processor received valid MLS data for a considerable distance prior to engagement of the MLS area navigation mode. Consequently, initial transients had subsided prior to the beginning of the MLS guidance usage. The mean and 2σ are somewhat less smooth locally because of the smaller sample size. Beginnings and endings of turns appear to cause the greatest perturbations of the mean lateral deviations. These deviations are generally less than 50 feet. The 2σ history also seems to be loosely correlated with the entries and exits of turns. In this case, the 2σ deviation about the mean is still generally 50 feet or less.

Mean and 2σ statistics for vertical deviation on the 130°-turn approach are shown in Figure 14. From the right hand side of this figure, it appears that vertical error was also affected by either the filter initialization transient or the step increase in guidance accuracy or both. Nevertheless, after the initial 6000 to 8000 feet, the maximum vertical position error is less than 20 feet and typically less than 10 feet. The 2σ value also remains less than 40 feet after the initial error decay.

Similar data for vertical deviation encountered during the S-turn approach are shown in Figure 15. In general, the mean error and the 2σ deviation are smaller than the values resulting from the 130°-turn approaches. The maximum mean vertical deviation is about 15 feet and occurs during the straight segment between the two 90° turns. The greatest 2σ deviation during the initial approach is about 30 feet from the mean. So far, both lateral and vertical deviation on the initial portions of both the 130°-turn and S-turn approaches have been presented. The following paragraphs will consider these tracking deviations on the final approach segment.

Since the final approach segments of both approaches were identical, the data from both approach types were combined into a single data set. The lateral deviation variable for this segment is DELYSK which was computed in the MLS signal processor. This lateral deviation is presented in a slightly different form in Figure 16. The center trace is the mean value as before. However, the 2σ value is added and subtracted from the mean giving both mean plus and mean minus 2σ traces. This is essentially the envelope within which the airplane normally remained. (The sign convention is reversed from that of HER on the initial approach segment.). At the right side of this figure the airplane has just completed the turn-to-final with an average overshoot to the right of less than 20 feet. The initial 2σ envelope is about 200 feet wide but collapses very rapidly to approximately 20 feet wide as the GPIP is neared. The distances of L = 3800 and L = 2000 feet correspond to heights of approximately 200 and 100 feet, respectively.

Careful examination of DELYSK at these positions reveals mean deviations of less than 7 feet and 5 feet, respectively, with associated 2σ dispersions of about 10 feet at both points.

The deviation variables presented thus far, XTK, HER, and DELYSK, were deviations computed from on-board receivers and sensors. As stated earlier, the ground-based theodolite at NAFEC was also employed to track the airplane.

In general, the independent theodolite tracking data agree well with the counterpart data generated on-board. The theodolite tracking data over the initial approach segments were often more variable than the on-board data largely because of weather related obstructions to visibility and the absence of photo-correction to the theodolite data.

Figure 17 presents the ground tracked lateral deviation, DYA, for the final approach course. The sign convention of this variable is opposite that of the on-board computed DELYSK. Data over the final two nautical miles of the approach show very close correspondence between these two data sources. The on-ground data show a greater mean overshoot following the turn to final. Note also that the 2σ values increase substantially at about 16,000 feet from GPIP. This is probably due to an optical loss of the airplane by the ground tracking in this region during one or more of the approaches.

The final type of tracking data to be presented in this paper is the vertical deviation on final approach as measured both on-board, DELHSK, and on-ground DZA, Figures 18 and 19, respectively. These variables exhibit similar behavior over the final two nautical miles or more. At the points corresponding to heights of 200 and 100 feet, mean deviations exhibited by the on-board data appear to be less than a foot while the on-ground data show approximately three foot deviations. In either case, the 2σ dispersion is less than 8 feet. The right hand portion of these two figures show the vertical deviations during roughly the last half of the turn-to-final. Transition to the MLS autoland mode occurred before intercept of the final approach course. Agreement between the two tracking variables is poorer during this portion of the turn-to-final. On-board data in Figure 18 show an initial error above the prescribed path with a ramp-like correction back to the path. This phenomenon is absent in the ground tracking data, Figure 19. This completes the brief examination of the tracking performance of the NASA TCV B-737 during the flight demonstration of the MLS.

9. WIND ENVIRONMENT

These flights were conducted to demonstrate MLS performance to the ICAO. They were flown on a schedule constrained by demonstration considerations and were not flown simply for flight test data generation. Consequently, the flights were conducted in weather conditions more diverse and adverse than would normally have been encountered in engineering flight testing. As a result, it becomes important to quantify and characterize the wind environment so that its effect on the flight performance can be accounted for.

During the post-flight data processing the airplane's inertial velocity vector and the velocity vector relative to the air mass were computed. The vector difference between these is the wind velocity vector. Malfunction of one of the data systems precluded computation for about 40% of the flights. Figures 20 and 21 present the wind speed and direction during the final approach segment. Mean wind velocity at the start of the final approach is approximately 20 knots and decreases to about 15 knots in the vicinity of the runway threshold. Concurrently, the 2σ also decreases from about 15 knots to about 8 knots near the ground. Note that a wind velocity of 15 knots near the ground corresponds to a velocity exceeded only 15% of the time, according to the FAA and CAA certificatory documents (References 3 and 4).

Figure 21 presents the corresponding mean and 2σ wind direction with respect to true north. The direction shown corresponds to the orientation of the wind vector; not the direction from which the wind is blowing. An average direction at low altitudes of about 50-60 degrees, as was the case during these flights, is especially significant since the runway direction was about 30°. Consequently, the average landing was flown with a left quartering tail wind of about 15 knots. This is far from a normal situation; the FAA certificatory requirements on autoland systems are limited to 10 knots tailwind at most.

10. CONCLUSIONS

This paper presents a brief summary of flight performance of the TCV B-737 Advanced Guidance and Control System (AGCS) operating in the MLS terminal area environment. The large number of flights in the same AGCS configuration during these demonstrations to the ICAO AWOP provided an unusual opportunity to analyze the flight performance on a statistical basis. In addition, the three dimensional navigation facility represented by the MLS presented another opportunity to examine flight on complex paths in the terminal area and to carefully assess the future operational potential of these kinds of flight paths for noise, congestion and interference alleviation. Because of the extensive data gathering capabilities of the TCV B-737 in conjunction with the NAFEC theodolite, ground-based tracking facility, very thorough and accurate flight data recordings were available. A further unusual aspect of this MLS flight demonstration series was the presence of an exceptionally adverse atmospheric environment which was described quantitatively from the flight data.

Finally, the flight performance data presented in this paper represents only a small portion of the data resulting from these flights. Data from over fifty flights were recorded. From the extensive recorded data, thirty variables describing the airplane's flight performance were analyzed and are available. These data include navigation, guidance, control, and tracking variables from both on-board and ground-based sources, and a complete description of the atmospheric wind velocity vector throughout the initial and final approach regions. For each of these thirty variables, the mean, standard deviation, and histogram statistical descriptions are available. In addition, an individual along-path history of each variable for each of the fifty-three approaches is available.

Of equal importance to the automatic flight performance were the advanced displays that allowed the flight crew and observers to follow the flight situation and aircraft tracking performance very accurately from the aft flight deck of the TCV B-737 research airplane without outside reference. Elements of these displays enabled the pilots to proceed after take-off toward the initial way point of the flight profiles, where automatic 3-D flight was initiated. During the initial phase of automatic 3-D navigation, elements of the displays were driven by conventional navigation signals. Upon entering the MLS coverage region, MLS signals were used to drive the display elements for monitoring of the automatic control system performance during transition from conventional RNAV to MLS RNAV; curved, descending flight; flare; touchdown; and roll-out.

The flights demonstrated the utility of the wide area coverage of the MLS for curved, descending paths commencing with a standard RNAV approach into a terminal area and continuation of this approach throughout the MLS coverage area and onto the runway. The ability to fly precision curved navigation paths with use of MLS signals highlights the potential of this system for design of noise alleviation and high-capacity flight paths in a terminal area.

REFERENCES

1. Reeder, John P.; Taylor, Robert T.; and Walsh, Thomas M.: New Design and Operating Techniques and Requirements for Improved Aircraft Terminal Area Operations. NASA TM X-72006, 1974.

2. Walsh, Thomas M.; Morello, Samuel A.; and Reeder, John P.: Review of Operational Aspects of Initial Experiments Utilizing the U.S. MLS. NASA SP-416, 1976.

3. "Automatic Landing Systems," FAA AC 20-57a, January 12, 1971.

4. "Airworthiness Requirements for Automatic Landing Including Automatic Landing in Restricted Visibility Down to Category 3," BCAR paper number 367, Issue 3, June 1970.

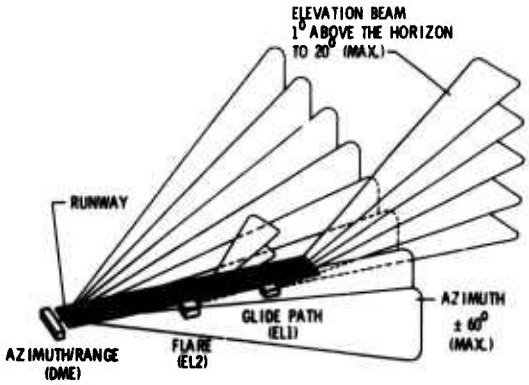

Figure 1 Microwave Landing System

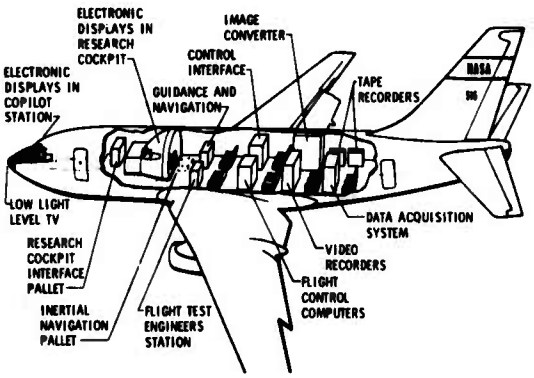

Figure 2 NASA TCV B-737 Research Airplane
(Internal Arrangements)

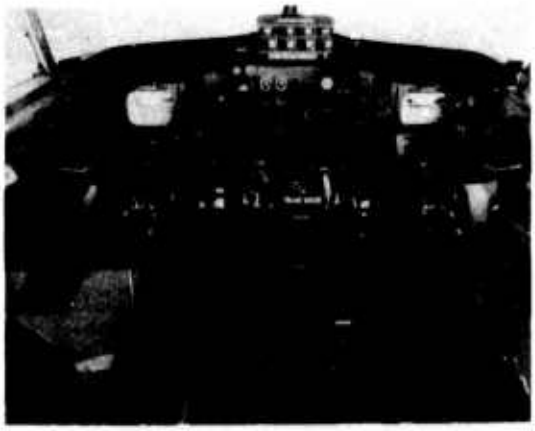

Figure 3 Aft Flight Deck Display Arrangement

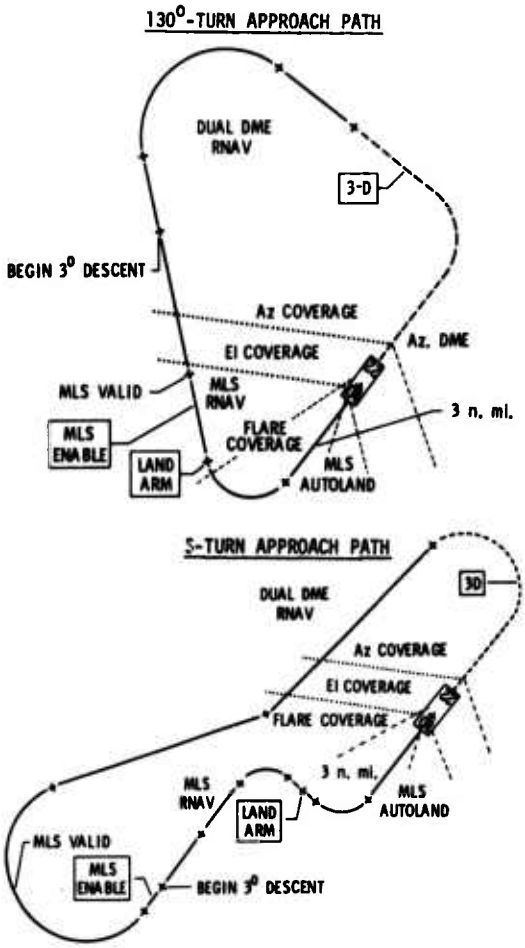

Figure 4 MLS Approach Paths

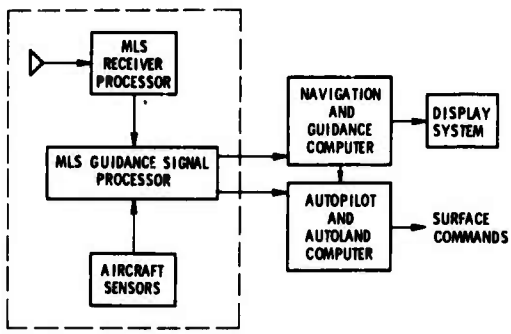

Figure 5 MLS Integration with TCV Airplane

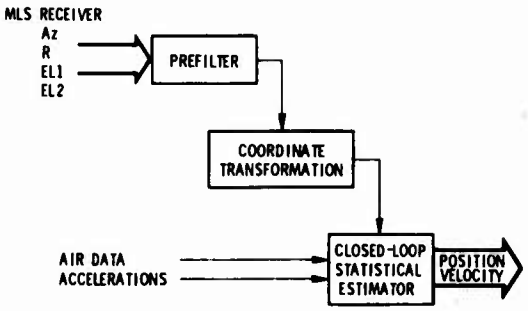

Figure 6 Major Functions of MLS Processor

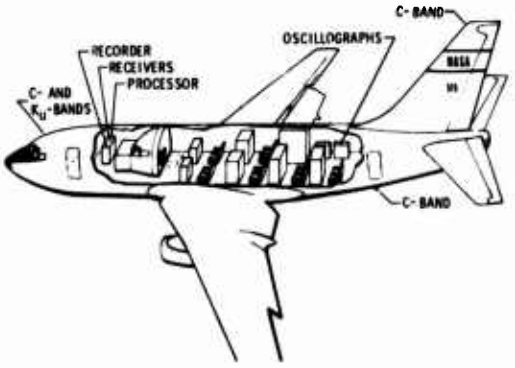

Figure 7 NASA TCV B-737 Research Airplane (Internal Arrangements with MLS)

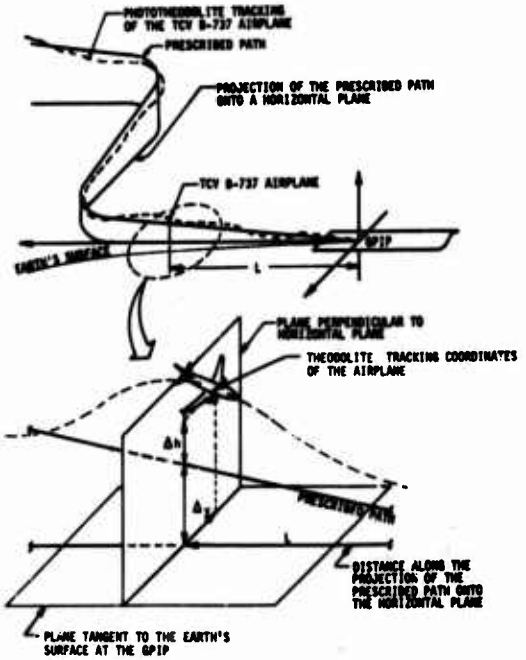

Figure 8 Definition of L

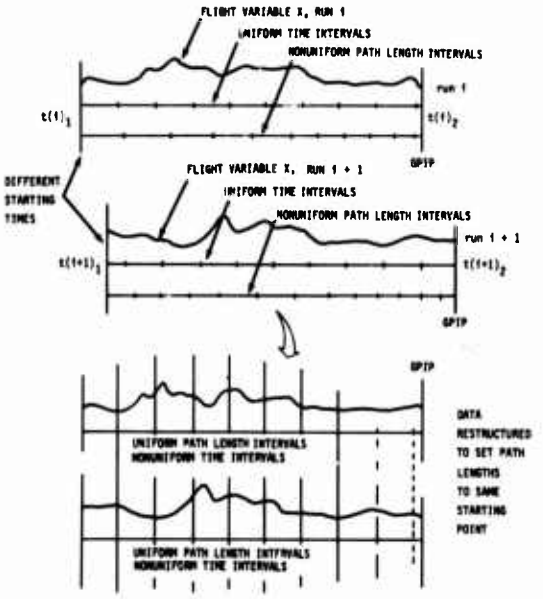

Figure 9 Flight Data Transformation from Time to Path Length and Subsequent Restructured Data Array

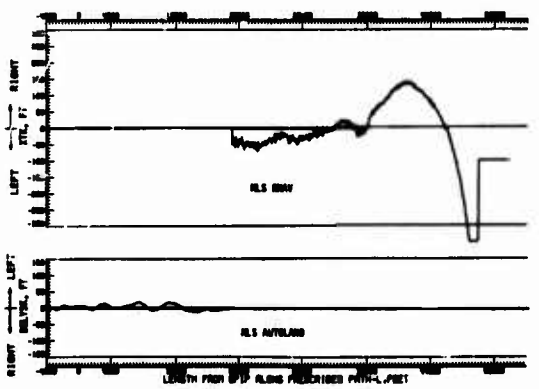

Figure 10 L - History Plots of XTK and DELYSK, Flight 122 Run A5

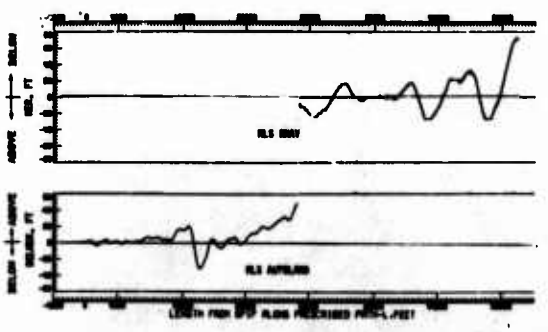

Figure 11 L - History Plots of HER and DELHSK, Flight 122 Run A5

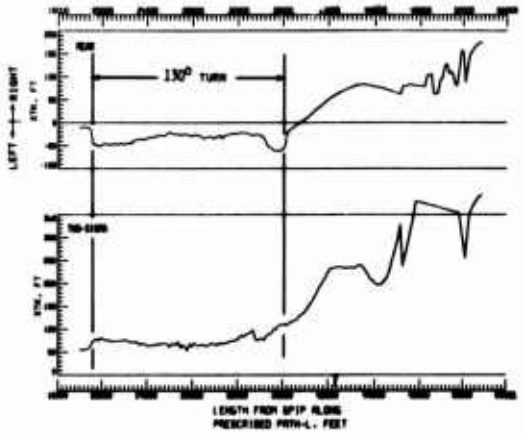

Figure 12 XTK, Mean and Two-Sigma Statistics, 130 Deg Turn Approach

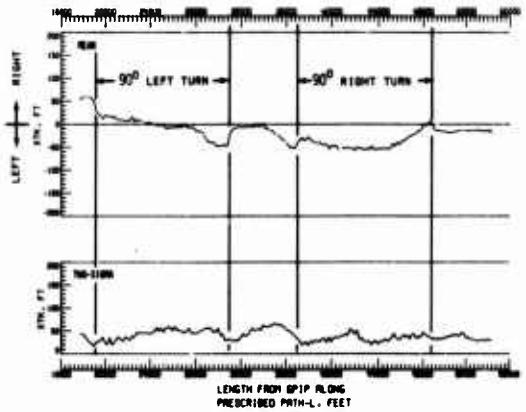

Figure 13 XTK, Mean and Two-Sigma Statistics, S-Turn Approach

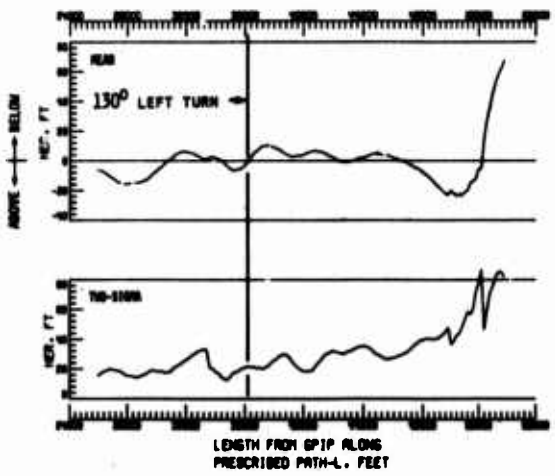

Figure 14 HER, Mean and Two-Sigma Statistics, 130 Deg-Turn Approach

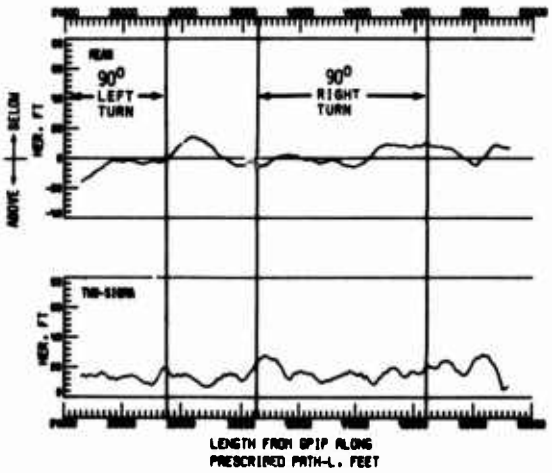

Figure 15 HER, Mean and Two-Sigma Statistics, S-Turn Approach

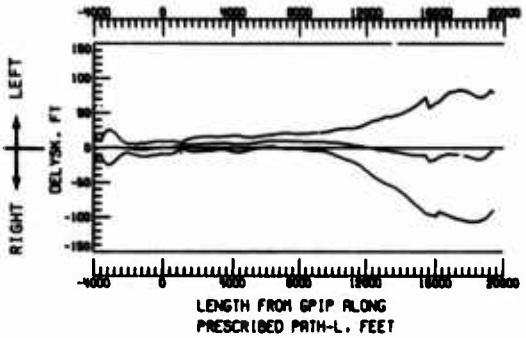

Figure 16 DELYSK, Mean and Mean ± Two-Sigma Statistics, Final Approach

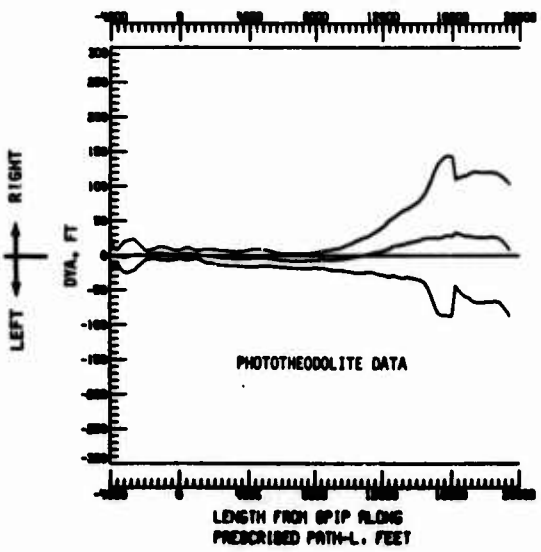

Figure 17 DYA, Mean and Mean ± Two-Sigma Statistics, Final Approach

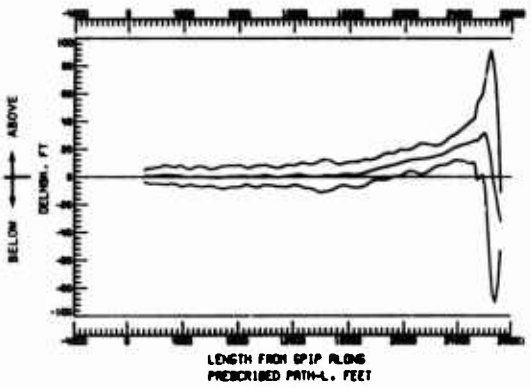

Figure 18 DELHSK, Mean and Mean ± Two-Sigma Statistics, Final Approach

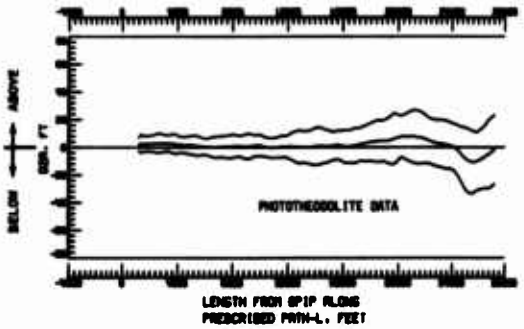

Figure 19 DZA, Mean and Mean ± Two-Sigma Statistics, Final Approach

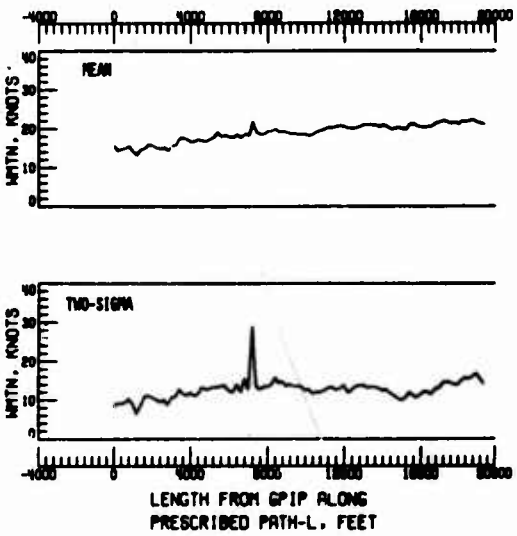

Figure 20 WMTN, Mean and Two-Sigma Statistics, Final Approach

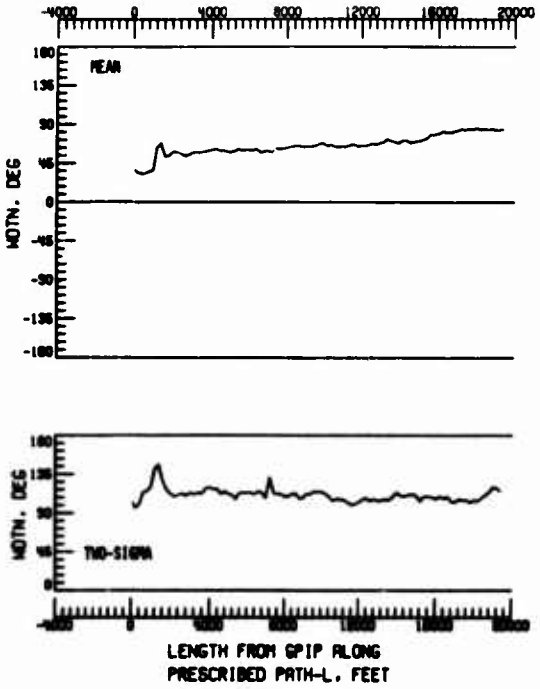

Figure 21 WDTN, Mean and Two-Sigma Statistics, Final Approach

ACCURATE TIMING IN LANDINGS THROUGH AIR TRAFFIC CONTROL

by

Marc PELEGRIN
Director of the 'Ecole Nationale Supérieure de l'Aéronautique et de l'Espace',
and of the 'Centre d'Etudes et de Recherches de Toulouse'
Boite Postale 40 25, 31055 TOULOUSE CEDEX, FRANCE

and

Nicole IMBERT
Engineer at the 'Centre d'Etudes et de Recherches de Toulouse (C.E.R.T.)
Boite Postale 40 25, 31055 TOULOUSE CEDEX, FRANCE

ABSTRACT

In order to increase the accuracy of the landing time, this paper proposes corrections of speed and heading to be made during the approach of the aircraft. Numerical simulations including instrumentation, localization, navigation errors and wind have been performed for four different aircraft on four approach trajectories. The comparison of the results of 200 simulations in each case,with and without the corrections, points out the improvement of the accuracy of the landing time due to these corrections. Flight tests also have been made on commercial flights and the result of these tests is included.

1. INTRODUCTION

In a previous paper [1] given at the AGARD Symposium on Plans and Developments for Air Traffic Control Systems (Cambridge, Massachusetts, May 1975), a method for increasing the rate of landings of aircraft was explained; shortly, it consisted in controlling the velocity and the heading of the aircraft while descending three times between the TMA entry and the ILS gate which has been chosen at 3 000' on the glide. It was then forecast that as soon as the plane entered into the TMA, a landing time was assigned to it and the three commands radioed to the pilot helped him to reach the gate at the proper time. The main object of the 1975 paper was to determine a policy of control which could be implemented within the present state of the art, without any modification, either on board or on ground control station, except a slight increase in the computer load ; the types of mathematical models of plane that had to be used in the computers and the type of numerical data to fill in when the plane entered the TMA were also anticipated.

The purpose of this paper is to compute the estimated accuracy which can be expected with such a control and give the results of some flights which have been performed on commercial planes of regular lines, i.e with planes and ground control Centers as they exist now without any additional equipment.

The studies about the optimal model have been completed and improved. The optimal model is such that :

a) it is of the lowest order

b) the errors in distance at the end of a 21 km trajectory (case of one path in Orly TMA) is a part of the width of the ILS entry gate. It is recalled that for most of ILS beams, the linear width of the localizer is 640 m (± 320 m) for the linear zone (± 1.8°) and 3 600 m (± 1800 m) for the wide capture zone (± 10°). In the previous paper, we compared a high order model (16th order) (that of the Mystère 20 - Falcon 20 - equipped with a Tapir automatic pilot) with a collection of degraded models up to the simplest first order model that is :

$$\dot{\psi} = \frac{g}{V} \operatorname{tg} \phi_c$$

where ψ is the heading of the a/c and ϕ_c the roll angle. It was shown that between the highest order model and the simplest one, the error was 340m (on the reference - path trajectory in the Paris - Orly TMA the length of which is 21 068m), i.e. about 50% of the linear zone of the ILS beam.

This work was supported by the Service Technique de la Navigation Aérienne under Convention STNA 3/75/3B Clauses 6987 : "Etude de la précision de Navigation en zone terminale d'aérodrome"

2. OPTIMAL MODEL ADOPTED

These computations have been considered because they are at the heart of the problem. Two hundred simulations will be computed for each of the 4 aircraft considered and the 4 trajectories. A too high order model will lead to unnecessary computer time, a too-low order model will lead to unacceptable errors.

To reach the best trade off, and on behalf of the previous studies [2] we start from a complete non-linear model (model n° 1) including longitudinal and lateral coupling. It is a 18th order model (between a roll command ϕ and the X Y Z motion of the plane). We then consider a 8th order model at constant speed (no coupling between longitudinal and lateral motions) and finally a 3rd order model which does not take care of the dynamic of the plane during a roll motion (see Table 1)

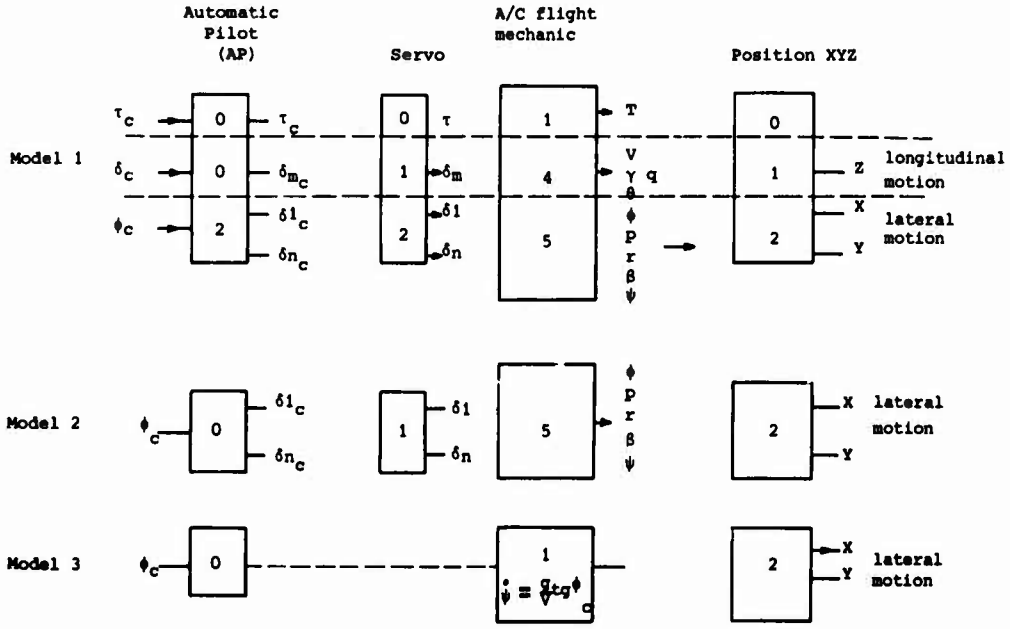

TABLE 1

The tests were conducted over 4 procedures :

a. a roll sequence made of 3 time-slots of 15, 50 and 30 s duration with gradient of 4°/s

b. a heading sequence represented by :

360° during 10 s)
330° during 65 s)
220° during 75 s) made by the A.P. according to $\phi_c = K (\psi - \psi_c)$
150° during 80 s)

c. a navigation with VOR/DME represented by :

. initialisation at heading 360°

. capture of a 315° radial (VOR at a distance of 80 km)

. capture of a 225° radial (VOR at a distance of 40 km)

. capture of a 150° radial (VOR at a distance of 15 km)

d. navigation along real approach routes

These routes called C_1, L_1 (C for short trajectories, i.e 54 km - L for long trajectories, i.e 120 km) will be defined later (see paragraph 4)

The results are summarized in Table 2 (next page).

Then the adopted model is defined by the following equations :

- in the vertical plane at constant heading :

$$\frac{1}{2} \rho S V_a^2 C_z = mg \cos \gamma - F \sin (\alpha + \omega) - m V_a \frac{d\gamma}{dt} \quad \text{(lift)}$$

$$\frac{1}{2} \rho S V_a^2 C_x = F \cos (\alpha + \omega) + mg \sin \gamma - m \frac{dV_a}{dt} \quad \text{(drag)}$$

$$\dot{z} = V_a \sin \gamma + V_{vz}$$

- during a turn :

$$\frac{1}{2}\rho S V_a^2 C_z = mg\frac{\cos\gamma}{\cos\phi} - F\sin(\alpha+\omega) - m V_a \frac{d\gamma}{dt}$$

$$\frac{1}{2}\rho S V_a^2 C_x = F\cos(\alpha+\omega) + mg\sin\gamma - m\frac{dV_a}{dt}$$

$$\dot{\psi} = \frac{g}{V_a} tg\phi$$

$$\dot{x} = V_a \cos\psi\cos\gamma + V_{vx}$$

$$\dot{y} = V_a \sin\psi\cos\gamma + V_{vy}$$

the following notations have been used :

ρ : air density

S : surface of reference

V_a : aerodynamic velocity

V_{vx})
V_{vy}) wind component on the 3 axis
V_{vz})

C_x)
C_z) coefficients (function of the angle of attack)

ω : engine setting angle

γ : slope

F : thrust (total)

m : mass of a/c

ϕ : roll angle

ψ : heading

These equations suppose known the drag-lift curve of the plane, the thrust-consumption curve of the engines, and the characteristic of the real atmosphere.

	test 1 ϕ_c sequence	test 2 ψ_c sequence	test 3	test 4	
				short trajectory	long trajectory
Length of trajectory	17 km	17 km	17 km	54 km	120 km
Time flight (w/model n°1)	230 s	230 s	230 s		
errors between models n° 1 - 2	500 m	50 m	50 m	Long.error : 70 m Lateral error : 50 m	long. error: 40 m Lateral error : 10 m
errors between models n° 1 - 3	1 250 m	460 m	250 m	Long.error : 200 m Lateral error :170 m	Long. error: 30 m Lateral error : 50 m

TABLE 2

(Note : These comparisons have been made in standard atmosphere. It is assumed that errors due to variations of atmosphere parameters are of the second order and do not modify the conclusions)

3. ATMOSPHERE MODEL

This is a very important point; all the previous data concerned the a/c with regard to the air, whereas the problem concerns the motion of the plane with regard to the ground. Many parameters depend on the local air density, temperature and pressure, some of them are sensitive to the hygrometry of the air and all the data collected on board are linked to these local parameters. A good atmosphere modelisation needs three phases :

1) the standard atmosphere model
2) the modelisation of the real atmosphere with regard to the standard atmosphere
3) the modelisation of the motions of the real atmosphere with regard to ground (winds and turbulence)

It is recalled that the standard atmosphere assumes that : the air is dry, the sea level pressure is 1013.25 mb and the temperature 15°C; the temperature gradient is -6.5°C/1000 m up tc 11 000m; above, the temperature is constant : -53°C. These models are worldwide utilized.

In this paper, we modelize the real atmosphere by introducing three variables modifying the standard atmosphere :

- the ground pressure on the runway from which a sea level standard atmosphere is computed
- the deviation from standard temperature
- for computation of temperature at flight level, it is assumed that the temperature gradient is the same in real and standard atmospheres.

The wind is basically represented by a fixed vector (of random direction and speed between $\pm$ 10 kts) to which a random vector is added. The two components of this vector are supposed gaussian with a σ of 10 kts and a correlation time of 600 s. No vertical component is considered. It is worth to note that the winds which are introduced in the simulations of approaches have a "fixed vector" belonging to a random space.

4. ROUTES CONSIDERED

The trajectories are defined by their ground projection and constraints on the height of the plane. Four ground tracks have been considered [3] :

- two long trajectories L1 and L3 with entry level of :

  190 for B 707
  210 for B 747 TMA Orly (see Fig. 1)

- two short trajectories C1, C3, the starting point being the exit of the stacking of Melun at flight level 70

Altitude constraints are : Z = 3 000' at point C
Z = 4 000' at point D

The simulations have been made :
- on trajectories L1 and L3 for B 747 and B 707
- on C1 and C3 (injection in A) for B 727 and N 262

In this paper, only the results obtained on trajectories C1 and C3 are commented.

For each plane, the currently used descent trajectories have been considered for the simulations.

For example, in the case of the B 727, on trajectory C1, the basic computations have been made with the following assumptions (Fig.2) :

- standard atmosphere
- aircraft mass at entry point 65T
- flight level 50
- entry speed 250 kts
- procedure :
  - flight along 360 MEL (VOR "from")) flight level at constant CAS
  - constant heading 308) descent at constant CAS - Residual thrust up to 3 000 ft
  - capture of 76.3 of OL)
  - flight along 76.3 of OL) level off, deceleration up to 170 kts with 15° flaps at 220 kts up to glide interception at 3000 ft

5. MODELISATION OF ERRORS DURING THE SIMULATED FLIGHTS

Six types of errors have been considered, the two first are due to the pilot when he is fully responsible of the flight plane, the three last one are due to the ground controllers when they interact with the pilot to monitor the navigation in the terminal area, the last one is the error made on meteorological conditions estimation.

5.1 - Errors resulting from the control of the a/c

They are :

- a standard deviation σ of 3 kts is assigned to the prescribed velocity

- the error on the slope is proportional to the slope angle with a σ of 0.125° in level and a σ of 0.50 for a 5° slope

- a σ of 75 feet is assigned to the altitude

5.2 Errors due the on-board navigation instruments :

- for a constant heading on a VOR the error has a σ of 1.15° and for segment at constant heading not pointed on a VOR, an error of 1° for σ has been introduced in the heading

- for the ILS, we take 0.2° at σ

- for the DME, we take 0.1 NM at σ

5.3 Error attached to the moment of injection in the terminal area

Assuming that the arrival of the plane in the TMA is known a few minutes ahead, we take a precision of 10 s at 3 σ for the injection time

5.4 Error of location of the plane with regard to the ground grid reference

The error is supposed isotrope and constant along the trajectory 0.25 NM at 3 σ

5.5 Error due to the reaction time of the pilot

We consider the time elapsed between the moment at which the controller has a correct measurement of the position of the plane and the moment at which the pilot reacts to the command transmitted by the controller to the crew after the computation of this order.

A constant delay of 20 s to which a random delay of $\pm$ 10 s at 3σ is added takes care of the time for computation, time for transmission and time before the pilot reacts.

5.6 Errors due to the wind

The winds indicated by the Meteorology are injected in the computer as a first approach; errors are attached to these basic data. They are :

- a constant error along the trajectory with a random direction and a velocity uniformly distributed between - 10 kts and + 10 kts
- two variable components along the two axes, with a zero mean value, a deviation of 10 kts at 3 σ and a correlation time of 600 s.

- In the simulation, the meteo wind is supposed null.

6. PROPOSED CONTROL PROCEDURES

The basic assumptions are :

- the corrections, if necessary, are computed by the ground equipments because the prescribed trajectory is known and assigned by the ground controller staff

- the data are transmitted by the normal VHF (voice channels)

- due to the occupancy of the frequencies allowed to the ground Control, we assumed that only three reset commands can be radioed during the approach, the duration of which is of the order of 250 - 350 s for short trajectories C1 or C3 and fast a/c (330 - 500 s for turboprop. slow planes) or 500 - 700 s for long trajectories (4 or L3) and fast a/c.

- the resets must be easy to realize, i.e they can concern only corrections in velocity (with a threshold of 3 kts) or corrections in heading (with a threshold of 1°)

For the best accuracy, on the expected time of arrival and easy control of the a/c we suggest that the 3 corrections be distributed as follows :

- a velocity correction during the level flight at the entry of the terminal zone

- a velocity correction during the descent

- a heading correction in level flight prior to the ILS capture

These corrections are referred to moments counted from the time of entry in the zone of the a/c; then, if an error is noticed at the time of control, the flight profile including these corrections is as follows (Fig 3.)

- acceleration (or deceleration) from the nominal speed V_N to a new speed V_1, computed by using the mathematical model of the plane for which the actual parameters have

been injected in the computer.

- level flight at V_1

- descent at V_1 with idle thrust down to 3000 feet on C_1 (or 4000' on C_3)

- deceleration in level flight up to point X at 230 kts

The chart $t(\Delta V_i)$: time to accelerate from V_N to V_i, descent at V_i, deceleration from V_i to V_F and the chart $d(\Delta V_i)$ giving the distances have been modelized by polynomial expansions of the 4th and 3rd degree, respectively.

If the correction is equal or inferior to 3 kts, the controller does not transmit any correction.

For the second velocity correction, it is necessary to take into account both the longitudinal error and the altitude error - Again, the functions $t(V_2,V_1,h)$ and $d(V_2, V_1,h)$ are represented by polynomial expansions (3rd degree). The new profile of descent is then as shown in Figure 4.

For the heading correction, the longitudinal and the lateral errors are taken into account. If d_1 and d_2 (Figure 5) are the projections along the ILS beam and along the nominal trajectory, the heading correction $\Delta\psi$ to be assigned is derived from :

$$\Delta t = f_1 (\Delta\psi, d_1) + f_2(\Delta\psi, d_2)$$

with f_1 parabolic in $\Delta\psi$

f_2 linear with $\Delta\psi$

The correction must be lower than 15°

Fig. 6a and 6b indicate the times of corrections in roman figures (I,II,III) and the measurement points on the route profile and height profiles (1,2,3,4,5) for one of the plane simulated (B 727) of one of the trajectories (C_1)

7. RESULTS OF THE SIMULATIONS

For each type of the a/c and each approach trajectory, 200 simulations have been computed : with the various errors described above, the dispersion of the time of arrival results from these 200 cases [4]

The deviation σ has been computed for the 5 points indicated at Fig. 6. These points are always the same for the different types of planes. Points 1,2,3 and 4 are fixed with regard to time, point 5 is a geographical point located at 3000 ft on the glide. Point 1 is 20 s after the forecast time of entry of the plane, into the TMA. Point 2 is located after the first velocity correction, point 3 after the second correction. Point 4 is the point named X in paragraph 6; in this point, the fast a/c are supposed to be at 230 kts and the slow a/c (N 262) at 150 kts.

For each point, the distribution of errors in altitude, velocity, heading, position (longitudinal and transversal) are represented. For point 5, the longitudinal error is represented by the dispersion of the time of arrival.

It would be tedious to give the results of all planes considered and the 4 trajectories.

Below, one case (B 727 on trajectory C_1) is partially represented :

- Table 3 indicates the σ for the above parameters in points 1 to 5

Point	Altitude	Speed	B.727 on C_1 Heading	lateral error	Longitudinal error
1	0.2 m	2.9 kts	0.6 °	21 m	460 m
2	37 m	8.7 kts	0.8 °	36 m	365 m
3	36 m	10. kts	6.8 °	204 m	528 m
4	9.9 m	5.3 kts	11.3 °	368 m	515 m
5	17.6 m	3 kts	9.1 °	391 m	251 m(242.5) 9 s = 810 m

Table 3

-In each case, σ of the recorded error is indicated
- At point 5, for the longitudinal error, the following additional parameters are indicated:
  - average time in seconds
  - between brackets, the nominal time
  - σ in seconds and its equivalence in distance

- Figures 7, 8, 9, 10 and 11 give the deviation in point 5 only for the above parameters.

8. FLIGHT TEST

In order to verify in flight the results obtained by simulation, two series of measurements were effected during regular flights, thanks to the collaboration of the on-board officer M. Leluc.

For the first series, the following trajectories had been chosen :

Toulouse/Bordeaux	(IT 7030)	06.45	07.25	)
Bordeaux/Roissy	(IT 7030)	07.45	09.00	)
Roissy/Bordeaux	(IT 039)	09.35	10.45	) 16 March 1977
Bordeaux/Toulouse	(IT 039)	11.00	11.35	)

Flights were made on Caravelle III (F-BNKJ), an aircraft for which the mathematical model was not available. We therefore decided to simulate on Caravelle III the B 727 descent conditions for which simulation tests had already been made.

To that effect, we defined a descent rate(ft/mn) as a function of descent speed and level. The on board mechanical engineer had therefor a table, an extract of which is given below:

levels	Speed = 270	260	250	240	230
150	2023	1917	1820	1735	1659
140	2005	1899	1802	1716	1640
130	1986	1880	1783	1696	1620

Table 4

The pilot kept constant the speed by acting on the slope; the mechanical engineer set the descent rate in terms of the Table by acting on the throttle.

A special authorization had been requested to the ground controllers before the TMA entry in order to release the a/c of other traffic constraints.

The OK for descent and the two corrections during flight were given by a person (one of the authors) located behind the pilot viewing directly the DME indicator, the anemometer and having a chronometer.

Tables established for a quiet atmosphere allowed to give the necessary corrections to be made to the pilot (the wind corrections were made later on according to the meteorological forecasts and ground local meteorology) the extracts of which are given in the following paragraphs.

For the second series of measurements effected on the 24th June, the same trajectory had been kept but to avoid the simulation of a B 727 on a Caravelle (with on-board passengers), it was decided to make a rough longitudinal model of Caravelle III.

The same procedure was followed : during approach, the pilot maintained a full-reduced speed (the mechanical engineer was not acting); the OK for descent and the 2 corrections were given to him by a person (the other author)in terms of the DME, the anemometer and the chronometer.

On the whole, these two series of flight, after corrections due to the wind, have given almost similar results to those computed despite the difficulties of setting the descent rate and the rather simplified computations (if compared with the ones made for the N 262, B 747 and a B 727) in the second series of flights.

With respect to the first series of measurements, a few details are given below on two trajectories (short ones requiring only two corrections) :

- the first one is the Toulouse Bordeaux flight for which the 1st correction was made on speed and the second one on heading
- the second one was the Bordeaux Toulouse flight for which the two corrections were made on speed.

Analysis of the Toulouse/Bordeaux flight :

a. Meteorological conditions : QNH 1017 mb
Winds 20.000 ft 180-200° 40-45 kts
Ground 160° 10-12 kts

b. Landing runway in service : 23

c. Forecast procedure : all distances are counted from the Bordeaux DME (114.4 MHz)

- Setting of descent : level : 160 - 31.1 NM
  " 150 - 28.5 NM
  140 - 25.9 NM

- Point of Entry in TMA : t = 0 located at 25.9 NM; then arrival forecast at t = 455 s (7'35"") at point Z = 3 000' on the glide

- First set-up at t = 58 s : set-up of speed
  nominal distance : 23.1 NM
  - if the real distance is :

    22.5 22.9 23.1 22.3 21.6

  - then take (kts)

    270 260 250 240 230

- Second set-up at t = 133 s (2'13"") : resetting of heading
  - initial heading : 345°
  - speed : 270 - nominal distance 21 NM

real distance	19.8	20.4	21	21.6	22.2
new heading	330	338	345	352	360

  - speed : 260 - nominal distance 20.9 NM

real distance	19.7	20.3	20.9	21.5	22.1
new heading	330	338	345	352	360

  - speed : 250 - nominal distance 20.8 NM

real distance	19.6	20.2	20.8	21.4	22.0
new heading	330	338	345	352	360

  - speed : 240 - nominal distance 20.5 NM

real distance	19.3	19.9	20.5	21.3	21.7
new heading	330	338	345	352	360

  - speed : 230 - nominal distance 20.2

real distance	19	19.6	20.2	21	21.4
new heading	330	338	345	352	360

d. Flight development

The a/c reached the TMA entry at level 140 to 350 kts with a mass of 38.12 T; the OK for descent had been given at 25.9 NM.This point agreed also with the TMA entry, t = 0 of time reference (local hour 07 16 58). The ETA (estimated time of arrival) (3000' on the glide) was 7'35".

At t = 58 s, the a/c was exactly at 23.1 NM (as to DME precision) so no correction was necessary (speed was kept at 250 kts)

At t = 133 s, the real distance was 21.4 NM. The heading 352 was given to the pilot.

The a/c, after lining up with the ILS, was 3000' up at 07 24 30, i.e 7'42" after the TMA entry.

Correction due to the wind

The meteorological forecast was indicating an altitude wind of 40 to 45 kts (180 - 200)

The a/c was at 07:14 at Sauveterre's beacon. It had therefore received a 3/4 behind wind whose axis component was about 28 kts for about 250 seconds.

Then, it received a front wind at 45°/55° on the left.

After computation, it was estimated that the net gain of time was about 20".

The correction on the a/c load (38.12 T) did not seem to be of great importance on this approach (it was less than 5")

Finally, the analysis of the on-board recorder had shown a good stabilisation of the descent rate but some fluctuations on the speed (- 5, + 1 kts) around 250 kts; then, after correcting the heading (352 instead of 345) a slight decrease of the average speed was observed : about 242 kts to which a slightly greater oscillation of about ± 5 kts had always to be added. Then the a/c had lost about 2% of the total time, i.e about 9 seconds with reference to the prescribed time.

To conclude, we will say that the excellent rough coincidence (7'42" for 7'35") stated) must be brought back to an error of about 18 s (7 + 20 - 9) for a nominal time flight with all corrections made of 7'55", i.e 475 s (3,79%)

Analysis of flight on Caravelle FBNKJ (flight IT 039 Bordeaux - Toulouse on 16.03.77)

a. Meteorological conditions : QNH 1020 mb - clear sky (CAVOK)
winds : 20 000ft 180-200° 20 kts
Ground : (at landing) 140° - 14 kts

b. Landing runway in service : 15

c. Forecast procedure : all distances are counted from the Toulouse DME (117.7 MHz)

- setting of descent : level 160 - 44.9 NM
150 42 NM
140 39.2 NM

250 kts had to be kept

- point of entry in the TMA : t = 0 located at 36.6 NM
then arrival forecast at t = 404 s (6'44") at point Z = 3 000'
on the glide

- 1st resetting at t = 100 s (1'40") set-up of speed

Nominal distance : 28.4 NM

- if real distance is	29.1	28.6	28.4	27.5	26.4
then take	270	260	250	240	230

- 2nd resetting at t = 194 s (3'14") : set up of speed

Speed : 270 kts - Nominal distance : 21.8

- real distance	21.8	21.5	21.1	20.9	20.7
new speed	270	260	250	240	230

Speed : 260 kts - Nominal distance : 21.4

- real distance	21.8	21.4	21.1	20.7	20.4
new speed	270	260	250	240	230

Speed : 250 kts - Nominal distance : 21

- real distance	21.8	21.4	21	20.6	20.3
new speed	270	260	250	240	230

Speed : 240 kts - Nominal distance : 20.6

- real distance	21.6	21.3	21	20.6	20.1
new speed	270	260	250	240	230

Speed : 230 kts - Nominal distance : 20.1

- real distance	21.3	21.1	20.9	20.5	20.1
new speed	270	260	250	240	230

d. flight process : without entering into details, let us say that the a/c was at level 150. The OK for descent was at 42 NM. Entry in TMA was at 36.6 NM (reference time t = 0), then ETA = 404 s (6'44") later. The 1st set up at 100 s brought the speed to 255 kts. The 2nd set-up at 194 s (3'14") brought the speed to 245 kts. The a/c was at the rendez-vous point (3000' on the glide) 6'40" after the point of reference t = 0

The wind corrections and lack of holding speed (recorder) lead to a 12" error, i.e 2.97% (it is to be noted that this was the fourth flight test made by the same aircrew : the operating process was better especially the simulation of B 727 on Caravelle III used for these flights)

e. Analysis of other flights : they have given similar results, the error being included between 3 to 4.2%. When writing this paper, the flight tape recordings on 24th June flight were not yet available, therefore not allowing a precise analysis. The rough results remain coherent with the previous ones and show a slight improvement (2.5 to 4%), that is, of course, if the tape recordings confirm this.

9. COMMENTS AND CONCLUSIONS

In the previous study, when neither error was introduced in the wind nor in the time of injection, the dispersion for a B.727 on C_1 was 28 seconds. After the three corrections, it amounted to only 9 seconds in spite of the additional errors introduced (injection time and wind)

We have noticed that the average time of arrival was a little delayed with regard to the nominal time : the corrections increased the average duration of an approach of about one sigma. The results were about the same for aircraft of same velocity.

To analyze in detail the influence of the wind and the influence of the delay between the time at which the measurement had been made by the controller and the time at which the pilot reacted, two additional series of simulation had been performed (B. 727 on C3). The conclusions were that the arrival time was not perturbed. Without wind, the duration of the approach was 341 s, with a σ of 7 s (instead of 6.7 s). Some results (343 s instead of 341 s; σ of 7.5 s) were obtained when no delay was introduced in the simulations.

This means that the main cause of dispersion on the arrival time is the velocity control and its follow-up by the pilot : simulations have shown that the dispersion could be divided by 3 when corrections are accepted on a precast manner during the approach (3 corrections); two sets of flights with regular commercial planes have shown that the order of magnitude of the errors computed was correct though the flight conditions were not ideal (the SE 210 - Caravelle - was not modelized; its descent was adjusted like the one of a B 727)

This type of control made of 3 resets during the approach could be implemented soon because it doesnot need any additional equipment. It is an intermediary step before the automatic data link air to ground and ground to air appears .

10. REFERENCES

[1] M. PELEGRIN : "Navigation 4D en zone terminale considérée comme un problème d'Automatique" AGARD, 1975

[2] M. CLIQUE, J.B. FILLEAU and al : "Etude de la précision de navigation en zone terminale d'aérodrome" - Rapport préliminaire 1 a/7101 DERA-CERT - Nov. 1975

[3] N. IMBERT, J.B. FILLEAU, A. FOSSARD : "Etude de la précision de navigation en zone terminale d'aérodrome" - Rapport principal intermédiaire n° 7101/2 RA - CERT - July 1976

[4] N. IMBERT, A. FOSSARD, B. LOTH : "Etude de la précision de navigation en zone terminale d'aérodrome" - Rapport final n° 3/7101/DERA - CERT - May 1977

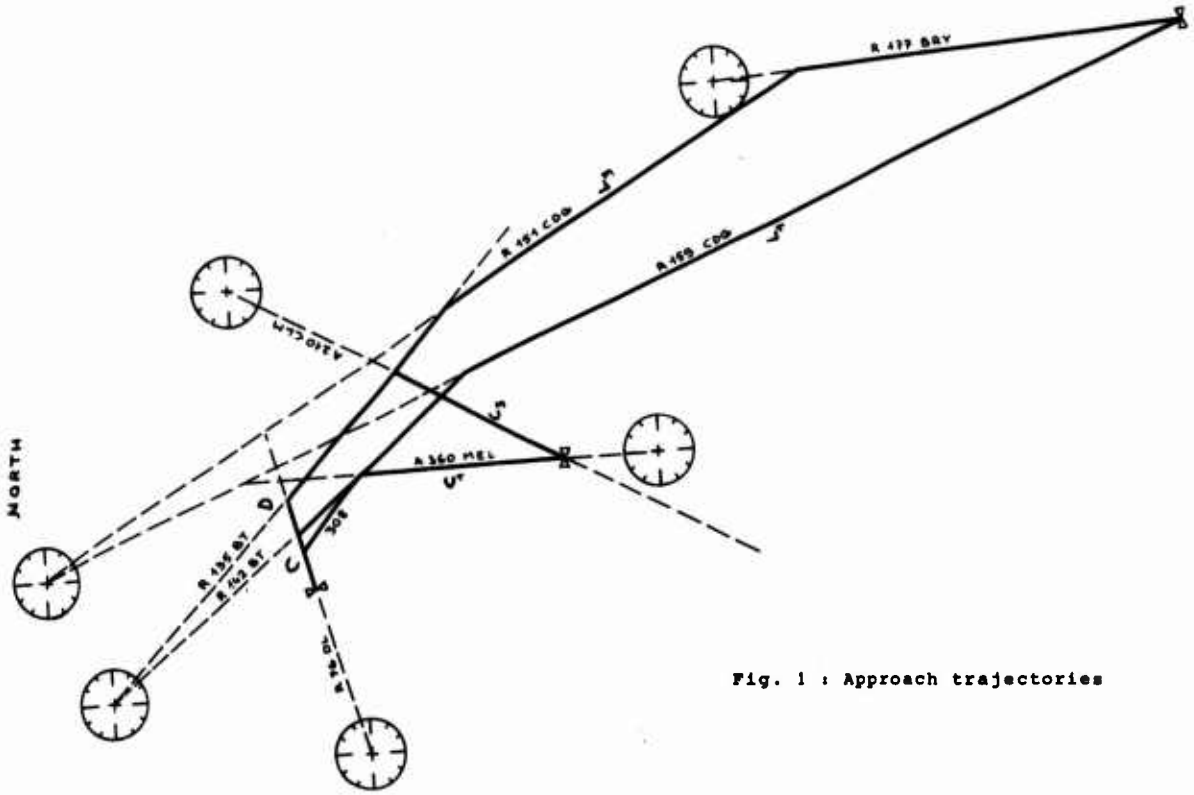

Fig. 1 : Approach trajectories

Fig. 2 : Flight Procedure of a B 727 on trajectory C1

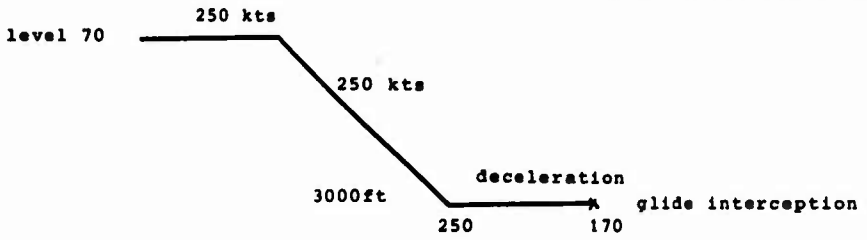

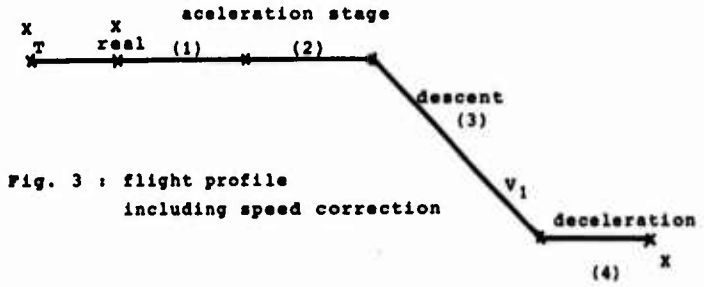

Fig. 3 : flight profile
including speed correction

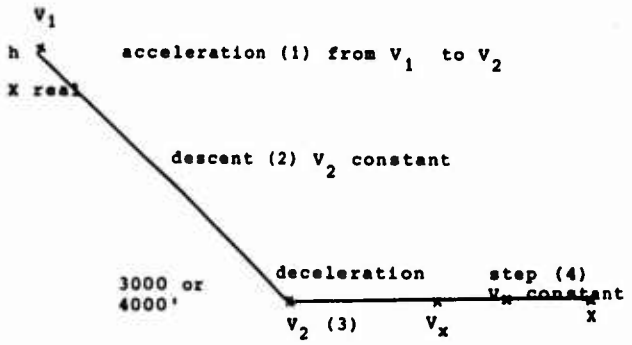

Fig. 4

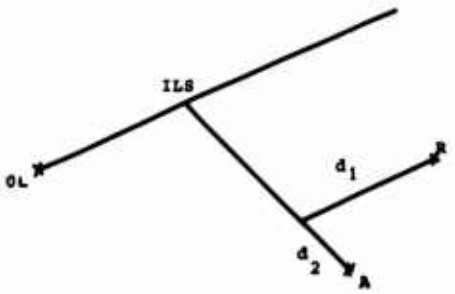

Fig. 5 : Definition of longitudinal and lateral errors for heading correction
A : theoretical position
B : real position

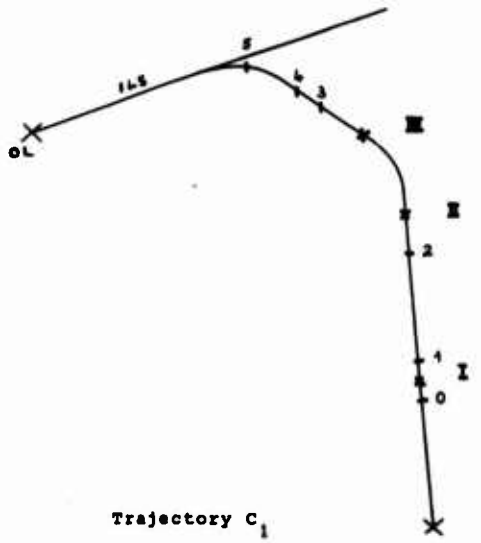

Trajectory C_1

Fig. 6 a : correction points (roman figures) and measurement points

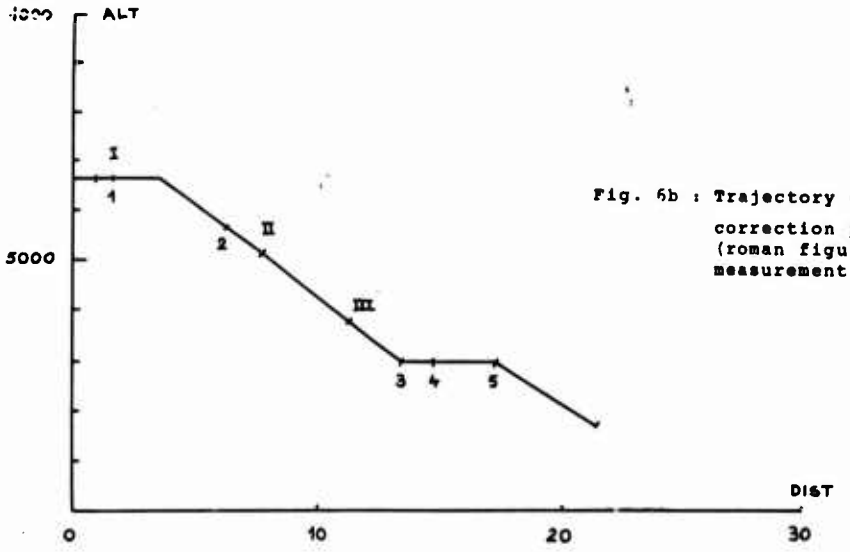

Fig. 6b : Trajectory C_1
correction points
(roman figures) and
measurement points

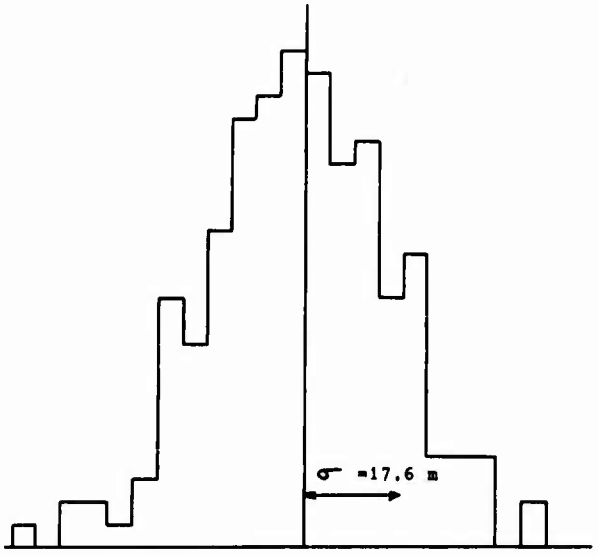

Fig 7 : Altitude deviation at point 5

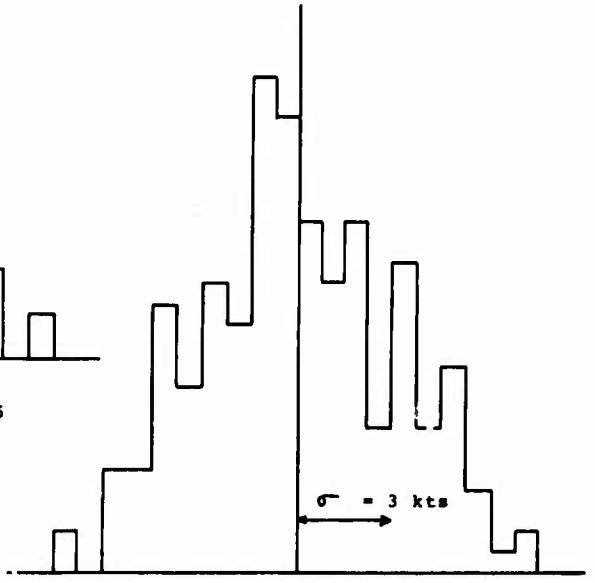

Fig 8 : Speed deviation at point 5

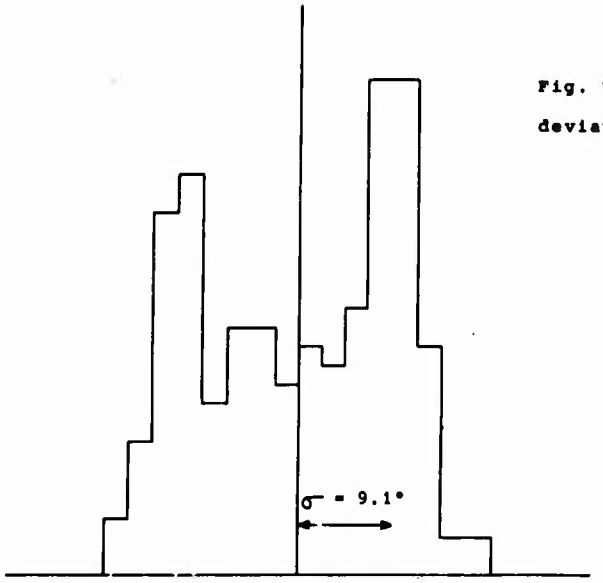

Fig. 9 : heading deviation at point 5

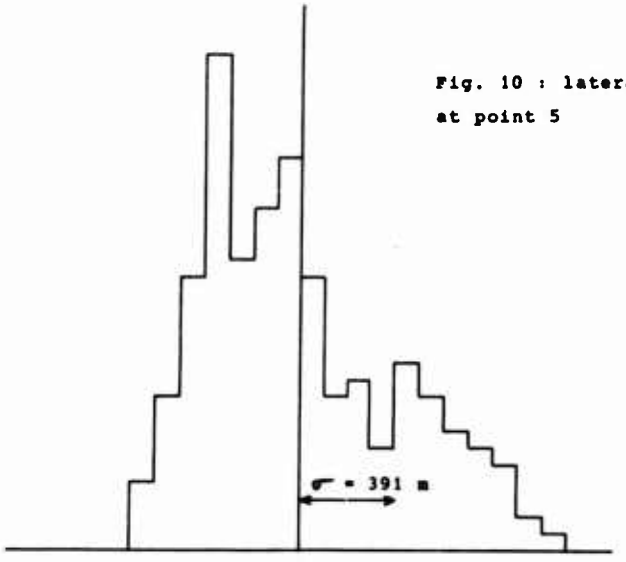

Fig. 10 : lateral deviation at point 5

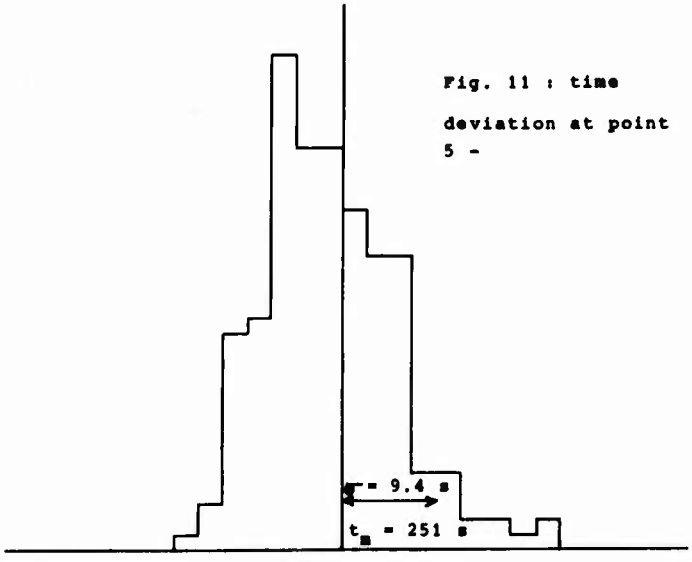

Fig. 11 : time deviation at point 5 -

PROPAGATION INTEGRITY FOR MICROWAVE INSTRUMENT LANDING SYSTEMS

Paul S. Demko
US Army Avionics Research and Development Activity*
Fort Monmouth, New Jersey 07703

SUMMARY

Testing at airfields at microwave landing system frequencies, using typical realistic multipath geometries and prototypical microwave landing system antenna radiation patterns, has indicated the existence of a multipath problem that must be reckoned with if our next generation microwave landing system, whatever it may be, is to provide the utmost in operational utility and safety. There is strong evidence to support a contention that the choice of the correct polarization is fundamentally the surest way to relieve our next generation precision approach and landing systems from the burden of unnecessary multipath signals. The data weigh heavily in favor of circular polarization.

*Formerly US Army Avionics Laboratory
US Army Electronics Command
Fort Monmouth, NJ

Now Part of US Army Aviation Research and Development Command
St. Louis, MO

INTRODUCTION:

Microwave landing systems require signals of the highest integrity if the utility and safety of the system is not to be compromised. It has become obvious through our multipath research over the last seven years that the microwave landing system environment, in spite of the advantages offered by higher microwave frequencies (when compared with ILS), is not a clean one. There will be, with few exceptions, difficult and unique multipath situations to cope with wherever microwave landing systems will be employed. Certain system design problems we will be able to solve in a straightforward manner. One phenomenon, ground lobing or ground multipath, can be controlled by proper antenna aperture size, height and tilt for any frequency or polarization. Also, the required airborne antenna coverage can likely be achieved with any polarization using contemporary designs and techniques. There is one adverse effect remaining, that is, multipath generated by vertical structures or obstacles on the ground. It is this problem that poses the single greatest challenge to microwave landing system designers and should compel these designers to take advantage of every possible means to reduce multipath effects to tolerable levels. The choice of the correct polarization to reduce multipath is fundamental. It is hoped that the evidence presented in this paper will aid in making that choice.

I. Rationale or Purpose for Performing Propagation/Multipath Research for Microwave Landing Systems

It was determined prudent to investigate, as throughly as possible, the extent to which microwave landing systems might be disturbed by multipath. It followed naturally that an investigation of the relative merits of signal polarization should be a priority part of such an investigation, to determine if one polarization or another could perform a useful role in reducing multipath interference to tolerable levels. A successful multipath investigation would provide the sound data base from which an informed choice of polarization could be made. Such a choice might determine whether or not the advantages inherent in our next generation microwave landing system could be utilized in a severe multipath environment.

II. Specific Objectives of Research Performed

The primary objective of the microwave landing system propagation research was to provide a comprehensive data base for aiding system designers to choose the correct system polarization. To produce such a data base, it would be essential to develop reliable techniques for performing "real world" multipath measurements at actual microwave landing system landing sites and to reduce the voluminous amounts of data from such measurements. If this could be accomplished, the tools would exist that would allow the system designers to make the correct polarization choice.

III. Technical Approach Selected and the Reason for its Selection

The approach selected to accomplish the stated program objective was not as straightforward as one might be led to believe from the stated objective. The first substantive test performed was a field test in which signals from a pulse modulated Ku-band landing system were reflected from an airport hangar door (Ref 1). This test was performed for two reasons: first to identify any multipath problem, if indeed a problem did exist, and second, to demonstrate, if possible, any differences in multipath intensity between vertical and horizontal polarization.

Results from this test indicated that the next logical step would be to determine and to catalog, in some quantitative manner, the reflection coefficients of various practical building materials for those grazing angles which might be encountered in real world multipath situations. This was accomplished by performing tests at Ku-band in an anechoic chamber (Ref 1).

Having now achieved some quantitative "feel" for the practical multipath physics and some "feel" also for the values of reflection coefficients for various building surfaces, it was next decided to see if multipath and polarization had any real significance in real, "live" microwave landing system precision approach situations. Flight tests were therefore conducted by the Army Avionics Laboratory at Lakehurst Naval Air Station, N.J., at Ku-band with a pulse modulated scanning beam landing system with horizontal and vertical polarization (Ref 1). For these flight tests the microwave landing system receiver processor was configured with video recording apparatus to record the beam envelope data and a strip chart recorder to document the quality of guidance data presented to the pilot's flight instruments. The United States Air Force has performed similar experiments at C-band using a vertically polarized doppler landing system at Wright Patterson Air Force Base, OH (Ref 2).

The principal reflecting surface for the Army's Ku-band flight tests was a large metal corrugated hangar wall. A site survey of civil and military airfields has revealed that a variety of corrugated surfaces is quite common in all sorts of civil and military airfield environments. Therefore, it was decided at this point in the research program to perform a rigorous analysis of the reflection properties of periodic surfaces at microwave frequencies (Ref 3, 4, 5). The analyses performed applied to all three system polarization possibilities, vertical, horizontal and circular and principally to system frequencies of C-band and Ku-band. The behavior of both the specular and space harmonic modes of reflection was thoroughly examined. Analysis was also performed for smooth dielectric surfaces (Ref 6).

In the preceding tests, the location of the multipath zones was predicted by assuming the simple ray theory of radio propagation and applying trigonometric techniques to the computation of the reflection geometry. This seemed to be quite reliable. In fact, through analysis and computational techniques developed during the study of periodic surfaces, even the location of the space harmonic reflections from corrugated surfaces could be predicted with great accuracy. However, to verify this procedure and to predict the behavior of microwave landing system propagation over runway humps or other such anomalies, an optical modeling experiment was performed (Ref 7, 8). The optical modeling was later expanded to physical millimeter wave radio frequency scale modeling of microwave landing system multipath effects at 70 GHz for both linear and circular polarizations (Ref 5). The principal reason for the 70 GHz tests was to obtain a manageable means of expanding the reflection coefficient data base for periodic surfaces and to verify the theoretical analysis of periodic surfaces performed earlier.

Up to now, no major consideration had been given to the use of circular polarization to reduce microwave landing system multipath effects. It seemed that there might be some merit to the use of circular polarization, particularly for reducing multipath reflections from smooth metallic surfaces. Therefore, the next major work unit accomplished was a detailed system analysis of circular polarization (Ref 9). This analysis, performed by Meyer Associates, Inc., under contract to the Army Avionics Laboratory, considered, in detail, circular polarization (CP) variables such as CP reflection coefficients, system degradation due to antenna ellipticity and the feasibility of practical ground and airborne circularly polarized antennas. During this analysis, a low speed computer technique was developed for determining the characteristics of reflections from composite surfaces for any form of polarization. As will be seen, this technique was later expanded into a high speed data reduction and simulation tool for determining the multipath signatures of landing areas serviced by a microwave landing system.

All of the preceding tests and analyses did, of course, produce a great deal of significant data, but, even more importantly, they provided the background required to finally attack, in earnest, the stated program objective. We were now prepared to conduct full scale microwave landing system multipath tests with realistic system geometries, polarizations and frequencies at operational airfields of the type that would most likely have a requirement for a microwave landing system. This was accomplished through a joint program between the US Air Force Flight Dynamics Laboratory and the US Army Avionics Laboratory with contractor support from the Illinois Institute of Technology Research Institute (IITRI) (Ref 10). The following measurement techniques were developed and used for this program: first, a necessarily precise method of performing physical surveys of candidate microwave landing system sites suitable for use with multipath analysis schemes; second, a method of performing short range static reflection coefficient measurements of airport structures; third, a method of performing short range dynamic reflectometry measurements of airport structures; and fourth, a method of performing long range, practical geometry multipath ratio tests with test antennas optimized to produce microwave landing system quality radiation patterns. Also, through this effort, the low speed computer technique, developed during the circular polarization analysis (Ref 9) was streamlined and expanded to operate as a high speed data reduction and simulation technique for determining the multipath signatures of airports to be equipped with microwave landing systems. With this joint effort, the techniques and data were produced so that the designers could justify a polarization choice (for whatever system evolved) on the basis of providing the cleanest signal in space.

IV. Highlights of Work Performed

Early microwave landing system multipath tests were clearly significant in that they demonstrated the existence of a multipath problem and provided some hints for the solution to those problems. Data produced has been used and corroborated by others such as the US Federal Aviation Agency and the U.K. Royal Aircraft Establishment (Ref 11, 12, 13).

The highlight of the overall effort was the joint US Army/US Air Force test program (Ref 10) which provided, with contractor support from IITRI and Guidance Systems, Inc. (GSI), an expanded microwave landing system multipath data base, a reliable technique for making multipath measurements at actual airfields, and an efficient computer technique for reducing multipath data and modeling of the multipath signatures of airfields. This technique has been tried and the initial results are encouraging. The computer program is in place, the program runs, and, so far, seems to generate valid answers. However, the technique does need to be exercised and validated. Nevertheless, the means have finally been made avail-

able for analyzing the real world microwave landing system multipath situation in a quantitative manner. This joint test program revealed two additional important facts: microwave landing system multipath from a supposedly benign airfield (WPAFB in this case) could indeed be severe and actual system siting could indeed be a problem as can be shown in the results which follow.

V. Results of Work Performed, Application of Results, and Problems and Difficulties Encountered

Overall, the results of the test program show a clear preference for the use of circular polarization, rather than either kind of linear polarization, to reduce microwave landing system multipath to tolerable levels. For linear polarizations, horizontal usually offers a significant advantage in terms of multipath reduction over vertical. The results show, further, that microwave landing system siting may not be as straightforward as initially expected because of multipath and that multipath could be much less severe with the use of Ku-band rather than C-band.

First indications of the superiority of horizontal polarization over vertical polarization in reducing the effects of multipath on microwave landing system performance were provided from the exploratory investigations, anechoic chamber reflection coefficient tests, and the Army Ku-band flight tests described earlier in part III (Ref 1). In an operational sense, the Army's Ku-band flight tests indicated that even a very simple receiver processor without sophisticated time gates or tracking filters would be able to perform successfully with horizontal polarization but not with more severe multipath from vertical polarization. Flight tests at Wright Patterson Air Force Base by the Air Force at C-band, described in part III, demonstrated that any microwave landing system, without sophisticated and reliable receiver processing, could fail completely because of severe multipath with vertical polarization (Ref 2). It is significant to note that this Air Force test was performed on an existing, active instrument runway. The test was in no way contrived especially to produce multipath and, in fact, the multipath occurred in what was thought to be a multipath free environment at microwave frequencies.

While these results, so far, are indeed significant it is the following real world results from the joint Army/Air Force test program which demonstrated the direct relevance of polarization to the performance of a microwave landing system with regard to multipath. The operational airfields selected for this joint test program were Felker Army Airfield, Ft Eustis, Virginia, Cairns Army Airfield, Ft Rucker, Alabama, and, since microwave landing system multipath was earlier demonstrated there, Wright Patterson Air Force Base, Ohio. The short range reflection coefficient data from airport structures at these airfields show that circular polarization can show an improvement of up to 25 db over the worst of the two linear polarizations. Horizontal polarization was always superior to vertical in rejecting multipath from vertical dielectric surfaces. For other surfaces, such as metallic corrugated surfaces, there is a statistical advantage in using horizontal rather than vertical polarization. However, in some cases, particularly for those metallic corrugated materials where the distance between corrugation peaks was large with respect to the wavelength (ratio of 5 to 16) and grazing angles were larger than ten or twelve degrees, horizontal polarization did produce more intense multipath than vertical polarization in the specular direction. Such was the case at Felker Army Airfield. In all cases, multipath could be reduced to acceptable levels by selecting circular polarization over the worst linear polarization.

Figure 1 depicts the typical multipath test geometry employed for the long range tests. In this case, the test geometry for Wright Patterson Air Force Base, runway 23, is illustrated.

It must be clearly understood that the reflecting surface (hangar 206, reflector) is within the coverage of a typical microwave landing system and that an aircraft approaching the touchdown zone can receive both the correct direct guidance beam and the erroneous reflected beam (similar situations existed for the Felker Army Airfield and Cairns Army Airfield test sites). Figures 2 through 4 and Tables 1 through 3 provide a brief summary of long range data for the three airfields tested. The "specular multipath ratio" number is the ratio in amplitude between the reflected and direct beams at the receiver antenna height indicated, in the specular multipath region along the runway centerline. This specular multipath is dangerously near the touchdown zones for the Felker Army Airfield and Wright Patterson Air Force Base tests.

Data for Cairns Army Airfield in Figure 2 and Table 1 show that, for the particular test case chosen Cairns appears to be relatively free from multipath that would be critically harmful to microwave landing system guidance (See Figure 2 and Table 1). Nevertheless, it is clear that a substantial protection margin can be gained by the use of other than vertical polarization for a guidance system which must rely on the integrity of the radiated guidance beam for accuracy and optimum safety and reliability.

Data presented in Table 2 show the superiority of circular over linear polarization for the multipath situation tested at Felker Army Airfield (See Figure 3 and Table 2). The comparison of circular to linear polarization is intentional, at this point, because in making the overall data comparisons for Cairns Army Airfield (Figure 2 and Table 1), Felker Army Airfield (Figure 3 and Table 2), and Wright Patterson Air Force Base (Figure 4 and Table 3), it begins to become apparent that the use of circular polarization offers the least risk solution for reducing multipath radiations to acceptable levels. As stated earlier, even though short range data from all test sites indicate a statistical advantage for using horizontal linear rather than vertical linear polarization to reduce multipath, more importantly, it shows that the use of circular polarization always provides substantial protection from multipath while one or the other of the linear polarizations may not. The long range data, likewise, show this to be the case.

Data from Figure 4 and Table 3 for Wright Patterson Air Force Base is the most dramatic example of destructive multipath for linear polarization for the cases tested (See Figure 4 and Table 3). As at Felker Army Airfield, the use of circular polarization guarantees that multipath will be acceptably low (additional supporting data indicates that, for Felker Army Airfield, for some reflection geometries other than noted in Figure 3 and Table 2, horizontal could produce less intense multipath than vertical polarization but circular polarization still guaranteed that multipath would be acceptably low — See Ref 4, 5, 10). It is important to note that at Wright Patterson Air Force Base the severe multipath occurs at the most critical part of a Category III (zero-zero) instrument approach, i.e., during the transition from the flare to the touchdown maneuver. Unless circular polarization is employed, even the best signal

processors are likely to be challenged or defeated by such intense multipath. Additional supporting data (Ref 2) shows that this multipath region lasts for about 20 seconds for an aircraft at typical approach speeds. The multipath would last even longer for low speed STOL aircraft or helicopters performing decelerating approaches to a hover.

The Wright Patterson data illustrates another important point. Very subtle undulations in runway profiles and terrain along the transmitter-reflector-receiver path can cause multipath and vertical beam lobing effects to combine in such a manner as to turn the seemingly benign airfield into a hostile multipath environment. This would indicate that the need for exact surveys and careful testing and site analysis for multipath is indeed crucial. If anything, the multipath situation at Wright Patterson is a relatively simple one in comparison with the potential multipath situations which might exist at some of our large jetports such as JFK, Philadelphia International or Washington National.

V. Conclusions

At some point in the future, both civil and military operators will most likely have a microwave landing system of some type. This system will have the potential of providing truly advanced operational capabilities, reliability and safety for all users. Whether this system, in reality, will achieve its maximum potential will depend on how carefully the system designers assess every system parameter and use the best possible engineering judgement to achieve the required performance. Our testing reveals that the microwave landing system propagation environment is not as benign as perhaps previously believed. While a 10 to 150 times increase in frequencies over ILS offers some potential advantages in terms of antenna aperture sizes, site preparation, beam control, and overall multipath reduction, the existence of problems because of severe multipath is a virtual certainty unless advantage is taken of all known means, first, to reduce multipath to the lowest levels possible and, then, to nullify the adverse effects of the remaining multipath without restricting system coverage and utility.

Tracking filters, time gates and other receiver processing techniques intended to nullify the effects of existing multipath can be successful to a certain degree in the right situations. However, these processing techniques cannot be depended upon to reliably solve all the guidance problems which could result from the frequent, high level multipath possible during microwave landing system approaches. The worst must be expected. Accordingly, system designers have the responsibility to generate the "cleanest" possible signals in space. Polarization must be considered. Known system deficiencies such as multipath vulnerable polarizations must not be designed into our next generation microwave landing systems. The cost of doing it correctly the first time is trivial in comparison with the cost and the hazard of suffering with less than optimum performance from a system with such enormous potential.

FIGURE 1.

TEST GEOMETRY FOR LONG RANGE MULTIPATH TEST

WRIGHT PATTERSON AIR FORCE BASE

RUNWAY 23*

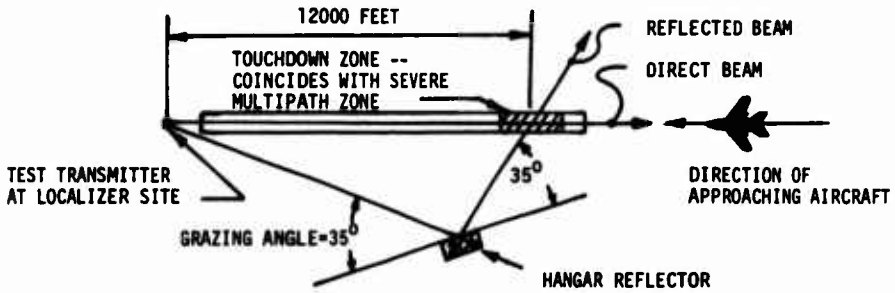

*RUNWAY 23 - ACTIVE, PRECISION APPROACH, INSTRUMENT RUNWAY

FIGURE 2.

SUMMARY OF LONG RANGE DATA

CAIRNS ARMY AIRFIELD

GRAZING ANGLE: 33.4 DEGREES.

REFLECTING STRUCTURE: COMPLEX BUILDING, MEDIUM SIZED SINUSOIDAL CORRUGATIONS.

RUNWAY: 13, ACTIVE ROTARY WING.

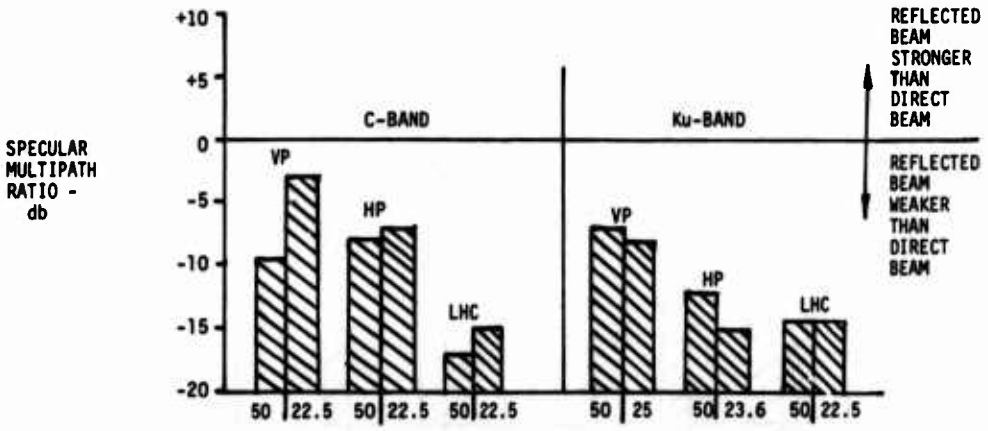

FIGURE 3.

SUMMARY OF LONG RANGE DATA

FELKER ARMY AIRFIELD

GRAZING ANGLE: 25.5 DEGREES.

REFLECTING STRUCTURE: SIMPLE BUILDING, TRAPEZOIDAL CORRUGATIONS, 12 INCHES BETWEEN CORRUGATION PEAKS, RELATIVELY FLAT METAL BETWEEN CORRUGATION PEAKS.

RUNWAY: 14, ACTIVE FIXED WING AND ROTARY WING INSTRUMENT.

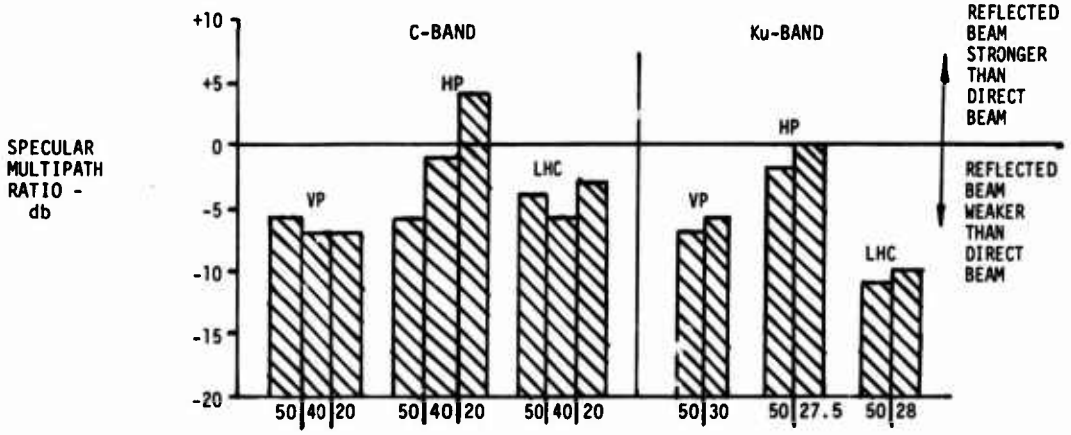

FIGURE 4.

SUMMARY OF LONG RANGE DATA

WRIGHT PATTERSON AIR FORCE BASE

GRAZING ANGLE: 34.6 DEGREES.

REFLECTING STRUCTURE: MODERATELY COMPLEX FLIGHT LINE HANGAR, LARGE DOORS, MOSTLY FLAT METAL.

RUNWAY: 23, ACTIVE PRECISION INSTRUMENT, 12,000 FEET LONG.

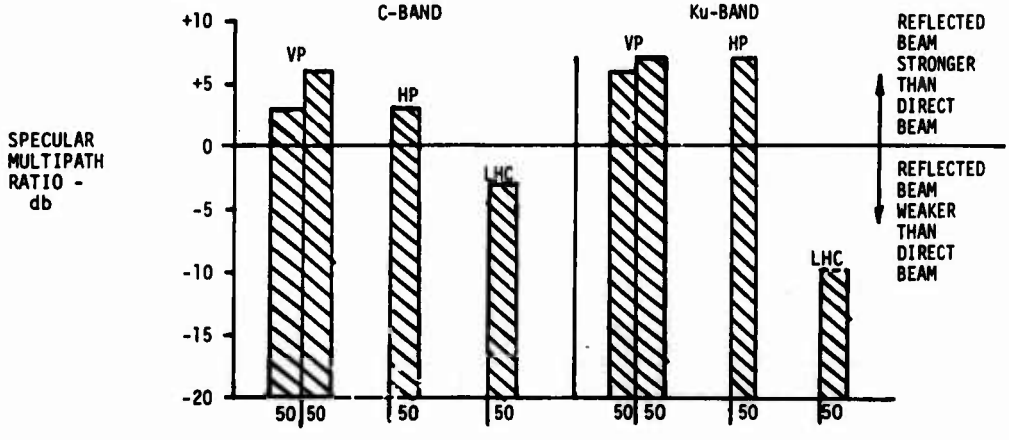

TABLE 1

SUMMARY OF LONG RANGE DATA, CAIRNS ARMY AIRFIELD

Grazing Angle: 33.4 degrees

Reflecting Structure: Complex building, medium sized sinusoidal corrugations.

Runway: 13-active rotary wing runway.

Band	Polarization	Receive Antenna Height	*Specular Multipath Ratio
C	Vertical	50 Ft	-9db
C	Vertical	22.5 Ft	-3db
C	Horizontal	50 Ft	-8db
C	Horizontal	22.5 Ft	-7db
C	Left Circular	50 Ft	-17db
C	Left Circular	22.5 Ft	-15db
Ku	Vertical	50 Ft	-7db
Ku	Vertical	25 Ft	-8db
Ku	Horizontal	50 Ft	-12db
Ku	Horizontal	23.6 Ft	-15db
Ku	Left Circular	50 Ft	-14db
Ku	Left Circular	22.5 Ft	-14db

*-db Indicates Reflected Beam Weaker Than Direct Beam.

TABLE 2

SUMMARY OF LONG RANGE DATA, FELKER ARMY AIRFIELD

Grazing Angle: 25.5 degrees.

Reflecting Structure: Simple building, trapezoidal corrugations, 12 inches between corrugation peaks, relatively flat metal between corrugation peaks.

Runway: 14-active fixed wing and rotary wing instrument runway.

Band	Polarization	Receive Antenna Height	*Specular Multipath Ratio
C	Vertical	50 Ft	-6db
C	Vertical	40 Ft	-7db
C	Vertical	20 Ft	-7db
C	Horizontal	50 Ft	-6db
C	Horizontal	40 Ft	-1db
C	Horizontal	20 Ft	+4db
C	Left Circular	50 Ft	-4db
C	Left Circular	40 Ft	-6db
C	Left Circular	20 Ft	-3db
Ku	Vertical	50 Ft	-7db
Ku	Vertical	30 Ft	-6db
Ku	Horizontal	50 Ft	-2db
Ku	Horizontal	27.5 Ft	0db
Ku	Left Circular	50 Ft	-11db
Ku	Left Circular	28 Ft	-10db

*-db Indicates Reflected Beam Weaker Than Direct Beam, +db Indicates Reflected Beam Stronger Than Direct Beam.

TABLE 3

SUMMARY OF LONG RANGE DATA, WRIGHT PATTERSON AIR FORCE BASE

Grazing Angle: 34.6 degrees

Reflecting Structure: Moderately complex flight line hanger, large doors, mostly flat metal.

Runway: 23-active instrument runway, 12000 feet long.

Band	Polarization	Receive Antenna Height	*Specular Multipath Ratio
C	Vertical	50 Ft	+3 to +6db
C	Horizontal	50 Ft	+3db
C	Left Circular	50 Ft	-3db
Ku	Vertical	50 Ft	+6db to +7db
Ku	Horizontal	50 Ft	+7db
Ku	Left Circular	50 Ft	-10db**

*-db Indicated Reflected Beam Weaker Than Direct Beam, +db Indicates Reflected Beam Stronger Than Direct Beam.

**Reflected Beam At Least 10db Weaker Than Direct Beam, Multipath Amplitude Lower Than Receiver Noise Threshold.

REFERENCES

1. Demko, Paul S., CPT., US Army Avionics Laboratory, US Army Electronics Command, Fort Monmouth,NJ 07703, "Polarization Multipath Study", August 1971 through June 1972, Report VL-5-72

2. Brindley, A.E., Calhoun, L.C., Patton, T.N., Valcik, L., IIT Research Institute, for US Air Force Flight Dynamics Laboratory, "Analysis, Test and Evaluation Support to the USAF Advanced Landing System Program ", August 1974, Technical Report AFFDL-TR-74-62, Vol I, Program Description and Results, section 7.4.4, page 131

3. Hessel, A., Schmoys, J., Polytechnic Institute of Brooklyn, Farmingdale, NY 11735, for US Army Electronics Command, "Computer Analysis of Propagation/ Reflection Phenomena", 20 August 1973, Final Report for Contract DAABO7-73-M-2716

4. Schwering, F., Comm/ADP Laboratory, Whitman, G., NJ Institute of Technology, for US Army Electronics Command, "A Theory of Scattering by Sinusoidal Metal Surfaces", May 1977, R&D Technical Report ECOMR-4496

5. Mink, J.W., Communications Research Technical Area, Comm/ADP Laboratory, US Army Electronics Command, "Energy Considerations of Beams Reflected from Periodic Surfaces", 29 August 1975, Technical Memorandum

6. Mink, J.W., Communications Research Technical Area, Comm/ADP Laboratory, US Army Electronics Command, for US Army Avionics Laboratory, "Reflection Properties of Various Building Materials for Linear, Circular and Elliptical Polarization", 22 July 1974, Memorandum for Record for Landing Team

7. Mink, J.W., Communications Research Technical Area, Comm/ADP Laboratory, US Army Electronics Command, for US Army Avionics Laboratory, "Optical Modeling Experiment for Tactical Landing System (TLS)", 8 January 1974, Memorandum for Record for Landing Team

8. Mink, J.W., Comm/ADP Laboratory, US Army Electronics Command, for US Army Avionics Laboratory, "Some Humped Runway Problems and Considerations for MLS", 20 August 1975, Memorandum for Landing Team

9. Ploussious, G., Meyer Associates, Inc., for US Army Electronics Command, "Circular Polarization Analysis for the Microwave Landing System (MLS)", February 1976, R&D Technical Report ECOM-75-0801F

10. Brindley, A.E., Calhoun, L.C., Patton, T.N., IIT Research Institute, for US Air Force Flight Dynamics Laboratory and US Army Avionics Laboratory, "A Joint Army/Air Force Investigation of Reflection Coefficients at C and Ku Bands for Vertical, Horizontal and Circular System Polarizations", July 1976, Final Report for Period November 1975 to February 1976, AFFDL-TR-76-67

    NOTE: This reference represents approximately 15 percent of the work accomplished under the joint Army/Air Force test program. The remaining 85 percent of the work accomplished under this joint effort, to date (October 1977), is documented in a draft report prepared by the IIT Research Institute for the Air Force Flight Dynamics Laboratory and the Army Avionics Laboratory (currently the US Army Avionics Research and Development Activity). This report is currently being prepared for publication and should be released during December 1977.

11. Evans, J.E., et al, Lincoln Laboratory, Massachusetts Institute of Technology, for the Federal Aviation Administration, "MLS Multipath Studies, Volume II: Application of Multipath Model to Key MLS Performance Issues", 25 February 1976, Project Report ATC-63 Volume II, Report No. FAA-RD-76-3, II, in particular Section IX pages 9-1, 9-8, 9-13, 9-16, 9-21, 9-23 through 9-25, 9-26, 9-27

12. Walker, D., Bennett, G.J., Royal Aircraft Establishment, "Building Surface Reflection Measurements at C-Band", February 1974, Technical Memo RAD1048

13. Benjamin, J., Peake, G.E.J., Editors, Royal Aircraft Establishment, "Contributions to the UK Microwave Landing System Study (Phase I)", June 1974, Technical Report 74050, in particular page 47, section 3.6, paragraph 3.6.1 and page 48, paragraph 3.6.2

ACKNOWLEDGEMENTS

I would be remiss, in having presented this paper, not to have acknowledged the work of those who contributed to the overall effort. Indeed, nothing would have been possible without their support. Everyones help is deeply appreciated. In particular I would like to thank Mr. Joseph Saganowich, my tech area chief, and Mr. Walt Melnick of the Air Force Flight Dynamics Laboratory for their continued encouragement and contributions. Dr. Jim Mink, formerly with the US Army Electronics Command (USAECOM) and now with the Army Research Office (ARO), provided nearly all of the essential modeling and theoretical analysis, along with support from Dr. Felix Schwering of ECOM. Their contributions are deeply appreciated. Mr. L.C. Calhoun of IITRI, our prime contractor, was singularly dedicated to the joint Army/Air Force research effort and gave much more of himself than obliged to under the terms of the contracts. Mrs. Kay Trezza, our tech area secretary, along with the other girls, has performed admirably and has tolerated much aggravation from me in my anxiety to get things done. Finally, and most important, I would like to thank my beautiful wife, daughter and son in surviving my long absences from home which were required in order to perform the field tests and in giving me priceless moral support.

DME-BASED SYSTEM FOR ENROUTE/TERMINAL NAVIGATION, ALL-WEATHER LANDING AND AIR TRAFFIC CONTROL

by
K. D. Eckert

Standard Elektrik Lorenz AG (ITT)
7000 Stuttgart 40
Germany

SUMMARY

The DME system, which has found a wide spread worldwide application in the civil and military area as well, includes, due to its ingenious signal format and the very economic channeling scheme, a considerable potential for additional applications. Todays navigation and air traffic control systems have at least partly reached its limits of improvement and extension as the call for a MLS proves. The growth potential of the ICAO-standardized DME allows for various operational extensions by improving the distance measuring system to PDME and using DME interrogations by direction finders on the ground, measuring azimuth and elevation. The operational applications of these features are the DME-based Landing System DLS, the FRGs contribution to the international MLS competition of ICAO, the additional use of the DLS-A groundsubsystem as TMA-navaid, the extension of this principle to the enroute-navigation called DENS for DME-based Enroute Navigation System, the universal DLS/DME/DENS = DLENS airborne equipment and last but not least the step into the ATC/CAS-field with DACS (DME-based Air traffic Control System).

The paper explains the systematic and technical background of this aeronavigational system. An analysis of the various subsystems detailing this advantages compared to today's installations dealing with the areas of operational performance and economic efficiency mainly, is given. The integrated aeronautical system, designed on the foundation of the standardized DME-system, is the right answer to the challenge of ICAOs 7th Air Navigation Conference, which initiating the international MLS competition asked for "a total system planning approach with due regard to operational needs, technical feasibility and cost effectiveness, and that new systems be well integrated within the total aeronautical system".

1. INTRODUCTION

Todays air traffic particularly in the high density areas can only be mastered by the use of high sophisticated navigation and air traffic control systems. For en-route navigation of the civil aviation VOR radio beacons combined with the distance measuring equipment DME are in general use since more than two decades; the military aviation applies the TACAN system, which incorporates the same DME system as an integral part. The problem of landing guidance was solved by the implementation and standardization of the instrument landing system ILS, providing one single approach path to the touchdown point for all approaching aircraft. The airforces overcame this problem by application of the Precision Approach Radar (PAR). The air traffic control net relies mainly on radar systems as the Surveillance Radar Equipment SRE and the Secondary Surveillance Radar SSR.

All these systems operating at least partly since decades have continuously been adapted to extended requirements by a steady running process of development and improvement. However, the growth potential of some of these systems is limited so that a substitution of these systems by more powerful candidates within a foreseeable period of time has to be considered seriously. Qualification criteria for these new systems concern items as mission success (accuracy, coverage, capacity etc.), integrity and safety of flight, environmental protection and costs. Some additional tasks unsolved hitherto concern roll-guidance, collision avoidance, ground-air-ground data exchange as well as special tactical or operational military demands which have to be added to the catalogue of requirements.

The internationally standardized system for distance measurement DME, which has found a wide spread world wide application in the civil and military field as well, contains a considerable potential for additional applications. Due to the ingenious signal format of DME and a very economic channeling scheme the DME system can be extended in an organic way without creating conflicts with its basic application. Thus it is designated to form the foundation of an integrated system for aircraft guidance capable of satisfying most of the above mentioned criteria.

2. DME CONSIDERATIONS

Since the DME is in widespread operation all over the world in civil and military aircraft as well, a description of the DME fundamentals being specified in ICAO's Annex 10 can be saved in this context. Some important topics however shall be recollected shortly in catchwords (Fig 1):

- Two way interrogation system, L-band operation;

- Airborne interrogator - ground transponder;

- Gaussian shaped pulse pairs;
- Random access system;
- Simultaneous operation of more than 100 a/c by one transponder;
- Airborne search/tracksystem substitutes addressing system;
- Average system accuracy about ± 0.1 NM;
- Integral part of military TACAN system.

This standard DME-system contains a considerable amount of potential for improvement of the distance measuring function as well as for application in other areas by using the DME signals and frequencies.

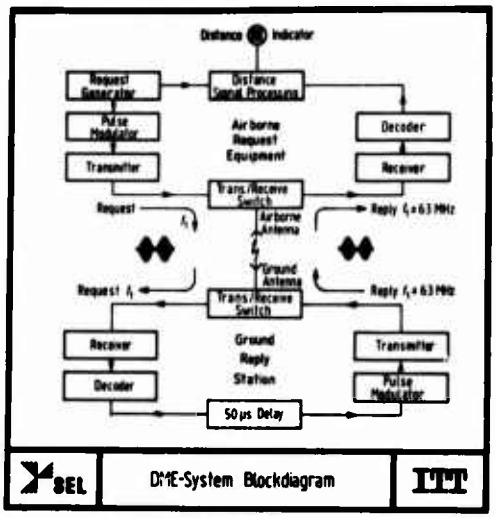

Fig. 1

3. DISCUSSION OF THE DME GROWTH-POTENTIAL

Channeling, signalformat and the DME principle present a lot of features, which illustrate the growth potential inherent in the DME system. The following advantages are underlining this statements:

* The DME frequency band, as shown in Fig 2, has 126 x-mode plus 126 y-mode channels, each consisting of an interrogation-down- and a reply-uplink, a well allocated and internationally agreed set of rf-channels, which can be employ for various other services provided that international DME-standards are kept.

* By introduction of different spacings or other additional codings the DME system offers the possibility of co-channel operation resulting in a further increase in the number of operational channels.

* The DME uplink and the down link are operating with very small duty cycles. This fact opens the chance of a time division multiplex use of both links.

* DME operates with a random access mode serving several users simultaneously by the same ground transponder. This principle in combination with the ground-to-air TDM-transmission allows for the parallel implementation of additional services without limiting the basic DME-service.

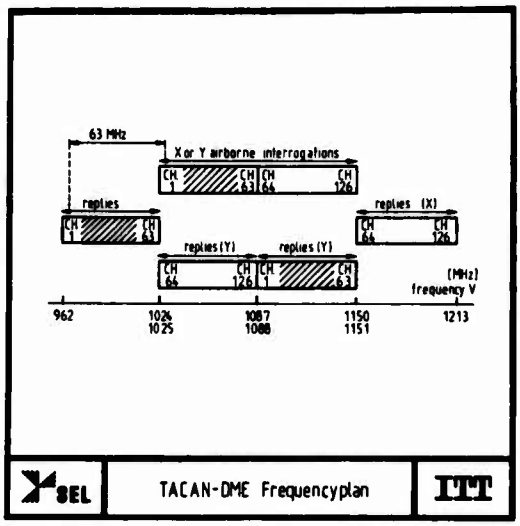

Fig. 2

* DME operates at L-band. This frequency is best suited for purposes requiring precise propagation, long range, negligible weather penetration, while allowing simple and small omnidirectional antennas as well as directional radiating elements.

* The L-band technology does not present difficulties. Sufficient experience is available, indicating that the technical risk for a system operating at about 1 GHz can be kept very small.

* One of the biggest advantages of the DME is its capability of improvement with regard to higher accuracy while keeping all figures of ICAO's DME specifications.

While this list probably is still not complete, one has to look at the disadvantages of the DME-system too, which might restrict its growth capability. Here it must be recognized, that the DME system can be saturated by principle, that it operates with the relativ small bandwidth of 400 kHz and that with respect to large aperture applications a wavelength of 30 cm may be a restrictive factor.

The next paragraphs nevertheless will prove, that DME has a remarkable growth

potential in showing, that the operational and technical advantages are overriding the possible draw backs of the system.

4. EXTENSIONS OF THE DME SYSTEM

In the context of this report three essential extensions of the standard DME system will be discussed in a certain detail:

- The Precision DME - PDME,
- the application of direction finding principles, using the DME signal format,
- the ground-to-air data transfer being integrated into the DME-system.

A survey on these extensions detailing PDME requirements, applications and realization as well as principles and applications of ground derived direction finding using DME interrogations and feeding back guidance data to the airborne equipment will be discussed now.

4.1 The Precision DME (PDME), applications and requirements

Today's DME does a satisfying job with respect to accuracy as far as standard en-route navigation is concerned. For some applications however such as landing guidance, and $\varphi - \varphi$-area navigation an error of more than 0.1 NM ($\sim$ 200 m) is unacceptable. If the DME system shall become somewhat like a backbone of an integrated navigation system, its performance must satisfy the most stringend requirements a subsystem of that integrated navigation system would ask for. This demand can be derived from the operational requirements for a microwave landing system MLS, if such a landing aid is part of the integrated navigation system. Obviously the DME needs a significant improvement in order to meet the MLS accuracy requirements. It has to be investigated how this improvement can be achieved without getting in conflict with ICAO's DME specifications.

4.1.1 PDME realization

In order to reach DME-errors an order of magnitude smaller than those of the en-route DME today (the MLS-OR asks for a 2σ-guidance error of 12 meters) the error sources have to be analyzed very carefully. This exercise was done covering the three possible error areas:

* The airborne DME interrogator hardware,
* the a/g- and g/a-transmission path,
* the DME-ground transponder hardware.

This basic investigations showed, that performance improvements could be achieved by

- accuracy improvements of DME-hardware, and
- reduction of signal interferences mainly caused by multipath propagation.

To reach this goal various measures have been taken at the airborne DME interrogator and at the DME ground transponder, some of them being worthwhile to be looked at in more detail:

- o It is essential for a PDME system to use DME-signals following the most stringend requirements. DME pulses, which satisfy this demand have reduced tolerances regarding the pulse-shape, as it is asked for by the new STANAG-specifications 5034 for the DME.
- o The technological progress rendered the introduction of digital search- and track systems as well possible as the application of high frequency- and high stability-clocks being mandatory for high precision time measurements as the basis of precise slant range determination. Similar considerations too apply for low noise-figure receivers, fast AGC-systems and accurate and stable local oscillators.
- o In order to result in a DME-hardware not depending on instable subsystem delays (i.e. transponder delay) pilot pulse loops were introduced in ground- and airborne equipment including the if-part of the receiver, the video part and the transmitter. This measure

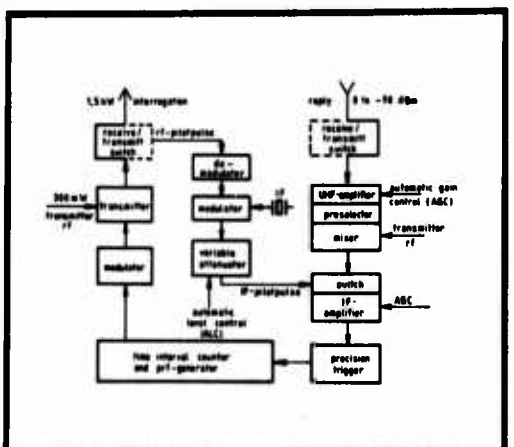

Fig. 3

reduced the bias error part drastically (Fig 3).

The reduction of multipath interferences was successfully attacked by the introduction of

* first-pulse-timing and

* the use of precision triggers.

While the first measure allows for a time-discrimination against multipath signals arriving at the receiver antenna always somewhat later than the direct signal, the precision trigger ensures the proper derivation of the trigger mark at the 50 %-amplitude point of the leading edge of a DME pulse independent of the pulse-amplitude.

The realization of all these measures could be conducted without doing any harm to the DME signal format being internationally agreed and specified by ICAO.

4.1.2 PDME performance

Following this results, SEL designed and built PDME ground- and airborne units. In the course of the development of the German contender to the international MLS competition ground- and flight tests were run for the PDME parameter too. The results of these tests confirmed the predictions made for PDME-accuracy. Fig 4 shows as an example the PDME-error referenced to a radar-cine-theodolite-tracking system for a 10 nautical miles radial. The result in this case is a bias error of +1.2 m superimposed by a 2σ-noise error of ± 15 m.

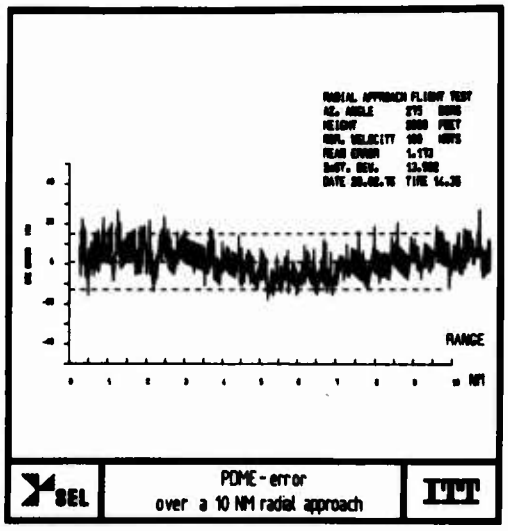

Fig. 4

Thus the first extension of the DME system was proven successfully, opening the gate to a wide field of additional applications, which can be handled while fully keeping the ICAO DME specifications.

4.2 Direction finders using DME interrogations

The second and even more important extension of the DME-system is the combination of DME interrogation signals and direction finding equipment on the ground. This principle permitts determination of the angle of incidence of DME signals, thus amending the distance measurement by an angle measurement. By this step the DME-system, originally designed for range determination only, gets completed to a system capable of delivering full position information.

4.2.1 Basic principles of ground derived position determination

The ground equipment capable of determining the angle of incidence azimuth and/or elevation of an airborne DME-interrogation consists of the following modules (Fig 5):

- o One- or twodimensional antenna array,
- o receiver multiple,
- o interface network,
- o digital processor,
- o output and encoding network.

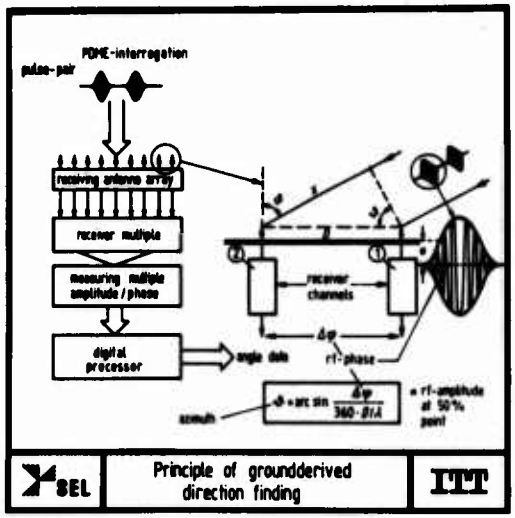

Fig. 5

Each element of the antenna array is connected to its individual receiver for digital rf-amplitude and rf-phase measurement. This is carried out simultaneously at all receiver channels sampling the rf-DME-interrogation at the leading edge of the first pulse. The resulting data are then transferred to a digital processor, where the necessary calculations for determination of the angle of incidence of the DME-interrogation (azimuth and/or elevation) are carried out. In the next step, the output and encoding network allocates the result of

this exercise to the correct DME reply pulse, thus initiating the ground-to-air angle data transmission.

While accuracy and multipath resistance of the direction finding process heavily depends on the aperture of the antenna array in charge, which means on the number of receiving channels, the capacity of the system, which is the number of aircraft to be served simultaneously, can be increased by parallel operation of several digital processors. A failure of a single receiver channel therefore does not cause a break-down up the whole system, but only a slight degradation in the system's performance. A failure of a digital processor however has no effect on system-accuracy but causes a slight reduction of the system capacity only.

The mathematical methods to be applied for evaluation of the angle of incidence are not specially related to a particular design of the direction finding ground system, but can vary widely in their complexity from simple interferometer methods to complex algorithms for reduction of multipath effects. More sophisticated evaluation methods apply procedures as Fast Fourier Transformations, application of virtual antenna patterns and adaptive beam steering.

New ideas in the direction finding techniques as for instance the "lateral diversity antenna" can be integrated into the system at any time without demanding changes to the overall system concept. These facts indicate, that the ground-derived direction finder extension of the DME-system ensures optimal matching of software- and hardware effort to individual requirements resulting from the operational target and the multipath environment.

4.2.1.1 Azimuth Measurement

The groundsystems employed for measurement of azimuth or elevation are nearly identical. Differences concern the antenna systems and the processor program software. Due to the horizontal orientation of the information gradient, ground derived direction finders measuring azimuth apply horizontal antenna systems. Basically two types have to be considered, linear arrays and circular arrays. While the first delivers "conical" azimuth, the circular array generates "planar" coordinates by principle. The circular array always allows for an omnidirectional coverage. To achieve this with linear arrays two of them installed in a perpendicular mode must be applied, which then are capable to deliver "planar" azimuth data too.

The determination of azimuth basically is executed by application of interferometer procedures, which might be refined by additional real or virtual antenna pattern shaping. The azimuth accuracy achieved depends on the aperture of the antenna array and on the degree of multipath contamination. Even at large apertures, which principally result in excellent accuracy data, heavy multipath signals can lead to a complete break down of the azimuth measurement due to a break down in rf-phase ambiguity resolution. Thus particular effort was spent in solving this problem by application of "phase-scanning"- and "amplitude-scanning" procedures as Fast Fourier Transformations (FFT).

4.2.1.2 Elevation Measurement

Determination of elevation has its biggest importance in the field of generation of approach and landing guidance information. Because of the vertical orientation of the elevation information gradient the elevation direction finding ground system normally applies vertical antenna systems. They are formed by linear arrays of different apertures or of so called "lateral diversity"-antennas in the case of high performance systems operating in heavy multipath environments. Besides this difference in antennae the direction finder groundsystem hardware applied for elevation measurement does not differ from that for azimuth measurement. Even regarding the program software there are several similarities.

In the elevation case too interferometer processing refined by virtual beam forming and shifting is applied. The elevation measurement is a strong challenge regarding suppression of multipath signals due to the relative low separation angles between wanted and unwanted signals in azimuth and elevation. In heavy multipath environment the empolyment of a lateral diversity antenna is recommended. Corresponding to Fig 6 this antenna comprises a vertical and horizontal aperture as well, while keeping the number of aerials and receiver channels compared to linear array of the same vertical aperture. The picture also shows the antenna pattern of such a lateral diversity antenna, which can be scanned virtually in the vertical and horizontal direction.

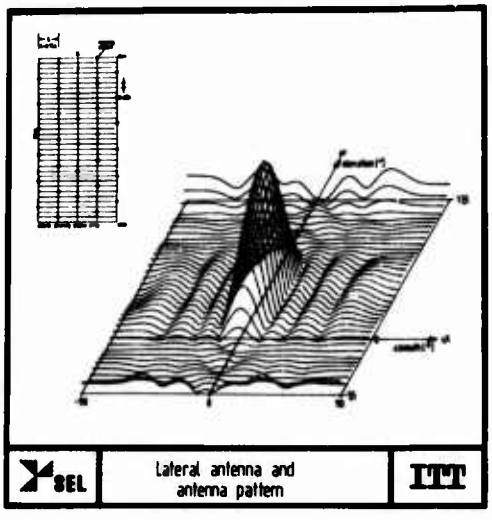

Fig. 6

4.3 Ground-to-air Data transfer integrated into the DME system

Position data, determined as described above, are required at the airborne equipment mainly. In a three step process this angle data transfer can be managed using the DME-reply-link:

- Allocation of angle data (azimuth/elevation) to the corresponding DME reply,
- Angle data encoding and transmission to the airborne equipment,
- Decoding and processing (search/track/average) in the airborne equipment.

Angle data ground-to-air transmission is executed by transmission of additional double pulses having a position on the time axis with reference to the DME-reply, which corresponds to the measured angle (Fig 7). After a basic time delay, a time proportional to the measured angle is counted and the angle reply is then initiated. The azimuth and elevation replies are transmitted in sequence, each double pulse occupying a seperate time slot.

Using the process as shown in Fig 7 permitts the g/a-data transfer being completely integrated into the DME-reply uplink and without the need for a special address-system.

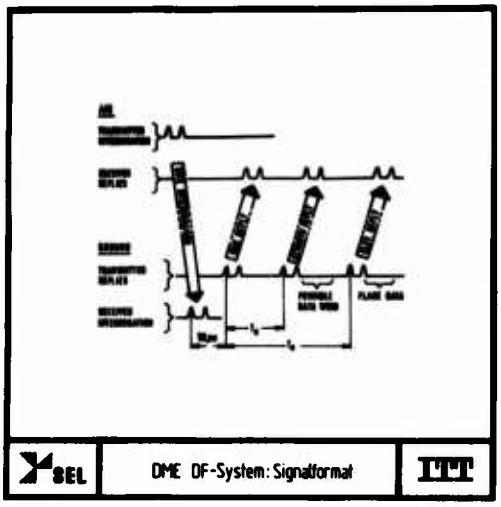

Fig. 7

4.4 Airborne Date receiver

The airborne unit of a system, which has been scetched in the preceding sections has to handle the following basic tasks:

* Precision distance measurement to the cooperating groundstation, which comprises
  - transmission of DME interrogations,
  - pilot pulse service,
  - receipt of groundstation replies,
  - evaluation of distance information using search-track-and filter systems;
* Angle Data determination consisting of
  - receipt and decode of angle replies (azimuth/elevation),
  - time intervall measurement,
  - angle data evaluation using search-track- and filter systems.

Two different airborne concepts are under consideration. The first consists of a standard airborne DME, which preferrably should easily be capable of being PDME-modified, supplemented by an airborne attachment containing a random logic time intervall measurement loop combined with a search-track- and filter system for angle data determination. This concept is designated for retrofit installations.

The second concept is an integrated airborne unit comprising all functions mentioned above in one box having form and fit of a standard airborne DME. In difference to the retrofit version however, the integrated unit, being similar at the rf-part, employs a small but powerful digital processor for evaluation of distance and angle. Except time interval measurements carried out between each twin of received pulses the decoding-, search-, track- and filtering task is completely solved by a much more flexible software solution. This approach gives the first impression of the outstanding economy of this concept, which combines the airborne DME- and angle-functions in one equipment beiny much less expensive than a conventional VOR-DME- or TACAN-DME combination.

5. OPERATIONAL APPLICATIONS OF THESE PRINCIPLES

The combination of precision distance measurement (PDME) and ground derived direction finding (GDF) has found a multiplicity of possible operational applications in the field of radio navigation and air traffic control. Examples to be explained in the next paragraphs will deal with:

- the microwave landing system DLS,
- the TMA- and enroute navigation system DENS,
- the superiority of the combined DLENS airborne equipment and
- the potential of this combination for ATC- and CAS-purposes.

5.1 The DME-based landing system DLS

The DME-based Landing System DLS is that operational application of the PDME and GDF principles, which got the most attention including the development and test of a trialssystem plus a big number of additional theoretical investigations. As the contribution of the Federal Republic of Germany to ICAO's international MLS competition DLS was subjected on thorough assessment, which proved the claimed advantages in system integrity, system cost, growth potential and several operational items as coverage and coverage control, capability of self-calibration, frequency economy and unbeatable economy of airborne installations.

5.1.1 Basic concept of DLS (Fig 8)

DLS approach and landing guidance data are obtained by

* use of improved ICAO-DME (PDME) for omnidirectional distance measurement,
* position determination in azimuth, elevation or height of each individual DME interrogation by the two DLS-groundstations for azimuth/PDME (DLS-A) and elevation/flare-height (DLS-E),
* angle data transfer to the DLS airborne unit synchronized with the related PDME-reply,
* transmission of auxiliary data (DLS-A to airborne unit) using further pulse triples added to the DME-replies,
* acquisition, tracking and display of position and aux-data after decoding in the airborne equipment.

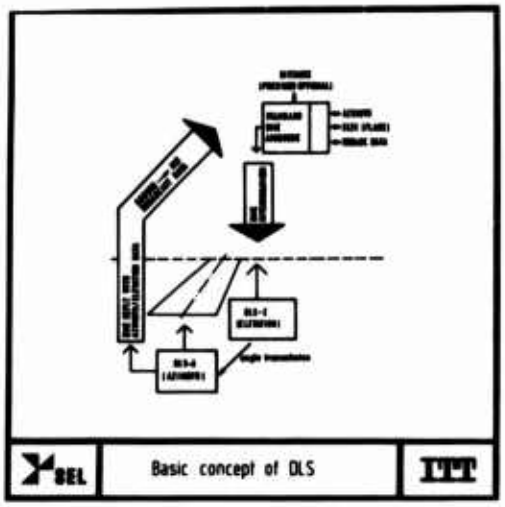

Fig. 8

The signal flow of DLS starts with the transmission of a DME interrogation pulse pair. (Rate: 15 Hz randomly jittered and increased to 50 Hz on final approach.) As described earlier, the interrogation pulses are received and measured simultaneously (rf-amplitude and rf-phase) at each element of the DLS-A- and DLS-E-antenna systems. There elevation and azimuth are calculated. The elevation data are then transferred to the DLS-A station. The PDME reply pulspair transmitted from DLS-A after the specified transponder delay is followed by pulse pairs additionally transmitted from DLS-A such that the spacing to the preciding DME reply is proportional to the measured angle or height. The DLS airborne unit is fully identical to that described above (sec. 4.4).

This short illustration of the basic concept of DLS indicates the extreme simplicity of the DLS, which caused its superiority regarding cost effectiveness and integrity.

5.1.2 The DLS-A groundstation (Fig 9)

The azimuth subsystem DLS-A consists in its most sophisticated version of two horizontal linear arrays installed orthogonally, with a maximum aperture of wavelengths. Each individual receiving element, which is formed by vertically staggered dipoles giving omnidirectional coverage and vertical beam shaping, is connected to a receiver for individually measuring rf-amplitude and rf-phase of the received signal. These measured values are fed into a processor unit in digitized form to calculate the angle of incidence by interferometric rules and virtual antenna pattern shaping. The improved precision DME transponder is incorporated in the DLS-A station for transmitting DME replies together with the coded angle, height and auxiliary data. The achieved coverage is nearly hemispherical with increased high precision angle data in the front and back azimuth sectors (± 40° from centreline) and to a distance of 30 NM.

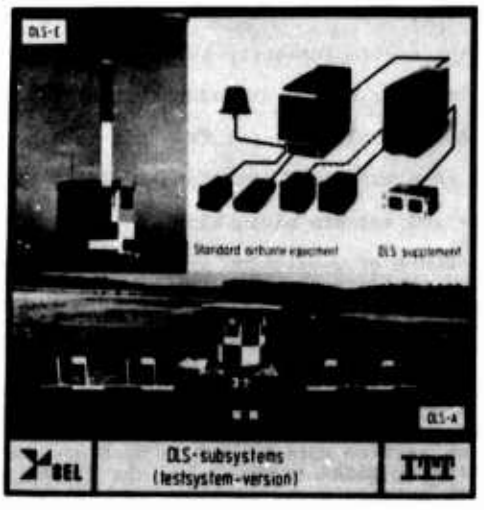

Fig. 9

5.1.3 The DLS-E groundstation (Fig 9)

The elevation subsystem (DLS-E) contains a vertical arrangement of directive antenna elements forming either a linear or lateral diversity array with a maximum vertical aperture of 30 wavelength. The derivation of the elevation angle is performed similar to the process in DLS-A. The direct measurement of the aircraft height above touchdown is incorporated in DLS-E without the need for an additional ground station. Data transfer to the transmitter at DLS-A is made by use of a radio or cable synchronizing link. Coverage of elevation data comprises the approach sector within ± 75° from centreline and up to an angle of 75° to a distance of 30 NM. Flare height information is provided within this coverage out to a distance of 1800 metres (5900 feet) from threshold to allow for a smooth transition to radio altimeter guidance.

5.1.4 The DLS airborne equipment

The airborne subsystem consists of an integrated combination of the DLS and ICAO-DME functions maintaining full compatibility with the latter and providing for full retrofit capability with respect to present avionics. The basic function and the different concepts have already been detailed earlier. The advantage of this approach lies mainly in the concentration of all functions needed for approach and landing in one box. While airborne installation for the conventional ILS consists of localizer/VOR-equipment, glideslope equipment, marker receiver and DME, for DLS only one airborne equipment having form and fit of a standard airborne DME is required. This advantage becomes even more significant, if further operational tasks are undertaken by the same unit.

5.1.5 DLS performances and advantages

Although DLS had a late start in mid 1973, it achieved remarkable results in the international MLS competition, which is a real hard test for any MLS contender. In more than 20 areas the MLS candidates were checked against the MLS-ORs and against each other. DLS run very well in this contest, got a superior position in 7 of 22 topics, such as system integrity, system cost, system growth potential and some other. A lag in hardware realization, due to the relative late start of the FRG MLS program resulted in flight test data from a DLS trialssystem gained at a heavily multipath contaminated test site. These results combined with data, which stem from studies and simulation done with the final DLS-version clearly indicate, that DLS not only satisfies ICAO's MLS-OR, but moreover shows equivalence in operational performances as accuracy, multipath resistance and capacity with respect to its competitors.

However, there is one basic question AWOP did not answer satisfactorily till now: Is the approach to substitute todays ILS by a pure MLS, which, at least in the foreseeable future, will mainly be used like an ILS, the right way? We believe it is not, and that todays MLS requirements are guiding us a one-way route, which will finally come out as a blind alley.

A transition therefore from ILS to MLS will be justified only if the new system will also allow for other functions in an aeronautical system as originally required by ICAO's 7th Air Navigation Conference in 1972. If the provider and user on the ground and in the air, can get rid of existing equipment in the future, thereby increasing reliability, simplicity and cost-effectiveness of the system, only then such a change to new systems will be possible on a worldwide basis. Simply replacing ILS by MLS is not the right answer.

DLS as an organic step in the development of DME's growth potential is the right answer, we think, because its advantages as

- low system cost, minimal airborne effort,
- high system integrity in terms of MTBF and hazard probability,
- high flexibility and adaptability and
- the applicability for TMA- and enroute navigation,

makes it to a preferred candidate avoiding to enter the mentioned blind alley.

5.2 TMA- and enroute navigation

The DLS-A groundstation provides two dimensional position information - azimuth and distance - omnidirectinally. For approach and landing and for the missed approach, high precision azimuth sectors symmetrical to the RCL are added (Fig 10).

With a range of 30 NM the DLS-A groundstation does the same job, which today is done by a terminal VOR-DME combination or by TACAN, however not asking for an ILS or MLS to provide full TMA- and MLS-service. In addition not only the ground installation becomes simpler and much more economic, but also the airborne installation reduces to one DLENS-unit substituting several other airborne equipment. The combined MLS/TMA-navigation service moreover gives much more accurate TMA-navigation data than the VOR/DME combination or TACAN is doing and the DLS-A groundstation, equipped for instance with a circular antenna array of about 10 λ diameter (~3...4 meters), can easily be employed substituting VOR or DVOR and TACAN-beacons, while always offering combined precision DME (PDME) and azimuth service. This service can be used by the same DLENS airborne unit.

Let's have now a little bit more detailed view on the bunch of advantages offered by this system.

5.2.1 Advantages of applying DLS-A for TMA-Navigation

The DLS-A groundstation, which generally is installed behind the stop-end of the runway, offers advantages in several areas, when operated simultaneously as an MLS in the DLS-mode and as a TMA-aid in the DENS-mode (DENS = DME-based Enroute Navigation System). These areas concern operational performances, economical features and logistic considerations. Looking at the advantages in the operational field, one has to recognize the following facts:

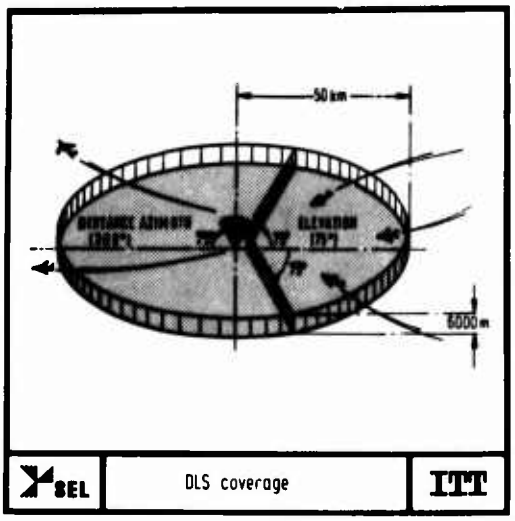

Fig. 10

* Guidance information for approach/landing and terminal navigation regarding azimuth and distance have the same source, the DLS-A groundstation. This is an operational advantage compared to conventional VOR-DME-ILS, TACAN-ILS, TACAN-PAR or VOR-DME (TACAN)-MLS solutions.

* The accuracy of TMA-guidance data generated by the DLS-A groundstation is much better than that of conventional navaids. DLS-A in cooperation with a DLENS airborne unit provides precision distance information with about ± 20 m (2σ)-error, which is at least 10 times better than that achieved with a conventional DME. The error of the planar azimuth delivered by DLS-A in its most capable version never exceeds ± 0.2° (2σ), which is at least an order of magnitude better than that of VOR or TACAN installations. These figures result from flight tests with a DLS-A test-system gained under multipath environment conditions.

* Compared to TACAN or VOR as todays TMA-navaids, which due to their small antenna aperture are rather sensitive against multipath interferences, the azimuth information of DLS-A is highly resistant against multipath contamination. Operating in its most capable version with a minimum of 80λ-aperture the DLS-A groundstation withstand multipath signal amplitude of more than 80 % of the desired signal without remarkable performance degradation. Thus DLS-A can be employed as a TMA-navaid at sites, where TACAN or VOR installations have to quit service.

* Further operational advantages of DLS-A or TMA-navaid are equally important for civil and military users:

  - DLS-A is basically a silent ground system. In contrast to TACAN-VOR, which are continuously transmitting, DLS-A stopps transmission, if there are no decodable interrogations. This fact might be of particular importance for tactical applications.

  - DLS-A adds a ground-to-air datalink to the azimuth-DME service for auxiliary data transmission. This way it becomes a self-announcing beacon, which, besides identity, transmitts characteristic groundstation data and can also transmitt tactical data of general interest.

This remarkable collection of operational advantages, which makes DLS-A superior to any existing TMA-/landing-aid combination, modern MLS included, must now be completed by adding all the economical and logistic advantages.

* First a simple comparison of hardware subsystems on the ground required for execution of the TMA- and landing guidance functions for todays service and for a DLS installation shall be discussed:

  - DLS installation

    DLS-A groundstation: PDME, Azimuth, Aux-Data (Omni)
    DLS-E groundstation: Elevation, Flare Guidance

  - Civil installation

    ILS-Localizer : Course
    ILS-Glideslope : Glidepath
    ILS-Marker : two distances

DME-Transponder : Continuous DME
(D)VOR-groundstation : omnidirectional azimuth

- Military installation

ILS LOC) : Course
ILS GS) PAR : Glidepath
ILS Marker) : two distances
TACAN-Terminal : omnidirectional azimuth and DME

- MLS installation (other than DLS)

MLS - AZ : Approach/missed approach-azimuth
MLS - EL1 : Elevation
MLS - EL2 : Flare Elevation
DME-Transponder : Enroute DME (omnidirectional)
(D)VOR-groundstation : omnidirectional azimuth

Already this rather rough comparision shows, that there must be a significant economic superiority of the DLS-solution, which does not need any further comment, if the following items are considered:

o purchase investments,
o cost of infrastructure efforts,
o life cycle cost,
o maintenance and logistic expenditures
o educational effort.

* Another point connected tc economy - in a little different sense indeed - needs attention, that is the frequency economy. Radio frequency bandwidth is like energy a very costly and even more rare element. Thus besides other items frequency economy must be one of the decisive issues, on which a system selection should be based. Here again the DLS solution is unbeatable (see Fig 11), because each installation occupies only one L-band-channel (uplink + downlink), while for instance the civil installation needs: VHF-Localizer frequency + VHF-VOR frequency (both ~100 MHz) + 300 MHz glide-slope-channel + 75 MHz Marker-frequency + L-band DME-channel. The MLS installation is even worse. This waste of bandwidth must be stopped and DLS shows how it can be achieved.

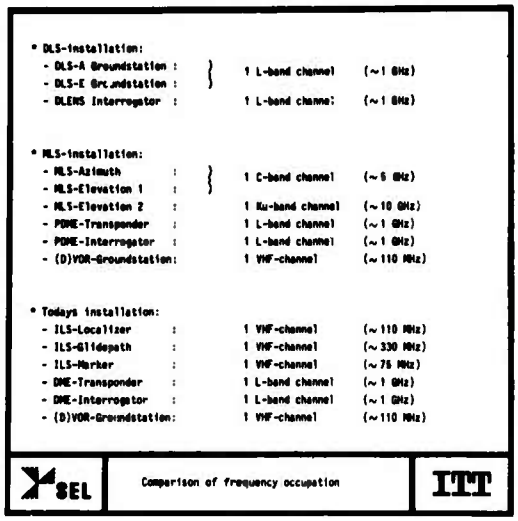

Fig. 11

5.2.2 Extension to Enroute Navigation

Most of the considerations just given for the DLS-A application as a TMA-navaid, applies for the DENS, the DME-based Enroute Navigation System too. Its basic concept is identical to that of the DLS-A groundstation. The DENS antenna system however is different. Instead of orthogonally crossed linear arrays, here a circular array of about 10 wavelengths diameter is employed. The DENS groundstation is rather similar to the trials system version of DLS-A, which also used a circular array and is shown in Fig 12.

The operational application of DENS can be compared to that of a Doppler-VOR system regarding the azimuth parameter. Both systems use circular arrays having a horizontal aperture of about 10 wavelengths, which results in about the same error margin of some tenth of a degree.(*)

With respect to multipath resistance

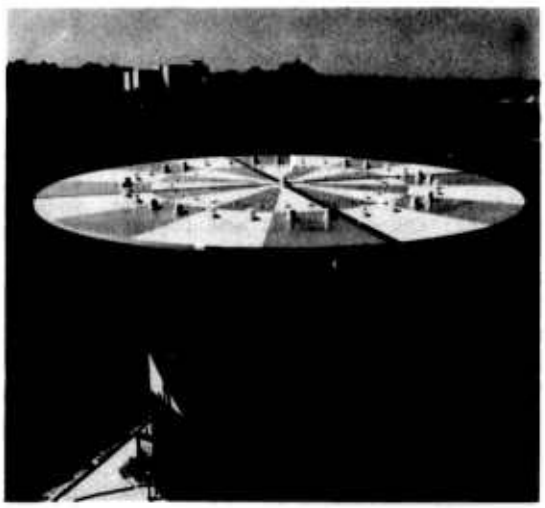

Fig. 12

(*) Ground- and flight tests with the DLS-A trialssystem confirmed these values.

DENS is somewhat superior to DVOR, because DENS is a pulsed system, which allows for time-discrimination against multipath signals, a measure not applicable to the CW-DVOR. Although the electrical aperture of both systems are about the same ($\sim 10\,\lambda$) the different radio frequencies cause significant differences in geometric sizes. While the DENS antenna has about 4 meters diameter, the DVOR antenna is more than 35 m wide.

The DENS - due to its nature - always incorporates the PDME-transponder function, thus delivering azimuth and distance information from the same source. Here DENS can be looked at like an enroute TACAN-beacon, however accuracy of both guidance parameters and their multipath insensitivity is much better for DENS than for TACAN.

The implementation of a DENS groundstation can be managed as an organic and smooth extension of a DME transponder operating for instance in colocation to VOR in a four-step-process:

* Improve DME to PDME,

* Complete PDME transponder by DENS-DF groundsystem,

* Substitute airborne DME by new airborne DLENS,

* Introduce full DENS service, delete VOR.

A similar procedure can be applied to TACAN ground beacons or even (D)VOR groundstations.

As DLS-A in the TMA-mode, DENS incorporates a ground-air-datalink for transfer of auxiliary data, giving DENS the capability of a self-announcing beacon. Due to the interrogation character of DENS, the system is basically a quiet one. It needs airborne interrogations to start transmission, a fact, which might be of importance to possible military applications.

Finally a short view to the economic pros and cons of the DENS. As a TACAN ground beacon DENS comprises all guidance parameters needed for enroute navigation in one equipment, which however will be less expensive. Besides the lower equipment cost, DENS gains its economic superiority from two facts:

- The identity of approach/landing aid, TMA- and enroute navigation aid, which simplifies maintenance and logistics remarkably, resulting in a low cost of ownership.

- The unique DLENS airborne equipment, which applies for approach/landing, enroute navigation including TMA and other tasks as well, minimizing the airborne effort and cost while optimizing system performance and integrity.

5.3 The DLS/DENS (DLENS) airborne equipment

The main features of this airborne equipment are already treated under section 4.4. Only some additional comments regarding the superiority of a DLENS airborne installation shall be given.

The use of the DLENS airborne unit for approach/landing, and TMA/enroute navigation need not to be recalled. An additional possibility however is the application of the processing part of the DLENS for R-nav calculations, which can be executed besides the tasks, for which the unit was provided originally. This calculations can rely upon the guidance data derived by the same equipment resulting for instance in a ϱ - ϱ- or ϱ ϑ - -area navigation, or, giving an other example, in a x-y-tracking system for DLS to smooth the transition from approach to missed approach.

Finally a comparison of airborne installations, which indicates the superiority of the DLENS equipment over operationally comparable installations regarding cost and integrity. It must be noted too, that the DLENS equipment, concerning angle- and aux-data, does neither limit the system accuracy nor add multipath distortions to the angle data performance.

The DLENS airborne equipment, serves for:

* Precision distance information,

* Azimuth data,

* Elevation data,

* Flare-height data and

* Auxiliary data.

This one equipment does the same job than 4 separate airborne equipment are doing in todays installation, in the future MLS-(other than DLS)-case and in todays military installations. Moreover DLENS supplies additional information as aux-data, which turn the DLS-/DENS-groundstations into self announcing ones, a feature available only in the MLS case. The following airborne effort is required to satisfy approach/landing,

TMA- and enroute navigation requirements:

a) DLS/DENS-service:

* DLENS airborne unit	+	L-band antenna

b) Todays radio navigation service:

* ILS-localizer / VOR-receiver	+	100 MHz-antenna
* ILS-glidepath receiver	+	300 MHz-antenna
* ILS-marker receiver	+	75 MHz-antenna
* (P)DME-airborne unit	+	L-band antenna

c) Military service using ILS:

* ILS-localizer / VOR-receiver	+	100 MHz-antenna
* ILS-glidepath receiver	+	300 MHz-antenna
* ILS-marker receiver	+	75 MHz-antenna
* TACAN airborne unit	+	L-band antenna

d) Future MLS service:

* Angle data receiver (az + el 1)	+	C-band antenna
* Elevation 2 receiver	+	Ku-band antenna
* PDME-airborne unit	+	L-band antenna
* (D)VOR receiver	+	100 MHz-antenna

5.4 Further growth aspects

Solving the most important navigation tasks using one basic system and one (1) airborne equipment (instead of four) in a reliable, extremely cost effective way giving high accuracy guidance data insensitive against multipath interferences, this is the essential step to the DME-based universal radio navigation system. However the growth potential of this proposal is not at all exhausted. Some other possible applications, partly perhaps a little bit more in future, shall round off the picture.

First the possibility to employ the DLS as an aid for roll-guidance shall be discussed. The demand for a roll-guidance aid is obvious, if a landing aid capable of Cat IIIc-operation is installed on an airport. If such a MLS has successfully guided an aircraft under extreme weather conditions to touchdown and roll-out, what happens then with the aircraft? A Cat IIIc-MLS does only make sense, if it is combined with a roll-guidance system, which enables the pilot to find the way to the allocated parking position under zero-visibility conditions safely and reliable.

Here again ground derived direction finders could help solve the problem. Several small DLS-A like groundstations installed distributed over the airport area, finding the direction to the interrogating aircraft transfer this information to a control center. Here position and velocity vector of the rolling aircraft is determined and together with the appropriate guidance instructions transferred to the rolling aircraft for suitable pilot's display. However it must be recognized, that a remarkable quantity of additional problems (as passive airport surveillance, airborne display problem etc.) have to be solved, before a roll-guidance system can be brought to operation, a consideration casting certain doubts on the justification of a Cat IIIc-MLS-requirement.

An other area, where the DME-based universal radio navigation system will become highly important in the future is the air traffic control (ATC) and collision avoidance (CAS). The application of ground derived direction finders incorporates the availability of at least the angle-coordinates of an interrogating aircraft on the ground. In order to make use of these ground derived position data, they need to be completed by at least three additional information:

- air derived distance information (slant range)
- air derived barometric height information and
- aircraft identification (address).

This requires an additional air-to-ground data link preferrably combined with the DME-interrogation. The groundsystem then is completely supplied with all information relevant for execution of the following tasks:

* Full ATC service, if ground derived angle-data plus air-to-ground transferred data are fed into central processing unit, programmed to
* Run each controlled aircraft in the observation volume as a dynamic model in the central processor, thus executing a full ground-tracking. Ground-tracking then results in a
* Reduction of number of aircraft interrogations to decrease the traffic capacity while keeping the performance data. Comparative ground-tracking and flight path extrapolations allow the

* Derivation of collision avoidance warnings, which then have to be retransmitted to the endangered aircraft.

While most of the problems dealing with the ATC-data processing are already solved the air-to-ground datalink combined with the DME-interrogation is the greatest technical challenge and therefore obtaines high attention and deep investigations.

As derivatives of the DME-system, the roll-guidance-aid and the ATC-system were denominated as:

- DRGA = DME-based Roll Guidance Aid

- DACS = DME-based Air traffic Control System

6. CONCLUSION

Todays ICAO-standardized distance measuring system DME has a manifold of additional radio navigational applications. Following the basic rule not to design a pure MLS, but to concept a universal radio navigation system as part of the overall aeronautical system, the DME was found to be a solid basis for an integrated system satisfying a lot of operational demands. Thus an integrated universal radio navigation system was composed and named

o MILECS = Microwave Integrate Landing Enroute-navigation and air traffic Control System.

The MILECS subsystems, which were explained in this paper, are:

* PDME: Precision DME - First DME-extension

* DLS : DME-based Landing System - Second DME-extension

* DENS: DME-based Enroute Navigation System - Third DME-extension

* DRGA: DME-based Roll Guidance Aid - Fourth DME-extension

* DACS: DME-based Air traffic Control System - Fifth DME-extension

All these subsystems operate with the same airborne equipment, the DLS/DENS-(DLENS) airborne unit.

This concept possesses a broad variety of advantages in the operational, the economic and the integrity area as well and therefore will obtain a growing attention in future.

THE ANALYSIS OF OPERATIONAL MISSION EXECUTION: AN ASSESSMENT OF LOW-ALTITUDE PERFORMANCE, NAVIGATION ACCURACY AND WEAPON DELIVERY PERFORMANCE

by

T.J. Stahlie
Operations Research Engineer
National Aerospace Laboratory NLR
Anthony Fokkerweg 2
1059 CM Amsterdam
The Netherlands

A description is given of characteristics of the mission analysis programs as carried out for the Royal Netherlands Air Force by the National Aerospace Laboratory (NLR). Although the program objectives can differ from trial to trial, they have a number of common properties: the use of on-board instrumentation/recording equipment, no need for ground equipment, specific, high accuracy, techniques for the determination of aircraft position with the aid of aerial photographs etc.

All the programs are aimed at the analysis of relevant mission parameters, e.g. low-altitude performance, navigation accuracy, execution of attack manoeuvre, score of the (simulated) attack. Apart from this primary objective, the additional intentions are: a realistic training opportunity for fighter pilots, the evaluation of new tactics and the acquisition of realistic input data for simulation studies.

In the paper the most important mission analysis programs are dealt with; main point in the description is not the military background of the exercises but the technical set-up including instrumentation and data reduction techniques, calculation techniques applied and typical results obtained.

1. INTRODUCTION

One of the most important problems related to the execution of low-altitude training missions with military aircraft in a (quasi) operational environment is the recording and analysis of relevant mission performance characteristics. If reliable data on the characteristics, e.g. low-altitude performance, navigation accuracy and the score of simulated bombing attacks are available, they can be used for many purposes, e.g.:

- objective assessment of the execution of specific mission tasks (valuable information both at Air Staff and at airbase level),
- improvement of pilot's mission performance (realistic training opportunity),
- evaluation of new tactics,
- use of the data as input for simulation studies,
- evaluation of new flight control, navigation or weapon delivery systems.

In this framework the National Aerospace Laboratory (NLR) has carried out a number of mission analysis programs for the Royal Netherlands Air Force (see table 1). Although the aims of the exercises may differ from trial to trial, they have one common approach in methodology: no use is made of ground equipment or data links in the operational training area. To this purpose special instrumentation and recording units have been developed which can be installed on-board operational RNLAF fighter aircraft (F-104 G, NF-5A/B) without interfering with the normal operational tasks and status of the aircraft. This implies a quick installation/removal capability and minimal modifications to the aircraft. The process of data-reduction associated with the analysis of the relevant mission characteristics under investigation is carried out after mission execution. The turn-around time is dependent on the objectives of the program: if a fast feed back of information to the pilot is required, an extensive analysis of the mission can be delivered within 2 hours after landing; if only scores of simulated attacks are of interest to the pilot a processing time of 1/2 hour can be realised. Although most of the analysis-programs in the past were set up for a limited period, recent developments are aimed at long-term projects incorporating regular reports and time histories of the mission results.

This paper gives a description of the most important exercises. Attention is paid to characteristics common to all programs as well as to specific aspects of instrumentation, recording and data-processing and the application of special calculation techniques. Typical results will be shown.

2. GENERAL MISSION ANALYSIS APPROACH

As has been stated in the previous section the RNLAF/NLR mission analysis programs have one common characteristic: no ground equipment in the operational training area. This aspect is considered to be very important, because:

- a wide spectrum of target types can be selected,
- undesired learning processes as occurring during missions to quite familiar Air Force training ranges can be avoided
- because no ground personnel is required, a relatively cheap and flexible set-up of the mission analysis program is possible

The absence of ground equipment implies special requirements to instrumentation and data analysis.

Instrumentation and recording units have been developed which can be mounted on-board operational aircraft without interfering with the normal operational status of the aircraft. Use is made of existing on-board systems as much as possible. For the realization of this approach the NLR is in the fortunate position of being an aerospace research and development organization with great experience in aircraft instrumentation; so expertise and facilities are amply available to solve the sometimes complicated technical problems associated with the set-up of mission analysis programs where airborne weapon systems play a central role.

Without ground equipment (e.g. radars, laser equipment, transponders) the determination of the aircraft position relative to the ground (target) must be realized in an alternative way. In particular this aspect is relevant for the analysis of the score of a simulated delivery; the aircraft position at the moment of delivery is an important and critical (accuracy!) parameter. To this aim use is made of (a) special photo-camera(s) installed in the aircraft. For the determination of the aircraft position a photogrammetric calculation technique has been developed which is described in detail in reference 1. The only ground information required for the application of this technique is the position of a number of reference points in the target area. For the reference points special features in the terrain are used (see figure 1). Only once, the co-ordinates of these reference points in the target area have to be measured in a local co-ordinate system. So, a large data base of targets can be created and all targets can be used at random in the mission analysis programs. It has been proven that with the photogrammetric technique the aircraft position can be determined with an accuracy of 0.1 m in XYZ co-ordinates and the attitude with an accuracy of 0.1 degree in Euler angles.

3. THE "INBREKER" (BURGLAR) EXERCISES

3.1 Introduction

The exercises "Inbreker" (transl.: "Burglar") were initiated in 1966 by the HQ-RNLAF in order to permit a systematic investigation of parameters which were felt to be of influence on the survivability resp. effectiveness of typical RNLAF military missions. Although similar looking exercises were held in the past by other Air Forces, it was doubted whether the results obtained were directly applicable to the RNLAF missions because of differences such as operational environment, aircraft type, and equipment, mission task and pilot experience. Moreover, the Military Operations Research group of the NLR started - on request of the RNLAF - a theoretical study towards mission optimisation (see also reference 2). Realistic input data in particular concerning the RNLAF pilot-airplane performance during typical low-altitude penetration missions were required.

Both phase I and II of exercise "Inbreker" provided the necessary data, while at the same time a better and objective impression was obtained of the operational execution of RNLAF reconnaissance- (phase I) and strike-mission (phase II) flown with RF- and F-104 G type aircraft respectively. The set-up and results of these two analysis-programs will not be dealt with in further detail in this paper.

When the RNLAF introduced the Canadair Northrop NF-5 A/B for the ground-attack role, the manoeuvrability and advanced navigation equipment of this aircraft were believed to permit a better low-altitude penetration performance. Also the need for an objective impression of execution and effectiveness of the ground-attack phase of the missions was a reason to initiate a third phase of exercise "Inbreker". This phase will be described in more detail in the following sections.

3.2 The "Inbreker" III exercise objectives

The following objectives were formulated:

a. quantification of operational low-level capability as a function of: air speed, terrain roughness, pilot experience, a/c configuration, a/c position in formation, mission phase,
b. analysis of navigation accuracy at initial and pull-up point,
c. measurement and analysis of a/c trajectories during standard RNLAF types of attack manoeuvre,
d. measurement and analysis of aiming accuracy during simulated conventional attacks.

A schematic lay-out of a typical pitch-up attack manoeuvre is shown in figure 2. The notion "aiming accuracy" is defined here as the qualification of a weapon delivery based on the distance between target and computed impact point.

The flight program consisted of a total of 31 missions flown with 2 instrumented a/c, 8 representative targets and 14 participating pilots (7 formations) with total jet experience varying between 400 and 4000 hours.

3.3 The operational realization

Measurement techniques

For the realization of the objectives formulated the following measurement techniques were applied:

a. The measurement of the low-altitude penetration performance was obtained by on-board recording of radar- and pressure altitude. The subtraction of the first from the latter also renders the corresponding terrain-profile (see figure 3a).
b. The analysis of the navigation accuracy was confined to the positional accuracy at those points of the mission, which were felt to be of influence on the mission success (e.g. Initial Point, Pull-Up Point). For this purpose aerial photographs, taken by the pilots as close as possible to these positions, were interpreted on standard geographical maps (see figure 3b). From Doppler registrations the distance-to-go and cross-track distance were analyzed.
c. For the measurement of the attack trajectories a special method, using a simple strap-down inertial system, was developed. The method, a detailed description of which can be found in the references 3 and 4, requires on-board recording of the aircraft accelerations and attitude as well as the accurate knowledge of two positions of the aircraft at the beginning resp. end of the trajectory to be measured. These positions were calculated from aerial photographs, taken at the appropriate moments during the

manoeuvres (Figure 3c). For this purpose a special developed photogrammetric method for aircraft position determination was used (Ref.1).

d. The calculated weapon impact position was obtained by taking into account the appropriate ballistic tables in combination with the "delivery parameters" being the initial conditions of the weapon trajectory. The delivery parameters (true airspeed, angle of pitch and heading) were recorded in-flight while the aircraft angle of attack was derived from the aircraft aerodynamic tables. The position of the aircraft relative to the target was calculated with the earlier mentioned photogrammetric method (see also figure 3d).

Aircraft instrumentation

The aircraft position relative to the target at the moment of weapon delivery was calculated from photographs, taken with a Perkin Elmer Minipan 35 mm panoramic camera; this camera was installed in such a way that it scanned the ground in a longitudinal direction; thus an excellent coverage of the target area could be achieved for a wide range of aircraft pitch attitudes.

For the recording of the aircraft position at those points where it could be assumed to be in approximately level attitude, photographs were taken with 2 standard 70 mm Oude Delft TA-7M reconnaissance cameras, looking in vertical resp. left-oblique direction.

The cameras were positioned in a specially modified centerline standard store, which will be discussed in more detail later on. The figures 4a and 4b present some typical examples of photographs taken with the Minipan and TA-7M cameras.

For the realization of the exercise objectives, as stated in section 3.2, an extensive data recording program was designed.

A distinction was made between the parameters to be used for the analysis of penetration and run-in phase of the missions and those for the analysis of the attack phase. The recording of the first group of parameters was performed with a digital system (Sperry wire recorder, sampling 46 channels/sec) for easier data reduction of the relatively long recordings with a duration between 45 and 90 minutes per aircraft and per mission. For "quick look" purposes and as a back-up this group of parameters was also recorded on a trace recorder (Beaudouin A-13).

The parameters necessary for the analysis of the attack-phase were recorded on a second trace recorder. This provided the flexibility of an optimal choice of the sampling frequency (= times per second that the traces are digitized) afterwards. Due to the relatively short duration of the attack manoeuvres the effort in digitizing the analogue recordings could be kept within reasonable limits.

The most important parameters which had to be recorded were: radar- and pressure-altitude, Doppler position (as determined by its components: cross-track-distance and distance-to-go), aircraft acceleration, aircraft attitude, true airspeed, groundspeed and drift angle. For correlation of both analogue recorders and the digital recorder a common time base was fed to each recorder.

Apart from the routine weapon release procedures additional actions had to be performed by the pilots in order to activate the relevant recording-equipment (see figure 2).

Summarized, the "Inbreker" III instrumentation unit consisted of the following elements:

- modified standard store, attached to the centerline pylon (see figures 5a and 5b), housing all cameras and the radar-altimeter.
- recorder-rack, mounted in the left hand gunbay (replacing the left hand ammunition box, see figures 6a and 6b); this rack contained the 3 data recorders, Haydon clock, signal converters and signal-conditioning electronics.
- accelerometer-unit, also mounted in the left hand gunbay (figures 6a and 6b); this unit contained the 3 accelerometers as well as counters, indicating the filmlength used in the trace-recorders and the number of frames made with the Minipan and TA-7M cameras.

Minor modifications of the NF-5A aircraft, mainly consisting of additional wiring, were required to install the instrumentation.

3.4 Results

The following results from the "Inbreker" III mission analysis program can be mentioned:

- a large amount of data was acquired concerning low-altitude performance during penetration and run-in. A typical example of a flight- and terrain-profile is given in figure 7a. All data together, split up in different terrain categories, permitted a spectral analytical approach for the calculation of power spectra of flight- and terrain-profiles (Ref.5). Figure 7b gives an impression of the groundclearance performance, averaged over all missions (16 hrs total recording time history) and the "highest" resp. "lowest" mission. Also, correlations between aircraft speed, pilot experience, terrain roughness etc. and groundclearance performance have been established.
- the navigation accuracy was in general good.
- the execution of the attack manoeuvres was analysed thoroughly; complete plots both in the horizontal and vertical plane were presented. An example of this presentation is given in figure 8. Correlations between type of manoeuvre, pilot experience, difficulty of target etc. and the "execution quality" (realized manoeuvre vs prescribed manoeuvre) were analyzed. As an example a registration has been taken into account which does not represent the average standard.
- From figure 8b it can be seen that apparently as a result of an inaccurate pull-up the pilot detected the target only after reaching apex. This explains the change in heading towards the target.
- the purpose of the weapon delivery analysis was to determine the delivery accuracy as achieved by the individual pilots in a (quasi) operational environment and to investigate possible deviations from the planned delivery conditions. Therefore a broad analysis was made concerning delivery scores and errors in

delivery parameters (i.e. deviations from planned conditions). The analysis of the delivery scores was split up for all targets and manoeuvre types. Interesting relations between delivery scores and manoeuvre execution, target detectibility, weapon type simulated etc. could be established.

4. THE "MISSION IMPROVEMENT PROGRAM"

4.1 Introduction

The results from "Inbreker" phase III incorporating a complete mission analysis provide a thorough insight in the operational execution of conventional ground-attack missions with the NF-5. It was realized that the data obtained could also be of great value for pilot training provided a quick turn-around time of the results could be realized. In fact, the instrumentation and recording principles as applied for "Inbreker" III needed only to be extended with an adequate set-up of data-processing. Such a "Mission Improvement Program" (MIP) would have to run for a rather long time in order to have optimal impact on pilot proficiency. Furthermore, the flight instrumentation hardware and data-processing facilities should be set up in such a way that servicing by airbase personnel would be possible.

By decision of the RNLAF the Mission Improvement Program had to be realized for the F-104 G type aircraft. The program started in 1975; more than 100 operational missions have been analyzed since.

4.2 Objectives of the program

The objectives of the Mission Improvement Program are as follows:

a. improvement of the execution and effectiveness of the visual-day air-to-ground missions of fighter bomber aircraft F-104 G equipped with conventional weapons, by a fast feed-back of the numerical mission results to the pilot,
b. collection of objective operational data of these ground-attack missions (related to mission aspects like: navigation accuracy, low-altitude performance, delivery score, manoeuvre execution etc; see also exercise "Inbreker" III). These data can be used for debriefing the individual pilots, for determining average operational proficiency of the pilots and as input for the RNLAF/NLR mission optimization studies concerning survivability aspects (Ref.2).

The same mission profiles were selected as for "Inbreker" phase III; for a schematic impression of a typical pitch-up profile one is again referred to figure 2.

Till now, the flight program consisted of 108 missions (ca. 200 attacks analyzed) with 1 instrumented aircraft and 8 representative targets.

4.3 The operational realization

Measurement techniques

The most important mission characteristics measured are: the low-altitude performance and the delivery score. The underlying calculation techniques are identical to those applied during exercise "Inbreker" III (see section 3.3). For a survey of the output parameters one is referred to table 2. The attack trajectory is calculated in a different way; for the F-104 G aircraft data from the LN-3 inertial navigation system could be obtained. Special updating techniques were not applied for trajectory calculations, since the LN-3 system furnishes data accurately enough for determining the trajectory during short time manoeuvres.

Aircraft instrumentation

One important requirement for the MIP F-104 G instrumentation is that the operational status of the participating aircraft should not be affected; remodifications have to be carried out within a very short time period (1/2 hour). This requirement was met by making use of "quick release units" and by avoiding extensive mechanical and electrical modifications to the aircraft.
The special instrumentation unit necessary to collect relevant flight data consists of:

- a forward-looking photo camera,
- a "Signal Conditioning Unit" (SCU) used as an interface device,
- a "Flight Data Acquisition Unit" (FDAU) which converts analog data (from SCU) into digital data,
- two magnetic cassette tape recorders.

The photo camera has been installed in the nose-section of a pod mounted at the aircraft's centre-line bomb rack.

The remaining instrumentation has been installed in two gas cans, connected to the T-rack in the electronic compartment.

The Signal Conditioning Unit has been built in one of the gas cans which is called the "Signal Conditioning Can".

The FDAU and the two magnetic cassette tape recorders have been mounted in the second gas can which is called the "FDAU Can".

The on-board wiring between the electronic compartment cover and a position close to the Centre-line Bomb rack, is used to connect the pod with the gas cans. The installation of the additional wiring between this point and the pod can be considered as a special modification.

The instrumentation system is supplied by the aircraft's power unit.

The camera and recorders are controlled with the aid of the trigger switch and bomb release button respectively, installed on the control stick; no additional pilot actions are required.

By using a "splicing cable" flight data are tapped from the inertial system LN3 and the air data computer for recording purposes.

The figures 9a up to 9d give an impression of the MIP instrumentation package.

Data processing

A survey of the data processing of a MIP mission is presented in figure 10.

After completion of the mission the recorded flight data are transmitted from the airbase to the data processing station (taking into account security aspects). This occurs via the public telephone network with the aid of a portable transmitter unit called PORDALI (portable data link). At the same time two aerial photos taken at IP and at weapon delivery are developed by the airbase personnel. From the former, the aircraft position at IP is determined and from the latter the co-ordinates of the reference points of the target area are measured. These data together with the information given by the pilot to the project officer during a debriefing (target attacked, weapon used and weather conditions) are additional input data for the mission analysis program and are telephoned to the data processing station (i.e. the Computer-centre of the NLR).

The results of the analysis program are telegraphed to the airbase (taking into account security aspects). These data enable the project officer together with the pilot involved to analyse the mission results within two hours after mission completion.

For statistical analysis the results are stored in a special data base which gives the possibility to determine the average operational proficiency over a number of MIP missions.

4.4 Results

Run-in phase

Groundspeed, low-altitude performance and navigation accuracy are available. As is shown in table 2 the minimum-, median- and maximum values of these parameters are given. Furthermore the actual run-in trajectory with respect to the planned trajectory is given in a graph.

Attack manoeuvre and weapon delivery

Aircraft's trajectory during the attack manoeuvre is given in a graph while delivery parameters such as altitude above target, slant range to target, dive angle, heading etc. are given in a table (see table 2).

Weapon impact

Weapon time of flight, weapon impact point (with and without wind) are presented. Aircraft's position at weapon impact (fragmentation envelope) is also given.

The weapon impact point is presented in a separate graph.

General remarks

It is evident that these objective results give the project officer and pilot involved valuable information for discussing and analyzing the execution of the mission in an extensive way.

5. NEW MISSION ANALYSIS PROGRAMS

As described in chapter 4 a special instrumentation unit has been developed for the F-104 G aircraft to analyse the execution and effectiveness of operational Fighter Bomber Attack trainings missions in the framework of the Mission Improvement Program. Apart from the objectives of MIP and the related specific data processing it is also possible to use the combination of F-104 G instrumentation set and data-handling computer programs for the acquisition of other data concerning the operational mission execution. These data can be related to the execution of standard F-104 G penetration and attack tactics and also of alternative e.g. new tactics for these mission phases. In this framework evasive manoeuvres can be recorded, low-altitude performance can be determined, the effectiveness of "range" missions can be assessed, the effect of new equipment (navigation systems, weapon delivery systems) can be analyzed, etc. This slightly modified MIP hardware system is called "Mission Data Acquisition System" (MIDAS) and is in operational use since the mid of 1977.

An other new program is the "Delivery and Impact Analysis System" (DIAS). This system is being developed for the RNLAF for the assessment of the score of conventional bomb deliveries. Basically it makes use of a single camera attached to the aircraft. With this camera a number of photo pictures is taken at the moment of (simulated) weapon delivery; these photo's are processed in such a way that reference points in the target area can be read out with the photogrammetric calculation technique as described in reference 1 (see also chapter 2). The system seems suitable for large scale installation. Data processing can be carried out at airbase level with the aid of some specific hardware such as: photo reading equipment, mini computer and a graphic display. Statistical analysis of stored mission data will be possible if data storage is realised.

6. THE BENEFITS OF MISSION ANALYSIS TECHNIQUES

In relation to the execution of low-altitude military missions, the approach of mission analysis as described in this paper has the following benefits:

. a thorough insight in the most relevant mission characteristics can be obtained. In particular low-altitude performance, navigation accuracy and weapon delivery of typical low-altitude military missions can be

analyzed.

- possible imperfections in both aircraft and pilot performance during low-altitude missions can be detected. If the process of data reduction is carried out fast the pilot has a detailed overview of the mission execution.
- bomb scoring systems, like DIAS, can be developed without any need of ground equipment. Hereby use is made of special photogrammetric calculation techniques for the determination of the aircraft position and attitude at the moment of simulated weapon delivery.
- new tactics with respect to low-altitude navigation, manoeuvring and weapon delivery with their impact on the execution of a mission can be evaluated.
- a large amount of data can be used for further investigation in the framework of other studies. For example, measured aircraft manoeuvres are used as input in computer simulation models of ground-based air defence systems in order to assess the vulnerability of aircraft executing those manoeuvres (see also reference 2).
- the effect of new flight control systems, navigation and weapon delivery systems on the operational mission execution can be established. In this way the evaluation of these systems can be carried out under (quasi) operational conditions.

7. POINTS OF CONTACT

Those who like to have more information on the mission programs are advised to contact one of the following points:

Royal Netherlands Air Force RNLAF
Assistent Chief of Staff for Operational Requirements (AOB)
Section Operations Research and Evaluation (ORE)
Prins Clauslaan 8
The Hague
The Netherlands

National Aerospace Laboratory NLR
Department of Flight
Military Operations Research Group
Ant. Fokkerweg 2
Amsterdam
The Netherlands

8. REFERENCES

1. v. Eck, M.A.A. The photogrammetric method as developed for the "Mission Improvement Program" to determine the aircraft position and heading at the moment of weapon delivery. NLR Memorandum VG-77-022 L, 1977.
2. Bovy, M.H.W. The "Ground-attack/Penetration" model: a Monte Carlo simulation model to assess the survivability and to evaluate tactics for low-altitude military missions in an environment of groundbased airdefence systems. Paper nr. 12 of Proceedings 25th GCP/AGARD meeting, Dayton, Ohio, USA.
3. Stahlie, T.J. and Veldhuyzen, R.P. The measurement of aircraft trajectories during manoeuvres of short duration with a simple strapdown inertial system. NLR Memorandum VG-72-031, 1972.
4. Stahlie, T.J. An updating technique for correcting measured positions of an aircraft trajectory. NLR Memorandum VG-72-040, 1972.
5. Veldhuyzen, R.P. and Hanekamp, J. A new approach to the generation of flight altitude profiles of low level penetration missions (Confidential). NLR Memorandum VM-71-048, 1971.

Name	Period	Mission type	Aircraft type
. "Inbreker" (Burglar) phase I	June - August 1966	Visual-day Recce	RF-104 G
. "Inbreker" (Burglar) phase II	April - June 1967	Visual-day Strike	F-104 G
. "Inbreker" (Burglar) phase III	May - August 1972	Visual-day ground-attack	NF-5A
. "Mission Improvement Program" (MIP)	1975/1976	Visual-day ground-attack	F-104 G
. "Delivery and Impact Analysis System" (DIAS)	1977... (under development)	Visual-day ground-attack	NF-5A
. "Mission Data Acquisition System" (MIDAS)	1977...	Recce/Strike	F-104 G

Table 1. Survey of RNLAF mission analysis programs.

MISSION IMPROVEMENT PROGRAM MIP AIR-TO-GROUND

ANALYSIS MISSION NO. _____

TARGET _____ WEAPON _____

RUN-IN			
GROUNDSPEED (KTS)		MEDIAN ____	
PRES. ALTITUDE ABOVE TARGET (FT)	MIN ____	MEDIAN ____	MAX ____
GROUNDCLEARANCE (FT)	MIN ____	MEDIAN ____	MAX ____
X-TRACK DEVIATION (FT)	MIN ____	MEDIAN ____	MAX ____
WEAPON DELIVERY 1)			
APEX ALTITUDE	____ FT		
SLANT RANGE TO TARGET	____ FT AT ____ FT OFFSET		
ALTITUDE ABOVE TARGET	____ FT		
VERTICAL ACCELERATION	____ G		
AMBIENT AIR TEMPERATURE	____ °C	TAS ____ KTS	
ROLL	____ DEG	IAS ____ KTS	
DIVE ANGLE	____ DEG		
UTM HEADING	____ DEG		
WEAPON TIME OF FLIGHT	____ SEC		
WEAPON IMPACT (WITHOUT WIND)	____ FT AT ____ DEG		
TAIL-WIND (KTS)	____ CROSS-WIND (KTS) ____		
WEAPON IMPACT (WITH WIND)	____ FT AT ____ DEG		
STRAFING ACCURACY (FT)	____		
PICKLE / TRIGGER TIME (SEC)	____		
A/C SLANT RANGE TO IMPACT AT WEAPON IMPACT (FT)	____		
A/C ALTITUDE ABOVE TARGET AT WEAPON IMPACT (FT)	____		
PIPPER POSITION ON "ROBOT" PHOTOGRAPH (MM)	X_r ____	Y_r ____	
IMPACT POSITION ON "ROBOT" PHOTOGRAPH (MM)	X_r ____	Y_r ____	

1) gunnery "open fire"

***Table 2** Example of the presentation of the results of the MIP F-104G mission analysis*

***Fig. 1** Photograph taken at weapon-delivery showing 5 reference points in the target area*

1 – 'PICKLE' FOR PHOTOGRAPHIC POSITION RECORDING (TA-7M CAMERAS) AND FOR INCREASED TRACE-RECORDER SPEED DURING 60 SECS.

2 – 'TRIGGER 2. DETENT' FOR ACTIVATING THE MINIPAN PANORAMIC CAMERA AND THE GUN-CAMERAS

3 – 'PICKLE'1) FOR INDICATING THE MOMENT OF SIMULATED WEAPON DELIVERY ON RECORDINGS PLUS 'TRIGGER'2. DETENT RELEASE' FOR STOPPING THE MINIPAN PANORAMIC CAMERA AND THE GUN-CAMERAS

1) IN AGREEMENT WITH STANDARD DELIVERY PROCEDURE

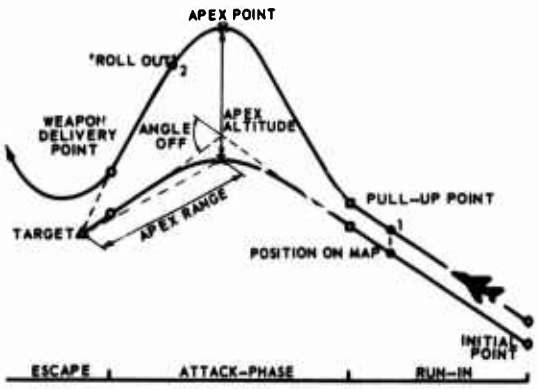

***Fig. 2** Schematic lay-out of pitch-up attacks with special pilot actions*

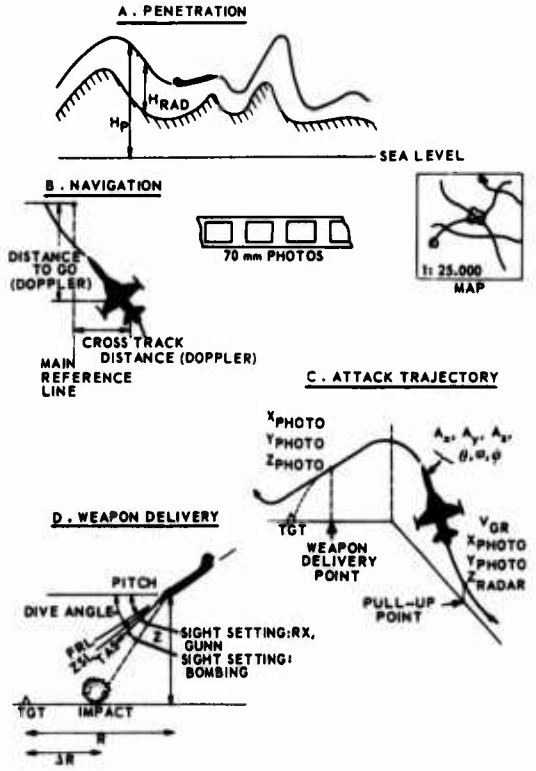

***Fig. 3** Inbroker III measurement techniques*

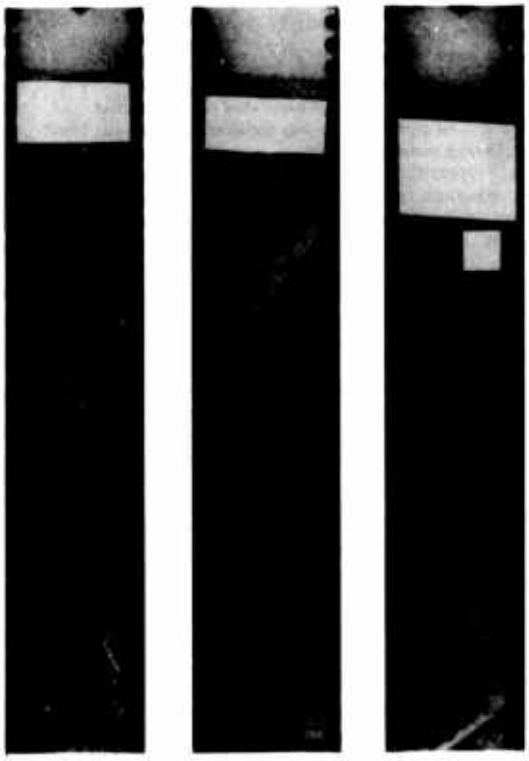

Fig 4a Typical minipan panoramic camera filmstrips

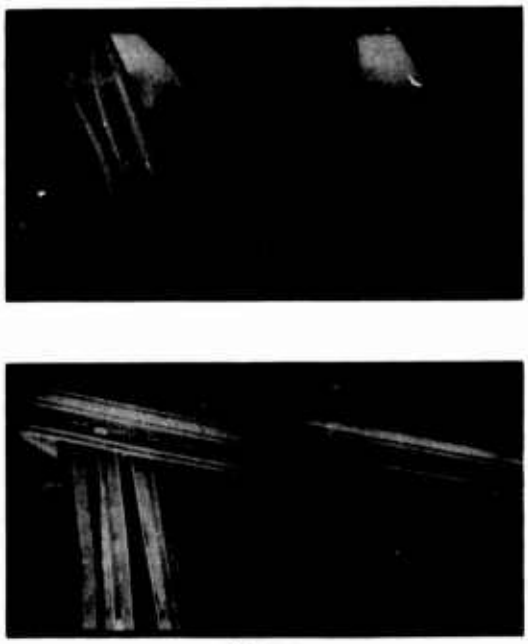

VERTICAL

Fig. 4b Typical recce-camera (TA-7M) filmstrips

Fig. 5a NF-5A with instrumented standard store

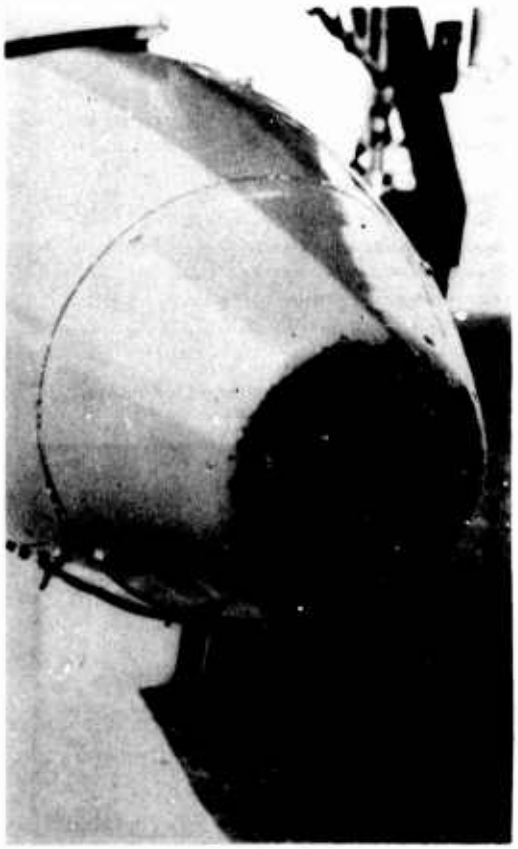

Fig. 5b Close-up of nose-section of standard store with Perkin Elmer Minipan panoramic camera

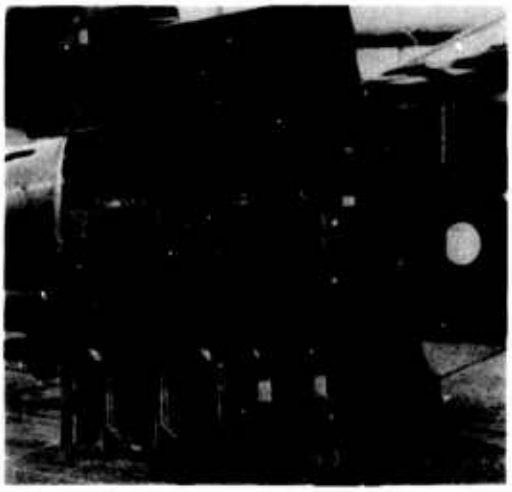

Fig. 6a NLR instrumentation in left hand gunbay of NF–5A

Fig. 6b Close–up of recorder–rack (left) with 2 'Beaudouin' trace recorders resp. 'Sperry' wire–recorder and accelerometer–unit (right)

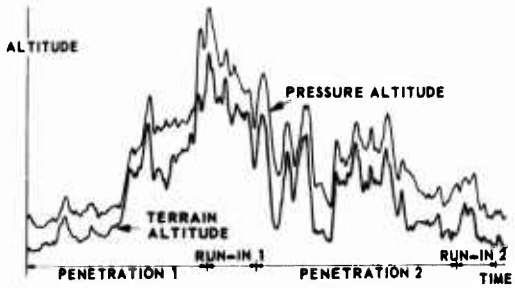

Fig. 7a Typical flight–and terrain –profile

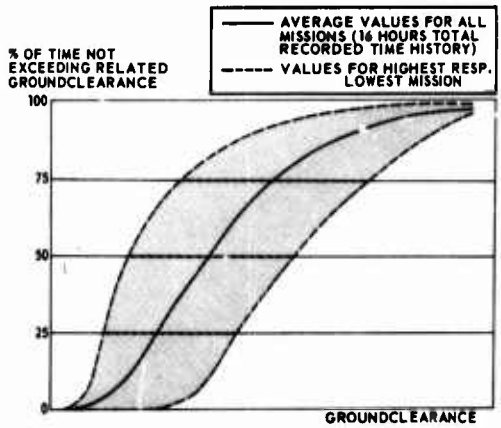

Fig. 7b Impression of 'Inbreker' III groundclearance performance

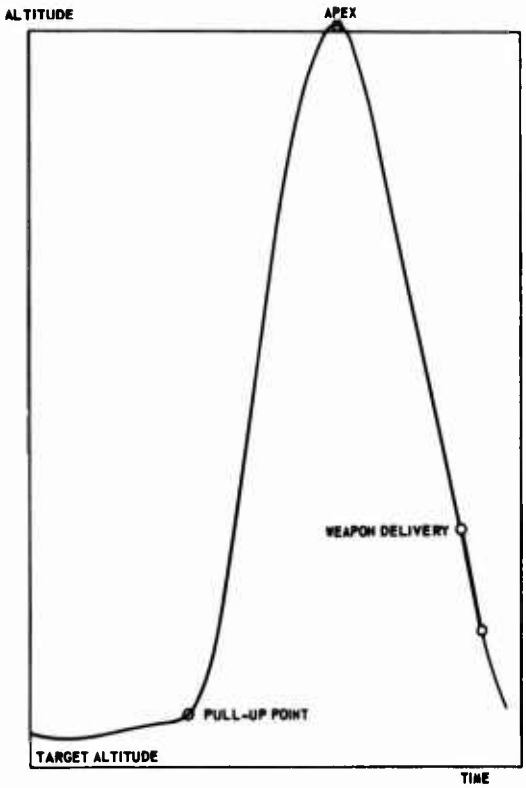

Fig. 8a Altitude profile of typical pitch–up attack

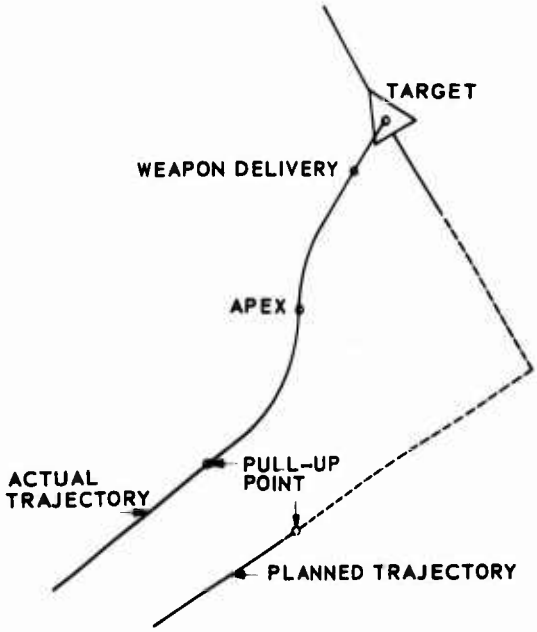

Fig. 8b Horizontal projection of A/C trajectory during execution of typical pitch–up attack (UTM–grid)

A. MIP-MODIFIED F-104G WITH INSTRUMENTED STANDARD STORE

B. CLOSE-UP OF STANDARD STORE WITH SPECIAL CAMERA

C. SIGNAL CONDITIONING UNIT AND FDAU-CAN

D. CASSETTE RECORDERS IN FDAU-CAN

Fig. 9 The MIP instrumentation unit

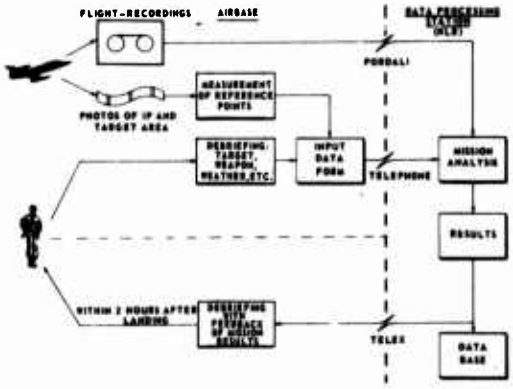

Fig. 10 Block diagram of the MIP data processing

EXPERIMENTAL DETERMINATION OF THE NAVIGATION ERROR OF THE 4-D NAVIGATION, GUIDANCE, AND CONTROL SYSTEMS ON THE NASA B-737 AIRPLANE

by

Charles E. Knox
NASA Langley Research Center
Hampton, VA 23665

SUMMARY

A series of flights were flown with the NASA B-737 airplane on an area navigation test path. Ground-based radar tracking information was utilized to compute the error of the airplane's position as estimated by an advanced experimental 4-D area navigation system onboard the airplane.

Navigation error data from these flights are presented in a format utilizing three independent axes - horizontal, vertical, and time. The navigation position estimate error term and the autopilot flight technical error term are combined to form the total navigation error in each axis. This method of error presentation allows comparisons to be made between other 2-, 3-, or 4-D navigation systems and allows experimental or theoretical determination of the navigation error terms.

Position estimate error data are presented with the navigation system position estimate based on dual DME radio updates that are smoothed with inertial velocities, dual DME radio updates that are smoothed with true airspeed and magnetic heading, and inertial velocity updates only. The normal mode of navigation with dual DME updates that are smoothed with inertial velocities resulted in a mean error of 390 m with a standard deviation of 150 m in the horizontal axis; a mean error of 1.5 m low with a standard deviation of less than 11 m in the vertical axis; and a mean error as low as 252 m (approximately 1.4 sec) with a standard deviation of 123 m (approximately 0.7 sec) in the time axis.

SYMBOLS

ADD	position estimate update mode based on dual DME radio inputs that are smoothed with true airspeed and magnetic heading inputs
AXX	position estimate update mode based on true airspeed and magnetic heading only
CADC	central air data computer
CPE	circular position error
CRT	cathode ray tube
DME	distance measuring equipment
D-DME	dual DME
FL230	flight level 230 (approximately 7010 m (23,000 ft) above sea level)
FTE	flight technical error, m
GS	ground speed, knots
HER	altitude flight technical error, m (see figure 8)
IDD	position estimate update mode based on dual DME radio inputs that are smoothed with inertially derived velocity inputs
INS	inertial navigation system
IXX	position estimate update mode based on inertially derived velocity inputs
LAT	latitude, deg
LONG	longitude, deg
MAG HDG	magnetic heading, deg
NCDU	navigation control display unit
$\bar{p}_1$	position vector

R	radius, m
SEPR	time axis flight technical error, m (see figure 8)
TACAN	tactical air navigation system
VOR	VHF omnidirectional range navigation system
WPT	way point
XTK	crosstrack flight technical error, m (see figure 8)
X,Y,Z	Earth-centered Cartesian coordinates
2-,3- & 4-D	horizontal, vertical, and time navigation, respectively
γ	flight-path angle, deg
σ	standard deviation

1. INTRODUCTION

The rapid advances in the state of the art of microprocessors have allowed significant advancement in the computational capabilities of navigation, guidance, and automatic-flight control systems. Area navigation systems may utilize a variety of inputs such as air data computers, inertial referenced platforms, doppler radar, low-frequency navigation systems, VOR, DME, TACAN, and satellite information to estimate the airplane's position in space. The navigation computer can calculate guidance in the lateral, vertical, and ground speed or time modes of flight. Guidance may be displayed directly to the pilot for manual flight or may be transferred to the flight control system for automatic flight.

Airplanes utilizing navigation systems and flight control systems of various levels of sophistication and automation will operate in the same airspace. It is, therefore, imperative that the navigation and flight control systems on board these airplanes assure compatible position estimates and delivery accuracy, both within the present separation criteria and possibly with reduced separation. The overall commonality of these systems must then be the navigation position estimate and the system's guidance and airplane response characteristics.

This report will present the results of flight tests where the accuracies of the experimental navigation system's position estimate and the flight technical error of the automatic-flight control system on board the NASA Boeing 737 airplane were experimentally measured during automatic 4-D flights. A circular position error concept was used to document the position estimate error so that the total navigation error could be specified in three axes independent of the flight-path geometry.

2. BACKGROUND

2.1 Terminal Configured Vehicle Program

The NASA Terminal Configured Vehicle (TCV) program was established to examine the airborne aspects of advanced aircraft systems and operational procedures for the fourth generation air traffic-control system. To accomplish the program's flight research in a realistic manner, NASA acquired a Boeing 737, twin-jet commercial-type transport airplane. The airplane is equipped with an advanced electronic display system, an advanced navigation and guidance system, an advanced flight control system, and an extensive data recording system. The research pilots interface with these advanced experimental systems in a separate, full-size research cockpit located aft of the conventional airplane cockpit.

The advanced navigation system is a highly sophisticated area navigation system which operationally satisfies ARINC Characteristic 582 (Mark 2 Air Transport Area Navigation System) but was designed as a research tool with flexibility achieved through software control.

The final test to determine the effects that software modifications have on the navigation and guidance system is the measurement of the airplane's navigational error. Hence, a method of obtaining and specifying the navigation position estimate and the guidance flight technical error was required.

2.2 Navigation Error Specification Guidelines

The total navigation error may be specified in various components to best suit the engineering and certification process and to facilitate the user and airspace planners. In choosing a method to specify navigation system error, it was desirable not only to be able to document the effects that software modifications have on navigational accuracy of the NASA B-737 navigation system, but also to be able to compare this system with other navigation systems. Hence, the following guidelines were followed for choosing a method to specify the navigation error: (1) Be able to provide independent, uniform accuracy specifications for horizontal navigation (2-D), vertical navigation (3-D), and time navigation (4-D). This will allow a sophisticated 4-D navigation system to be compared to a relatively simple 2-D navigation system in the 2-D mode of navigation; (2) Navigation

system error specifications would not be dependent upon sensor inputs (not dependent on rho/theta accuracies inputs such as with VOR/DME); (3) Navigation system error would not be path dependent (horizontal error would not necessarily cause an altitude error when on a climbing or descending flight path); and (4) Navigation system error could be obtained with either experimental measurement or theoretical analysis, or a combination of both.

3. DESCRIPTION OF THE AIRPLANE, EXPERIMENTAL SYSTEMS, AND RADAR TRACKING FACILITIES

3.1 Airplane

The NASA test airplane is a Boeing 737-100 twin-jet transport airplane shown in figure 1. This airplane was designed for short-haul commercial transport operations into minimum facility airports with short runways. Although the NASA B-737 airplane is used as a research vehicle with separate experimental navigation, guidance, flight control, and display systems, all of the normal flight systems (flight control, navigation, pressurization, etc.) and the conventional cockpit have been retained in a normal, functional state. This allows changes to occur to any of the experimental systems without affecting the operational safety of the airplane.

3.2 Experimental Research Flight Systems

The experimental research flight systems consist of a digital flight control system, an electronic cathode-ray-tube (CRT) display system, and a digital navigation and guidance system integrated into a separate two-member crew research cockpit. The research cockpit shown in figure 2 is full-size and is located in the airplane cabin just forward of the wing. The research cockpit is configured for two-man crew flight operations. All of the airplane's primary flight control surfaces (pitch, roll, and yaw axes) may be operated directly from the research cockpit through the three experimental flight control computers. The throttle, thrust reversers, flaps, and radios may also be operated from the research cockpit. Speed brakes, autobrakes, and the landing-gear position may be signaled from the research flight deck to the airplane's safety pilots in the conventional flight deck. The safety pilots must then engage these systems.

The research pilots may fly the airplane manually through two augmented control modes or they may select various degrees of automatic flight through the autopilot mode control panel shown in figure 3. Autopilot flight options range from track-angle select and flight-path angle select (or altitude hold) to fully automatic 4-D path tracking. The autothrottle may be utilized at any time in an airspeed or ground speed mode in conjunction with 4-D automatic path tracking.

Each of the research pilots has three CRT displays for airplane attitude, navigation and guidance information, and for addressing the navigation computer. The electronic attitude indicator (EADI) display gives the pilot basic airplane attitude, flight path angle, potential flight-path angle, and, at the pilot's discretion, flight director and navigation-situation information. The electronic horizontal situation indicator (EHSI) display gives the pilot an electronically drawn map of pertinent navigation information (routes, navaids, airports, etc.) relative to the airplane's position. The pilot may display other information such as other airports, obstacles, route altitudes and ground speeds, a time guidance box for 4-D navigation, and airplane horizontal-path trend information. The third CRT display is used by the research pilots as an input-output display unit which is used to address the navigation computer and to assist with navigation.

Figure 4 is a simplified functional block diagram of the navigation, guidance, and control process during automatic path tracking. The navigation and guidance calculations are performed in a single Litton C-4000 digital navigation computer. Various navigation sensor signals (including INS, CADC true airspeed, magnetic heading, VOR, and DME) are input to the navigation computer. The navigation computer computes an estimate of the airplane's position based on combinations of the sensor inputs. Horizontal, vertical, and time (thrust) commands based on the airplane's estimated position, velocity, and path tracking errors are computed and transferred to the flight control system 20 times/sec. The flight control system then commands the flight control surface servos.

3.3 Airborne Data Acquisition System

Data were recorded on board the airplane on a wide-band magnetic tape recorder at 40 samples/sec using the NASA Langley Piloted Aircraft Data System (PADS). This data included ninety-three parameters describing the airplane's configuration, attitude, and control surface activity. Thirty-two additional channels were used for recording parameters calculated in the navigation computer. Video recordings of the EADI and EHSI displays were also made throughout the flights. All recorded data on the airplane are time correlated.

3.4 Radar Tracking System

Radar tracking was provided by the AN/FPS-16 ground-based radar tracking facility at the NASA Wallops Flight Center. The radar utilizes a 4.2 m antenna for improved accuracy. Slant range, azimuth angle, and elevation angle data were recorded continuously on magnetic tape for postflight analysis. Postflight analysis consisted of a linear removal of

position drift as determined by a radar calibration at the beginning and end of each flight and conversion to latitude, longitude, and altitude coordinates. An oblate spheroid Earth model was used during these conversions.

4. THE NAVIGATION COMPUTER AND MAJOR SOFTWARE FUNCTIONS

4.1 Computer Processor Unit

The navigation computer is a Litton C-4000 general purpose digital computer designed for airborne computations and data processing tasks. It utilizes a 24-bit word length and has a 32,000-word core memory which is directly addressable.

Major software routines in the C-4000 computer include the navigation position estimate, automatic tuning of the navigation radios, guidance commands to the flight control computer system, flight route definition, pilot input/output control, piloting display system computations, and flight data storage for navigation purposes.

4.2 Automatic Navigation Radio Tuning

The normal mode of radio updating of the navigation position estimate on the NASA B-737 airplane is dual DME (D-DME). The DME's may be manually tuned or automatically tuned. In the automatic radio tuning mode, the first DME is selected based on the way points that define the flight path. If no flight path has been programed, this DME must be manually selected.

The second DME selected must pass a geometry check in which the angle between the airplane and the two DME's must be between 30° and 150°. This geometry check will be applied first to all known DME's within a 40 n.mi. radius of the airplane. If no DME's are available within 40 n.mi., the radius is increased in 40 n.mi. increments up to 200 n.mi. If no DME's are available, VOR inputs may be selected. The geometry check is made four to five times per second.

Before using the DME inputs of a selected station, a check is performed to determine the difference between the estimated position of the airplane from the DME and the measured distance from the DME. If this difference is more than 5 n.mi., the DME station will be rejected and another one tuned. This check precludes an erroneously defined DME station from influencing the navigation position estimate or selecting a DME station from a position where frequency protection from other stations is weak.

A validity check is made on each radio input to determine that the signal is strong enough to use. If the validity check fails, the input will not be used and another DME station will be selected. Neither DME inputs will be used when the airplane is banked more than 15° because of the possible effects from airborne antenna blockage. However, neither DME will be reselected unless required by a geometry check.

4.3 Navigation Position Estimate

An estimate of the airplane's horizontal position in terms of latitude, longitude, and vertical position above mean sea level is made by the navigation computer 20 times/sec (ref. 1). The horizontal position estimate is obtained by first calculating the north and east components of the position error determined from both radio inputs (normally D-DME) and the previous position estimate. A system velocity is then derived from inertial north and east velocity components summed with an error term developed from the radio position error. Next, latitude and longitude update terms based on an oblate spheroid Earth are calculated from the system velocity and the radio position error. These update terms are added to the previous latitude and longitude terms to obtain a new position estimate. The inertially smoothed, dual DME updated position, designated IDD, is the normal mode of position calculations.

If radio inputs are not available, the position error is set to zero. The position estimate calculations continue with the solution becoming entirely inertially referenced. This position estimate update mode is designated as IXX. If the inertial system velocity inputs are not usable, true airspeed from the CADC system and magnetic heading will be used to generate north and east velocity components. This position estimate update mode is designated as ADD or AXX.

The vertical position (altitude) estimate is based on a combination of vertical acceleration and barometric altitude. The quick dynamic characteristics of the inertial signal are utilized during vertical flight-path changes to produce a more responsive estimate of altitude. The long-term stability of barometric altimeter signals is utilized so that the vertical position estimate is primarily based on barometric pressure. This produces a quickened response to altitude changes but retains the necessary vertical compatibility with other barometric altitude-referenced aircraft operating in the airspace.

4.4 Guidance Calculations

The guidance commands for horizontal, vertical, and time navigations are developed in the navigation computer. In all three axes (roll, pitch, and thrust), path-tracking errors are computed and combined to give an acceleration command which, when obeyed, nulls the tracking errors. In the roll axis, bank angle is associated with lateral accelaration so that the lateral steering signal sent from the navigation computer is in the form of bank-

angle command. In the pitch axis, the steering signal is commanded directly as vertical acceleration. In the thrust axis, longitudinal acceleration is in the form of throttle position command.

The path-tracking errors used in generating steering signals are computed by vector mathematics (ref. 2) by assuming a round Earth with a right-hand orthogonal coordinate system in its center, as shown in figure 5. Though the position estimate made by the navigation computer is based on the Earth represented as an oblate spheroid, path definition and guidance calculations are greatly simplified by assuming a round Earth. Errors in great circle distances and vector lengths that are used during guidance calculations are caused by using the round Earth simplication and are less than 0.33 percent (6 m/n.mi.). These errors were considered negligible.

5. EXPERIMENT DESIGN AND PROCEDURES

5.1 Design

The NASA B-737 airplane was to be flown on a predefined, self-contained 4-D flight path. The navigation-position estimate error was to be determined from a comparison of the airplane's estimated position with the airplane's true position as defined by a ground-based radar. Autopilot flight technical error (FTE) was to be established during automatic flight from path-tracking parameters used in the guidance calculations. The position estimate error and the FTE were to be combined statistically to form the total navigation error.

The navigation-position estimate accuracy utilizing various navigation sensor inputs was to be made for comparison purposes. These sensor inputs included D-DME with inertial velocity smoothing (IDD), D-DME with CADC true airspeed and magnetic heading smoothing (ADD), and inertial velocity inputs only (IXX).

5.2 Flight Procedures

At the beginning of each flight, the airplane would be positioned on a known reference point on the runway for radar calibration. Once airborned, control of the airplane would be shifted from the conventional flight deck to the research flight cockpit as soon as possible for navigation to the start of the test path. Before passing the first way point of the test path, the airplane would be stabilized in 4-D flight. During the automatic 4-D flights, the autopilot and autothrottles would be engaged before passing the first way point of the test path. After the test path was completed, the airplane was returned to the reference point on the runway for postflight radar calibration.

5.3 Flight Test Path

The flight test path is a preprogramed, self-contained 4-D flight path. The path is defined three dimensionally by latitude and longitude referenced way points with altitude assignments. A ground speed is also assigned to each way point. For 4-D flight, a time profile from which time guidance can be calculated is developed by the navigation computer from the ground speeds at each way point when a desired arrival time is specified by the pilot for any one of the way points defining the path.

The flight path, shown in figure 6 requires approximately one hour to fly and varies in altitude between 1829 m (6000 ft) and FL230. The routing of the flight path was chosen due to radar coverage limitations, airspace restrictions, and air-traffic control considerations. A large number of DME radio facilities were also available for good radio updating.

Due to the local traffic-flow considerations, a rapid climb to FL230 after take-off was required. This required a 300^{0} turn while climbing at the airplane's maximum performance capabilities. If the winds aloft were above 20 knots while the airplane was in the turn, a large time error would develop since the airplane did not have enough thrust available to increase its ground speed to catch the time guidance box. This was considered a path design problem rather than an airplane system deficiency.

6. TOTAL NAVIGATION ERROR AND ITS COMPONENTS

6.1 Error Axes

The total airplane navigation error is the difference between the airplane's actual position and the desired position. The total airplane navigational error was specified in three axes - horizontal, vertical, and time, as shown in figure 7. Error specification for each axis is independent to eliminate cross coupling effects of the error between axes due to path dependence.

Each axis contains two types of error components. One type is associated with the navigation sensor inputs and position estimate calculations. The other types are flight technical errors associated with guidance and control of the airplane in either the manual or automatic mode of flight. Each of these components can be determined analytically or measured experimentally and then statistically combined in a root-sum-square function $(\sigma = \sqrt{\sigma_1^2 + \sigma_2^2 + \ldots + \sigma_n^2})$ to define the total navigation error for each axis.

6.2 Position Estimate Error

The error component associated with the navigation sensor input and position estimate in the horizontal axis is described as a circular position error, CPE. The CPE concept is not limited to rho/theta (VOR/DME) type sensor inputs and may be uniformly utilized for all types of navigation sensor inputs including self-contained (INS, Doppler radar, etc.) inputs. The CPE is the horizontal distance between the airplane's actual position and its navigation systems position estimate. Direction of th CPE may be obtained for diagnostic purposes. However, the random nature of the CPE direction will require airspace utilization to be based on a circular boundary of position error. The equations and method of determining CPE and its direction for a latitude/longitude derived position estimate are presented in the appendix.

The CPE component consists of airborne receiver errors, navigation ground station errors, and navigation computer calculation errors. These errors may be determined analytically and then statistically combined in a root-sum-square fashion to obtain the CPE component. However, no attempt was made in this report to determine the magnitudes of these errors since CPE was determined from radar tracking data.

When direct measurement of CPE is employed, any additional error caused by the system that is used to determine the airplane's true position must be accounted for in the CPE error. During the navigation tests described in this report, a ground-based radar was used to determine the airplane's true position.

The tracking errors attributed to the radar are given in the following table.

	Bias	Noise
Range	2 m	2 m
Azimuth angle	0.05 mrad	0.1 mrad
Elevation angle	0.05 mrad	0.1 mrad

Based on a maximum range from the radar of 60 n.mi., these angular errors are 5.5 m bias and 11.1 m noise. The bias error was added to the CPE mean and the noise error was added to the CPE standard deviation in a root-sum-square fashion.

In the vertical axis, true altitude may be obtained in several different manners. However, true-altitude information is not generally useful for specifying the vertical axis error since all airplanes operating in the airspace use barometric altitude references. Some of the more sophisticated navigation systems may employ vertical acceleration or velocity to augment the altitude estimate, but this is only to improve the short-term barometric response to altitude changes. Since the vertical estimate of altitude is based primarily on the barometric altimeter, the sensor input error in the vertical axis can be obtained from a standard altimeter calibration. In the NASA B-737 airplane, this altimeter calibration showed an error of less than 6 m at FL230.

The sensor error in the time axis comes from the time error produced by the systems time mechanism and the CPE. Most navigation systems that are sophisticated enough to provide 4-D navigation capabilities will use a digital time clock. These mechanisms provide a relatively error-free time reference. However, the time sensor error input from a particular system may be determined from calibration. On the NASA B-737 airplane, the time drift was less than 28 msec/h and was considered negligible.

Since the CPE must be thought of as a circle of error, its effects must be added to the time axis navigation error. This necessitates that the CPE be converted to units of time or that the time error be expressed in distance. In this report, time error is expressed in length since the time axis guidance is derived from the distance between the airplane and its desired point of time position.

6.3 FTE

Flight technical error (FTE) is defined as the accuracy with which the pilot or autopilot controls the airplane, as measured in the success in causing the indicated airplane position to match the desired position. During automatic flight, FTE includes the guidance calculations errors and the autopilot/airplane response to commands which will nullify path-tracking errors. Flight technical error was reported for the autopilot controlled flights during the navigation system tests.

Three of the path-tracking errors used to develop path steering signals for the autopilot were used to describe the FTE. These path-tracking errors, shown in figure 8, include the crosstrack error (XTK) for the horizontal axis, the altitude error (HER) for the vertical axis, and the separation error (SEPR) between the airplane and its desired "time box" position for the time axis.

Crosstrack error is the perpendicular distance from the path to the airplane. On a curved leg segment, crosstrack error is the airplane's radial distance from the path. The altitude error is the difference between the airplane's altitude and the altitude of the programed path at the abeam point (the point on the path from which the crosstrack error is defined). The separation error is the along track distance between the abeam point on the path to the desired point on the path defined by the path ground speed profile and selected way point times.

The separation error is specified in units of distance rather than time so that the effects of the CPE may be added to obtain the total navigation error in the time axis. In addition, the time guidance algorithms in the NASA B-737 uses the separation parameter to determine the time error. The separation error may be converted to units of time by dividing by the programed ground speed.

7. RESULTS AND DISCUSSION

7.1 Flight Summary

Table I summarizes the flight control mode and type of radio update and smoothing inputs that were used to estimate the airplane's position for each of the navigation test flights. Remarks were added for each flight where an anomaly that invalidated or adversely influenced flight or radar data occurred.

Eight data flights were flown. Six flights utilized D-DME radio inputs smoothed with inertial velocities (IDD) to determine the position estimate; one flight utilized D-DME with true airspeed and magnetic heading for smoothing (ADD); and one flight utilized inertial velocities with no radio updating (IXX).

Four flights were flown with the autopilot in the 4-D mode although one of these flights was flown with manual throttles. The remaining flights were flown manually. The FTE was not reported for the manually flown flights.

7.2 Horizontal Axis Autopilot FTE

Figure 9 shows that the mean crosstrack FTE on the four automatic flights were all less than 150 m. This mean value is consistent with the crosstrack errors obtained on previous flights that were conducted to document the NASA B-737 guidance and flight-control systems. When the crosstrack FTE mean is not zero, it is normally caused by a constant standoff error due to airplane mistrim (fuel imbalance, thrust differential, etc.).

If the airplane is mistrimed, the airplane will roll to a small bank angle and slowly fly away from the desired course. As a crosstrack error develops, the navigation computer will command a small bank angle toward the path. However, the commanded bank angle will be just enough to compensate for the mistrim and the airplane will fly wings level with a constant crosstrack error. With the horizontal-path control law gains used on the flight, the standoff error is equal to 110 m/deg (364 ft/deg) of bank angle mistrim.

The crosstrack FTE standard deviation was less than 100 m on all flights except flight 5. This flight utilized true airspeed and magnetic heading inputs with DME updating to determine the navigation position estimate. In the ADD update mode, the position estimate changed sufficiently fast and with large enough magnitudes that the flight control system/airplane response could not react fast enough to null the guidance errors. This is the only flight where the condition was noted.

The standard deviation of the crosstrack FTE can be reduced by increasing the gains in the horizontal-path guidance equations. The horizontal path gains used in this flight test were typical of those to be used for en-route flight where precision tracking, such as required on an approach to landing, is not necessary. The mean crosstrack FTE can be nulled by incorporating a forward path integrator in the horizontal path guidance equations. Both of these methods of reducing the crosstrack FTE have been flight demonstrated for use in the terminal area.

7.3 Vertical Axis

The mean and standard deviation for the vertical-path deviations experienced on the automatic, 4-D flights are shown in figure 10. The mean altitude FTE due to the autopilot/airplane response was less than 3 m. The standard deviation of the altitude FTE for all the automatic flights was less than 5 m except for flight 1. The standard deviation for this flight was 10.8 m. On this flight the standard deviation was higher due to a noisy signal on the recording system.

A slight altitude deviation occurred at way points where there was a change in the programed flight-path angle. This was a normal characteristic of this system since no programed flight-path-angle change lead information is used by the vertical guidance algorithms. As the airplane would pass a way point where the flight-path angle changed, a vertical-path error would have to develop before the vertical-path guidance control law could command a flight-path-angle change. The magnitude of the vertical error was a function of the airplane's ground speed and the amount of flight-path-angle change but has not been observed to be greater than 60 m (200 ft) in the en-route operation.

7.4 Time Axis

Three of the automatic 4-D flights utilized the autothrottle. However, time guidance problems developed in one of these flights and resulted in no usable separation FTE data. Figure 11 shows the mean and standard deviation of the separation FTE for these two flights. For flight 1, the mean and standard deviation was 356 m (2 sec) and 1066 m (5.9 sec) respectively, and for flight 2 the mean was -9 m (0.05 sec) and the standard deviation 73 m (0.4 sec). The times specified above are based on a constant ground speed of 350 knots.

Although both flights demonstrated good time delivery accuracies, the relatively large differences in the separation FTE were due to winds aloft coupled with large path direction changes. A separation error would occur on the second leg of the test path (fig. 6) where a 300° climbing turn was programed. As the airplane would make the climbing turn, a tail wind would develop from the predominantly westerly winds aloft and the airplane would pull ahead of the time guidance box. As a result, the autothrottle would reduce the thrust and airplane's ground speed to recapture the time box. As the airplane continued around the turn, a head-wind condition would develop and the airplane would then have to increase its ground speed by an amount more than double the wind aloft speed (tail wind to head wind) to remain with the time guidance box. (The recorded inertial winds aloft for flight 1 were 45 knots, for flight 2, 20 knots, and for some of the other navigation flights, greater than 100 knots. Since the throttles were almost at maximum thrust settings to make good the climb and programed ground speed increase between the way points, little excess thrust was available to stay with the time guidance box.

A large separation error also developed on flight 1 on the last leg of the navigation test path. It was found that the airplane did not have enough drag to slow down and descend as required by the programed path unless the pilot extended the speed brakes, flaps, or landing gear to increase drag. Unless the drag was increased just as the airplane started the last leg of the path, a separation error would build quickly.

Of the three navigation error axes, the FTE in the time axis was most sensitive to path design and wind effects. Time-axis performance must be analyzed with consideration of the airplane's capabilities with respect to the flight-path design and environmental conditions.

7.5 Navigation Position Estimate Error Results

The mean and standard deviation of CPE for all the flights except flight 4 are presented in figure 12. The CPE in flight 4 cannot be calculated since a time error occurred in the airplane's data recording system during the initialization of the airborne systems. While the FTE data are usable, it is not possible to accurately correlate the ground-based radar data and the airborne data to calculate CPE.

Flights 1,2,6,7, and 8 used D-DME updating with inertial velocity smoothing to obtain the navigation position estimate. The mean CPE for these flights was approximately 276 m and the standard deviation approximately 131 m. Examination of the CPE vector for each leg of the path did not show any error trends due to path geometry. No particular inaccuracy trends were noted during turns where the DME inputs were not used because the airplane was banked steeper than 15°.

The CPE mean and standard deviation for flight 3, where only inertial velocity inputs were used to derive the position estimate, were 924 m and 478 m, respectively. While the standard deviation appears large for the entire flight, the standard deviation for each of the paths legs was less than 180 m and indicated a steady drift to the west.

Flight 5 utilized D-DME updating, smoothed with true airspeed and magnetic heading inputs. The mean CPE for flight 5 was 1350 m and the standard deviation was 1295 m. Part of the large mean and standard deviation was attributed to the automatic navigation radio tuner. The radio tuner malfunctioned intermittently, which resulted in only a single DME, or no DME, input updating the navigation position estimate during much of the flight. D-DME updating was accomplished on 40 percent of the flight, single DME accomplished 28 percent, and no DME accomplished 32 percent.

The CPE vector data were examined to see if the radio updating or the true airspeed/magnetic heading inputs were causing the large errors and rapid changes of the position estimate. It was found that the navigation position estimate was quite sensitive to small fluctuations of the DME inputs while in the D-DME update mode. This was caused by more weight being put upon the radio inputs when deriving the navigation position estimate while utilizing true airspeed and magnetic heading for smoothing rather than the more stable inertial velocity inputs.

While in the single DME and no DME update mode, the navigation estimate is based on true airspeed and magnetic heading. Little or no compensation for winds aloft is made and can result in substantial error of the navigation position estimate. This error is proportional to the amount of time that no radio updates occur and the magnitudes of the wind aloft. The wind aloft at FL230 for this flight was from the west at 30 knots.

The CPE magnitude and rapid changes were substantial enough that smooth path guidance commands could not be generated. Possible solutions to smoothing the navigation position estimate while in the ADD update mode include filtering the DME inputs before using them in the position update, changing the gains of the radio inputs, and, when D-DME inputs are not utilized, incorporating the last known winds aloft into the position estimate calculations.

7.6 Inertial System Drift

Table II shows the total flight time from the preflight to postflight radar calibrations for the navigation test flights using D-DME updates with inertial smoothing to obtain the navigation position estimate. The final radio updated position error may be compared to inertial system position drift for the total flight. Though only velocity inputs from INS 2 are used by the navigation computer for position updating purposes, the internally computed positions of all three of the inertial systems may be compared. It can readily be seen that the inertial drift is considerably greater than the final radio update position estimate.

Flights 1 and 7 are of particular interest since the inertial system used by the navigation computer had an excessive amount of drift; 2.25 n.mi. and 7.13 n.m., respectively. Inertial long-term errors do not significantly affect the navigation solution when radio updates are applied. This implies that the very accurate inertial acceleration inputs required for inertially derived position are not required to derive a position estimate when D-DME radio updating is also used.

7.7 Total Navigation Error

Table III shows the total navigation error for the horizontal, vertical, and time axes for the flights flown by the autopilot (flights 1, 2, and 5). The total navigation error in the horizontal axis was calculated by summing the crosstrack FTE and CPE means with the radar bias error. The standard deviations of these parameters were combined in a root-sum-square fashion.

Flights 1 and 2 were representative of D-DME updating with inertial velocity smoothing flights (IDD). Based on previous navigation flights to document autopilot FTE, the expected error in the horizontal axis would have been less than 390 m for the mean and less than 150 m for the standard deviation had all the flights been flown in the automatic mode.

Flight 5 utilized the D-DME update with true airspeed and magnetic heading inputs for smoothing (ADD). The large mean and standard deviation for the horizontal and time axes were due to the large and rapidly changing navigation position estimate.

The total navigation error in the vertical axis for all flights was found by summing the means of altitude FTE and the barometric altimeter error for FL230. The standard deviation is the same as that obtained for the altitude FTE since the barometric altitude correction was treated as a bias.

The total navigation error in the time axis was found by summing the means of the CPE and separation FTE with the radar bias error. The standard deviation was found by combining the CPE, separation FTE, and radar error in root-sum-square fashion.

8. SUMMARY OF RESULTS

A method of specifying total aircraft navigation error into independent horizontal, vertical, and time axes by utilizing circular position error and flight technical error was presented. Some of the important features of this method include the ability to directly compare navigation accuracies of both sophisticated and relatively non-sophisticated navigation systems in 2-, 3-, or 4-D modes of flight. The navigation error specifications for each axis are not dependent upon particular types of navigation sensor inputs such as rho/theta (VOR/DME) nor upon path geometry. The errors may be determined experimentally or theoretically.

All three axes, including the time axis, have their errors specified in units of length. It was advantageous to specify the time axis with units of length since time guidance was derived based on distance between the airplane and desired position and speed rather than directly by time. The units of length were easily converted to time units by dividing by speed.

Navigation accuracy data were presented for flights with the NASA B-737 airplane utilizing its experimental navigation, guidance, and flight control systems. The data showed that D-DME radio updating with inertial velocity smoothing results in a mean navigation position estimate error of approximately 276 m with a standard deviation of approximately 131 m.

The inertial system drift data implied that low-quality inertial inputs can be used with D-DME radio updating to obtain an acceptable navigation solution.

REFERENCES

1. Martin, A.J.; and Cosley, D.H.: ADEDS Functional/Software Requirements. Phase II - SST Technology Follow-On Program. D6-60296, Boeing Commercial Airplane Company, 1973. (Available from DOT as FAA-SS-73-19).

2. McKinstry, R. Gill: Guidance Algorithms and Non-Critical Control Laws for ADEDS and the AGCS Model NASA 515. D6-41565, The Boeing Company, 1974.

3. Approval of Area Navigation Systems for Use in the U.S. National Airspace System. Advisory Circular 90-45A. Department of Transportation, Federal Aviation Administration. February 21, 1975.

TABLE I. FLIGHT CONTROL AND NAVIGATION MODES AND SYSTEMS STATUS AND EFFECTS SUMMARY.

Flight	Flight control mode	Navigation estimate update	Remarks
1	4-D, automatic	Inertial, D-DME	None
2	4-D, automatic	Inertial, D-DME	None
3	4-D, manual	Inertial only	None
4	4-D, automatic	Inertial, D-DME	Time correlation problem, navigation estimate data invalid. Time path guidance problem, SEPR invalid; XTK and HER okay.
5	3-D, automatic Manual throttle	Air data computer, D-DME	Autotuning malfunction intermittently; caused portions of flight to utilize no or a single DME update only.
6	4-D, manual	Inertial, D-DME	Several flight control-system anomalies occurred, FTE data invalid on certain legs. Navigation estimate data okay.
7	4-D, manual	Inertial, D-DME	None
8	4-D, manual	Inertial, D-DME	None

TABLE II. TOTAL DRIFT ENCOUNTERED ON AREA NAVIGATION FLIGHT TESTS UTILIZING DUAL DME UPDATES WITH INERTIAL SMOOTHING.

Flight number	Flight time (hours)	Total Drift, n.mi.			
		Navigation estimate (a)	INS 1	INS 2	INS 3
1	1.43	0.19	Inoperative	2.25	0.86
2	1.59	0.25	1.40	1.07	0.82
4	1.62	0.10	5.81	0.57	1.58
7	1.56	0.57	1.72	7.13	0.81
8	1.27	0.38	1.81	0.41	10.04

[a]Navigation estimate uses inertial velocity inputs from INS 2 only.

TABLE III. COMBINED ERRORS OF THE NAVIGATION POSITION ESTIMATE, AUTOPILOT FLIGHT TECHNICAL ERROR, AND RADAR TRACKING ERROR FOR THE TOTAL AREA NAVIGATION TEST PATH.

Flight	Total error in horizontal axis, m		Total error in time axis, m		Total error in vertical axis, m	
	mean	σ	mean	σ	mean	σ
1	392.0	153.1	709.8	1074.2	-1.5	10.8
2	250.1	131.7	252.1	123.5	-1.0	2.6
5	1451.5	1391.2	1597.2	1733.9	0.2	5.2

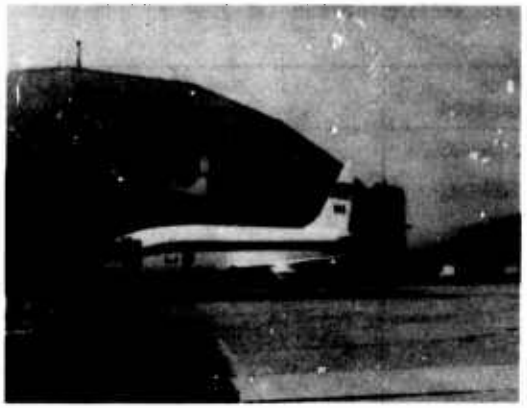

Figure 1.- Twin-jet commercial type transport test airplane.

Figure 2.- Research flight deck.

Figure 3.- Autopilot control mode panel.

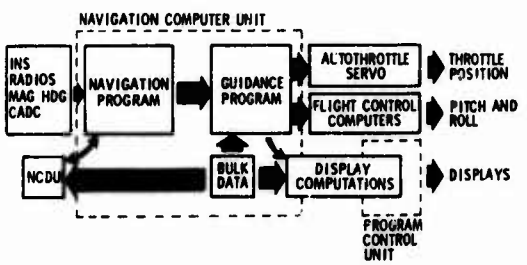

Figure 4.- Navigation, guidance, and control systems.

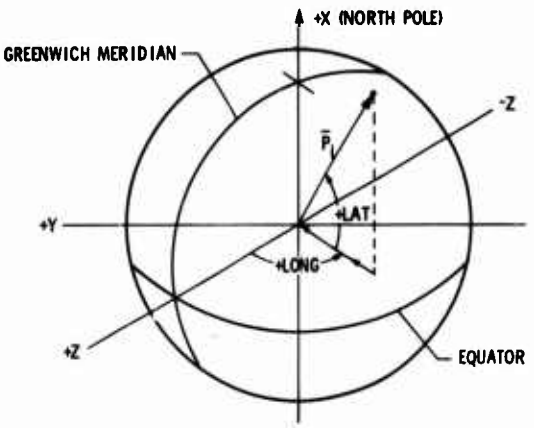

Figure 5.- Round earth and Cartesian reference system used in the navigation computer.

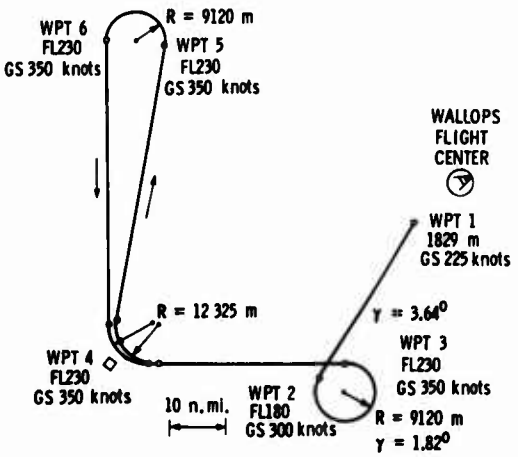

Figure 6.- Self-contained 4-D navigation flight test path.

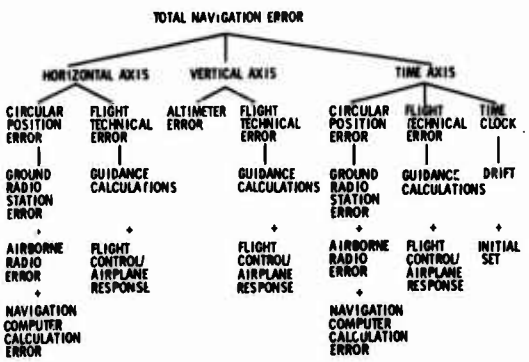

Figure 7.- Total navigation error and its axes, components, and subcomponents.

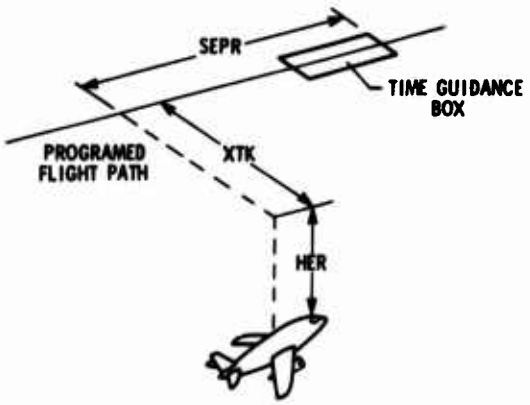

Figure 8.- Autopilot and autothrottle flight technical error.

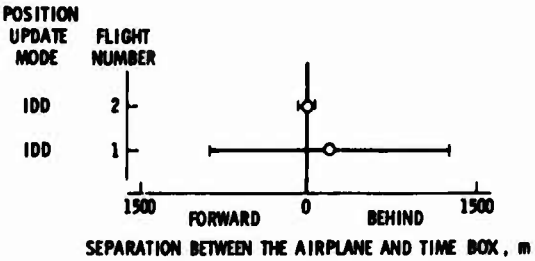

Figure 11.- Mean and standard deviation of autothrottle flight technical error for total navigation test path.

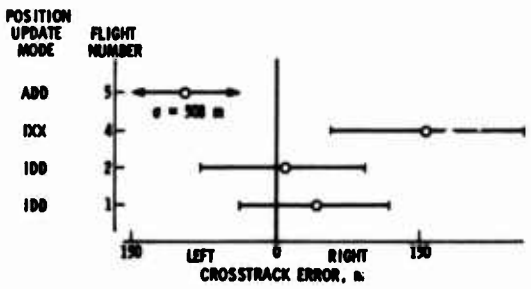

Figure 9.- Mean and standard deviation of autopilot lateral axis flight technical error for total navigation test path.

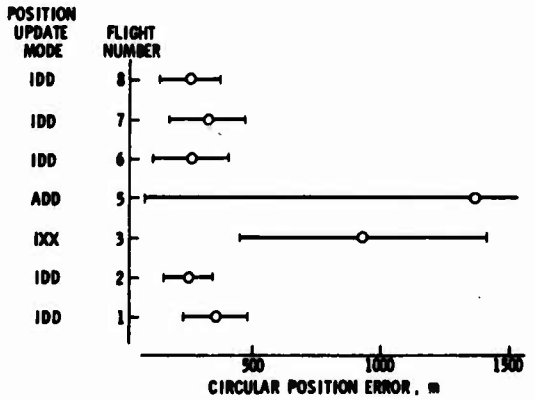

Figure 12.- Mean and standard deviation of navigation position estimate circular position error for total navigation test path.

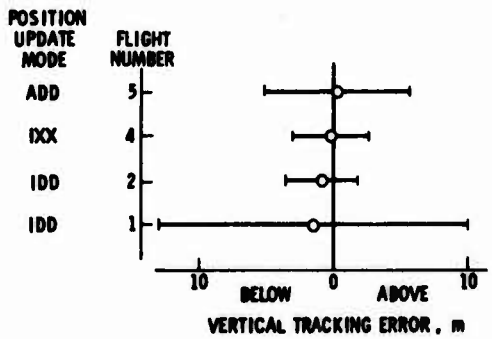

Figure 10.- Mean and standard deviation of autopilot vertical axis flight technical error for total navigation test path.

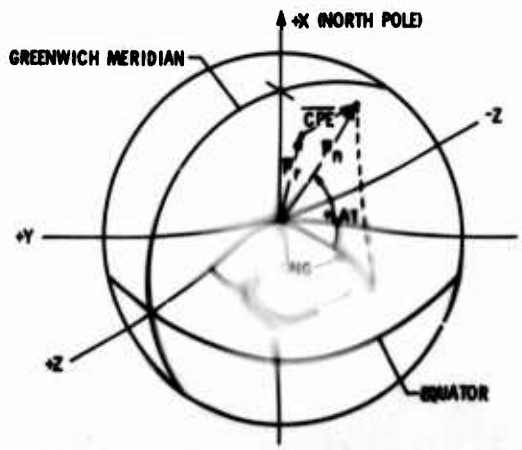

Figure 13.- Definition of the circular position error vector, CPE.

APPENDIX

CALCULATION OF $\overline{CPE}$ AND ITS DIRECTION

Calculation of $\overline{CPE}$.

$$\overline{CPE} = \overline{P}_n - \overline{P}_r$$

in which

$\overline{P}_n$ is a position vector (fig. 13) drawn from the origin of the Earth-centered Cartesin coordinate system to the navigation computer's estimated latitude/longitude position of the airplane

$\overline{P}_r$ is a similarly drawn position vector to the radar defined airplane position.

$$\overline{P}_i = (R_E + H)\{\sin(LAT_i)\hat{i} - \sin(LONG_i)\cos(LAT_i)\hat{j} + \cos(LONG_i)\cos(LAT_i)\hat{k}\}$$

where

i = r for radar defined airplane LAT/LONG

i = n for nav computer defined airplane LAT/LONG

R_E = Earth's radius (6,366,753.2 m)

H = airplane's altitude above sea level

Calculation of $\overline{CPE}$ Direction with respect to True North

$$\overline{CPE} \text{ direction} = \cos^{-1}\left[\frac{\overline{NV}\ \overline{CPE}}{|\overline{CPE}|}\right]$$

where the North pointing unit vector $\overline{NV}$ is

$$\overline{NV} = \cos(LAT)\hat{i} + \sin(LAT)\sin(LONG)\hat{j} - \sin(LAT)\cos(LONG)\hat{k}$$

DIRECT LIFT CONTROL

FOR

FLIGHT PATH CONTROL AND GUST ALLEVIATION*)

BY

GUNTHER SCHÄNZER

DIRECTOR OF THE INSTITUTE OF FLIGHT MECHANICS

TECHNICAL UNIVERSITY OF BRUNSWICK

D 3300 BRAUNSCHWEIG GERMANY

CONTENTS

*)This investigation has been sponsored by

- Ministry of Defense (ZTL)
- Ministry of Research and Technology (ZKP)
- Bodenseewerk Gerätetechnik GmbH, Überlingen
- Department of Research "Guidance and Control" at the Technical University of Brunswick, Germany (Sonderforschungsbereich 58)

1. INTRODUCTION

Direct lift control (DLC) means control of wing circulation by flap or spoiler deflections without any remarkable change in angle of attack. A change in circulations results primarily in a corresponding variation of lift besides some effects on drag and pitch moment.

Transport and fighter aircrafts are usually equipped with direct lift control surfaces such as flaps, slats or spoilers. In conventional operations (e.g. landing approach) these direct lift controlsare only set into certain discrete positions but not used in a continuous control.

In principle two essential advantages of DLC can be expected: improvement of handling qualities and gust alleviation.

- Particularly quick variation in lift, accompanied by fast vertical acceleration can be realised by DLC without remarkable pitch deviations; this will result in improvements of handling qualities, especially for heavy transport aircraft.

- Compensation of gust induced lift variation should be possible during flight in turbulent air; this will alleviate undesirable vertical acceleration and will improve passenger comfort and handling qualities. In addition the aerodynamic load of the aircraft structure due to the gusts can be reduced.

Many scientists and engeneers have become involved in order to make use of DLC. However, most of the results have not been very encouraging. What are the reasons for this poor outcome? The main reason is the coupling of desirable lift change with undesirable change of drag and pitch moment. This leads to unfavourable cross couplings with respect to handling qualities. Another reason is a design problem that can occur due to the high actuator rate, required for the DLC device. High actuator rate leads to high costs of the control actuator and actuator power supply as well as to drawbacks in the reliability of the system.

The purpose of this paper is to illustrate some of the problems, to point out the main cause of these problems and to indicate when DLC can be used successfully.

2. LIST OF SYMBOLS

$\ddot{h}$	initial acceleration normal to the flight path
L	lift
W	weight
g	gravity acceleration
t	time
ρ	air density
V	air speed
S	wing area
C_L	lift coefficient
$\Delta\alpha$	angle of attack deviation from the steady state value
δ_{DL}	direct lift device deviation from the steady state value
C_D	drag coefficient
γ	flight path angle
$\dot{V}$	steady state acceleration parallel to the flight path
k	change of drag to lift ratio due to a direct lift device deflection (see equation (8))
k_1	$= 1 - \frac{C_{D\delta DL}}{C_{L\delta DL}} \frac{C_{L\alpha}}{C_{D\alpha}}$ (see equation (18))
U_g	horizontal gust velocity
W_g	vertical gust velocity

$\dot{\delta}_{DLmax}$	max. DLC deviation rate
ω_g	efficient gust frequency
λ_{min}	shortest gust wave length
L	characteristical gust wave length
D	drag
Δ	deviation from the steady state
Q	ratio of r.m.s. cost values of integrated control system with and without DLC

SUSCRIPTS

e	equilibrium (steady state)
α	angle of attack
δ_{DL}	direct lift device deflection

3. HANDLING QUALITIES

A good quality criterion for a DLC system is the response of the aircraft flight path resulting from a step input deflection of the direct lift device.

The flight path response can be simply described, if only the initial response (high frequency response) and the steady state is considered. The initial vertical acceleration h (t=o) is proportional to the difference between lift L and weight W

$$(1) \qquad \left(\frac{\ddot{h}}{g}\right)_{t=o} = \frac{L}{W} - 1 = \frac{\Delta L}{W} \quad ,$$

where the lift is defined as

$$(2) \qquad L = \frac{\rho}{2} V^2 S(C_{Le} + C_{L\alpha}\,\Delta\alpha + C_{L\delta DL}\,\delta_{DL}) \quad ,$$

and where $\Delta\alpha$ and δ_{DL} are the deviations of the angle of attack and the direct lift device deflections from the steady state value. At the constant angle of attack the initial vertical acceleration is proportional to the direct lift device deflection.

$$(3) \qquad \left(\frac{\ddot{h}}{g}\right)_{t=o} = \frac{\rho}{2} V^2 \frac{S}{W} C_{L\delta DL}\,\delta_{DL}$$

The resulting initial flight path h(t) can be approximated by a parabola (fig 1, part I). The steady state response of the flight depends on the forces parallel to the flight path. The steady state flight path angle $\gamma_{t=\infty}$ is

$$(4) \qquad \gamma_{t=\infty} = -\frac{\dot{V}}{g} + \frac{F}{W} - \frac{C_D}{C_L}$$

where the drag coefficient C_D is defined as

$$(5) \qquad C_D = C_{De} + C_{D\alpha}\Delta\alpha + C_{D\delta DL}\,\delta_{DL} \quad .$$

Equ. (4) shows that the steady state flight path angle is proportional to the lift to drag ratio, which depends mainly on the aerodynamic properties of the DLC. For small flap or spoiler deflections, the lift to drag ratio can by liniarised as

$$(6) \qquad \frac{C_D}{C_L} = \frac{C_{De} + C_{D\delta DL}\,\delta_{DL}}{C_{Le} + C_{L\delta DL}\,\delta_{DL}} \sim \frac{C_{De}}{C_{Le}}\left(1 + \frac{C_{D\delta DL}}{C_{De}}\,\delta_{DL} - \frac{C_{L\delta DL}}{C_{Le}}\,\delta_{DL}\right)$$

A change of the lift to drag ratio as a result of a flap or spoiler deflection leads to the following change of steady state flight path angle

$$(7) \qquad \Delta\gamma = -\Delta\frac{C_D}{C_L} = -\frac{C_{De}}{C_{Le}}\left(\frac{C_{D\delta DL}}{C_{De}} - \frac{C_{L\delta DL}}{C_{Le}}\,\delta_{DL}\right)$$

$$= \frac{C_{L\delta DL}}{C_{Le}} \cdot \frac{C_{De}}{C_{Le}}\underbrace{\left(1 - \frac{C_{D\delta DL}}{C_{L\delta DL}} \cdot \frac{C_{Le}}{C_{De}}\right)}_{k}\delta_{DL}$$

which is a function of k.

$$(8) \qquad k = 1 - \frac{C_{D\delta DL}}{C_{L\delta DL}}\,\frac{C_{Le}}{C_{De}}$$

$$(7a) \qquad \Delta\gamma = \frac{C_{L\delta DL}}{C_{Le}} \cdot \frac{C_{De}}{C_{Le}}\,k\,\delta_{DL}$$

Positive values of k result in a positive change of flight path angle (fig.1). It is obvious, that negative values of k lead to non minimum phase response, which reduces the handling qualities. It can be expected for proper handling qualities, that a direct lift control system using spoilers ($C_{D\delta DL}/C_{L\delta DL} < 0$) gives better results than a system operating with flaps ($C_{D\delta DL}/C_{L\delta DL} > 0$).

4. GUST COMPENSATION

After the brief discussion of the influence of DLC on the handling qualities, a short introduction of gust compensation by means of DLC will be given.

Theoretically, an increase of lift, caused by atmospheric disturbance can be eliminated by a proper deflection of the direct lift device, such, that the resulting lift remains constant ($\Delta L=0$).

Corresponding to equ. (2), the deviation of lift is a function of the horizontal (U_g) and vertical (W_g) gust velocities.

$$(9) \qquad L = L_e + \Delta L = \frac{\rho}{2}(V_e + U_g)^2\, S\left(C_{Le} - C_{L\alpha}\frac{W_g}{V_e} + C_{L\delta DL}\,\delta_{DL}\right)$$

for ideal gust compensation ($\Delta L=0$),

$$(10) \qquad \frac{\Delta L}{L_e} = 2\frac{U_g}{V_e} - \frac{C_{L\alpha}}{C_{Le}} \cdot \frac{W_g}{V_e} + \frac{C_{L\delta DL}}{C_{Le}}\,\delta_{DL} \overset{!}{=} 0$$

the required change of lift device deflection δ_{DL} is

$$(10a) \qquad \delta_{DL} = -\frac{2\,C_{Le}}{C_{L\delta DL}}\,\frac{U_g}{V_e} + \frac{C_{L\alpha}}{C_{L\delta DL}}\,\frac{W_g}{V_e}$$

From equ. (10a) it becomes apparent, that for

$$(11) \qquad 2\,C_{Le} = C_{L\alpha}$$

the horizontal as well as the vertical gust components effect the lift to the same amount. Extremely slow aircraft (e.g. STOL) primarily responds to horizontal gust. Common fighter and transport aircrafts operate on $C_{L\alpha}$ values greater than $2\,C_{Le}$. In this case, the vertical gust portion of lift change is predominant.

$$(10b) \qquad \delta_{DL} \sim \frac{C_{L\alpha}}{C_{L\delta DL}} \cdot \frac{W_g}{V_e} \qquad \text{for } C_{L\alpha} \gg 2\,C_{Le}$$

The required deflection of the DLC surface δ_{DL} is proportional to the gust induced angle of attack

$$\alpha_g = -\frac{w_g}{V_e}$$

which is high at low airspeed. The required maximum DLC deviation rate $\dot{\delta}_{DLmax}$ for ideal gust compensation is proportional to the maximum DLC deviation and the highest efficient gust frequency ω_g.

(12) $$\dot{\delta}_{DLmax} = \omega_g \quad \delta_{DLmax}$$

where the gust frequency depends on the airspeed and the minimum gust wave length λ_{min}

(13) $$\omega_g = \frac{2\pi}{\lambda_{min}} V$$

Therefore, the required rate for complete gust compensation can be derived from equ. (10b), (12) and (13)

(14) $$\dot{\delta}_{DLmax} = \frac{C_{L\alpha}}{C_{L\delta DL}} \frac{2\pi}{\lambda_{min}} w_g$$

Equ. (14) shows, that the required DLC rate is independent of the airspeed.

The shortest efficient gust wave length is about 0,3 of the characteristical gust wavelength [1,2]

(15) $$\lambda_{min} \approx 0.3\ L$$

At flight levels higher than 300 m, the characteristic wavelength is about L = 150 m for average weather conditions [3,4]. Therefrom the shortest efficient wavelenght can be calculated as $\lambda_{min} \approx 45$ m.

The required DLC deviation and rate is given in table 1 for medium turbulence [2,3,4] and a common transport aircraft in final approach configuration

	r.m.s.-value	max. value
$\lambda_{min} = 45$ m $E\{w_g\} = 0{,}9$ m s^{-1} $V_e = 65$ m s^{-1} $\frac{C_{L\alpha}}{C_{L\delta DL}} = 4$	$E\{\delta_{DL}\} = 3{,}2^\circ$ $E\{\dot{\delta}_{DL}\} = 26^\circ$ s^{-1}	$\delta_{DL} \approx 10^\circ$ $\dot{\delta}_{DL} \approx 80^\circ$ s^{-1}

Table 1

Table 1 shows that the required DLC surface deviation will not necessarily exceed the operational limits whereas the rate can become unrealistically high. For servere turbulence ($E\{w_g = 1{,}8$ m s$^{-1}\}$) the required values are twice as much.

The DLC deviation δ_{DL} required for gust compensation with respect to constant lift (Equ. (10a)) as well as the direct influence of the horizontal and vertical gust leads to the following change in drag (similar as equ. (10))

(16) $$\frac{\Delta D}{D_e} = 2\frac{u_g}{V_e} - \frac{C_{D\alpha}}{C_{De}}\frac{w_g}{V_e} + \frac{C_{D\delta DL}}{C_{De}}\delta_{DL}$$

Substituting δ_{DL} by use of equ. (10a), results in

(17) $$\frac{\Delta D}{D_e} = 2\underbrace{\left(1 - \frac{C_{D\delta DL}}{C_{L\delta DL}}\frac{C_{Le}}{C_{De}}\right)}_{k}\frac{u_g}{V_e} - \frac{C_{D\alpha}}{C_{De}}\underbrace{\left(1 - \frac{C_{D\delta DL}}{C_{L\delta DL}}\frac{C_{L\alpha}}{C_{D\alpha}}\right)}_{k_1}\frac{w_g}{V_e}$$

The change in drag results in a forward-backward acceleration, accompanied by poor passenger comfort. If an autothrottle system is in operation, the throttle-activity will be increased by the change in drag.

The effect of horizontal gusts is compensated, if k=0 (see also equ. (8)). The drag response to vertical gust disappears, if

$$(18) \qquad k_1 = 1 - \frac{C_{D\delta DL}}{C_{L\delta DL}} \frac{C_{L\alpha}}{C_{D\alpha}} ! = 0$$

This means, that a complete gust compensation ($k=k_1=0$) can be expected only if the aircraft is flying with minimum drag speed $\frac{C_D}{C_L} = \frac{C_{D\alpha}}{C_{L\alpha}}$.

Discussing the flight path response (chapter 3) and the gust compensation, the importance of the change in the lift to drag ratio as a function of DLC deviation is obvious. Guidance and gust alleviation will be improved, if $\frac{C_{D\delta DL}}{C_{L\delta DL}} < 0$. This indicates, that a DLC system using spoilers will give better results than a system using flaps.

5. DIRECT LIFT CONTROL AS A PART OF AN INTEGRATED FLIGHT CONTROL SYSTEM

5.1 CROSS COUPLED CONTROL OF ELEVATOR THROTTLE AND DLC

The discussions of handling qualities and gust compensation have pointed out that the drag characteristics of the direct lift device are of great importance. The effect of pitch moment is obvious. The strong cross coupling between flight path to aircraft velocity and pitch attitude requires DLC elevator and throttle actuation at the same time. The question has to be answered: what is the ideal combination of elevator, throttle, flaps and spoilers and which efficiency with respect to handling qualities and gust compensation can be achieved.

The combination and cross coupling of different control surfaces demand additional signal processing and control design effort. The modern control theory gives hints for optimal control structures and calculation methods. The optimal structure of a controller is the complet tate vector feed back. This can be accomplished within an integrated flight contro system [5]. Fig.2 shows the control law structure of the integrated flight control system FRG70 of Bodenseewerk [5]. The optimal integrated flight control system is based on a certain quality criterion and particular input functions for guidance-commands and turbulence. Fig.3 shows typical input functions for a curved steep approach at medium turbulence. There is also a windshear of about 7 kn/100 ft. An adequate quality criterion has to include a fair compromise of accuracy in flight path, airspeed and angle of attack as well as in throttle activity and passenger comfort. The appendix gives a detailled description of this quality criterion.

The quality criterion can be expressed in terms of r.p.m.-cost value. For example, a Dornier Do 28 D aircraft controlled by the Bodenseewerk FRG70 integrated Flight Control System without DLC will react due to the different input functions as discribed in fig.3 in the following portions of r.m.s cost values

change in flight path command	3 %
change in angle of attack command	3 %
wind shear	10 %
horizontal and vertical gust	84 %
	100 %

Table 2. Portions of the r.m.s. cost value

This relation is realistic for curved flight path, medium turbulence and strong wind shear. Under heavy turbulence and a conventional rectiliniar flight path, the relative r.m.s. cost value due to gust increases from 84 % to 95 %. Therefore the performance of gust alleviation appears to be a very important property of an integrated flight control system.
Taking this strong influence of gust alleviation into account, the important question is: How is the reduction of the r.m.s. cost value of a control system including DLC compared to a system without DLC, when the input functions, the quality criterion and the aircraft are the same?

Because of the complexity of the integrated flight control systems it is difficult to describe the performance gain in an explicite form, which can be achieved by use of DLC. But the comparison of the results for both systems with and without DLC leads to some important answers.

All influences with respect to DLC have been investigated in a parameter study. Both, parameter of the aircraft and the control system (including sensors, control parameters, actuators) have been considered. The individual systems are optimized (minimum r.p.m. cost value). It is a surprising result, that only three of the great amount of parameters are of significant influences:

1. Compensation of pitch moment,
2. drag to lift ratio of the direct lift device,
3. limitation of the DLC control surface deflection and its maximum rate.

5.2 PITCH MOMENT COMPENSATION

Pitch moments, as a side product of DLC, must be compensated by adequate elevator deflection. In the design process for an integrated flight control system the pitch moment compensation will be effected by the optimisation procedure. The result is much dependent on the control surface layout. This explains the disadvantages of some gust alleviation systems, especially those of tailless delta wing aircraft, where the pitch moment compensation is limited because of the control surface configuration. DLC systems including strong pitch moment couplings cannot operate without a proper pitch moment compensation.

5.3 DRAG TO LIFT RATIO

The influence of drag to lift ratio of the DLC device on the control quality is extremely strong. This result could be expected from the discussions on handlung qualities (chapter 2, fig.1) and gust compensation (chapter 3). In fig.4 the ratio Q of r.m.s cost values in an optimal integrated control system with and without DLC is plotted versus k (see equ. (8)), a function of the drag to lift ratio of the DLC device. The strong influence of the drag to lift ratio on the relative r.m.s cost value Q is obvious. The best control quality, which is represented by the minimum point in fig.4 can be obtained with $k \approx 3$ and Q = 40 %. This optimal amount of cost reduction and the corresponding improvement in control qualities are rather high. The desirable value of $k \approx 3$ can be realised with drag spoilers only. The smallest reduction of cost value (maximum in fig.4) is obtained by Q = 90 % and k = -4. A value k = -4 can occur when landing flaps are used. The amount of cost reduction is so small, that the additional expense for the DLC system is not worthwhile. In case of a conventional autopilot and a DLC subsystem using landing flaps, the result can be even worse than with an integrated control system using no DLC ($Q \geq 100$ %). This explains the disadvantages experienced by such DLC systems.

When the drag to lift ratio increases considerably ($|k| > 15$), the relative cost value Q approaches a value of about 0,5 (asymptote in fig.4). This means, even with the use of plain drag flaps ($C_{L\delta DL} = 0, |k| = \infty$), the relative cost value can be reduced down to 50 %.

The surprising result, plottet in fig.4 is difficult to analyse in all its consequences. Two important outcomes shall be pointed out.

1. non minimum phase-effect in flight path control
2. phase correct drag forces to reduce throttle ativity.

5.3.1 NON MINIMUM PHASE EFFECT

The non minimum phase effect in flight path control has been discussed in principle in chapter 2, fig.1. This effect shall be discussed more in detail with regard to a step input in flight path command. A typical step response in flight path of an integrated flight control system is plotted in fig.5. The corresponding DLC deflection δ_{DL} is plotted in fig.6 for different values of k. It can be seen, that optimal DLC δ_{DL} deflection is roughly proportional to the commanded vertical acceleration $\dot{h}$. The greatest DLC movement is obtained at k = 2 (spoiler), a value that is close to the optimum value of $k \approx 3$ (see fig.4). At k = -3 (landing flaps) the DLC movement is small. Stronger DLC-activity at k = -3 would only decrease the result. At k = -7 the flaps are even retracted if the aircraft is forced to accellerate the climb.

5.3.2 PHASE CORRECT DRAG FORCE

In contrast to pure gust compensation systems, as discussed in chapter 3, only the medium and lower frequencies are weighted particularly in an integrated flight control system. Seeing the results, one should have in mind, that the integrated flight control system is designed for a major portion for gust alleviation by a strong weighing of throttle activity (table 2).

It has become evident for integrated flight control systems without DLC, that there is a close coupling between flight path accuracy and throttle activity [5] (see equ. (4)). The more accurately flight path control is required, the higher throttle activity has to be tolerated and vice versa. This coupling can be eliminated by DLC. Therefore the DLC system can take over the part of the autothrottle control system if medium and high frequency forces parallel to the flight path ($|k| > 15$) are produced.

An optimal combination of low and medium frequency autothrottle function (equ. (4) and high frequency gust compensation function (equ. (7) and (17)) can be obtained by DLC systems using spoilers ($k \approx 3$). A DLC system using high drag landing flaps ($k \approx -4$) operates its autothrottle function and its gust compensation function in the wrong phase.

5.3.3 REALISATION OF THE OPTIMAL DRAG TO LIFT RATIO

The optimal drag to lift ratio of the DLC device at $k \approx 3$ can be realised via

- the design of the DLC device
- combined deflection of flaps and spoilers

Assuming, the deflections of spoilers δ_{Sp} and flaps δ_{Fl} are proportional to δ_{DL}

$$\delta_{Sp} = \delta_{DL} \qquad \delta_{Fl} = m\,\delta_{DL}$$

then lift and drag derevatives can be termed as

(19) $$C_{L\delta DL} = C_{L\delta Sp} + m\,C_{L\delta Fl}$$

(20) $$C_{D\delta DL} = C_{D\delta Sp} + m\,C_{D\delta Fl}$$

(21) $$k = 1 - \frac{C_{Le}}{C_{De}} \frac{C_{D\delta Sp} + m\,C_{D\delta Fl}}{C_{L\delta Sp} + m\,C_{L\delta Fl}}$$

By the choise of m, desirable values of k can be adjusted as long as

(21a) $$\frac{C_{D\delta Sp}}{C_{L\delta Sp}} \neq \frac{C_{D\delta Fl}}{C_{L\delta Fl}}$$

No problems occure for combinations of flaps and spoilers, because the drag to lift ratio of spoilers is $C_{D\delta Sp}/C_{L\delta Sp} > 0$ and of flaps is $C_{D\delta Fl}/C_{L\delta Fl} < 0$. This can be achieved, if the flap and spoiler interference is small enough.

5.4 LIMITATIONS OF THE DLC CONTROL SURFACE DEFLECTION AND RATE

The investigations discussed previously are based on unlimited control surface deflection and rate. It is obvious that a limitation in deflection and rate will strongly influence the control quality and therefore the Q-value. In the extreme case of $\delta_{DLmax} = \dot{\delta}_{DLmax} = 0$ the DLC system is without any effect (Q = 100 %). Principially the function between the degree of limitation and Q can be seen as plotted in fig.7. For an unlimited system ($|\delta_{DLmax}| = \infty \quad |\dot{\delta}_{DLmax}| = \infty$) the Q-value is identical with that of fig.4. The effect of the limitation will be marked as significant, if the value of Q is increased by more than 10 %.

The integrated flight control system FRG 70 with DLC has been flight tested in an airplane type Dornier 'Do 28 D Skyservant'. This airplane operates during landing approach on k = 0,5 (see triangle in fig.4). The corresponding value of Q is 60 %. The significant influence of limitations is given in table 3.

	δ_{DLmax}	$\dot{\delta}_{DLmax}$	$\ddot{\delta}_{DLmax}$
integrated control system	6^o	$2{,}5^o\ s^{-1}$	$3{,}5^o\ s^{-2}$
ideal gust compensation (from table 1)	10^o	$80^o\ s^{-1}$	—
ratio	1,7	32	—

Table 3. Significant influence of limitation

The required actuator deflection and rate of the DLC-system are remarkably small in comparison to those required for total gust compensation. Even the required maximum acceleration with $|\ddot{\delta}_{DLmax}| = 3{,}5^o\ s^{-2}$ is so small that the effect of the inertia forces of the DLC system can be neglected.

There arises some doubt that the requirements, usually known for the DLC actuation, are effected by unrealistic requirements for ideal gust compensation.

Remarks

The datas presented here are proved for o n e example of airplains. Simulation-results confirm the effects for other types of aircraft.

6. CONCLUSION

It can be stated that control quality, especially gust alleviation, can be improved remarkably by direct lift control, if its drag to lift ratio is optimal. Spoilers are to be recommended compared with flaps. Using flaps with a high drag to lift ratio the control quality improvement is negligible. This explains the disadvantages experienced by this type of DLC. For all DLC systems a pitch moment compensation has to be included.

The required DLC activity can be kept much smaller than it is expected for ideal gust compensation. Therefore, direct lift control can be applied successfully and economically.

7. BIBLIOGRAPHY

[1] W.R. Sears : Some aspects of non stationary airfoil theory and its practical applications. J. Aeron. Sci. 8 (1941), p. 104-108

[2] G. Schänzer : Gust model for applications in flight dynamics (in German), Z. Flugwiss. Weltraumforsch. 1 (1977) Heft 3

[3] F.E. Pritchard et al.: Spectral and exeedance probability models ot atmospheric turbulence for use in aircraft design and operation. Air Force Flight Dynamics Laboratory, Wright-Patterson Air Force Base, Ohio, Rep. AFFDL-TR-65-122 (1965)

[4] C.R. Chalk et al. : Background Information and User Guide for MIL-F-8785 B (ASG) "Military Specification - Flying qualities of piloted airplanes" Air Force Flight Dynamics Laboratory Wright-Patterson Air Force Base, Ohio, Rep. AFFDL-TR-69-72 (1969)

[5] G. Schänzer, H. Böhret : Integrated Flight Control System for Steep Approach and Short Landing AGARD-CP-137 Conference Proceedings, 1973

[6] G. Coupry : Some Results on Gust Alleviation. International Conference at Atmospheric Turbulence, R. Ae. S. London, May 1971 and ONERA Rep. T.P. n° 925 (1971)

[7] G.L. Nelsen, R.C. Lorenzetti : Direct lift control for LAMS B-52 AFTI-Thesis GGC/EE/68-8, March 1968

[8] J.W. Stickle, J.M. Patton, R.C. Henry : Flight test of a direct lift control system during approach and landing NASA TN D-4854, Nov. 1968

[9] T.W. Chase, V.L. Falkner, R.F. Helfinsline : Study and simulator program to investigate the mechanisation of an aircraft flight control system that employs direct lift. Technical Rep. AFFDL-TR-68-69, Vol I-III, June 1968, Wright-Patterson AFB, Ohio

APPENDIX QUALITY CRITERION [5]

A flight control system will always be a compromise between conflicting requirements. It is required from a flight-control system that any deviations from the commanded flight path and the commanded lift coefficient are as low as possible and that, at the same time, a sufficient low throttle activity and an adequate passenger comfort will be obtained. These contradictory requirements can be defined by quality criteria. The control system structure and control parameters can be such determined, that the control system will in the best manner meet the requirements, defined in the quality criterion by means of an automatic optimization procedure. Thereby, the response to command inputs and to disturbances as well as the system stability will be determined. For the determination of the quality criterion by weighting factors an arbitary devision is made concerning the relation which shall exist between the individual cost items. In this way the priorities are defined for competitive control parameters. We have to decide for instance, whether a deviation of the lift coefficient of $\Delta C_L = 0.05$ and a flight path deviation of $\Delta h = 12$ ft have the same unfavourable effects. Increasing the weighting of the C_L-value will improve the precision of the C_L-value control but at the same time the quality of altitude hold may be deteriorated and vice versa.

The control of the C_L-value and the flight path by means of an integrated flight control system provides high accuracy also for curved steep approaches.
A control system based on extreme control accuracy however may be poor with respect to passenger comfort and low throttle activity. The requirements for low throttle activity is based almost exclusively on psychological reasons because engines roaring up and down

a) disturb the pilot as any frequent changing of the engine thrust is considered as a typical indication of an inexpert pilot;

b) alarm the passengers who suspect engine failures. This impression is still increased if the cabine pressure changes in synchronisn with the engine changes;

c) disturb the residents in the neighbourhood of the airport. Investigations made in Berlin have shown that constantly changing engine noises are perceived by the residents living in the vicinity of the airport to be much more troublesome than uniform noises of constant intensity;

d) increase the fuel consumption and reduce the life of the engines.

A suitable measure for throttle activity is the thrust rate.

Besides throttle activity and guidance accuracy in flight path and aerodynamics, the pilot and passenger comfort is the fourth important performance for the quality of a flight control system. The pilot and passenger comfort consists of two elements independent of each other:

a) translational accelerations on the pilot and passenger seats (h_p) whereby the passengers far behind the centre of gravity are particularly troubled due to gust.

b) pitching motions. The pilot is disturbed by pitching motions induced by gust especially under good visibility conditions, if the apparently moving horizon is clearly perceptible. During bad visibility conditions the pilot reacts more to the feel of vertical accelerations.

Both elements of the pilot and passenger comfort can be described by the modified C^*-criterion [5]

$$\tilde{C}^{*2} = \ddot{\tilde{h}}_p^{\,2} + (U_p\, q)^2$$

where $\tilde{h}_p$ is the weighted acceleration on a typical passenger seat, q the pitch rate and U_p the speed at which both elements have formally the same value. The relation between vertical acceleration and pitch angle rate is fixed by U_p which is independent of the aircraft type and the mission range.

The requirements of low throttle activity and high passenger comfort, and the opposing requirements for very accurate C_L-value and flight path control, are contradictory since very accurate guidance in flight path and aerodynamics call for more elevator and throttle activity. The combination of these contradicting requirements is made by a compromise based on the specifications of the user. Passenger comfort and low throttle activity must be given priority in passenger aircraft as the control system would otherwise get a bad pilot rating and be rejected. In this case, the weighting factors for low throttle activity and high passenger comfort must be increased to the inevitable detriment of the accuracy of C_L-value and flight path hold. In military aircraft priority is however frequently

given to a high guidance control accuracy disgarding the pilot's comfort. The weighting factors can only be determined on the basis of flight tests particularly for throttle activity and passenger comfort. Simulations and flight tests with different weighting factors for the quality criterion show that there is a very close relation between the C_L-value accuracy and the pitching rate (pilot's comfort) on the one hand, and the flight path control accuracy and low throttle activity on the other hand. The close correlation between accuracy of the C_L-value or the angle of attack and the pitching rate is dependent on the relation between flight path angle, angle of attack, pitch angle and the vertical gusts. High frequency disturbances of the angle of attack can only be balanced by violent and undesired pitching motions. By an appropriate selection of the weighting factors it will be possible to ensure that the medium and low frequency disturbances of the angle of attack and the C_L-value will be smoothed out accurately and that any undesired high frequency pitch attitude changes will be avoided by the use of an integrated flight control system. The relation between flight path control accuracy and low throttle activity can be shown in a simple manner by means of the known equation for forces parallel to the flight path.

$$T = W \left(\frac{C_D}{C_L} + \gamma\right)$$

Any flight path disturbance results in a change of the flight path angle whose compensation requires a thrust variation for a constant aerodynamic flow condition (C_D/C_L = const.). High frequency flight path changes inevitably cause undesired rapid thrust variations and the associated throttle activity. In contrast to conventional flight control systems consisting of damper, autopilot and autothrottle, an optimal integrated flight control system provides the desired frequency distribution between elevator and thrust [5]. An optimized integrated flight control system operates according to the principle of generally balancing the high-frequency disturbances of flight path and aerodynamics via the elevator and using the thrust only for low frequency disturbances if energy variations are necessary.

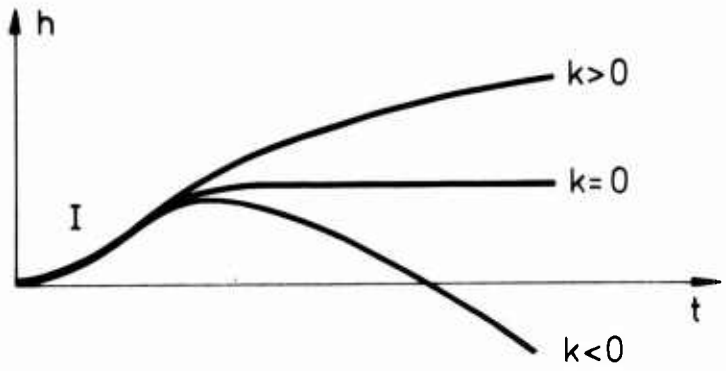

Fig. 1: Simplified height response on a step input on the direct lift control

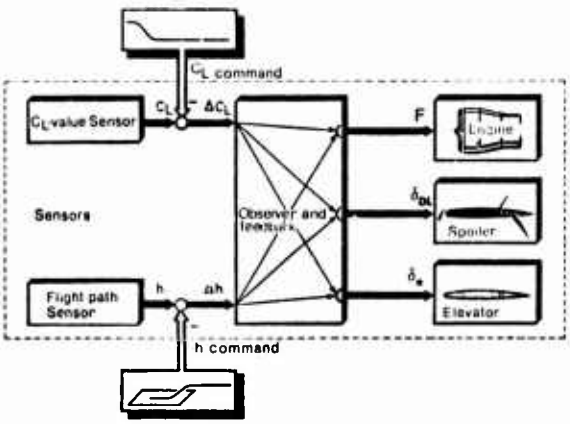

Fig. 2: Block diagramm of an Integratet Flight Control System

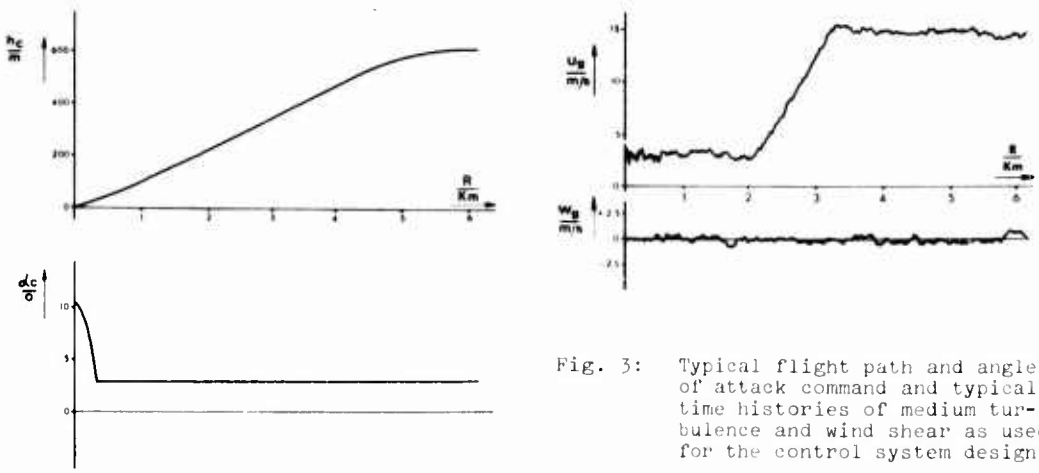

Fig. 3: Typical flight path and angle of attack command and typical time histories of medium turbulence and wind shear as used for the control system design

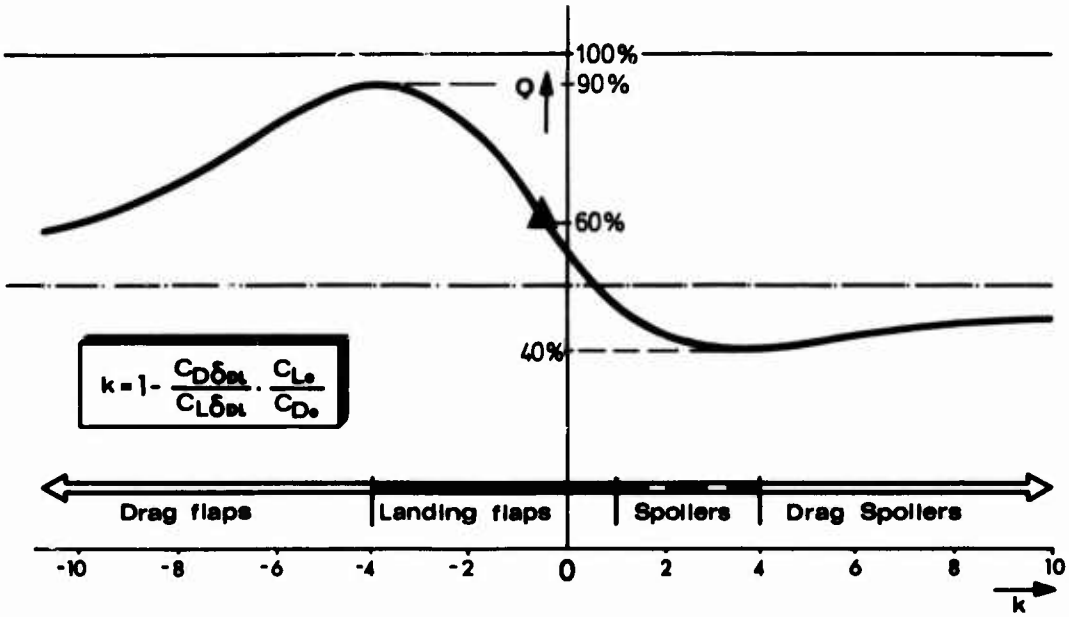

Fig. 4: Control quality as a function of the drag to lift ratio

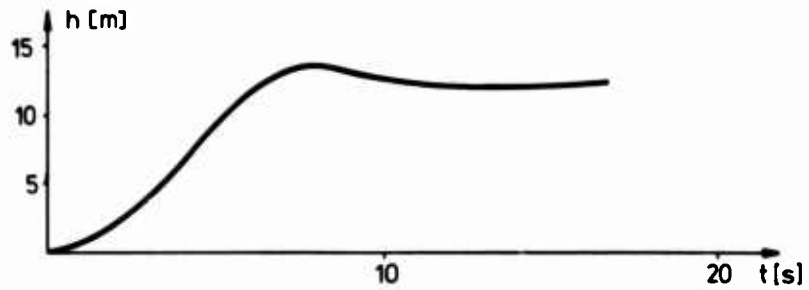

Fig. 5: Typical height response

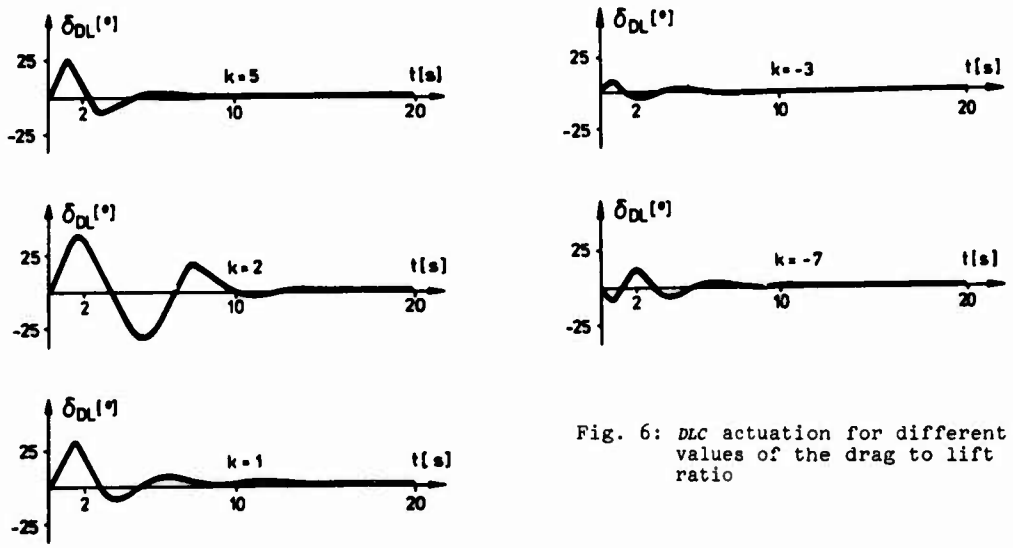

Fig. 6: *DLC* actuation for different values of the drag to lift ratio

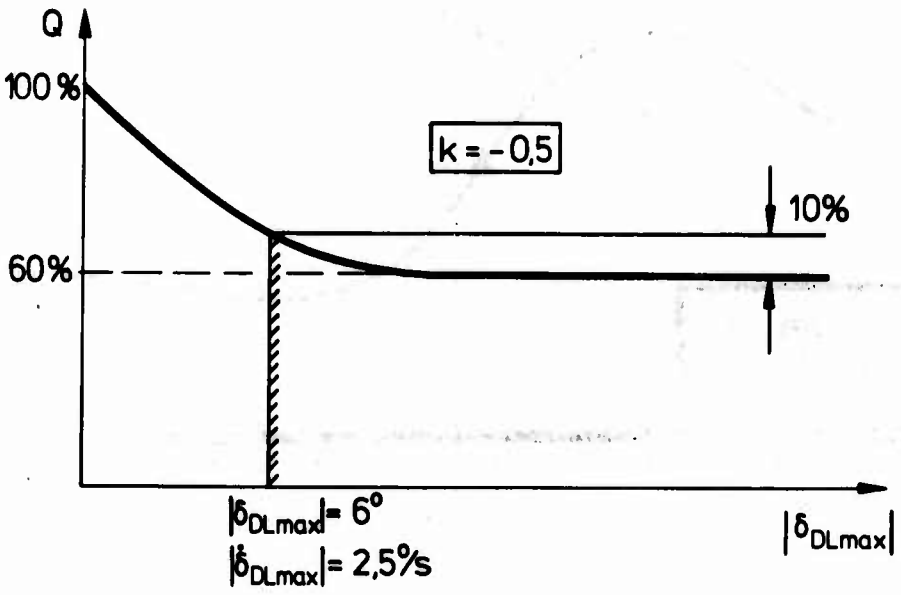

Fig. 7: Effect of limitation in δ_{DLC} deflection on the control quality reduction

NAVIGATION SYSTEM ASPECTS OF LOW ALTITUDE FLIGHT

by

Paul A. Bross
Dipl.-Physicist
ESG Elektronik-System-GmbH
Arabellastraße 4
8000 München 81
West Germany

SUMMARY

The paper considers the navigation task in low altitude missions. It first examines the requirements deriving from accurate weapon delivery in enemy controlled areas. It investigates in detail the requirements imposed on precision, integrity and safety and stresses the need for an integrated navigation system. Principal design criteria for low altitude flight are suggested.

Deriving from mission task and integrity requirements a typical system will be deployed. The importance of combining navigation as the master in the horizontal plane with Terrain Following/Radar Height Hold as the master in the vertical plane will be outlined.

The paper will then examine the requirements for a high integrity system, necessary to avoid ground hazards and to achieve mission success in low level operations. Conclusions are drawn only in connection with the navigation task, the flight control system itself not being subject of this paper. The redundancies required in their varying importance for either crossmonitoring or reversionary purposes are described.

The monitoring task will then be diversified into test circuitry designed to trace detectable failures and those for undetectable ones. The need for system monitors will be deduced, stressing their effect on system integrity and safety. The navigational parameters like attitude, speed, drift, incidence etc. and the vertical parameters like TF elevation or Radar altitude, which are of particular interest in that aspect, will be discussed in detail. Also some views are cast on the Pilot and his displays in the loop to assist in this particular duty.

From the daily technical experience arising when developing such a system to maturity and from flight test results providing inputs on dynamic properties of the system, design steps are described which have been used to overcome the impact of sensor behaviour on the system concept, that is for the crossmonitored or unmonitored reversionary case. It will be stressed in that context, that nuisance pull-ups can impair safety as much as ground proximity and the reduced requirements for the unmonitored reversion will be pointed out.

The limitations of the system are described and suggestions are made on future trends, e.g. how nuisance pull-ups can be avoided, how sensors can monitor each other in highly integrated systems.

1. INTRODUCTION

The paper considers the navigational task in low altitude missions and the requirements deriving from accurate weapon delivery in enemy controlled areas.

The Navigation System here is understood as support for the flight control system in both the horizontal and the vertical plane. It shall control the flight profile and execute the flight to avoid hazards from enemy defences on one side and ground contract on the other.
It shall therefore be precise, integer and safe. (The design of the Flight Control System itself is not subject of this paper.)

The display system is understood to assist the Navigation System in performing this task by presenting head-up and head-down information, which can also be used for further improvement of the integrity.

The following presentation is based on the design, development and partly flight test of the Tornado-Multi Role Combat Aircraft program, but outlines also proposals and future trends as seen with the personal view of the author.

2. DEFINITION OF THE MISSION TASK

To carry out single pass attacks at high speed and deliver stores with high accuracy is a need for modern air combat, as worldwide experience has shown recently. You can no longer afford to pull-up in order to acquire targets and perform a dive attack on them. If you remain at low height and near sonic speed or above, you can be certain that it will be difficult to detect or even hit you, even for advanced low level air defence systems. Therefore it is a vital need to reduce vulnerability to enemy defences in penetrating enemy controlled areas only at the lowest height possible and at high speed. There is of course a physical height restriction to about 200 ft over land due to power cables, television areals, etc.. Over sea this limit may be reduced to about 100 ft. There is no limitation on speed up to the aircrafts performance limits (Fig. 1).

Battlefield hazards can be partly avoided by selection of an appropriate track. However, tactical defence systems cannot be overcome that easy and deviations from planned track is not always possible nor desirable as the overall timing for the strike might suffer. Therefore it is important to fly as much as possible on the planned track, which in turn requires low height, high speed and precise knowledge of present position. An important factor lies here with those, who are responsible to plan the aircrafts route, possibly in between through two enemy defence areas.

Therefore we had to design a system, which is precise, integer and safe enough to get the aircraft at low height and fast to the planned target on time. This implies precise Navigation in the horizontal and in the vertical plane (Fig. 2).
Especially at low heights, the problem is one of continuous dynamic control in both horizontal and vertical planes relative to the terrain.

2.1 Horizontal Plane Considerations

For various operational reasons, such as avoidance of enemy defences, intelligence points, etc. a carefully chosen flight plan is needed. The final track for instance will be selected to facilitate target acquisition taking account of tactics being used, stores to deliver. Although increasing vulnerability, in some cases an initiating vertical manoeuvre might be required for some attacks either for visual acquisition, position fixing/target aiming or just as transition from Terrain following to a dive attack. In these cases the timing must be perfect to minimise exposure during that transition phase.

Therefore the navigation task is, to control the flight path in the horizontal plane very accurately. Position fix techniques may or may not be available or usable during the last phase of the mission, what has to be born in mind when choosing the navigational sensors and defining the Navigation System. Steering has to be equally precise in keeping the aircraft on the planned track and allow prediction of time-on-target or time-to-go within the accuracy required. Vital navigational parameters here are position (latitude, longitude), track and speed.

2.2 Vertical Plane Considerations

For the control in the vertical plane, commonly available navigational information like baro/inertial altitude or radio height are unusable. For precision reasons, a Terrain Following System will be used over land and a Radar Altimeter System over sea (i.e. Radar Height Hold). The choice of sensors is here already apparent. The vital parameters are inclination, bank, vertical speed and height.

3. INTEGRITY CONSIDERATIONS (Fig. 3)

Low level operations require a high integrity system. For the flight control system itself this is usually achieved by multiplex sensors and computations. The Navigation System which provides the basic navigation inputs could on its side also contain multiplex sensors to achieve integrity. We have, however, for cost and other reasons adopted the philosophy to choose a dissimilar redundancy concept, which offers the advantage of crossmonitoring between sensors of differing error behaviour thereby minimising the chance of a faulty monitoring process and easying the possibility of deciding (with the help of the crew, but automatically too) which the faulty sensor was. In an assimilar redundancy concept the method of majority voting must be used. However, this increases complexity even further.

As long as the monitor does not signal a discrepancy, this solution offers a high confidence level, however, if it does the disadvantage of this concept lies in the fact, that continuation of the mission is deferred to a lower confidence level.

This leads either to less safer heights, as system performance may have been reduced whereas system functions have been maintained. Also the monitoring function is lost, if the situation leading to the warning is not recoverable. (Note: We will see later in the paper what sort of problems can turn up to cause recoverable and non-recoverable monitor flags.) Without the monitoring confidence again greater heights must be adopted, which in turn are less safe from the enemy defence point of view.

Only a narrow gateway leads to an optimum design of an integer system. If the TF-system would fail (vertical situation), only an immediate escape manoeuvre is possible to climb to a safer clearance height. As this again is dangerous in rendering the aircraft vulnerable to enemy air defence, a highly integer system is required. Nuisance pull-ups must be avoided. Of course, the supporting navigation data need to be as integer as the rest of the system, as accurate navigation and track keeping were still required even with a failed TF-system. On the other hand, a proper working TF-system still protects from ground impact, even when the navigation performance is degraded.

3.1 Consequences on Navigation

For low level flight, the following parameters are essential for control of the vertical plane:

Bank angle - The TF-Radar is rollstabilised.

Drift angle - The scanning centreline of the TF must be offset by drift to look along track.

Turn rate - In turning flight special turn rate allowance is required.

Inclination - As the aircraft is pitching, this parameter is needed to derive TF elevation (depression angle).

Incidence and groundspeed are needed for calculation of commands.
TF elevation angle and Radar Altimeter height are required from the Terrain Following System for computation of commands.

For control of the horizontal plane the following parameters are of major importance:

Present Position - to stay on route
Track - to keep it
Velocity - to compute correct time and arrive in time.

All these parameters need to be integer. Therefore they are at least derived from two different sensors and monitored/or updated.

3.2 Concept for Monitoring

Principally the following requirements emerge for every system and sensor involved in-flight control. The probability of the occurence of a hazardous situation should be low. An equipment failure shall be detected with high probability. Therefore, every sensor must have a built-in-test monitor, which detects any type of equipment/sensor failure. However, the rate of undetected failures which is still an accountable percentage of the detectable ones needs to be low, as undetected failures of above parameters may lead to dangerous situations. They are at least involved in flight safety, if not safety-critical. Therefore additional system monitors have been provided, which either crossmonitor the critical parameters directly or use other system outputs to detect potentially hazardous situations. This monitoring can be split into three categories.

i) Sensor self monitoring (BITE) which will serve for

- prime mode integrity, where no redundancy is provided
- reversionary mode selection, if redundancy is provided
- reversionary mode integrity.

Therefore the overall system integrity depends on the self monitoring facilities provided within the sensors.

ii) Signal cross monitoring which provides integrity with respect to BITE-undetected errors.

iii) System performance monitor, also taking the crew within the monitoring loop. This provides decision aids for pilot (replacing sensor majority voting) and of course warnings (reminders of unobeyed commands).

3.3 Safety Aspects

For mission safety it is vital to detect errors, but the warning generated could cause the abandoning of the mission. Therefore we have tried to diversify the various warnings in those which require to abandon mission and those which still provide a safe system but also guarantee mission success.

Sometimes it may even be safer to continue the mission at low level, than abandon and pull-up. The redundancy required must be such, that you may continue with reasonable accuracy at medium confidence.

The monitoring required must be such, that all possible warnings are given but that they do not necessarily cause a pull-up and that nuisance pull-ups by faulty monitors are completely avoided.

Therefore the redundant navigation sensor provides for three important requirements:

- cross-monitoring of flight safety important parameters
- achieve mission success upon sensor failure in providing reversionary, but unmonitored modes
- avoid nuisance pull-up.

It is therefore apparent, that in the prime mode monitored data will be available; if the monitor or BITE signal warning then simplex data from either source or a reversion to fixed values will be available.

The reversionary mode of course is degraded apart from the missing monitoring functions and a compromise for the set clearance height has to be found, respecting safety implications on one and mission success on the other side.

For the three reasons above, the secondary redundant navigation sensor should be of a different type (not two Inertial Navigators) but not of a too different quality (maximum of factor 3 is accepted).

3.4 Crew Assistance in Monitoring

Some less safety involved parameters may also be cross-checked by the crew using head-up and head-down displays (HUD-HSI-ADI) in order to gain additional confidence. This of course implies that the data displayed derive from different sensors. The parameters concerned are A/C bank angle (cross-check HUD-ADI), any sort of track keeping or track acquiring information (cross-check HUD-HSI) and flight director information (HUD-ADI).

Such a highly integer system, using different sensors to achieve redundancy for reversionary and monitoring purposes, and in addition to that requiring supplementary system monitors can only be achieved by an integrated navigation system.

4. DEFINITION OF CHOSEN SYSTEM (Fig. 4)

Summing up all the aforesaid, the Navigation System supporting a Terrain Following System is made up as follows.

Primary navigation information is provided by an Inertial Navigator. Secondary navigational information is provided by an Attitude and Heading Reference and a Doppler System, all data being fed to a central computer. The Navigation computer processes all data to provide optimal steering information, which in turn feeds a Flight Director and Autopilot or serves the pilot via head-up and head-down displays to control the aircraft in the horizontal plane. It carries out additional functions like navigation updating and moding, i.e. it selects automatically the next reversionary navigation mode, if the prime mode fails indicated by an equipment BITE. As will be described further down this computer also serves in a monitoring function. For improvement of navigation data itself an open-loop Kalman Filter has been implemented, which works on the basis of velocity comparison between Doppler and Inertial Platform as well as on navigation fixing data. This filter mechanism will be used to provide useful monitoring information for the Terrain Following System.

On the other side, all information in the vertical plane are dealt within the Terrain Following Computer, where data from the Radar Altimeter and Terrain Following Radar are used to provide control information for the Flight Director and Pilot/Autopilot in the vertical plane. We know now the principal sensors needed in the system to provide a functioning Terrain Following System. We also know from previous explanations the criticality of some of the parameters in order to obtain a successful and secure TF System. And we also know that some of these parameters may fail or at least show unexpected error behaviour, which could corrupt the system. The possible error sources will be dealt with in detail later. Here we want to outline the monitors designed to make the system safe.

4.1 The Attitude (-Signal) Monitor

Bank and Inclination angles are important parameters in flying low level missions. First, because the Radar antenna is rollstabilised and second, because inclination is an important parameter when computing TF commands together with the TF Radar scan angle. Therefore we have actually implemented two attitude monitors, one in the TF computer and one in the Autopilot/Flight Director Computer. The principal monitor is build as shown in Fig. 5 for the Autopilot. First the status of the information source is checked for internally detected or transmission faults. The reason for checking the central computer status will be seen further down when talking about the derivation of secondary parameters in the computer for monitoring purposes. When every status is good the attitude monitor is entered. If the monitor yields positive results the best available data, i.e. Inertial Navigator data will be used on a monitored basis. If the attitude heading reference or the computer fail, then unmonitored single source IN data will be used, whereas upon failure of the Inertial Navigator, unmonitored AHR data are the only ones available. Only in the case of an all sensor failure or with a genuine monitor failure with no indication of a sensor BITE an Autopilot disengagement will be initiated and a pull-up commanded. A manual re-engagement on single data source is possible. If the autopilot was not engaged a fly-up command will be displayed on the Attitude Director Indicator and Head-Up-Display for Pilot's action.

The philosophy previously outlined is such, that only in case of total data loss or in case of uncertainty about the reason for the monitor discrepancy, a pull-up will be initiated. The special System Monitor-IN Data will be described later. At this stage it is only important to say that it provides an additional mean to decide, whether to use unmonitored IN data or rather not. If unmonitored data are used the clearance height for the low level flight is usually increased to a safer value accounting for the unmonitored signal and its relative accuracy. A similar attitude monitor is contained in the processor unit for the Terrain Following Radar but will be described in the context of the overall TFR monitoring circuit.

4.2 Independence of Primary/Secondary Data for Monitoring

As apparent from previous considerations the attitude signals from the Inertial Navigator and the Attitude and Heading Reference are compared with each other. The failure detection probability of the BITE for both equipments is about 80 % which leaves a certain amount of undetectable errors, i.e. slowly changing attitude by unexpectedly high drift behaviour of the vertical gyro. In order to detect discrepancies caused in such a manner on the safe side, the AHR needs to be indepedent of any IN data. This is done by

resolving the Doppler velocities (airframe fixed coordinates) with the attitude and heading information provided by the AHR and computing earth rate and transport rate compensation terms for the AHR in using these velocities. Although the attitude is slaved to the local vertical by eletrolytic switches the use of these compensation terms are necessary to improve and achieve the required attitude performance, which allows to make a cross comparison with good quality inertial data. The heading is also slaved to a magnetic compass, however in its directional gyro mode highly accurate compensation terms are also required. Thus the Doppler and Attitude/Heading Reference are a closed loop, integrated system making use of the central computer (Fig. 6).

Also latitude, which is required for earth rate corrections, will not be taken from the Inertial Navigator but integrated velocities from Doppler/AHR will be used. Defining the system in this manner renders all secondary navigation data completely independent from the primary ones. In addition, a secondary, reversionary navigation mode is automatically available in the computer and can be entered at any time, when required, i.e. failure of the Inertial Navigator.

Here we would like to outline some further properties of this secondary navigation mode. As this mode is a complete navigation mode in every sense it certainly offers to calculate any sort of parameters which would be needed other than only latitude/longitude, velocities, heading and attitude. For instance drift, incidence, vertical and ground speed or turn rate might be derived. For a low level flight (Terrain Following) all these parameters are of vital importance. Therefore we designed the system such, that these additional parameters will be used to crossmonitor the corresponding prime data from the Inertial Navigator. To compute a good turn rate, however, we used input data from the aircraft strap-down gyros, otherwise needed for the Control Stability and Augmentation System. Because all these computations are done in a computer we also implemented a Doppler noise check. This guaranteed that no Doppler data would be used for further computations if they were not noisy. This was achieved by comparing the follow-up data for change within a certain limit. In addition, the Doppler indicated itself when it went into memory. This is a double safeguard against using wrong data.

4.3 The TF System Monitor (Figures 7 and 8)

Apart from the attitude being monitored in the autopilot/flight director computer, the attitude is again monitored within the Terrain Following Computer, respective Mapping Radar which are sharing a processor unit with each other. In addition, we want to monitor system data like Drift, Incidence, Groundspeed and Turn rate. Drift is required to stabilise the antenna in the track direction and turn rate is needed to stabilise the antenna correctly when turning, i.e. looking ahead in sidewise direction. Incidence and Groundspeed are required for computation of Terrain Following commands and also define the flight vector, which is itself an important property.

Therefore the TF system monitor for the horizontal plane actually consists of two parts, an attitude signal monitoring part and a monitor for primary and secondary navigation data. The attitude monitoring part is principally identical to the one in the autopilot, except for the fact that the IN channel to the Terrain Following Computer is duplicated in order to avoid safety implications by transmission problems on one line. The same strategy has been implemented as before, that is, a pull-up is only commanded, when either both data sources (IN Primary) or Doppler, Attitude/Heading Reference, Computer (Secondary) have failed, or a monitor trip occurred when all equipment signalled functioning. If one data source only fails (Computer and Attitude/Heading Reference taken as an entity), TF may be continued on single source information being unmonitored. However, in case of an Inertial Navigator failure the set clearance height shall be increased to account for the reduced performance of the secondary data source and Warning will be given accordingly.

If primary and secondary data sources are available and functioning properly, which is always checked by BITE-Information, transmission parity and special discretes signalling the alignment state or lock-on state of the relevant equipment, a system monitor will be entered to cross compare primary and secondary information on Groundspeed, Drift, Incidence and Turn rate. If this monitor fails fixed data will be used to continue TF, although of course with increased clearance height to account for the incorrectness of fixed data. If the monitor performs as expected primary data will be used for computations of TF commands. The turn rate itself will be furthermore checked for exceedance of a set maximum value. In case it does the pilot has to take action to bring the aircraft back to the maximum rate allowed.

The TF system monitor for the vertical plane shall only be outlined here for completeness, as the TF system itself it not subject of this paper. After Radar Altimeter BITE and data crossmonitoring of the two Radar Altimeter channels a low height monitor will be entered to check Radar Height against the set clearance height. If this is too low, a warning is generated and pull-up initiated. If good and TF data are available then TF commands are computed using TF data, speed, attitude etc. to achieve a desired flight path. The Radar Altimeter as back-up itself generates also commands using the set clearance height. The most nose-up signal will be used to generate the vertical acceleration demand for use by the autopilot. If the Radar Altimeter has failed TF may be continued exercising the required care when flying without Radar Altimeter back-up, especially when flying in bad weather or over grounds with low reflectivity such as water.

4.4 The Kalman Filter-Inertial Navigator-System Monitor

In Figure 7 an IN Data Good-Monitor was mentioned which shall now be explained in more detail (Fig. 9).

The fact that we had already implemented an open-loop Kalman Filter in our central processor unit led us to an additional system monitor which is quite useful. As we have seen before, the Inertial Navigator can show an undetected, unexpected error behaviour by slow drifting vertical gyro. This might happen due to various IN-internal reasons such as badly stabilised temperature, corruption of drift compensation etc. but will not be detected by the Built-in-Test-Equipment. The attitude monitor will, due to its wide limits, not even have spotted this discrepancy. However, the Kalman Filter which is based on velocity comparison between IN and Doppler to establish a measurement vector will actually see a growing disparity between the velocities of the two sensors much earlier than a relative unsensitive attitude monitor will see. The Kalman Filter's state vector of the most predominant error variables which we modelled contained misalignment error, Doppler scale factor error and others. The initial covariance matrix Po was propagated through time and at a certain time after the last measurement the expectance for any error, for instance velocity error was limited by a circular error probability. If this error limit was vastly exceeded by the measurement, then an indication for a strange behaviour was given. We have checked the Doppler input for BITE detected errors, lock/unlock condition, made the noise and a drift value check (Drift was to be expected smaller than 30^{0}) in order to prove the reasonability of the Doppler data. We also checked the inputs from the Inertial Navigator for BITE errors and Navigation mode being correctly selected. If all data were good and still the error covariances were exceeding the set limit for a certain amount of repetitions then a visual warning was given. If the situation did not recover after an additional time the KF auto-deselected itself thereby reverting to the next available Navigation mode. In this case we assume, that the IN was causing the effect and therefore IN data for Terrain Following were declared faulty. If a genuine IN Drift fault occurs, this indication is useful, as it is given well in advance of a consequently following attitude monitor trip.

This is also the philosophy we pursued. In case of an IN Data Good failure detected by the Kalman Filter nothing is done at first. However, if the Attitude Monitor fails we check the IN Data Good Information. This serves as a decision aid whether to engage on primary (IN) or secondary (AHR) data source for the following unmonitored flight. The feature of the Doppler to be a longterm reliable velocity source has here been used to also monitor the IN outputs in the long run. A drift-corrupted Inertial Navigator exhibiting for instance a velocity error of 15 feet/sec. after a short time would have auto-deselected the Kalman Filtering processes very soon. The warning of the immanent KF deselection again provides the crew the possibility to check for any sort of faulty operation, i.e. land/sea switch of Doppler in wrong position. If everything is set up correctly but the warning persists, then this is a powerful mean to detect a possible problem and you are not surprised when sometimes later this velocity error has integrated to an attitude error of sufficient amount to make the attitude monitor trip.

4.5 Monitor for Horizontal Navigation Data

As previously outlined some lesser safety involved parameters are navigation parameter like present position derived from velocities, velocity itself and heading/track. Apart from the velocity monitor which is implemented in the Kalman Filter and which has been described already above, there is no similar monitor for present position. Therefore it will be updated at regular intervals by highly accurate position fixes which also serve for updating of best drift and heading. All these update programs are processed through the Kalman Filter to obtain optimum estimates. The improvement which we obtained on Inertial Navigator position accuracy was 70 % in using both velocity and fix information for update.

5. IMPACT OF SENSOR BEHAVIOUR ON INTENDED DESIGN

So far it looks like a perfect system. Once you come to see the practical aspects of such a highly integrated and mutually monitored system you find more problems to solve. Therefore I would like to outline now some of the interesting problems which showed up during the development and flight test of this system and how we tried to cope with it.

Therefore let us have a look at the various navigation sensors which were involved in our system and outline their particular failure behaviour which became apparent during the development and let us also describe their impact on the system as it was designed.

5.1 Inertial Navigator (Fig. 10)

The detectable errors by Built-in-Test Equipment are no longer of any concern here, because the system enables detection and provides redundancy. The usually known undetectable error, i.e. azimuth or attitude drift caused by faulty temperature stabilisation or erroneous drift compensation will now at least be detected by the Kalman Filter, as long as the Doppler works. Therefore it is now reduced to an undetectable equipment error but no longer constitutes an undetectable system error. Still, as it reduces overall system capabilities it is not acceptable that such shortcomings show up too often and therefore need to be reduced to within the limit of 20 % undetectable equipment errors. During development testing of the IN we found some unacceptably high drifting platforms probably due to drift corruption problems. This affects navigation performance in general as well as the attitude monitor, where it will cause a monitor trip, but has been rectified by hardware modifications.

The next problem we found was a high level of noise on digital outputs. This may affect the system in two ways. First it might cause a nuisance monitor trip of any sort of monitor where it is involved, or when used in conjunction with a stabilisation loop as the bank angle stabilising the Radar antenna or with a display system, like attitude angles, climb angles being displayed on the Head-up-Display, it will cause an unacceptable jittering. Here is no remedy other than reducing the digital noise to an acceptable level.

The next problem encountered during tests is the stiffness of the servo loop of the outer Roll, which is a problem directly related to other hardware, the attitude and heading reference. As this one is a three gimbal version, the roll servo of that platform may have a high gain and is therefore providing a stiff servo loop. The Inertial Navigator, however, uses a four-gimbal platform and has to cope with the non-linearities of a gimbal flip. Therefore the gain of this loop is smaller and a discrepancy may occur when flying a fast turn with high rates of changes of bank angles. Comparing the two information results in a possible monitor trip because the output from the Inertial Navigator is lagging the one from the attitude reference system.

Another not less important problem was encountered with the IN in the vertical channel (Fig. 11).

The inertial velocities and height are mixed with an input from the Air Data Computer, i.e. pressure altitude. Interesting enough, this pressure altitude was fairly good during the flight and did not give any raise to problems then. However, in the initial alignment phase due to power switch over from ground to a/c power, a short invalid altitude input would corrupt the whole vertical channel. Even if the pressure altitude input was corrected immediately thereafter, the velocity was still wrong up to 10 feet/sec. vertical speed when standing on ground. Due to the rather large time constant involved in the vertical channel loop, it took a rather long time to reduce that error. Also we had mechanised a vertical channel capable to assess error characteristics of the vertical accelerometer during the gyro-compass-alignment phase of the platform. Any acceleration error deriving from comparison with the pressure altitude on ground and the knowledge, that velocity in the vertical is zero was attributed to the accelerometer bias. Having indeed inserted faulty information from the Air Data Computer these estimates were wrong and would lead to faulty information during the whole flight. Faulty information in the vertical channel, however, influence elevation incidence, climb angle via vertical speed which in turn may cause a monitor trip in the TF system.

The last IN problem was associated with the threshold setting in the vertical channel for switching between the level flight mode (as shown in Fig. 11) and the climb/dive mode. In the climb/dive mode the height output is mainly derived from inertial data although a certain amount of slaving to the barometric input is still available. In the level flight mode the inertial output is damped by the pressure altitude input. Due to noise on the digital output signals and actual vertical aircraft excursions the original setting of 9.6 ft/sec. vertical speed was not high enough and a permanent change of modes occurred. After extensive investigations we had to raise the threshold setting to 26.4 ft/sec. which then provided an optimum vertical channel.

5.2 Doppler Radar (Fig. 10)

Here we were faced again with development errors or problems. What was uncompensated drift data, noise, servo loop or vertical channel problems there, here it was lock-on to internally reflected signals, transient outputs or scale factor errors.

Due to the fact that the Doppler Radome was not an integral part of the Doppler antenna but part of the aircraft skin and therefore separately mounted, it was important that this radome was properly harmonised. A skewed mounting can cause beam deflections which result in a faulty scale factor. Isolation problems caused internal reflections which gave a fixed velocity output when normal returns were too weak. This could be cured by hardware modifications.

A problem, however, which can not be cured is of course the fact, that the Doppler may lock on to clouds, when flying well above them. In para. 6 we will propose a possible solution to overcome this problem in making use of our Kalman Filter. However, so far we considered this problem small, as flying Terrain Following missions is usually at low level and either well below the clouds or within, but not above. Then we found intermittent transients on one or two beams which might have been caused by terrain of different reflectivity (Fig. 12). For instance flying over sea with little wind, the water surface is very smooth. If one beam now hits an island or the coast line we find transients in this beam, usually affecting two velocity outputs. These transients were of short duration (approximately up to 20 seconds) but could be large in amplitude up to 200 ft/sec.. Navigation basically was not affected, however, the secondary Navigation data which were used in TF monitoring encountered the very same transients on Vertical speed and Groundspeed and therefore caused monitor trips which were not justified.

Both this and the locking to clouds are normal Doppler phenomena and little can be done in the Doppler itself, unless you change to beam-lobing techniques. The system consequences for the Kalman Filter were negligible as the Kalman Filter would not accept large transients as valid measurement values. The effects on Transport Rate Compensation terms for the attitude and heading reference are probably also small as time duration is short. The effects, however, on the Terrain Following System are of more importance and shall be highlighted in the next two subparas.

5.2.1 Effects of Doppler Transients on Crossmonitoring

In prime mode operation of Terrain Following the Inertial Navigator data are crossmonitored by the secondary Doppler derived navigation data. If the data diverge significantly exceeding the set monitor threshold, then a fixed value reversion is selected and of course a rather poor Terrain Following performance will be obtained. Depending on flight condition, particularly at high speed the degradation in performance is extreme and safety is impaired if the pilot does not take action. Over rough undulated terrain this is even more important.

5.2.2 Effects of Doppler Transients on TF Calculations/Performance

If due to any reason the prime sensor has already failed, then secondary data derived from Doppler are the only information available. In view of the reduced system performance, this mode is only allowed at a higher set clearance height. Still, a large error on ground speed can cause significant degradation especially over rough terrain. At low speed simulations show, that a maximum negative fixed error of 80 ft/sec. is acceptable. At higher speed, this value may be increased. Errors, however, up to 200 ft/sec. especially if they occur in the negative sense are significantly impairing Terrain Following performance.

A large positive ground speed error is critical if performing let downs over very smooth water under Radar Altimeter control. At high speed, excessive undershoots may occur.

Incidence of course is also effected by errors in ground speed or vertical speed and simulations show that an error of 1.5^{o} in incidence cause a noticeable variation in the clearance height. Even at higher set clearance height an undetected transient on Doppler data is causing significant performance degradation.

Next affected by Doppler transients is the drift angle, which in turn causes a wrong positioning of the Radar antenna in the azimuth plane; any error larger than a predefined value would cause the radar beamwidth not to illuminate the terrain ahead of the aircraft in straight flight.

It is quite apparent that these errors can impair the Terrain Following performance. Even though they might occur very rarely, the circumstances prevailing when these transients occur cannot be dismissed completely, as the TF system will operate both in blind and over water coastal area conditions! Reverting to fixed value or pull-up is also not the optimal solution. We will see in para. 6 what solutions can be proposed to detect this occurrence and to optimise the reaction.

Another problem, which we found during flight tests was the along-heading scale factor. Having been established on ground during tower measurements the so found scale factor was known exactly to within 0.01 % and measurements showed repeatedly the same value. However in real world, the effective beam centre does not seem to be the geometric centre, but somewhat lower in the order of 8 '-10' boresight angle. This causes an average scale factor error of about -0.64 % which we found out with our Kalman Filter.

The state vector contained scale factor error as a variable and during all flights a mean value of about -0.6 % was found. Therefore the Kalman Filter has found an unexpected function as aid in Doppler development flight test. The scale factor could be corrected by hardware therefore improving secondary navigation data significantly and bringing their accuracy within specification limits.

5.3 Attitude and Heading Reference (Fig. 10)

The last sensor which contributes one way or the other to the TF performance is the attitude and heading reference. The AHR is operating in two modes, a directional or free gyro mode and a magnetically slaved mode. The mechanization is shortly outlined in Figure 13. In slaved mode the signal from the flux gate is used to drive the heading gyro. The synchro reference excitation signal is gain scheduled in such a manner, that the lowest possible field strength of the earth magnetic field which will be sensed amounts to 0.1 Oersted. Operationally this covers most of the earth except for polar regions, where the horizontal component of the earth field vector reduces, of course, to lower values. In order to obtain a test facility for a proper functioning of the flux gate and a valid input for the heading gyro, this horizontal field strength, as measured, was used to indicate failure, when below 0.1 Oersted. Under dynamic flight conditions, however, with a dip angle of the field vector of 60^{o} - 70^{o}, there are specific heading angles when the flux gate's measurement plane will be perpendicular to the field vector and no field will be sensed. In such an occasion the BITE will provide a warning and fail the slaved mode. This in turn fails the secondary Doppler/AHR mode which is to provide secondary navigation data for Terrain Following.

In the prime mode condition of TF this means, that unmonitored IN data will be used without crossmonitoring and a warning will be given. This of course is a nuisance, as really nothing has gone wrong.

In the reversionary mode after an IN failure this would even lead to a pull-up command, which is unacceptable. Therefore we changed the mechanization of the AHR.

Whenever a bank or inclination angle larger than 5^{o} was detected by the electrolytic switches, the FLUX GATE BITE SIGNAL was disengaged and could not affect the validity of the Doppler/AHR mode. The Flux Gate signal itself was of course disengaged as well.

Transients on digital data output for bank or inclination have been recorded. They were caused by an overload situation in the synchro-to-digital converter combined with the Flux Gate BITE warning and led to monitor trips of the attitude monitor.

Disregarding the small problems usually encountered in a development program, we have only highlighted the most significant ones affecting the availability and performance of the Terrain Following mode. In the next para. we will outline the proposals to cure the shortcomings of the system, where a hardware modification could not solve the problem.

6. EFFECT ON MONITORS AND PROPOSED DESIGN CHANGES

Those parameters which are safety involved or critical have been engaged in crossmonitors. In the original design these monitors had a set threshold limit which was mainly derived by theoretical investigations. Conclusions for the threshold settings have mainly been drawn from the allowable error limits in connection with a certain confidence height and speed and of course from the relative equipment accuracies given as specification values. Apart from the fact that specification values do not always reflect the real world behaviour particularly under dynamic conditions, as it is for instance for the attitude and heading reference, they also do not account for particular error behaviours as outlined above.

It is therefore not surprising that the initial bandwidth setting of the monitor is not optimal. During our flight tests we sampled plenty of results which we shall review now briefly.

6.1 Monitor Threshold

The relative performance of the secondary and primary navigation data sources have been assessed when the aircraft was flying in a typical "TF environment". We were interested to see the number of samples for the different intervals and of course the number of exceedances for the set monitor bandwidth. Therefore we plotted histograms of the concerned parameters using as much flight data as possible in order to obtain a good statistical meaning (Fig. 14).

This allowed also to evaluate the effect of varying the limit settings for the threshold. The figure shows a typical example for the differences between attitude angles from the Inertial Navigator and the attitude and heading reference. The quantised differences were used to draw the histogram. They were also used to produce probability curves which provided statistical data on the crossmonitoring performance. Also it could be seen, that the differences between secondary and primary data approximated to a normal distribution and a standard deviation figure could be obtained. For a good TF system operation thresholds should be as low as possible, but still for correct system operation all results should fall within these limits. It is obvious that by widening the limits, exceedances would be completely banned but the monitor would become ineffective. Therefore we had to set the limits such, that good performance was always ensured and the normal error distribution of the parameter as found during flight test, was lying within the setting of the upper and lower threshold limits.

For the bank angle for instance a wide threshold can be accepted, as the performance tolerances on this parameter are expected to be large. A nuisance trip from this parameter should no longer occur. Not so with inclination, where the threshold setting must be smaller.

6.2 Monitor Timer

Due to the previously described transients or ordinary threshold exceedances, a single transient can cause an unwanted monitor trip, if the data are not filtered. Therefore one idea we pursued was to change the monitors to introduce a timer of a set limit which again we tried to find by using data from flight test. A typical time histrogram is shown in Figure 15 which shows the number of exceedances of the set threshold value and the duration for which it lasted. They were related to three different flights, when the inclination monitor exceeded, in one flight, however, twice. Introducing a half a second filter in the monitor would remove the two short duration transients, however, the 1.5 sec. transient would still cause a break-away cross. It is apparent that a very well balanced approach between monitor limit setting and monitor timer (filter time constant) has to be adopted in order to define a correctly working system.

Bank and inclination results have been described above. A similar behaviour could be established for drift angle, elevation incidence, turn rate, ground speed and vertical velocity. However, even after having re-defined monitor thresholds and/or timer some monitor trips occurred. They were associated with degrading Doppler velocities before unlocking or Doppler noise or due to the Doppler transients described above. Use of an prolonged time filter would not reduce the likelihood of this form of monitor trip. Therefore we had to devise means to overcome that remaining problem.

6.3 System Changes and Future Trends (Fig. 16)

The basic idea here is, to make use of the system's capabilities to detect invalid signals from either source before the monitoring process is entered and to declare them invalid.

The second basic idea is, to avoid the pull-up command, when either the monitor threshold was exceeded or the signal from one source was declared invalid, by timing the warning flag or introducing an escalation theory.

The third basic idea is to ask the crew for additional assistance in visually cross-monitoring the information on redundant displays, like for instance attitude being displayed on the self-contained Attitude Director Indicator and on the Head-up Display, there deriving from the Inertial Navigator.

Coming back to the first part, it is important to recall that some rare transients on ground speed, drift or elevation incidence have been caused by Doppler transients, which in fact seem to be related to physical phenomena. Having mechanised a Kalman Filter processor on the basis of velocity comparison between Inertial Navigator and Doppler, this can be used to monitor Doppler velocities on short term, as opposed to using the Doppler velocities to monitor IN data in the long term. Therefore a Kalman Filter monitoring flag would be provided which gives a warning to the Terrain Following monitor whenever it detects unreasonable exceedance of a set bandwidth within the Kalman Filter. In such a case, a monitor trip would be disregarded. If the exceedance of the monitor threshold endured, then of course a genuine problem of either of the two equipment seems to show up and a warning was provided to the crew to check for correct mode settings etc..

Due to the attitude performance of the Doppler especially over water, we have modelled the Kalman Filter such, that Doppler gain was a function of attitude and altitude and even cut-out, when a certain bank or inclination angle was exceeded, even when the Doppler itself still showed lock-on. This was provided in order to avoid a possible corruption of the Kalman Filter and thereby the IN Data Good Information.

Last not least what can be done in that area is to introduce a special software which makes account for faulty Doppler measurement over water due to water surface movement caused by wind. This is principally not so important for Terrain Following as this is usually not lasting for a long time over water surfaces, however, for let-downs over cliffs and a following Radar Height Hold mode over sea leads to similar requirements.

Talking about the second idea and in view of the marginal performance of the present monitor mechanization, it has been considered to change the monitor so, that after exceedance of the first threshold the warning is not yet given. Either a reversion to single source IN data is being considered for a limited time before reverting to fixed values or a two level comparator where the most nose-up signal from either primary or secondary data source is used after exceeding the first threshold and a system disconnect after the second wider limit. This second wider threshold has been chosen to give a reasonable performance degradation in the safe side, but cannot completely avoid nuisance monitor trips, if the difference is excessive. However, the fixed value reversion for a possibly only short term nuisance trip is a big penalty, because higher set clearance height will be required and pilot's action as well. Therefore, because a nuisance trip is much more likely than a genuine one, we have chosen to adopt the two level comparator for certain parameters where the flight test results indicated its use. This one will reduce effects of nuisance trips on overall mission success, but still not endanger the aircraft when a real fault has occurred.

Concerning the crew assistance, it is important to indicate to the crew in which mode they are:

- Primary, monitored
- Single source, unmonitored, either IN or Doppler/AHR
- FIXED VALUE
- DISCONNECT.

It is also important for the crew that they use every additional crossmonitor information which they may obtain themselves when monitoring the displays (HUD-ADI) in order to distinguish between genuine or nuisance trips. The Kalman Filter indications here are of vital importance, because they provide the crew with information of possible discrepancies at an early stage or if this warning does not show, they provide the crew with trust that the short term nuisance trip was only caused by a transient condition.

7. CONCLUSION

In order to define a highly integrated redundant Navigation System for Terrain Following missions, an approach of dissimilar redundancy was chosen. The disadvantages encountered by using the different sensors could be used advantageously to improve the integrity of the whole system, not only from the point of view of safety but also of fulfilling the mission success rather than abandoning it or expose unnecessarily to the enemy. The price for it is complexity, however, in software only.

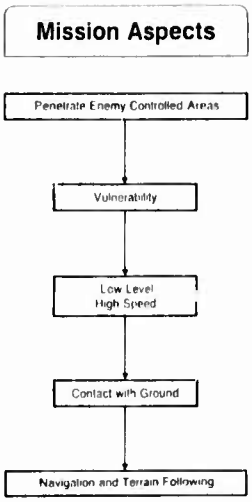

Fig 1

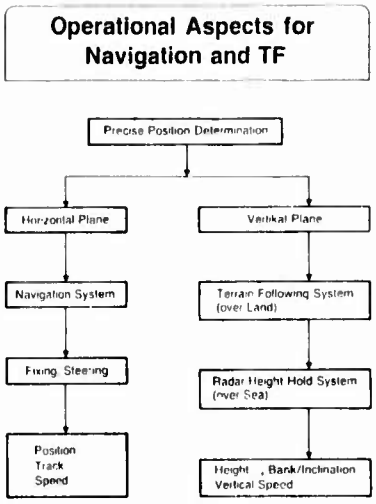

Fig 2

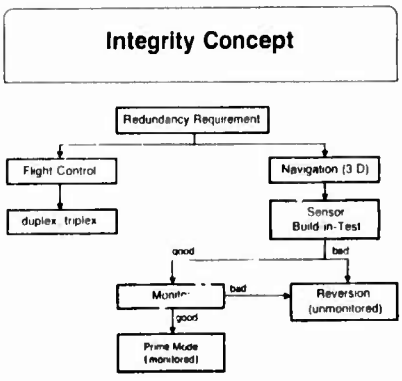

Fig.3

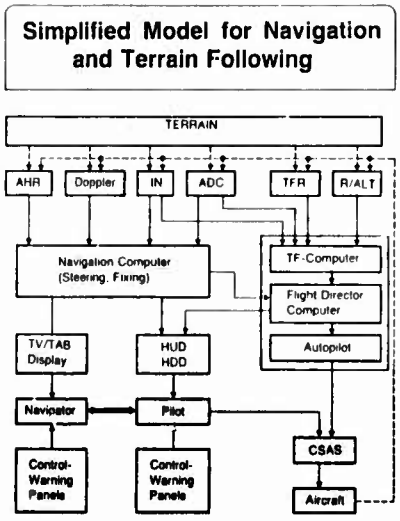

Fig.4

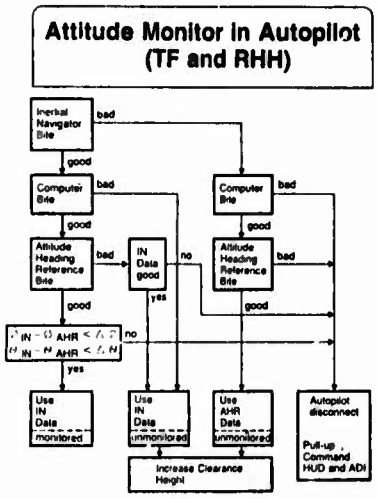

Fig. 5

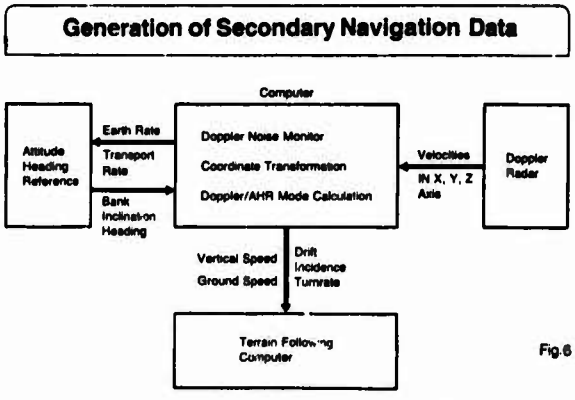

Fig.6

TF-System Mon..or Horizontal Plane

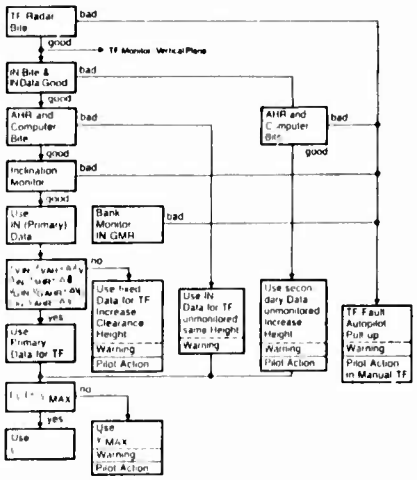

Fig 7

TF-System Monitor Vertical Plane

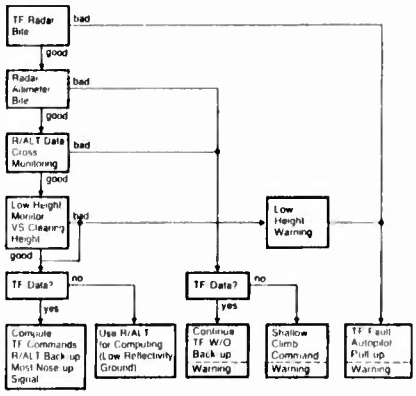

Fig 8

KALMAN FILTER – I.N. – SYSTEMMONITOR

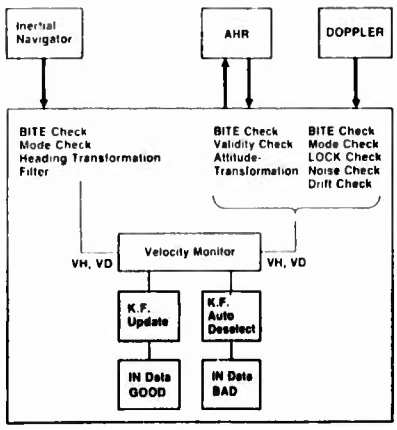

Fig.9

I.N.- DOPPLER AND AHR-ERRORS

I.N.	Platform Drift Digital Output Noise Truncation Errors Servoloop Gain Outer Roll Vertical Channel Errors
DOPPLER	False LOCK-ON LOCK-ON to clouds Velocity: TRANSIENTS: – Effects on Cross Monitoring – Effects on TF-Performance Scaling Factor Error
AHR	FLUX GATE Test Signal (0.1 OE level) Transients on Digital Data

Fig.10

INERTIAL NAVIGATOR – VERTICAL CHANNEL

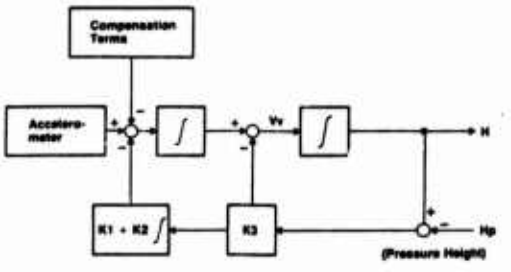

(LEVEL FLIGHT MODE)

Fig.11

DOPPLER TRANSIENTS

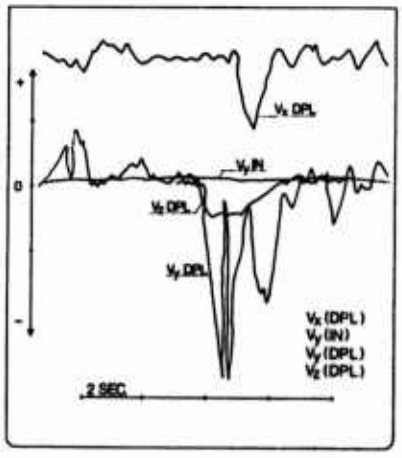

AHR – AZIMUTH CHANNEL

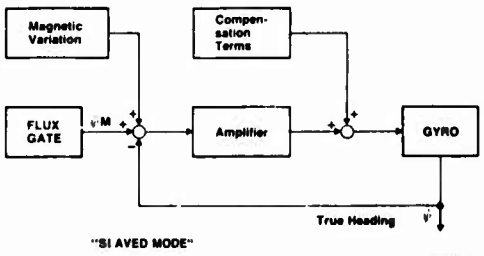

Fig. 13

HISTOGRAMM OF IN-AHR ATTITUDES

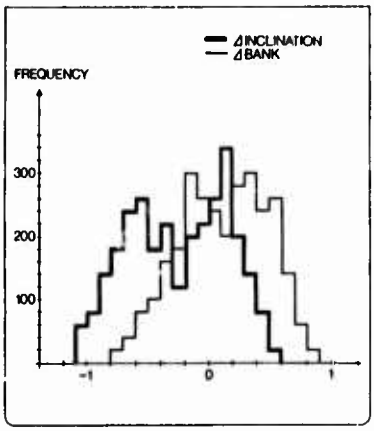

Fig.14

TIME HISTOGRAM – INCLINATION

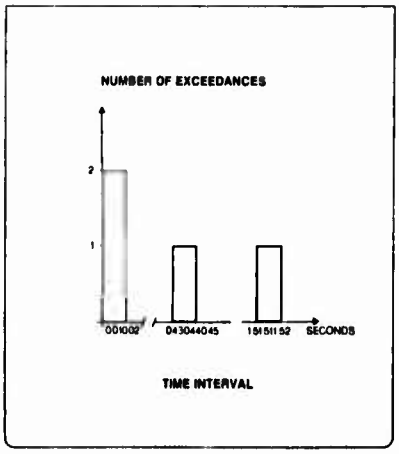

Fig.15

SYSTEM IMPROVEMENT

DETECT INVALID SIGNALS:

KF Monitors DOPPLER Data
DOPPLER Attitude Performance

AVOID NUISANCE MONITOR TRIPS:

Widen THRESHOLD on Safe Side
Introduce TIMER
Revert to SINGLE SOURCE Timelimited
Introduce TWO LEVEL COMPARATOR

CREW ASSISTANCE:

Mode Indication
Display Crossmonitoring

Fig 16

REPORT DOCUMENTATION PAGE			
1. Recipient's Reference	2. Originator's Reference AGARD-CP-240	3. Further Reference ISBN 92-835-1278-2	4. Security Classification of Document UNCLASSIFIED
5. Originator	Advisory Group for Aerospace Research and Development North Atlantic Treaty Organization 7 rue Ancelle, 92200 Neuilly sur Seine, France		
6. Title	GUIDANCE AND CONTROL DESIGN CONSIDERATIONS FOR LOW-ALTITUDE AND TERMINAL-AREA FLIGHT		
7. Presented at	the Guidance and Control Panel Symposium held in Dayton, Ohio, USA, 17–20 October 1977.		
8. Author(s) Various			9. Date April 1978
10. Author's Address Various			11. Pages 330
12. Distribution Statement	This document is distributed in accordance with AGARD policies and regulations, which are outlined on the Outside Back Covers of all AGARD publications.		

13. Keywords/Descriptors

Low level flight	Terrain avoidance	Terminal guidance
Aircraft landing	Airborne operations	Weapon delivery
Flight control		

14. Abstract

The Proceedings include papers presented at a symposium of the AGARD Guidance and Control Panel, held in Dayton, Ohio, USA, 17–20 October 1977. Twenty six papers were presented on the following topics: Operational Problems and Considerations, Terrain Following, Terminal-Area and Landing Considerations, Weapon Delivery, System Intergration

AGARD Conference Proceedings No.240
Advisory Group for Aerospace Research and Development, NATO
GUIDANCE AND CONTROL DESIGN CONSIDERATIONS FOR LOW-ALTITUDE AND TERMINAL-AREA FLIGHT
Published April 1978
330 pages

The Proceedings include papers presented at a symposium of the AGARD Guidance and Control Panel, held in Dayton, Ohio, USA, 17–20 October 1977. Twenty six papers were presented on the following topics: Operational Problems and Considerations, Terrain Following, Terminal-Area and Landing Considerations, Weapon Delivery, System Integration.

P.T.O.

AGARD-CP-240

Low level flight
Aircraft landing
Flight control
Terrain avoidance
Airborne operations
Terminal guidance
Weapon delivery

AGARD Conference Proceedings No.240
Advisory Group for Aerospace Research and Development, NATO
GUIDANCE AND CONTROL DESIGN CONSIDERATIONS FOR LOW-ALTITUDE AND TERMINAL-AREA FLIGHT
Published April 1978
330 pages

The Proceedings include papers presented at a symposium of the AGARD Guidance and Control Panel, held in Dayton, Ohio, USA, 17–20 October 1977. Twenty six papers were presented on the following topics: Operational Problems and Considerations, Terrain Following, Terminal-Area and Landing Considerations, Weapon Delivery, System Integration.

P.T.O.

AGARD-CP-240

Low level flight
Aircraft landing
Flight control
Terrain avoidance
Airborne operations
Terminal guidance
Weapon delivery

AGARD Conference Proceedings No.240
Advisory Group for Aerospace Research and Development, NATO
GUIDANCE AND CONTROL DESIGN CONSIDERATIONS FOR LOW-ALTITUDE AND TERMINAL-AREA FLIGHT
Published April 1978
330 pages

The Proceedings include papers presented at a symposium of the AGARD Guidance and Control Panel, held in Dayton, Ohio, USA, 17–20 October 1977. Twenty six papers were presented on the following topics: Operational Problems and Considerations, Terrain Following, Terminal-Area and Landing Considerations, Weapon Delivery, System Integration.

P.T.O.

AGARD-CP-240

Low level flight
Aircraft landing
Flight control
Terrain avoidance
Airborne operations
Terminal guidance
Weapon delivery

AGARD Conference Proceedings No.240
Advisory Group for Aerospace Research and Development, NATO
GUIDANCE AND CONTROL DESIGN CONSIDERATIONS FOR LOW-ALTITUDE AND TERMINAL-AREA FLIGHT
Published April 1978
330 pages

The Proceedings include papers presented at a symposium of the AGARD Guidance and Control Panel, held in Dayton, Ohio, USA, 17–20 October 1977. Twenty six papers were presented on the following topics: Operational Problems and Considerations, Terrain Following, Terminal-Area and Landing Considerations, Weapon Delivery, System Integration.

P.T.O.

AGARD-CP-240

Low level flight
Aircraft landing
Flight control
Terrain avoidance
Airborne operations
Terminal guidance
Weapon delivery

Papers presented at the Guidance and Control Panel Symposium held in Dayton, Ohio, USA, 17–20 October 1977.

ISBN 92-835-1278-2

Papers presented at the Guidance and Control Panel Symposium held in Dayton, Ohio, USA, 17–20 October 1977.

ISBN 92-835-1278-2

Papers presented at the Guidance and Control Panel Symposium held in Dayton, Ohio, USA, 17–20 October 1977.

ISBN 92-835-1278-2

Papers presented at the Guidance and Control Panel Symposium held in Dayton, Ohio, USA, 17–20 October 1977.

ISBN 92-835-1278-2

AGARD
NATO OTAN
7 RUE ANCELLE · 92200 NEUILLY-SUR-SEINE
FRANCE
Telephone 745.08.10 · Telex 610176

DISTRIBUTION OF UNCLASSIFIED AGARD PUBLICATIONS

AGARD does NOT hold stocks of AGARD publications at the above address for general distribution. Initial distribution of AGARD publications is made to AGARD Member Nations through the following National Distribution Centres. Further copies are sometimes available from these Centres, but if not may be purchased in Microfiche or Photocopy form from the Purchase Agencies listed below.

NATIONAL DISTRIBUTION CENTRES

BELGIUM
Coordonnateur AGARD – VSL
Etat-Major de la Force Aérienne
Quartier Reine Elisabeth
Rue d'Evere, 1140 Bruxelles

CANADA
Defence Scientific Information Service
Department of National Defence
Ottawa, Ontario K1A OZ2

DENMARK
Danish Defence Research Board
Østerbrogades Kaserne
Copenhagen Ø

FRANCE
O.N.E.R.A. (Direction)
29 Avenue de la Division Leclerc
92 Châtillon sous Bagneux

GERMANY
Zentralstelle für Luft- und Raumfahrt-
dokumentation und -information
c/o Fachinformationszentrum Energie,
Physik, Mathematik GmbH
Kernforschungszentrum
7514 Eggenstein-Leopoldshafen 2

GREECE
Hellenic Armed Forces Command
D Branch, Athens

ICELAND
Director of Aviation
c/o Flugrad
Reykjavik

ITALY
Aeronautica Militare
Ufficio del Delegato Nazionale all'AGARD
3, Piazzale Adenauer
Roma/EUR

LUXEMBOURG
See Belgium

NETHERLANDS
Netherlands Delegation to AGARD
National Aerospace Laboratory, NLR
P.O. Box 126
Delft

NORWAY
Norwegian Defence Research Establishment
Main Library
P.O. Box 25
N-2007 Kjeller

PORTUGAL
Direcção do Serviço de Material
da Força Aerea
Rua da Escola Politecnica 42
Lisboa
Attn: AGARD National Delegate

TURKEY
Department of Research and Development (ARGE)
Ministry of National Defence, Ankara

UNITED KINGDOM
Defence Research Information Centre
Station Square House
St. Mary Cray
Orpington, Kent BR5 3RE

UNITED STATES
National Aeronautics and Space Administration (NASA)
Langley Field, Virginia 23365
Attn: Report Distribution and Storage Unit

THE UNITED STATES NATIONAL DISTRIBUTION CENTRE (NASA) DOES NOT HOLD STOCKS OF AGARD PUBLICATIONS, AND APPLICATIONS FOR COPIES SHOULD BE MADE DIRECT TO THE NATIONAL TECHNICAL INFORMATION SERVICE (NTIS) AT THE ADDRESS BELOW.

PURCHASE AGENCIES

Microfiche or Photocopy
National Technical
Information Service (NTIS)
5285 Port Royal Road
Springfield
Virginia 22151, USA

Microfiche
Space Documentation Service
European Space Agency
10, rue Mario Nikis
75015 Paris, France

Microfiche
Technology Reports
Centre (DTI)
Station Square House
St. Mary Cray
Orpington, Kent BR5 3RF
England

Requests for microfiche or photocopies of AGARD documents should include the AGARD serial number, title, author or editor, and publication date. Requests to NTIS should include the NASA accession report number. Full bibliographical references and abstracts of AGARD publications are given in the following journals:

Scientific and Technical Aerospace Reports (STAR)
published by NASA Scientific and Technical
Information Facility
Post Office Box 8757
Baltimore/Washington International Airport
Maryland 21240, USA

Government Reports Announcements (GRA)
published by the National Technical
Information Services, Springfield
Virginia 22151, USA

Printed by Technical Editing and Reproduction Ltd
Harford House, 7–9 Charlotte St, London W1P 1HD

ISBN 92-835-1278-2